EMERGING INFECTIOUS DISEASES®

U.S. CENTERS FOR DISEASE CONTROL AND PREVENTION

Tuberculosis

March 2025

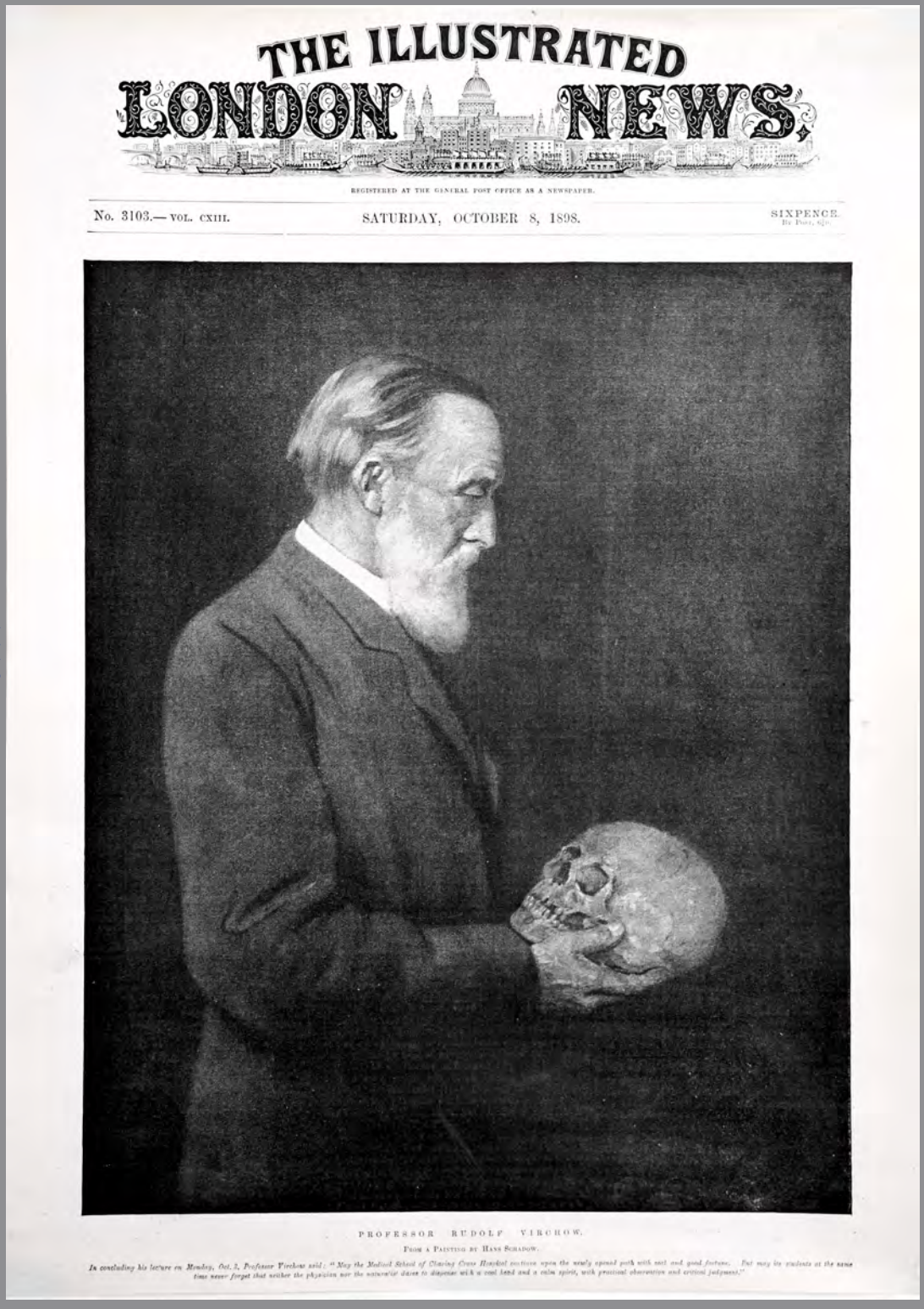

Hans Schadow (1862–1924), print of original oil on canvas portrait of Rudolf Virchow (1896). The Illustrated London News (London, UK; October 8, 1898). Private collection, Atlanta, Georgia, USA. Photography by Will Breedlove

EMERGING INFECTIOUS DISEASES®

EDITOR-IN-CHIEF
D. Peter Drotman

ASSOCIATE EDITORS

Charles Ben Beard, Fort Collins, Colorado, USA
Ermias Belay, Atlanta, Georgia, USA
Sharon Bloom, Atlanta, Georgia, USA
Richard S. Bradbury, Townsville, Queensland, Australia
Corrie Brown, Athens, Georgia, USA
Benjamin J. Cowling, Hong Kong, China
Michel Drancourt, Marseille, France
Paul V. Effler, Perth, Western Australia, Australia
Anthony Fiore, Atlanta, Georgia, USA
David O. Freedman, Birmingham, Alabama, USA
Isaac Chun-Hai Fung, Statesboro, Georgia, USA
Peter Gerner-Smidt, Atlanta, Georgia, USA
Stephen Hadler, Atlanta, Georgia, USA
Shawn Lockhart, Atlanta, Georgia, USA
Nina Marano, Atlanta, Georgia, USA
Martin I. Meltzer, Atlanta, Georgia, USA
Nkuchia M. M'ikanatha, Harrisburg, Pennsylvania, USA
David Morens, Bethesda, Maryland, USA
J. Glenn Morris, Jr., Gainesville, Florida, USA
Patrice Nordmann, Fribourg, Switzerland
Johann D.D. Pitout, Calgary, Alberta, Canada
Ann Powers, Fort Collins, Colorado, USA
Didier Raoult, Marseille, France
Pierre E. Rollin, Atlanta, Georgia, USA
Frederic E. Shaw, Atlanta, Georgia, USA
Neil M. Vora, New York, New York, USA
David H. Walker, Galveston, Texas, USA
J. Scott Weese, Guelph, Ontario, Canada

Deputy Editor-in-Chief
Matthew J. Kuehnert, Westfield, New Jersey, USA

Managing Editor
Byron Breedlove, Atlanta, Georgia, USA

Technical Writer-Editors Shannon O'Connor, Team Lead; Dana Dolan, Amy J. Guinn, Jill Russell, Jude Rutledge, Cheryl Salerno, Bryce Simons, P. Lynne Stockton, Denise Welk, Susan Zunino

Production, Graphics, and Information Technology Staff
Reginald Tucker, Team Lead; William Hale, Tae Kim, Barbara Segal

Journal Administrators J. McLean Boggess, Claudia Johnson

Editorial Assistants, Nell Stultz, Jeffrey Terrell

Communications/Social Media Candice Hoffmann, Team Lead; Patricia A. Carrington-Adkins, Heidi Floyd

Associate Editor Emeritus
Charles H. Calisher, Fort Collins, Colorado, USA

Founding Editor
Joseph E. McDade, Rome, Georgia, USA

EDITORIAL BOARD

Barry J. Beaty, Fort Collins, Colorado, USA
David M. Bell, Atlanta, Georgia, USA
Martin J. Blaser, New York, New York, USA
Andrea Boggild, Toronto, Ontario, Canada
Christopher Braden, Atlanta, Georgia, USA
Arturo Casadevall, New York, New York, USA
Kenneth G. Castro, Atlanta, Georgia, USA
Gerardo Chowell, Atlanta, Georgia, USA
Adam Cohen, Atlanta, Georgia USA
Christian Drosten, Berlin, Germany
Clare A. Dykewicz, Atlanta, Georgia, USA
Kathleen Gensheimer, Phippsburg, Maine, USA
Rachel Gorwitz, Atlanta, Georgia, USA
Patricia M. Griffin, Decatur, Georgia, USA
Duane J. Gubler, Singapore
Scott Halstead, Westwood, Massachusetts, USA
David L. Heymann, London, UK
Keith Klugman, Seattle, Washington, USA
S.K. Lam, Kuala Lumpur, Malaysia
Ajit P. Limaye, Seattle, Washington, USA
Alexandre Macedo de Oliveira, Atlanta, Georgia, USA
John S. Mackenzie, Perth, Western Australia, Australia
Jennifer H. McQuiston, Atlanta, Georgia, USA
Joel Montgomery, Lilburn, GA, USA
Frederick A. Murphy, Bethesda, Maryland, USA
Kristy O. Murray, Atlanta, Georgia, USA
Stephen M. Ostroff, Silver Spring, Maryland, USA
Christopher D. Paddock, Atlanta, Georgia, USA
W. Clyde Partin, Jr., Atlanta, Georgia, USA
David A. Pegues, Philadelphia, Pennsylvania, USA
Mario Raviglione, Milan, Italy, and Geneva, Switzerland
David Relman, Palo Alto, California, USA
Connie Schmaljohn, Frederick, Maryland, USA
Tom Schwan, Hamilton, Montana, USA
Wun-Ju Shieh, Taipei, Taiwan
Rosemary Soave, New York, New York, USA
Robert Swanepoel, Pretoria, South Africa
David E. Swayne, Athens, Georgia, USA
Kathrine R. Tan, Atlanta, Georgia, USA
Phillip Tarr, St. Louis, Missouri, USA
Kenneth L. Tyler, Aurora, Colorado, USA
Duc Vugia, Richmond, California, USA
Mary Edythe Wilson, Iowa City, Iowa, USA

Emerging Infectious Diseases is published monthly by the Centers for Disease Control and Prevention, 1600 Clifton Rd NE, Mailstop H16-2, Atlanta, GA 30329-4018, USA. Telephone 404-639-1960; email, eideditor@cdc.gov

The conclusions, findings, and opinions expressed by authors contributing to this journal do not necessarily reflect the official position of the U.S. Department of Health and Human Services, the Public Health Service, the Centers for Disease Control and Prevention, or the authors' affiliated institutions. Use of trade names is for identification only and does not imply endorsement by any of the groups named above.

All material published in *Emerging Infectious Diseases* is in the public domain and may be used and reprinted without special permission; proper citation, however, is required.

Use of trade names is for identification only and does not imply endorsement by the Public Health Service or by the U.S. Department of Health and Human Services.

EMERGING INFECTIOUS DISEASES is a registered service mark of the U.S. Department of Health & Human Services (HHS).

EMERGING INFECTIOUS DISEASES®

Tuberculosis **March 2025**

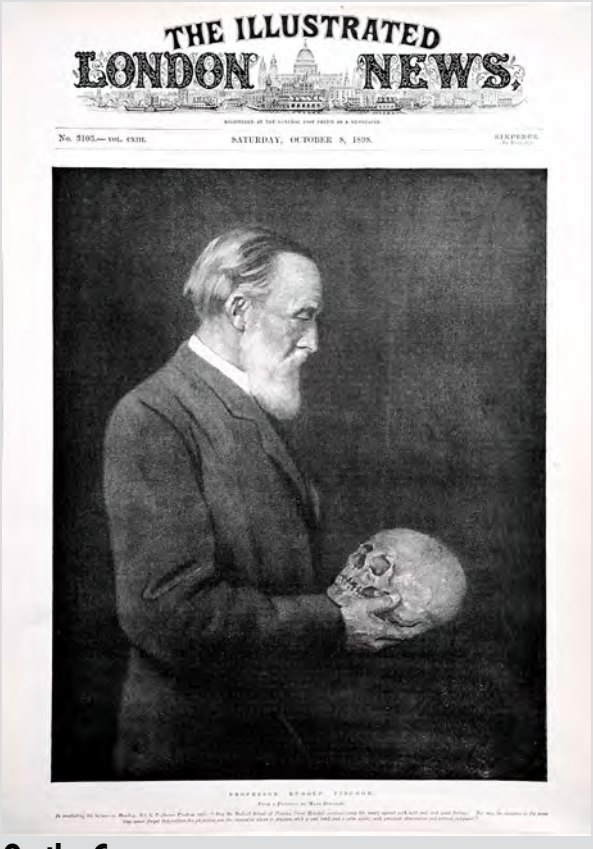

On the Cover

Hans Schadow (1862–1924), print of original oil on canvas portrait of Rudolf Virchow (1896). The Illustrated London News (London, UK; October 8, 1898). Private collection, Atlanta, Georgia, USA. Photography by Will Breedlove.

About the Cover p. 639

Synopses

Research

Medscape EDUCATION ACTIVITY

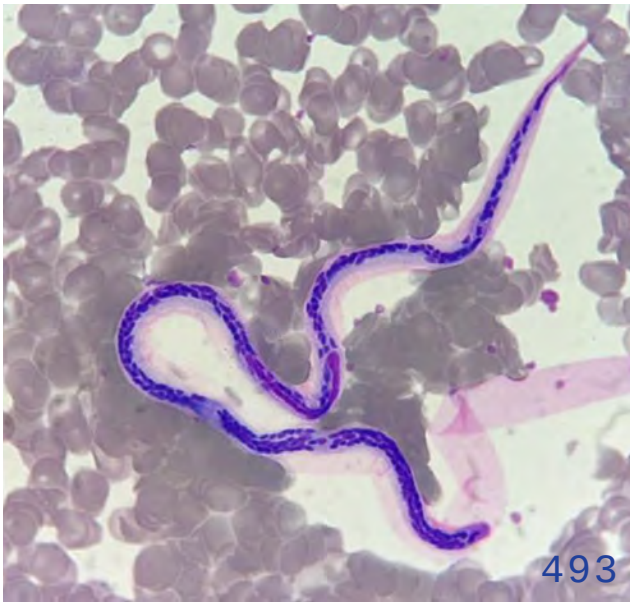

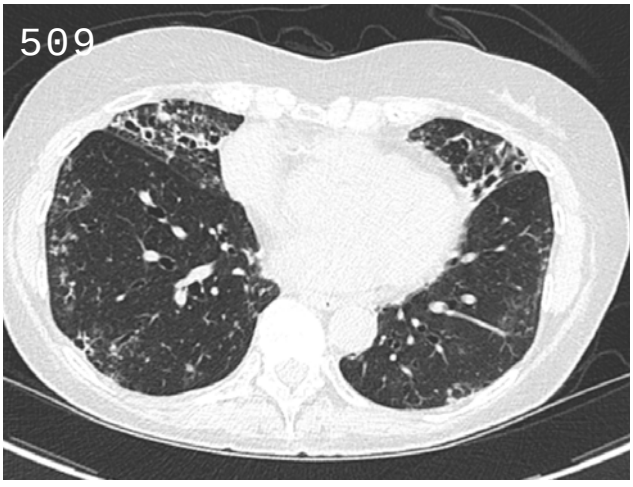

EMERGING INFECTIOUS DISEASES®
March 2025

Dispatches

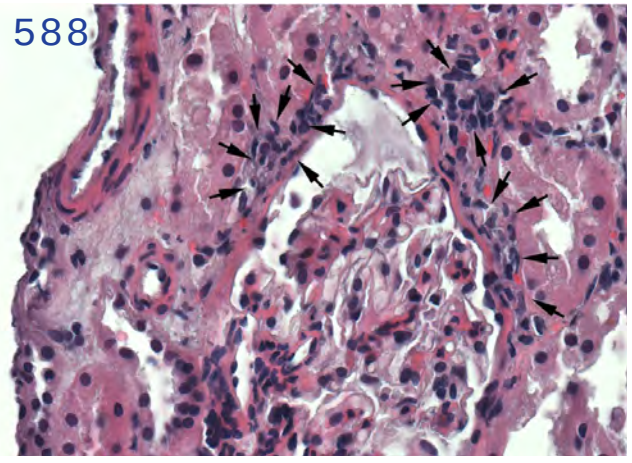

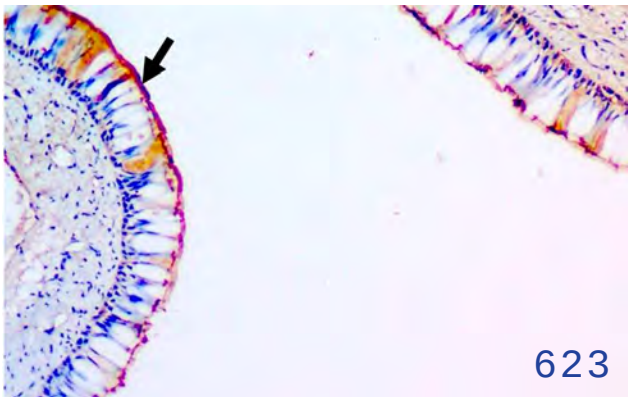

EMERGING INFECTIOUS DISEASES®
March 2025

Another Dimension

Research Letters

About the Cover

Etymologia

Online Report

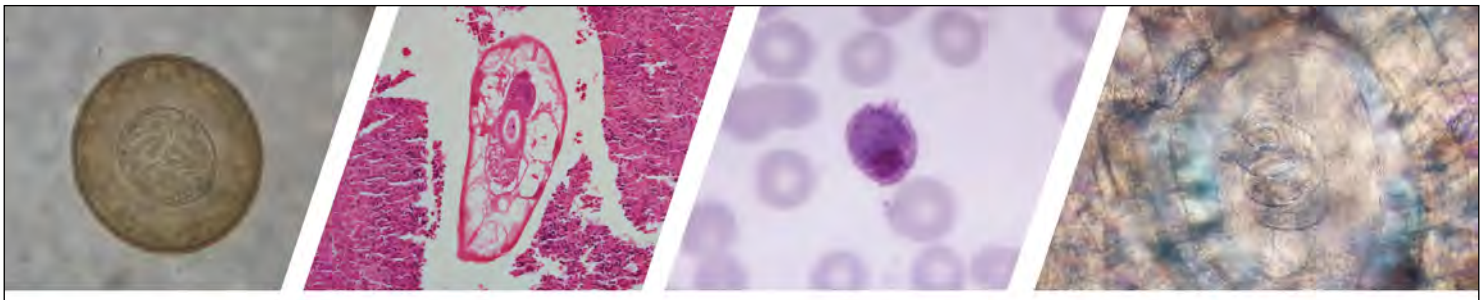

DPDx

Diagnostic Assistance and Training in Laboratory Identification of Parasites

A free service of CDC available to laboratorians, pathologists, and other health professionals in the United States and abroad

- Diagnosis from photographs of worms, histological sections, fecal, blood, and other specimen types
- Expert diagnostic review
- Formal diagnostic laboratory report
- Submission of samples via secure file share

Visit the DPDx website for information on laboratory diagnosis, geographic distribution, clinical features, parasite life cycles, and training via Monthly Case Studies of parasitic diseases.

www.cdc.gov/dpdx
dpdx@cdc.gov

U.S. Department of Health and Human Services
Centers for Disease Control and Prevention

CS272346-DE

Corynebacterium diphtheriae Infections, South Africa, 2015–2023

Mignon du Plessis, Rito Mikhari, Linda de Gouveia, Noluthando Duma, Tamsin Lovelock, Charlene Lawrence, Prasha Mahabeer, Yesholata Mahabeer, Nevashan Govender, Susan Nzenze, Jonathan Featherston, Mishalan Moodley, Jocelyn Moyes, Sibongile Walaza, Cheryl Cohen, Anne von Gottberg

We reviewed *Corynebacterium* spp. infection cases reported in South Africa during 2015–2023. We analyzed 84 isolates from 83 patients with *C. diphtheriae*, as well as 1 *C. belfantii* and 3 *C. ulcerans* isolates. Among *C. diphtheriae* cases, we observed respiratory diphtheria (26/83 patients [31%]), endocarditis (14/83 [17%]), cutaneous diphtheria (22/83 [27%]), nonspecific respiratory illnesses (5/83 [6%]), and asymptomatic carriage (16/83 [19%]). The median patient age was 19 (range 0–88) years. Diphtheria-tetanus-pertussis vaccination was incomplete for 26% (5/19) or unknown for 68% (13/19) of children 0–9 years of age. *C. diphtheriae* was intermediately resistant to penicillin (82/84 [98%] isolates; MIC_{90} 0.5 μg/mL) but susceptible to erythromycin (83/84 [99%] isolates). Eighteen unique sequence types were identified, corroborating *C. diphtheriae* heterogeneity. Toxin-producing strains were detected among cutaneous and respiratory diphtheria cases, indicating all forms of disease require monitoring and prompt public health action to curb transmission.

Diphtheria is a potentially fatal disease caused by toxigenic strains of *Corynebacterium diphtheriae*, *C. ulcerans*, or *C. pseudotuberculosis*. Diphtheria-tetanus-pertussis (DTP) vaccination has led to declines in the global incidence of diphtheria. However, since the early 1990s, a global resurgence in *C. diphtheriae* infections has occurred. Since 2023, an increase in diphtheria cases has been recorded in 4 countries (Guinea, Mauritania, Niger, Nigeria) in Africa, all of which have been experiencing ongoing, active outbreaks (*1*).

Resurgence of diphtheria has been caused by several factors, including disruptions in vaccination programs in countries with low socioeconomic status or political instability (*2*,*3*), increased awareness and reporting of nontoxigenic infections (*4*,*5*), and changing epidemiology in some settings (*6*). Adolescents and adults whose vaccine-induced or naturally induced protection wanes in the absence of sustained transmission of toxigenic strains or adequate booster immunization are particularly vulnerable during diphtheria outbreaks (*7*). Vaccine coverage of 80%–85% has been previously recommended to maintain herd immunity at the population level (*8*); however, more recent data recommend a coverage threshold of >90% (*9*).

Diphtheria toxin is the primary virulence factor in toxigenic *Corynebacterium* spp., inhibiting protein synthesis in target host cells (*10*). The phage-encoded toxin gene, *tox*, integrates into the bacterial genome by site-specific recombination. Nontoxigenic *C. diphtheriae* can produce toxin if they are lysogenized with a toxin gene–carrying corynephage. Some nontoxigenic *C. diphtheriae* isolates harbor the *tox* gene but are not able to express toxin because of a frameshift mutation or insertion sequence in this gene (referred to as nontoxigenic, toxin gene–bearing [NTTB] *C. diphtheriae*) (*11*). Although rare, NTTB *C. diphtheriae* has been reported as an emerging pathogen in some countries (*11*,*12*).

Classical respiratory diphtheria caused by toxigenic *Corynebacterium* strains is characterized by sore throat, low-grade fever, a swollen neck, and the presence of a gray/white pseudomembrane covering

Author affiliations: National Health Laboratory Service, Johannesburg, South Africa (M. du Plessis, R. Mikhari, L. de Gouveia, N. Duma, N. Govender, S. Nzenze, J. Featherston, M. Moodley, J. Moyes, S. Walaza, C. Cohen, A. von Gottberg); University of the Witwatersrand, Johannesburg (M. du Plessis, R. Mikhari, S. Walaza, C. Cohen, A. von Gottberg); Stellenbosch University and Tygerberg Hospital, Cape Town, South Africa (T. Lovelock); Western Cape Department of Health, Cape Town (C. Lawrence); National Health Laboratory Service, Durban, South Africa (P. Mahabeer, Y. Mahabeer); University of Kwazulu-Natal, Durban (P. Mahabeer, Y. Mahabeer); University of Cape Town, Cape Town (A. von Gottberg)

DOI: https://doi.org/10.3201/eid3103.241211

the tonsils, pharynx, or larynx that can cause airway obstruction and suffocation. Reports of invasive infections caused by nontoxigenic *C. diphtheriae* have notably increased and can manifest as bacteremia, endocarditis, and other more unusual clinical syndromes (*13*,*14*). Cutaneous diphtheria, also caused by *C. diphtheriae* (toxigenic or nontoxigenic) in skin lesions or nonhealing ulcers, is often less severe but might serve as a potential reservoir for transmission of toxigenic and nontoxigenic *C. diphtheriae* (*15*).

Treatment for toxigenic diphtheria involves administering diphtheria antitoxin (DAT) to neutralize circulating toxin and antimicrobial drugs (β-lactams or macrolides) to eradicate the bacterium in patients and close contacts. However, a global shortage of DAT and bacterial resistance to first-line antimicrobial drugs have been reported, potentially complicating clinical management of *C. diphtheriae* infections (*16*–*18*). Genomic data can clarify the distribution of resistance determinants and their association with phenotype or lineage. We evaluated characteristics of isolates from reported *C. diphtheriae* infections in South Africa during 2015–2023 by using epidemiologic and molecular methods.

Methods

Ethics Approval

Investigations related to notifiable medical conditions, including access to medical records, are allowable in South Africa under the terms of the National Health Act 2003 (Act No. 61 of 2003): Regulations Relating to the Surveillance and Control of Notifiable Medical Conditions. Furthermore, the South Africa National Institute for Communicable Diseases of the National Health Laboratory Service is subject to oversight by the Human Research Ethics Committee of the University of the Witwatersrand, Johannesburg, regarding the application of good clinical and laboratory practice while serving the interests of public health in the collection, analysis, and interpretation of communicable diseases data (ethics certification no. M160667).

Disease Classification/Category

Diphtheria is a category 1 legally notifiable medical condition in South Africa. Diagnostic laboratories send clinical specimens and isolates of *C. diphtheriae*, *C. ulcerans*, and *C. pseudotuberculosis* from patients with suspected respiratory or cutaneous diphtheria, or any other clinical manifestation, to the national reference laboratory for confirmation and toxin production analysis.

We classified infections as respiratory diphtheria (detection of toxigenic *C. diphtheriae/ulcerans/pseudotuberculosis* in nose or throat samples of patients with respiratory illness), cutaneous diphtheria (detection of toxigenic or nontoxigenic *C. diphtheriae/ulcerans/pseudotuberculosis* in a nonhealing ulcer or wound), or endocarditis (detection of *C. diphtheriae* in blood and clinical signs compatible with endocarditis). We classified patients with nonspecific respiratory disease as those with nontoxigenic *C. diphtheriae* infections incidentally isolated during routine microbiology laboratory workup. We classified persons as asymptomatic if they were carriers of *C. diphtheriae* (in the nose or throat) and in close contact with symptomatic patients who had laboratory-confirmed *C. diphtheriae* infections.

Laboratory Methods

We confirmed species identification of isolates by using matrix-assisted laser desorption/ionization time-of-flight mass spectrometry (*19*); we used a Microflex LT/SH analyzer with FlexControl version 3.4.135 and FlexAnalysis version 3.4.76.00 software (Bruker Daltonics, https://www.bruker.com). In addition, we performed PCR to identify the *rpoB* gene specific for *C. diphtheriae*, the *rpoB* gene specific for *C. ulcerans*/*pseudotuberculosis*, and the *tox* gene for all 3 species (*20*). We used a modified Elek test to measure toxin production (*21*). We performed antimicrobial susceptibility testing by using the broth microdilution method according to Clinical and Laboratory Standards Institute (CLSI) guidelines (*22*). We used Sensititer STP6F MIC panels (Thermo Fisher Scientific, https://www.thermofisher.com) to test susceptibility to 20 antimicrobial drugs (Appendix 1 Table, https://wwwnc.cdc.gov/EID/article/31/3/24-1211-App1.xlsx). We used the API Coryne kit (bioMérieux, https://www.biomerieux.com) to measure nitrate reduction. When they were available, we extracted basic patient demographic and clinical data from medical records, including year of symptom onset, patient sex, region (province), specimen type, clinical diagnosis, DTP vaccination history, hospitalization, and outcome.

Genome Sequencing and Characterization

We extracted and sequenced DNA from *C. diphtheriae* as previously described (*23*) by using an Illumina NextSeq 1000/2000 instrument (Illumina, https://www.illumina.com); coverage depth was ≥100×. We trimmed raw reads by using Trim Galore version 0.6.2 (Babraham Bioinformatics, https://www.bioinformatics.babraham.ac.uk) and de novo assembled the reads by using SPAdes version 3.12.0 (*24*). We performed assembly quality checks by using BUSCO version 5.8; assembly completeness of >90% was the cutoff for inclusion

(*25*). We deposited raw sequences in the National Center for Biotechnology Information BioSample database (https://www.ncbi.nlm.nih.gov/biosample; accession nos. SAMN45099837–922) (Appendix 1 Table). We submitted assembled genomes to the Insitut Pasteur Bacterial Isolate Genome Sequence *C. diphtheriae* database (https://bigsdb.pasteur.fr/diphtheria) for curation and sequence type (ST) assignments. We used core genome multilocus sequence typing (cgMLST) of 1,305 loci for sublineage (SL) classification within the database by using a 500-allelic mismatch threshold (*26*,*27*).

We analyzed genomic features, such as antimicrobial resistance genes (*pbp2m* for penicillin and *ermX* for erythromycin resistance), biovar (the presence of the *spuA* gene [DIP0357 locus] indicated biovar gravis; absence of *spuA* indicated biovar mitis), and known virulence genes, by using the diphtOscan framework with assembled genomes as inputs (*17*,*27*). To verify the presence or absence of antimicrobial resistance genes, we scanned raw reads by using DeepARG version 1.0.4 after converting reads from fastq format to fasta with SeqKit (*28*,*29*).

Phylogeny

Using JolyTree version 2.1, we generated an alignment-free, distance-based tree for phylogenetic inference of 84 assembled genomes (*30*) and 2 additional genomes from clinical isolates collected in South Africa during the 1980s (for which no clinical or demographic data were available). We used the tree alongside a cgMLST-based MAFFT alignment generated by using Genome Comparator to serve as input for ClonalFrameML version 1.2 (*31*); we visualized and annotated the tree by using iTOL (https://itol.embl.de). To enhance resolution among outbreak clusters, we determined single-nucleotide polymorphisms (SNPs) and SNP distances by mapping assembled reads of each genome to a *C. diphtheriae* reference strain (GenBank accession no. NCTC13129) by using the Split Kmer analysis tool (S.R. Harris, unpub. data, https://doi.org/10.1101/453142).

Results

During the study period, 83 *C. diphtheriae*, 1 *C. belfantii*, and 3 *C. ulcerans* infection cases were reported nationally. No cases of *C. pseudotuberculosis* were reported.

C. diphtheriae Infections

The clinical categories for 83 *C. diphtheriae* culture-positive cases were as follows: toxigenic respiratory diphtheria (26/83 [31%] patients), cutaneous diphtheria (22/83 [27%]), nontoxigenic infective endocarditis (14/83 [17%]), asymptomatic (16/83 [19%]), and nonspecific respiratory illness (5/83 [6%]) (Table 1; Figure 1). Of the 83 patients, 50 (61%) were male and 32 (39%) female; sex was not recorded for 1 person. Median age was 19 years (range 6 months–88 years). DTP vaccination status was incomplete for 26% (5/19) or unknown for 68% (13/19) of children <10 years of age (only 1 child was fully vaccinated). One patient's throat was colonized with 2 different strains (*23*), resulting in a total of 84 *C. diphtheriae* cultures. PCR and culture results were 100% concordant for all samples. The Elek tests correlated with PCR *tox* gene results for all cultures; no NTTB isolates were identified.

Other *Corynebacterium* spp. Infections

Toxin-producing *C. ulcerans* was detected in 1 patient >65 years of age who had suspected diphtheria in 2016. In 2017, *C. ulcerans* was reported in an elderly patient with a pituitary adenoma; however, that isolate was not available for further characterization. In 2020, nontoxigenic *C. ulcerans* was isolated from a uterine tissue sample from a 37-year-old patient with a history of miscarriage. No information regarding animal exposure, outcome, or DAT administration was available for *C. ulcerans* cases.

C. belfantii (nontoxigenic) was isolated in 2023 from a sputum sample from an elderly patient with nonspecific respiratory illness. We identified the isolate as *C. diphtheriae* by using mass spectrometry and PCR. We classified the isolate as *C. belfantii* according to the absence of nitrate reductase genes and corresponding inability to reduce nitrates, characteristic of *C. belfantii* (*32*). Because *C. belfantii* has been reclassified from a biovar to a separate *Corynebacterium* species (*33*), we excluded this species from the *C. diphtheriae* dataset.

Respiratory Diphtheria

Respiratory diphtheria was diagnosed in 26 patients. The case-fatality ratio among *C. diphtheriae* cases with known outcomes was 35% (8/23) (Table 1). Eleven cases, all toxigenic ST378, were from a community outbreak in KwaZulu-Natal during 2015 (*23*,*34*). A second cluster of 3 diphtheria cases occurred in a correctional services facility in the Western Cape in 2023, caused by toxigenic ST906. The median patient ages were 10 (range 4–41) years in KwaZulu-Natal and 19 (range 18–20) years in Western Cape. The remaining 12 diphtheria cases were sporadic and occurred in the same 2 provinces; bacteria strains were identified as ST378 (n = 9), ST905 (n = 1), and ST906 (n = 2) (Table 2; Figure 2).

Infective Endocarditis

Endocarditis cases (n = 14) were caused by nontoxigenic *C. diphtheriae*; the case-fatality ratio was 60% (6/10) among patients with known outcomes (Table 1).

Table 1. Characteristics of *Corynebacterium diphtheriae* infection cases, South Africa, 2015–2023*

Characteristics	Respiratory diphtheria	Endocarditis	Cutaneous diphtheria	Nonspecific respiratory illness	Asymptomatic
No. patients/group	26	14	22	5	16
Toxin positive	26 (100)	0	2 (9)	0	14 (88)
Year of bacteria isolation					
2015	11 (42)	2 (14)	1 (5)	1 (20)	7 (44)
2016	2 (8)	0	0	0	0
2017	4 (15)	2 (14)	1 (5)	2 (40)	0
2018	2 (8)	0	4 (18)	0	1 (6)
2019	0	0	2 (9)	1 (20)	0
2020	1 (4)	0	3 (14)	0	0
2021	0	6 (43)	3 (14)	1 (20)	1 (6)
2022	0	1 (7)	4 (18)	0	0
2023	6 (23)	3 (21)	4 (18)	0	7 (44)
Province					
Gauteng	0	0	3 (14)	1 (20)	0
Western Cape	9 (35)	14 (100)	2 (9)	2 (40)	8 (50)
Eastern Cape	0	0	12 (55)	1 (20)	0
KwaZulu-Natal	17 (65)	0	4 (18)	1 (20)	8 (50)
North West	0	0	1 (5)	0	0
Age category, y					
0–4	3 (12)	0	0	2 (40)	1 (6)
5–9	4 (15)	4 (29)	0	0	4 (25)
10–19	10 (38	5 (36)	2 (9)	1 (20)	6 (38)
20–45	9 (35)	5 (36)	12 (55)	2 (40)	5 (31)
>45	0	0	8 (36)	0	0
Patient sex					
M	16 (62)	9 (64)	14 (64)	2 (50)†	9 (56)
F	10 (38)	5 (36)	8 (36)	2 (50)	7 (44)
Outcome					
Died	8 (31)	6 (43)	0	0	0
Survived	15 (58)	4 (29)	9 (41)	1 (20)	16 (100)
Unknown	3 (12)	4 (29)	13 (59)	4 (80)	0
Hospitalization					
Inpatient	23 (88)	14 (100)	11 (50)	2 (40)	0
Outpatient	2 (8)	0	10 (45)	2 (40)	16 (100)
Unknown	1 (4)	0	1 (5)	1 (20)	0
Vaccine history					
Fully vaccinated for age	1 (4)	1	0	1 (20)	0
Incomplete/unvaccinated	7 (27)	0	0	0	0
Unknown/not recorded	18 (69)	13 (93)	22 (100)	4 (80)	16 (100)

*Values are no. (%). Total number of cases was 83.
†Sex unknown for 1 person.

The median patient age was 14 (range 5–38) years, and all cases were reported from the Western Cape. Five of those cases were geographically and temporally linked, and detailed clinical aspects have been previously described (*35*); 1 patient from the cluster reported substance abuse (not intravenous), 1 had undergone a mitral valve replacement, and the remaining 3 did not have a known underlying illness or report a history of substance/alcohol abuse. Among the remaining 9 endocarditis cases, 5 patients had underlying illness or were substance abusers; underlying illnesses were not captured for 4 of those patients. Although 6 STs were identified, most (57% [8/14]) cases were caused by *C. diphtheriae* ST885 (Table 2; Figure 2).

Cutaneous Diphtheria

Cutaneous diphtheria accounted for 27% (22/83) of *C. diphtheriae* infections, reported from 5 of 9 provinces (Table 1). The median patient age was 38 (range 15–88) years. Two cases, reported in 2020 (Eastern Cape) and 2023 (KwaZulu Natal) were caused by toxigenic ST378. The other 20 cases were a mixture of 10 nontoxigenic (mostly unrelated) STs (Table 2; Figure 2).

Nonspecific Respiratory Illness and Asymptomatic Carriers

Incidental isolation of nontoxigenic *C. diphtheriae* was reported in 5/83 (6%) patients during routine diagnostic testing, representing 4 different sequence types; *C. diphtheriae* was isolated from 16/83 (19%) asymptomatic contacts of symptomatic patients who had laboratory-confirmed *C. diphtheriae* (Tables 1, 2). During the outbreak investigations, *C. diphtheriae* was isolated from 8/145 (6%) close contacts in KwaZulu-Natal during 2015 and 6/151 (4%) close contacts in Western Cape during 2023. During the KwaZulu-Natal

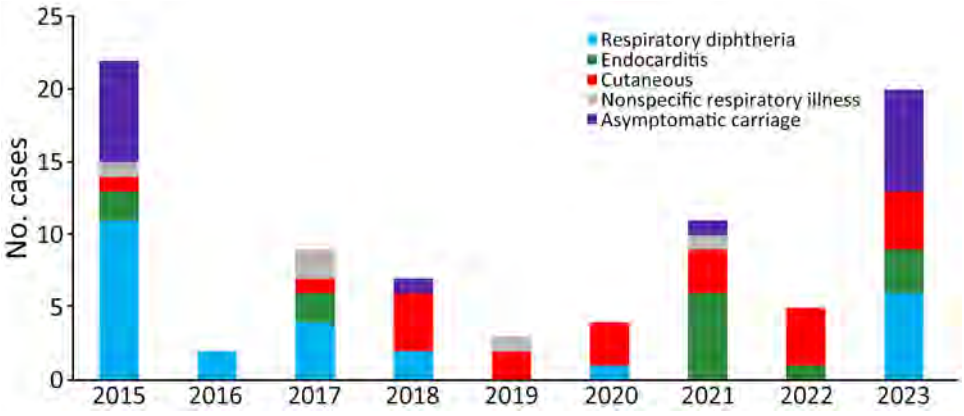

Figure 1. *Corynebacterium diphtheriae* infections according to year and clinical illness category, South Africa, 2015–2023. Total number of cases was 83.

outbreak, 6/8 (75%) asymptomatic contacts carried the toxigenic outbreak strain (ST378) in their throats; during the Western Cape outbreak, all asymptomatic contacts carried the same toxigenic strain (ST906) as the symptomatic patients. Asymptomatic contacts did not develop respiratory symptoms.

Antimicrobial Susceptibility Profiles

Almost all *C. diphtheriae* isolates were intermediately resistant to penicillin (82/84 [98%]), amoxicillin (83/84 [99%]), and cefotaxime (83/84 [99%]) (Appendix 1 Table). For penicillin, MIC_{50} was 0.25 μg/mL and MIC_{90} was 0.5 μg/mL. For cefotaxime, MIC_{50} and MIC_{90} were 2 μg/mL. Eleven (13%) isolates were intermediately resistant to tetracycline (MIC 8 μg/mL) and belonged to lineage ST885/SL31. All isolates were susceptible to linezolid, meropenem, and vancomycin. The 2 isolates from 1980 were susceptible to penicillin, amoxicillin, and cefotaxime (penicillin, MIC 0.03 μg/mL; amoxicillin and cefotaxime, MIC 0.12 μg/mL). Four nontoxigenic isolates belonging to different lineages were nonsusceptible to ≥3 drug classes. *C. diphtheriae* from 1 fatal case of infective endocarditis was nonsusceptible to 5 antimicrobial drugs, including penicillin (MIC 0.25 μg/mL) and erythromycin (MIC 2 μg/mL), and was the only isolate that was nonsusceptible to erythromycin and also harbored the *pbp2m* gene.

C. diphtheriae Population Structure and Phylogeny

We identified 18 novel STs among 84 genomes from 83 patients (Table 2; Figure 2). The most prevalent STs were toxigenic ST378 (29/84 [35%] isolates) and ST906 (12/84 [14%]) and nontoxigenic ST885 (11/84 [13%])

Table 2. Clinical characteristics of *Corynebacterium diphtheriae* isolates, South Africa, 2015–2023*

Clinical category	No. isolates/total (%)	Sequence type/sublineage†
Total no. isolates	84	NA
Respiratory diphtheria	27/84 (32)	NA
Toxin positive	26/27 (96)	ST378/SL265, n = 20; ST905/SL393, n = 1; ST906/SL394, n = 5
Toxin negative‡	1/27 (4)	ST395/SL31, n = 1
Endocarditis	14/84 (17)	NA
Toxin positive	0	NA
Toxin negative	14/14 (100)	ST391/SL52, n = 1; ST395/SL31, n = 2; ST743/SL31, n = 1; ST885/SL31, n = 8; ST887/SL31, n = 1; ST924/SL396, n = 1
Cutaneous diphtheria	22/84 (26)	NA
Toxin positive	2/22 (9)	ST378/SL265, n = 2
Toxin negative	20/22 (91)	ST395/SL31, n = 5; ST608/SL259, n = 2§; ST885/SL31, n = 2; ST886/SL389, n = 3; ST888/SL31, n = 2; ST890/SL390, n = 1; ST891/SL391, n = 2; ST894/SL392, n = 1; ST896/SL31, n = 1; ST964/SL397, n = 1
Nonspecific respiratory illness	5/84 (6)	NA
Toxin positive	0	NA
Toxin negative	5/5 (100)	ST395/SL31, n = 1; ST886/SL389, n = 1; ST888/SL31, n = 1; ST904/SL31, n = 2
Asymptomatic carrier¶	16/84 (19)	NA
Toxin positive	14/16 (88)	ST378/SL265, n = 7; ST906/SL394, n = 7
Toxin negative	2/16 (13)	ST395/SL31, n = 1; ST885/SL31, n = 1

*Total number of isolates was 84 from 83 patients. NA, not applicable; SL, sublineage; ST, sequence type.
†Sublineage identified by using core genome multilocus sequence typing (*26*).
‡One patient with respiratory diphtheria harbored toxigenic ST378 and nontoxigenic ST395 in their throat.
§Sublineage not assigned for 1 isolate.
¶Contacts of symptomatic patients (did not develop respiratory symptoms).

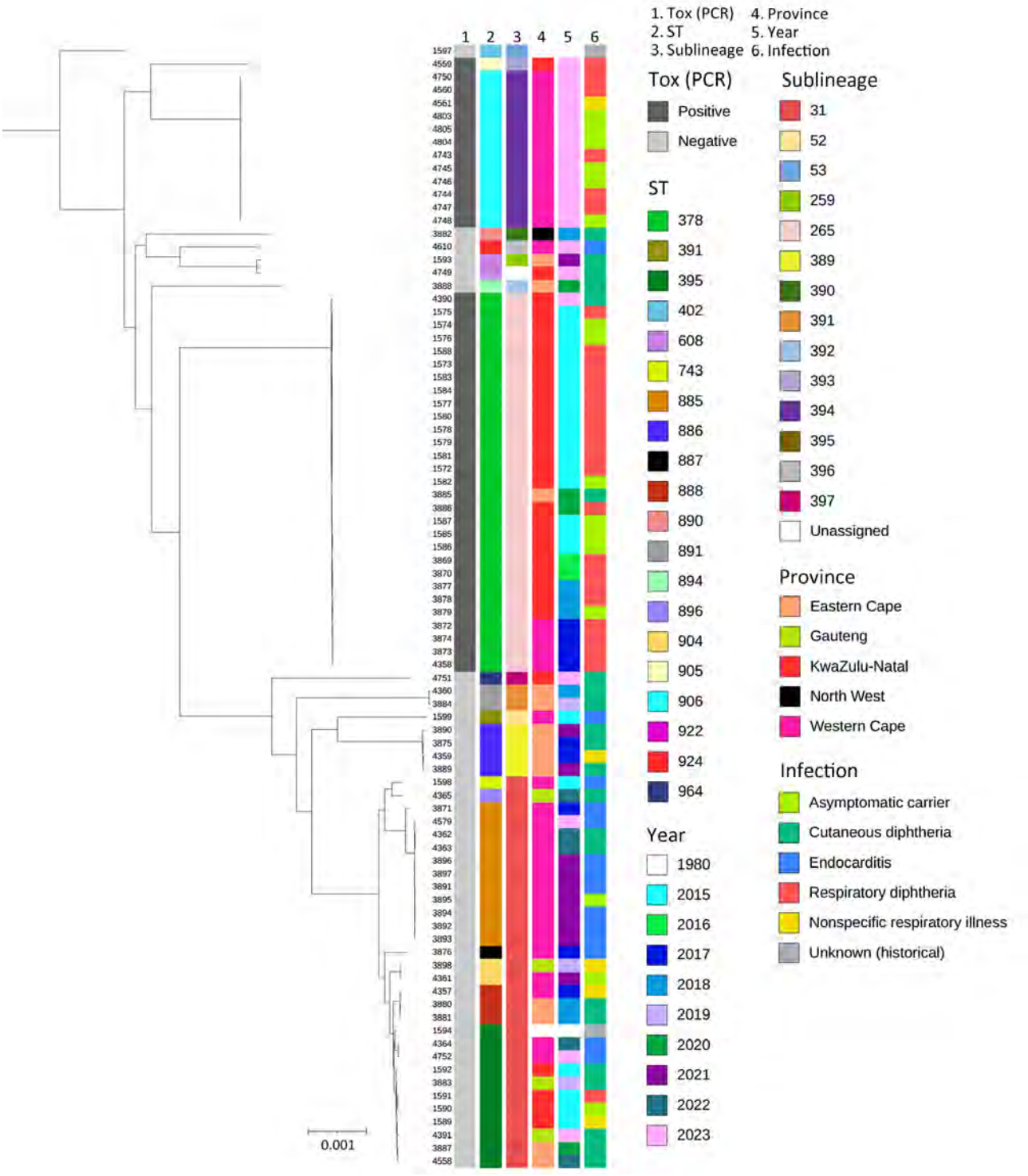

Figure 2. Phylogenetic analysis of *Corynebacterium diphtheriae* isolates, South Africa, 2015–2023. Total number of isolates was 84 from 83 patients. Isolate identification numbers are listed on the right side of the colored bars. Colored columns indicate presence/absence of the *tox* gene, sequence type, sublineage, location of isolate, year isolate was collected, and clinical infection type. Neighbor-joining tree was generated by using the core genome multilocus sequence typing scheme in the Insitut Pasteur Bacterial Isolate Genome Sequence *C. diphtheriae* database (https://bigsdb.pasteur.fr/diphtheria). Tree was visualized by using iTOL (https://itol.embl.de) and rooted by using a *tox* gene–negative *C. diphtheriae* genome (no. 1597 at top) isolated from South Africa circa 1980 (clinical isolate with no available clinical or demographic data). Scale bar indicates nucleotide substitutions per site. ST, sequence type.

and ST395 (10/84 [12%]). Toxigenic and nontoxigenic isolates had mutually exclusive STs with no overlap. We identified 12 SLs among 83 isolates (an SL was not assigned for 1 isolate because of poor sequence quality) by using cgMLST (Table 2). SL265 (29/83 [35%]) was exclusively found in ST378 isolates, and SL394 (12/83 [14%]) was only found in ST906 isolates. Pairwise SNP distances were <100 SNPs for both ST378 and ST906 isolates. We observed the same pairwise SNP distance for ST885 isolates except for 1 isolate (from 2017), which differed by 1,632–1,646 SNPs from other ST885 isolates (Appendix 2 Table 1, https://wwwnc.cdc.gov/EID/article/31/3/24-1211-App2.pdf).

spuA and Virulence-Associated Genes

PCR and the diphtOscan pipeline confirmed the presence of the *tox* gene in 42/84 (50%) isolates (Appendix 1). We assessed the potential effect of amino acid mutations on toxin structure as previously described (*36*) and identified 3 toxin variants: *tox* gene variant 6 (toxin group 8) associated with ST378 (n = 29), *tox* variant 16 (toxin group 7) associated with ST905 (n = 1), and *tox* variant 29 (not assigned to a toxin group) associated with ST906 (n = 12). *tox* variants 6 and 16 shared a low impact mutation (T262A), and *tox* variant 16 had an additional moderate impact mutation (V233A). Using the *spuA* gene as a proxy for biovar gravis, 20/42 (48%) nontoxigenic isolates harbored *spuA* and represented a mixture of 8 STs. All toxigenic isolates were classified as biovar mitis according to the absence of *spuA*. The *spa*-like pili (adhesin) genes *spaA*, *spaH*, and *spaD* and *chtAB* (iron uptake) were absent from all toxin-positive isolates but were present in most toxin-negative isolates (*spaA*, 37/42 [88%]; *spaH*, 20/42 [48%]; *spaD*, 33/42 [79%]; and *chtAB*, 37/42 [88%]) (Appendix 2 Table 2).

Virulence gene profiles were mostly conserved among isolates representing the predominant, outbreak-associated ST378 and ST 906 (respiratory diphtheria) and ST885 (endocarditis) lineages. The *spaA*, *spaH*, *spaD*, and *chtAB* genes were absent in ST378 and ST906, whereas all (with the exception of *spaH*) were present in ST885 (Appendix 2 Table 3). *Irp2ABCDEFGHI* (siderophore biosynthesis) and iron uptake system genes *irp2JKLMN* and *htaA-hmuTUV-htaBC* were present in all ST378 and ST906 genomes but absent in ST885.

Discussion

We provide insight into the types, pathogenicity, and characteristics of *C. diphtheriae* infections after their reemergence in South Africa in 2015. Intermediate resistance to penicillin for almost all isolates indicates real-time monitoring of treatment outcomes is critical to identify emerging clinically significant resistance. Infections were caused by diverse and novel genotypes, confirming the genetic heterogeneity and phylogeographic clustering of *C. diphtheriae* described in other countries (*17*,*36*); however, outbreak-associated lineages were highly conserved even among sporadic cases. Patients with cutaneous diphtheria and nonspecific respiratory illness and asymptomatic carriers promote ongoing transmission, providing a reservoir of strains for genetic exchange. The reemergence of diphtheria has increased awareness among clinicians and diagnostic laboratories in South Africa and highlights the importance of surveillance and active case management for all *C. diphtheriae* cases irrespective of clinical symptoms.

Diphtheria-related deaths in our study were higher (6%–24%) than those reported in other settings (*37*,*38*), likely caused by several factors, such as incomplete vaccination and lack of booster doses, delays in seeking healthcare, lack of accurate symptom onset dates, and limited availability and timely administration of DAT. Our findings highlight the lack of systematic data collection (often unknown or not captured in detail). Data collection methods need improvement to properly assess risk factors associated with diphtheria-related deaths in our setting.

Diphtheria outbreaks are usually associated with inadequate vaccination coverage (*39*). During the KwaZulu-Natal community outbreak in 2015, coverage for the primary series of diphtheria vaccinations in the province was high (96%); however, coverage was substantially lower for the 18-month (83%), 6-year (56%), and 12-year (20%) booster doses (*23*). Vaccination coverage during the second diphtheria cluster in the Western Cape in 2021–2023 was >80% for the primary series, declining to <80% for the 18-month dose; tetanus-diphtheria boosters at 6 and 12 years were inadequate at <50% (C. Lawrence, unpub. data). Vaccine coverage in KwaZulu-Natal and the Western Cape was comparable to that in other provinces (*40*), and increased clinical awareness in those 2 regions might have contributed to the higher number of detected cases. The World Health Organization and United Nations Children's Fund (https://immunizationdata.who.int) have estimated that DTP3 vaccination coverage in South Africa has been consistently >80% since 2014; however, inaccuracies in data reporting and data quality exist in South Africa, and coverage might be lower. Similar to the case for other countries, disruption in immunization services and changes in healthcare-seeking behavior occurred in South Africa during the COVID-19 pandemic. The number of reported cases of *C. diphtheriae* is too low to directly measure the effects of the COVID-19 pandemic. However, transmission of other respiratory pathogens was interrupted because of social distancing and

nonpharmaceutical interventions (*41*), which likely holds true for *C. diphtheriae* transmission.

A cluster of geographically linked cases of *C. diphtheriae* endocarditis among young adults in 2021 with a high death rate indicates that nontoxigenic *C. diphtheriae* infections should not be overlooked (*35*). Although infective endocarditis cases are mostly sporadic, outbreaks caused by single clones have been reported and, similar to our cases, risk factors included drug use, homelessness, and underlying illnesses (*42*,*43*).

In South Africa, toxin production confirmation is usually performed at the national reference laboratory, making it possible to monitor all forms of disease and detect other *Corynebacterium* spp. Cutaneous *C. diphtheriae* and *C. ulcerans* cases have been increasingly reported in Europe, partly because of changes in laboratory testing methods and guidelines (*6*). *C. ulcerans* is predominantly zoonotic but can also cause diphtheria-like illness and be toxigenic, requiring treatment and public health actions similar to those used for *C. diphtheriae* infections.

NTTB strains have not been reported in South Africa, and we did not identify clones that had both toxigenic and nontoxigenic properties. Poland and Germany have both reported nontoxigenic ST8 strains isolated from blood, cutaneous, and respiratory tract specimens (*4*,*44*). Toxigenic *C. diphtheriae* ST8 was responsible for the extensive respiratory diphtheria outbreak in the former Soviet Union in the 1990s (*4*,*44*). ST8 has transformed to a less virulent, nontoxigenic variant, which presumably sustains its spread among highly vaccinated populations in Europe. Molecular typing data from Africa are limited, but nontoxigenic and toxigenic isolates with the same genotype (ST377) were recently isolated from 2 immigrants from West Africa who had cutaneous diphtheria (*18*). Those findings stress the importance of monitoring all manifestations of *C. diphtheriae* disease.

In South Africa, diphtheria case management and prophylaxis for close contacts of diphtheria patients involves administering either penicillin or macrolides. Emerging penicillin resistance in different countries prompted the World Health Organization to update its guidelines in 2024 to recommend the use of macrolides in preference to β-lactams (https://www.who.int/teams/health-care-readiness/clinical-management-of-diphtheria). Until recently, MIC breakpoints for antimicrobial resistance have been undefined; however, CLSI updated its guidelines in 2015 to include interpretative criteria to define nonsusceptibility. Interpretation is complicated by different breakpoints to determine penicillin nonsusceptibility (MIC ≥4 μg/mL in CLSI guidelines and >1 μg/mL in EUCAST guidelines; https://www.eucast.org/clinical_breakpoints). Two genomic studies using geographically representative datasets demonstrated that the *pbp2m* gene correlates with a penicillin-resistant phenotype (*17*,*27*); however, other studies showed intermediate-resistant isolates did not necessarily harbor *pbp2m* (*18*,*45*,*46*). The contribution of other *pbp* genes to β-lactam resistance and increased MICs has not been conclusively established (*46*). Furthermore, the clinical significance of intermediate resistance to penicillin is not fully understood, and it remains critical to monitor treatment failures (for symptomatic cases) and failure to eradicate carriage in close contacts of diphtheria patients.

C. diphtheriae is subdivided into biochemically distinct biovars that could be associated with increased severity (*47*). Differentiation can be technically challenging and earlier genomic studies could not confidently differentiate biovars (*48*). Studies have shown concordance between the *spuA* gene and biovar gravis (*17*,*49*). Gravis isolates are largely nontoxigenic (mitis isolates are mostly toxigenic) (*18*), which was consistent with our findings. We did not find a clear distinction among mitis and gravis virulence gene profiles among nontoxigenic isolates in our dataset. We observed an absence of *spa*-type pili genes in toxigenic isolates, which were present in the nontoxigenic endocarditis clone ST885. The *spa*-type pili are adhesins that play a major role in host cell invasion (*50*). Genomic data can identify toxin variants and predict the extent to which amino acid mutations might affect virulence and vaccine toxoid match (*36*). None of the toxin variants in our isolates harbored mutations likely to cause vaccine escape.

Our findings help elucidate *C. diphtheriae* disease epidemiology, pathogen characteristics, and transmission networks in South Africa. The high case-fatality ratio and ongoing circulation of toxigenic strains among asymptomatic carriers and cutaneous diphtheria patients stresses the importance of notifying all suspected and laboratory-confirmed cases and implementing prompt public health action and treatment to reduce transmission and death. Improved DTP vaccination coverage and improved coverage for booster doses is urgently needed and aligns with the life-course immunization model, which promotes the idea that prevention is better than cure by vaccinating persons throughout their lifespan.

The study was supported by a Fogarty International Center Global Infectious Disease research training grant, US National Institutes of Health, awarded to the University of Pittsburgh, and the South Africa National Institute for Communicable Diseases (grant no. D43TW011255).

Whole-genome sequencing was supported by the SEQAFRICA project, funded by the Department of Health and Social Care's Fleming Fund, UK Health Security Agency. PubMLST is funded by a Biomedical Resources grant from The Wellcome Trust (no. 218205/Z/19/Z).

About the Author

Dr. du Plessis is a medical laboratory scientist at the National Institute for Communicable Diseases, National Health Laboratory Service, Johannesburg, South Africa. Her research interests focus on pathogens causing respiratory disease and meningitis and pathogen detection and characterization using molecular epidemiologic and genomic methods.

References

1. World Health Organization. Diphtheria outbreaks: comprehensive guidance for the public health preparedness and response in the WHO African Region. 2024 [cited 2024 Mar 6]. https://iris.who.int/handle/10665/376838
2. Agrawal R, Murmu J, Kanungo S, Pati S. "Nigeria on alert: diphtheria outbreaks require urgent action"—a critical look at the current situation and potential solutions. New Microbes New Infect. 2023;52:101100. https://doi.org/10.1016/j.nmni.2023.101100
3. Finger F, Funk S, White K, Siddiqui MR, Edmunds WJ, Kucharski AJ. Real-time analysis of the diphtheria outbreak in forcibly displaced Myanmar nationals in Bangladesh. BMC Med. 2019;17:58. https://doi.org/10.1186/s12916-019-1288-7
4. Dangel A, Berger A, Konrad R, Bischoff H, Sing A. Geographically diverse clusters of nontoxigenic *Corynebacterium diphtheriae* infection, Germany, 2016–2017. Emerg Infect Dis. 2018;24:1239–45. https://doi.org/10.3201/eid2407.172026
5. Hoefer A, Pampaka D, Herrera-León S, Peiró S, Varona S, López-Perea N, et al. Molecular and epidemiological characterization of toxigenic and nontoxigenic *Corynebacterium diphtheriae, Corynebacterium belfantii*, *Corynebacterium rouxii*, and *Corynebacterium ulcerans* isolates identified in Spain from 2014 to 2019. J Clin Microbiol. 2021;59:e02410-20. https://doi.org/10.1128/JCM.02410-20
6. Gower CM, Scobie A, Fry NK, Litt DJ, Cameron JC, Chand MA, et al. The changing epidemiology of diphtheria in the United Kingdom, 2009 to 2017. Euro Surveill. 2020;25:1900462. https://doi.org/10.2807/1560-7917.ES.2020.25.11.1900462
7. Gao H, Lau EHY, Cowling BJ. Waning immunity after receipt of pertussis, diphtheria, tetanus, and polio-related vaccines: a systematic review and meta-analysis. J Infect Dis. 2022;225:557–66. https://doi.org/10.1093/infdis/jiab480
8. Anderson RM. The concept of herd immunity and the design of community-based immunization programmes. Vaccine. 1992;10:928–35. https://doi.org/10.1016/0264-410X(92)90327-G
9. Truelove SA, Keegan LT, Moss WJ, Chaisson LH, Macher E, Azman AS, et al. Clinical and epidemiological aspects of diphtheria: a systematic review and pooled analysis. Clin Infect Dis. 2020;71:89–97. https://doi.org/10.1093/cid/ciz808
10. Holmes RK. Biology and molecular epidemiology of diphtheria toxin and the *tox* gene. J Infect Dis. 2000;181:S156–67. https://doi.org/10.1086/315554
11. Zakikhany K, Neal S, Efstratiou A. Emergence and molecular characterisation of non-toxigenic *tox* gene-bearing *Corynebacterium diphtheriae* biovar mitis in the United Kingdom, 2003–2012. Euro Surveill. 2014;19:20819. https://doi.org/10.2807/1560-7917.ES2014.19.22.20819
12. Billard-Pomares T, Rouyer C, Walewski V, Badell-Ocando E, Dumas M, Zumelzu C, et al. Diagnosis in France of a non-toxigenic *tox* gene–bearing strain of *Corynebacterium diphtheriae* in a young male back from Senegal. Open Forum Infect Dis. 2017;4:ofw271. https://doi.org/10.1093/ofid/ofw271
13. Clinton LK, Bankowski MJ, Shimasaki T, Sae-Ow W, Whelen AC, O'Connor N, et al. Culture-negative prosthetic valve endocarditis with concomitant septicemia due to a nontoxigenic *Corynebacterium diphtheriae* biotype gravis isolate in a patient with multiple risk factors. J Clin Microbiol. 2013;51:3900–2. https://doi.org/10.1128/JCM.01403-13
14. Wojewoda CM, Koval CE, Wilson DA, Chakos MH, Harrington SM. Bloodstream infection caused by nontoxigenic *Corynebacterium diphtheriae* in an immunocompromised host in the United States. J Clin Microbiol. 2012;50:2170–2. https://doi.org/10.1128/JCM.00237-12
15. Belsey MA, LeBlanc DR. Skin infections and the epidemiology of diphtheria: acquisition and persistence of *C. diphtheriae* infections. Am J Epidemiol. 1975;102:179–84. https://doi.org/10.1093/oxfordjournals.aje.a112145
16. Forde BM, Henderson A, Playford EG, Looke D, Henderson BC, Watson C, et al. Fatal respiratory diphtheria caused by ß-lactam–resistant *Corynebacterium diphtheriae*. Clin Infect Dis. 2021;73:e4531–8. https://doi.org/10.1093/cid/ciaa1147
17. Hennart M, Panunzi LG, Rodrigues C, Gaday Q, Baines SL, Barros-Pinkelnig M, et al. Population genomics and antimicrobial resistance in *Corynebacterium diphtheriae*. Genome Med. 2020;12:107. https://doi.org/10.1186/s13073-020-00805-7
18. Brémont S, Passet V, Hennart M, Fonteneau L, Toubiana J, Badell E, et al. Multidrug-resistant *Corynebacterium diphtheriae* in people with travel history from West Africa to France, March to September 2023. Euro Surveill. 2023;28:2300615. https://doi.org/10.2807/1560-7917.ES.2023.28.46.2300615
19. Konrad R, Berger A, Huber I, Boschert V, Hörmansdorfer S, Busch U, et al. Matrix-assisted laser desorption/ionisation time-of-flight (MALDI-TOF) mass spectrometry as a tool for rapid diagnosis of potentially toxigenic *Corynebacterium* species in the laboratory management of diphtheria-associated bacteria. Euro Surveill. 2010;15:19699. https://doi.org/10.2807/ese.15.43.19699-en
20. Williams MM, Waller JL, Aneke JS, Weigand MR, Diaz MH, Bowden KE, et al. Detection and characterization of diphtheria toxin gene-bearing *Corynebacterium* species through a new real-time PCR assay. J Clin Microbiol. 2020;58:e00639-20. https://doi.org/10.1128/JCM.00639-20
21. Engler KH, Glushkevich T, Mazurova IK, George RC, Efstratiou A. A modified Elek test for detection of toxigenic corynebacteria in the diagnostic laboratory. J Clin Microbiol. 1997;35:495–8. https://doi.org/10.1128/jcm.35.2.495-498.1997
22. Clinical and Laboratory Standards Institute. Methods for antimicrobial dilution and disk susceptibility testing of infrequently isolated or fastidious bacteria; third edition (M45). Wayne (PA): The Institute; 2015.
23. du Plessis M, Wolter N, Allam M, de Gouveia L, Moosa F, Ntshoe G, et al. Molecular characterization of *Corynebacterium diphtheriae* outbreak isolates, South Africa, March–June 2015. Emerg Infect Dis. 2017;23:1308–15. https://doi.org/10.3201/eid2308.162039

24. Bankevich A, Nurk S, Antipov D, Gurevich AA, Dvorkin M, Kulikov AS, et al. SPAdes: a new genome assembly algorithm and its applications to single-cell sequencing. J Comput Biol. 2012;19:455–77. https://doi.org/10.1089/cmb.2012.0021
25. Manni M, Berkeley MR, Seppey M, Zdobnov EM. BUSCO: assessing genomic data quality and beyond. Curr Protoc. 2021;1:e323. https://doi.org/10.1002/cpz1.323
26. Guglielmini J, Hennart M, Badell E, Toubiana J, Criscuolo A, Brisse S. Genomic epidemiology and strain taxonomy of *Corynebacterium diphtheriae*. J Clin Microbiol. 2021;59:e0158121. https://doi.org/10.1128/JCM.01581-21
27. Hennart M, Crestani C, Bridel S, Armatys N, Brémont S, Carmi-Leroy A, et al. A global *Corynebacterium diphtheriae* genomic framework sheds light on current diphtheria re-emergence. Peer Community J. 2023;3:e76. https://doi.org/10.24072/pcjournal.307
28. Arango-Argoty G, Garner E, Pruden A, Heath LS, Vikesland P, Zhang L. DeepARG: a deep learning approach for predicting antibiotic resistance genes from metagenomic data. Microbiome. 2018;6:23. https://doi.org/10.1186/s40168-018-0401-z
29. Shen W, Le S, Li Y, Hu F. SeqKit: a cross-platform and ultrafast toolkit for FASTA/Q file manipulation. PLoS One. 2016;11:e0163962. https://doi.org/10.1371/journal.pone.0163962
30. Criscuolo A. A fast alignment-free bioinformatics procedure to infer accurate distance-based phylogenetic trees from genome assemblies. Res Ideas Outcomes. 2019;5:e36178. https://doi.org/10.3897/rio.5.e36178
31. Didelot X, Falush D. Inference of bacterial microevolution using multilocus sequence data. Genetics. 2007;175:1251–66. https://doi.org/10.1534/genetics.106.063305
32. Dazas M, Badell E, Carmi-Leroy A, Criscuolo A, Brisse S. Taxonomic status of *Corynebacterium diphtheriae* biovar Belfanti and proposal of *Corynebacterium belfantii* sp. nov. Int J Syst Evol Microbiol. 2018;68:3826–31. https://doi.org/10.1099/ijsem.0.003069
33. Oren A, Garrity GM. Notification that new names of prokaryotes, new combinations, and new taxonomic opinions have appeared in volume 68, part 12, of the IJSEM. Int J Syst Evol Microbiol. 2019;69:600–1. https://doi.org/10.1099/ijsem.0.003197
34. Mahomed S, Archary M, Mutevedzi P, Mahabeer Y, Govender P, Ntshoe G, et al. An isolated outbreak of diphtheria in South Africa, 2015. Epidemiol Infect. 2017;145:2100–8. https://doi.org/10.1017/S0950268817000851
35. Lovelock T, du Plessis M, van der Westhuizen C, Janson JT, Lawrence C, Parker A, et al. Non-toxigenic *Corynebacterium diphtheriae* endocarditis: a cluster of five cases. S Afr J Infect Dis. 2024;39:539. https://doi.org/10.4102/sajid.v39i1.539
36. Will RC, Ramamurthy T, Sharma NC, Veeraraghavan B, Sangal L, Haldar P, et al. Spatiotemporal persistence of multiple, diverse clades and toxins of *Corynebacterium diphtheriae*. Nat Commun. 2021;12:1500. https://doi.org/10.1038/s41467-021-21870-5
37. Adegboye OA, Alele FO, Pak A, Castellanos ME, Abdullahi MAS, Okeke MI, et al. A resurgence and re-emergence of diphtheria in Nigeria, 2023. Ther Adv Infect Dis. 2023;10:20499361231161936. https://doi.org/10.1177/20499361231161936
38. Al-Dar AA, Al-Qassimi M, Ezzadeen FH, Qassime M, Al murtadha AM, Ghaleb Y. Diphtheria resurgence in Sada'a-Yemen, 2017–2020. BMC Infect Dis. 2022;22:46. https://doi.org/10.1186/s12879-022-07033-x
39. Clarke KEN, MacNeil A, Hadler S, Scott C, Tiwari TSP, Cherian T. Global epidemiology of diphtheria, 2000–2017. Emerg Infect Dis. 2019;25:1834–42. https://doi.org/10.3201/eid2510.190271
40. Republic of South Africa Department of Health. Expanded programme on immunisation (EPI) national coverage survey report, 2020 [cited 2024 Mar 6]. https://www.health.gov.za/wp-content/uploads/2022/03/National-EPI-Coverage-Survey_Final-full-report-Dec-2020.pdf
41. Shaw D, Abad R, Amin-Chowdhury Z, Bautista A, Bennett D, Broughton K, et al. Trends in invasive bacterial diseases during the first 2 years of the COVID-19 pandemic: analyses of prospective surveillance data from 30 countries and territories in the IRIS Consortium. Lancet Digit Health. 2023;5:e582–93. https://doi.org/10.1016/S2589-7500(23)00108-5
42. Gubler J, Huber-Schneider C, Gruner E, Altwegg M. An outbreak of nontoxigenic *Corynebacterium diphtheriae* infection: single bacterial clone causing invasive infection among Swiss drug users. Clin Infect Dis. 1998;27:1295–8. https://doi.org/10.1086/514997
43. Karmarkar EN, Fitzpatrick T, Himmelfarb ST, Chow EJ, Smith HZ, Lan KF, et al. Cluster of nontoxigenic *Corynebacterium diphtheriae* infective endocarditis and rising background *C. diphtheriae* cases—Seattle, Washington, 2020–2023. Clin Infect Dis. 2024;78:1214–21. https://doi.org/10.1093/cid/ciae094
44. Wołkowicz T, Zacharczuk K, Zasada AA. Genomic analysis of *Corynebacterium diphtheriae* strains isolated in the years 2007–2022 with a report on the identification of the first non-toxigenic *tox* gene-bearing strain in Poland. Int J Mol Sci. 2023;24:4612. https://doi.org/10.3390/ijms24054612
45. Arcari G, Hennart M, Badell E, Brisse S. Multidrug-resistant toxigenic *Corynebacterium diphtheriae* sublineage 453 with two novel resistance genomic islands. Microb Genom. 2023;9:mgen000923. https://doi.org/10.1099/mgen.0.000923
46. Xiaoli L, Peng Y, Williams MM, Lawrence M, Cassiday PK, Aneke JS, et al. Genomic characterization of cocirculating *Corynebacterium diphtheriae* and non-diphtheritic *Corynebacterium* species among forcibly displaced Myanmar nationals, 2017–2019. Microb Genom. 2023;9:001085. https://doi.org/10.1099/mgen.0.001085
47. McLeod JW. The types mitis, intermedius and gravis of *Corynebacterium diphtheriae*: a review of observations during the past ten years. Bacteriol Rev. 1943;7:1–41. https://doi.org/10.1128/br.7.1.1-41.1943
48. Sangal V, Burkovski A, Hunt AC, Edwards B, Blom J, Hoskisson PA. A lack of genetic basis for biovar differentiation in clinically important *Corynebacterium diphtheriae* from whole genome sequencing. Infect Genet Evol. 2014;21:54–7. https://doi.org/10.1016/j.meegid.2013.10.019
49. Santos AS, Ramos RT, Silva A, Hirata R Jr, Mattos-Guaraldi AL, Meyer R, et al. Searching whole genome sequences for biochemical identification features of emerging and reemerging pathogenic *Corynebacterium* species. Funct Integr Genomics. 2018;18:593–610. https://doi.org/10.1007/s10142-018-0610-3
50. Ott L, Möller J, Burkovski A. Interactions between the re-emerging pathogen *Corynebacterium diphtheriae* and host cells. Int J Mol Sci. 2022;23:3298. https://doi.org/10.3390/ijms23063298

Address for correspondence: Mignon du Plessis, Centre for Respiratory Diseases and Meningitis, National Institute for Communicable Diseases, National Health Laboratory Service, 1 Modderfontein Rd, Sandringham, 2192, Johannesburg, South Africa; email: mignond@nicd.ac.za

Genetic Diversity and Geographic Spread of Henipaviruses

Yakhouba Kane, Betty Nalikka, Alexander Tendu, Victor Omondi, Kathrina Mae Bienes, Abdou Padane, Veasna Duong, Nicolas Berthet, Gary Wong

Henipaviruses, such as Hendra and Nipah viruses, are major zoonotic pathogens that cause encephalitis and respiratory infections in humans and animals. The recent emergence of Langya virus in China highlights the need to understand henipavirus host diversity and geographic spread to prevent future outbreaks. Our analysis of the National Center for Biotechnology Information Virus and VIRION databases revealed ≈1,117 henipavirus sequences and 142 complete genomes. Bats (64.7%) and shrews (11.7%) dominated the host species record, and the genera *Pteropus* and *Crocidura* contained key henipavirus hosts in Asia, Australia, and Africa. Henipaviruses found in the *Eidolon* bat genus exhibited the highest within-host genetic distance. Phylogenetic analysis revealed batborne and rodent- or shrew-derived henipaviruses diverged ≈11,000 years ago and the first known lineage originating in *Eidolon* genus bats ≈9,900 years ago. Pathogenic henipaviruses diverged from their ancestors 2,800–1,200 years ago. Including atypical hosts and regions in future investigations is necessary to control future outbreaks.

Henipaviruses belong to the family *Paramyxoviridae*, a group of enveloped, single-stranded RNA viruses (*1*). During the past 3 decades, henipaviruses have gained considerable attention because of their zoonotic potential, causing severe and often fatal encephalitis and respiratory disease in humans and animals (*2*). Outbreaks caused by Hendra virus (HeV) and Nipah virus (NiV) were linked to bats and are particularly deadly to humans, exhibiting case-fatality rates of 75% for HeV infection and 40%–80% for NiV infection (*3*,*4*). The emergence of HeV in Australia in 1994 and of NiV in Malaysia during 1998–1999, Bangladesh and India beginning in 2001, and the Philippines in 2014 demonstrated the viruses' ability to infect humans and various domestic animals, causing devastating effects (*5*–*12*).

Henipaviruses ecology and distribution patterns rely on reservoir host circulation, with spillover leading to sporadic outbreaks (*13*,*14*). Studies focusing on pteropid bats revealed diverse henipaviruses and henipa-like viruses in South and Southeast Asia, China, Australia, and Africa and recently in Europe and South America (*5*,*15*–*22*). Most HeV and NiV infections in humans come from contact with contaminated fruits or domestic animals (*13*,*23*). The broad distribution of henipaviruses and discovery of new hosts suggests inconsistent surveillance and unidentified potential hosts.

The discovery of emerging henipaviruses, such as Mojiang virus (MojV) and Langya virus (LayV), highlights the threat to humans might extend beyond HeV and NiV (*20*,*24*). MojV is a nonbat henipavirus that was detected in a cave-rat in the Yunnan Province of China after 3 miners died in 2012 from a severe pneumonia with unknown etiology (*24*). LayV, a recently discovered shrewborne henipavirus, was detected in febrile patients in China in 2018, and spillover events were estimated to have occurred during 2018–2022 (*20*). In Africa, molecular and serologic data supported the circulation of henipaviruses in bats and domestic animals, with evidence of spillover into humans without observable clinical disease (*16*,*25*,*26*).

Efforts to develop henipavirus vaccines and antiviral drugs led to promising candidates in various stages of development, including DNA- and mRNA-based vaccines and neutralizing antibody products (*27*–*30*). However, no licensed vaccine is available for human use, and treatments remain limited to supportive care. Since 2012, only the Equivac vaccine is licensed for horses in Australia (*31*). The growing threat of henipaviruses and the possibility of human-to-human transmission

Author affiliations: Shanghai Public Health Clinical Center, Fudan University, Shanghai, China (Y. Kane); Institut Pasteur, Phnom Penh, Cambodia (B. Nalikka, A. Tendu, V. Omondi, K.M. Bienes, V. Duong, G. Wong); Institut de Recherche en Santé, de Surveillance Épidémiologique et de Formation, Dakar, Senegal (A. Padane); Institut Pasteur, Paris, France (N. Berthet); Institut Pasteur, Vientiane, Laos (G. Wong)

DOI: https://doi.org/10.3201/eid3103.241134

underscore the importance of studying henipavirus host distribution and assessing outbreak risks (*7*).

In this study, we aimed to increase understanding of the henipavirus host spectrum and distribution patterns by analyzing existing data from public repositories. We focused on henipavirus infections in nonhuman mammals to assess the spatial distribution of these viruses and the diversity of their associated hosts. We further assessed the origin, diversification, and cross-species transmission of henipaviruses. In this article, we have defined the term reservoir or reservoir host as the animal species that repeatedly tested positive for henipavirus, shed infectious viruses, and supported long-term viral maintenance across locations. We have defined an accidental host as an animal species that tested positive for henipavirus but does not necessarily support its sustained transmission or maintenance, often acting as a dead-end host.

Materials and Methods

Data Collection and Processing

We searched for available sequence data of the family *Paramyxoviridae* in the National Center for Biotechnology Information (NCBI) Virus database (https://www.ncbi.nlm.nih.gov/labs/virus) on December 11, 2023, by using the keyword "Paramyxoviridae,taxid:11158" and downloaded the results. We downloaded the sequence metadata and included the columns relevant for this study (Appendix Table 1, https://wwwnc.cdc.gov/EID/article/31/3/24-1134-App1.xlsx). We removed the rows corresponding to accessions without confirmed host and laboratory generated sequences. We excluded animal-derived henipavirus sequences <100 bp from the analysis because of frequent lack of host or country information. We collected host data for henipaviruses from the VIRION database, the atlas of vertebrate viromes (*32*). We removed records from the analysis that were not taxonomically resolved to the NCBI backbone or had uncertainty in host identification.

We performed a descriptive analysis of henipavirus hosts by using R packages dplyr and ggplot2 v.3.5.1 (https://ggplot2.tidyverse.org). This analysis included filtering and summarizing the metadata, saving unique host data, and creating visualizations, including a temporal trend of sequence submission and a heatmap to represent host species distribution. We created a choropleth map visualizing total henipavirus sequences by country and the number of unique host genera of henipavirus across countries by using Python packages geopandas (Zenodo, https://zenodo.org/records/3946761), matplotlib, and pandas (Python, https://pandas.pydata.org) to filter and group metadata and merge with world shapefile.

Evolutionary Divergence and Spread of Henipaviruses

We screened a total of 167 henipavirus sequences (>14,000 bp), including 142 complete genomes, to filter out sequences with unknown nucleotides >0.05% and aligned by using MAFFT version 7.505 with the default parameters (*33*). We trimmed the alignment by using TrimAl 1.2rev57 and the duplicated sequences dropped with Seqkit version 2.8 (*34*,*35*). We used ModelFinder implemented in IQ-TREE2 to detect the best-fit model (*36*). To assess the relatedness of henipaviruses across host groups, we computed the mean genetic distance of henipaviruses within and between host genera by using MEGA version 11.0.13 (https://www.megasoftware.net) with the following settings: 500 bootstrap replications, Kimura 2-parameter model, gamma distributed with gamma parameter set to 4 (*37*).

We performed a Bayesian time-resolved phylogeny and ancestral host reconstruction by using BEAST version 1.10.4 with host genus and country as discrete characters (*38*). We used Bayesian discrete phylogeographic method implemented in BEAST to construct the ancestral hosts. Because we found no temporal signature, BEAST analysis was based on a fixed substitution rate of 1.0 substitutions per site per unit of time. We ran the analysis for a total of 200 million iterations and collected samples every 20,000 generations. We used the Hasegawa-Kishino-Yano substitution model, a strict molecular clock, and a constant size coalescent prior (*39*). We chose those settings to ensure comprehensive sampling of the posterior distribution. We assessed convergence of the Markov Chain Monte Carlo chains by using Tracer version 1.7, where parameters were checked for sufficient effective sample sizes and the first 10% of iterations were discarded as burn-in (*40*). We used the remaining samples to generate maximum clade credibility trees, which were visualized by using FigTree version 1.4.4 (http://tree.bio.ed.ac.uk/software/figtree) to interpret the phylogenetic relationships and divergence times within the dataset. In addition, we performed ancestral sequence reconstruction by using the empirical Bayesian method implemented in IQ-TREE 2.3.2 with the following parameters: the ModelFinder Plus model selection, DNA sequence type, ancestral sequence reconstruction, and 1,000 ultrafast bootstrap replicates (*41*). This method enables the reconstruction of the most likely ancestral states at each node of the tree,

accounting for model uncertainty and providing robust support for inferred ancestral sequences.

Results

Temporal Trend and Major Host Groups of Paramyxoviruses

We visualized the temporal trend of paramyxovirus sequences in GenBank (Figure 1, panel A). A total of ≈69,000 paramyxovirus sequences were identified, and 8.6% (n = 5,841) were complete genomes. Sequences of *Morbillivirus*, *Orthorubulavirus*, and *Respirovirus* are predominantly human-associated, whereas *Orthoavulavirus* sequences primarily originate from avian hosts and henipavirus sequences primarily originate from nonhuman mammal hosts (Figure 1, panel B). Since 2002, paramyxovirus sequences have increased exponentially, with noted reductions in 2012, 2015, 2018, and 2020 (Figure 1, panel A). Henipaviruses accounted for ≈1,117 nucleotide sequences, including 859 from nonhuman mammals. Among the 142 complete henipavirus genomes recorded, 90 originated from nonhuman animals, largely from the genera *Crocidura* and *Pteropus* (*20*).

Henipavirus Host Range

Henipaviruses showed the potential to infect diverse mammalian taxonomic groups. Our analysis revealed 668 henipavirus records involving 51 unique mammal species distributed among 25 genera and 13 families (Figures 2, 3; Appendix Table 2). Most henipavirus host records were associated with wild mammals and bats and shrews identified as the key animal group hosts. Although henipavirus detection spans 51 species, not all species act as competent hosts with virus-shedding and transmission capabilities.

The proportions of henipavirus detection rate across host families and genera vary (Figure 3). Bats (order Chiroptera) represent the most diverse host group for henipaviruses, comprising 64.7% of the total host species (Figure 2; Appendix Table 2). Those records involve 4 bat families: Hipposideridae, Pteropodidae, Rhinolophidae, and Vespertilionidae. Of note, ≈65% of NiV detection involved the Pteropodidae family, and other bat families had a relatively low detection rate: 5.6% for Hipposideridae, 3.7% for Rhinolophidae, and 6.6% for Vespertilionidae (Figure 3, panel A).

The family Pteropodidae is the most diverse, encompassing 8 genera previously known to host henipaviruses: *Cynopterus*, *Dobsonia*, *Eidolon*, *Eonycteris*, *Epomophorus*, *Hypsignathus*, *Pteropus*, and *Rousettus*. Within those genera, henipaviruses were detected in 25 species, with the genus *Pteropus* displaying detection records of 28.8% for HeV and 40.3% for NiV, involving various species such as *P. vampyrus*, *P. hypomelanus*, and *P. medius* (formerly *P. giganteus*) (Figure 3, panel B). The family Vespertilionidae comprised 2 genera, *Myotis*, with a detection record of ≈3%, and *Scotophilus*, with a detection record of <2%, and 3 species, *Myotis daubentonii*, *Myotis ricketti*, and *Scotophilus kuhlii*. The family Hipposideridae includes the single genus *Hipposideros*, accounting for 3.7% of NiV instances, with 3 involved species: *H. armiger*, *H. larvatus*, and *H. pomona*. The family Rhinolophidae consists of the

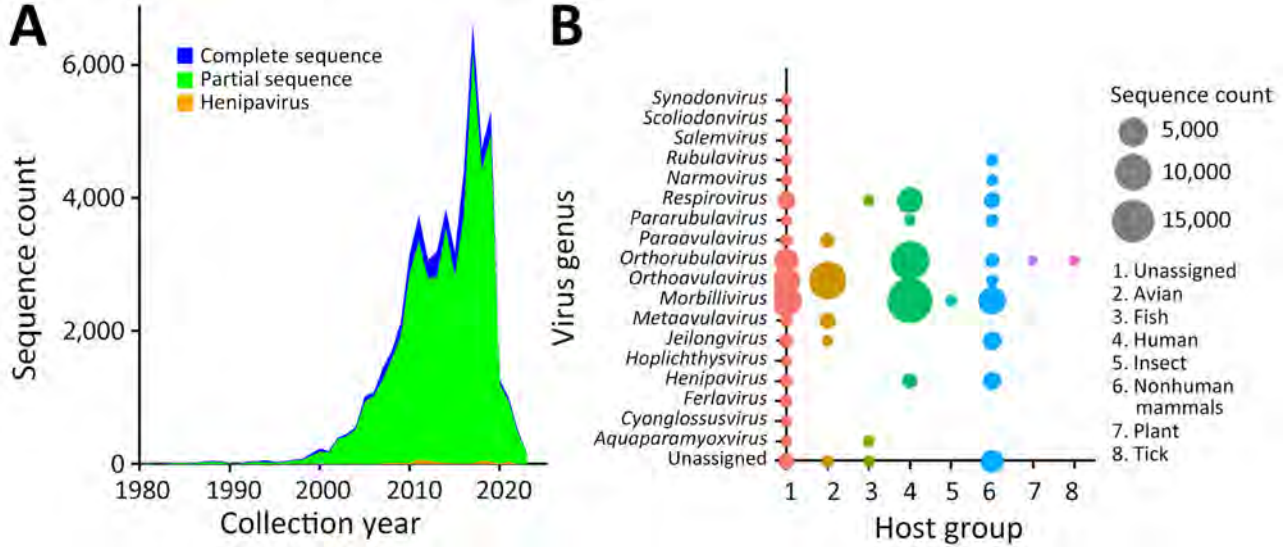

Figure 1. Trend in paramyxovirus sequences submitted to the National Center for Biotechnology Information Virus database (https://www.ncbi.nlm.nih.gov/labs/virus), 1980–2023. A) Sequence count by collection year, showing all complete and partial sequences compared with all henipaviruses. B) Virus genera and sequence counts by major host group from the VIRION database (*32*).

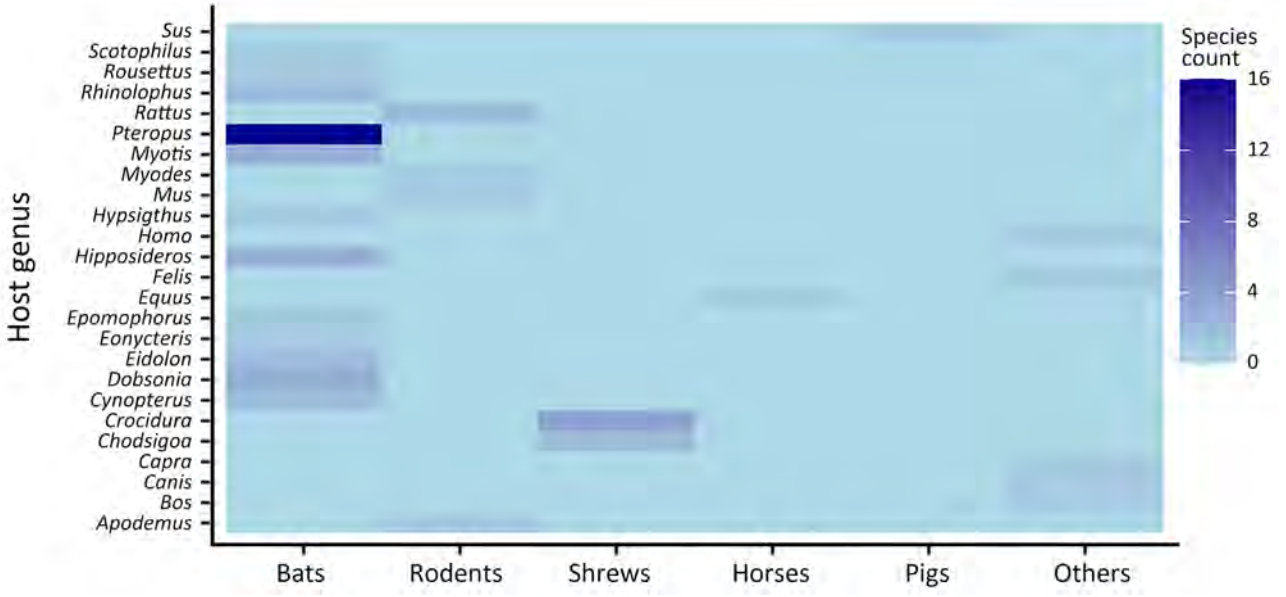

Figure 2. Numbers of henipavirus species by host group for sequences submitted to the National Center for Biotechnology Information Virus database (https://www.ncbi.nlm.nih.gov/labs/virus), 1980–2023. Host groups from the VIRION database (*32*) are represented at the genus level.

genus *Rhinolophus* and exhibits 2.5% NiV detection records with 2 species: *R. affinis* and *R. sinicus*.

Shrews (family Soricidae) have emerged as a major group of *Henipavirus* hosts, accounting for 11.7% of recorded henipavirus host species (Figures 2, 3; Appendix Table 2). They are distributed across 2 genera: *Chodsigoa*, with 2 species (*C. hypsibia* and *C. smithii)*, and *Crocidura*, with 4 species (*C. attenuata*, *C. lasiura*, *C. shantungensis*, and *C. tanakae*). Of note, >85% of LayV instances were recorded in shrews of the genus *Crocidura*.

Rodents (order Rodentia) represented ≈9.8% of henipavirus host species records, involving 2 families, Cricetidae and Muridae. The family Muridae is more diverse, comprising 3 genera: *Apodemus*, *Mus*, and *Rattus*. The identified species within those genera are *A. agrarius*, *M. musculus*, *R. rattus*, and *R. tanezumi*. The family Cricetidae includes the genus *Myodes*, and the single species *M. rutilus* is associated with >14% of LayV detection record.

Our data revealed a spectrum of domestic animals with evidence of henipavirus infection. Bovids (Bovidae) and swine (Suidae) each accounted for ≈3.9% of the host species records. Bovines encompassed 2 genera: *Bos* (*B. taurus*) and *Capra* (*C. hircus*), with 3.7% of NiV instances, whereas swine are represented by the single genus, *Sus* (*S. scrofa* and *S. crofa domesticus*), accounting for 6.6% of NiV.

Canids (Canidae), equids (Equidae), and felids (Felidae) each represent ≈1.9% of the host species records. Canids are represented by the genus *Canis* and the species *C. lupus*, in which 2.8% NiV instances were identified. Equids included the single genus *Equus*, specifically *E. caballus* (the domestic horse). Of note, HeV was predominantly detected in domestic horses, with over 72.8% occurrences, compared with

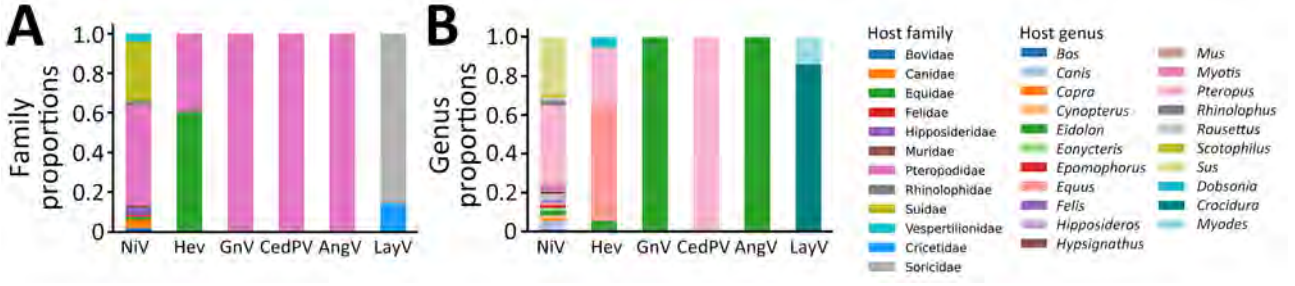

Figure 3. Proportional counts of henipaviruses by host family and genus for sequences submitted to the National Center for Biotechnology Information Virus database (https://www.ncbi.nlm.nih.gov/labs/virus), 1980–2023. A) Virus detection proportions across host families. B) Virus detection proportions across host genera. AngV, Angavokely virus; CedPV, Cedar virus; GnV, Ghana virus; HeV, Hendra virus; LayV, Langya virus; NiV, Nipah virus.

1.8% for NiV. Felids were represented by the genus *Felis*; the species *F. catus* (the domestic cat) was involved in 1.8% of NiV instances.

Geographic Distribution of Henipavirus Hosts

Our analysis is on the basis of henipavirus sequence records across many countries from the NCBI Virus database. The dataset comprises information on the geographic occurrence of potential henipavirus hosts. We identified a total of 806 of 859 henipavirus records involving diverse animal host species spanning ≈11 mammal genera from 13 countries (Figure 4). Although the presence of henipavirus sequences in a host species may indicate exposure or infection, the reservoir status for many of those hosts remains unverified.

China contributed >50% (446) of henipavirus sequence records with a diverse array of hosts including 1 bat genus (*Eonycteris*), 3 rodent genera (*Apodemus*, *Myodes*, *Rattus*), and 2 shrew genera (*Chodsigoa*, *Crocidura*). Of note, most of those records involve shrews, particularly the genus *Crocidura* and the species *C. lasiura*, suggesting those small mammals are major henipavirus carriers in China. In addition, 2 shrew species, *C. lasiura* and *C. shantungensis*, were found infected with henipaviruses in South Korea.

In mainland Southeast Asia, bat species of the genus *Pteropus* emerged as a primary host group for henipaviruses. In Bangladesh and India, the Indian flying fox (*P. medius*) is the reservoir of henipaviruses. Henipavirus instances in Malaysia were linked to 2 *Pteropus* species, *P. hypomelanus* and *P. vampyrus*, although some occurrences were noted in domestic animals including pigs (*S. scrofa*, *S. scrofa domesticus*) and dogs (*C. lupus familiaris*). In Indonesia, the large flying fox (*P. vampyrus*) was identified as a henipavirus host. In Cambodia and Thailand, henipavirus occurrences were primarily associated with the common fruit bat (*P. lylei*). *P. hypomelanus* bats also contributed to a small portion of henipavirus records in Thailand.

In Australia, henipaviruses are primarily linked to bat species within the genus *Pteropus*. The black flying fox (*P. alecto*), the spectacled flying fox (*P. scapulatus*), and the gray-headed flying fox (*P. poliocephalus*) are prominent reservoir host species

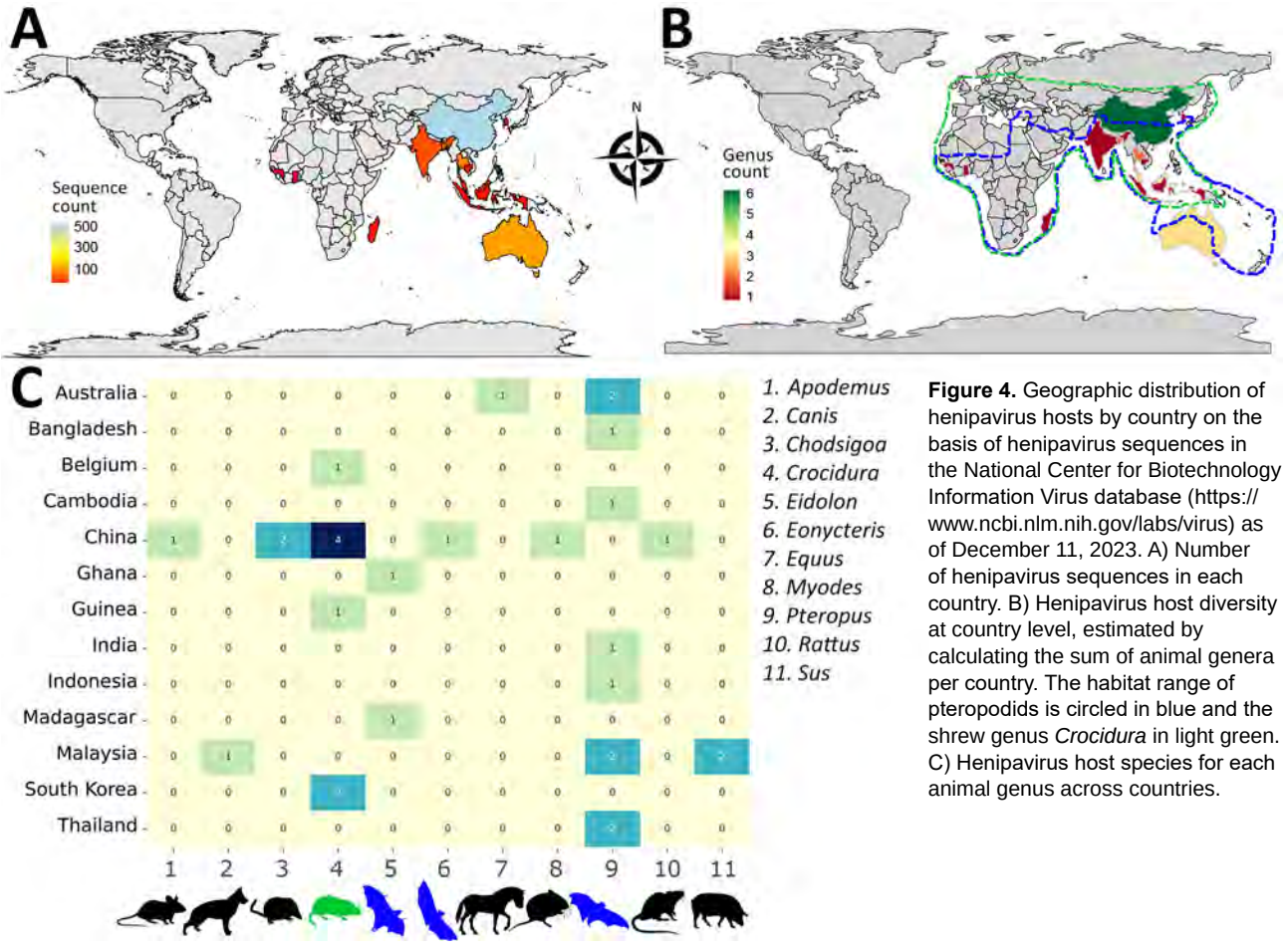

Figure 4. Geographic distribution of henipavirus hosts by country on the basis of henipavirus sequences in the National Center for Biotechnology Information Virus database (https://www.ncbi.nlm.nih.gov/labs/virus) as of December 11, 2023. A) Number of henipavirus sequences in each country. B) Henipavirus host diversity at country level, estimated by calculating the sum of animal genera per country. The habitat range of pteropodids is circled in blue and the shrew genus *Crocidura* in light green. C) Henipavirus host species for each animal genus across countries.

for henipaviruses in this region. In addition, equids such as *E. caballus* are henipavirus hosts of note in this region.

In Africa, we identified the bat genus *Eidolon* as a critical host group of henipaviruses. In Madagascar, the Madagascan fruit bat (*E. dupreanum*), an endemic and vulnerable species, is a prominent host for henipaviruses. In West Africa, henipaviruses occurrences were noted in the straw-colored fruit bat (*E. helvum*) in Ghana and in the shrew species *C. grandiceps* in Guinea. In Europe, henipaviruses occurrence has also been confirmed with another shrew species, *C. russula*, as the only identified host in Belgium.

Evolutionary Divergence and Cross-Species Transmission of Henipaviruses

We investigated the evolutionary distances of henipaviruses within and between their diverse hosts (Figure 5, panels A, B). Henipaviruses from the bat genus *Eidolon* exhibited the highest within-host genetic distance (D = 0.92), followed by those from the shrew genera *Chodsigoa* (D = 0.62) and *Crocidura* (D = 0.49) (Figure 5, panel A). In contrast, the bat genus *Pteropus* showed relatively low within-host genetic distance (D = 0.18) for henipaviruses, and henipaviruses from swine and equid showed almost no diversity (D<0.1). The analysis of the genetic distances of henipaviruses between host groups showed a clear dichotomy between small nonflying and flying mammal henipaviruses (Figure 5, panel B). Rodents and shrews shared more closely related henipaviruses, whereas bats of the genus *Pteropus* had henipaviruses similar to those found in domestic animals. Of note, henipaviruses from *Eidolon* genus bats appeared distantly related to all other host groups.

We performed ancestral host reconstruction of henipaviruses by using both a Bayesian discrete phylogeographic approach in BEAST and an empirical Bayesian method in IQ-TREE. Because both methods yielded similar results, we generated the phylogenetic tree from IQ-TREE and a BEAST-derived tree (Figure 6, panels A, B). Phylogenetic analysis supported the results of the genetic distances of henipaviruses, displaying 2 main branches: 1 consisting of batborne henipaviruses and another of rodent- and shrew-derived henipaviruses.

The time-calibrated Bayesian phylogeny supported the divergence of 2 main clades ≈11,000 years ago (95% highest posterior density [HPD] 15,500–8,200 years) (Figure 6, panel B). Considering host genera as discrete character states, henipaviruses likely originated in African fruit bats of the genus *Eidolon* (Figure 6, panels A, B; Appendix Table 1). The Madagascan fruit bat hosts the earliest known henipavirus lineage, other lineages in bats likely emerged from these early lineages ≈9,900 years ago (95% HPD 14,010–7,400 years). Pathogenic henipaviruses, including HeV, LayV, NiV, and MojV, showed a recent divergence from their sister clades ≈2,800–1,200 years ago (Figure 6, panel B). Rodent and shrew henipaviruses displayed an evolutionary origin in the shrew genus *Crocidura*.

Bat-derived henipaviruses, including NiV and HeV, emerged from the bat genus *Pteropus*. The zoonotic transmission of those viruses involved

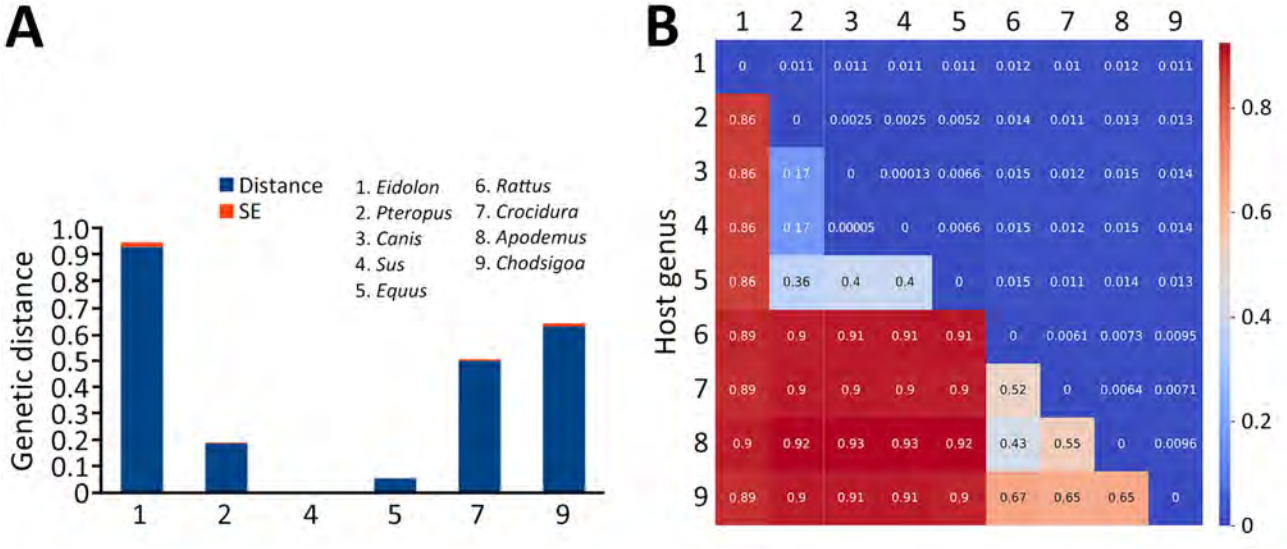

Figure 5. Evolutionary divergence and spread of henipaviruses for sequences submitted to the National Center for Biotechnology Information Virus database (https://www.ncbi.nlm.nih.gov/labs/virus), 1980–2023. A) Genetic distance of henipaviruses within host genera. B) Genetic distance of henipaviruses between host genera. SE, standard error.

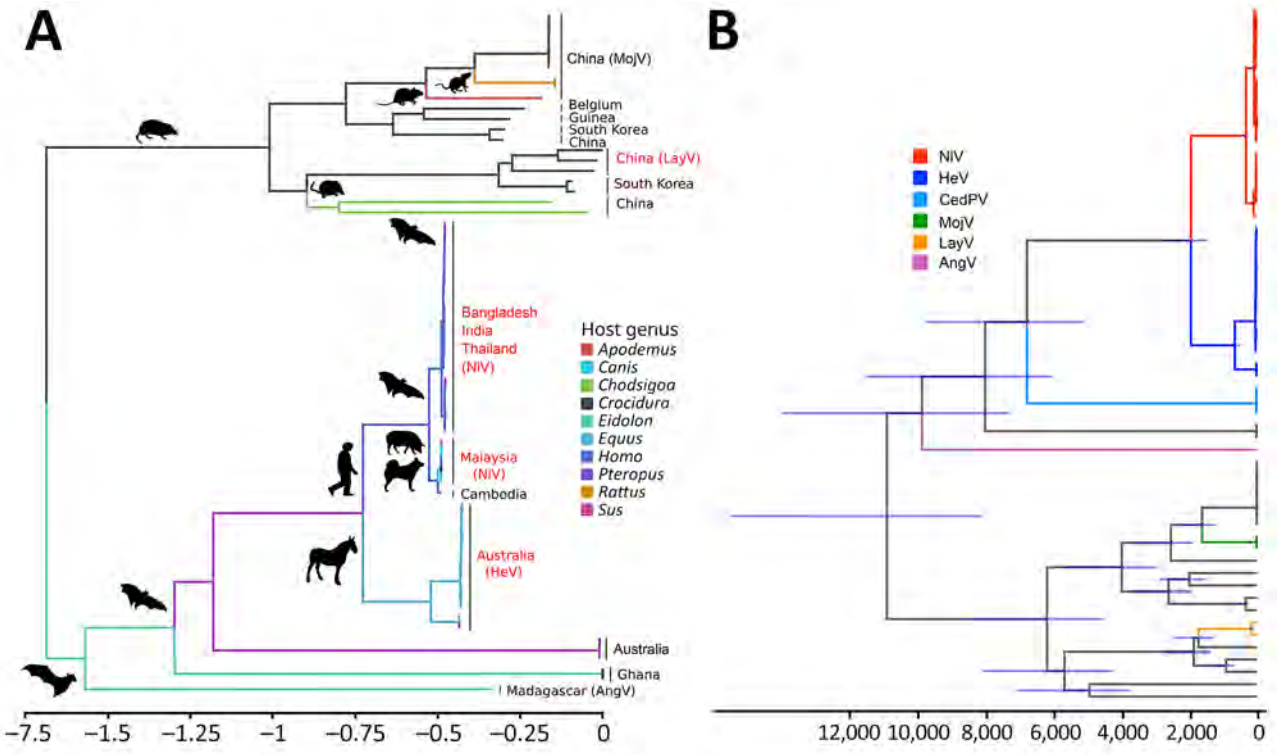

Figure 6. Time-calibrated phylogenetic trees showing the evolutionary divergence and spread of henipaviruses for sequences submitted to the National Center for Biotechnology Information Virus database (https://www.ncbi.nlm.nih.gov/labs/virus), 1980–2023. A) Ancestral host tree demonstrating divergence of hosts and countries of origin. Scale bar indicates relative number of substitution events per site per unit of time. B) Time-calibrated Bayesian phylogeny showing the divergence times for henipaviruses. The node bars indicate 95% HPD. The divergence between batborne and shrewborne henipaviruses occurred ≈11,000 (95% HPD 15,500–8,200) years ago. AngV, Angavokely virus; CedPV, Cedar virus; HeV, Hendra virus; HPD, highest posterior density; LayV, Langya virus; MojV, Mojiang virus, NiV, Nipah virus.

various domestic animals such as horses for HeV and dogs and pigs for NiV, which indicates potential cross-species transmission of henipaviruses (Figure 6, panels A, B). Furthermore, the increased diversity of *Crocidura* shrew henipavirus lineages, along with their close phylogenetic relatedness to other shrew and rodent henipaviruses, suggests shrews might play a critical role as reservoirs and vectors (Figure 6, panels A, B).

Discussion

In this study, we analyzed the host and geographic range of henipaviruses by using data from public repositories. Henipaviruses showed a broad host range infecting ≈13 mammal families, including bats, rodents, and shrews, predominantly in Africa, Australia, East Asia, South Asia, and Southeast Asia. Megabats within the genus *Pteropus* displayed a high diversity of henipavirus host species. Because most sampling events targeted pteropodid bats, comprehensive studies are needed to accurately assess the roles of species from other bat families (*42*). Shrews and rodents have emerged as major nonbat hosts, which is critical because of their widespread distribution and ability to host zoonotic pathogens such as hantaviruses and bornaviruses (*43*). Shrews and rodents' ability to host henipaviruses suggests a broader ecologic and epidemiologic role for those animals than previously recognized, and further study would be beneficial to understanding factors leading to henipavirus maintenance and transmission among these animals.

The geographic spread and discovery of novel nonbat hosts, particularly in China, suggests increased global attention of henipaviruses (*18*,*44*). China likely contains more henipavirus sequence records with a high diversity of nonbat hosts involving shrews and rodents. The emergence of LayV as the first nonbat henipavirus to cause disease in humans indicates potential roles for shrews in zoonotic transmission (Figure 7). Moreover, the prominence and the extensive distribution of shrews, particularly of the genus *Crocidura*, suggests those small mammals as a potential reservoir for henipaviruses in East Asia.

Of note, the antigenic profile of LayV and MojV were found to be distinct from NiV, emphasizing the effect of henipavirus diversification along their hosts and the potential difficulty to develop a vaccine that can cover both bat and rodent or shrew derived-henipaviruses (*45*). In addition, the route for the zoonotic transmission of LayV and its geographic extent necessitates further study.

In regions highly affected by pathogenic henipavirus diseases, including South and Southeast Asia and Australia, henipavirus records mostly involve bats of the genus *Pteropus*, although other bat genera may play roles in the maintenance of henipaviruses. Expanding henipavirus sampling to Africa, Europe, and South America has improved understanding of host range, thereby expanding the geographic extent of henipavirus endemicity from its traditionally known regions (*17*–*19*,*25*,*42*–*44*). Even with those efforts, henipavirus studies outside of Asia and Australia remain scarce, potentially overlooking other henipavirus reservoirs.

Henipaviruses from *Eidolon* genus bats showed increased genetic diversity, likely because of their wide geographic distribution and diverse ecologic niches. Rodents and shrews share closely related henipaviruses, whereas bats, particularly from the genus *Pteropus*, harbor henipaviruses related to those found in domestic animals. This relation suggests host-specific adaptations and evolutionary pressures. Ancestral host reconstruction pointed to the African fruit bats (genus *Eidolon*) as the henipavirus origin. The earliest known henipavirus lineage dates back ≈9,900 years, suggesting a longstanding association with African fruit bats (*16*,*45*). The recent divergence of pathogenic henipaviruses aligns with their emergence as major zoonotic threats, emphasizing the dynamic nature of henipavirus evolution and the potential for sudden outbreaks. Rodent and shrew henipaviruses likely originated in *Crocidura* shrews. The close phylogenetic relationship between henipaviruses from those animal groups highlights active host-switching events (Figure 6, panel A). Moreover, the hopping of bat-derived henipaviruses from pteropodid bats to diverse domestic animals underscores the need for monitoring regions with major reservoirs (Figure 7).

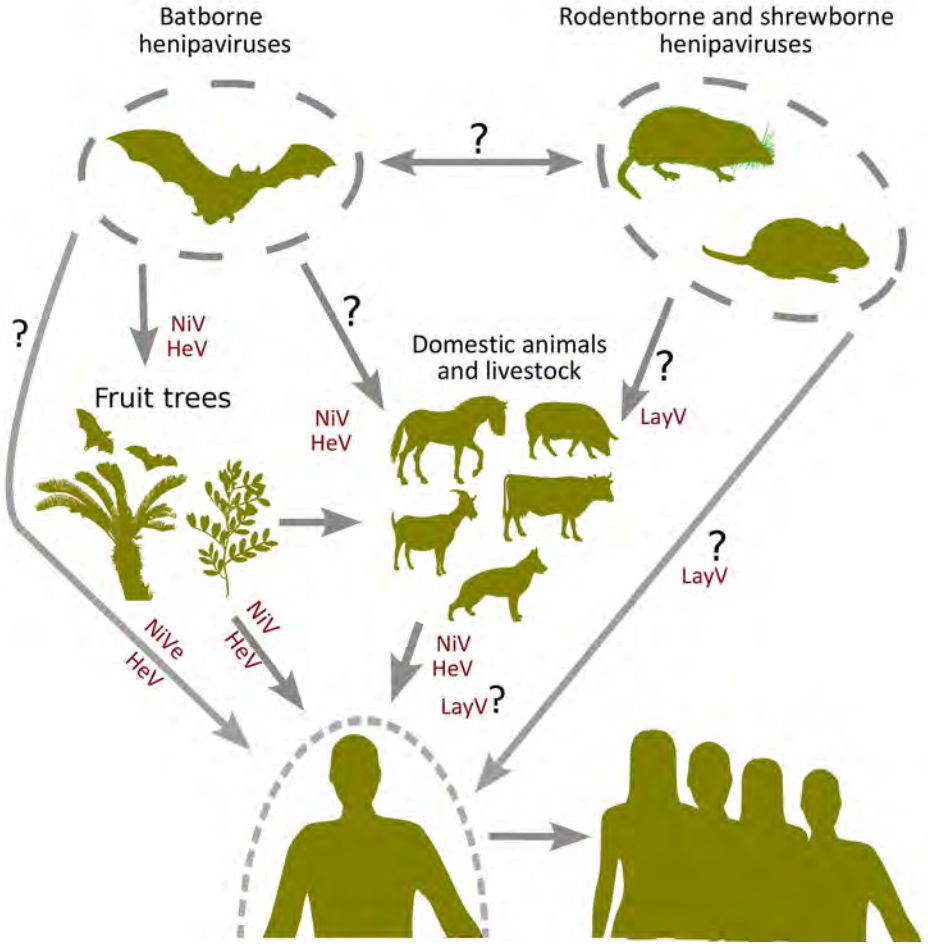

Figure 7. Flowchart showing the potential for host switching of henipaviruses and the routes for potential spillover events. The question marks indicate unconfirmed transmission routes. HeV, Hendra virus; LayV, Langya virus; NiV, Nipah virus.

Despite increased paramyxovirus data, several abrupt declines during major events (severe acute respiratory syndrome in 2002, Middle East respiratory syndrome in 2012, Ebola and Zika in 2014–2016, Ebola in 2018, and COVID-19 in 2020) were noted (Figure 1, panel A). Those observations suggest the effect of global outbreaks on existing surveillance efforts. The limited number of henipavirus sequences, specifically complete genome sequences, limits the understanding of their diversity and evolution. Of note, despite evidence of zoonotic spillover of henipaviruses in Africa, only 2 full genomes were publicly available during this study.

Public repositories in virus research led to various challenges because of incomplete data and reporting inconsistencies. During data collection, the first marsupialborne henipavirus sequence was not available online (18). Regions may be underrepresented because of serologic method or PCR use without GenBank records, as observed in the Republic of the Congo, the Democratic Republic of the Congo, Cameroon, and South Africa (*16*,*44*). Those challenges with public data collection highlight the importance of improving online repositories to provide more comprehensive and accurate information. However, it is crucial to recognize that most of those limitations are consequences of the limited resources and logistic challenges faced by field researchers and affecting their data collection. Because of those challenges, it is difficult to expect standardized collection of surveillance data from all regions. However, focusing efforts on long-term monitoring and including less-explored hosts like shrews and rodents is essential for a better understanding of henipavirus epidemiology. Enhanced collaboration and resource sharing between local and international institutions could help mitigate those challenges and improve the overall quality of henipavirus research.

In conclusion, the concentration of henipavirus data from countries such as China and Australia highlights their laboratory infrastructure and robust surveillance capacities, which enable extensive data collection and sequencing. This data concentration emphasizes the need to increase the capacity of research facilities and surveillance in other regions to achieve a more globally representative understanding of henipavirus dynamics. We stress the importance of noninvasive methods in virological surveillance. Practices such as culling bat populations and destroying their habitats are harmful and unethical. Approaches that protect both conservation efforts and biodiversity are necessary.

About the Author

Dr. Kane is a postdoctoral researcher at Shanghai Public Health Clinical Center, Fudan University, in Shanghai, China. His main interests are human and animal microbiomes and viromes, virus evolution, and genomic epidemiology.

References

1. Wang L, Harcourt BH, Yu M, Tamin A, Rota PA, Bellini WJ, et al. Molecular biology of hendra and Nipah viruses. Microbes Infect. 2001;3:279–87. https://doi.org/10.1016/S1286-4579(01)01381-8
2. Quarleri J, Galvan V, Delpino MV. Henipaviruses: an expanding global public health concern? Geroscience. 2022;44:2447–59. https://doi.org/10.1007/s11357-022-00670-9
3. Aljofan M. Hendra and Nipah infection: emerging paramyxoviruses. Virus Res. 2013;177:119–26. https://doi.org/10.1016/j.virusres.2013.08.002
4. Gazal S, Sharma N, Gazal S, Tikoo M, Shikha D, Badroo GA, et al. Nipah and Hendra viruses: deadly zoonotic paramyxoviruses with the potential to cause the next pandemic. Pathogens. 2022;11:1419. https://doi.org/10.3390/pathogens11121419
5. Breed AC, Meers J, Sendow I, Bossart KN, Barr JA, Smith I, et al. The distribution of henipaviruses in Southeast Asia and Australasia: is Wallace's line a barrier to Nipah virus? PLoS One. 2013;8:e61316. https://doi.org/10.1371/journal.pone.0061316
6. Chen JM, Yu M, Morrissy C, Zhao YG, Meehan G, Sun YX, et al. A comparative indirect ELISA for the detection of henipavirus antibodies based on a recombinant nucleocapsid protein expressed in Escherichia coli. J Virol Methods. 2006;136:273–6. https://doi.org/10.1016/j.jviromet.2006.05.003
7. Parashar UD, Sunn LM, Ong F, Mounts AW, Arif MT, Ksiazek TG, et al. Case-control study of risk factors for human infection with a new zoonotic paramyxovirus, Nipah virus, during a 1998–1999 outbreak of severe encephalitis in Malaysia. J Infect Dis. 2000;181:1755–9. https://doi.org/10.1086/315457
8. Luby SP, Gurley ES, Hossain MJ. Transmission of human infection with Nipah virus. Clin Infect Dis. 2009;49:1743–8. https://doi.org/10.1086/647951
9. Taylor J, Thompson K, Annand EJ, Massey PD, Bennett J, Eden JS, et al. Novel variant Hendra virus genotype 2 infection in a horse in the greater Newcastle region, New South Wales, Australia. One Health. 2022;15:100423. https://doi.org/10.1016/j.onehlt.2022.100423
10. Smith C, Skelly C, Kung N, Roberts B, Field H. Flying-fox species density—a spatial risk factor for Hendra virus infection in horses in eastern Australia. PLoS One. 2014;9:e99965. https://doi.org/10.1371/journal.pone.0099965
11. Edson D, Peel AJ, Huth L, Mayer DG, Vidgen ME, McMichael L, et al. Time of year, age class and body condition predict Hendra virus infection in Australian black flying foxes (*Pteropus alecto*). Epidemiol Infect. 2019;147:e240. https://doi.org/10.1017/S0950268819001237
12. Ching PKG, de los Reyes VC, Sucaldito MN, Tayag E, Columna-Vingno AB, Malbas FF Jr, et al. Outbreak of henipavirus infection, Philippines, 2014. Emerg Infect Dis. 2015;21:328–31. https://doi.org/10.3201/eid2102.141433

13. Islam A, Cannon DL, Rahman MZ, Khan SU, Epstein JH, Daszak P, et al. Nipah virus exposure in domestic and peridomestic animals living in human outbreak sites, Bangladesh, 2013–2015. Emerg Infect Dis. 2023;29:393–6. https://doi.org/10.3201/eid2902.221379
14. Becker DJ, Crowley DE, Washburne AD, Plowright RK. Temporal and spatial limitations in global surveillance for bat filoviruses and henipaviruses. Biol Lett. 2019;15:20190423. https://doi.org/10.1098/rsbl.2019.0423
15. Li Y, Wang J, Hickey AC, Zhang Y, Li Y, Wu Y, et al. Antibodies to Nipah or Nipah-like viruses in bats, China. Emerg Infect Dis. 2008;14:1974–6. https://doi.org/10.3201/eid1412.080359
16. Hayman DTS, Suu-Ire R, Breed AC, McEachern JA, Wang L, Wood JLN, et al. Evidence of henipavirus infection in West African fruit bats. PLoS One. 2008;3:e2739. https://doi.org/10.1371/journal.pone.0002739
17. Madera S, Kistler A, Ranaivoson HC, Ahyong V, Andrianiaina A, Andry S, et al. Discovery and genomic characterization of a novel henipavirus, Angavokely virus, from fruit bats in Madagascar. J Virol. 2022;96:e0092122. https://doi.org/10.1128/jvi.00921-22
18. Hernández LHA, da Paz TYB, Silva SPD, Silva FSD, Barros BCV, Nunes BTD, et al. First genomic evidence of a henipa-like virus in Brazil. Viruses. 2022;14:2167. https://doi.org/10.3390/v14102167
19. Horemans M, Van Bets J, Joly Maes T, Maes P, Vanmechelen B. Discovery and genome characterization of six new orthoparamyxoviruses in small Belgian mammals. Virus Evol. 2023;9:vead065. https://doi.org/10.1093/ve/vead065
20. Zhang X-A, Li H, Jiang F-C, Zhu F, Zhang Y-F, Chen J-J, et al. A zoonotic henipavirus in febrile patients in China. N Engl J Med. 2022;387:470–2. https://doi.org/10.1056/NEJMc2202705
21. Lee SH, Kim K, Kim J, No JS, Park K, Budhathoki S, et al. Discovery and genetic characterization of novel paramyxoviruses related to the genus *Henipavirus* in *Crocidura* species in the Republic of Korea. Viruses. 2021;13:2020. https://doi.org/10.3390/v13102020
22. Chakraborty S, Chandran D, Mohapatra RK, Islam MA, Alagawany M, Bhattacharya M, et al. Langya virus, a newly identified Henipavirus in China—zoonotic pathogen causing febrile illness in humans, and its health concerns: current knowledge and counteracting strategies—correspondence. Int J Surg. 2022;105:106882. https://doi.org/10.1016/j.ijsu.2022.106882
23. Weatherman S, Feldmann H, de Wit E. Transmission of henipaviruses. Curr Opin Virol. 2018;28:7–11. https://doi.org/10.1016/j.coviro.2017.09.004
24. Wu Z, Yang L, Yang F, Ren X, Jiang J, Dong J, et al. Novel henipa-like virus, Mojiang paramyxovirus, in rats, China, 2012. Emerg Infect Dis. 2014;20:1064–6. https://doi.org/10.3201/eid2006.131022
25. Hayman DTS, Wang LF, Barr J, Baker KS, Suu-Ire R, Broder CC, et al. Antibodies to henipavirus or henipa-like viruses in domestic pigs in Ghana, West Africa. PLoS One. 2011;6:e25256. https://doi.org/10.1371/journal.pone.0025256
26. Baker KS, Leggett RM, Bexfield NH, Alston M, Daly G, Todd S, et al. Metagenomic study of the viruses of African straw-coloured fruit bats: detection of a chiropteran poxvirus and isolation of a novel adenovirus. Virology. 2013;441:95–106. https://doi.org/10.1016/j.virol.2013.03.014
27. Lu M, Yao Y, Zhang X, Liu H, Gao G, Peng Y, et al. Both chimpanzee adenovirus-vectored and DNA vaccines induced long-term immunity against Nipah virus infection. NPJ Vaccines. 2023;8:170. https://doi.org/10.1038/s41541-023-00762-3
28. Mire CE, Geisbert JB, Agans KN, Feng YR, Fenton KA, Bossart KN, et al. A recombinant Hendra virus G glycoprotein subunit vaccine protects nonhuman primates against Hendra virus challenge. J Virol. 2014;88:4624–31. https://doi.org/10.1128/JVI.00005-14
29. Huang X, Li Y, Li R, Wang S, Yang L, Wang S, et al. Nipah virus attachment glycoprotein ectodomain delivered by type 5 adenovirus vector elicits broad immune response against NiV and HeV. Front Cell Infect Microbiol. 2023;13:1180344. https://doi.org/10.3389/fcimb.2023.1180344
30. Naveed M, Mehmood S, Aziz T, Hammad Arif M, Ali U, Nouroz F, et al. An mRNA-based reverse-vaccinology strategy to stimulate the immune response against Nipah virus in humans using fusion glycoproteins. Acta Biochim Pol. 2023;70:623–31. https://doi.org/10.18388/abp.2020_6721
31. Broder CC, Xu K, Nikolov DB, Zhu Z, Dimitrov DS, Middleton D, et al. A treatment for and vaccine against the deadly Hendra and Nipah viruses. Antiviral Res. 2013;100:8–13. https://doi.org/10.1016/j.antiviral.2013.06.012
32. Carlson CJ, Gibb RJ, Albery GF, Brierley L, Connor RP, Dallas TA, et al. The global virome in one Network (VIRION): an atlas of vertebrate-virus associations. MBio. 2022;13:e0298521. https://doi.org/10.1128/mbio.02985-21
33. Katoh K, Standley DM. MAFFT multiple sequence alignment software version 7: improvements in performance and usability. Mol Biol Evol. 2013;30:772–80. https://doi.org/10.1093/molbev/mst010
34. Capella-Gutiérrez S, Silla-Martínez JM, Gabaldón T. trimAl: a tool for automated alignment trimming in large-scale phylogenetic analyses. Bioinformatics. 2009;25:1972–3. https://doi.org/10.1093/bioinformatics/btp348
35. Shen W, Sipos B, Zhao L. SeqKit2: a Swiss army knife for sequence and alignment processing. iMeta. 2024;3:e191. https://doi.org/10.1002/imt2.191
36. Minh BQ, Schmidt HA, Chernomor O, Schrempf D, Woodhams MD, von Haeseler A, et al. IQ-TREE 2: new models and efficient methods for phylogenetic inference in the genomic era. Mol Biol Evol. 2020;37:1530–4. https://doi.org/10.1093/molbev/msaa015
37. Tamura K, Stecher G, Kumar S. MEGA11: Molecular Evolutionary Genetics Analysis Version 11. Mol Biol Evol. 2021;38:3022–7. https://doi.org/10.1093/molbev/msab120
38. Drummond AJ, Suchard MA, Xie D, Rambaut A. Bayesian phylogenetics with BEAUti and the BEAST 1.7. Mol Biol Evol. 2012;29:1969–73. https://doi.org/10.1093/molbev/mss075
39. Hasegawa M, Kishino H, Yano T. Dating of the human-ape splitting by a molecular clock of mitochondrial DNA. J Mol Evol. 1985;22:160–74. https://doi.org/10.1007/BF02101694
40. Rambaut A, Drummond AJ, Xie D, Baele G, Suchard MA. Posterior summarization in Bayesian phylogenetics using Tracer 1.7. Syst Biol. 2018;67:901–4. https://doi.org/10.1093/sysbio/syy032
41. Kalyaanamoorthy S, Minh BQ, Wong TKF, von Haeseler A, Jermiin LS. ModelFinder: fast model selection for accurate phylogenetic estimates. Nat Methods. 2017;14:587–9. https://doi.org/10.1038/nmeth.4285
42. Crowley D, Becker D, Washburne A, Plowright R. Identifying suspect bat reservoirs of emerging infections. Vaccines (Basel). 2020;8:228. https://doi.org/10.3390/vaccines8020228

43. Gu SH, Nicolas V, Lalis A, Sathirapongsasuti N, Yanagihara R. Complete genome sequence and molecular phylogeny of a newfound hantavirus harbored by the Doucet's musk shrew (*Crocidura douceti*) in Guinea. Infect Genet Evol. 2013;20:118–23. https://doi.org/10.1016/j.meegid.2013.08.016
44. Mortlock M, Geldenhuys M, Dietrich M, Epstein JH, Weyer J, Pawęska JT, et al. Seasonal shedding patterns of diverse henipavirus-related paramyxoviruses in Egyptian rousette bats. Sci Rep. 2021;11:24262. https://doi.org/10.1038/s41598-021-03641-w
45. Isaacs A, Low YS, Macauslane KLL, Seitanidou J, Pegg CLL, Cheung STM, et al. Structure and antigenicity of divergent henipavirus fusion glycoproteins. Nat Commun. 2023;14:3577. https://doi.org/10.1038/s41467-023-39278-8

Address for correspondence: Gary Wong, Institut Pasteur du Laos, Samsenthai Road, Ban Kao-Gnot, Sisattanak district, P.O. Box 3560, Vientiane, Laos; email: g.wong@pasteur.la

etymologia revisited

Haematospirillum jordania

[Hae.ma.to.spi.ril'lum jor.da'ni.ae]

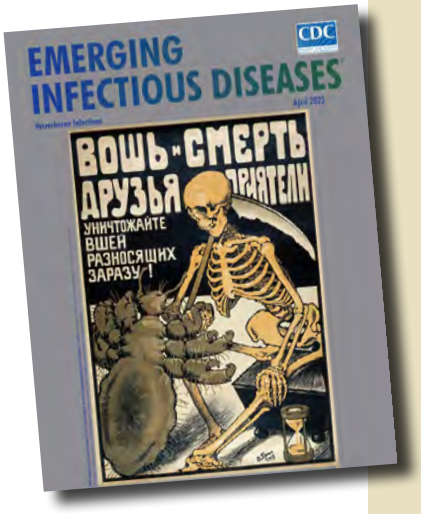

Originally published in April 2023

For the sesquipedalian term *Haematospirillum*, *Haema* is derived from the Greek haima, meaning blood. *Spirillum* is derived from Medieval Latin in the mid-13th century Latin (*spiralis*), French in the 1550s (*spiral*), and Greek (*speira*). All suggest a winding or coil. A New Latin reference book entry in 1875 implied a little coil.

Isolated from human blood, Haematospirillum jordaniae was reported as a novel genus and species in 2016 by Centers for Disease Control and Prevention (CDC) scientist Ben W. Humrighouse and his laboratory team, which included Jean G. Jordan, a microbiologist. This gram-negative bacterium was isolated 14 times in 10 states during 2003–2012 before its identification in 2016.

H. jordaniae was previously considered an environmental bacterium with limited pathogenicity, but increasing numbers of isolates indicated a possible emerging pathogen. All cases occurred in male patients, and the pathogen showed a predilection for infecting lower leg injuries. In 2018, Hovan and Hollinger reported a case of infection in a Delaware man who, in 2016, had sepsis from a lower leg wound. The organism isolated was identified at the CDC Special Bacteriology Reference Laboratory (SBRL) in the Division of High-Consequence Pathogens and Pathology, National Center for Emerging and Zoonotic Infectious Diseases.

References:

1. Hovan G, Hollinger A. Clinical isolation and identification of *Haematospirillum jordaniae*. Emerg Infect Dis. 2018;24:1955–6.
2. Humrighouse BW, Emery BD, Kelly AJ, Metcalfe MG, Mbizo J, McQuiston JR. *Haematospirillum jordaniae* gen. nov., sp. nov., isolated from human blood samples. Antonie van Leeuwenhoek. 2016;109:493–500.
3. LPSN List of prokaryotic names with standing in nomenclature. Species *Haematospirillum jordaniae* [cited 2022 May 21]. https://lpsn.dsmz.de/species/haematospirillum-jordaniae
4. Jean Jordan obituary. Published by the Atlanta Journal-Constitution on May 28, 2014. [cited 2022 Oct 17]. https://www.legacy.com/us/obituaries/atlanta/name/jean-jordan94
5. Pal E, Štrumbelj I, Kišek TC, Kolenc M, Pirš M, Rus KR, et al. *Haematospirillum jordaniae* cellulitis and bacteremia. Emerg Infect Dis. 2022;28:2116–9.
6. Persiana (1875) (Latin Edition): Heckmanns, Alexius. *Spirillum* (n.) [cited 2022 May 21]. https://www.etymoline.com/word/spirillum
7. Weyant RS, Moss CW, Weaver RE. Hollis, Jordan JG, Cook E, et al.; Centers for Disease Control and Prevention. Identification of unusual pathogenic gram-negative aerobic and facultatively anaerobic bacteria. The Orange Book, 2nd ed. Philadelphia: Lippincott Williams and Wilkins; 1996 1.

https://wwwnc.cdc.gov/eid/article/29/4/et-2904_article

Candida auris Outbreak and Epidemiologic Response in Burn Intensive Care Unit, Illinois, USA, 2021–2023

Hannah J. Barbian,[1] Louise Lie,[1] Alyse Kittner, Amanda Harrington, Joshua Carson, Mabel Frias, David H. Slade, Do Young Kim, Stephanie Black, Jorge P. Parada,[2] Mary K. Hayden[2]

Candida auris is an emerging fungal pathogen associated with outbreaks in healthcare settings. We report a multiyear outbreak of *C. auris* in a burn intensive care unit in Illinois, USA, during 2021–2023. We identified 28 *C. auris* cases in the unit over a 2-year period, despite outbreak response and multimodal mitigation measures. Of the 28 case-patients, 15 (53.6%) were considered colonized and 13 (46.4%) had clinical infections. Phylogenetic analysis of whole-genome sequences revealed 4 distinct clusters of closely related (0–6 SNP differences) genomes containing 3–6 cases. Clusters generally contained temporally related isolates from patients with epidemiologic links; this finding suggests that multiple introductions and within-unit spread over a limited time were responsible for the outbreak, rather than transmission from a long-term source (e.g., persistent environmental contamination or staff carriage). Here, integrated traditional and genomic epidemiology supported *C. auris* outbreak investigation and response and informed targeted interventions.

Candida auris is a fungal pathogen associated with colonization and high-mortality invasive infections in persons with underlying medical conditions, especially those who are hospitalized or reside in long-term care facilities (*1*,*2*). Prolonged skin colonization and environmental contamination likely contribute to within-facility persistence and spread (*2*–*5*). *C. auris* often displays extensive antifungal resistance and can acquire resistance rapidly during antifungal treatment (*6*–*8*).

Intensive care units (ICUs) are particularly vulnerable to *C. auris* outbreaks because of prolonged patient stays, high medical acuity, and extensive use of medical devices that can encourage pathogen spread (*9*–*12*). Effective infection prevention strategies are key to curbing the spread of *C. auris*; those strategies include contact screening, strict hand hygiene procedures, appropriate use of personal protective equipment (PPE) and transmission-based precaution by healthcare providers, use of single-patient equipment, environmental cleaning and disinfection, and private-room isolation (*13*). However, *C. auris* colonization and transmission have been reported to persist despite aggressive infection prevention interventions, making *C. auris* control a long-term burden in affected facilities (*12*,*14*,*15*).

In burn ICUs (BICUs), patients are at increased risk for healthcare-acquired infections because of breakdown of the skin barrier and the immunocompromising effects of burns; infection is the leading cause of death after burn injury (*16*). Fungal wound infections are reported in 6%–45% of all burn admissions; candidemia develops in up to 5% of patients with severe burns. Unlike most *Candida* species, *C. auris* has a tropism for skin (*17*), and it can readily colonize or infect adjacent large, open, nutrient-rich burn wounds. Furthermore, because they have frequent infections and large, open wounds, burn patients often require treatment with systemic and topical antimicrobials, both of which have capacity to eliminate competitive microbiota and encourage colonization

Author affiliations: Rush University Medical Center, Chicago, Illinois, USA (H.J. Barbian, M.K. Hayden); Loyola University Medical Center, Maywood, Illinois, USA (L. Lie, A. Harrington, J. Carson, D.H. Slade, J.P. Parada); Chicago Department of Public Health, Chicago (A. Kittner, D.Y. Kim, S. Black); Cook County Department of Public Health, Forest Park, Illinois, USA (M. Frias)

DOI: https://doi.org/10.3201/eid3103.241195

[1]These first authors contributed equally to this article.

[2]These authors contributed equally to this article.

with resistant organisms such as *C. auris*. Care provided in BICUs, such as skin debridement, may disperse colonized or infected skin cells into the environment, which contributes to transmission.

We describe a *C. auris* outbreak and response in a BICU in Illinois beginning in 2021. We used whole-genome sequencing (WGS) to help refine epidemiologic inferences and direct interventions. WGS has been used to support epidemiologic investigations of *C. auris* infection, including hospital outbreaks (*9*,*18*–*23*). Outbreak sequences generally form a unique clade with limited diversity (*9*,*18*); close relationships have been observed between epidemiologically linked cases (median 7 SNPs) and isolates from the same person (median 2 SNPs) (*21*). WGS can also detect antifungal resistance mutations (*19*,*24*,*25*). Thus, WGS may be a powerful tool to support *C. auris* outbreak investigations.

Methods

Study Setting and Participants

The Burn Center is a 10-bed intensive care unit caring for pediatric and adult burn patients at a 547-bed academic tertiary care medical center in the Chicago metropolitan area, Illinois, USA. The unit accommodates ICU overflow from other services, including medical and surgical ICUs. The unit practices universal contact precautions (gowns, gloves, masks, and eye protection) for all patients, staff, and visitors to the unit. We abstracted patient data via retrospective review of the hospital electronic medical records.

The Institutional Review Board of Loyola University (Chicago, IL, USA) reviewed and approved the protocol for this study (LU218571). Informed consent was waived.

Case Identification and Investigation

The outbreak investigation, led by the infection prevention team, consisted of admission screening and weekly point prevalence surveys of all patients in the unit. We defined a hospital-acquired case of *C. auris* as any illness in patient who, after a negative *C. auris* admission screen, tested positive for *C. auris* on subsequent weekly point prevalence screens or in any clinical specimen. We defined colonized cases as patients who had *C. auris* identified from surveillance cultures but no detection of *C. auris* in any clinical specimens. Clinical cultures refer to blood, wound, respiratory, or urine cultures.

We conducted epidemiologic investigations to identify commonalities between cases, including healthcare workers, medical equipment, prior room occupancies, and exposure locations outside of the BICU, including the operating room, tub room, and procedural areas such as the interventional radiology and gastroenterology suites. We reviewed patients' history of *C. auris* through query of the Illinois extensively drug-resistant organism registry (*34*).

Infection Control Measures

Universal contact precautions and masks are used for all BICU patients; further containment strategies implemented in response to this outbreak involved increased observation of isolation compliance, education of nursing and ancillary staff about *C. auris* transmission and control, environmental cleaning validation, enhanced environmental cleaning with ultraviolet (UV) light, observation and training regarding correct use of PPE, and proper hand hygiene. In addition, the local health department performed an infection control assessment and response to identify and address infection control gaps.

Microbiologic Identification of Cases

We isolated *C. auris* fungus from screening samples collected from the axilla and groin of patients using a BBL CultureSwab EZ Collection and Transport System (BD, https://www.bd.com). We then inoculated samples onto HardyCHROM Candida (Hardy Diagnostics, https://hardydiagnostics.com) and incubated aerobically, protected from light, at 35°C for 72 hours. We isolated *C. auris* from clinical samples submitted for routine diagnostic testing on standard microbiologic media including sheep blood agar, chocolate agar, inhibitory mold agar (BBL prepared plated media; BD), and blood culture media (BACTEC Plus Aerobic and Lytic Anaerobic media; BD). We performed species identification by using Biotyper matrix-assisted laser desorption/ionization time-of-flight (MALDI-TOF) mass spectrometry with the MBT Compass Library version 12 Revision K (Bruker Daltonics, https://bruker.com).

Whole-Genome Sequencing

We suspended available *C. auris* isolates in DNA/RNAshield (Zymo, https://zymoresearch.com) and transported them to the Regional Innovative Public Health Laboratory at Rush University Medical Center (Chicago, IL, USA). We extracted nucleic acids using the Cultured Cells DNA Kit and Maxwell extraction system (Promega, https://promega.com) and prepared sequencing libraries using 1 ng DNA extract and Nextera XT DNA Library Preparation

Kit (Illumina, https://illumina.com). We barcoded genome libraries by using IDT for Illumina DNA/RNA UD Indexes (Illumina) and balanced using a small-scale sequencing run of an equivolume pool (Illumina iSeq). We subjected final libraries to 2 × 150 paired-end sequencing on NovaSeq6000 (Illumina). We submitted data to the National Center for Biotechnology Information Short Read Archive (Appendix Table 1, https://wwwnc.cdc.gov/EID/article/31/3/24-1195-App1.pdf).

Bioinformatic and Statistical Analysis

We downloaded all publicly available Illinois *C. auris* sequences for comparison to outbreak sequences (Appendix Table 1). We analyzed paired-end sequences with the MycoSNP-nf pipeline version 1.4 (https://github.com/CDCgov/mycosnp-nf) by using clade IV reference B11243 (Genbank accession no. GCA_003014415.1) and implemented on Terra as previously described (*20*,*27*,*28*), excluding isolates with estimated coverage depth <25. We determined *C. auris* clade using phylogenetics with clade I–IV reference sequences. We used SNP differences between all samples and the reference to build a neighbor-joining tree using MEGA 11 (*29*) as previously described with 1,000 bootstrap replicates (*21*,*30*). To compare SNP differences, we used SNP distance matrices with all available Illinois sequences. To identify potential antifungal-resistance mutations, we used Snippy (*31*) to query for mutations in the *FKS1, ERG11, TAC1b, MRR1, ERG3,* and *FUR1* genes. We compared mean SNP differences using Kruskal-Wallis nonparametric testing with adjusted significance between individual groups calculated using the Dunn multiple comparisons test.

Results

Outbreak Investigation

The first clinical *C. auris* isolate in a BICU patient was identified from blood culture in 2021. Three additional case-patients with hospital-acquired *C. auris* were identified in the subsequent 2 months (Figure 1). Admission screening in the BICU was initiated 3 months after the first case-patient was detected (Figure 1). A fifth case-patient, who originally screened negative on admission, was identified from a wound culture 83 days after admission; that case was notable because it was the first confirmed hospital acquisition of *C. auris*. A point prevalence survey 5 months after first case detection identified a sixth case. Weekly point prevalence screening was initiated 6 months after first case detection; 22 additional cases were identified 6–21 months after first case identification (Figure 1). Weekly point prevalence surveys were discontinued 28 days after discharge of the last patient with *C. auris*.

We reviewed case records to identify documented epidemiologic links; specifically, common locations (rooms), procedures, and staff exposures. Intensive observation of infection control practices throughout the BICU identified breaches that may have contributed to *C. auris* transmission, including poor hand hygiene compliance, improper PPE donning and doffing, cluttered patient care areas preventing thorough environmental cleaning, poor auditing of environmental cleaning, and inconsistent cleaning and disinfection practices for shared equipment. Shared equipment within the unit included bladder scanners, forced-air patient warming devices, vascular Dopplers, EKG machines, point-of-care ultrasounds,

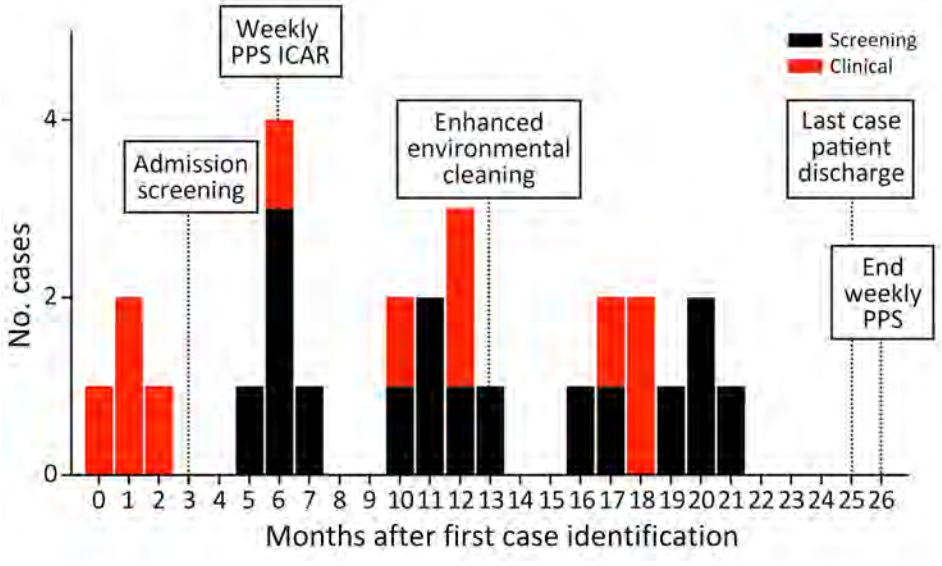

Figure 1. Epidemiologic curve of *Candida auris* outbreak cases in burn intensive care unit, Illinois, USA, 2021–2023. Color indicates whether case was identified by screening or clinical isolates. PPS, point prevalence survey.

and recliners. Particular attention was given to staff whose patient care activities were extended to areas in the medical center outside of the BICU, including physical, occupational, speech and respiratory therapy, and radiology staff. The hospital infection control team and the local health department observed infection control breaches during the infection control assessment performed 6 months after the first case of *C. auris* was detected.

Outbreak Mitigation Measures

Early in the outbreak, a multidisciplinary *C. auris* response team, including staff from infection prevention, environmental services, nursing, facilities management, BICU physicians and hospital leadership, convened to create and implement a structured plan. All patients in the BICU with positive *C. auris* culture results were placed on contact precautions; signs were placed on the patients' room doors, and their electronic medical records were flagged for *C. auris* and an isolation order. The team implemented outbreak mitigation measures universally in the BICU and centered on communication, education, and process improvement, focusing on environmental cleaning and hand hygiene. Education on *C. auris* transmission and necessary precautions were extended to the BICU nursing staff, with special attention on ancillary groups, particularly those also providing care to units outside of the BICU: environmental service, respiratory therapy, physical and occupational therapy, food and nutrition services, radiology, and pastoral care.

The team reviewed cleaning responsibilities between nursing and environmental service, including method of cleaning and frequency. Standard cleaning practices include floor and surface cleaning with a disinfectant effective against *C. auris,* bleach-wipe cleaning of equipment, and a log to track cleaning of shared equipment. Storage cabinets were installed in patient rooms. Black-light audits on discharge cleans were required on every terminal discharge to monitor cleaning practices, and environmental service staff received coaching when cleaning failures were identified. Germicidal ultraviolet disinfection was performed in patient rooms and above the unit's nursing station beginning 9 months after first case detection. Thirteen months after first case detection, terminal cleaning of patient rooms incorporated high-intensity UV disinfection.

Unobtrusive-observer audits revealed that overall hand hygiene compliance was 78%–93% during the outbreak period. Most observations were of nursing staff; the greatest opportunities for improvement in compliance were among patient transporters (32% compliance), food and nutrition services (35% compliance), and physicians (67% compliance). The team increased hand hygiene promotion signage and efforts to normalize just-in-time coaching for hand hygiene and PPE breaches among staff and visitors.

Patient Characteristics

During the 21-month investigation, 28 patients were colonized or infected with *C. auris* (Table); 4 patients had invasive *C. auris* before admission screening. The average patient age was 49 years (range 16–81 years). Most patients were admitted with burns (64%), 9 patients (32%) were admitted with soft-tissue infections, and 1 patient was on medical ICU service. None of the patients had a history of *C. auris* infection, determined by chart review and query of the Illinois extensively drug-resistant organism registry. Seven patients were admitted from outside hospitals or had a hospitalization ≤30 days before the BICU admission; none were admitted from skilled nursing facilities. The mean length of stay in the BICU before identification of *C. auris* was 26 days (range 7–83 days). *C. auris* was identified in clinical cultures from 13 patients, some of which had *C. auris* in multiple cultures; 8 had *C. auris* identified in blood culture, 6 in respiratory culture, 8 in wound culture, and 3 in urine culture. The mean total length of stay in the BICU was 67 days (Figure 2).

Genomic Analysis of Outbreak Isolates

To investigate the genetic relationship of *C. auris* among cases, we conducted WGS on available isolates from the BICU outbreak, including isolates from 22 (79%) of 28 case-patients and 8 longitudinal isolates from 3 of those patients (Figure 2). Isolates from the remaining 6 case-patients were not available for analysis. We also sequenced available contemporaneous isolates from the same facility (n = 19) or another healthcare facility within the medical system (n = 31) to estimate diversity of hospital *C. auris* isolates and identify potential links outside of BICU. Of 80 isolates, 78 (97.5%) had sufficient genome quality for analysis; all were *C. auris* clade IV. Comparison with publicly available *C. auris* sequences from Illinois (n = 364) revealed that genomes from the BICU and related facilities were interspersed throughout other Illinois *C. auris* sequences (Appendix Figure 1), indicating multiple transmissions to the BICU facility from the broader diversity in the region.

BICU isolates formed 4 clusters within Illinois sequences (Figure 3, panel A). Clusters contained

3–6 unique patients and closely related genomes (0–8 SNP differences) (Figure 3, panels B-E). Three BICU isolates did not cluster closely with any other BICU or Illinois isolate, differing by 7–39 SNPs from the closest non-BICU and 21–49 SNPs from the closest BICU isolate (Figure 3, panel A; Appendix Figure 1). We identified a mean 1.9 (range 0–8) SNP differences within BICU clusters, which was not significantly different from SNP differences from isolates collected from the same patient (p>0.9999) (Figure 4). However, SNP differences among all BICU isolates were significantly higher (mean 34.6; p<0.0001), but not significantly different from, mean SNP differences among isolates collected within the same timeframe elsewhere within the medical center (mean 35.8) or all Illinois (mean 37.9). Those findings indicate that BICU clusters were very closely related among isolates within the cluster but not more closely related among clusters than for other regional isolates, consistent with multiple independent introductions from regional *C. auris* followed by within-unit spread.

Table. Characteristics of 28 *Candida auris* outbreak case-patients in BICU, Illinois, USA, 2021–2023*

Characteristic	Value
Sex	
F	13 (46)
M	15 (54)
Average age, y (range)	49 (16–81)
Admission diagnosis	
Burn	18 (64)
Soft tissue infection not including burns	9 (32)
COVID-19†	1 (4)
C. auris culture source	
Axillary/inguinal screening culture‡	24 (86)
Clinical culture§	14 (50)
Blood	8 (29)
Respiratory	6 (21)
Wound	8 (29)
Urine	3 (11)
Co-infection with multidrug-resistant organism¶	13 (46)
Mean length of stay from admission to first positive *C. auris* culture, d (range)	26 (7–83)
Recent hospitalization ≤1 month before hospitalization	8 (29)
Medical devices used ≤1 week before positive *C. auris* culture	
Central venous catheter	24 (86)
Ventilator	18 (64)
Urinary catheter	24 (86)
Ancillary medical services received ≤1 week before first positive *C. auris* culture	
Occupational therapy	23 (82)
Physical therapy	18 (64)
Speech therapy	5 (18)
Mean length of stay in BICU, d (range)	67 (6–442)
C. auris outcome	
Colonization	14 (50)
Infection	13 (46)
Discharge disposition	
Skilled nursing facility, acute rehab or other hospital	17 (61)
Home	5 (18)
Deceased	6 (21)

*Values are no. (%) except as indicated. BICU, burn intensive care unit.
†Medical intensive care unit service patient on overflow to BICU.
‡Ten of the 24 patients with a positive axillary/inguinal screen also had *C. auris* identified from a clinical culture.
§Of the clinical cultures, 4 patients had *C. auris* identified only in blood, 3 had *C. auris* only from wound infections, 1 had *C. auris* only from respiratory source, and the remaining 6 had *C. auris* identified in >1 clinical culture source.
¶A total of 13 patients were co-infected or co-colonized with 19 other multidrug-resistant organisms: 6 vancomycin-resistant enterococci, 5 extended-spectrum β-lactamase–producing organisms, 3 methicillin-resistant *Staphylococcus aureus*, 2 multidrug-resistant *Pseudomonas aeruginosa* (MDR-PA), 1 carbapenem-resistant *Acinetobacter baumannii*, 1 carbapenem-resistant Enterobacterales, 1 AmpC β-lactamase–producing organism.

Integrated Genomic and Epidemiologic Investigation of Outbreak Clusters

Clusters 2 and 4 contained exclusively BICU isolates (Figure 3, panels C, E), whereas clusters 1 and 3 contained sequences collected within the medical center but outside of the BICU (Figure 3, panels B, D). In one instance, in cluster 1, Figure 3, panel B), 1 sequence from the same facility collected 4 months before the first BICU case was identical to the first BICU case's genome (patient 1). No epidemiologic links to BICU patients in this cluster were identified, and facility stays were separated by 123 days. In cluster 3 (Figure 3, panel D), 1 sequence from another unit within the facility and 1 sequence from elsewhere in the medical system collected 1 month before and 1 month after the first BICU case clustered with BICU isolates (patients 14, 15, 16, 18). No epidemiologic links were identified between the cases from the same facility. The case-patient from elsewhere in the medical system had been hospitalized at the BICU facility the month before, overlapping with other patients in this cluster. In addition, this patient and another BICU patient with *C. auris* from this cluster were both exposed to the same healthcare worker (speech therapist) during overlapping timeframes. Contextual isolates from institutions outside of the medical system did not fall in BICU clusters (≥8 SNPs) (Figure 3; Appendix Figure 1).

BICU sequences clustered by collection date; clusters generally contained isolates collected within 3–6 months of each other (Figure 3, panels B–E). Clustering patients had overlapping BICU admission dates in all but 1 instance (Figure 2). In the exception, a patient (patient 9) from cluster 1 was admitted to the BICU 91 days after other patients in cluster 1 were discharged, but the *C. auris* isolate was not sequenced. This patient was then discharged to the same long-term acute care hospital

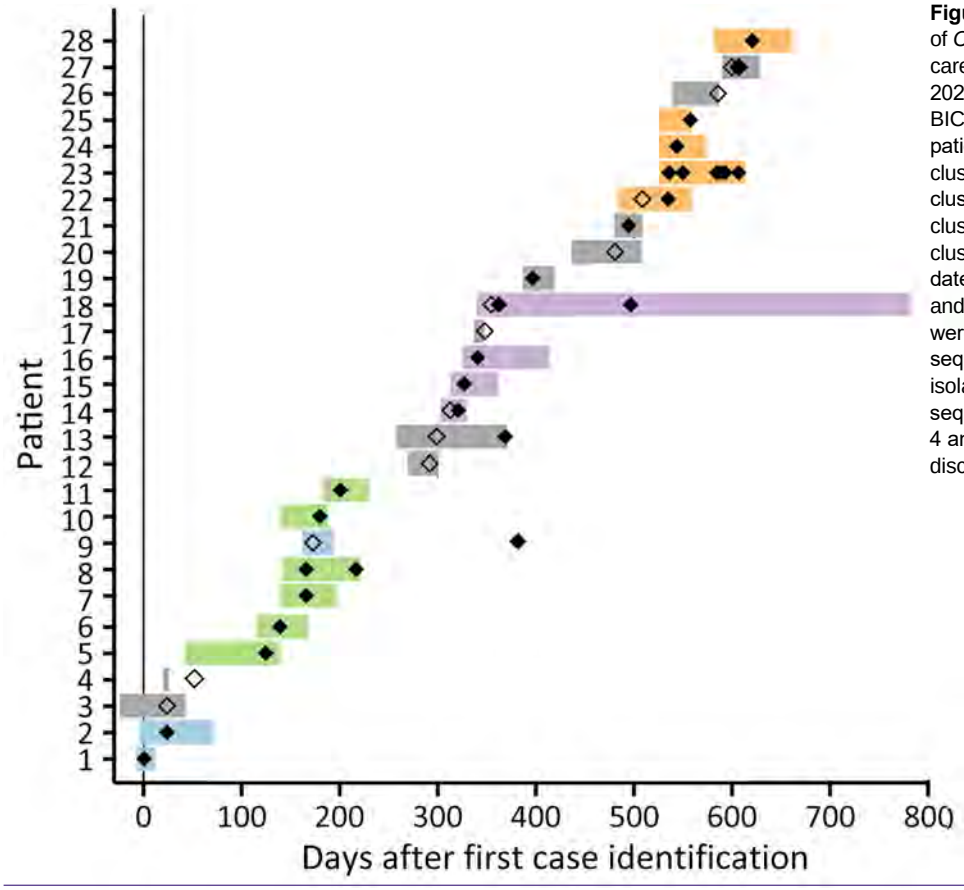

Figure 2. Case timeline for outbreak of *Candida auris* in burn intensive care unit (BICU), Illinois, USA, 2021–2023. Horizontal bars indicate BICU admission duration for each patient; bar colors indicate genomic cluster (blue, cluster 1; green, cluster 2; purple, cluster 3; orange, cluster 4; gray, not sequenced or no cluster). Diamonds indicate collection date of the first *C. auris* isolate and any subsequent isolates that were subjected to whole-genome sequencing; filled diamonds mean the isolate was sequenced, unfilled, not sequenced. In 2 instances (patient 4 and 9), *C. auris* was isolated after discharge from the BICU.

as another patient in cluster 1 (Figure 3, panel B). The isolate belonging to cluster 1 was identified in an admission screening culture 8 months later, when the patient was admitted to another unit within the BICU facility. Thus, *C. auris* transmission may have occurred either on the BICU or at the long-term acute care hospital.

Analysis of Longitudinal Outbreak Isolates

Longitudinal isolates were collected from 3 patients over 51 (n = 2), 63 (n = 6), and 135 (n = 3) days and included both clinical and screening isolates. All longitudinal sequences clustered closely with other sequences from the same patient. Six of 11 longitudinal sequences were identical to another sequence from the same person; clinical and screening isolates were often identical to one another (Figure 3, panels C–E). Specimens collected from the same person had a mean 1.2 (range 1–4) SNP differences (Figure 4).

We investigated mutations in antifungal resistance–associated genes to look for longitudinal acquisition of antifungal resistance mutations. We identified a mutation associated with azole resistance in the *TAC1b* gene (I187T) in the last isolate collected from 1 patient; the 2 isolates obtained from this person earlier did not contain this mutation (Figure 3, panel D) (*32*,*33*). The patient received voriconazole therapy after collection of the isolates lacking the mutation but before the emergence of the *TAC1b* mutation. The isolate was not subjected to phenotypic antifungal susceptibility testing.

Discussion

We describe a *C. auris* outbreak in a BICU that resulted in 28 patients colonized or infected over 2 years. We initially hypothesized that this was one continuous outbreak with possible environmental reservoirs on the unit contributing to ongoing transmission. WGS revealed 4 distinct clusters and 7 distinct genotypes; integration with epidemiologic information identified a complex outbreak that was driven both by importation of new strains and by within-BICU cross-transmission. Two phylogenetic clusters that included 7 (32%) of the sequenced case patient isolates contained isolates from both BICU patients and patients who were cared for in other units within the medical center, suggesting that *C. auris* might have been imported into the BICU from elsewhere in the facility by contaminated

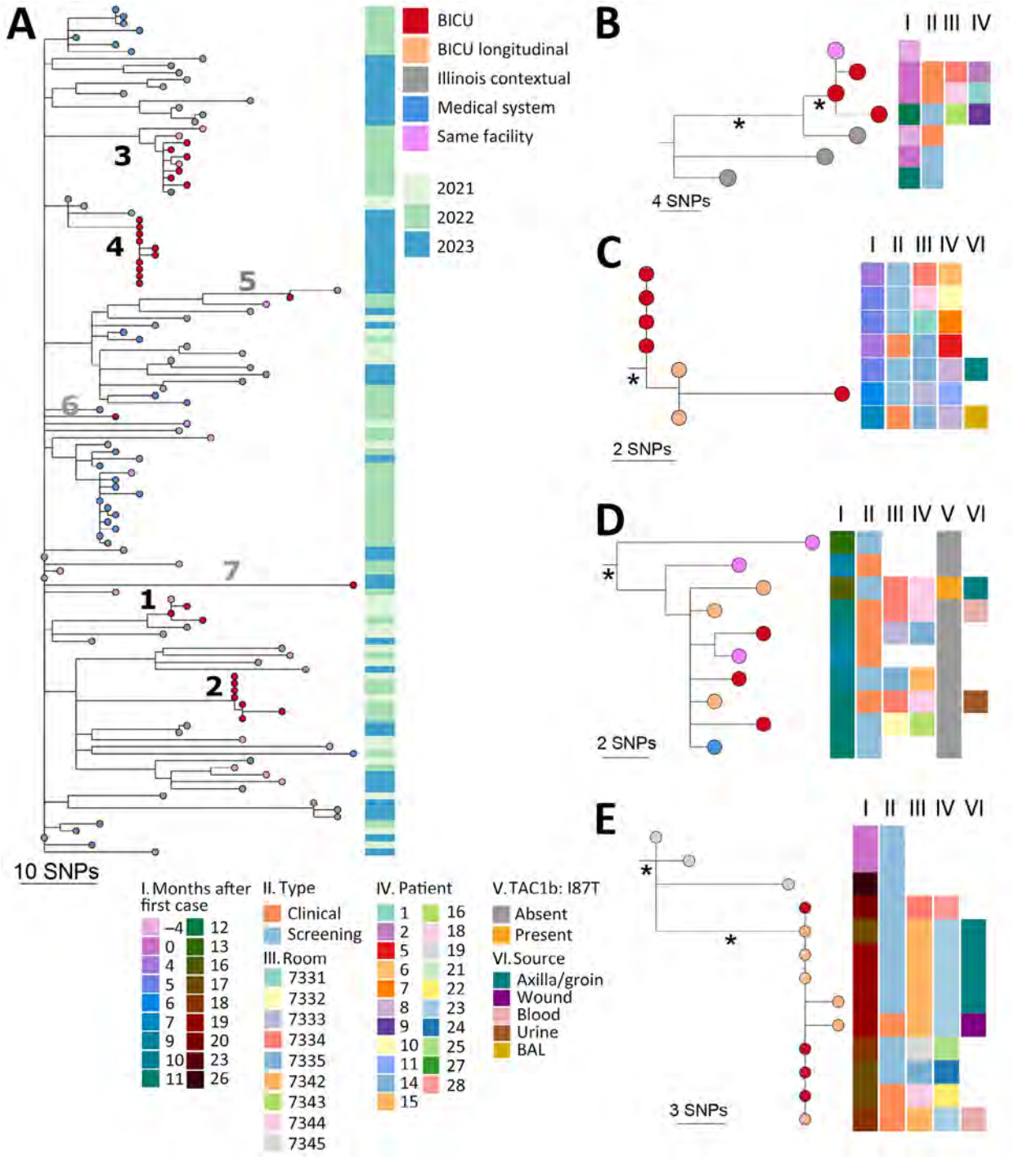

Figure 3. Genomic analysis of outbreak and contemporaneous contextual *Candida auris* isolates in outbreak of *C. auris* in BICU, Illinois, USA, 2021–2023. A) Neighbor-joining SNP-based phylogenetic tree of sequences from BICU isolates, isolates collected from the same facility or another facility within the medical system, and publicly available Illinois sequences collected in 2021–2023. Facility source for 31 of 43 Illinois contextual sequences was confirmed as not within the BICU medical system. The facility source of the remaining 12 isolate sequences was not known. Branch lengths are SNP distances. Isolate collection year is indicated in metadata column to the right. Numbers 1–4 indicate branches leading to BICU clusters; numbers 5–7 indicate branches leading to BICU isolates that do not cluster with others. B–E) Subtrees from BICU cluster 1 (B), cluster 2 (C), cluster 3 (D), and cluster 4 (E). Relevant isolate and patient metadata are indicated in the columns to the right of tree tips; key at bottom shows metadata coding for panels B–E. Orange tips indicate isolates collected from the same person. Isolate collection date is shown as months after the first BICU case. Asterisks (*) indicate branches with >95% bootstrap support. Scale bars indicate SNPs. BICU, burn intensive care unit; SNP, single-nucleotide polymorphism.

healthcare provider hands or clothing or by shared equipment. Alternatively, a BICU patient might have acquired *C. auris* upon exposure to contaminated surfaces or equipment in a common diagnostic or procedure area outside of the BICU. Either of those pathways could have led to the index BICU case; the index isolate genome was identical to an isolate collected from a patient in a unit elsewhere in the medical center 4 months earlier. However, epidemiologic links between new case-patients on the BICU and other patients in the hospital were not always identified.

Occult colonization, or colonization at low level or unsampled sites that results in nondetection by surveillance culture, of newly admitted patients might also have contributed to importation of *C. auris* into the BICU. Although all patients underwent axilla or groin screening for *C. auris* at the time of BICU admission, the sensitivity of this approach has been reported at ≈62%; to detect 100% of colonized patients, ≥6 body sites needed to be screened (*15*). Indeed, 3 patients were colonized with unique isolates that did not fall into any of the 4 clusters. Further, 11 of 22 case-patients whose isolates were sequenced and who had temporally overlapping BICU stays were included in 2 clusters that included only BICU patient isolates, suggesting within-BICU transmission of *C. auris*. Thus, undetected colonization at the time of admission and infection control breaches likely enabled introduction and transmission of *C. auris* to occur on the BICU. As our study demonstrated, *C. auris* is transmitted easily in healthcare facilities, and regional transmission can be hastened by patient transfers; in this outbreak, 61% of colonized or infected patients were discharged to other healthcare facilities. Interfacility communication and strict infection control measures are necessary to limit spread to other patient populations.

Once *C. auris* was introduced on the BICU, transmission was likely exacerbated by observed infection control breaches, particularly poor hand hygiene practices and lapses in cleaning of shared equipment. The prolonged lengths of stay of the patients (mean 67 days) also pose infection prevention and control challenges; *C. auris* rooms are recontaminated in as little as 4 hours after disinfection (*34*), emphasizing the need for stringent long-term adherence to cleaning and basic infection control practices.

The first limitation of our study is that it was conducted retrospectively; we selected samples for WGS on the basis of availability of stored isolates, and not all isolates from the outbreak were sequenced. Second, in most cases, only 1 isolate per patient was

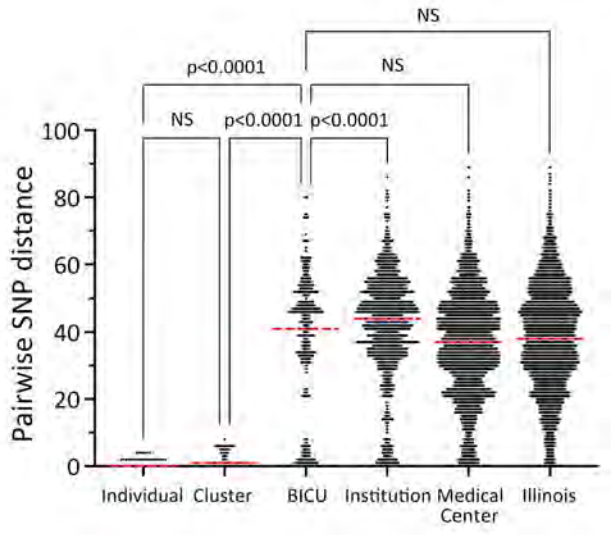

Figure 4. Pairwise SNP distances within different *Candida auris* populations in study of outbreak in burn intensive care unit, Illinois, USA, 2021–2023. Black points (which appear as lines for the large datasets) are pairwise SNP distances between 2 isolate sequences; horizontal red dashed lines indicate medians. BICU, burn intensive care unit; NS, not significant (adjusted p>0.05); SNP, single-nucleotide polymorphism.

available for sequencing. Although some studies have found that patients can carry multiple genetically distinct *C. auris* isolates, genetically similar isolates may be more likely in an acute outbreak setting (*9*,*21*). In our study, all isolates collected from the same patient were closely related. Third, collection of epidemiologic metadata was limited to medical record review; some activities would not be recorded in the medical record. Further, contamination of portable unit-based equipment that is shared between patients might have contributed to ongoing *C. auris* transmission, but this possibility could not be verified through medical record review, and we conducted no environmental culturing.

WGS refined our understanding of this *C. auris* outbreak. The discovery that the outbreak included multiple introductions of *C. auris* onto the unit influenced our current approach to *C. auris* investigation and response; we focus now on between-unit transmission, including the possible role of ancillary personnel who move throughout the hospital, and not just on within-unit infection prevention measures. Furthermore, we conduct admission screening as well as point prevalence survey protocols in response to a *C. auris* case to identify and isolate colonized patients quickly. Integrated WGS and epidemiologic investigation is a powerful tool for identifying drivers of transmission in nosocomial outbreaks.

Acknowledgments

We thank Stefan Green, Sofiya Bobrovska, and members of the Rush University Medical Center Genomics and Microbiome Core Facility for whole-genome sequencing and data management. We thank Michael Bauer and members of the Loyola University Medical Center clinical microbiology laboratory for generation, storage, and transport of isolates. We thank Isaac Ghinai and the Chicago Department of Public Health Laboratory-Based Surveillance and Healthcare Settings teams. We thank Robert Garcia for manuscript review.

This project was supported by the Centers for Disease Control and Prevention (CDC) of the US Department of Health and Human Services (HHS) as part of a financial assistance award totaling $11,162,000 with 100% funded by CDC/HHS. The contents are those of the authors and do not necessarily represent the official views of, nor an endorsement by, CDC/HHS or the US government.

About the Author

Dr. Barbian is an assistant professor and genomic epidemiologist at Rush University Medical Center Regional Innovative Public Health Laboratory. Her primary research interests are public health genomics, genomic surveillance, and pathogen evolution.

References

1. Tsay S, Welsh RM, Adams EH, Chow NA, Gade L, Berkow EL, et al. Notes from the field: ongoing transmission of *Candida auris* in health care facilities—United States, June 2016–May 2017. MMWR Morb Mortal Wkly Rep. 2017;66:514–5. https://doi.org/10.15585/mmwr.mm6619a7
2. Vallabhaneni S, Kallen A, Tsay S, Chow N, Welsh R, Kerins J, et al. Investigation of the first seven reported cases of *Candida auris,* a globally emerging invasive, multidrug-resistant fungus-United States, May 2013–August 2016. Am J Transplant. 2017;17:296–9. https://doi.org/10.1111/ajt.14121
3. Piedrahita CT, Cadnum JL, Jencson AL, Shaikh AA, Ghannoum MA, Donskey CJ. Environmental surfaces in healthcare facilities are a potential source for transmission of *Candida auris* and other *Candida* species. Infect Control Hosp Epidemiol. 2017;38:1107–9. https://doi.org/10.1017/ice.2017.127
4. Sexton DJ, Bentz ML, Welsh RM, Derado G, Furin W, Rose LJ, et al. Positive correlation between *Candida auris* skin-colonization burden and environmental contamination at a ventilator-capable skilled nursing facility in Chicago. Clin Infect Dis. 2021;73:1142–8. https://doi.org/10.1093/cid/ciab327
5. Horton MV, Johnson CJ, Kernien JF, Patel TD, Lam BC, Cheong JZA, et al. *Candida auris* forms high-burden biofilms in skin niche conditions and on porcine skin. MSphere. 2020;5:e00910-19. https://doi.org/10.1128/mSphere.00910-19
6. Lockhart SR, Etienne KA, Vallabhaneni S, Farooqi J, Chowdhary A, Govender NP, et al. Simultaneous emergence of multidrug-resistant *Candida auris* on 3 continents confirmed by whole-genome sequencing and epidemiological analyses. Clin Infect Dis. 2017;64:134–40. https://doi.org/10.1093/cid/ciw691
7. Biagi MJ, Wiederhold NP, Gibas C, Wickes BL, Lozano V, Bleasdale SC, et al. Development of high-level echinocandin resistance in a patient with recurrent *Candida auris* candidemia secondary to chronic candiduria. Open Forum Infect Dis. 2019;6:ofz262. https://doi.org/10.1093/ofid/ofz262
8. Rybak JM, Barker KS, Muñoz JF, Parker JE, Ahmad S, Mokaddas E, et al. In vivo emergence of high-level resistance during treatment reveals the first identified mechanism of amphotericin B resistance in *Candida auris*. Clin Microbiol Infect. 2022;28:838–43. https://doi.org/10.1016/j.cmi.2021.11.024
9. Eyre DW, Sheppard AE, Madder H, Moir I, Moroney R, Quan TP, et al. A *Candida auris* outbreak and its control in an intensive care setting. N Engl J Med. 2018;379:1322–31. https://doi.org/10.1056/NEJMoa1714373
10. Ruiz-Gaitán A, Moret AM, Tasias-Pitarch M, Aleixandre-López AI, Martínez-Morel H, Calabuig E, et al. An outbreak due to *Candida auris* with prolonged colonisation and candidaemia in a tertiary care European hospital. Mycoses. 2018;61:498–505. https://doi.org/10.1111/myc.12781
11. Armstrong PA, Rivera SM, Escandon P, Caceres DH, Chow N, Stuckey MJ, et al. Hospital-associated multicenter outbreak of emerging fungus *Candida auris,* Colombia, 2016. Emerg Infect Dis. 2019;25:1339–46. https://doi.org/10.3201/eid2507.180491
12. Schelenz S, Hagen F, Rhodes JL, Abdolrasouli A, Chowdhary A, Hall A, et al. First hospital outbreak of the globally emerging *Candida auris* in a European hospital. Antimicrob Resist Infect Control. 2016;5:35. https://doi.org/10.1186/s13756-016-0132-5
13. Jeffery-Smith A, Taori SK, Schelenz S, Jeffery K, Johnson EM, Borman A, et al.; Candida auris Incident Management Team. *Candida auris*: a review of the literature. Clin Microbiol Rev. 2018;31:e00029-17. https://doi.org/10.1128/CMR.00029-17
14. Pacilli M, Kerins JL, Clegg WJ, Walblay KA, Adil H, Kemble SK, et al. Regional emergence of *Candida auris* in Chicago and lessons learned from intensive follow-up at 1 ventilator-capable skilled nursing facility. Clin Infect Dis. 2020;71:e718–25. https://doi.org/10.1093/cid/ciaa435
15. Proctor DM, Dangana T, Sexton DJ, Fukuda C, Yelin RD, Stanley M, et al.; NISC Comparative Sequencing Program. Integrated genomic, epidemiologic investigation of *Candida auris* skin colonization in a skilled nursing facility. Nat Med. 2021;27:1401–9. https://doi.org/10.1038/s41591-021-01383-w
16. Escandón-Vargas K, Tangua AR, Medina P, Zorrilla-Vaca A, Briceño E, Clavijo-Martínez T, et al. Healthcare-associated infections in burn patients: timeline and risk factors. Burns. 2020;46:1775–86. https://doi.org/10.1016/j.burns.2020.04.031
17. Huang X, Hurabielle C, Drummond RA, Bouladoux N, Desai JV, Sim CK, et al. Murine model of colonization with fungal pathogen *Candida auris* to explore skin tropism, host risk factors and therapeutic strategies. Cell Host Microbe. 2021;29:210–221.e6. https://doi.org/10.1016/j.chom.2020.12.002
18. Eckbo EJ, Wong T, Bharat A, Cameron-Lane M, Hoang L, Dawar M, et al. First reported outbreak of the emerging pathogen *Candida auris* in Canada. Am J Infect Control. 2021;49:804–7. https://doi.org/10.1016/j.ajic.2021.01.013
19. Rhodes J, Abdolrasouli A, Farrer RA, Cuomo CA, Aanensen DM, Armstrong-James D, et al. Genomic epidemiology of the UK outbreak of the emerging human

fungal pathogen *Candida auris*. Emerg Microbes Infect. 2018;7:1–12. https://doi.org/10.1038/s41426-018-0045-x
20. Gorzalski A, Ambrosio FJ III, Massic L, Scribner MR, Siao DD, Hua C, et al. The use of whole-genome sequencing and development of bioinformatics to monitor overlapping outbreaks of *Candida auris* in southern Nevada. Front Public Health. 2023;11:1198189. https://doi.org/10.3389/fpubh.2023.1198189
21. Chow NA, Gade L, Tsay SV, Forsberg K, Greenko JA, Southwick KL, et al.; US Candida auris Investigation Team. Multiple introductions and subsequent transmission of multidrug-resistant *Candida auris* in the USA: a molecular epidemiological survey. Lancet Infect Dis. 2018;18:1377–84. https://doi.org/10.1016/S1473-3099(18)30597-8
22. Chow NA, Muñoz JF, Gade L, Berkow EL, Li X, Welsh RM, et al. Tracing the evolutionary history and global expansion of *Candida auris* using population genomic analyses. MBio. 2020;11:e03364-19. https://doi.org/10.1128/mBio.03364-19
23. Escandón P, Chow NA, Caceres DH, Gade L, Berkow EL, Armstrong P, et al. Molecular epidemiology of *Candida auris* in Colombia reveals a highly related, countrywide colonization with regional patterns in amphotericin B resistance. Clin Infect Dis. 2019;68:15–21. https://doi.org/10.1093/cid/ciy411
24. Naicker SD, Maphanga TG, Chow NA, Allam M, Kwenda S, Ismail A, et al. Clade distribution of *Candida auris* in South Africa using whole-genome sequencing of clinical and environmental isolates. Emerg Microbes Infect. 2021;10:1300–8. https://doi.org/10.1080/22221751.2021.1944323
25. Misas E, Escandón PL, Gade L, Caceres DH, Hurst S, Le N, et al. Genomic epidemiology and antifungal-resistant characterization of *Candida auris*, Colombia, 2016–2021. MSphere. 2024;9:e0057723. https://doi.org/10.1128/msphere.00577-23
26. Trick WE, Lin MY, Cheng-Leidig R, Driscoll M, Tang AS, Gao W, et al. Electronic public health registry of extensively drug-resistant organisms, Illinois, USA. Emerg Infect Dis. 2015;21:1725–32. https://doi.org/10.3201/eid2110.150538
27. Libuit KG, Doughty EL, Otieno JR, Ambrosio F, Kapsak CJ, Smith EA, et al. Accelerating bioinformatics implementation in public health. Microb Genom. 2023;9:mgen001051. https://doi.org/10.1099/mgen.0.001051
28. Bagal UR, Phan J, Welsh RM, Misas E, Wagner D, Gade L, et al. MycoSNP: a portable workflow for performing whole-genome sequencing analysis of *Candida auris*. Methods Mol Biol. 2022;2517:215–28. https://doi.org/10.1007/978-1-0716-2417-3_17
29. Tamura K, Stecher G, Kumar S. MEGA11: Molecular Evolutionary Genetics Analysis version 11. Mol Biol Evol. 2021;38:3022–7. https://doi.org/10.1093/molbev/msab120
30. Welsh RM, Misas E, Forsberg K, Lyman M, Chow NA. *Candida auris* whole-genome sequence benchmark dataset for phylogenomic pipelines. J Fungi (Basel). 2021;7:214. https://doi.org/10.3390/jof7030214
31. Seemann T. Snippy: rapid haploid variant calling and core genome alignment. Github [cited 2025 Jan 29]. https://github.com/tseemann/snippy
32. Rybak JM, Muñoz JF, Barker KS, Parker JE, Esquivel BD, Berkow EL, et al. Mutations in *TAC1B*: a novel genetic determinant of clinical fluconazole resistance in *Candida auris*. MBio. 2020;11:e00365-20. https://doi.org/10.1128/mBio.00365-20
33. Carolus H, Pierson S, Muñoz JF, Subotić A, Cruz RB, Cuomo CA, et al. Genome-wide analysis of experimentally evolved *Candida auris* reveals multiple novel mechanisms of multidrug resistance. MBio. 2021;12:e03333-20. https://doi.org/10.1128/mBio.03333-20
34. Sansom SE, Gussin GM, Schoeny M, Singh RD, Adil H, Bell P, et al. Rapid environmental contamination with *Candida auris* and multidrug-resistant bacterial pathogens near colonized patients. Clin Infect Dis. 2024; 78:1276–84.

Address for correspondence: Hannah Barbian, Rush University Medical Center, Jelke 1412, 1750 W Harrison St, Chicago, IL 60612, USA; email: Hannah_J_Barbian@rush.edu

Epidemiology of Buruli Ulcer in Victoria, Australia, 2017–2022

Bhavi Ravindran, Daneeta Hennessy, Miriam O'Hara, Ee Laine Tay, Rosalina Sa'aga Banuve, Jodie McVernon, Kylie Carville

Buruli ulcer (BU) is a rare, neglected tropical disease caused by *Mycobacterium ulcerans* that can lead to severe skin ulcers. To determine the epidemiology of BU in Victoria, Australia, during 2017–2022 we analyzed surveillance data. A total of 1,751 cases of BU were notified; 968 (55%) patients were male and 781 (45%) female (2 were missing sex data), and 984 (56%) resided in established BU-endemic areas, although an increasing number were in new BU-endemic areas. Most cases (83%, 1,301) were classified as category I. Multivariate modeling demonstrated that factors for severe BU included being male, being older, and living in a new BU-endemic or non–BU-endemic area. A relatively shorter interval between first visit to a clinician and receipt of diagnosis was protective against severe disease. The expansion of BU-endemic areas throughout Victoria remains a public health concern and calls for targeted action, particularly for patients and clinicians in new BU-endemic areas.

Buruli ulcer (BU) is a devastating skin and tissue infection caused by *Mycobacterium ulcerans* (*1*). BU is prevalent mainly in tropical sub-Saharan Africa, although ≈30 countries have reported cases (*2*). Although the number of cases has decreased worldwide, local epidemics in Australia have countered that trend (*3*,*4*). BU-endemic regions in Australia include the Daintree Rainforest and the Capricorn region in tropical Queensland and the East Gippsland and metropolitan Greater Melbourne/Bellarine regions in the state of Victoria in southeastern Australia (*3*,*5*,*6*). The climate in the southeastern state of Victoria is temperate; temperature and weather vary substantially throughout the year (*7*).

BU is usually exhibited initially as a painless skin nodule that predominantly affects the distal limbs and, if left untreated, forms a characteristic ulcer with undermined edges (*8*). The average incubation period for BU is ≈4–5 months, and the average delay between symptom onset and diagnosis is 1–2 months (*9*). Although the BU mortality rate is low, the illness can result in substantial socioeconomic effects on individual persons and communities (*2*,*10*).

Residence in or visitation to a BU-endemic area remains a significant risk factor for *M. ulcerans* acquisition; previous BU outbreaks have occurred as geographically defined infections (*11*). In the temperate climates of Australia, transmission research has focused on mosquitoes as vectors and small Australia native marsupials (possums) as animal reservoirs (*12*,*13*). Mosquitoes are infected by biting possums that carry the bacteria, after which they directly inoculate humans, causing clinical disease (*13*,*14*). An environmental study has shown a correlation between rainfall and BU, as is seen for other vectorborne diseases in the region, including Barmah Forest and Ross River fevers, which further supports the role of mosquitoes (*15*). Definitive evidence was provided through an extensive field survey and genomic analysis that indicated that mosquitoes transmit *M. ulcerans* in southeastern Australia from a reservoir of possums (*16*).

BU was first identified in Victoria in 1948, and only 50 cases were recorded before 1990 (*17*). Since then, the pattern of disease has changed substantially, from low numbers in fixed geographic regions to more widespread transmission (*3*,*18*). New areas of endemicity have emerged, and cases have increased continually since 2011 (*11*,*19*). Within Melbourne, the emergence, continued propagation, and expansion of BU-endemic areas remains a public health concern (*10*).

Author affiliations: Victorian Infectious Diseases Reference Laboratory, Royal Melbourne Hospital, at the Peter Doherty Institute for Infection and Immunity, Melbourne, Victoria, Australia (B. Ravindran, K. Carville); Australian National University, Canberra, Australian Capital Territory, Australia (B. Ravindran, R. Sa'aga Banuve); Department of Health, Melbourne (D. Hennessy, M. O'Hara, E.L. Tay); University of Melbourne Department of Microbiology and Immunology, at the Peter Doherty Institute for Infection and Immunity, Melbourne (J. McVernon, K. Carville)

DOI: https://doi.org/10.3201/eid3103.240938

Using routinely collected surveillance data, we analyzed the epidemiology of BU in Victoria during 2017–2022, identifying factors that influence disease severity and mapping the ongoing spread of the disease. Ethics approval was provided by the Australian National University Human Research Ethics Committee (protocol 2017/909).

Methods

In Victoria, BU has been a notifiable condition since 2004; reporting has been required by laboratories and clinicians under the Public Health and Wellbeing Regulations of 2019 (*20*). The study population included all patients with confirmed cases notified to the Victoria Department of Health during 2017–2022.

Data Sources

We obtained case data from the Public Health Event Surveillance System database of Victoria. Since January 1, 2011, the Victoria Department of Health has collected enhanced surveillance forms that are completed by notifying clinicians or by public health officers from case interviews. Information collected included patients' date of birth, sex, residential address, history of travel to or residence in BU-endemic areas in the 12 months before symptom onset, date of symptom onset, date of first visit to a clinician, date when a clinician first suspected BU, form of the disease, size of the affected area (World Health Organization [WHO] categories I, II or III), lesion location, laboratory results (PCR or culture), and treatment details. To determine the rate of BU per 100,000 population, we obtained information about the population of Victoria from the Australian Bureau of Statistics (*21*).

Definitions

Before July 2021, a confirmed case of BU was defined by definitive laboratory evidence of infection as either PCR detection of IS2404 insertion sequences or culture identification of *M. ulcerans* from a tissue specimen or lesion swab sample (*22*). After July 2021, a confirmed case was defined by definite laboratory evidence as above and by clinical evidence as a clinical diagnosis of BU made by a clinician experienced in the management of BU, including clinical follow-up to ensure a consistent clinical course (*22*).

The Australia Department of Health has defined BU-endemic areas (*11*,*19*) as places where ≥2 residents had BU without recalled travel to another BU-endemic area in the previous year, places adjacent to an endemic area with ≥1 affected residents or visitors without recalled travel history, or places where *M. ulcerans* has been detected in the environment (*22*). We classified BU-endemic areas in Victoria into 3 categories: established BU-endemic, new BU-endemic, and non–BU-endemic areas. Established areas were Mornington Peninsula, Bellarine Peninsula, Phillip Island, East Gippsland, South Eastern Bayside suburbs, and Frankston region because they had been described in previous analyses (*11*,*19*). New BU-endemic areas included Surf Coast and Geelong (first identified in 2017) and Inner Melbourne (first identified in 2019) (Appendix, https://wwwnc.cdc.gov/EID/article/31/2/24-0983-App1.pdf). Non–BU-endemic areas were all other areas in Victoria not previously listed (Figure 1). The Department of Health recorded primary exposure as the most likely area of BU acquisition, considering the duration and frequency of exposure to known BU-endemic areas and

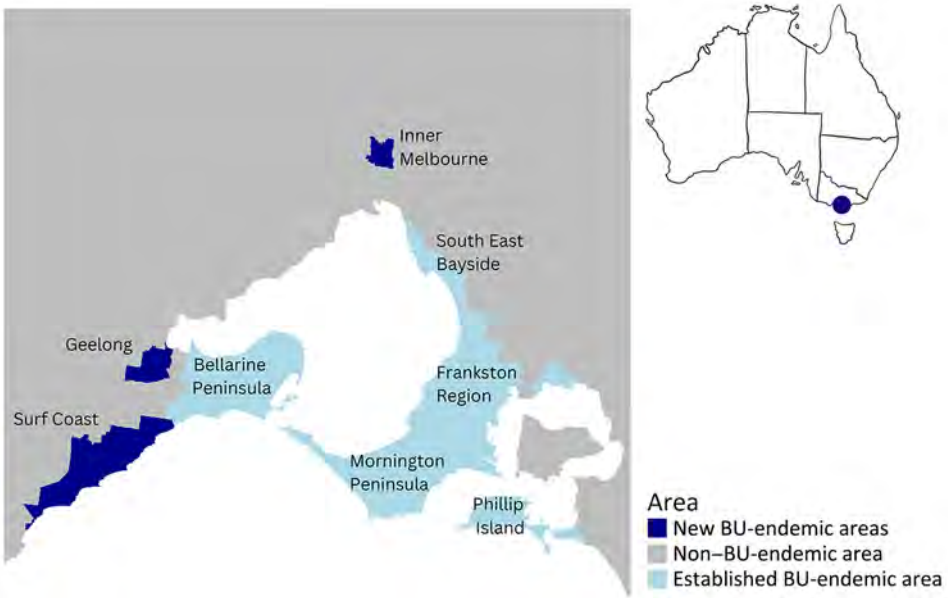

Figure 1. Geographic areas in Greater Melbourne and Bellarine region, Australia, highlighting new (Inner Melbourne, Geelong and Surf Coast), established (Mornington Peninsula, Bellarine Peninsula, South East Bayside, Frankston region, Philip Island), and non–BU-endemic areas, 2017–2022. Not shown: East Gippsland BU-endemic area, which is to the east of the state. BU, Buruli ulcer.

exposure timing relative to symptom onset. If a case-patient resided in a BU-endemic area, the primary exposure was considered to be the patient's home address, given the assumed duration and frequency of exposure. For case-patients who reported no history of residence in or travel to known BU-endemic areas, primary exposure was considered to be the home address at the time of diagnosis.

Lesion severity was classified according to WHO definitions (*23*). Category I comprises single, small lesions <5 cm in diameter; category II comprises single lesions of 5–15 cm in diameter; and category III comprises single extensive lesions >15 cm in diameter, multiple lesions, lesions at critical sites (e.g., eye, genitalia, joints), and osteomyelitis. Severe disease was classified as category II or category III lesions.

Similar to previous studies, delay to first visit was calculated as days from symptom onset to first visit to a healthcare practitioner (*19*). Diagnosis delay was days from first visit to a healthcare practitioner to diagnosis date, approximated by the date of notification to the Department of Health (*19*).

Statistical Analyses

We imported de-identified data into R version 4.3.2 (The R Project for Statistical Computing, https://www.r-project.org) for analysis. To illustrate the study population, we descriptively analyzed data. We described first visit, diagnosis, and total delays by using the median and interquartile range. To explore differences between groups, we used χ^2 or Fischer exacts tests for categorical variables and Kruskal-Wallis or Mann-Whitney U tests for continuous variables. We excluded cases from multivariate analysis if WHO lesion severity outcome, lesion location, or manifestation of BU was missing or if diagnosis or first visit delay could not be calculated because of missing information. We assessed risk factors of disease severity by using logistic regression between independent variables (patient sex, age, residential location at time of notification; first visit delay; and diagnosis delay) and the outcome variable of severe disease. We included area of residence, as opposed to primary exposure location, because that reflected where case-patients would access healthcare. We considered all independent variables for which univariate analysis indicated $p<0.25$ for inclusion in the multivariate model. To identify differences between included and excluded case-patients that were used in the final multivariate model, we conducted sensitivity analyses.

Results

During 2017–2022, a total of 1,751 confirmed cases of BU were notified to the Australia Department of Health (Table 1). More than half of the patients were male (968 [55%] male and 781 [45%] female; data on sex were missing for 2); most were 16–60 (883 [50%]) or ≥60 (721 [40%]) years of age. Approximately half of the patients lived in an established BU-endemic area (984 [56%]). The most common lesion location was the lower limbs (74%); a small number of patients had lesions at multiple sites (2%). Most lesions were category I (1,301 [83%]). After a drop in case numbers in 2020, case numbers in 2021 and 2022 were similar to those before the COVID-19 pandemic; case numbers for 2022 (334 [19% of notified cases in the study period]) were similar to the previous high number from 2018 (340 [19%]). Of the 1,604 patients for whom treatment was recorded, most patients received antimicrobial therapy alone as treatment (1,144 [71%]) followed by a combination of surgery and antimicrobial drug treatment (332 [21%]). The median time to seeking care was 28 days (95% CI 11–50 days), and the median time between seeking care and diagnosis was 19 days (95% CI 7–42 days). Of the 1,614 patients with a recorded manifestation, the most common manifestation was ulcers (1,227 [76%]) (Table 1). Of the 387 nonulcerous manifestations of BU, most common were cellulitis (126 [33%]), nodules (108 [28%]), and papules (89 [23%]).

The overall rate of BU diagnosis in Victoria was 4.48 cases/100,000 population during the study period. The lowest annual rate was 3.28 cases/100,000 population in 2020, and the highest rate was 5.29 cases/100,000 population in 2018.

Demographic Differences by Area of Residence

We found significant differences in sex, age grouping, WHO severity score, diagnosis delay, manifestation delay, and manifestation between residents in new, established, and non–BU-endemic areas. Compared with new and non–BU-endemic areas, case-patients residing in established areas were more likely to be older (48% >60 years of age in established areas, 32% in non–BU-endemic areas, 35% in new areas; $p<0.001$); to have category I disease (85% in established areas, 81% in non–BU-endemic areas, 77% in new areas; $p = 0.006$); to have a shorter diagnosis delay ($p<0.001$) and shorter delay before first visit ($p<0.001$) (Table 1). The location of lesions also differed; case-patients in non–BU-endemic areas were more likely than those in other areas to have a lesion on their lower limbs (78% in non–BU-endemic areas, 71% in established areas, and 68% in new areas; $p = 0.027$) and more likely to have different treatments recorded at the time of public health follow-up visits (66% received antimicrobial drugs

Table 1. Characteristics of BU cases notified to the Victoria Department of Health, overall and by location of residence, Victoria, Australia, 2017–2022*

Variable	Overall, n = 1,751	BU area			p value
		New, n = 163	Non–BU-endemic, n = 604	Established, n = 984	
Sex					<0.05
F	781 (45)	78 (48)	244 (40)	459 (47)	
M	968 (55)	84 (52)	359 (60)	525 (53)	
Missing	2	1	1	0	
Age group, y					<0.001
0-15	148 (8.5)	16 (9.8)	58 (9.6)	74 (7.5)	
16-60	883 (50)	90 (55)	352 (58)	441 (45)	
>60	720 (41)	57 (35)	194 (32)	469 (48)	
Lesion location					<0.05
Arm	350 (21)	41 (27)	101 (17)	208 (23)	
Leg	1,206 (74)	103 (68)	460 (78)	643 (71)	
Multiple	37 (2.3)	4 (2.6)	15 (2.6)	18 (2.0)	
Other	47 (2.9)	4 (2.6)	12 (2.0)	31 (3.4)	
Missing	111	11	16	84	
WHO lesion category					<0.05
I	1,301 (83)	114 (77)	462 (81)	725 (85)	
II	176 (11)	21 (14)	77 (13)	78 (9.2)	
III	95 (6.0)	14 (9.4)	32 (5.6)	49 (5.8)	
Missing	179	14	33	132	
Year of notification					0.001
2017	277 (16)	12 (7.4)	110 (18)	155 (16)	
2018	340 (19)	10 (6.1)	125 (21)	205 (21)	
2019	299 (17)	19 (12)	115 (19)	165 (17)	
2020	217 (12)	16 (9.8)	69 (11)	132 (13)	
2021	284 (16)	41 (25)	78 (13)	165 (17)	
2022	334 (19)	65 (40)	107 (18)	162 (16)	
Treatment					0.001
Antibiotics	1,144 (71)	111 (73)	386 (66)	647 (75)	
Antibiotics and surgery	332 (21)	34 (22)	159 (27)	139 (15)	
Other	90 (5.6)	6 (3.9)	21 (3.6)	63 (7.3)	
Surgical	38 (2.4)	1 (0.7)	16 (2.7)	21 (2.4)	
Missing	147	11	22	114	
Diagnosis delay, d, median (IQR)	19 (7–42)	22 (9–44)	31 (13–58)	13 (6–31)	<0.001
Missing	209	20	48	141	
Presentation d, median, (IQR)	28 (11–50)	27 (9–45)	30 (14–61)	24 (10–47)	0.001
Missing	251	21	60	170	
Manifestation					<0.05
Nonulcer	387 (24)	50 (33)	129 (22)	208 (24)	
Ulcer	1,227 (76)	102 (67)	454 (78)	671 (76)	
Missing	137	11	21	105	

*Values are no. (%) except as indicated. Percentages exclude missing data. BU, Buruli ulcer; IQR, interquartile range; WHO, World Health Organization.

in non–BU-endemic areas, 75% in established areas, and 73% in new areas; p = 0.027) (Table 1).

When compared with non–BU-endemic and established areas, case-patients in new BU-endemic areas were more likely to be notified in 2021 and 2022 (p<0.001) and to not have an ulcer (33% in new, 24% in established, and 22% in non–BU-endemic areas; p = 0.022) The proportions of male and female case-patients differed by area of residence (p = 0.036) (Table 1).

Demographic Differences by Age and Sex

With respect to age, we noted significant differences in lesion severity, area of residence, and first visit delay. Patients >60 years of age were more likely to have category II or category III ulcers (19% of patients >60 years of age, 16% of patients 16–60 years of age, 17% of patients 0–15 years of age; p = 0.002) and to live in an established BU-endemic area (65% of patients >60 years of age, 50% of patients 16–60 years of age, 50% of patients 0–15 years of age; p<0.001) (Table 2). Patients who were 16–60 years of age were more likely to have a longer delay to first visit (p<0.001) and to have received more antimicrobial drugs without surgery (p = 0.01) than were patients who were older and younger. We found no significant differences by age group in terms of sex, year of diagnosis, diagnosis delay, or manifestation type (Table 2).

With respect to patient sex, we found significant differences in lesion category, area of residence, diagnosis delay, and having an ulcer compared with other manifestations. Male patients were more likely than female patients to have category II or category III ulcers

(7.1% of lesions in male vs. 4.6% of lesions in female patients were category III; p = 0.036); reside in different areas (p = 0.036); have a shorter delay to diagnosis (p = 0.06); or have an ulcer (79% male vs. 72% female; p<0.001) (Table 2). We found no significant differences by sex between age group, lesion location, area of residence, treatment, or delay to first visit (Table 2).

Notifications by Residence

Patient places of residence, by endemicity classification, were similar during 2017–2019. In 2020, the proportion of cases from non–BU-endemic areas dropped substantially. Patients residing in new BU-endemic areas increased relative to non–BU-endemic and established areas from 2020 (7% [16/217] of patients to 19% [65/334] of patients in 2022) (Figure 2). The increased cases in the new BU-endemic areas primarily resulted from patients residing in the inner Melbourne BU-endemic area.

Notifications by Primary Exposure Location

Primary exposure location was available for 1,700 (97.1%) case-patients. Over the study period, the most common primary exposure area continued to be

Table 2. Characteristics of BU cases notified to the Victoria Department of Health, by age group and sex, Victoria, Australia, 2017–2022*

		Age group, y				Sex	
Variable	No.	0–15, n = 148	16–60, n = 883	>60, n = 720	No.	F, n = 781	M, n = 968
Sex	1,749						
F		69 (47)	378 (43)	334 (46)		NA	NA
M		78 (53)	504 (57)	386 (54)		NA	NA
Missing		1	1	0			
Lesion location	1,640				1,638		
Upper limb		19 (13)	147 (18)	184 (27)		169 (23)	181 (20)
Lower limb		120 (84)	628 (76)	458 (68)		524 (72)	680 (75)
Multiple		2 (1.4)	21 (2.5)	14 (2.1)		12 (1.6)	25 (2.8)
Other		2 (1.4)	28 (3.4)	17 (2.5)		24 (3.3)	23 (2.5)
Missing		5	59	47		52	59
WHO lesion category	1,572 (p<0.01)				1,570 (p<0.05)		
I		116 (83)	671 (84)	514 (81)		599 (85)	701 (81)
II		20 (14)	88 (11)	68 (11)		71 (10)	105 (12)
III		3 (2.2)	36 (4.5)	56 (8.8)		32 (4.6)	62 (7.1)
Missing		9	88	82		79	100
Area of residence	1,751 (p<0.001)				1,749 (p<0.05)		
New		16 (11)	90 (10)	57 (7.9)		78 (10.0)	84 (8.7)
Non–BU-endemic		58 (39)	352 (40)	194 (27)		244 (31)	359 (37)
Established		74 (50)	441 (50)	469 (65)		459 (59)	525 (54)
Year	1,751				1,749		
2017		27 (18)	131 (15)	119 (17)		132 (17)	143 (15)
2018		31 (21)	173 (20)	136 (19)		142 (18)	198 (20)
2019		32 (22)	149 (17)	118 (16)		122 (16)	177 (18)
2020		11 (7.4)	102 (12)	104 (14)		94 (12)	123 (13)
2021		24 (16)	159 (18)	101 (14)		130 (17)	154 (16)
2022		23 (16)	169 (19)	142 (20)		161 (21)	173 (18)
Treatment	1,604 (p<0.05)				1,602		
Antibiotics		99 (70)	600 (75)	445 (67)		494 (70)	650 (73)
Both		37 (26)	141 (18)	154 (23)		146 (21)	184 (21)
Dressings/other		5 (3.5)	43 (5.4)	42 (6.4)		43 (6.1)	47 (5.3)
Surgical		0 (0)	19 (2.4)	19 (2.9)		24 (3.4)	14 (1.6)
Missing		7	80	60		74	73
Diagnosis delay, d, median (IQR)	1,542	17 (10–36)	21 (8–46)	16 (7–38)	1,540 (p<0.01)	20 (8–44)	17 (7–42)
Missing		17	115	77		92	117
First visit delay, d, median (IQR)	1,500 (p<0.001)	22 (12–35)	30 (14–60)	21 (7–45)	1,498	28 (9–54)	28 (13–48)
Missing		18	134	99		109	142
Manifestation	1,614				1,612 (p<0.001)		
Nonulcer		40 (28)	177 (22)	170 (26)		203 (28)	184 (21)
Ulcer		101 (72)	633 (78)	493 (74)		514 (72)	711 (79)
Missing		7	73	57		64	73

*Values are no. (%) except as indicated. Percentages exclude missing data. BU, Buruli ulcer; IQR, interquartile range; NA, not applicable; WHO, World Health Organization.

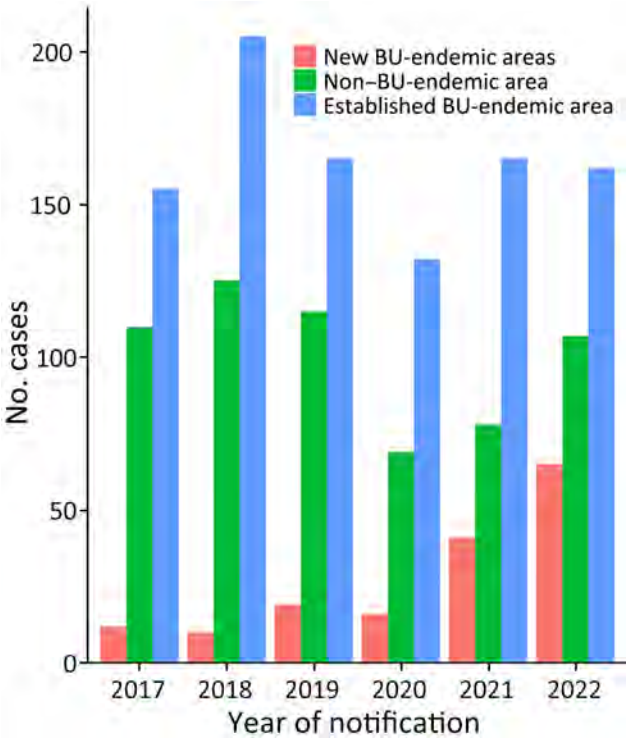

Figure 2. Cases of BU notified to the Victoria Department of Health, by area of residence and year, Victoria, Australia, 2017–2022. BU, Buruli ulcer.

established areas (1,427 [84%]), followed by new BU-endemic areas (216 [13%]) and then non–BU-endemic areas (57 [3%]). The proportion of patients whose primary exposure location was a new BU-endemic area increased substantially from 2017 to 2022 (4% [9/230] of exposures to 18% [61/330] of exposures), mirrored by a decrease in a primary exposure location in established endemic areas (93% [215/230] of exposures to 78% [256/330] of exposures (Figure 3).

During the study period, the higher number of primary exposures were in the Mornington Peninsula (1,028 [60%]), followed by the Bellarine Peninsula (223 [13%]) and the Frankston Area (116 [7%]). For 57 (3%) patients, no travel to BU-endemic areas was reported (Figure 4). Although still relatively low compared with the Mornington Peninsula, of note is the emergence of the inner-city Melbourne area, in which primary exposure locations substantially increased in from 2019 (0 exposures) to 2022 (37 exposures, 11%) (Figure 4).

Seasonality

The date of symptom onset was available for 1,573 (89.8%) patients, and the date of first visit was available for 1,541 (88.1%) of patients. Symptom onset was most frequent in July (winter in Victoria) and least often in January (summer in Victoria). The peak for healthcare visitation was August, and the peak for BU diagnosis was October (Figure 5).

Risk Factors for Severe Disease

Of the 1,751 cases, we excluded 357 (20%) from the regression model because information was missing for either the dependent variable; WHO lesion category; or the independent variables sex, delay to first visit, delay to diagnosis, or manifestation. Included patients were less likely to be from an established BU-endemic area ($p<0.001$), have a longer delay to diagnosis where recorded ($p<0.001$), and to have been notified in 2021 ($p<0.001$). We found no differences in sex, age grouping, delay to first visit, manifestation with an ulcer, or lesion category (Table 3).

Multivariate regression revealed increased odds of severe BU disease among male patients (odds ratio [OR] 1.44 [95% CI 1.08–1.94]; $p = 0.014$) with increasing age per year (OR 1.01 [95% CI 1.00–1.01]; $p = 0.015$), residence in a new area (OR 1.69 [95% CI 1.02–2.73]; $p = 0.035$) or non–BU-endemic area (OR 1.38 [95% CI 1.01–1.88]; $p = 0.042$), or a longer delay to diagnosis per day (OR 1.00 [95% CI 1.00–1.01]; $p<0.001$) (Table 4). Notifications received in 2018 (OR 0.61 [95% CI 0.39–0.97]; $p = 0.036$) and 2021 (OR 0.41 [95% CI 0.23–0.71]; $p = 0.002$) were associated with significantly less severe disease than were cases notified in 2017.

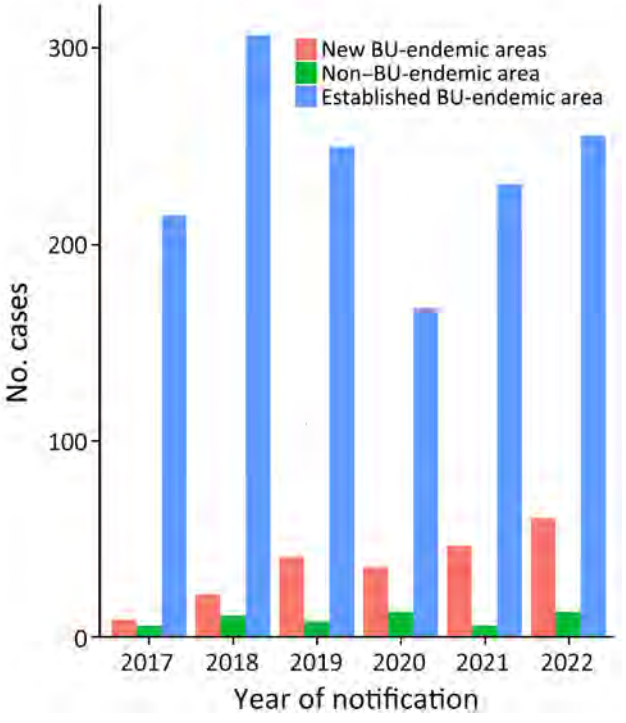

Figure 3. BU primary exposure locations, by region and year, Victoria, Australia, 2017–2022. BU, Buruli ulcer.

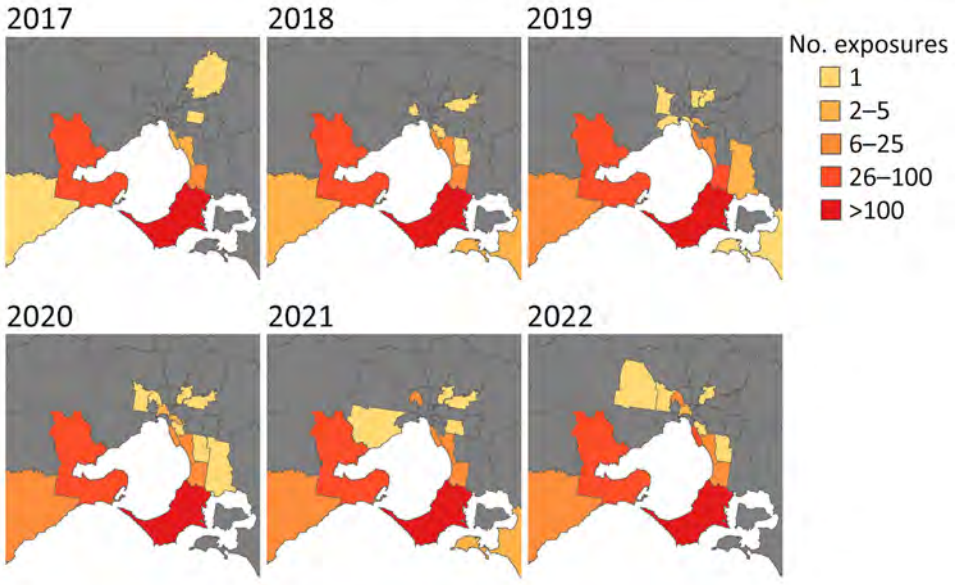

Figure 4. Change in Buruli ulcer primary exposures areas in Greater Melbourne and Bellarine region over time by local government area, Victoria, Australia, 2017–2022.

Discussion

The continued increase of BU cases in Victoria demonstrates BU progression from a localized disease in small geographic clusters to further expansion and emergence of endemic areas (*24*). Although the Geelong and Surf Coast regions are contiguous to the well-established BU-endemic area of the Bellarine Peninsula, the inner Melbourne area is not coastal and shares no boundaries with known BU-endemic areas.

The expansion of BU-endemic areas is a public health concern, and monitoring the emergence of new areas is still needed. Current research provides evidence for possums as a reservoir and mosquitoes as vectors; thus, environmental surveillance through possum fecal excreta and mosquito surveys with screening for *M. ulcerans* may help supplement current activities for monitoring spread (*16*,*25*). *M. ulcerans* is probably introduced into new environments and then expands rather than emerging from a dormant pathogen reservoir; however, initial *M. ulcerans* introduction into new BU-endemic areas is unclear (*26*).

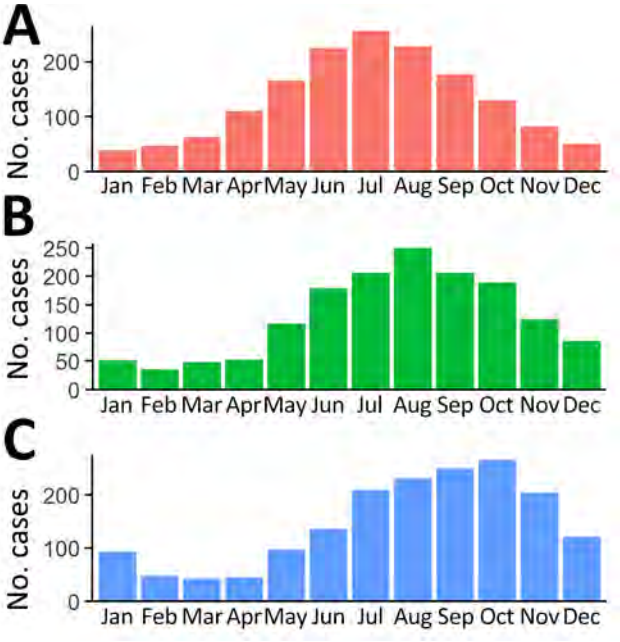

Figure 5. Timing of symptom onset (A), first visit to a clinician (B), and notification of Buruli ulcer (C) among cases notified to Victoria Department of Health, Victoria, Australia, 2017–2022.

Demographics, clinical signs, and diagnosis delays differ by area of residence. Patient and clinician understanding of BU disease in established areas may be greater than that in new or non–BU-endemic areas, particularly with respect to care seeking and consideration of treatment options.

Similar to previous work, our study demonstrates that older age (*11*,*18*) and living in a new or non–BU-endemic area are associated with severe BU lesions (*11*). Of note, the multivariate model demonstrated that diagnosis delay, and not first visit delay, was associated with severe disease. Median delays between first visit (3 weeks) and diagnosis (4 weeks) in Victoria are considerably shorter than in other settings such as Nigeria (median delay of 29 weeks) and Cameroon (median delay of 12 weeks) (*27*,*28*). Factors that contributed to a longer delays in first visit and diagnosis in those countries include geography and inaccessibility to healthcare, which are unlikely to be factors in Victoria (*27*).

The temporal relationship between symptom onset, first visit, and notification of BU followed the previously described seasonal patterns: symptom onset peaking mid-winter and dipping mid-summer (*29*).

Table 3. Characteristics of BU cases notified to the Victoria Department of Health, by exclusion or inclusion from logistic regression, Victoria, Australia, 2017–2022*

Variable	Excluded, n = 357	Included, n = 1,394	p value
Sex			0.3
F	149 (42)	632 (45)	
M	206 (58)	762 (55)	
Unknown	2	0	
Age, y, continuous	54 (35,70)	53 (36,69)	0.5
Area of residence			<0.001
New BU-endemic	30 (8.4)	133 (9.5)	
Non–BU-endemic	91 (25)	513 (37)	
Established BU-endemic	236 (66)	748 (54)	
Year			<0.001
2017	56 (16)	221 (16)	
2018	56 (16)	284 (20)	
2019	53 (15)	246 (18)	
2020	55 (15)	162 (12)	
2021	83 (23)	201 (14)	
2022	54 (15)	280 (20)	
Diagnosis delay, d, median (IQR)	13 (5, 33)	20 (8, 43)	<0.001
Unknown	209	0	
Presentation delay, d, median (IQR)	21 (2, 60)	28 (12, 50)	0.2
Unknown	251	0	
WHO lesion category			
I	145 (83)	1156 (81)	0.2
II/III	33 (17)	238 (19)	
Unknown	179	0	

*Values are no. (%) except as indicated. Percentages exclude missing data. BU, Buruli ulcer; WHO, World Health Organization.

The mosquito season in Victoria is November–April, which, given the median incubation period of 4–5 months, supports acquisition during the summer in Victoria (*9*). Therefore, targeted messages to the public in the warmer months with regard to prevention and to patients and clinicians in the autumn/winter months with regard to early disease recognition and diagnosis should be strengthened (*30*).

Our study period encompasses the COVID-19 pandemic, and the effect of nonpharmaceutical control measures on transmission and public health follow-up was apparent. The state of Victoria experienced prolonged lockdowns and movement restrictions (*31*), which resulted in a low number of BU cases in 2020 and exclusion of several cases in 2021 from the regression model because of missing data. Competing public health priorities meant that BU patient follow-up could not always be consistently performed during that period.

Before the COVID-19 pandemic, we observed a lower proportion of patients with severe disease in 2018, possibly associated with increased public messaging within established areas (*32*). Another effect of the COVID-19 pandemic was the increased proportion of patients with severe disease in 2020. However, further public health messaging may have improved awareness among the public and clinicians,

Table 4. Univariate and multivariate associations between risk factors and severity of BU, Victoria, Australia, 2017–2022*

	WHO severity		Univariate analysis				Multivariate analysis	
Variable	I, n = 1,156	II/III, n = 238	OR	95% CI	p value	aOR	95% CI	p value
Sex								
F	541 (47)	91 (38)	1.00	NA	NA	1.00	NA	NA
M	615 (53)	147 (62)	1.42	1.07–1.90	0.016	1.44	1.08–1.94	0.014
Age, y, continuous	53 (35–69)	56 (41–74)	1.01	1.00–1.01	0.021	1.01	1.00–1.01	0.015
BU-endemic area								
New BU-endemic	105 (9.1)	28 (12)	1.56	0.97–2.46	0.059	1.69	1.02–2.73	0.035
Non–BU-endemic	416 (36)	105 (44)	1.44	1.07–1.94	0.017	1.38	1.01–1.88	0.042
Established BU-endemic	635 (55)	105 (44)	1.00	NA	NA	1.00	NA	NA
Year								
2017	171 (15)	50 (21)	1.00	NA	NA	1.00	NA	NA
2018	241 (21)	43 (18)	0.61	0.39–0.96	0.032	0.61	0.39–0.97	0.036
2019	203 (18)	43 (18)	0.72	0.46–1.14	0.2	0.68	0.43–1.09	0.11
2020	132 (11)	30 (13)	0.78	0.46–1.28	0.3	0.71	0.42–1.18	0.2
2021	179 (15)	22 (9.2)	0.42	0.24–0.72	0.002	0.41	0.23–0.71	0.002
2022	230 (20)	50 (21)	0.74	0.48–1.15	0.2	0.69	0.44–1.09	0.11
Diagnosis delay, d	18 (7–41)	28 (12–57)	1.03	1.01–1.04	<0.001	1.00	1.00–1.01	<0.001
First visit delay, d	28 (12–51)	26 (10–40)	1.00	1.00–1.00	0.7	NA	NA	NA

*Values are no. (%) except as indicated. aOR, adjusted odds ratio; BU, Buruli ulcer; NA, not applicable; OR, odds ratio; WHO, World Health Organization.

particularly in newly identified areas, and resulted in reduction of severe disease in 2021 (*33*).

Among the strengths of our study is inclusion of the extensive public health surveillance database. Limitations included exclusion of cases because of missing information. Because excluded case-patients were more likely to live in a BU-endemic area, have a shorter delay to diagnosis, and be notified in 2020 and 2021, disease might have been less severe for those case-patients, which might have biased the multivariate model to show a stronger association between independent variables and severe BU lesions. Furthermore, because the data were from a notifiable public health disease database, data on other factors that could have influenced the severity of disease were not available, including medical comorbidities, socioeconomic status, or access to healthcare facilities. Last, primary exposure information was not collected consistently across established, new, or non–BU-endemic areas over the study period, potentially resulting in misclassification.

Our study findings contribute to the substantial body of work on BU in Victoria. However, several findings are concerning, including the near tripling of cases during 2017–2022 compared with 2011–2016 and the emergence of multiple new BU-endemic areas (*11*). The continued propagation and increased case numbers call for clear, targeted, and effective public health action, which may include continued surveillance of human cases, enhanced surveillance of mosquitoes and possum excreta, mosquito control activities, public health messaging, and clinician education.

About the Author

Dr. Ravindran is a Master of Applied Epidemiology Scholar and Public Health Registrar at the Victorian Infectious Diseases Reference Laboratory, at the Peter Doherty Institute for Infection and Immunity. His research interests include infectious disease surveillance and field epidemiology.

References

1. Johnson PDR. Buruli ulcer: here today but where tomorrow? Lancet Glob Health. 2019;7:e821–2. https://doi.org/10.1016/S2214-109X(19)30233-5
2. Omansen TF, Erbowor-Becksen A, Yotsu R, van der Werf TS, Tiendrebeogo A, Grout L, et al. Global epidemiology of Buruli ulcer, 2010–2017, and analysis of 2014 WHO programmatic targets. Emerg Infect Dis. 2019;25:2183–90. https://doi.org/10.3201/eid2512.190427
3. Johnson PDR. In: Pluschke G, Roltgen K, editors. Buruli ulcer: *Mycobacterium ulcerans* disease. Cham (CH): Springer; 2019. p. 61–76.
4. O'Brien DP, Jeanne I, Blasdell K, Avumegah M, Athan E. The changing epidemiology worldwide of *Mycobacterium ulcerans.* Epidemiol Infect. 2018;147:e19. https://doi.org/10.1017/S0950268818002662
5. Steffen CM, Freeborn H. *Mycobacterium ulcerans* in the Daintree 2009–2015 and the mini-epidemic of 2011. ANZ J Surg. 2018;88:E289–93. https://doi.org/10.1111/ans.13817
6. Boyd SC, Athan E, Friedman ND, Hughes A, Walton A, Callan P, et al. Epidemiology, clinical features and diagnosis of *Mycobacterium ulcerans* in an Australian population. Med J Aust. 2012;196:341–4. https://doi.org/10.5694/mja12.10087
7. Yerramilli A, Tay EL, Stewardson AJ, Fyfe J, O'Brien DP, Johnson PDR. The association of rainfall and Buruli ulcer in southeastern Australia. PLoS Negl Trop Dis. 2018;12:e0006757. https://doi.org/10.1371/journal.pntd.0006757
8. Bravo FG. Emerging infections: mimickers of common patterns seen in dermatopathology. Mod Pathol. 2020;33(Suppl 1):118–27. https://doi.org/10.1038/s41379-019-0399-1
9. Loftus MJ, Trubiano JA, Tay EL, Lavender CJ, Globan M, Fyfe JAM, et al. The incubation period of Buruli ulcer (*Mycobacterium ulcerans* infection) in Victoria, Australia—remains similar despite changing geographic distribution of disease. PLoS Negl Trop Dis. 2018;12:e0006323. https://doi.org/10.1371/journal.pntd.0006323
10. O'Brien DP, Athan E, Blasdell K, De Barro P. Tackling the worsening epidemic of Buruli ulcer in Australia in an information void: time for an urgent scientific response. Med J Aust. 2018;208:287–9. https://doi.org/10.5694/mja17.00879
11. Loftus MJ, Tay EL, Globan M, Lavender CJ, Crouch SR, Johnson PDR, et al. Epidemiology of Buruli ulcer infections, Victoria, Australia, 2011–2016. Emerg Infect Dis. 2018;24:1988–97. https://doi.org/10.3201/eid2411.171593
12. Fyfe JA, Lavender CJ, Handasyde KA, Legione AR, O'Brien CR, Stinear TP, et al. A major role for mammals in the ecology of *Mycobacterium ulcerans*. PLoS Negl Trop Dis. 2010;4:e791. https://doi.org/10.1371/journal.pntd.0000791
13. Blasdell KR, McNamara B, O'Brien DP, Tachedjian M, Boyd V, Dunn M, et al. Environmental risk factors associated with the presence of *Mycobacterium ulcerans* in Victoria, Australia. PLoS One. 2022;17:e0274627. https://doi.org/10.1371/journal.pone.0274627
14. Wallace JR, Mangas KM, Porter JL, Marcsisin R, Pidot SJ, Howden B, et al. *Mycobacterium ulcerans* low infectious dose and mechanical transmission support insect bites and puncturing injuries in the spread of Buruli ulcer. PLoS Negl Trop Dis. 2017;11:e0005553. https://doi.org/10.1371/journal.pntd.0005553
15. Linke JA, Athan E, Friedman ND. Correlation between Buruli ulcer incidence and vectorborne diseases, southeastern Australia, 2000–2020. Emerg Infect Dis. 2021;27:3191–2. https://doi.org/10.3201/eid2712.203182
16. Mee PT, Buultjens AH, Oliver J, Brown K, Crowder JC, Porter JL, et al. Mosquitoes provide a transmission route between possums and humans for Buruli ulcer in southeastern Australia. Nat Microbiol. 2024;9:377–89.
17. Mac CP, Tolhurst JC, Buckle G, Sissons HA. A new mycobacterial infection in man. J Pathol Bacteriol. 1948;60:93–122. https://doi.org/10.1002/path.1700600111
18. Tai AYC, Athan E, Friedman ND, Hughes A, Walton A, O'Brien DP. Increased severity and spread of *Mycobacterium ulcerans*, southeastern Australia. Emerg Infect Dis. 2018;24:58–64. https://doi.org/10.3201/eid2401.171070
19. Coutts SP, Lau CL, Field EJ, Loftus MJ, Tay EL. Delays in patient presentation and diagnosis for Buruli ulcer (*Mycobacterium ulcerans* infection) in Victoria, Australia, 2011–2017. Trop Med Infect Dis. 2019;4:100. https://doi.org/10.3390/tropicalmed4030100

20. Public Health and Wellbeing Regulations. 2019 (Authorised Version No. 022) [cited 2023 Aug 4]. https://www.legislation.vic.gov.au/in-force/statutory-rules/public-health-and-wellbeing-regulations-2019/022
21. Australian Bureau of Statistics. National, State and Territory population [cited 2024 Jun 30]. https://www.abs.gov.au/statistics/people/population/national-state-and-territory-population/latest-release
22. Betts JM, Tay EL, Johnson PDR, Lavender CJ, Gibney KB, O'Brien DP, et al. Buruli ulcer: a new case definition for Victoria. Commun Dis Intell. 2018;2020:44.
23. World Health Organization. Treatment of *Mycobacterium ulcerans* disease (Buruli ulcer): guidance for health workers. Geneva: WHO Press; 2012.
24. Kurcheid J, Gordon CA, Clarke NE, Wangdi K, Kelly M, Lal A, et al. Neglected tropical diseases in Australia: a narrative review. Med J Aust. 2022;216:532–8. https://doi.org/10.5694/mja2.51533
25. Vandelannoote K, Buultjens AH, Porter JL, Velink A, Wallace JR, Blasdell KR, et al. Statistical modeling based on structured surveys of Australian native possum excreta harboring *Mycobacterium ulcerans* predicts Buruli ulcer occurrence in humans. eLife. 2023;12:e84983. https://doi.org/10.7554/eLife.84983
26. Buultjens AH, Vandelannoote K, Meehan CJ, Eddyani M, de Jong BC, Fyfe JAM, et al. Comparative genomics shows that *Mycobacterium ulcerans* migration and expansion preceded the rise of Buruli ulcer in Southeastern Australia. Appl Environ Microbiol. 2018;84:e02612-17. https://doi.org/10.1128/AEM.02612-17
27. Ayelo GA, Anagonou E, Wadagni AC, Barogui YT, Dossou AD, Houezo JG, et al. Report of a series of 82 cases of Buruli ulcer from Nigeria treated in Benin, from 2006 to 2016. PLoS Negl Trop Dis. 2018;12:e0006358. https://doi.org/10.1371/journal.pntd.0006358
28. Porten K, Sailor K, Comte E, Njikap A, Sobry A, Sihom F, et al. Prevalence of Buruli ulcer in Akonolinga health district, Cameroon: results of a cross sectional survey. PLoS Negl Trop Dis. 2009;3:e466. https://doi.org/10.1371/journal.pntd.0000466
29. Quek TY, Henry MJ, Pasco JA, O'Brien DP, Johnson PD, Hughes A, et al. *Mycobacterium ulcerans* infection: factors influencing diagnostic delay. Med J Aust. 2007;187:561–3. https://doi.org/10.5694/j.1326-5377.2007.tb01416.x
30. Quek TY, Athan E, Henry MJ, Pasco JA, Redden-Hoare J, Hughes A, et al. Risk factors for *Mycobacterium ulcerans* infection, southeastern Australia. Emerg Infect Dis. 2007;13:1661–6. https://doi.org/10.3201/eid1311.061206
31. Macreadie I. Reflections from Melbourne, the world's most locked-down city, through the COVID-19 pandemic and beyond. Microbiol Aust. 2022;43:3–4. https://doi.org/10.1071/MA22002
32. O'Brien DP, Athan E, Blasdell K, De Barro P. Tackling the worsening epidemic of Buruli ulcer in Australia in an information void: time for an urgent scientific response. Med J Aust. 2018;208:287–9. https://doi.org/10.5694/mja17.00879.
33. Lewin E. Melbourne GPs told to consider Buruli ulcers when assessing lesions [cited 2024 May 9]. https://www1.racgp.org.au/newsgp/clinical/buruli-ulcers-discovered-in-non-coastal-areas-in-v

Address for correspondence: Bhavi Ravindran, The Peter Doherty Institute for Infection and Immunity, 792 Elizabeth St, Melbourne, VIC 3000, Australia; email: bhavi.ravindran@mh.org.au

EID Podcast

Thelazia callipaeda Eyeworms in American Black Bear, Pennsylvania, USA, 2023

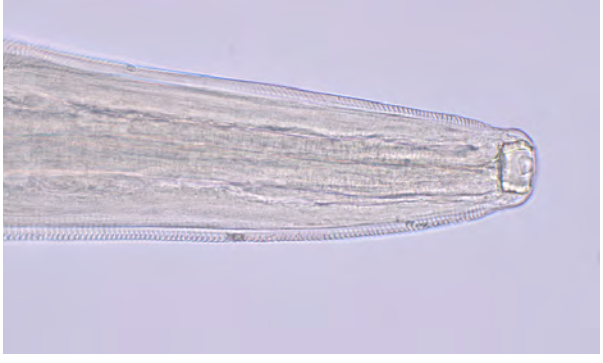

In November 2023, an American black bear was legally harvested in Coolbaugh Township, Monroe County, Pennsylvania. Multiple linear nematodes observed behind the third eyelid were later identified as *Thelazia callipaeda*. The presence of adult *T. callipaeda* eyeworms in an American black bear suggests the establishment of a sylvatic transmission cycle in the United States and expansion of the number of definitive host species used by the zoonotic nematode.

In this EID podcast, Dr. Carol Sobotyk, an assistant professor of clinical parasitology and director of the Clinical Parasitology Laboratory at the University of Pennsylvania, discusses *T. callipaeda* eyeworms in an American black bear.

Visit our website to listen: https://bit.ly/3P5bj94

EMERGING INFECTIOUS DISEASES®

Effect of Prior Influenza A(H1N1)pdm09 Virus Infection on Pathogenesis and Transmission of Influenza A(H5N1) Clade 2.3.4.4b Virus in Ferret Model

Xiangjie Sun, Jessica A. Belser, Zhu-Nan Li, Nicole Brock, Joanna A. Pulit-Penaloza, Troy J. Kieran, Claudia Pappas, Hui Zeng, Jessie C. Chang, Paul J. Carney, Brandon L. Bradley-Ferrell, James Stevens, Terrence M. Tumpey, Min Z. Levine, Taronna R. Maines

Reports of human infections with influenza A(H5N1) clade 2.3.4.4b viruses associated with outbreaks in dairy cows in the United States underscore the need to assess the potential cross-protection conferred by existing influenza immunity. We serologically evaluated ferrets previously infected with an influenza A(H1N1)pdm09 virus for cross-reactive antibodies and then challenged 3 months later with either highly pathogenic H5N1 clade 2.3.4.4b or low pathogenicity H7N9 virus. Our results showed that prior influenza A(H1N1)pdm09 virus infection more effectively reduced the replication and transmission of the H5N1 virus than did the H7N9 virus, a finding supported by the presence of group 1 hemagglutinin stalk and N1 neuraminidase antibodies in preimmune ferrets. Our findings suggest that prior influenza A(H1N1)pdm09 virus infection may confer some level of protection against influenza A(H5N1) clade 2.3.4.4.b virus.

Highly pathogenic avian influenza A(H5N1) clade 2.3.4.4b viruses have exhibited rapid global spread in wild birds since 2021 (*1*,*2*). That spread has resulted in numerous outbreaks in domestic poultry and sporadic infections in nonavian hosts (*1*,*2*), including >20 mammal species in the United States alone since January 2022 (*3*). On March 25, 2024, H5N1 clade 2.3.4.4b virus was reported in dairy cows in Texas and Kansas (*4*), and the virus was subsequently detected in dairy herds from over a dozen states within 5 months (*5*). Those outbreaks resulted in several confirmed human infections, primarily after exposure to infected dairy cows or poultry (*6*). Although human cases from 2024 generally exhibited mild symptoms (*7*,*8*), clade 2.3.4.4b viruses can cause severe infection in humans (*9*). Viruses isolated before and concurrent with ongoing dairy farm outbreaks possess an efficient capacity for replicating in mammalian hosts and are capable of systemic spread and lethal infection in both mouse and ferret models (*10*–*13*). Furthermore, some clade 2.3.4.4b viruses, including viruses isolated from dairy farm workers in 2024, exhibit a limited capacity for airborne transmission between ferrets, suggesting a heightened risk to public health (*10*–*12*,*14*). Those incidents highlight the ongoing threat posed by H5N1 viruses and underscore the need for comprehensive risk assessments to evaluate the capacity of clade 2.3.4.4b viruses to cause infection and disease in diverse human populations.

Although almost all influenza A(H5N1) human cases in the United States have been associated with mild disease, and no human-to-human transmission has been reported, assessing whether the human population has cross-reactive antibodies that can provide protection against the disease caused by H5N1 virus infection is critical. Despite previous serologic surveys indicating very low (0%–1.9%) seropositivity against H5N1 virus in the general population (*15*), recent findings have shown relatively high levels of cross-reactive neuraminidase inhibition antibodies to H5N1 clade 2.3.4.4b viruses in healthy adults, likely because of prior exposure to influenza A(H1N1) pdm09 (pH1N1) virus (*16*). In addition, broadly reactive hemagglutinin (HA) stalk antibodies induced by seasonal influenza A(H1N1) and A(H3N2) virus infections in humans have been suggested to provide some level of protection against zoonotic H5N1 and H7N9 virus infections (*17*,*18*).

Author affiliation: Centers for Disease Control and Prevention, Atlanta, Georgia, USA

DOI: https://doi.org/10.3201/eid3103.241489

Well-controlled studies in mammalian models can provide crucial insight into the ability of prior influenza A virus (IAV) exposure to modulate subsequent disease after homologous or heterologous viral challenge (*19*). Cross-protection against H5N1 clade 1 viruses induced by prior human seasonal IAV infection has been previously shown in the ferret model (*20*,*21*). However, those studies have not assessed the role of preexisting immunity in modulating transmission outcomes and have not explored the extent of cross-protection or the specific types of cross-reactive antibodies in preimmune animals. We used a ferret model to evaluate viral replication and transmission of the H5N1 clade 2.3.4.4b virus in ferrets with or without prior immunity against pH1N1 virus.

Materials and Methods

Viruses

We propagated stocks of 3 virus strains: pH1N1 A/Nebraska/14/2019 (Neb/14); highly pathogenic H5N1 clade 2.3.4.4b A/Texas/37/2024 (Texas/37); and low pathogenicity H7N9 A/Anhui/1/2013 (Anhui/1), which was isolated from the first wave of human infections in China in 2013, as described previously (*11*,*22*,*23*). All virus preparation and animal infection experiments were conducted in Biosecurity Level 3 containment laboratories including enhancements required by the US Department of Agriculture and the Federal Select Agent Program. All animal studies were approved by the Institutional Animal Care and Use Committee of the Centers for Disease Control and Prevention (CDC) and were conducted under the guidance of the CDC's Institutional Animal Care and Use Committee in an AAALAC-accredited animal facility.

Primary Intranasal Infection with pH1N1 Virus

We serologically tested twelve 8-month-old ferrets by using the 2023–2024 World Health Organization influenza reagent kit; all tested negative for circulating influenza viruses, including A/Victoria/2570/2019 (H1N1)pdm09, A/Delaware/01/2021 (H3N2), B/Phuket/3073/2013 (Yamagata lineage), and B/Michigan/01/2021 (Victoria lineage). We then intranasally inoculated the ferrets with $\geq 10^2$ PFU Neb/14 virus per ferret in 1 mL phosphate-buffered saline under ketamine/xylazine anesthesia. All 12 ferrets developed productive infection and exhibited hemagglutination inhibition (HI) titers of 80–320 against homologous virus by day 93 postinoculation. We termed that group of ferrets as preimmune.

Ferret Inoculation and Evaluation of Viral Replication and Transmission

We then inoculated groups of the preimmune ferrets and naive ferrets by respiratory inhalation of aerosolized virus for 15 minutes, as previously described (*24*), and used an elevated relative humidity (≈65%) to better emulate environmental conditions on dairy farms. We administered doses varying from $10^{0.5}$ to $10^{2.8}$ PFU (Table). At 24 hours postinoculation, we pair-housed

Table. Pathogenicity and transmissibility of influenza viruses in naive and preimmune ferrets in study of the effect of prior influenza A(H1N1)pdm09 virus infection on pathogenesis and transmission of human influenza A(H5N1) clade 2.3.4.4b virus in ferret model*

Challenge virus	Status†		Inoculated animals‡					Contact animals	
	Donor	Contact	Dose, PFU§	Lethargy¶	Temp. rise, °C#	% Weight loss**	Peak titer (SD)††	Peak titer (SD)††	Transmission/ inoculation‡‡
Texas/37	Naive	Naive	$10^{0.5}$	1.5	2.4 (2/2)	7.3 (2/2)	5.5 (0.7)	2.5 (0.6)	2/2
Texas/37	Naive	Preimmune	$10^{2.4}$	1.9	1.7 (3/3)	7.9 (3/3)	4.2 (0.4)	NA	0/3
Texas/37	Preimmune	Naive	$10^{2.4–2.5}$	1.7	1.5 (2/3)	5.5 (2/3)	2.5 (1.8)	NA	0/3
Anhui/1	Naive	Naive	$10^{2.7}$	1.2	1.9 (2/3)	4.7 (3/3)	5.7 (0.8)	6.1 (1.5)	3/3
Anhui/1	Naive	Preimmune	$10^{2.8}$	1.1	1.5 (2/3)	5.4 (1/3)	6.5 (0.4)	5.4 (0.8)	3/3
Anhui/1	Preimmune	Naive	$10^{2.6}$	1.1	1.6 (2/3)	5.4 (2/3)	6.3 (0.2)	3.3 (1.5)	2/3

*Preimmune ferrets were those inoculated with influenza A(H1N1)pdm09 (A/Nebraska/14/2019). Naive and preimmune ferrets were challenged with highly pathogenic influenza A(H5N1) clade 2.3.4.4b A/Texas/37/2024 (Texas/37) and low pathogenicity influenza A(H7N9) A/Anhui/1/2013 (Anhui/1). NA, not applicable because titers were below the limit of detection; temp., temperature.
†Ferrets were serologically naive to contemporary influenza A viruses (naive) or inoculated with A/Nebraska/14/2019 influenza A(H1N1)pdm09 virus 3 months before use in this study (preimmune).
‡Inoculated ferrets were monitored for clinical signs of disease for 3 days for the Texas/37 virus and 4 days for the Anhui/1 virus. All animals that were productively infected after aerosol exposure are shown (n = 3 for all groups except Texas/37 naive donor/naive contact, which is n = 2).
§Presented dose of virus to ferrets following 15-min inhalation exposure to aerosolized virus.
¶Relative inactivity index of ferrets inoculated with the challenge virus specified.
#Values in parentheses are no. affected/no. inoculated. Mean maximum temperature rise $\geq$1°C among all inoculated animals in degrees centigrade; number of ferrets with temperature rise $\geq$1°C in all productively infected ferrets was shown in parentheses.
**Values in parentheses are no. affected/no. inoculated. Mean maximum weight loss >1% among all inoculated animals expressed as a percentage; number of ferrets with weight loss >1% in all productively infected ferrets was shown in parentheses.
††Mean maximum nasal wash titer $\pm$SD reported as $\log_{10}$ PFU/mL among ferrets with positive virus shedding; for NA, titers for all ferrets were below limit of detection of 10 PFU.
‡‡Values are no. affected/no. inoculated. Transmission was defined as both the detection of productive virus shedding and seroconversion of surviving animals to homologous challenge virus or confirmed infection requiring euthanasia. Two contact ferrets, each co-housed with a ferret productively infected with the Texas/37 virus, were humanely euthanized on days 3 and 4 postcontact; all contact ferrets co-housed with ferrets inoculated with Anhui/1 virus survived through day 21 postcontact.

groups of 3 naive or preimmune ferrets with inoculated ferrets at a 1:1 donor:contact ratio to assess virus transmission in a direct contact setting. We observed all ferrets daily for clinical signs of infection, including temperature rise, weight loss, and lethargy, and collected nasal wash daily until day 3 postinoculation for Texas/37 or day 4 postinoculation for Anhui/1 virus, as previously described (*11*,*22*), at which time we humanely euthanized inoculated animals to evaluate virus replication and systemic spread. We monitored contact ferrets for virus shedding and seroconversion at day 21 postinoculation as determined by HI titers using 0.5% turkey red blood cells. We determined productive transmission by detection of infectious virus in nasal wash specimens and seroconversion to homologous challenge virus.

All samples collected for infectious virus determination were frozen at −80°C until titration by standard plaque assay in Madin-Darby canine kidney cells (limit of detection 10 PFU/mL or g of tissue). We used a 2-way analysis of variance test in Prism 7.05 (GraphPad Software Inc., https://www.graphpad.com) to assess viral titer differences between naive and preimmune groups. We considered $p<0.05$ statistically significant.

Serologic Assessment of Cross-Reactive Antibodies after Primary pH1N1 Virus Challenge

We developed and performed a high-throughput multiplex influenza antibody detection assay, as described previously (*25*,*26*). In brief, we included HA globular head, HA stalk, neuraminidase (NA), and nucleoprotein (NP) antigens from IAVs and HA globular head from influenza B viruses in this study (Appendix 1 Table, https://wwwnc.cdc.gov/EID/article/31/2/24-1489-App1.xlsx). We obtained antigens from Sino Biological U.S. Inc. (https://www.sinobiological.com), the International Reagent Resource (https://www.internationalreagentresource.org), or by using an in-house baculovirus expression system to express and purify our own reagents (*27*,*28*).

To each well of a black-wall 96-well plate, we added 50 μL of microsphere suspension containing 2,000 microspheres for each of the 32 bead regions in an assay buffer comprising 1× PBS with 0.05% Tween 20, 1% bovine serum albumin (BSA), and 0.5 mol sodium chloride (total 64,000 microspheres/well). We then added 1:200 diluted naive or preimmune ferret serum in assay buffer to appropriate wells in duplicates, including 2 serum pools on each plate as intraassay and interassay controls. We incubated plates in the dark at room temperature for 60 minutes on an orbital shaker, then washed plates 3 times with 100 μL of assay buffer by using Bio-Plex Handheld Magnetic Washer (Bio-Rad Laboratories, https://www.bio-rad.com). We then added 100 μL of protein A–phycoerythrin conjugate and incubated plates in the dark at room temperature for 60 minutes on an orbital shaker. Then, we washed plates 3 times with 100 μL of reading buffer comprising 1× PBS with 0.05% Tween 20, 1% BSA and read the plates by using a Bio-Plex MAGPIX Multiplex Reader (Bio-Rad Laboratories). We calculated median fluorescence intensities by using GraphPad 7.05 software (GraphPad Software Inc.).

Results

Cross-Reactive Antibodies Induced by pH1N1 Virus Infection

We tested serum samples collected 93 days after primary pH1N1 virus infection for reactivity against various HA, NA, and NP antigens (Figure 1). We found the highest serum antibody levels detected were against the HA globular head from pH1N1 viruses predating the challenge strain, but we consistently detected antibodies against all 6 H1 HA targets assessed. We also detected antibodies reactive to the N1 NA, which were derived from either H1N1 or H5N1 virus isolates, including Texas/37, in all preimmune animals. Moreover, we detected antibodies against NP protein of pH1N1 virus A/Brisbane/10/2007 in preimmune ferrets. The NP proteins between Texas/37 and Neb/14 viruses share 94% similarity. However, we detected no antibodies against the HA globular head of H3, H5, or H7 viruses, or the NA from H3N2 or H7N9 viruses. In addition, Neb/14 virus infection induced antibodies reactive to group 1, but not group 2, HA stalks (Figure 1). Furthermore, alignments of surface exposed residues in the HA, including HA1 head and HA2 stalk, and NA proteins of Neb/14 and Texas/37 virus revealed higher similarities in NA surface residues (83.4%, 186/223) and in the HA2 stalk (80.4%, 111/138) compared with HA1 surface exposed residues (45%, 107/238) (Appendix 2 Figures 1, 2, https://wwwnc.cdc.gov/EID/article/31/2/24-1489-App2.pdf). That finding supports the observed cross-reactivity to the HA2 stalk and Texas/37 NA but not to the Texas/37 HA head in preimmune ferrets. Our serologic findings demonstrated that pH1N1 infection can induce low levels of cross-reactive antibodies to H5N1 NA and the HA stalk from the group 1 H5N1 but not to group 2 H7N9, virus where cross-reactive antibodies remained at undetectable levels.

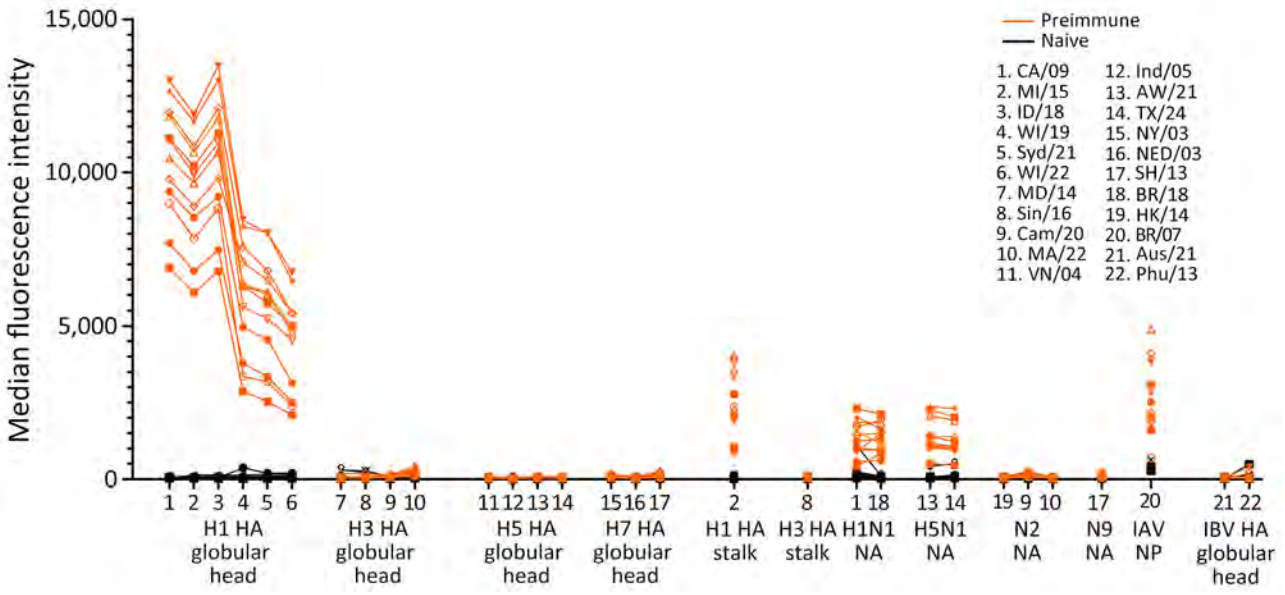

Figure 1. Detection of cross-reactive antibodies in study of the effect of prior influenza A(H1N1)pdm09 virus infection on pathogenesis and transmission of human influenza A(H5N1) clade 2.3.4.4b virus in ferret model. After primary pH1N1 infection, we detected cross-reactive antibodies by using a high-throughput multiplex influenza antibody detection assay. Serum samples from naive and preimmune ferrets were prediluted 200-fold and added to plates containing antigen-coated microspheres, then plates were incubated with protein A–phycoerythrin conjugate. Reported values represent the mean of duplicate assays. Antibody titers were expressed as median fluorescence intensity. Full virus strain names and sources of all antigens are provided (Appendix 1 Table, https://wwwnc.cdc.gov/EID/article/31/3/24-1489-App1.pdf). HA, hemagglutinin; IAV, influenza A virus; IBV, influenza B virus; NA, neuraminidase; NP, nucleoprotein.

Attenuation of Texas/37 Virulence and Transmission in pH1N1 Preimmune Ferrets

To assess if cross-reactive antibodies elicited in ferrets after pH1N1 infection could reduce H5N1 clade 2.3.4.4b virus virulence and transmissibility, we challenged preimmune and naive control ferrets via respiratory inhalation of aerosolized Texas/37 virus, to closely emulate natural mammalian exposure to IAV. First, we exposed a group of 3 ferrets to a low (≈3 PFU) dose of aerosolized Texas/37 virus. In agreement with prior work (*29*), we productively infected 2/3 ferrets, which led to a severe and fatal infection in serologically naive ferrets. In addition, after 48 hours of sustained contact, we detected successful transmission to cohoused naive animals in direct contact with infected animals (Table). To provide a robust challenge, both naive and preimmune ferrets received inhaled doses of $10^{2.4}$–$10^{2.5}$ PFU of H5N1 virus; then, preimmune ferrets served as either donors or contacts in direct contact transmission experiments. We humanely euthanized all donor ferrets on day 3 postinoculation to assess systemic dissemination of virus.

Serologically naive ferrets inoculated by the aerosol inhalation route with Texas/37 virus exhibited a rapid and severe infection within 3 days postinoculation (Table). As with the inoculated naive ferrets, preimmune ferrets exhibited clinical symptoms by day 3 postinoculation, but clinical signs were less severe, and lethargy, temperature rise, and weight loss were less pronounced. Virus shedding in nasal wash specimens from the preimmune ferrets was delayed (Figures 2, 3), and only 1/3 ferrets had detectable virus shedding on days 1 and 2 postinoculation, compared with 2/3 and 3/3 ferrets in the inoculated naive group at those timepoints (Figure 2, panel A). Although viral titers in day 3 postinoculation nasal wash and tissues proximal to the upper respiratory tract (i.e., nasal turbinate, ethmoid turbinate, soft palate) were comparable between the preimmune and naive ferret groups, virus was either undetectable in the lower respiratory tract (trachea, lung), extrapulmonary tissues (spleen, kidney), and blood, or detected at lower frequency in other tissues (brain, olfactory bulb, intestines, liver) in preimmune ferrets relative to naive animals (Figure 2, panel C).

Unlike the efficient transmissibility of Texas/37 virus during direct contact when both donor and contact animals were serologically naive (Table; Figure 3, panel A), Texas/37 did not transmit by that route when preimmune ferrets served as either donor or recipient animals. We did not recover infectious virus from nasal wash specimens collected

from contact animals nor did those animals seroconvert to H5N1 virus (Table, Figure 3 panels C, E). Thus, we found that prior exposure to a 2019 pH1N1 virus in ferrets reduced disease severity and limited viral spread to the lower respiratory tract and extrapulmonary tissues after rechallenge with Texas/37 virus via respiratory inhalation compared with serologically naive animals. We also observed reduced transmissibility of Texas/37 virus during direct contact when either the donor or recipient animals had prior pH1N1 exposure.

Effect of Preexisting pH1N1 Immunity on H7N9 Virus Pathogenesis and Transmission

Because we detected antibodies against antigens other than HA and NA, such as NP, in preimmune serum samples (Figure 1), we performed a parallel experiment, to better understand the breadth and magnitude of cross-protection. For that experiment we used the group 2 low pathogenicity (H7N9 Anhui/1 virus, which has distinct HA and NA subtypes to which pH1N1 convalescent serum does not react. Anhui/1 virus has previously been reported to cause milder disease and exhibit lower replication capacity in ferrets compared with the Texas/37 virus (*11*,*22*). Donor ferrets received an aerosol inhalation dose of $10^{2.6}$–$10^{2.8}$ PFU of Anhui/1 virus. Donor and contact animals cohoused for 72 hours before donor animals were humanely euthanized on day 4 postinoculation, which was a sufficient time for efficient transmission to occur in direct contact between serologically naive donor and contact animals (Table; Figure 3, panel B).

Upon Anhui/1 virus respiratory inhalation challenge, only mild clinical signs were observed in both naive and preimmune ferrets (Table). Virus shedding in nasal wash specimens and systemic tissues were generally similar across naive and preimmune

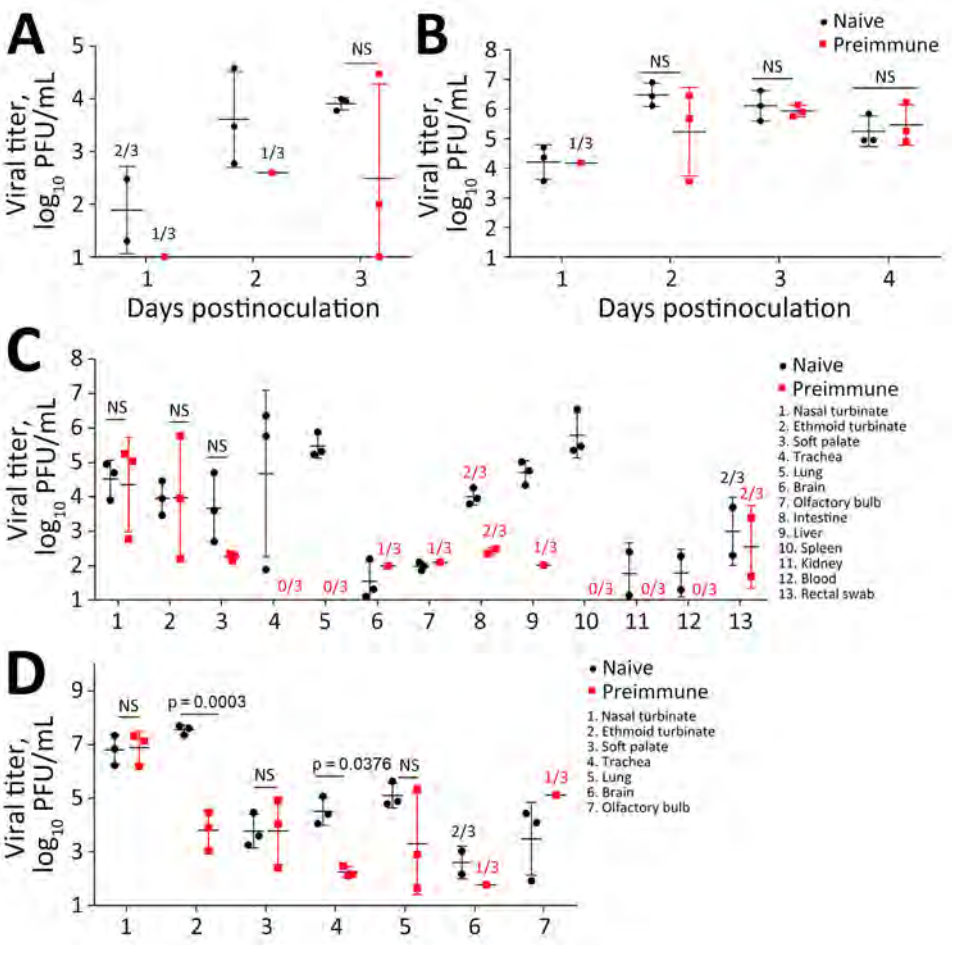

Figure 2. Virus shedding in study of the effect of prior influenza A(H1N1)pdm09 virus infection on pathogenesis and transmission of human influenza A(H5N1) clade 2.3.4.4b virus in ferret model. A, B) Nasal wash viral titers for influenza A(H5N1) Texas/37 virus (A) and influenza A(H7N9) Anhui/1 virus (B). C, D) Virus titers from tissues for Texas/37 H5N1 virus collected 3 days postinoculation (C) and Anhui/1 H7N9 virus collected 4 days postinoculation (D). Horizontal bars indicate median, dots indicate individual titers, whiskers indicate range of positive titers. Three naive and 3 pH1N1 preimmune ferrets were inoculated via respiratory inhalation with Texas/37 or Anhui/1 virus (Table). Nasal wash specimens (A, B) were collected daily. Virus titers were determined by standard plaque assay in MDCK cells. Tissue samples collected from nasal turbinate, ethmoid turbinate, soft palate, blood, and rectal swabs were reported in $\log_{10}$ PFU/mL. Tissues collected from lung, brain, olfactory bulb, intestines, liver, spleen, kidney were reported in $\log_{10}$ PFU/g. The limit of detection was 10 PFU per mL or g. Statistical analyses were performed using 2-way analysis of variance test when samples were positive for viral titers in all 3 inoculated animals; we considered $p<0.05$ statistically significant. When <3 inoculated ferrets had detectable virus, the detection frequency is indicated above the corresponding positions. Anhui/1, low pathogenicity influenza A(H7N9) A/Anhui/1/2013; NS, not statistically significant; Texas/37, highly pathogenic influenza A(H5N1) clade 2.3.4.4b A/Texas/37/2024.

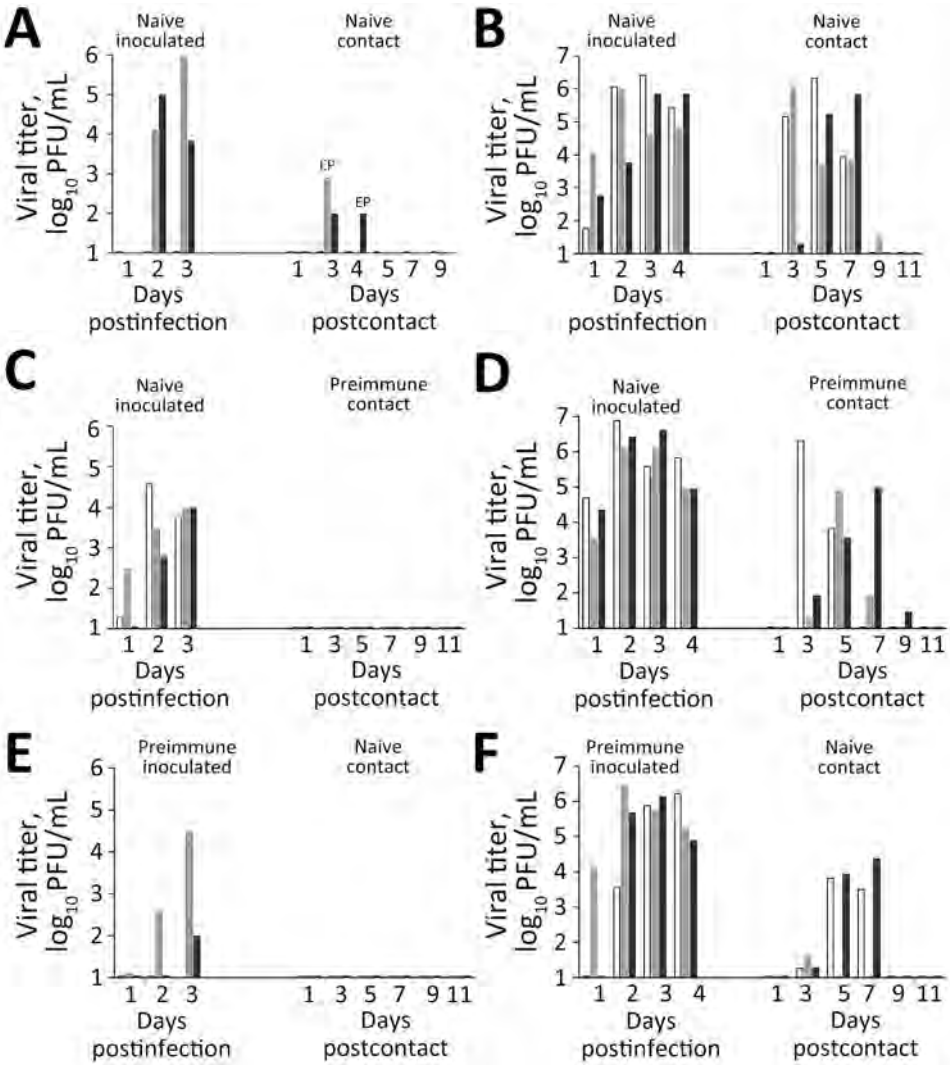

Figure 3. Contact transmission of Texas/37 influenza A(H5N1) virus and Anhui/1 influenza A(H7N9) virus in study of the effect of prior influenza A(H1N1)pdm09 virus infection on pathogenesis and transmission of human influenza A(H5N1) clade 2.3.4.4b virus in ferret model. A, C, E) Transmission of Texas/37 H5N1 virus among ferrets; B, D, F) transmission of Anhui/1 H7N9 virus among ferrets. Different shades indicate individual animals. We inoculated 3 naive ferrets per virus (A–D) and 3 preimmune ferrets per virus (E, F) by respiratory inhalation exposure (Table). Each inoculated ferret was pair-housed with a contact recipient, with (C, D) or without preimmunity (A, B, E, F); contact was sustained for 48 hours for Texas/37 and for 72 hours for Anhui/1 before inoculated animals were humanely euthanized. Nasal wash samples were collected daily from inoculated ferrets (days 1–4 postinfection) and on alternate days from the contact animals (days 1–11 postcontact). The limit of detection was 10 PFU/mL. Two naive contact ferrets (panel A) reached humane endpoints and were euthanized on days 3 and 4 postinfection. Anhui/1, low pathogenicity influenza A(H7N9) A/Anhui/1/2013; EP, endpoint; NS, not statistically significant; Texas/37, highly pathogenic influenza A(H5N1) clade 2.3.4.4b A/Texas/37/2024.

donor animals, except for day 4 postinoculation ethmoid turbinate and trachea titers, which were significantly higher in naive ferrets ($p<0.05$) (Figure 2, panels B, D). Efficient virus transmission during direct contact was observed when preimmune ferrets served as either donor or contact animals (Figure 3, panels D, F). Overall, we found that prior exposure to pH1N1 virus had no substantial effect on H7N9 virus shedding, replication, or transmission during direct contact, in contrast to viral challenge with H5N1 virus.

Discussion

Key elements in the risk assessment of emerging IAVs include evaluating virus transmissibility in animal models, assessing population immunity against novel IAVs, and determining disease severity and pathogenesis in humans and animals after infection (*30*). Assessing the risk for human infection and human-to-human transmission of emerging HPAI H5N1 clade 2.4.4.4b virus, which has caused sporadic human infections among poultry and dairy farm workers in the United States, is crucial for pandemic preparedness. We showed that ferrets with existing pH1N1 virus immunity had reduced disease severity and limited viral systemic spread after aerosol inhalation exposure to Texas/37 virus. Moreover, direct-contact transmission was abolished when either the donor or recipient animals had prior H1N1 immunity. However, the protective effect of pH1N1 immunity did not extend to the virus with an HA from different phylogenetic group and NA from a distinct subtype, as evidenced by the minimal effect that pH1N1 immunity had on infection and transmission after challenge with a group 2 H7N9 virus.

This study builds upon a growing body of literature on ferrets previously exposed to seasonal IAVs and subsequently challenged with either

seasonal or zoonotic IAV (*19*,*21*,*31*). Use of ferrets with existing IAV immunity from prior infection with wild-type viruses can provide contextual data for risk assessment studies (*31*). Of note, we used a contemporary 2019 pH1N1 strain to establish prior immunity, which could influence the subsequent preimmune profile of animals, as supported by varying serum H1 HA and N1 NA antibody levels depending on the year of virus isolation (Figure 1). Our findings from use of 2019 pH1N1 virus underscores the importance of considering the specific pH1N1 strain used for primary infection in such studies, and conducting future work that explores the full breadth of diverse infection histories seen in humans.

Our findings extend the understanding of cross-protective effects of pH1N1 immunity against H5N1 clade 2.3.4.4b viruses by challenging animals with a recent human isolate, Texas/37. Unlike other US isolates, Texas/37 carries a PB2–627K mutation, likely contributing to enhanced virulence in ferrets (*7*). In line with a similar study using a bovine isolate (*32*), we observed reduced disease severity and systemic viral spread in pH1N1 preimmune ferrets relative to naive controls. In addition, we found that while virus shedding in nasal wash specimens was delayed in preimmune animals early (days 1–2) after infection relative to naive animals, titers from both groups reached comparable levels by day 3 postinoculation in specimens from the upper respiratory tract (nasal wash, nasal and ethmoid turbinates) and the surrounding milieu (soft palate). Of note, a previous study also reported that H1N1-preimmune ferrets exhibited substantially reduced virus shedding in nasal secretions and viral replication in both upper and lower respiratory tissues compared with naive ferrets when challenged with an H5N1 bovine isolate (*32*). The differences between that study and ours could be attributed to variation in H5N1 challenge strains, cross-protective antibody levels, or differences in inoculation doses and routes. Beyond examination of directly inoculated animals, transmission in the presence of direct contact was reduced when either donor or recipient ferrets were preimmune, likely the result of altered host susceptibility and delayed virus shedding. Although we did not assess respiratory droplet transmission in this study, we anticipate that droplet transmission would be unlikely under this more stringent transmission setting. Of note, we used inhalation of aerosolized virus to challenge the animals, which is known to delay onset of detectable virus replication and peak titers in nasal wash specimens (*24*), more closely emulating the kinetics of natural human exposure to IAVs.

In our study, using a comprehensive panel of antigens in serologic tests, we identified antibodies that reacted to H5N1 NA and the group 1 HA stalk, but not to the HA heads of H5 and H7 viruses or the group 2 HA stalk. Broadly reactive NA and HA stalk antibodies have been shown to play a key role in cross-heterosubtypic protection in animal models (*33*,*34*), which likely contributed to the cross-protection observed in our study. In addition, human epidemiologic studies have demonstrated that populations with previous exposure to pH1N1 might experience less severe outcomes from H5N1 infection (*18*). However, we only explored cross-protective immunity at approximately 3 months after seasonal pH1N1 primary infection. The duration of such immunity and correlation between the level of NA or HA stalk antibodies, specifically H5 HA stalk antibodies, and protection efficacy warrant further study, as do comprehensive evaluations of how prior vaccination may contribute to modulating disease severity.

Our experimental evidence from the ferret model underscores the potential role of cross-reactive HA stalk and NA antibodies in reducing disease severity and transmission after H5N1 virus infection. However, future studies of larger group sizes are warranted, as are studies investigating how antibodies targeting internal influenza virus proteins, such as NP, or cellular immunity, contribute to cross-protection. In addition, a single seasonal virus infection in naive ferrets cannot fully recapitulate the complexity of human IAV immune history. Future studies involving ferrets vaccinated with different types of influenza vaccines or repeatedly exposed to seasonal viruses more closely mirroring the varied infection histories in humans will help provide deeper insights into cross-immunity elicited across different IAV subtypes. Furthermore, inclusion of multiple zoonotic strains to assess relative contributions of nonspecific effects in preimmune animals, as demonstrated here by performing tandem challenge studies and serology assessments with both H5N1 and H7N9 viruses, is a practice not typically used in the field yet shown to be a key provider of essential contextual information.

In conclusion, our results showed that prior pH1N1 virus infection more effectively reduced the replication and transmission of H5N1 virus than it did H7N9 virus in a ferret model. Those results suggest that pH1N1 virus immunity may confer some level of protection against H5N1 clade 2.3.4.4.b virus in humans.

About the Author

Dr. Sun is a microbiologist in the Influenza Division, National Center for Immunization and Respiratory Diseases, Centers for Disease Control and Prevention, Atlanta, Georgia, USA. Her research primarily focuses on using the ferret model to understand influenza virus pathogenicity and transmissibility.

References

1. Bevins SN, Shriner SA, Cumbee JC Jr, Dilione KE, Douglass KE, Ellis JW, et al. Intercontinental movement of highly pathogenic avian influenza A(H5N1) clade 2.3.4.4 virus to the United States, 2021. Emerg Infect Dis. 2022;28:1006–11. https://doi.org/10.3201/eid2805.220318
2. Caliendo V, Lewis NS, Pohlmann A, Baillie SR, Banyard AC, Beer M, et al. Transatlantic spread of highly pathogenic avian influenza H5N1 by wild birds from Europe to North America in 2021. Sci Rep. 2022;12:11729. https://doi.org/10.1038/s41598-022-13447-z
3. Elsmo EJ, Wünschmann A, Beckmen KB, Broughton-Neiswanger LE, Buckles EL, Ellis J, et al. Highly pathogenic avian influenza A(H5N1) virus clade 2.3.4.4b infections in wild terrestrial mammals, United States, 2022. Emerg Infect Dis. 2023;29:2451–60. https://doi.org/10.3201/eid2912.230464
4. Burrough ER, Magstadt DR, Petersen B, Timmermans SJ, Gauger PC, Zhang J, et al. Highly pathogenic avian influenza A(H5N1) clade 2.3.4.4b virus infection in domestic dairy cattle and cats, United States, 2024. Emerg Infect Dis. 2024;30:1335–43. https://doi.org/10.3201/eid3007.240508
5. US Department of Agriculture. HPAI confirmed cases in livestock [cited 2024 Aug 30]. https://www.aphis.usda.gov/livestock-poultry-disease/avian/avian-influenza/hpai-detections/hpai-confirmed-cases-livestock
6. Centers for Disease Control and Prevention. CDC reports fourth human case of H5 bird flu tied to dairy cow outbreak [cited 2024 Aug 30]. https://www.cdc.gov/media/releases/2024/p-0703-4th-human-case-h5.html
7. Uyeki TM, Milton S, Abdul Hamid C, Reinoso Webb C, Presley SM, Shetty V, et al. Highly pathogenic avian influenza A(H5N1) virus infection in a dairy farm worker. N Engl J Med. 2024;390:2028–9. https://doi.org/10.1056/NEJMc2405371
8. Morse J, Coyle J, Mikesell L, Stoddard B, Eckel S, Weinberg M, et al. Influenza A(H5N1) virus infection in two dairy farm workers in Michigan. N Engl J Med. 2024;391:963–4. https://doi.org/10.1056/NEJMc2407264
9. World Health Organization. Disease outbreak news: human infection caused by avian influenza A(H5N1)—Chile, 21 April 2023 [cited 2024 Sep 10]. https://www.who.int/emergencies/disease-outbreak-news/item/2023-DON461
10. Eisfeld AJ, Biswas A, Guan L, Gu C, Maemura T, Trifkovic S, et al. Pathogenicity and transmissibility of bovine H5N1 influenza virus. Nature. 2024;633:426–32. https://doi.org/10.1038/s41586-024-07766-6
11. Pulit-Penaloza JA, Belser JA, Brock N, Kieran TJ, Sun X, Pappas C, et al. Transmission of a human isolate of clade 2.3.4.4b A(H5N1) virus in ferrets. Nature. 2024;636:705–10. https://doi.org/10.1038/s41586-024-08246-7
12. Restori KH, Septer KM, Field CJ, Patel DR, VanInsberghe D, Raghunathan V, et al. Risk assessment of a highly pathogenic H5N1 influenza virus from mink. Nat Commun. 2024;15:4112. https://doi.org/10.1038/s41467-024-48475-y
13. Kandeil A, Patton C, Jones JC, Jeevan T, Harrington WN, Trifkovic S, et al. Rapid evolution of A(H5N1) influenza viruses after intercontinental spread to North America. Nat Commun. 2023;14:3082. https://doi.org/10.1038/s41467-023-38415-7
14. Gu C, Maemura T, Guan L, Eisfeld AJ, Biswas A, Kiso M, et al. A human isolate of bovine H5N1 is transmissible and lethal in animal models. Nature. 2024;636:711–8. https://doi.org/10.1038/s41586-024-08254-7
15. Chen X, Wang W, Wang Y, Lai S, Yang J, Cowling BJ, et al. Serological evidence of human infections with highly pathogenic avian influenza A(H5N1) virus: a systematic review and meta-analysis. BMC Med. 2020;18:377. https://doi.org/10.1186/s12916-020-01836-y
16. Daulagala P, Cheng SMS, Chin A, Luk LLH, Leung K, Wu JT, et al. Avian influenza A(H5N1) neuraminidase inhibition antibodies in healthy adults after exposure to influenza A(H1N1)pdm09. Emerg Infect Dis. 2024;30:168–71. https://doi.org/10.3201/eid3001.230756
17. Ekiert DC, Friesen RH, Bhabha G, Kwaks T, Jongeneelen M, Yu W, et al. A highly conserved neutralizing epitope on group 2 influenza A viruses. Science. 2011;333:843–50. https://doi.org/10.1126/science.1204839
18. Gostic KM, Ambrose M, Worobey M, Lloyd-Smith JO. Potent protection against H5N1 and H7N9 influenza via childhood hemagglutinin imprinting. Science. 2016;354:722–6. https://doi.org/10.1126/science.aag1322
19. Skarlupka AL, Ross TM. Immune imprinting in the influenza ferret model. Vaccines (Basel). 2020;8:173. https://doi.org/10.3390/vaccines8020173
20. Bissel SJ, Wang G, Carter DM, Crevar CJ, Ross TM, Wiley CA. H1N1, but not H3N2, influenza A virus infection protects ferrets from H5N1 encephalitis. J Virol. 2014;88:3077–91. https://doi.org/10.1128/JVI.01840-13
21. Nuñez IA, Jang H, Huang Y, Kelvin A, Ross TM. Influenza virus immune imprinting dictates the clinical outcomes in ferrets challenged with highly pathogenic avian influenza virus H5N1. Front Vet Sci. 2023;10:1286758. https://doi.org/10.3389/fvets.2023.1286758
22. Belser JA, Gustin KM, Pearce MB, Maines TR, Zeng H, Pappas C, et al. Pathogenesis and transmission of avian influenza A (H7N9) virus in ferrets and mice. Nature. 2013;501:556–9. https://doi.org/10.1038/nature12391
23. Pulit-Penaloza JA, Brock N, Jones J, Belser JA, Jang Y, Sun X, et al. Pathogenesis and transmission of human seasonal and swine-origin A(H1) influenza viruses in the ferret model. Emerg Microbes Infect. 2022;11:1452–9. https://doi.org/10.1080/22221751.2022.2076615
24. Gustin KM, Belser JA, Wadford DA, Pearce MB, Katz JM, Tumpey TM, et al. Influenza virus aerosol exposure and analytical system for ferrets. Proc Natl Acad Sci U S A. 2011;108:8432–7. https://doi.org/10.1073/pnas.1100768108
25. Li ZN, Weber KM, Limmer RA, Horne BJ, Stevens J, Schwerzmann J, et al. Evaluation of multiplex assay platforms for detection of influenza hemagglutinin subtype specific antibody responses. J Virol Methods. 2017;243:61–7. https://doi.org/10.1016/j.jviromet. 2017.01.008
26. Li ZN, Liu F, Gross FL, Kim L, Ferdinands J, Carney P, et al. Antibody landscape analysis following influenza vaccination and natural infection in humans with a high-throughput multiplex influenza antibody detection assay. MBio. 2021;12:e02808-20. https://doi.org/10.1128/mBio.02808-20
27. Yang H, Carney P, Stevens J. Structure and receptor binding properties of a pandemic H1N1 virus hemagglutinin.

PLoS Curr. 2010;2:RRN1152. https://doi.org/10.1371/currents.RRN1152
28. Yang H, Carney PJ, Chang JC, Villanueva JM, Stevens J. Structure and receptor binding preferences of recombinant hemagglutinins from avian and human H6 and H10 influenza A virus subtypes. J Virol. 2015;89:4612–23. https://doi.org/10.1128/JVI.03456-14
29. Belser JA, Pulit-Penaloza JA, Brock N, Sun X, Kieran TJ, Pappas C, et al. Ocular infectivity and replication of an A(H5N1) clade 2.3.4.4b influenza virus associated with human conjunctivitis in a dairy farm worker: an in vitro and ferret study. Lancet Microbe. In press 2025.
30. Centers for Disease Control and Prevention. CDC's influenza risk assessment tool (IRAT) [cited 2024 Aug 30]. https://www.cdc.gov/ncird/whats-new/cdcs-influenza-risk-assessment-tool.html
31. Le Sage V, Rockey NC, French AJ, McBride R, McCarthy KR, Rigatti LH, et al. Potential pandemic risk of circulating swine H1N2 influenza viruses. Nat Commun. 2024;15:5025. https://doi.org/10.1038/s41467-024-49117-z
32. Le Sage V, Werner BD, Merrback GA, Petnuch SE, O'Connell AK, Simmons HC, et al. Influenza A(H5N1) immune response among ferrets with existing influenza A(H1N1) immunity. Emerg Infect Dis. 2025;31. https://doi.org/10.3201/eid3103.241485
33. Rockman S, Brown LE, Barr IG, Gilbertson B, Lowther S, Kachurin A, et al. Neuraminidase-inhibiting antibody is a correlate of cross-protection against lethal H5N1 influenza virus in ferrets immunized with seasonal influenza vaccine. J Virol. 2013;87:3053–61. https://doi.org/10.1128/JVI.02434-12
34. Sandbulte MR, Jimenez GS, Boon AC, Smith LR, Treanor JJ, Webby RJ. Cross-reactive neuraminidase antibodies afford partial protection against H5N1 in mice and are present in unexposed humans. PLoS Med. 2007;4:e59. https://doi.org/10.1371/journal.pmed.0040059

Address for correspondence: Xiangjie Sun, Centers for Disease Control and Prevention, 1600 Clifton Rd NE, Mailstop H17-5, Atlanta, GA 30329-4018, USA; email: jgz1@cdc.gov

etymologia revisited

Nipah Virus

[ne´-pə vī´-rəs]

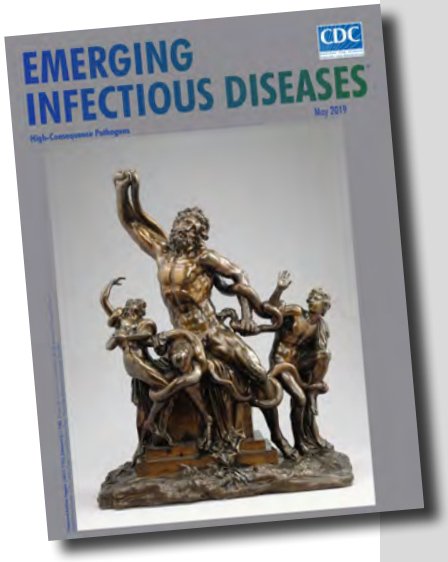

Originally published in May 2019

In 1994, a newly described virus, initially called equine morbillivirus, killed 13 horses and a trainer in Hendra, a suburb of Brisbane, Australia. The reservoir was subsequently identified as flying foxes, bats of the genus *Pteropus* (Greek pteron ["wing"] + *pous* ["foot"]). In 1999, scientists investigated reports of febrile encephalitis and respiratory illness among workers exposed to pigs in Malaysia and Singapore. (The pigs were believed to have consumed partially eaten fruit discarded by bats.)

The causative agent was determined to be closely related to Hendra virus and was later named for the Malaysian village of Kampung Sungai Nipah. The 2 viruses were combined into the genus *Henipavirus*, in the family *Paramyxoviridae*. Three additional species of *Henipavirus*—Cedar virus, Ghanaian bat virus, and Mojiang virus—have since been described, but none is known to cause human disease. Outbreaks of Nipah virus occur almost annually in India and Bangladesh, but *Pteropus* bats can be found throughout the tropics and subtropics, and henipaviruses have been isolated from them in Central and South America, Asia, Oceania, and East Africa.

References:

1. Centers for Disease Control and Prevention. Outbreak of Hendra-like virus—Malaysia and Singapore, 1998–1999. MMWR Morb Mortal Wkly Rep. 1999;48:265–9.
2. Selvey LA, Wells RM, McCormack JG, Ansford AJ, Murray K, Rogers RJ, et al. Infection of humans and horses by a newly described morbillivirus. Med J Aust. 1995;162:642–5.

https://wwwnc.cdc.gov/eid/article/25/5/et-2505_article

Efficacy and Safety of 4-Month Rifapentine-Based Tuberculosis Treatments in Persons with Diabetes

Ekaterina V. Kurbatova, William C. Whitworth, Lakshmi Praveena Peddareddy, Patrick P.J. Phillips, Nigel A. Scott, Kia E. Bryant, Rodney Dawson, Sandra Wagner Cardoso, Wadzanai Samaneka, Melissa Engle, Ziyaad Waja, Erin Sizemore, Wendy Carr, Kelly E. Dooley, Radojka Savic, Susan Swindells, Richard E. Chaisson, Susan E. Dorman, Payam Nahid, Nhung V. Nguyen, AIDS Clinical Trials Group A5349,[1] Tuberculosis Trials Consortium Study 31[2]

Medscape CME Activity

In support of improving patient care, this activity has been planned and implemented by Medscape, LLC and Emerging Infectious Diseases. Medscape, LLC is jointly accredited with commendation by the Accreditation Council for Continuing Medical Education (ACCME), the Accreditation Council for Pharmacy Education (ACPE), and the American Nurses Credentialing Center (ANCC), to provide continuing education for the healthcare team.

Medscape, LLC designates this Journal-based CME activity for a maximum of 1.00 ***AMA PRA Category 1 Credit(s)™***. Physicians should claim only the credit commensurate with the extent of their participation in the activity.

Successful completion of this CME activity, which includes participation in the evaluation component, enables the participant to earn up to 1.0 MOC points in the American Board of Internal Medicine's (ABIM) Maintenance of Certification (MOC) program. Participants will earn MOC points equivalent to the amount of CME credits claimed for the activity. It is the CME activity provider's responsibility to submit participant completion information to ACCME for the purpose of granting ABIM MOC credit.

All other clinicians completing this activity will be issued a certificate of participation. To participate in this journal CME activity: (1) review the learning objectives and author disclosures; (2) study the education content; (3) take the post-test with a 75% minimum passing score and complete the evaluation at https://www.medscape.org/qna/processor/73653?showStandAlone=true&src=prt_jcme_eid_mscpedu; and (4) view/print certificate. For CME questions, see page 643.

NOTE: It is Medscape's policy to avoid the use of Brand names in accredited activities. However, in an effort to be as clear as possible, trade names are used in this activity to distinguish between the mixtures and different tests. It is not meant to promote any particular product.

Release date: February 24, 2025; Expiration date: February 24, 2026

Learning Objectives

Upon completion of this activity, participants will be able to:

- Assess treatment efficacy of a 4-month regimen of rifapentine-moxifloxacin vs control treatment for tuberculosis
- Analyze treatment efficacy of 4-month vs 6-month treatment regimens for tuberculosis among patients with diabetes
- Evaluate time to tuberculosis culture conversion to negative with different treatment regimens for tuberculosis among patients with diabetes
- Assess adverse events associated with different treatment regimens for tuberculosis among patients with diabetes

CME Editor

Jude Rutledge, BA, Technical Writer/Editor, Emerging Infectious Diseases. *Disclosure: Jude Rutledge, BA, has no relevant financial relationships.*

CME Author

Charles P. Vega, MD, Health Sciences Clinical Professor of Family Medicine, University of California, Irvine School of Medicine, Irvine, California. *Disclosure: Charles P. Vega, MD, has the following relevant financial relationships: served as consultant or advisor for Boehringer Ingelheim; GlaxoSmithKline.*

Authors

Ekaterina V. Kurbatova, MD, PhD, MPH; William C. Whitworth, MPH; Lakshmi Praveena Peddareddy, MBBS, MPH; Patrick P.J. Phillips, PhD; Nigel A. Scott, MS; Kia E. Bryant, MPH; Rodney Dawson, MD; Sandra Wagner Cardoso, MD, PhD; Wadzanai Samaneka, MBChB, MSc; Melissa Engle, CRT, CCRC; Ziyaad Waja, MD; Erin Sizemore, MPH; Wendy Carr, PhD; Kelly E. Dooley, MD, PhD; Radojka Savic, PhD; Susan Swindells, MD; Richard E. Chaisson, MD; Susan E. Dorman, MD; Payam Nahid, MD, MPH; Nhung V. Nguyen, MD, PhD.

A previous study demonstrated noninferior efficacy of 4-month rifapentine/moxifloxacin regimen for tuberculosis (TB) treatment compared with the standard regimen. We explored results among study participants with diabetes. Among 2,516 randomized participants, 181 (7.2%) had diabetes. Of 166 participants with diabetes in the microbiologically eligible analysis group, 26.3% (15/57) had unfavorable outcomes in the control regimen, 13.8% (8/58) in the rifapentine/moxifloxacin regimen, and 29.4% (15/51) in the rifapentine regimen. The difference in proportion of unfavorable outcomes between the control and rifapentine/moxifloxacin arms in the microbiologically eligible analysis group was –12.5% (95% CI –27.0% to 1.9%); the difference between the control and rifapentine arms was 3.1% (95% CI –13.8% to 20.0%). Safety outcomes were similar in the rifapentine/moxifloxacin regimen and control arms. Among participants with TB and diabetes, the rifapentine/moxifloxacin arm had fewest unfavorable outcomes and was safe. Our findings indicate that the rifapentine/moxifloxacin regimen can be used in persons with TB and diabetes.

Tuberculosis (TB) and diabetes are important public health concerns because they have high global prevalence and high mortality rates (*1*). The presence of diabetes in patients with TB has been shown to be associated with poor TB treatment outcomes, such as prolonged times for sputum smear or sputum culture conversion, treatment failure, relapse, and an increased mortality rate (*2*–*11*). Worse treatment outcomes in persons with diabetes might be attributable to several interwoven factors, including immune dysregulation, lower drug exposures, and higher frequency of underlying conditions (*12*–*14*).

The Tuberculosis Trials Consortium Study 31/AIDS Clinical Trials Group A5349 (https://clinicaltrials.gov/study/NCT02410772) was a randomized, controlled, noninferiority phase 3 trial that examined two 4-month treatment-shortening rifapentine containing regimens compared with the standard 6-month control regimen for treatment of drug-susceptible pulmonary TB in adults and adolescents (*15*). One investigational regimen contained rifapentine, moxifloxacin, and isoniazid administered for 4 months plus pyrazinamide administered during the first 2 months (rifapentine/moxifloxacin regimen). The other investigational regimen contained rifapentine plus isoniazid administered for 4 months plus pyrazinamide and ethambutol administered during the first 2 months (rifapentine regimen). The trial demonstrated that the 4-month rifapentine/moxifloxacin regimen had efficacy that was noninferior to that of the control and was safe and well-tolerated. The rifapentine regimen did not meet the noninferiority criteria for efficacy. In that study, the time to stable sputum culture conversion to negative was shorter in participants treated with each of the investigational 4-month regimens compared with the control regimen (*15*).

On the basis of the trial results, the rifapentine/moxifloxacin regimen has been recommended by the World Health Organization (WHO) and Centers for Disease Control and Prevention (CDC) for use for the treatment of drug-susceptible pulmonary tuberculosis (*16*,*17*). Given the importance of the TB and diabetes syndemic, we compared the efficacy and safety across study regimens for the subgroup of participants with diabetes.

Methods

Study Design, Participant Enrollment, Randomization, and Follow-up

Full details of the parent study design, eligibility criteria, enrollment and randomization, safety monitoring, and study outcomes have been previously published (*15*). In brief, we enrolled participants ≥12 years of age with newly diagnosed pulmonary TB during January 2016–October 2018. We randomly assigned enrolled participants in a 1:1:1 ratio to 1 of the 3 regimens (i.e., control, rifapentine, or

Author affiliations: Centers for Disease Control and Prevention, Atlanta, Georgia, USA (E.V. Kurbatova, W.C. Whitworth, L.P. Peddareddy, N.A. Scott, K.E. Bryant, E. Sizemore, W. Carr); University of California– San Francisco Center for Tuberculosis, San Francisco, California, USA (P.P.J. Phillips, R. Savic, P. Nahid); University of Cape Town Lung Institute, Cape Town, South Africa (R. Dawson); Fundação Oswaldo Cruz Insituto Nacional de Infectologia Evandro Chagas, Rio de Janeiro, Brazil (S. Wagner Cardoso); Milton Park Clinical Research Site, Harare, Zimbabwe (W. Samaneka); Audie L. Murphy Veterans Administration Medical Center, San Antonio, Texas, USA (M. Engle); Wits Health Consortium Perinatal HIV Research Unit, Johannesburg, South Africa (Z. Waja); Vanderbilt University Medical Center, Nashville, Tennessee, USA (K.E. Dooley); University of Nebraska Medical Center, Omaha, Nebraska, USA (S. Swindells); Johns Hopkins University School of Medicine, Baltimore, Maryland, USA (R.E. Chaisson); Medical University of South Carolina, Charleston, South Carolina, USA (S.E. Dorman); Vietnam National Tuberculosis Program/University of California–San Francisco Research Collaboration Unit, Hanoi, Vietnam (N.V. Nguyen)

DOI: https://doi.org/10.3201/eid3103.241634

[1]Members of group listed at the end of this article.

[2]Members of group listed at the end of this article.

rifapentine/moxifloxacin). We administered study drugs once daily, by directly observed therapy, on ≥5 of 7 days/week.

The study protocol required diabetes screening before enrollment. Hemoglobin A1c (HgbA1c) was the preferred test. If such testing was not available, we collected readings of fasting blood glucose (defined as no caloric intake for ≥8 hours) or nonfasting blood glucose. A prior diagnosis of diabetes at the time of TB diagnosis was self-reported by the study participants and verified with medical documentation when available. Concomitant medications taken during the study were routinely recorded by the study sites on the concomitant medications case report form and thereafter coded and characterized by using the WHO Drug Dictionary's anatomic therapeutic classification system (*18*). We used the WHO Drug Dictionary's standardized drug groupings to identify class 2 category drugs used in diabetes (*18*).

Because we used different approaches in different sites for capturing data on diabetes, we developed a consensus definition of diabetes. We classified participants as having diabetes if any of the following case selection criteria were met at baseline: a prior diagnosis of diabetes, receipt of insulin or any other diabetes medications, HgbA1c ≥6.5%, fasting blood glucose ≥126 mg/dL, or nonfasting blood glucose ≥200 mg/dL.

All participants had study visits at baseline, at weeks 2, 4, 8, 12, 17, 22, and 26, and at months 9, 12, 15, and 18 after randomization (*15*). During study visits, we evaluated participants for adverse events, collected blood samples for complete blood count and biochemical analyses through week 22, and collected sputum samples for mycobacterial culture through the follow up. We collected adverse event reports through the 18 months of the study follow-up period. We graded adverse events severity on the basis of Common Terminology Criteria for Adverse Events criteria version 4.03 (*19*).

The study was approved by the CDC institutional review board. Each participating institution provided for the review and approval of protocol and its informed consent documents by a local institutional or ethics committee or relied formally on the CDC institutional review board's approval. All participants provided written informed consent. The study data were monitored by a data safety monitoring board coordinated by the study sponsor.

Definitions of Outcomes

The primary efficacy outcome was TB disease–free survival 12 months after randomization. For each participant, we assigned a primary outcome status of favorable, unfavorable, or not assessable, as described previously; we further classified unfavorable outcomes as TB-related or not TB-related (*15*). We defined time to stable culture conversion as the time to the first of 2 consecutive negative sputum cultures without an intervening positive culture.

The primary safety outcome was the proportion of participants with grade ≥3 adverse events during treatment (with onset up to 14 days after the last dose of study medication). Tolerability was a secondary safety outcome and was defined as premature discontinuation of the assigned regimen for any reason other than microbiologic ineligibility.

Analysis Populations

The microbiologically eligible analysis population included participants with culture-confirmed TB without resistance to isoniazid, rifampin, and fluoroquinolones. The assessable analysis population excluded those without an assessable outcome. We considered microbiologically eligible and assessable as primary analysis populations. Secondary analysis populations included participants who completed ≥75% and ≥95% of treatment doses (2 per protocol analysis populations), and all participants randomized (intention to treat). We included all randomized participants that started study treatment in safety analyses.

Statistical Analysis

We used descriptive statistics to summarize the demographic and clinical characteristics among participants with diabetes. For primary efficacy and safety secondary subgroup analysis, we calculated the risk difference between the regimens and their respective 95% CIs.

Pharmacokinetics

We sampled all participants who underwent randomization for pharmacokinetic analysis. All participants had 1–3 sparse pharmacokinetic samples (timepoints were at 0.5, 5, and 24 hours postdose), and at some sites participants had 7 intensive pharmacokinetic sampling (timepoints were at 0.5, 3, 5, 9, 12, and 24 hours postdose), conducted during weeks 2–8 of TB treatment. We determined plasma concentrations of rifapentine, 25-desacetyl-rifapentine, rifampin, isoniazid, pyrazinamide, ethambutol, and moxifloxacin by using validated high-performance liquid chromatography assays. We developed population pharmacokinetic models for each of the 6 drugs, and we calculated the individual area under the concentration time curve from 0–24 hours (AUC_{0-24h}) and maximal

plasma concentration (C_{max}) for each drug (*20*). We compared $AUC_{0–24h}$ and C_{max} for each drug by using *t*-tests by diabetes.

Results

Study Population

Of 2,516 randomized participants in the full study, 181 (7.2%) we classified as having diabetes (Table 1; Appendix Figure, https://wwwnc.cdc.gov/EID/article/31/3/24-1634-App1.pdf). Among 181 participants who were classified as having diabetes, 83 (45.8%) reported a prior diabetes diagnosis at enrollment. Participants with diabetes were from study sites in 12 countries (Brazil, Haiti, India, Kenya, Malawi, Peru, South Africa, Thailand, Uganda, United States, Vietnam, and Zimbabwe). The percentage of participants with diabetes among the enrolled sites was 19.3% (17/88) in sites located in South America, 15.5% (45/290) in Asia, 5.7% (104/1832) in Africa, and 4.9% (15/306) in North America.

We examined baseline demographics and clinical characteristics of participants with diabetes by regimen (Appendix Table 1). Overall, 67.4% were male and 32.6% female, the median age was 46 years, 16 (8.8%) participants were HIV-positive, 132 (72.9%) had baseline cavitation on chest radiograph, and the median body mass index was 21 kg/m^2. A total of 146 (80.1%) of 181 participants had available HgbA1c results at baseline (median value 7%). Sixty-two participants (34.3%) reported receiving medications for diabetes. Among the 83 participants reporting a prior diagnosis of diabetes at baseline, 8 (9.6%) reported having diabetes mellitus type 1 and 73 (88.0%) reported having diabetes mellitus type 2; for 2 (2.4%), the type of diabetes was unknown. Twenty participants were classified as having diabetes on the basis of blood glucose test results only.

Compared with participants without diabetes, participants with diabetes were older (median age 46 vs. 30 years); more often reported Asian race (25.9% vs. 10.3%), White race (8.4% vs. 1.0%), ≥1 race (18.1% vs. 13.0%), or Hispanic ethnicity (13.3% vs. 2.4%); were more often enrolled at study sites in Asia (25.9% vs. 10.1%) or South America (9.6% vs. 3.1%); had higher bodyweight (56 vs. 53 kg); had smaller (<4 cm) cavity size (44.6% vs. 32.2%); and had lower (negative to 1+) smear positivity grade (55.4% vs. 42.2%) (all p<0.005) (Appendix Table 2). The presence of baseline cavitation on chest radiograph was similar (72.9% of participants with diabetes had cavitary disease vs. 72.3% participants without diabetes). We observed a shorter time-to-detection in liquid media in participants with diabetes compared with those without diabetes (8.27 days vs. 8.82 days; p = 0.03).

Efficacy

We included 166 participants with diabetes (91.7%) in the microbiologically eligible analysis population and 155 (85.6%) participants in the assessable analysis population (Figure 1; Appendix Table 3). Among participants in the microbiologically eligible population, unfavorable outcomes occurred in 26.3% of participants in the control regimen and 13.8% of participants in the rifapentine/moxifloxacin regimen, indicating a risk difference from control of –12.5% (95% CI –27.0% to 1.9%). Unfavorable outcomes occurred in 29.4% of participants in the rifapentine regimen, indicating a risk difference from control of 3.1% (95% CI –13.8% to 20.0%). For the assessable analysis population, unfavorable outcomes occurred in 17.6% of participants in the control regimen and 12.3% of participants in the rifapentine/moxifloxacin regimen, indicating an absolute difference from control of –5.4% (95% CI –18.9% to 8.1%). Unfavorable outcomes occurred in 23.4% of participants in the rifapentine regimen, indicating an absolute risk difference from control of 5.8% (95% CI –10.2% to 21.8%). The percentage of participants with TB-related unfavorable outcome was 5.3% in the control arm, 3.4% in the rifapentine/moxifloxacin regimen, and 19.6% in the rifapentine regimen in the microbiologically eligible population and 5.9% in the control arm, 3.5% in the rifapentine/moxifloxacin regimen, and 21.3% in the rifapentine regimen

Table 1. Diabetes status of 181 participants at enrollment, by tuberculosis drug regimen, in a study assessing efficacy and safety of 4-month rifapentine-based tuberculosis treatments in persons with diabetes at sites in 12 countries,* January 2016–October 2018

	No. patients (%)			
Criterion†	Control, n = 59	Rifapentine/moxifloxacin, n = 66	Rifapentine, n = 56	Total, N = 181
Hemoglobin A1c ≥6.5%	49 (83.1)	43 (65.2)	43 (76.8)	135 (74.6)
Prior reported diagnosis of diabetes	31 (52.5)	36 (54.5)	16 (28.6)	83 (45.9)
Receiving antidiabetic drugs‡	22 (37.3)	29 (43.9)	11 (19.6)	62 (34.3)
Fasting blood glucose ≥126 mg/dL	14 (23.7)	18 (27.3)	13 (23.2)	45 (24.9)
Nonfasting blood glucose ≥200 mg/dL	5 (8.5)	13 (19.7)	4 (7.1)	22 (12.2)

*Brazil, Haiti, India, Kenya, Malawi, Peru, South Africa, Thailand, Uganda, United States, Vietnam, and Zimbabwe.
†Diabetes criteria were assessed at enrollment (baseline). Randomized trial participants meeting ≥1 of these criteria at enrollment were included in these analyses.
†World Health Organization Drug Dictionary's standardized drug groupings were used to identify class 2 category drugs used in diabetes (*18*).

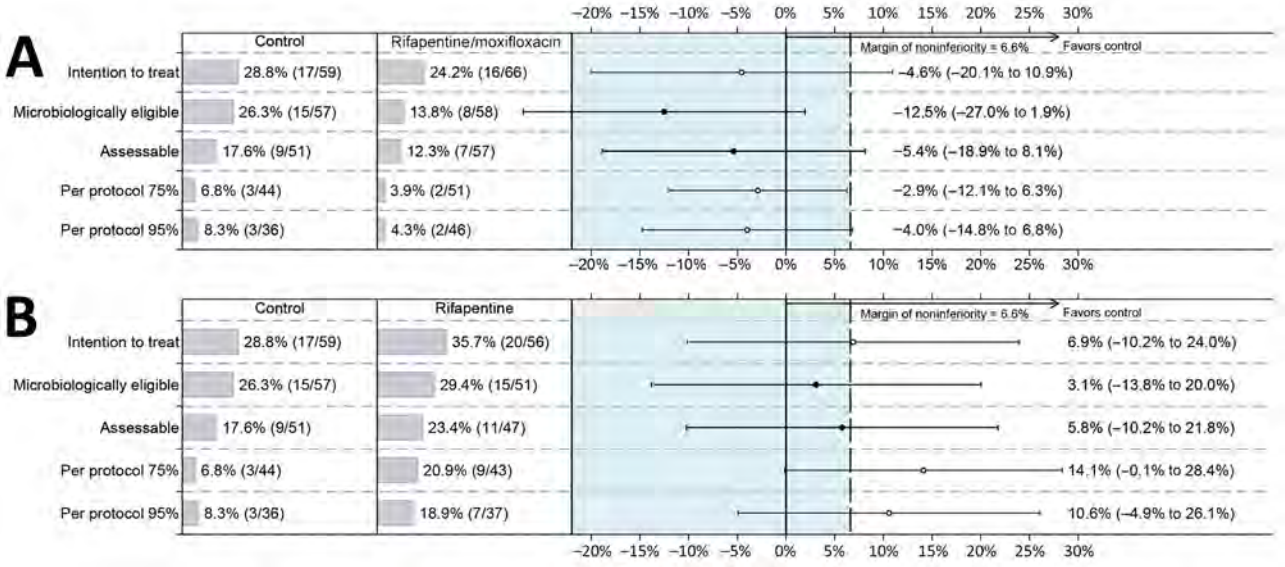

Figure 1. Unadjusted differences in unfavorable outcomes in each analysis population among participants with diabetes in a study assessing efficacy and safety of 4-month rifapentine-based tuberculosis treatments in persons with diabetes at sites in 12 countries (Brazil, Haiti, India, Kenya, Malawi, Peru, South Africa, Thailand, Uganda, United States, Vietnam, and Zimbabwe), January 2016–October 2018. Results of the efficacy results in all 5 analysis populations are shown: rifapentine/moxifloxacin regimen versus control regimen (A) and rifapentine regimen versus control regimen (B). Solid dots indicate primary results, open dots indicate secondary results, and error bars indicate 95% CIs. Dashed vertical line indicates the noninferiority margin of 6.6% for overall results in the randomized trial (*18*).

in the assessable population (Appendix Table 3). We observed no cases of acquired TB drug resistance in participants with diabetes.

In sensitivity analysis limited to the 83 participants with prior diabetes diagnosis, proportions of unfavorable outcome were slightly higher than in analysis of all participants classified as having diabetes, but differences between regimens were similar (Appendix Table 4). Participants with diabetes had higher overall proportion of unfavorable outcomes compared with participants without diabetes (microbiologically eligible population, 22.9% vs. 15.4%; assessable population, 17.4% vs. 11.4%).

Time to Culture Conversion

We found no statistically significant difference in time to stable sputum culture conversion to negative in participants with diabetes treated with each of the experimental regimens compared with the control regimen: rifapentine/moxifloxacin regimen hazard ratio 1.3 (95% CI 0.9–1.9) in liquid media and 1.4 (95% CI 1.0–2.1) on solid media; rifapentine regimen hazard ratio 1.0 (95% CI 0.7–1.5) in liquid media and 1.1 (95% CI 0.8–1.7) on solid media (Figure 2). CIs were wide, and the point estimates of the hazard ratios were similar to those previously reported for the whole study population (*15*). In the microbiologically eligible population in participants with diabetes, culture conversion was achieved by the 8-week follow-up visit in liquid media in 62.3% in the control arm, 84.2% in the rifapentine/moxifloxacin arm, and 75.1% in the rifapentine arm and, on solid media, in 67.3% in the control arm, 91.2% in the rifapentine/moxifloxacin arm, and 85.6% in the rifapentine arm.

Safety and Tolerability

Of 178 participants with diabetes included in the safety analysis population, 24.7% experienced grade ≥3 adverse events during treatment (31.6% in the control arm, 23.1% the in the rifapentine/moxifloxacin arm, and 19.6% in the rifapentine arm) (Table 2). The difference in proportion of participants with grade 3–5 adverse events between the control and rifapentine/moxifloxacin arm was –8.7% (95% CI –24.5 to 7.1), and the difference between the control and rifapentine arm was –11.0% (95% CI –26.7 to 4.8).

Serious adverse events during treatment were experienced by 14% participants with diabetes (17.5% in the control arm, 10.8% in the rifapentine/moxifloxacin arm, and 14.3% in the rifapentine arm) (Table 2). Two deaths (3.5%) occurred in participants in the control arm and none in the rifapentine or rifapentine/moxifloxacin arms. Six participants permanently discontinued study treatment (6.2% the in the rifapentine/moxifloxacin arm and 3.6% in the rifapentine arm) (Table 2). The percentage of participants

that had any transaminase value during treatment of ≥5-fold the upper limit of normal was highest in the rifapentine/moxifloxacin arm (6.2%, 4/65) compared with the rifapentine arm (3.6%, 2/56) and the control arm (3.5%, 2/57) (Table 2). No participants in the control regimen had any transaminase value of ≥10-fold the upper limit of the reference range, compared with 3.6% in the rifapentine arm and 3.1% in rifapentine/moxifloxacin arm. The most frequent adverse events among participants with diabetes were hepatitis (n = 14), hypertension (n = 9), and diabetes mellitus under inadequate control (n = 8) (Appendix Table 5). One case of peripheral neuropathy was reported in a participant in the rifapentine arm (Appendix Table 5).

Discontinuation of assigned treatment for any reason (tolerability) in microbiologically eligible analysis population was 19.3% in the control arm, 13.8% in the rifapentine/moxifloxacin arm, and 13.7% in the rifapentine arm (Table 2). The difference in proportion of discontinuation of assigned treatment for any reason between the control and rifapentine/moxifloxacin arm was –4.9% (95% CI –18.0% to 8.2%), and the difference between the control and rifapentine arm was –4.7% (95% CI –18.4% to 9.0%).

In a sensitivity safety analysis limited to participants with prior diabetes diagnosis, point estimates of grade >3 adverse events were higher than in analysis of all participants classified as having diabetes but showed similar findings across the regimens (Appendix Table 6). The proportion of participants with grade ≥3 adverse events was higher in participants with diabetes compared with those without diabetes (24.7% vs. 16.9%; p = 0.01).

Pharmacokinetics

We compared model-estimated mean AUC_{0-24h} and C_{max} in participants classified with diabetes with those of participants without diabetes for each of the study drugs (Table 3). Rifamycin (rifampin and rifapentine) AUC_{0-24h} and C_{max} were similar among participants with diabetes and participants without diabetes. Participants with diabetes compared with participants without diabetes had lower AUC_{0-24h} values for moxifloxacin and ethambutol and higher C_{max} values for pyrazinamide, but the magnitude of these differences was modest.

Discussion

In this prespecified subgroup analysis among participants with diabetes enrolled in the parent TB study, the efficacy of the 4-month rifapentine/moxifloxacin regimen was comparable to that of the control regimen: 13.8% (8/58) unfavorable outcomes in microbiologically eligible and 12.3% (7/57) unfavorable outcomes in assessable populations, among participants in the 4-month rifapentine/moxifloxacin regimen, compared with 26.3% (15/57) in microbiologically eligible and 17.6% (9/51) in assessable populations, for the control regimen. The 4-month rifapentine regimen without moxifloxacin had more unfavorable outcomes among participants with diabetes (29.4% [15/51]) compared with the control group (23.4% [11/47]). Thus, moxifloxacin was essential for the success of the 4-month regimen, including among persons with diabetes.

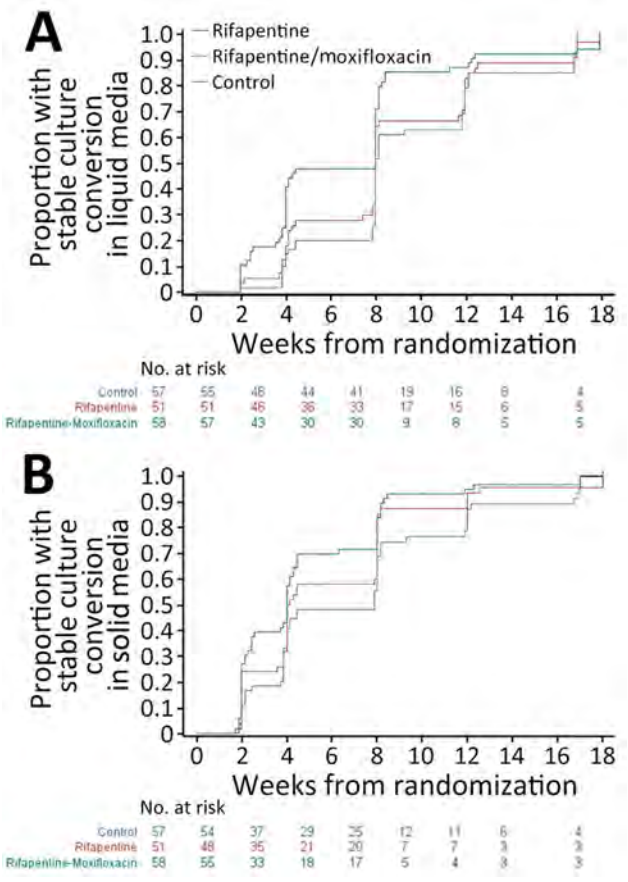

Figure 2. Analysis of time to sputum culture conversion (number of weeks from randomization) in liquid (A) and solid media (B) among participants with diabetes, by tuberculosis drug regimen, in the microbiologically eligible analysis population in a study assessing efficacy and safety of 4-month rifapentine-based tuberculosis treatments in persons with diabetes at sites in 12 countries (Brazil, Haiti, India, Kenya, Malawi, Peru, South Africa, Thailand, Uganda, United States, Vietnam, and Zimbabwe), January 2016–October 2018. Because scheduled study visits did not necessarily occur exactly at 8 weeks, the proportion of participants with culture conversion at 8 weeks is estimated from the Kaplan-Meier estimator at t = 10 weeks. Differences were not statistically significant for any comparisons.

Participants with diabetes had higher overall proportion of unfavorable outcomes compared with participants without diabetes. The presence of severe TB disease, as indicated by baseline cavities on chest radiograph, was similar between participants with and without diabetes (72.9% vs. 72.3%), although some indication of a higher bacillary load was observed in participants with diabetes at baseline because of shorter time-to-detection in liquid media. With regard to the study drug concentrations in participants with and without diabetes, rifamycin exposures unexpectedly were not different between persons with versus without diabetes, and differences in the pharmacokinetics of moxifloxacin, ethambutol, and pyrazinamide were modest. Of note, the proportion with unfavorable outcomes by arm was 14.6% in the control arm and 15.5% in the rifapentine/moxifloxacin arm in the overall study population (*15*) but 26.3% in the control and 13.8% in rifapentine/moxifloxacin arms among people with diabetes. The percentage of participants with TB-related unfavorable outcomes was 5.3% in the control and 3.5% in rifapentine/moxifloxacin arms. Those findings suggest that the high potency of the moxifloxacin and optimally dosed rifapentine in the experimental regimen might have played an important role in successful TB treatment in persons with diabetes.

Among participants with diabetes, both 4-month investigational rifapentine regimens appeared to have comparable (and perhaps even better) safety compared with the 6-month control regimen, including the proportion of participants with grade ≥3 adverse events, serious adverse events, and all-cause discontinuations. Mortality rates during TB treatment were low among participants with diabetes (1.1%), and no deaths were observed in the rifapentine/moxifloxacin and rifapentine arms. Mortality rates were also low in the overall study population (0.6%) (*15*). We did not observe an imbalance

Table 2. Safety and tolerability among 178 participants with diabetes (safety analysis population*), by tuberculosis drug regimen, in a study assessing efficacy and safety of 4-month rifapentine-based tuberculosis treatments in persons with diabetes at sites in 12 countries,† January 2016–October 2018‡

Characteristic	Control, n = 57	Rifapentine/ moxifloxacin, n = 65	Rifapentine, n = 56	Total, N = 178
Primary safety outcome				
Participants with grade ≥3 adverse event, no. (%)	18 (31.6)	15 (23.1)	11 (19.6)	44 (24.7)
Unadjusted risk difference compared with control (95% CI)		–8.7% (–24.5 to 7.1)	–11.0% (–26.7 to 4.8)	
Secondary safety outcome				
Participants with treatment-related grade ≥3 adverse event, no. (%)	4 (7.0)	7 (10.8)	4 (7.1)	15 (8.4)
Unadjusted risk difference compared with control (95% CI)		3.3% (–6.7 to13.2)	0.5% (–9.2 to 10.1)	
Other safety outcomes, no. (%)				
Participants with any serious adverse event during treatment	10 (17.5)	7 (10.8)	8 (14.3)	25 (14.0)
Participants who died§	2 (3.5)	0	0	2 (1.1)
Participants with any adverse event resulting in discontinuation of study treatment¶	0	4 (6.2)	2 (3.6)	6 (3.4)
Participants with any grade ≥3 adverse event during 28 weeks after randomization	18 (31.6)	19 (29.2)	13 (23.2)	50 (28.1)
Liver function test values, no. (%)				
ALT or AST ≥5-fold upper limit of normal#	2 (3.5)	4 (6.2)	2 (3.6)	8 (4.5)
ALT or AST ≥10-fold upper limit of normal	0	2 (3.1)	2 (3.6)	4 (2.2)
Serum total bilirubin ≥3-fold upper limit of normal**	1 (1.8)	5 (7.7)	3 (5.4)	9 (5.1)
ALT or AST ≥3-fold upper limit of normal plus serum total bilirubin ≥2-fold upper limit of normal (Hy's Law)	1 (1.8)	3 (4.6)	2 (3.6)	6 (3.4)
Tolerability among microbiologically eligible analysis population, n = 166				
Discontinuation of assigned treatment for any reason, no. (%)	11/57 (19.3)	8/58 (13.8)	7/51 (13.7)	26/166 (15.7)
Unadjusted risk difference compared with control (95% CI)		–4.9 (–18.0 to 8.2)	–4.7 (–18.4 to 9.0)	

*The safety analysis population included all participants who underwent randomization and received ≥1 dose of the assigned treatment. Safety was assessed during the on-treatment period (the time during which the participants were receiving the study treatment and up to 14 days after the last dose), unless otherwise specified. Adverse events were graded by the site investigators on the basis of the Common Terminology Criteria for Adverse Events criteria, version 4.03 (*19*).
†Brazil, Haiti, India, Kenya, Malawi, Peru, South Africa, Thailand, Uganda, United States, Vietnam, and Zimbabwe.
‡ALT, alanine aminotransferase; AST, aspartate aminotransferase.
§In the control regimen group, 2 participants died from pulmonary tuberculosis.
¶In the rifapentine/moxifloxacin regimen group, 4 participants had hepatitis. In the rifapentine regimen group, 2 participants had hepatitis.
#ALT or AST ≥5-fold upper limit of normal corresponds to grade ≥3.
**Total bilirubin ≥3-fold upper limit of normal corresponds to grade ≥3.

Table 3. $AUC_{0–24h}$ and C_{max} in participants with and without diabetes, by tuberculosis drug, in a study assessing efficacy and safety of 4-month rifapentine-based tuberculosis treatments in persons with diabetes at sites in 12 countries,* January 2016–October 2018†

Value	Diabetes status	No. participants	Mean	SD	p value‡
$AUC_{0–24h}$, μg × h/mL					
Rifapentine	No	1,565	572.44	183.8	0.25
	Yes	122	553.98	169.1	
Moxifloxacin	No	783	25.51	7.0	0.0001
	Yes	66	22.34	6.0	
Rifampin	No	770	53.32	37.5	0.94
	Yes	59	53.69	35.2	
Isoniazid	No	2,335	16.52	12.1	0.51
	Yes	181	15.80	14.5	
Ethambutol	No	1,552	15.93	3.2	0.0002
	Yes	115	14.89	2.8	
Pyrazinamide	No	2,335	346.14	91.5	0.48
	Yes	181	340.77	99.2	
C_{max}, μg/mL					
Rifapentine	No	1,565	33.10	8.7	0.17
	Yes	122	31.97	8.7	
Moxifloxacin	No	783	2.67	0.7	0.23
	Yes	66	2.55	0.8	
Rifampin	No	770	10.20	4.8	0.60
	Yes	59	10.52	4.5	
Isoniazid	No	2,335	2.83	0.9	0.25
	Yes	181	2.75	0.9	
Ethambutol	No	1,552	1.82	0.6	0.43
	Yes	115	1.87	0.6	
Pyrazinamide	No	2,335	30.34	7.2	0.008
	Yes	181	32.05	8.3	

*Brazil, Haiti, India, Kenya, Malawi, Peru, South Africa, Thailand, Uganda, United States, Vietnam, and Zimbabwe.
†$AUC_{0–24h}$, area under the concentration time curve from 0–24 hours; C_{max}, maximal plasma concentration.
‡A *t*-test was used to compare pharmacokinetic parameters between participants classified as having or not having diabetes at enrollment.

across study arms in diabetes-associated adverse events, such as diabetes mellitus under inadequate control, hyperglycemia, diabetic ketoacidosis, diabetic neuropathy, or diabetic retinopathy.

The percentage of participants with grade ≥3 adverse events was higher in participants with diabetes compared with those without diabetes (24.7% [44/178] vs. 16.9% (393/2,328). This increase might be attributable to age-related factors and underlying conditions in the diabetes population, given than participants with diabetes, compared with participants without diabetes, were older (median age 46 years vs. 33 years), and also might be attributable to diabete-related adverse events, such as inadequate glucose control.

A limitation of our study is that testing for diabetes was only required at the time of enrollment, and not all study participants had HgbA1c tests done. Some participants were classified in this analysis to have diabetes solely on the basis of a laboratory test result (hemoglobin or random or fasting glucose test), and we recognize potential for transient hyperglycemia induced by acute illness (stress hyperglycemia) among patients with TB disease (*21*). However, we performed sensitivity analyses limited to participants with a prior established diabetes diagnosis, and efficacy and safety results were consistent. The parent trial was not powered for this subgroup analysis and had relatively few participants with diabetes (*18*). Thus, correspondingly large CIs around point estimates occurred for efficacy and safety outcomes. The prevalence of diabetes was relatively low (7.2%) among trial participants; however, it appears to be similar the comparative age-adjusted diabetes prevalence in the populations of Africa (5.3%) and general global populations (9.8%) (*22*). We noted an imbalance in numbers of participants with diabetes among the regimens; slightly more were randomized in the rifapentine/moxifloxacin arm, given that randomization was stratified by the site, cavitation, and HIV status at the baseline, but not by diabetes. Furthermore, because study protocol did not require blood glucose testing after enrollment, we could not assess the affect of glycemic control on TB treatment outcomes in participants with diabetes.

In conclusion, among participants in a larger TB treatment trial who had diabetes, we found the study's rifapentine/moxifloxacin regimen had improved culture conversion on solid media and a numerically better point estimate for efficacy and similar safety to control. Further studies of TB treatment using the rifapentine/moxifloxacin regimen in larger numbers of patients with diabetes

is needed. Our findings suggest that persons with diabetes are good candidates for the rifapentine/moxifloxacin regimen.

Members of the AIDS Clinical Trials Group A5349: TASK, South Africa; University of Cape Town Lung Institute, South Africa; Les Centre GHESKIO INLR, Haiti; Parirenyatwa Clinical Research Site, Zimbabwe; South African Tuberculosis Vaccine Initiative, South Africa; Wits Helen Joseph Clinical Research Site Department of Medicine, South Africa; Les Centre GHESKIO IMIS, Haiti; Soweto ACTG Clinical Research Site, South Africa; Byramjee Jeejeebhoy Medical College, India; University of North Carolina Project Tidziwe Centre, Malawi; Kisumu Clinical Research Site, Kenya; Instituto Nacional de Pesquisa Clinica Evandro Chagas, Brazil; Blantyre Clinical Research Site/Johns Hopkins Research Project, Malawi; Family Clinical Research Unit (FAMCRU), South Africa; Durban International Clinical Research Site, South Africa; Moi University Clinical Research Site, Kenya; San Miguel Clinical Research Site, Peru; Asociacion Civil Impacta Salud y Educacion, Peru; Joint Clinical Research Center, Kampala Clinical Research Site, Uganda; Kenya Medical Research Institute/Walter Reed Project Clinical Research Center, Kenya; The Thai Red Cross AIDS Research Centre, Thailand; Chiang Mai University HIV Treatment Clinical Research Site, Thailand; Hospital Conceicao Porto Alegre, Brazil; and University of California San Francisco Clinical Research Site, USA.

Members of the Tuberculosis Trials Consortium Study 31: Uganda-Case Western Reserve University Research Collaboration, Uganda; Vietnam National Tuberculosis Program/University of California San Francisco Research Collaboration, Vietnam; Wits Health Consortium Perinatal HIV Research Unit (PHRU), South Africa; Tuberculosis and Chest Service of Hong Kong, China; San Antonio Veterans Administration Medical Center, USA; Universidad Peruana Cayetano Heredia, Peru; University of North Texas Health Science Center, USA; Columbia University, USA; Austin Tuberculosis Clinic, USA; and Baylor College of Medicine and Affiliated Hospitals/VA, USA.

Acknowledgments

We are grateful to the study participants who contributed their time to this trial and site and local tuberculosis program staff who assisted in the clinical management of study participants. Support from Andrew A. Vernon, Lara Hosey, Richard Hafner, Kristine Coughlin, Akbar Shahkolahi, and Christopher Lane is also appreciated. We thank Phil LoBue, Carla Winston, and Jonathan Mermin for continued support of the Tuberculosis Trials Consortium Study 31 within the Centers for Disease Control and Prevention. We thank Westat, Inc., and PPD, Inc., for onsite monitoring.

Funding support for this trial was provided by the Centers for Disease Control and Prevention, National Center for HIV, Viral Hepatitis, STD, and Tuberculosis Prevention, Division of Tuberculosis Elimination (contract nos. 200-2009-32582, 200-2009-32593, 200-2009-32594, 200-2009-32589, 200-2009-32597, 200-2009-32598, 75D30119C06702, 75D30119C06701, 75D30119C06703, 75D30119C06222, 75D30119C06225, and 5D30119C06010) and by the National Institute of Allergy and Infectious Diseases of the National Institutes of Health (award nos. UM1 AI068634, UM1 AI068636, and UM1 AI106701).

Sanofi donated rifapentine and all other study drugs, supported shipping of study drugs to all sites, and provided funding support for pharmacokinetic testing and preparation of the final clinical study in this collaborative study.

Authors contributions: study conception and design (E.V.K., L.P.P., P.J.P.P., N.A.S., S.S., R.E.C., S.E.D., and P.N.); data collection (E.V.K., W.C.W., L.P.P., N.A.S., K.E.B., N.V.N., R.D., S.W.C., W.S., M.W., Z.W., E.S., W.C., S.S., R.E.C., S.E.D., and P.N.); data analysis (W.C.W., L.P.P., P.J.P.P., N.A.S., and K.E.B.); data interpretation (E.V.K., W.C.W., L.P.P., P.J.P.P., N.A.S., K.E.B., W.C., K.E.D., S.S., R.E.C., S.E.D., and P.N.); drafting of the initial manuscript (E.V.K., W.C.W., L.P.P., and P.J.P.P.); critical review of the final draft of the manuscript (E.V.K., W.C.W., L.P.P., P.J.P.P., N.A.S., K.E.B., N.V.N., R.D., S.W.C., W.S., M.W., Z.W., E.S., W.C., K.E.D., S.S., R.E.C., S.E.D., and P.N.); and access and verification of underlying data (W.C.W., L.P.P., P.J.P.P., N.A.S., and K.E.B.).

The authorship team members have declared any potential conflicts of interest with respect to the research, authorship, or publication of this article. Sanofi commercial interests did not influence the study design; the collection, analysis, or interpretation of data; the preparation of this manuscript; or the decision to submit this manuscript for publication. A Sanofi technical expert served on the protocol team.

About the Author

Dr. Kurbatova is health scientist in the Clinical Research Branch, Division of Tuberculosis Elimination, National Center for HIV, Viral Hepatitis, STD, and Tuberculosis Prevention, Centers for Disease Control and Prevention. Her primary research interests include tuberculosis epidemiology and treatment shortening.

References

1. World Health Organization. Global tuberculosis report 2023. 2023 Nov 7 [cited 2024 Aug 2]. https://www.who.int/teams/global-tuberculosis-programme/tb-reports/global-tuberculosis-report-2023
2. Baker MA, Harries AD, Jeon CY, Hart JE, Kapur A, Lönnroth K, et al. The impact of diabetes on tuberculosis treatment outcomes: a systematic review. BMC Med. 2011;9:81. https://doi.org/10.1186/1741-7015-9-81
3. Alisjahbana B, Sahiratmadja E, Nelwan EJ, Purwa AM, Ahmad Y, Ottenhoff TH, et al. The effect of type 2 diabetes mellitus on the presentation and treatment response of pulmonary tuberculosis. Clin Infect Dis. 2007;45:428–35. https://doi.org/10.1086/519841
4. Salindri AD, Kipiani M, Kempker RR, Gandhi NR, Darchia L, Tukvadze N, et al. Diabetes reduces the rate of sputum culture conversion in patients with newly diagnosed multidrug-resistant tuberculosis. Open Forum Infect Dis. 2016;3:ofw126. https://doi.org/10.1093/ofid/ofw126
5. Workneh MH, Bjune GA, Yimer SA. Diabetes mellitus is associated with increased mortality during tuberculosis treatment: a prospective cohort study among tuberculosis patients in South-Eastern Amahra Region, Ethiopia. Infect Dis Poverty. 2016;5:22. https://doi.org/10.1186/s40249-016-0115-z
6. Ma Y, Huang ML, Li T, Du J, Shu W, Xie SH, et al. Role of diabetes mellitus on treatment effects in drug-susceptible initial pulmonary tuberculosis patients in China. Biomed Environ Sci. 2017;30:671–5.
7. Güler M, Unsal E, Dursun B, Aydln O, Capan N. Factors influencing sputum smear and culture conversion time among patients with new case pulmonary tuberculosis. Int J Clin Pract. 2007;61:231–5. https://doi.org/10.1111/j.1742-1241.2006.01131.x
8. Dooley KE, Chaisson RE. Tuberculosis and diabetes mellitus: convergence of two epidemics. Lancet Infect Dis. 2009;9:737–46. https://doi.org/10.1016/S1473-3099(09)70282-8
9. Jiménez-Corona ME, Cruz-Hervert LP, García-García L, Ferreyra-Reyes L, Delgado-Sánchez G, Bobadilla-Del-Valle M, et al. Association of diabetes and tuberculosis: impact on treatment and post-treatment outcomes. Thorax. 2013;68:214–20. https://doi.org/10.1136/thoraxjnl-2012-201756
10. Restrepo BI, Schlesinger LS. Impact of diabetes on the natural history of tuberculosis. Diabetes Res Clin Pract. 2014;106:191–9. https://doi.org/10.1016/j.diabres.2014.06.011
11. Hodgson K, Morris J, Bridson T, Govan B, Rush C, Ketheesan N. Immunological mechanisms contributing to the double burden of diabetes and intracellular bacterial infections. Immunology. 2015;144:171–85. https://doi.org/10.1111/imm.12394
12. Martinez N, Smulan LJ, Jameson ML, Smith CM, Cavallo K, Bellerose M, et al. Glycerol contributes to tuberculosis susceptibility in male mice with type 2 diabetes. Nat Commun. 2023;14:5840. https://doi.org/10.1038/s41467-023-41519-9
13. Alfarisi O, Mave V, Gaikwad S, Sahasrabudhe T, Ramachandran G, Kumar H, et al. Effect of diabetes mellitus on the pharmacokinetics and pharmacodynamics of tuberculosis treatment. Antimicrob Agents Chemother. 2018;62:e01383-18. https://doi.org/10.1128/AAC.01383-18
14. Chiang CY, Bai KJ, Lin HH, Chien ST, Lee JJ, Enarson DA, et al. The influence of diabetes, glycemic control, and diabetes-related comorbidities on pulmonary tuberculosis. PLoS One. 2015;10:e0121698. https://doi.org/10.1371/journal.pone.0121698
15. Dorman SE, Nahid P, Kurbatova EV, Phillips PPJ, Bryant K, Dooley KE, et al.; AIDS Clinical Trials Group; Tuberculosis Trials Consortium. Four-month rifapentine regimens with or without moxifloxacin for tuberculosis. N Engl J Med. 2021;384:1705–18. https://doi.org/10.1056/NEJMoa2033400
16. Carr W, Kurbatova E, Starks A, Goswami N, Allen L, Winston C. Interim guidance: 4-month rifapentine-moxifloxacin regimen for the treatment of drug-susceptible pulmonary tuberculosis—United States, 2022. MMWR Morb Mortal Wkly Rep. 2022;71:285–9. https://doi.org/10.15585/mmwr.mm7108a1
17. World Health Organization. Treatment of drug-susceptible tuberculosis: rapid communication. 2021 Jun 14 [cited 2024 Aug 2]. https://www.who.int/publications/i/item/9789240028678
18. Lagerlund O, Strese S, Fladvad M, Lindquist M. WHODrug: a global, validated and updated dictionary for medicinal information. Ther Innov Regul Sci. 2020;54:1116–22. https://doi.org/10.1007/s43441-020-00130-6
19. National Clinical Trials Network. Common Terminology Criteria for Adverse Events (CTCAE). 2021 Apr 19 [cited 2024 Aug 2]. https://ctep.cancer.gov/protocoldevelopment/electronic_applications/ctc.htm
20. US Food and Drug Administration. Population pharmacokinetics: guidance for industry. 2022 Feb 3 [cited 2024 Aug 2]. https://www.fda.gov/regulatory-information/search-fda-guidance-documents/population-pharmacokinetics
21. Magee MJ, Salindri AD, Kyaw NTT, Auld SC, Haw JS, Umpierrez GE. Stress hyperglycemia in patients with tuberculosis disease: epidemiology and clinical implications. Curr Diab Rep. 2018;18:71. https://doi.org/10.1007/s11892-018-1036-y
22. International Diabetes Federation. International Diabetes Federation diabetes atlas. 10th edition. 2021 [cited 2024 Aug 2]. https://diabetesatlas.org/atlas/tenth-edition

Address for correspondence: Ekaterina Kurbatova, Centers for Disease Control and Prevention, 1600 Clifton Rd NE, Mailstop US 12-4, Atlanta, GA 30329-4018, USA; email: ies3@cdc.gov

Influenza A(H5N1) Immune Response among Ferrets with Influenza A(H1N1)pdm09 Immunity

Valerie Le Sage, Bailee D. Werner, Grace A. Merrbach, Sarah E. Petnuch, Aoife K. O'Connell, Holly C. Simmons, Kevin R. McCarthy, Douglas S. Reed, Louise H. Moncla, Disha Bhavsar, Florian Krammer, Nicholas A. Crossland, Anita K. McElroy, W. Paul Duprex, Seema S. Lakdawala

The emergence of highly pathogenic avian influenza A(H5N1) virus in dairy cattle herds across the United States in 2024 caused several human infections. Understanding the risk for spillover infections into humans is crucial for protecting public health. We investigated whether immunity from influenza A(H1N1) pdm09 (pH1N1) virus would provide protection from death and severe clinical disease among ferrets intranasally infected with H5N1 virus from dairy cows from the 2024 outbreak. We observed differential tissue tropism among pH1N1-immune ferrets. pH1N1-immune ferrets also had little H5N1 viral dissemination to organs outside the respiratory tract and much less H5N1 virus in nasal secretions and the respiratory tract than naive ferrets. In addition, ferrets with pH1N1 immunity produced antibodies that cross-reacted with H5N1 neuraminidase protein. Taken together, our results suggest that humans with immunity to human seasonal influenza viruses may experience milder disease from the 2024 influenza A(H5N1) virus strain.

In March 2024, an outbreak of highly pathogenic avian influenza A(H5N1) clade 2.3.4.4b virus was identified in dairy cattle herds in Texas, USA, and then spread to >400 herds in ≥15 states (*1*). That spread emphasized the need to monitor H5N1 clade 2.3.4.4b for pandemic potential. H5N1 clade 2.3.4.4b virus infections of various mammals resulted in severe disease and death, including among foxes, mink, cats, cetaceans, pinnipeds, and cows (*2*,*3*). In early April 2024, a case of human infection was identified in Texas (*4*), and more human H5N1 cases were identified among workers associated with poultry or dairy farms in California, Missouri, Michigan, Colorado, and Washington (*5*). In August 2024, human infections in the United States were characterized by conjunctivitis and mild respiratory symptoms, and most did not require hospitalization (*5*).

Most persons experience their first influenza virus infection by 5 years of age (*6*). Thus, current H5N1 human infections are occurring among persons with prior influenza A virus (IAV) immunity. The reduced disease severity among persons infected with the 2024 H5N1 virus might be driven by immunity to human seasonal influenza viruses. Statistical modeling analysis of known human cases of H5N1 and H7N9 infection indicated that childhood hemagglutinin (HA) imprinting may provide lifelong protection against severe infection and death from those viruses (*7*). Specifically, previous research has suggested that immune imprinting with human seasonal H1N1 or H2N2 influenza viruses would reduce disease severity to H5N1 because H5, H1, and H2 share a similar group 1 HA stalk domain (*7*). Despite the potential effects such immunity could have to reduce H5N1 replication and pathogenesis, risk assessment of the 2024 H5N1 outbreak strain has only been performed in immunologically naive ferrets (*8*). We investigated whether ferrets with H1N1 immunity would experience reduced virus replication and disease severity from dairy cow H5N1 virus.

Author affiliations: University of Pittsburgh, Pittsburgh, Pennsylvania, USA (V. Le Sage, B.D. Werner, G.A. Merrbach, S.E. Petnuch, H.C. Simmons, K.R. McCarthy, D.S. Reed, L.H. Moncla, A.K. McElroy, W.P. Duprex); Boston University, Boston, Massachusetts, USA (A.K. O'Connell, N.A. Crossland); Icahn School of Medicine at Mount Sinai, New York, New York, USA (D. Bhavsar, F. Krammer); Medical University of Vienna, Vienna, Austria (F. Krammer); Boston University Chobanian & Avedisian School of Medicine, Boston, Massachusetts, USA (N.A. Crossland); Emory University, Atlanta, Georgia, USA (S.S. Lakdawala)

DOI: https://doi.org/10.3201/eid3103.241485

Methods

Cell Preparation

We obtained MDCK cells and human 293T cells from the American Type Culture Collection (https://www.atcc.org). We maintained the MDCK cells in minimum essential medium and the 293T cells in Dulbecco Modified Eagle Medium. We supplemented both cell media with 10% fetal bovine serum, 2 mmol L-glutamine, 100 U/mL penicillin, and 100 mg/mL streptomycin. We incubated cells at 37°C with 5% carbon dioxide (CO_2). We obtained human 293F cells Medium (Thermo Fisher Scientific, https://www.fishersci.com) and maintained cells at 37°C with 5%–8% CO_2 in FreeStyle 293 Expression (Thermo Fisher Scientific) supplemented with 100 U/mL penicillin and 100 mg/mL streptomycin.

Virus Generation

We generated A/dairy cattle/Texas/24-008749-001/2024(H5N1) (GISAID accession no. EPI_ISL_19014384) virus from 8 plasmid reverse genetics system and propagated in MDCK cells (Appendix, https://wwwnc.cdc.gov/EID/article/31/3/24-1485-App1.pdf). We determined noncoding regions for each segment from consensus alignment of H5N1 strains from the 2.3.4.4b clade viruses.

Human Subjects Research and Ethics Statement

As part of this research, we assessed human serum samples for cross-reactive antibodies to H5N1 virus (Figure 1). The University of Pittsburgh institutional review board approved collection of serum samples from healthy adult donors who provided written informed consent for their samples to be used in infectious disease research (protocol approval no. STUDY20030228). All participants self-reported age, sex, ethnicity, and race.

Ferret Infections

We screened ferrets before this study to ensure no influenza immunity before they arrived at University of Pittsburgh (Appendix). Using our previously developed preimmune ferret model (*9*,*10*), we infected 5 ferrets with recombinant influenza A(H1N1)pdm09 (pH1N1) virus by using the A/California/07/2009 strain. We infected ferrets either experimentally by intranasal introduction of A/California/07/2009 or naturally by exposure to an experimentally infected ferret in a controlled transmission study conducted at the University of Pittsburgh.

pH1N1-immune animals then recovered from acquired infections and were housed for 98 days before we infected 5 pH1N1-immune and 5 immunologically naive ferrets with A/dairy cattle/Texas/24-008749-001/2024(H5N1), termed cow/Tx/24 H5N1. We intranasally inoculated all 10 ferrets with 10^4 50% tissue culture infectious dose ($TCID_{50}$) cow/Tx/24 H5N1 virus in 500 µL of L-15 media (250 µL in each nostril). We monitored ferrets daily during the postinoculation period and recorded clinical signs, including weight loss, temperature, activity, sneezing,

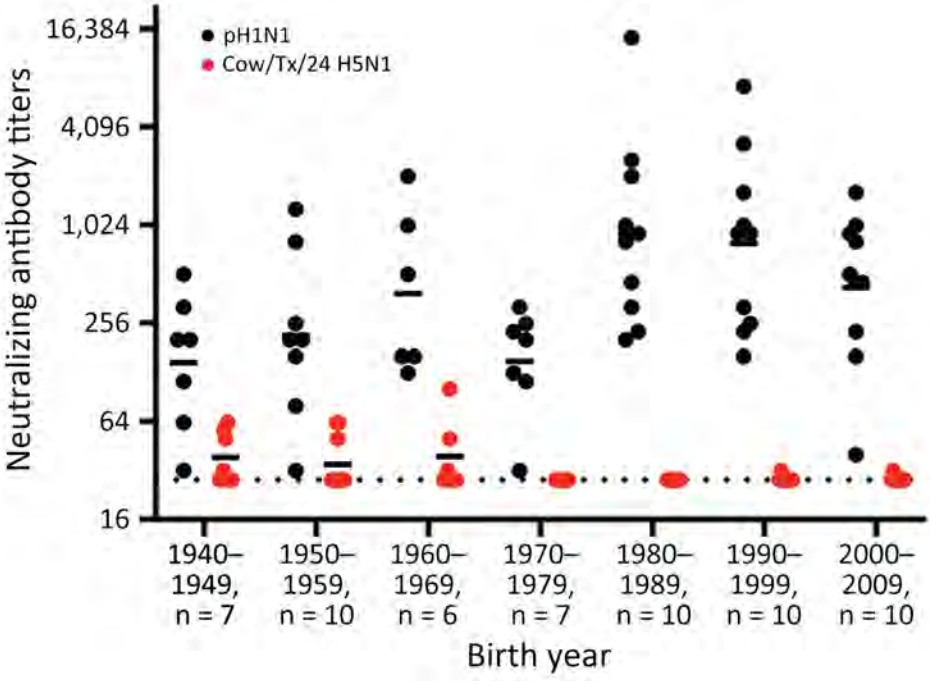

Figure 1. Neutralizing antibody titers in human serum used in a study of influenza A(H5N1) immune response among ferrets with pH1N1 immunity. We used serum samples collected from healthy persons during 2020–2021 with birth years ranging from 1940–2009. We tested serum for neutralizing antibodies against pH1N1 virus and 2024 outbreak virus A/dairy cattle/Texas/24-008749-001/2024(H5N1). Each dot represents the neutralizing antibody titer of a single person to neutralize 100 $TCID_{50}$ of pH1N1 or cow/Tx/24 H5N1 on Madin-Darby canine kidney cells. Solid horizontal lines indicate the geometric mean value each birth decade; dotted line represents the limit of detection for the assay. cow/Tx/24, A/dairy cattle/Texas/24-008749-001/2024(H5N1); pH1N1, influenza A(H1N1)pdm09; $TCID_{50}$, 50% tissue culture infectious dose.

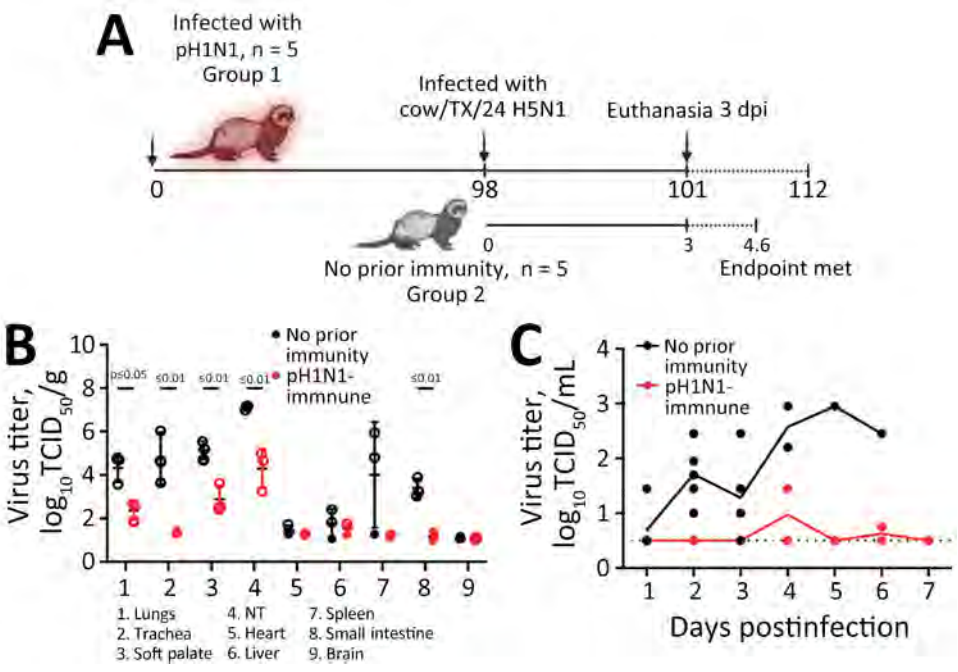

Figure 2. Infection timeline and virus replication titers in a study of influenza A(H5N1) immune response among ferrets with pH1N1 immunity. A) Schematic of experimental timeline for 2 groups of ferrets intranasally infected with H5N1 strain cow/Tx/24. Group 1 (n = 5) was previously infected with pH1N1 98 days before H5N1 infection and group 2 (n = 5) was immunologically naive. At 3 dpi, 3 animals from each group were humanely euthanized. We monitored the remaining ferrets from groups 1 and 2 until 14 dpi or until the endpoint criteria were reached. Schematic was created in BioRender (https://www.biorender.com). B, C) Viral titers from ferret tissues (B) and nasal secretions (C). B) Tissues were collected from H5N1-infected ferrets without (n = 3) and with (n = 3) pH1N1 immunity at 3 days postinfection. Unpaired *t*-test analysis was used to determine statistically significant ($p \leq 0.05$) differences: lungs, p = 0.0124; trachea, p<0.008; soft palate, p = 0.0072; nasal turbinate, p = 0.0061; small intestine, p = 0.0014. C) Nasal wash samples were collected from H5N1-infected ferrets without (n = 5) and with (n = 5) pH1N1 immunity on the indicated dpi: 1–3 dpi, n = 5 from each group; 4 dpi, n = 2 from each group; 5 and 6 dpi, n = 2 for immune group and n = 1 from the naive group; 7 dpi, n = 2 from the immune group . Each circle represents a single ferret. Open circles indicate values above the limit of detection. Horizontal bars indicate means; whiskers indicate SDs of viral titers; dashed line represents the limit of detection. cow/Tx/24, A/dairy cattle/Texas/24-008749-001/2024(H5N1); dpi, days postinfection; NT, nasal turbinate; pH1N1, influenza A(H1N1)pdm09; $TCID_{50}$, 50% tissue culture infectious dose.

coughing, and nasal discharge, as previously described (*11*). For animals that reached ≥10% weight loss, we provided urgent care diet cat food 2×/day to entice eating.

Humane endpoints for this study included bodyweight loss >20% (relative to weight at challenge) and a prolonged inactivity as assessed by trained veterinary staff. Three animals from each group were euthanized 3 days postinoculation (dpi) for tissue titration; the other 2 ferrets from each group were kept for ≥14 days or until they reached endpoint criteria (Figure 2, panel A).

Ferret Sample Collection and Preparation

We collected nasal wash from each ferret at 1–7 days postinoculation (dpi). To examine whether pH1N1 altered cow/Tx/24 H5N1 tissue tropism, we euthanized 3 intranasally infected ferrets from each group at 3 dpi to collect tissues (lungs, trachea, soft palate, nasal turbinates, heart, liver, spleen, small intestine, and brain) and determined virus titers (Appendix).

We titered nasal wash and organ samples in MDCK cell cultures. We made 10-fold serial dilutions and inoculated dilutions on 96-well plates by using 4 wells/dilution. We observed the MDCK cells at 4 dpi for cytopathic effect (CPE). We calculated viral titers by using the Reed and Muench method (*12*) and expressed the results as $\log_{10}$ $TCID_{50}$/mL.

Animal Ethics Statement

Ferret experiments were conducted in Biosecurity Level 2 and 3 facilities at the University of Pittsburgh in compliance with the guidelines of the Institutional Animal Care and Use Committee (approved protocol nos. 22061230 and 21089461). For all nasal washes and survival blood draws, animals were sedated with isoflurane following approved methods. Ketamine and xylazine were used for sedation for all terminal procedures, followed by cardiac administration of euthanasia solution. Approved University of Pittsburgh Division of Laboratory Animal Resources staff administered euthanasia. H5N1 studies were performed in accordance with the University of Pittsburgh select agent permit no. 20230320-074008.

Microneutralization Assays

We heat inactivated human and ferret serum samples at 56°C for 30 minutes. We determined the titer

of neutralizing antibodies by incubating 2-fold serial dilutions of the heat-inactivated serum samples with $10^{3.3}$ $TCID_{50}$ of influenza virus for 1 hour at room temperature with continuous rocking. We added media with tosyl phenylalanyl chloromethyl ketone–treated trypsin to 96-well plates with confluent MDCKs before adding the virus-serum mixture. After 4 days, we determined the CPE and expressed the neutralizing antibody titer as the reciprocal of the highest dilution of serum required to completely neutralize the infectivity of each virus on MDCK cells. We calculated the concentration of antibody required to neutralize 100 $TCID_{50}$ of virus on the basis of the neutralizing titer dilution divided by the initial dilution factor, multiplied by the antibody concentration.

Histology

We stained respiratory tissue sections collected from euthanized ferrets with hematoxylin and eosin for histopathologic analysis or influenza A nucleoprotein for immunohistochemistry (Appendix). We initially examined the prepared slides blinded to experimental groups to eliminate observer bias, then by unblinding for figure preparation. We developed an ordinal scoring system to summarize the histopathologic and immunohistochemical findings: 0, not observed; 1 (mild), <10% of parenchyma impacted; 2 (moderate), from 10%–25% of parenchyma affected; and 3 (severe), 25%–50% of parenchyma affected.

ELISA

We adhered 500 ng of recombinant HA full-length soluble ectodomains or recombinant neuraminidase (NA) to high-capacity binding 96 well-plates (Corning, https://www.corning.com) overnight in phosphate-buffered saline (PBS) at 4°C (Appendix). We then washed the HA- or NA-coated plates with a 0.05% vol/vol PBS-Tween-20 (PBS-T) buffer and then blocked with PBS-T containing 2% bovine serum albumin for 1 hour at room temperature. We removed the blocking solution and added 2-fold dilutions of ferret serum in blocking solution to the wells. We then incubated the plates for 1 hour at room temperature. We removed the primary antibody solution and washed the plates 3 times with PBS-T. We added a secondary Goat Anti-Ferret IgG H&L (HRP) (Abcam, https://www.abcam.com) diluted 1:10,000 in blocking solution to the wells and incubated for 30 minutes at room temperature. We then washed the plates 3 times with PBS-T. We developed the plates by using 150 µL 1-Step TMB Substrate (Thermo Fisher Scientific). After a brief incubation at room temperature, we stopped HRP reactions by adding 100 µL of 4N sulfuric acid solution. We read the plates by using a SpectraMax 340PC384 Microplate Reader (Molecular Devices, https://www.moleculardevices.com) at 450 nm. We performed all measurements in duplicate. We then graphed the average of the 2 measurements for each ferret sample as the mean absorbance at 450 nm by using Prism software version 9.0 (GraphPad, https://www.graphpad.com).

Results

Neutralizing Antibody Levels in Humans

H5N1 IAVs have not circulated widely in the human population, and major immunity against those strains likely does not exist. To assess whether any cross-reactive antibodies existed in the human population, we conducted neutralization assays with human serum against cow/Tx/24 H5N1 and pH1N1, and results revealed high levels of circulating antibodies against pH1N1 in persons of all ages (Figure 1). Of note, 12 of the 60 serum samples tested had detectable levels of cross-neutralizing antibodies against cow/Tx/24 H5N1 that were above the limit of detection. Of the 12 serum samples with cross-neutralizing antibodies, 10 were collected from persons born in the 1940s, 1950s, and 1960s and 2 were from persons born after 1970 (Figure 1), which correlates well with H5 cross-reactive antibodies in older persons (*13*). Those data suggests persons born after 1980 could be more susceptible to infection with H5N1 virus from dairy cows. We do not know the ages of persons with documented H5N1 infections since 2022.

Effect of pH1N1 Immunity on Viral Titers and Dissemination

We sought to extend our prior work (*9*,*10*) and examine the role of pH1N1 immunity on dairy cow H5N1 infection severity and replication in the ferret model. In ferrets without pH1N1 immunity, cow/Tx/24 H5N1 resulted in high viral loads in the respiratory tissues and produced a systemic infection, as observed by virus detection in the heart, liver, spleen, and intestine (Figure 2, panel B). In contrast, ferrets with pH1N1 immunity exhibited lower levels of virus replication that were limited to the respiratory tract and were statistically significant ($p \leq 0.01$) (Figure 2, panel B). The lack of virus in the brain of ferrets without pH1N1 immunity at 3 dpi is consistent with data reported from other groups (*8*).

Nasal wash titers were also drastically different between the 2 groups of ferrets. Virus was consistently detected over time in the nasal washes of

ferrets without prior immunity, whereas most pH1N1-immune ferrets had no detectable cow/Tx/24 H5N1 virus in nasal washes; the exceptions were 1 ferret at 4 dpi and a different ferret at 6 dpi (Figure 2, panel C). Of note, we detected virus in the nasal turbinates of the pH1N1-immune ferrets euthanized at 3 dpi, despite a lack of virus in the nasal wash; however, virus levels were much lower than among animals without prior immunity (Figure 2, panels B, C). That difference could be attributed to the methods of sample collection. Nasal washes are performed by pushing fluid through 1 nostril and collecting the liquid from the other nostril, which samples the tip of the turbinates. In contrast, the entire nasal turbinate tissue is collected at the time of necropsy and homogenized to collect any released and cell associated viruses; thus, turbinates would be expected to have higher virus levels.

Histopathological analysis of lung tissues harvested at 3 dpi indicated both groups of ferrets had similar lung injury (Figure 3, panel A). However, more detailed examination of the data indicated that ferrets with pH1N1 immunity had more residual mononuclear perivascular infiltrates and bronchus-associated lymphoid tissue (BALT) hyperplasia (Figure 3, panels B, C), which may play a role in preventing development of severe clinical disease. Immunohistochemistry with IAV nucleoprotein (NP) indicated that pH1N1-immune ferrets had limited NP-positive cells in the trachea, mainstem bronchi, and bronchioles than ferrets without prior immunity (Figure 4). In pH1N1-immune ferrets with areas of BALT hyperplasia, we detected limited viral antigen and necrotizing bronchointerstitial pneumonia (Figure 4, panel C). Furthermore, we observed IAV NP antigen in alveolar pneumocytes (both type 1 and 2) in ferrets irrespective of immune status (Figure 4, panel C). Those findings are in contrast to pH1N1 infection in ferrets, in which pH1N1 virus infected epithelial cells in the large and small airways (*14*–*18*).

Examination of the tracheobronchial lymph node histology revealed more lymphoid depletion, necrosis, fibrin, and edema in ferrets without pH1N1 immunity compared with pH1N1-immune ferrets (Figure 5). Overall, those data indicated that resident lymphoid changes in ferrets with pH1N1 immunity may have reduced cow/Tx/24 H5N1 replication and dissemination to other organs, which could affect disease severity.

Effects of pH1N1 Immunity on H5N1 Mortality and Severe Disease

We followed H5N1-infected ferrets with (n = 2) and without (n = 2) pH1N1 immunity to 14 dpi to examine death outcomes (Figure 6, panel A). The 2 animals with pH1N1 immunity survived challenge with cow/Tx/24 H5N1 virus, whereas the 2 immunologically naive ferrets were humanly euthanized at 4 dpi and 6 dpi because severe clinical signs developed (Figure 6, panel A). We observed that ferrets with pH1N1 immunity had ≤5% weight loss, whereas naive ferrets experienced ≥10% weight loss (Figure 6, panel B). Assessment of clinical signs, such as diarrhea, fever, nasal discharge and playfulness, revealed more severe clinical signs in all immunologically naive animals than among those with prior pH1N1 immunity (Figure 7).

Surviving ferrets with pH1N1 immunity seroconverted against cow/Tx/24 H5N1, albeit to low microneutralization titers of 20 and 80 (Table). In addition, neither of the 2 pH1N1-immune ferrets had a >4-fold rise in pH1N1 antibodies after cow/Tx/24 H5N1 challenge (Table). Taken together, those data indicated that pH1N1 immunity protects ferrets from severe clinical disease and death caused by cow/Tx/24 H5N1 infection.

Cross-Reactive NA Antibody Production

IAV infection induces antibody responses against HA and NA proteins that can provide varying levels of

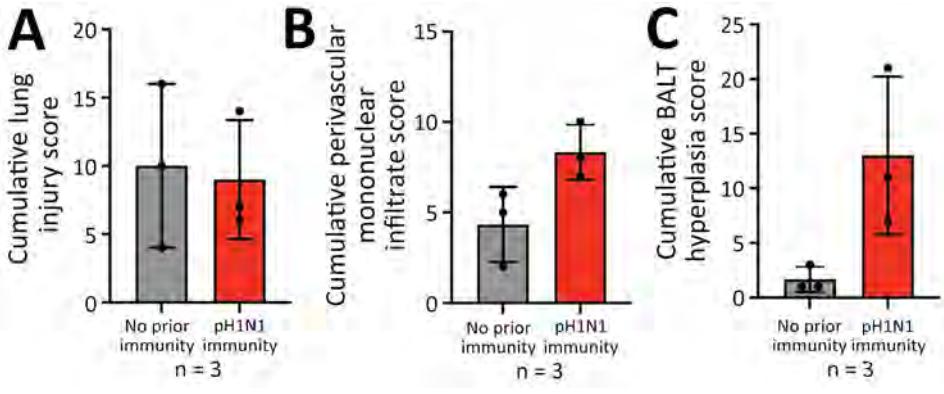

Figure 3. Lung infiltrates measured in a study of influenza A(H5N1) immune response among ferrets with pH1N1 immunity. We blindly scored 5 lung sections for ferrets with no prior or existing pH1N1 immunity for lung injury (A), perivascular mononuclear infiltrates (B), and BALT hyperplasia (C). Each dot represents the cumulative score of the 5 sections for each ferret. Bar values indicate means; whiskers indicate SDs. BALT, bronchus-associated lymphoid tissue; pH1N1, influenza A(H1N1)pdm09.

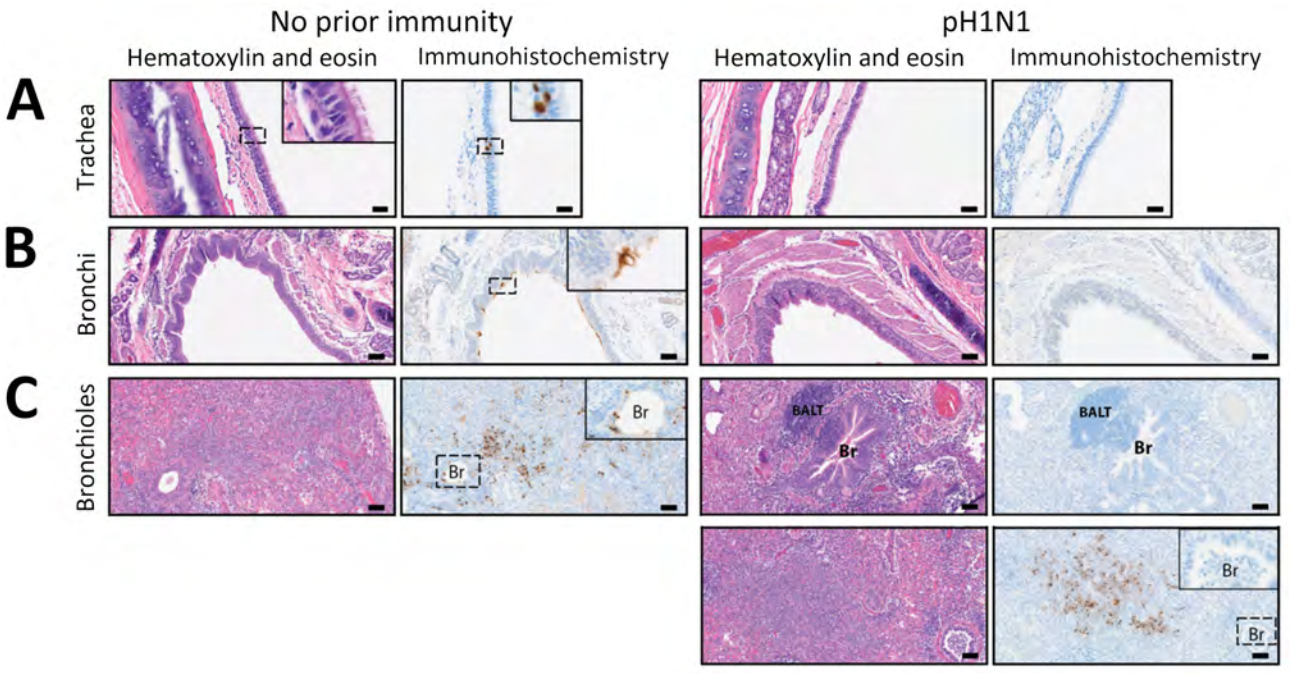

Figure 4. Hematoxylin and eosin–stained and immunohistochemistry tissue samples from a study of influenza A(H5N1) immune response among ferrets with pH1N1 immunity. A) Tracheal tissue. Scale bars indicate 20 mm; inset shows magnification ×400. B) Bronchial tissue. Scale bars indicate 50 mm; inset shows magnification ×200. C) Bronchiole tissue. Scale bars indicate 50 mm; inset shows magnification ×200. Ferrets with no prior immunity (left panels) or existing influenza A(H1N1)pdm09 immunity (right panels) were infected with 10^4 50% tissue culture infectious dose of H5N1 strain A/dairy cattle/Texas/24-008749-001/2024(H5N1) and humanely euthanized 3 days postinfection. Images show hematoxylin and eosin stained (purple) tissues and immunohistochemistry of influenza A nucleoprotein (blue). Dotted squares indicate areas that are magnified within the inset panel in tissues from ferrets with no prior immunity versus pH1N1-immune ferrets. BALT, bronchus-associated lymphoid tissue; Br, bronchiole; pH1N1, influenza A(H1N1)pdm09.

protection against subsequent infections (*19*). In addition, cross-reactive HA stalk-specific antibodies are able to play a role in reducing influenza virus disease severity (*20*–*22*). To identify immune factors that contribute to the protection of pH1N1-immune ferrets from severe disease, we measured neutralizing and total HA binding antibodies. Before challenge with cow/Tx/24 H5N1 virus, ferrets with pH1N1 immunity exhibited high levels of neutralizing antibodies against pH1N1 but no neutralizing antibodies above the limit of detection against cow/Tx/24 H5N1 (Figure 8, panel A).

To explore the production of nonneutralizing cross-reactive HA antibodies, we performed an ELISA with serum from ferrets with pH1N1 immunity by using the whole H1 (A/California/07/2009 H1N1) or H5 (A/dairy cattle/Texas/24008749001/2024 H5N1) HA protein (Figure 8, panel B). Ferrets with pH1N1 immunity produced antibodies that bound to H1 as expected but displayed the same background levels of antibody binding to the H5 HA protein as ferrets with no prior immunity (Figure 8, panel B), indicating no detectable cross-reactive HA antibodies against the avian H5 protein.

Finally, we performed an ELISA using NA from a human(A/Michigan/45/2015H1N1)oravian(A/mallard/New York/22-008760–007-original/2022 H5N1, which is 98.7% similar to cow/Tx/24 NA) IAV to determine whether pH1N1-immune ferrets had any cross-reacting NA antibodies that might contribute to the protection against severe disease before challenge with H5N1. Of note, serum samples from pH1N1-immune ferrets had antibodies that bound to both the

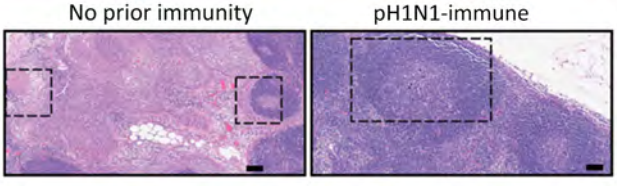

Figure 5. Hematoxylin and eosin–stained lymph node samples from a study of influenza A(H5N1) immune response among ferrets with pH1N1 immunity. Ferrets with no prior immunity (left panel) or pH1N1 (right panel) were infected with 10^4 50% tissue culture infectious dose of H5N1 strain A/dairy cattle/Texas/24-008749-001/2024(H5N1) and humanely euthanized 3 days postinfection. Dotted squares indicate areas that are with cortical lymphoid necrosis and depletion in tissues from ferrets with no prior immunity versus normal secondary germinal center in pH1N1-immune ferret. Scale bars indicate 100 mm. pH1N1, influenza A(H1N1)pdm09.

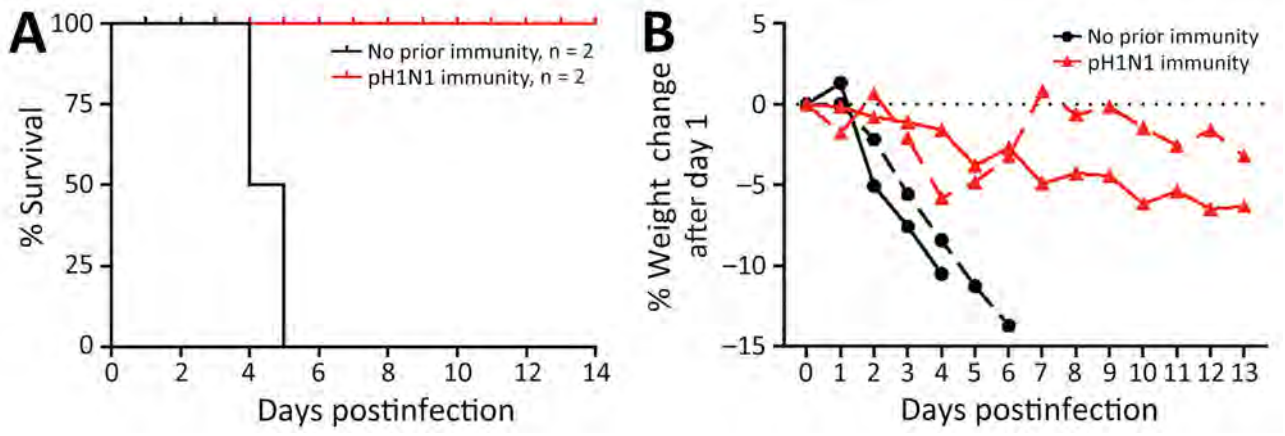

Figure 6. Mortality rates and weight change in a study of influenza A(H5N1) immune response among ferrets with pH1N1 immunity. A) Mortality rates; B) percentage weight change. We observed percentage of weight change as an indicator of severe disease in ferrets with or without pH1N1 immunity among ferrets intranasally infected with H5N1 strain A/dairy cattle/Texas/24-008749-001/2024(H5N1). pH1N1, influenza A(H1N1)pdm09.

human and avian NA antigens, but ferrets without immunity had background binding levels (Figure 8, panel C). Those data suggest that cross-reactive NA antibodies to avian N1 may be produced from a human seasonal pH1N1 infection.

Discussion

Influenza A(H1N1)pdm09 immunity in ferrets was sufficient to protect from severe disease and death from highly pathogenic avian influenza A(H5N1) virus from dairy cows. We also observed significantly reduced H5N1 viral titers in nasal secretions and respiratory tract tissues in the animals with pH1N1 immunity ($p<0.01$). Of note, protection from H5N1 infection was not due to cross-neutralizing antibodies in serum because ferrets with pH1N1 immunity did not generate systemic antibodies that cross-neutralized the cow/Tx/24 H5N1 virus (Figure 8, panel A). Rather, we found ferrets with pH1N1 immunity produced cross-reacting antibodies to H5N1 NA protein (Figure 8, panel C), which is consistent with observations reported from human serologic data (*23*). Immunity to NA has previously been implicated in providing protection during the 1968 H3N2 pandemic (*24*,*25*), and can reduce disease severity of naturally infected and experimentally challenged persons (*26*).

NA antibodies may be involved in protection from severe disease observed in the pH1N1-immune ferrets. However, further studies on the mechanisms of protection are clearly warranted and should include an examination of mucosal immunity from antibodies in the respiratory tract that have broad binding potential. Tissue-resident memory T cells may also help reduce the severity of disease, as is suspected in the case of H1 immunity protecting from

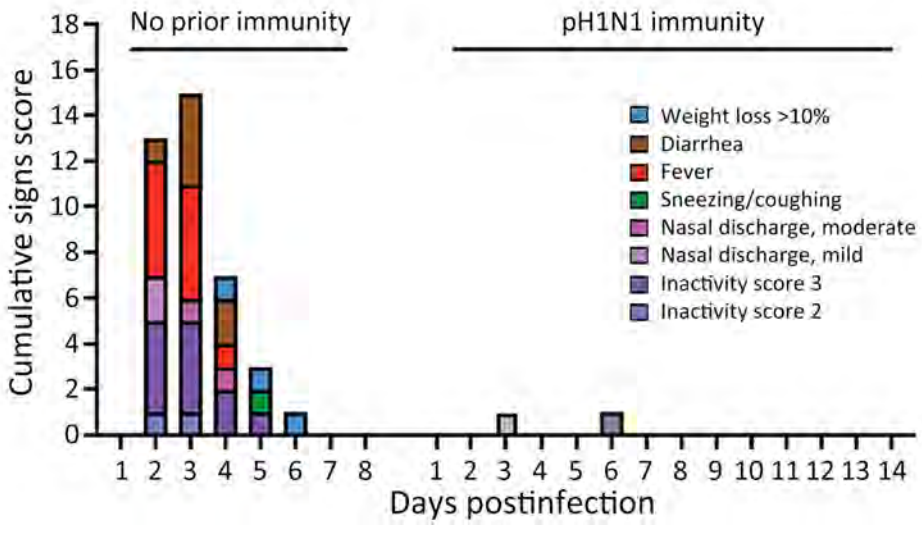

Figure 7. Cumulative clinical signs scores in a study of influenza A(H5N1) immune response among ferrets with pH1N1 immunity. Ferrets with or without pH1N1 immunity were intranasally infected with H5N1 strain A/dairy cattle/Texas/24-008749-001/2024(H5N1). Clinical signs of infection were monitored each day postinfection and quantified into a cumulative signs scores based on 5 ferrets on days 1–3 and 2 ferrets on days 4–14 postinfection or until euthanasia. pH1N1, influenza A(H1N1)pdm09.

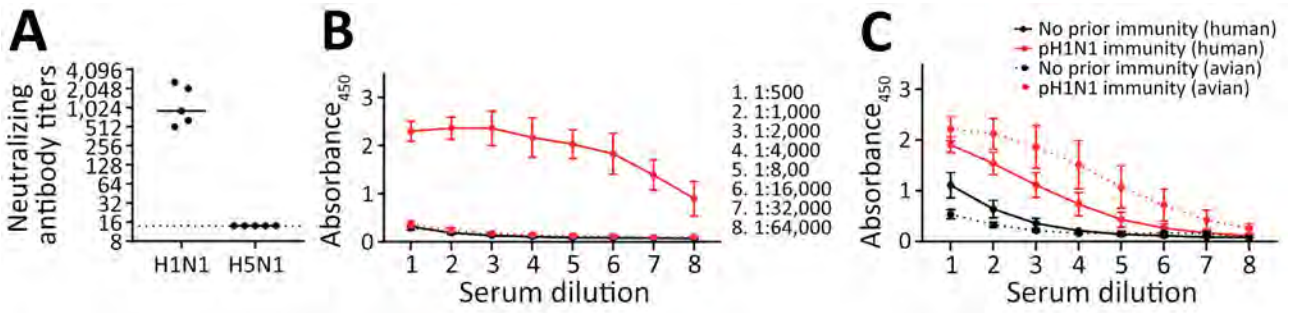

Figure 8. Cross-reactive NA binding antibodies in a study of influenza A(H5N1) immune response among ferrets with pH1N1. Ferrets with or without pH1N1 immunity were intranasally infected with H5N1 strain A/dairy cattle/Texas/24-008749-001/2024(H5N1). A) Serum samples were collected from 5 ferrets with pH1N1 immunity on day 98 postinfection and tested for neutralizing antibodies against pH1N1 and 2024 cow/Tx/24 H5N1 viruses. Each dot represents the antibody titer of a single ferret to neutralize 100 $TCID_{50}$ of pH1N1 or cow/Tx/24 H5N1 on MDCK cells. Solid line indicates the geometric mean value for each virus; dotted line represents the limit of detection for the assay. B) Serum IgG against purified HA proteins in ferrets with or without pH1N1 immunity. Solid lines show ferret serum reactivity to human HA (A/Michigan/45/2015 H1N1) and the dashed lines show ferret serum reactivity to dairy cow HA from A/dairy cattle/Texas/24008749001/2024(H5N1). Dots indicate means; whiskers indicate SDs. C) Serum IgG antibodies against purified NA proteins in ferrets with or without pH1N1 immunity. Solid lines show ferret serum reactivity to human NA (A/California/07/2009 H1N1); dashed lines show ferret serum reactivity to avian NA from A/mallard/New York/22–008760–007-original/2022(H5N1). Dots indicate means; whiskers indicate SDs. $Absorbance_{450}$, absorbance at 450 nm for each dilution; HA, hemagglutinin; NA, neuraminidase; pH1N1, influenza A(H1N1)pdm09; $TCID_{50}$, 50% tissue culture infectious dose.

airborne transmission of human seasonal H3N2 virus (*9*). A conservation of immunodominant T-cell epitopes between H5N1 and seasonal influenza viruses, including H1N1, was recently reported and suggested to potentially provide a level of cross-protective immunity (*27*). We did note that the lung tissues of ferrets with pH1N1 immunity had increased mononuclear perivascular infiltrates and BALT hyperplasia, consistent with tissue-specific T-cell responses, although additional investigation is required.

The mild infection noted in the 2 pH1N1-immune ferrets that survived until day 14 might account for the low levels of neutralizing antibodies against cow/Tx/24 H5N1 (Table). That observation may be critical to inform the use of H5 seroconversion as a detection mechanism for prevalence of H5 infections in farm workers because mild infections may not produce a robust systemic antibody immune response.

All adults have immunity from repeated influenza virus infections over their lifetimes, but how previous exposures translate into protection may be strain-dependent and change over time. Human H5N1 infections during 2003 had a 30%–50% mortality rate worldwide (*28*). However, since the emergence of the 2.3.4.4b clade in 2020, the mortality rate has been declining; during 2020–2024, at least 80 human infections with various H5N1 clades were reported, but only 8 deaths were reported (*28*). Of note, in 2024, at least 72 human infections and 2 deaths from H5N1 have occurred; both deaths were reported in Cambodia from 2.3.2.1c clade, which is distinct from 2.3.4.4b (*28*). The mild clinical manifestations of H5N1 human cases in the United States could be due to several factors, including changes in the viral genome that result in a less pathogenic virus, inoculation routes and doses,

Table. Serologic testing from a study of influenza A(H5N1) immune response among ferrets with pH1N1 immunity*

		Microneutralization titers			
		H5N1		pH1N1	
Ferret no.	Euthanasia, dpi	0 dpi	At euthanasia	0 dpi	At euthanasia
Naive group					
1	3	<20	<20	ND	ND
2	3	<20	<20	ND	ND
3	3	<20	<20	ND	ND
4	4	<20	<20	ND	ND
5	6	<20	<20	ND	ND
pH1N1-immune group					
1	3	<20	<20	905	1,016
2	3	<20	<20	508	320
3	3	<20	<20	2,032	508
4	14	<20	20	2,560	2,032
5	14	<20	80	640	2,032

*A/dairy cattle/Texas/24-008749-001/2024(H5N1) strain (GISAID accession no. EPI_ISL_19014384) was used for H5N1 inoculation. dpi, days postinoculation; ND, not done; pH1N1, influenza A(H1N1)pdm09.

immunity to H1N1 strains that circulated widely since 2010, or a combination of those factors. However, additional research into the level of protection afforded by other human seasonal influenza viruses, particularly currently circulating H1N1 viruses and those before the 2009 H1N1 pandemic, is needed to assess whether currently circulating H1N1 viruses produce a protective immune signature but other prior strains do not. In particular, understanding whether infection from H1N1 or H2N2 strains circulating before 1970 can produce antibodies that cross-react with H5N1 would be useful, given the presence of cross-neutralizing antibodies observed persons born before 1970. Finally, determining whether immunity to conserved regions of the NA or other viral proteins are driving the protection observed with pH1N1 infection is crucial because we detected no neutralizing antibodies in younger persons (Figure 1).

One limitation of this study is the small number of human serum samples used to test for cross-neutralizing antibodies against dairy cow H5N1. However, another group reported similar findings from a different assay (T.A. Garretson et al., unpub. data, https://doi.org/10.1101/2024.10.31.2431651. Other limitations that should be addressed in future work include the small number of animals used in our preimmune studies, use of only 1 subtype of human seasonal virus for the immune imprint, and challenge with only 1 strain of H5N1. Lethality after highly pathogenic avian A(H5N1) influenza infection can be strain specific, and published work has shown that another dairy cattle H5N1 strain was only partially lethal in immunologically naive ferrets (*30*), but a human H5N1 isolate from Texas was lethal in ferrets (*29*,*30*). Therefore, assessment of additional H5N1 strains isolated from dairy cows and human spillover infections is needed. Other groups have performed studies with ferrets having imprints from vaccination or seasonal human influenza virus infection and shown protection against different H5N1 strains (*31*–*35*; P.H. Brigleb et al., unpub. data, https://doi.org/10.1101/2024.10.23.619695).

In conclusion, we found ferrets with immunity to pH1N1 virus exhibited reduced H5N1 virus replication and dissemination, had less mortality and fewer disease symptoms from H5N1 infection, and expressed H5N1 cross-reacting antibodies to the NA protein. Those results suggest that immunity to heterotypic influenza viruses may explain the mild symptoms observed during 2024 H5N1 infection of dairy and poultry farm workers. Although human H5N1 infections from the 2024 outbreak resulted in mostly mild illnesses, additional research addressing the effects of prior influenza immunity on the pathogenesis and transmission of H5N1 could shed light on the 2024 outbreak strain and inform pandemic risk plans.

This article was preprinted at https://www.biorxiv.org/content/10.1101/2024.10.23.619881v1.

Acknowledgments

We would like to extend our deepest gratitude to Julian Arthur and Jessica Simendinger for their outstanding work in developing the Influenza A Nucleoprotein (NP) (F8L6X) Rabbit mAb #99797 (Cell Signaling Technology, Inc., https://www.cellsignal.com). Their expertise, dedication, and tireless efforts have been instrumental in the successful creation of this critical clone, and we are particularly grateful for their collaborative efforts with our team during the validation process. We thank Rachel Duron for critical review and feedback.

All source data are available on Figshare (https://doi.org/10.6084/m9.figshare.25843414).

This project has been funded in part with federal funds from the National Institute of Allergy and Infectious Diseases (NIAID), National Institutes of Health (NIH), Department of Health and Human Services, under contract no. 75N93021C00015. A.K.M. receives funding from Burroughs Wellcome Career Awards for Medical Scientists (award no. 1013362.02). The University of Pittsburgh Regional Biocontainment Laboratory within the Center for Vaccine Research is supported by an NIH award (no. UC7AI180311) from NIAID. N.A.C. is supported by NIH S10 instrumentation awards (nos. S10OD030269 and S10OD026983). Work in the Krammer laboratory was supported via an NIAID-funded Center of Excellence for Influenza Research and Response contract (no. 75N93021C00014).

The Icahn School of Medicine at Mount Sinai has filed patent applications relating to influenza virus vaccines and therapeutic vaccines which list F.K. as coinventor. Several of those patents have been licensed and F.K. has received royalty payments from commercial entities. F.K. has consulted for Merck, Pfizer, Seqirus, GlaxoSmithKline, and Curevac and is currently consulting for Gritstone, 3rd Rock Ventures, and Avimex, and he is a cofounder and scientific advisory board member of CastleVax. The Krammer laboratory is also collaborating with Dynavax on influenza virus vaccine development and with VIR on influenza therapeutics. All other authors declare no competing financial or nonfinancial interests in relation to the work described.

Author contributions: V.L. and S.S.L. designed the experiments, analyzed, interpreted the data, and wrote the manuscript. V.L., B.D.W., G.A.M., S.E.P., A.K.O., H.C.S., and N.A.C. performed the experiments. K.R.M., D.S.R., L.H.M., D.B., F.K., A.K.M., and W.P.D. contributed resources and analysis. All authors edited and approved the manuscript.

About the Author

Dr. Le Sage is a research assistant professor at the University of Pittsburgh Center for Vaccine Research. Her research interests include elucidating the requirements for influenza virus transmission and assessing the pandemic potential of emerging influenza viruses.

References

1. US Department of Agriculture. HPAI confirmed cases in livestock [cited 2024 Nov 9]. https://www.aphis.usda.gov/livestock-poultry-disease/avian/avian-influenza/hpai-detections/hpai-confirmed-cases-livestock
2. Koopmans MPG, Barton Behravesh C, Cunningham AA, Adisasmito WB, Almuhairi S, Bilivogui P, et al.; One Health High-Level Expert Panel. The panzootic spread of highly pathogenic avian influenza H5N1 sublineage 2.3.4.4b: a critical appraisal of One Health preparedness and prevention. Lancet Infect Dis. 2024;24:e774–81. https://doi.org/10.1016/S1473-3099(24)00438-9
3. Peacock TP, Moncla L, Dudas G, VanInsberghe D, Sukhova K, Lloyd-Smith JO, et al. The global H5N1 influenza panzootic in mammals. Nature. 2025;637:304–13. https://doi.org/10.1038/s41586-024-08054-z
4. Uyeki TM, Milton S, Abdul Hamid C, Reinoso Webb C, Presley SM, Shetty V, et al. Highly pathogenic avian influenza A(H5N1) virus infection in a dairy farm worker. N Engl J Med. 2024;390:2028–9. https://doi.org/10.1056/NEJMc2405371
5. Centers for Disease Control and Prevention. Avian influenza (bird flu) [cited 2024 Nov 9]. https://www.cdc.gov/bird-flu/spotlights/ah5n1-response-update.html
6. Bodewes R, de Mutsert G, van der Klis FR, Ventresca M, Wilks S, Smith DJ, et al. Prevalence of antibodies against seasonal influenza A and B viruses in children in Netherlands. Clin Vaccine Immunol. 2011;18:469–76. https://doi.org/10.1128/CVI.00396-10
7. Gostic KM, Ambrose M, Worobey M, Lloyd-Smith JO. Potent protection against H5N1 and H7N9 influenza via childhood hemagglutinin imprinting. Science. 2016;354:722–6. https://doi.org/10.1126/science.aag1322
8. Eisfeld AJ, Biswas A, Guan L, Gu C, Maemura T, Trifkovic S, et al. Pathogenicity and transmissibility of bovine H5N1 influenza virus. Nature. 2024;633:426–32. https://doi.org/10.1038/s41586-024-07766-6
9. Le Sage V, Jones JE, Kormuth KA, Fitzsimmons WJ, Nturibi E, Padovani GH, et al. Pre-existing heterosubtypic immunity provides a barrier to airborne transmission of influenza viruses. PLoS Pathog. 2021;17:e1009273. https://doi.org/10.1371/journal.ppat.1009273
10. Le Sage V, Rockey NC, French AJ, McBride R, McCarthy KR, Rigatti LH, et al. Potential pandemic risk of circulating swine H1N2 influenza viruses. Nat Commun. 2024;15:5025. https://doi.org/10.1038/s41467-024-49117-z
11. Mueller Brown K, Le Sage V, French AJ, Jones JE, Padovani GH, Avery AJ, et al. Secondary infection with *Streptococcus pneumoniae* decreases influenza virus replication and is linked to severe disease. FEMS Microbes. 2022;3:xtac007. https://doi.org/10.1093/femsmc/xtac007
12. Reed LJ, Muench H. A simple method of estimating fifty per cent endpoints. Am J Epidemiol. 1938;27:493–7. https://doi.org/10.1093/oxfordjournals.aje.a118408
13. Nachbagauer R, Choi A, Izikson R, Cox MM, Palese P, Krammer F. Age dependence and isotype specificity of influenza virus hemagglutinin stalk-reactive antibodies in humans. MBio. 2016;7:e01996-15. https://doi.org/10.1128/mBio.01996-15
14. Camp JV, Bagci U, Chu YK, Squier B, Fraig M, Uriarte SM, et al. Lower respiratory tract infection of the ferret by 2009 H1N1 pandemic influenza A virus triggers biphasic, dystemic, and local recruitment of neutrophils. J Virol. 2015;89:8733–48. https://doi.org/10.1128/JVI.00817-15
15. Lakdawala SS, Jayaraman A, Halpin RA, Lamirande EW, Shih AR, Stockwell TB, et al. The soft palate is an important site of adaptation for transmissible influenza viruses. Nature. 2015;526:122–5. https://doi.org/10.1038/nature15379
16. Lakdawala SS, Shih AR, Jayaraman A, Lamirande EW, Moore I, Paskel M, et al. Receptor specificity does not affect replication or virulence of the 2009 pandemic H1N1 influenza virus in mice and ferrets. Virology. 2013;446:349–56. https://doi.org/10.1016/j.virol.2013.08.011
17. Smith JH, Nagy T, Driskell E, Brooks P, Tompkins SM, Tripp RA. Comparative pathology in ferrets infected with H1N1 influenza A viruses isolated from different hosts. J Virol. 2011;85:7572–81. https://doi.org/10.1128/JVI.00512-11
18. Vidaña B, Martínez J, Martínez-Orellana P, García Migura L, Montoya M, Martorell J, et al. Heterogeneous pathological outcomes after experimental pH1N1 influenza infection i n ferrets correlate with viral replication and host immune responses in the lung. Vet Res. 2014;45:85. https://doi.org/10.1186/s13567-014-0085-8
19. Kosik I, Yewdell JW. Influenza hemagglutinin and neuraminidase: yin-yang proteins coevolving to thwart immunity. Viruses. 2019;11:346. https://doi.org/10.3390/v11040346
20. Pica N, Hai R, Krammer F, Wang TT, Maamary J, Eggink D, et al. Hemagglutinin stalk antibodies elicited by the 2009 pandemic influenza virus as a mechanism for the extinction of seasonal H1N1 viruses. Proc Natl Acad Sci U S A. 2012;109:2573–8. https://doi.org/10.1073/pnas.1200039109
21. Throsby M, van den Brink E, Jongeneelen M, Poon LL, Alard P, Cornelissen L, et al. Heterosubtypic neutralizing monoclonal antibodies cross-protective against H5N1 and H1N1 recovered from human IgM+ memory B cells. PLoS One. 2008;3:e3942. https://doi.org/10.1371/journal.pone.0003942
22. Wu NC, Wilson IA. Influenza hemagglutinin structures and antibody recognition. Cold Spring Harb Perspect Med. 2020;10:a038778. https://doi.org/10.1101/cshperspect.a038778
23. Daulagala P, Cheng SMS, Chin A, Luk LLH, Leung K, Wu JT, et al. Avian influenza A(H5N1) neuraminidase inhibition antibodies in healthy adults after exposure to influenza A(H1N1)pdm09. Emerg Infect Dis. 2024;30:168–71. https://doi.org/10.3201/eid3001.230756

24. Monto AS, Kendal AP. Effect of neuraminidase antibody on Hong Kong influenza. Lancet. 1973;301:623–5. https://doi.org/10.1016/S0140-6736(73)92196-X
25. Murphy BR, Kasel JA, Chanock RM. Association of serum anti-neuraminidase antibody with resistance to influenza in man. N Engl J Med. 1972;286:1329–32. https://doi.org/10.1056/NEJM197206222862502
26. Maier HE, Nachbagauer R, Kuan G, Ng S, Lopez R, Sanchez N, et al. Pre-existing antineuraminidase antibodies are associated with shortened duration of influenza A(H1N1) pdm virus shedding and illness in naturally infected adults. Clin Infect Dis. 2020;70:2290–7. https://doi.org/10.1093/cid/ciz639
27. Sidney J, Kim A-R, de Vries RD, Peters B, Meade PS, Krammer F, et al. Targets of influenza human T cell response are mostly conserved in H5N1. mBio. 2024 Dec 26 [Epub ahead of print]. https://doi.org/10.1128/mbio.03479-24
28. World Health Organization. Cumulative number of confirmed human cases for avian influenza A(H5N1) reported to WHO, 2003–2024, 26 February 2024. [cited 2025 Feb 3] https://www.who.int/publications/m/item/cumulative-number-of-confirmed-human-cases-for-avian-influenza-a(h5n1)-reported-to-who--2003-2024--20-december-2024
29. Eisfeld AJ, Biswas A, Guan L, Gu C, Maemura T, Trifkovic S, et al. Pathogenicity and transmissibility of bovine H5N1 influenza virus. Nature. 2024;633:426–32. https://doi.org/10.1038/s41586-024-07766-6
30. Gu C, Maemura T, Guan L, Eisfeld AJ, Biswas A, Kiso M, et al. A human isolate of bovine H5N1 is transmissible and lethal in animal models. Nature. 2024;636:711–8. https://doi.org/10.1038/s41586-024-08254-7
31. Pulit-Penaloza JA, Belser JA, Brock N, Kieran TJ, Sun X, Pappas C, et al. Transmission of a human isolate of clade 2.3.4.4b A(H5N1) virus in ferrets. Nature. 2024;636:705–10. https://doi.org/10.1038/s41586-024-08246-7
32. Nuñez IA, Jang H, Huang Y, Kelvin A, Ross TM. Influenza virus immune imprinting dictates the clinical outcomes in ferrets challenged with highly pathogenic avian influenza virus H5N1. Front Vet Sci. 2023;10:1286758. https://doi.org/10.3389/fvets.2023.1286758
33. Skarlupka AL, Zhang X, Blas-Machado U, Sumner SF, Ross TM. Multi-influenza HA subtype protection of ferrets vaccinated with an N1 COBRA-based neuraminidase. Viruses. 2023;15:184. https://doi.org/10.3390/v15010184
34. Uno N, Ebensen T, Guzman CA, Ross TM. Intranasal administration of octavalent next-generation influenza vaccine elicits protective immune responses against seasonal and pre-pandemic viruses. J Virol. 2024;98:e0035424. https://doi.org/10.1128/jvi.00354-24
35. Furey C, Scher G, Ye N, Kercher L, DeBeauchamp J, Crumpton JC, et al. Development of a nucleoside-modified mRNA vaccine against clade 2.3.4.4b H5 highly pathogenic avian influenza virus. Nat Commun. 2024;15:4350. https://doi.org/10.1038/s41467-024-48555-z

Address for correspondence: Valerie Le Sage, University of Pittsburgh, 3501 Fifth Ave, Pittsburgh, PA 15261, USA; email: valerie.lesage@pitt.edu; and Seema Lakdawala, Emory University, 1510 Clifton Rd, Atlanta, GA 30322, USA; email: seema.s.lakdawala@emory.edu

etymologia revisited

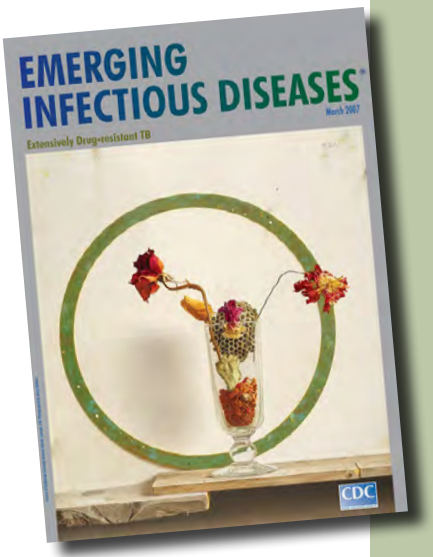

Originally published in March 2007

Norovirus

[nor′-o-vi′rəs]

Genus of viruses that cause viral gastroenteritis. Noroviruses are named after the original strain, "Norwalk virus," which caused an outbreak of acute gastroenteritis among children at an elementary school in Norwalk, Ohio, in 1968. Numerous outbreaks of disease with similar symptoms have been reported since, and the etiologic agents were called "Norwalk-like viruses" or "small round-structured viruses." Noroviruses are transmitted primarily through the fecal-oral route and are highly contagious; as few as 10 viral particles may infect a person.

Reference

Mahy BWJ. A dictionary of virology. London: Academic Press; 2001; http://www.cdc.gov/ncidod/dvrd/revb/gastro/norovirus-qa.htm; http://www.medicinenet.com/norovirus_infection/article.htm

https://wwwnc.cdc.gov/eid/article/13/3/e1-1303_article

Postelimination Cluster of Lymphatic Filariasis, Futuna, 2024

Clément Couteaux, Thibaut Demaneuf, Laurent Bien, Manuel Munoz, Bernadette Worms, Samuel Chésimar, Gwenael Takala, Atonio Lie, Vincent Jessop, Malia Kalemeli Selemago, Valelia Uhila, Monika Toa, Dominique Euller, Cyrille Goarant

After detection of 2 clinical lymphatic filariasis (LF) cases in a postelimination context in 2023 on the island of Futuna (Wallis and Futuna archipelago), the Wallis and Futuna Health Agency conducted a LF prevalence survey in Futuna in May 2024. This cross-sectional study, carried out among schoolchildren <18 years of age, identified 5 children with antigenemia, indicating an estimated antigenemia prevalence in Futuna children nearing 2%. The study also confirmed a spatial cluster of cases in the village of Taoa, where the child antigenemia prevalence reached 7.5% (95% CI 2.1%–18.2%), and demonstrated a link between infection and traditional housing. We observed microfilariae in contact cases during secondary investigations. These findings suggest resurgence of LF in a postelimination context, in which the expected child antigenemia prevalence should not exceed 1%. This situation should prompt a new mass drug administration campaign using triple therapy and the reinforcement of epidemiologic and entomologic surveillance.

Lymphatic filariasis (LF) is a vectorborne neglected tropical disease caused by nematode worms. Three worm species can cause the disease, *Brugia malayi*, *B. timori*, and *Wuchereria bancrofti*; the last of those is responsible for LF in Pacific Island countries and territories (PICTs). In 2018, ≈51 million people were infected with LF globally, and by 2021, ≈40 million cases of lymphoedema (i.e., elephantiasis of the lower limbs or hydrocele [scrotal edema] resulting from the blockage of lymph flow in lymphatic vessels) were reported (*1*,*2*).

In 2000, the World Health Organization (WHO) launched the Global Program for the Elimination of Lymphatic Filariasis (GPELF). This program's strategy is based on mapping LF-endemic areas, reducing filarial transmission through mass drug administration (MDA) of microfilaricides, conducting post-MDA surveillance to document elimination, and implementing postelimination surveillance (*2*,*3*). In 2022, a total of 8 PICTs had reached the "elimination as a public health problem" status, including Wallis and Futuna, and another 8 were in the process of MDA (*4*).

Wallis and Futuna (WF) is an overseas collectivity of France in the Pacific Ocean, 370 km east of Samoa and 800 km west of Fiji (Appendix Figure 1, https://wwwnc.cdc.gov/EID/article/31/3/24-1317-App1.pdf). The territory consists of 2 island groups: Wallis, locally named Uvea (74 km^2), and Futuna and Alofi (46 km^2), 230 km southwest of Wallis. Wallis is 1 kingdom with a population of 8,088, whereas Futuna has 2 kingdoms, Alo and Sigave, whose combined populations total 3,063 population, according to a 2023 census (*5*,*6*). The Health Agency (Agence de Santé) is the sole regulator and operator of healthcare services.

Until the 1980s, WF was a hyperendemic area for LF, which was transmitted locally by *Aedes polynesiensis* mosquitoes. Microfilaria prevalence rates were 20% in 1958 and 10% by the end of the 1970s (*7*,*8*). Diethylcarbamazine MDA campaigns were implemented throughout the archipelago during 1978–2007; unfortunately, however, no information regarding treatment is available. In 2001, WF joined the Pacific Program for the Elimination of Lymphatic Filariasis, the regional component of the WHO-led GPELF. After a survey reporting a 1% infection prevalence, 6 MDA campaigns with diethylcarbamazine and albendazole were implemented in 2002, 2003, 2004, 2005, 2006, and 2007; reported coverage rates ranged from 53% to 66% (*2*,*9*,*10*). Three transmission assessment surveys (TASs) (a pre-TAS in 2006 and TASs in 2012 and 2016) performed using immunochromatographic card tests

Author affiliations: Wallis and Futuna Health Agency, Mata'utu, Uvea, Wallis and Futuna (C. Couteaux, L. Bien, M. Munoz, B. Worms, S. Chésimar, G. Takala, A. Lie, V. Jessop, M.K. Selemago, V. Uhila, M. Toa, D. Euller); The Pacific Community, Noumea, New Caledonia (T. Demaneuf, C. Goarant)

DOI: https://doi.org/10.3201/eid3103.241317

reported child prevalence of filarial antigenemia <1% (*10*). In 2018, WHO declared the elimination status of LF (*10*,*11*). Subsequently, no postelimination surveillance was implemented.

In October 2023, a lower limb lymphedema was diagnosed and reported in Wallis in a 70-year-old man. A retrospective investigation of medical records identified another lower limb lymphedema in 2022 in a 34-year-old man and a hydrocele in an 11-year-old child in 2021, both of whom were living on the island of Futuna. All 3 cases were serologically positive for LF (Novalisa IgG ELISA Enzyme Linked Immunoabsorbent Assay; Gold Standard Diagnostics, https://www.goldstandarddiagnostics.cn) and showed marked hypereosinophilia (>1,500 cells/mm^3 [reference range 40–500 cells/mm^3]). A search of a laboratory information system identified 109 patients with marked hypereosinophilia during May 15, 2023–May 27, 2024; 57 cases were in Futuna, and 52 were in Wallis, indicating a prevalence of hypereosinophilia 3 times higher in Futuna.

A rapid diagnostic test (RDT) (Bioline Filariasis Test Strip; Abbott, https://www.abbott.com), typically used for TAS, was offered to patients identified on the basis of having hypereosinophilia, leading to the diagnosis of 15 cases of antigenemia (2 in Wallis and 13 in Futuna). In Futuna, 10 of the 13 cases were in patients who lived in the village of Taoa, and none had any clinical signs. Those findings triggered further investigation of the LF situation in Futuna. Our study aimed to assess the prevalence of LF in children <18 years of age in Futuna, specify the spatial distribution of LF cases, and identify factors associated with infection.

Methods

Study Design

We conducted a cross-sectional study in all Futuna schools to assess infection status by using an RDT, as recommended by WHO, for postelimination surveillance. We used a non-TAS methodology because WHO does not recommend TAS methodology for postelimination surveillance, given its lack of sensitivity in low-prevalence settings. We assessed possible risk factors for LF by administering a questionnaire and retrieved eosinophil counts from medical records when available. After the school-based study, we screened household contacts of LF-positive children by using secondary surveys.

Survey Population

We used data from the latest general population census (conducted in 2023). The target population consisted of children <18 years of age living in Futuna, totaling 808 persons, according to a 2023 census. The source population was children <18 years of age attending schools in Futuna, born after the last round of MDA in 2007. The territorial education directorate (Vice Rectorat) provided the list of schoolchildren in Futuna for 2024, which totaled 619 children.

We included children from the source population in the survey if they were enrolled in schools on Futuna Island from 1st grade (6 years of age) to 10th grade (15–16 years of age), if their parents completed the questionnaire and provided written informed consent for testing, and if they attended school on the day of the survey. We excluded children enrolled in special needs classes and those who declined to provide a blood sample. Given the small population size, all 448 eligible children were offered the test.

Data Collection

Three weeks before the screening, we distributed a survey questionnaire to be self-administered and filled in by parents. We defined LF disease status on the basis of the result of a prospective RDT from a drop of capillary blood taken from the child's fingertip. We collected information on variables related to exposure to the bites of *Ae. polynesiensis* mosquitoes (the vector of LF in WF), which included information on the type of housing (traditional, permanent house, or hut), the presence of mosquito window screens, and the use of topical mosquito repellents or fumigants. We also asked participants about their perception of mosquito biting intensities. Although other biting insects might contribute to this perception, the limited diversity of mosquito or biting midges species in Futuna mean that *Ae. polynesiensis* mosquitoes probably are the strongest contributor to the perception of biting intensities (*8*,*12*). To our knowledge, no precise evaluation of *Ae. polynesiensis* mosquitoes biting intensity has been conducted in Futuna. However, studies from other Pacific Islands where *Ae. polynesiensis* mosquitoes are present indicate that this species is the cause of a high biting intensity (*13*,*14*). We searched medical records for eosinophil counts from up to 5 years before.

The patient questionnaire included questions regarding a set of sociodemographic variables: identity (surname and first name), date of birth, sex, class, school, and test results with the date of the test. The surveillance team collected a geolocation variable of positive cases by using GPS during secondary surveys of household in which positive cases had been identified.

Organization of the Survey and Case Definition

We conducted screening in schools in Futuna during May 14–17, 2024, by deploying a team of 4 interviewers who had been formerly trained to perform the RDT. After interviewers verified the child's identity and parental consent, we provided the child with information about the purpose of the test and asked for oral consent. After obtaining consent, we took a capillary blood sample from the child's fingertip.

We used the Abbott Bioline Filariasis Test Strip for screening (*15*). We rechecked positive samples by using the same test performed in the laboratory from a venous puncture in the next 2 days to comply with the health regulations of France, which requires confirmation of the RDT in a laboratory setting. We defined a case of LF by a positive filariasis test strip antigenemic test confirmed in the laboratory. We did not evaluate microfilaremia because the technique for doing so was not available in the laboratory.

Survey of Case-Patient Contacts

After laboratory confirmation of the antigenemic cases detected in the schools, we offered all persons living in the same household as a positive case-patient an RDT on heparinized whole blood, in accordance with WHO recommendations. We also performed a qualitative search for microfilariae by direct search on fresh blood smear.

Information Flow and Analyses

We handwrote RDT results on each child questionnaire during the survey. We then entered all deidentified data into an Epi Info form (https://www.cdc.gov/epiinfo). We cleaned the data by using Excel (Microsoft, https://www.microsoft.com) and analyzed data by using R version 4.2.1 (The R Project for Statistical Computing, https://www.r-project.org) with R studio 2022.02.3+492 (https://rstudio-desktop.fr.download.it).

We described the dataset using the same terms as in the questionnaire. We combined some variables to create binary choices for the analysis (e.g., inhabitants of tin shacks and fale [a traditional Polynesian house with open sides and a thatched roof] were defined as living in traditional housing). We compared eosinophil counts on the basis of the test result as a quantitative variable, as we did for the child's age. We calculated prevalence of filarial antigenemia on the basis of the population screened and whether a valid positive or negative RDT result was obtained.

We used Fisher exact tests for qualitative variables and Mann–Whitney–Wilcoxon tests to compare the means of a child's age and eosinophil concentration. We considered differences with a p value <0.05 to be statistically significant. We used univariate logistic regression to study the association between screening results and risk factors. We excluded data on the presence of mosquito nets from the logistic regression analysis because it was a confounder with the type of habitat. In additionally, the low proportion of cases precluded the interpretation of a multivariate analysis. For the spatial analysis, we considered all known LF cases from Futuna on the basis of the school-based survey and positive contacts of antigenemic children, clinical cases, and antigenemic cases identified from the active eosinophilia-based surveillance, which totaled 21 cases.

We generated maps by using the Leaflet package in R (*16*). We used the global Moran *I* test, "spdep" R package (*17*) to detect the presence of spatial autocorrelation and to identify a possible cluster of cases. We used SaTScan software and the Kulforff method (*18*) based on a spatial Poisson discrete model to identify clusters by the Monte Carlo method and reported results with their radius, the number of observed and expected cases, the relative risk, and their statistical significance level. In addition, we calculated the barycenter (i.e., the arithmetic mean of the latitudes and longitudes) of the Taoa village cases. We used binomial distribution to estimate the LF prevalence in children.

Ethics Considerations

Wallis and Futuna does not have an ethics committee. This survey was presented to and received a favorable recommendation from the Health Agency Medical Committee, acting as an institutional review board, and from WHO. We offered antigenemic case-patients triple therapy with albendazole, diethylcarbamazine, and ivermectin, per WHO recommendations, free of charge.

Results

Study and Survey Populations

Of 448 eligible children, 353 returned the questionnaires, completed by their parents, yielding a 79% participation rate. Approximately 83% of the children in the population surveyed took part in the screening, making the screening rate in the eligible population just above 65%. The proportion of the eligible population who had an interpretable test, positive or negative, was 61% (Appendix Figure 2). The mean age of the children participating in the survey was 10.3 years (SD 2.8 years), and the mean eosinophil count was 571

cells/mm^3 (SD 623 cells/mm^3). Approximately 54% of participants were girls and 46% boys. Half were attending elementary schools, and half were attending junior high schools or high schools. Almost 60% of the pupils attended a school in the kingdom of Alo. The distribution by class, from 1st to 9th grade, was fairly even (at ≈10% per grade), whereas <5% attended 10th grade. Only 3 villages had >10% representation (Taoa, Ono, and Leava); children from Taoa accounted for ≈17% of the participants. In contrast, the villages of Fiua, Tamana, Tavai, and Vele each had <5% representation in the population sampled (Table 1). The sample proved to be a fair representation of the target population (Appendix Table 1).

The habitation type most reported was permanent house, accounting for 94% of the population studied; 80% of habitations did not report having mosquito nets. More than 30% of participants reported using topical mosquito repellents or pyrethroid-containing mosquito coils. The same proportion rated mosquito biting intensity as "fairly high" or above. Nearly 80% of households raised pigs; 30% of households had ≥10 pigs. Over 83% of the survey population took part in the infection screening, and nearly 4% were absent from school on the day of the survey. For the 293 children taking the RDT, 20 tests (6.8%) were invalid, 5 (1.7%) were positive, and 268 (91.5%) were negative (Table 2). The high rate of invalid tests was mainly attributable to insufficient sampling, given that the minimum volume of blood for the filariasis test strip test is 75 μL.

Estimated Prevalence in the Child Population

Based on the proportion of positive tests among valid readings, the prevalence estimate was 1.8% (95% CI 0.6%–4.2%). The prevalence was 2.4% (95% CI 0.7%–6.1%) in the kingdom of Alo, compared with 0.9% (95% CI 0.0%–5.1%]) in the kingdom of Sigave. Prevalence reached 7.5% (95% CI 2.1%–18.2%) in the village of Taoa (Figure 1).

Spatial Analysis

Global Moran index was significantly different from that expected (Moran *I* 0.353; p<0.001), indicating positive spatial autocorrelation and the presence of ≥1 LF cluster. Clustering analysis with SaTScan revealed a significant cluster in the village of Taoa (relative risk 18.91; p<0.001), which had 16 cases. All cases detected in Taoa were in children who lived 750 m from the barycenter (Figure 2). One case detected during the school survey had already been detected through the recently introduced active surveillance based on hypereosinophilia.

Table 1. Description of sociodemographic and biologic variables of children <18 years of age screened for lymphatic filariasis, Futuna, May 2024*

Variable	No. patients	Value
Age, y, mean (SD)	353	10.27 (2.79)
Eosinophil concentration, cells/mm^3, mean (SD)	114	571.00 (623.03)
Sex		
F	191	54.1
M	162	45.9
Elementary school level, 1st–5th grade	178	50.4
Location of school		
Fiua	69	19.6
Kolopelu	109	30.9
Sausau	69	19.5
Sisia	106	30.0
School grade		
10th grade	16	4.5
9th grade	37	10.5
8th grade	39	11.0
7th grade	39	11.1
6th grade	43	12.2
5th grade	30	8.5
4th grade	44	12.5
3rd grade	37	10.5
2nd grade	28	7.9
1st grade	40	11.3
Village of habitation (2023 census population [%])		
Fiua (245 [8.0])	16	4.6
Kolia (237 [7.7])	29	8.2
Leava (302 [9.9])	41	11.6
Malae (155 [5.1])	18	5.1
Nuku (202 [6.6])	28	7.9
Ono (504 [16.5])	46	13.0
Poi (165 [5.4])	19	5.4
Tamana (147 [4.8])	10	2.8
Taoa (443 [14.5])	59	16.7
Tavai (132 [4.3])	13	3.7
Toloke (168 [5.5])	33	9.4
Vaisei (139 [4.5])	13	3.7
Vele (222 [7.2])	28	7.9

*Values are % frequency except as indicated.

Factors Associated with Infection

We observed no effect of age on infection status and no difference by school grade (e.g., 1 case in each grade in elementary school except 1st grade and 1 case in 7th grade. One single case was in a child living in the kingdom of Sigave, compared with 4 in the kingdom of Alo. Fisher tests indicated significant differences for village of residence (p = 0.006) and habitation type (p = 0.030). We identified no positive cases in children from households with mosquito nets. In contrast, 15% of LF-negative schoolchildren's habitations had mosquito nets, a nonsignificant difference. We also observed no significant difference for the use of insect repellents, mosquito coils usage at home, or perceived mosquito biting intensity. All 5 case-patients and 78% of children testing negative reported raising pigs at home (p = 0.59 by Fisher test). Univariable logistic regression models identified associations

Table 2. Social and behavioral variables and lymphatic filariasis test results, Futuna, May 2024

Variable and test result	No. patients	Frequency, %
Habitation type		
Tin hut	2	0.6
Closed traditional fale*	6	1.7
Open traditional fale	12	3.4
Permanent house	330	94.3
Mosquito net at habitation		
No	273	77.8
Yes	47	13.4
Partial	31	8.8
Repellent or mosquito coil use		
Never	120	34.2
Sometimes	120	34.2
Often	60	17.1
Very often	15	4.3
Always	36	10.2
Perceived biting density		
Absence of bites	92	26.7
Low	155	44.9
Fairly high	70	20.3
High	19	5.5
Very high	9	2.6
No. pigs at household		
0	74	21.0
1–5	78	22.1
6–10	97	27.5
>10	104	29.4
Lymphatic filariasis rapid diagnostic result		
Negative	268	91.5
Positive	5	1.7
Invalid	20	6.8

*Fale, a traditional Polynesian house with open sides and a thatched roof.

between testing positive and living in Taoa (odds ratio 17.9 [95% CI 2.0–163.5]; p = 0.003) and living in a traditional habitation (OR 12.0 [95% CI 1.9–77.8]; p = 0.023) (Table 3).

Biologic Factors Associated with Infection

Eosinophil counts were 2.3 times higher in children testing positive compared with children testing negative for LF. However, this difference was not significant in our small dataset (p = 0.2 by Mann–Whitney–Wilcoxon test).

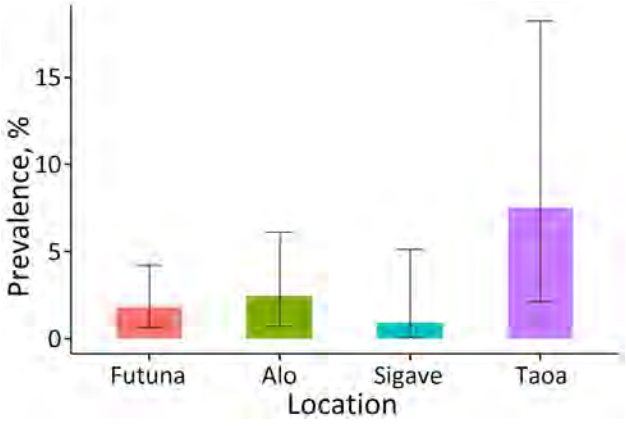

Figure 1. Estimated prevalence of lymphatic filariasis in schoolchildren in Futuna overall, in the kingdoms of Alo and Sigave, and in the village of Taoa, Futuna, May 2024. A total of 283 schoolchildren were screened. Error bars indicate 95% CIs.

Contact Investigations

After RDT confirmation of LF in 5 children in the school survey, we offered a screening test to all persons living in the same household as the children with antigenemia. Among these 10 contacts, the father of a 5-year-old child tested positive. A blood smear confirmed microfilaremia in this adult (Figure 3; Video, https://wwwnc.cdc.gov/EID/article/31/3/24-1317-V1.htm).

Discussion

In this postelimination LF prevalence assessment in Futuna, >60% of the eligible population was screened, showing a prevalence of nearly 2% among schoolchildren, twice the expected prevalence in the general population in a postelimination context (*19*). This estimate reached 7.5% in 1 village. Given that the survey population was born after the last MDA round, a much lower prevalence would be expected if transmission had been stopped. This study also identified a link between infection and traditional housing, which posed a significant risk (p = 0.023). The small number of cases limited multivariate analysis and led unprecise results with wide CIs. Although cases were identified through RDTs, microfilaremia was evidenced from fresh blood smears during contact investigations.

The youngest positive case-patient in this study was 7 years of age; earlier eosinophilia-based surveillance had also identified a case in a 6-year-old. Our results are robust and generalizable to the entire child population of Futuna and can be used for public health decision-making.

The 2012 and 2016 TAS surveys screened almost all primary school children, reaching coverage of 90% in 2012 and 88% in 2016, meaning prevalence underestimation is unlikely. In this 2024 study, systematic screening was extended to secondary school children, achieving a 61% screening rate. This reemergence probably has multifactorial causes. The effectiveness of the LF-elimination program depends on administering mass treatments to ≥65% of the eligible population. In WF, average MDA coverage during 2002–2007 was <58%. Unfortunately, island- or age-specific MDA coverage data is lacking, so whether Futuna had lower coverage or age-specific gaps remain uncertain (*10*). Age-specific MDA heterogeneities have been identified as possible drivers of LF resurgence in Madagascar (*20*).

Ae. polynesiensis mosquitoes, LF vectors in WF, are exophilic and reaching high densities in rural and

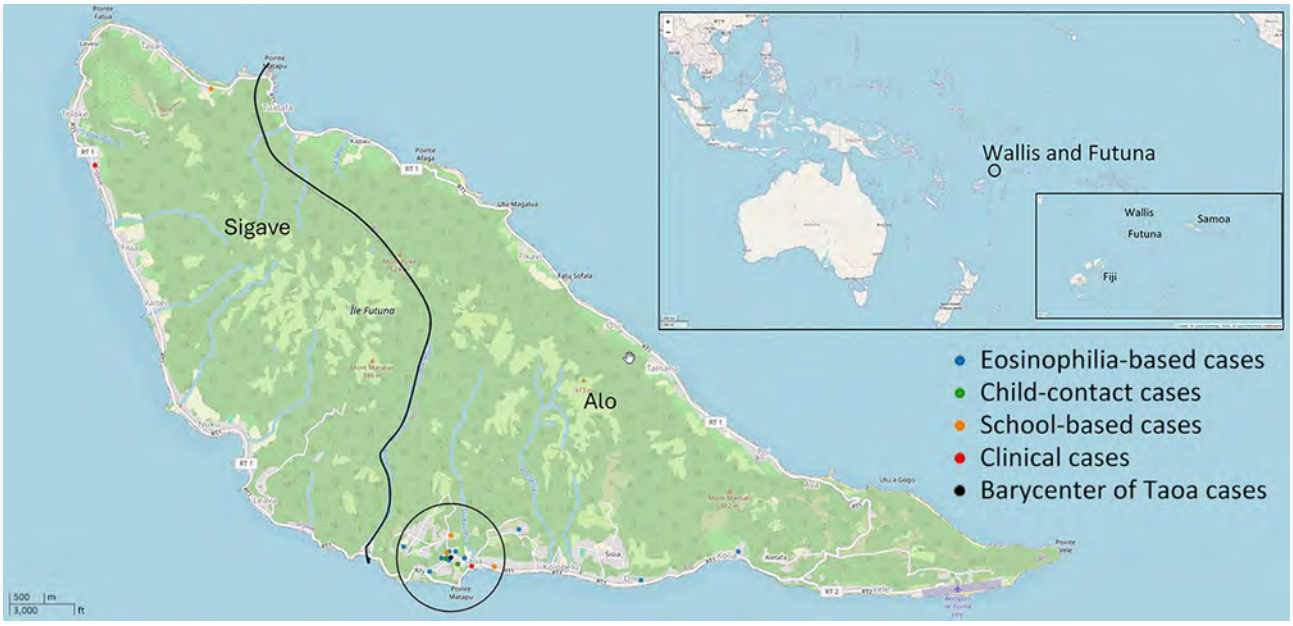

Figure 2. Geolocation of lymphatic filariasis cases detected in Futuna during October 2023–June 2024 and barycenter of Taoa cases. Kingdoms of Alo and Sigave are indicated. Inset maps show location of Wallis and Futuna in South Pacific.

sylvatic environments (*12*). This aggressive exophagous species feeds on humans and animals outdoors (*21*). In 1981, biting intensities nearing 100 bites/hour were reported at dusk in Wallis (*8*); similar findings were reported in Samoa (*13*). The vector's biology might explain the increased LF risk linked with traditional habitations like the Polynesian fale. The 3.3 male:female sex bias among 21 cases (clinical and antigenemic) since October 2023 probably reflects higher exposure during more male-centered activities, such as agriculture, farming, and sociocultural practices such as traditional kava-drinking ceremonies (Tauasu), during which men remain outdoors from dusk to early night.

No vector-control measures were implemented during 2013–2021 in Futuna, a highly favorable environment for *Ae. polynesiensis* mosquitoes, which are recognized as a good LF vector, even with low microfilaremia (*10*,*22*,*23*). Together with the high vector density and intense biting exposure, vector biology and ecology probably were strong determinants of this reemergence. Xenomonitoring could improve surveillance and guide much-needed vector-control strategies in post-MDA surveillance (*24*).

Furthermore, LF was not a target for postelimination surveillance. The shorter wording "elimination" used without "as a public health problem" probably caused confusion between "elimination" and "eradication." Consequently, medical staff might not have considered LF as a possible diagnosis in recent years, abandoning passive surveillance altogether.

Active surveillance based on hypereosinophilia initiated in October 2023 used a threshold value of 1,500 cells/mm^3 to evaluate LF using an RDT. A study in French Polynesia evaluated the predictive performance of eosinophilia for LF infection, establishing a lower threshold value of 500 cells/mm^3 for optimal sensitivity and specificity (*25*). According to the laboratory information system, 500 patients had eosinophilia above the 500 cell/mm^3 threshold during June 2023–June 2024, suggesting that many LF cases remain to be identified. Sustaining this surveillance while adopting the lower threshold could increase sensitivity.

Table 3. Univariable logistic regression model results for biologic and risk factors associated with lymphatic filariasis, Futuna, May 2024*

Variable	Univariate OR (95% CI)	p value
Eosinophil count, cells/mm^3	1.00 (1.00–1.00)	0.092
Age, y	0.87 (0.62–1.22)	0.415
Village of habitation		
Other	Referent	
Taoa	17.90 (2.0–163.5)	0.003
Habitation type		
Permanent house	Referent	
Traditional	12.00 (1.9–77.8)	0.023
Repellent or mosquito coil use		
No	Referent	
Yes	2.10 (0.2–18.6)	0.498
Perceived biting density		
High	Referent	
Low	1.50 (0.2–13.5)	0.715
Pigs at household		
No	Referent	
Yes	20,541,717 (0.0–∞)	0.113

*OR, odds ratio.

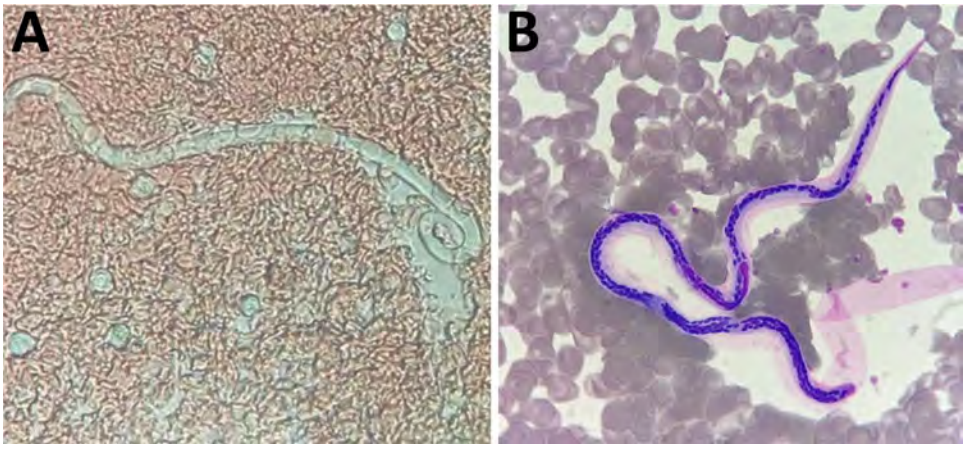

Figure 3. Microphotographs of microfilaria from a sample collected in Futuna, June 2024. A) Fresh blood smear from an antigen-positive child's close contact; original magnification ×40. B) Smear after May-Grunwald-Giemsa staining; original magnification ×100).

This LF surveillance could also be reinforced by integrating a LF RDT during standardized health population surveys aimed at monitoring behavioral risk factors for noncommunicable diseases, including the Global School-Based Health Survey for adolescents and STEPWise for adults conducted on average every 5 years (*26*,*27*). In addition, reinforcing vector-control activities, reducing breeding sites, and promoting individual protection against mosquito bites are essential measures, especially for vulnerable populations living in traditional habitations.

Furthermore, new rounds of MDA could be considered for Futuna, because active surveillance has not shown any resurgence in Wallis. Risk mapping could be refined through xenomonitoring to support this decision. Since 2017, WHO has recommended triple therapy within the GPELF framework (*28*). Adding ivermectin aims to provide longer microfilaricidal activity, further decreasing LF transmission. Ivermectin might also have co-benefits, notably protecting from helminthiases and scabies. However, although triple therapy safety has been reported, its efficacy for subperiodic diurnal LF was not properly evaluated (*29*).

A systematic bibliographic search on PubMed found no reported cluster or postelimination LF resurgence in the 8 PICTs that declared LF elimination since 2016. The reemergence evidenced in Futuna illustrates the importance of postelimination surveillance.

This cross-sectional study estimated LF prevalence in persons <18 years of age born after the last MDA round at ≈2%, much higher than the WHO elimination criterion of <1%. Child prevalence reached 2.5% in the kingdom of Alo and 7.5% in Taoa. Despite a localized cluster in Taoa, 1 case in a child from Sigave with no linkage to Taoa highlighted the need for islandwide interventions. The study also revealed an association between housing type and LF infection, suggesting traditional or precarious housing as a risk factor linked to *Ae. polynesiensis* mosquito biology.

Although hypereosinophilia might be a predictive marker of LF, our study lacked statistical significance, and further studies are required to confirm this predictive value in the specific context of Futuna. The low coverage of MDA administered during 2002–2007, the temporary absence of vector-control measures, and the absence of postelimination surveillance together might explain the resurgence.

These results should have implications on LF elimination programs because they illustrate the critical role of postelimination surveillance and the complexity of its implementation, through the introduction of targeted screening strategies, integrated with larger-scale surveys or xenomonitoring. For countries that have made considerable efforts to achieve elimination, sustaining the elimination status will require implementing efficient postelimination surveillance, particularly in areas where transmission of LF is ensured by *Ae. polynesiensis* mosquitoes. Our study points to the need to step up epidemiologic and entomologic postelimination surveillance and the probable benefits from implementing new rounds of MDA on the island of Futuna to tackle the reemergence of LF. Particular attention should be paid to vulnerable populations who are more affected by this neglected tropical disease, which was no longer considered as a public health problem. This LF reemergence is also a wake-up call for countries that have already reached the status of elimination as a public health problem.

Acknowledgments

The authors warmly thank the territorial education directorate (Vice Rectorat), school directors, and teachers, notably Catherine Le Riblair and Virginie Del Signore. We also thank Berlin Kafoa and Amy Simpson.

About the Author

Mr. Couteaux is an epidemiologist at the Wallis and Futuna Islands Health Agency, where he leads the Health Monitoring and Health Observatory Unit. His primary research interests include infectious diseases and multisource health surveillance.

References

1. Local Burden of Disease 2019 Neglected Tropical Diseases Collaborators. The global distribution of lymphatic filariasis, 2000–18: a geospatial analysis. Lancet Glob Health. 2020;8:e1186–94.
2. World Health Organization. Filariose lymphatique. 2024 Nov 21 [cited 2024 Mar 20]. https://www.who.int/fr/news-room/fact-sheets/detail/lymphatic-filariasis
3. World Health Organization. Global programme to eliminate lymphatic filariasis: progress report, 2020. Wkly Epidemiol Rec. 2022;96:513–24 [cited 2024 Jul 24]. https://iris.who.int/handle/10665/346577
4. World Health Organization. Global programme to eliminate lymphatic filariasis: progress report, 2022. Wkly Epidemiol Rec. 2023;98:489–502 [cited 2024 Jul 24]. https://www.who.int/publications/i/item/who-wer9841-489-502
5. Préfecture des Îles Wallis et Futuna. Résultats du recensement de la population 2023 de Wallis-et-Futuna. 2024 Mar 1 [cited 2024 Mar 27]. https://www.wallis-et-futuna.gouv.fr/Actualites/Les-chiffres-INSEE-du-recensement-2023-authentifies-sont-parus
6. Institut d'Emission Outre-Mer. Rapport annuel économique 2022 de l'IEOM Wallis-et-Futuna. 2023 [cited 2024 May 23]. https://www.ieom.fr/wallis-et-futuna/publications/rapports-annuels-economiques/rapports-annuels-economiques/article/rapport-annuel-economique-2022-de-l-ieom-wallis-et-futuna
7. Office de la Recherche Scientifique et Technique Outre-Mer. Enquête sur la filariose à Wallis. 1959 [cited 2024 Jul 24]. https://horizon.documentation.ird.fr/exl-doc/pleins_textes/divers14-10/12574.pdf
8. Fauran P, Lacoste J, Combes D, Marcille P, Charpin M. *Wuchereria bancrofti* human aperiodic filariasis in French territory of Wallis and Futuna [in French]. Med Trop (Mars). 1981;41:665–9.
9. Ichimori K, Graves PM. Overview of PacELF—the Pacific Programme for the Elimination of Lymphatic Filariasis. Trop Med Health. 2017;45:34. https://doi.org/10.1186/s41182-017-0075-4
10. Pezzoli L, Kim SH, Mathelin JP, Hennessey K, Eswara Aratchige P, Valiakolleri J. An expanded transmission assessment survey to confirm the interruption of lymphatic filariasis transmission in Wallis and Futuna. Am J Trop Med Hyg. 2019;101:1325–30. https://doi.org/10.4269/ajtmh.19-0476
11. Agence de Santé (Wallis et Futuna). Dossier documentant l'élimination de la filariose lymphatique. Wallis and Futuna: Agence de Santé; 2017.
12. Calvez E, Pocquet N, Malau A, Kilama S, Taugamoa A, Labrousse D, et al. Assessing entomological risk factors for arboviral disease transmission in the French Territory of the Wallis and Futuna Islands. PLoS Negl Trop Dis. 2020;14:e0008250. https://doi.org/10.1371/journal.pntd.0008250
13. Samarawickrema W, Sone F, Cummings R. Seasonal abundance, diel biting activity and parity of *Aedes polynesiensis* Marks and *A. samoanus* (Grünberg) (Diptera: Culicidae) in Samoa. Bull Entomol Res. 1987;77:191–200. https://doi.org/10.1017/S0007485300011676
14. Russell RC, Webb CE, Davies N. *Aedes aegypti* (L.) and *Aedes polynesiensis* Marks (Diptera: Culicidae) in Moorea, French Polynesia: a study of adult population structures and pathogen (*Wuchereria bancrofti* and *Dirofilaria immitis*) infection rates to indicate regional and seasonal epidemiological risk for dengue and filariasis. J Med Entomol. 2005;42:1045–56. https://doi.org/10.1093/jmedent/42.6.1045
15. Weil GJ, Curtis KC, Fakoli L, Fischer K, Gankpala L, Lammie PJ, et al. Laboratory and field evaluation of a new rapid test for detecting *Wuchereria bancrofti* antigen in human blood. Am J Trop Med Hyg. 2013;89:11–5. https://doi.org/10.4269/ajtmh.13-0089
16. Cheng J, Schloerke B, Karambelkar B, Xie Y. leaflet: Create interactive web maps with the JavaScript "Leaflet" library. R package version 2.2.2.9000. 2024 [cited 2024 Aug 21]. https://github.com/rstudio/leaflet
17. Bivand R. R packages for analyzing spatial data: a comparative case study with areal data. Geogr Anal. 2022;54:488–518. https://doi.org/10.1111/gean.12319
18. Kulldorff M. A spatial scan statistic. Commun Stat Theory Methods. 1997;26:1481–96. https://doi.org/10.1080/03610929708831995
19. World Health Organization. Monitoring and epidemiological assessment of mass drug administration in the global program to eliminate lymphatic filariasis: a manual for national elimination programs [in French]. 2013 [cited 2024 Jul 24]. https://iris.who.int/handle/10665/85616
20. Rajaonarifara E, Roche B, Chesnais CB, Rabenantoandro H, Evans M, Garchitorena A. Heterogeneity in elimination efforts could increase the risk of resurgence of lymphatic filariasis in Madagascar. Infect Genet Evol. 2024;120:105589. https://doi.org/10.1016/j.meegid.2024.105589
21. Rivière F. Ecologie de *Aedes* (*Stegomyia*) *polynesiensis*, Marks, 1951, et transmission de la filariose de Bancroft en Polynésie. Paris: Université de Paris Sud Centre d'Orsay; 1988.
22. Pichon G. Limitation and facilitation in the vectors and other aspects of the dynamics of filarial transmission: the need for vector control against *Anopheles*-transmitted filariasis. Ann Trop Med Parasitol. 2002;96(Suppl 2):S143–52. https://doi.org/10.1179/000349802125002509
23. Snow LC, Bockarie MJ, Michael E. Transmission dynamics of lymphatic filariasis: vector-specific density dependence in the development of *Wuchereria bancrofti* infective larvae in mosquitoes. Med Vet Entomol. 2006;20:261–72. https://doi.org/10.1111/j.1365-2915.2006.00629.x
24. Lau CL, Won KY, Lammie PJ, Graves PM. Lymphatic filariasis elimination in American Samoa: evaluation of molecular xenomonitoring as a surveillance tool in the endgame. PLoS Negl Trop Dis. 2016;10:e0005108. https://doi.org/10.1371/journal.pntd.0005108
25. Musso D, Vialette V. Predictive value of the eosinophil counts in the biological diagnosis of lymphatic filariasis in French Polynesia. Med Mal Infect. 2012;42:585–90. https://doi.org/10.1016/j.medmal.2012.09.006
26. World Health Organization. STEPwise approach to NCD risk factor surveillance (STEPS). 2025 [cited 2024 Dec 23]. https://www.who.int/teams/noncommunicable-diseases/surveillance/systems-tools/steps
27. World Health Organization. Global school-based student health survey. 2025 [cited 2024 Dec 23]. https://www.who.int/teams/noncommunicable-diseases/surveillance/systems-tools/global-school-based-student-health-survey

28. World Health Organization. Guideline: alternative mass drug administration regimens to eliminate lymphatic filariasis. 2017 [cited 2024 Jul 26]. https://iris.who.int/handle/10665/259381
29. Hardy M, Samuela J, Kama M, Tuicakau M, Romani L, Whitfeld MJ, et al. Individual efficacy and community impact of ivermectin, diethylcarbamazine, and albendazole mass drug administration for lymphatic filariasis control in Fiji: a cluster randomized trial. Clin Infect Dis. 2021;73:994–1002. https://doi.org/10.1093/cid/ciab202

Address for correspondence: Clément Couteaux, Health Agency of Wallis and Futuna, BP-4G, UVEA, Wallis and Futuna; email: clement.couteaux@adswf.fr

January 2025

Antimicrobial Resistance

- Global Health's Evolution and Search for Identity
- Pneumococcal Septic Arthritis among Adults, France, 2010–2018
- *Rickettsia sibirica mongolitimonae* Infections in Spain and Case Review of the Literature
- The Rise of Mpox in a Post-Smallpox World
- Meningococcal C Disease Outbreak Caused by Multidrug-Resistant *Neisseria meningitidis*, Fiji
- Cluster of Legionellosis Cases Associated with Manufacturing Process, South Carolina, USA, 2022
- Systematic Review of Avian Influenza Virus Infection and Outcomes during Pregnancy
- Ongoing Evolution of Middle East Respiratory Syndrome Coronavirus, Saudi Arabia, 2023–2024
- Population-Based Study of Emergence and Spread of *Escherichia coli* Producing OXA-48–Like Carbapenemases, Israel, 2007–2023
- Social Contact Patterns in and Age Mixing before and during COVID-19 Pandemic, Greece, January 2020–October 2021
- *Neisseria meningitidis* Serogroup Y Sequence Type 1466 and Urogenital Infections
- Social Contact Patterns in Rural and Urban Settings, Mozambique, 2021–2022

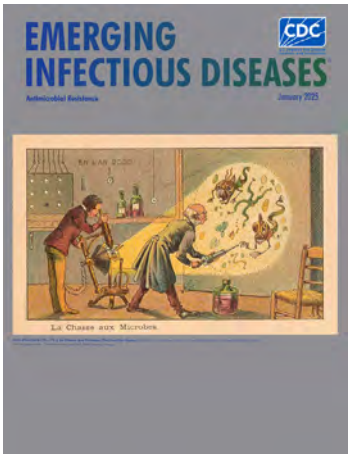

- Trichuriasis in Human Patients from Côte d'Ivoire Caused by Novel *Trichuris incognita* Species with Low Sensitivity to Albendazole/Ivermectin Combination Treatment
- Surveillance Strategy in Duck Flocks Vaccinated against Highly Pathogenic Avian Influenza Virus
- Cefiderocol Resistance Conferred by Plasmid-Located Ferric Citrate Transport System in KPC–Producing *Klebsiella pneumoniae*
- Influenza A(H5N1) Virus Clade 2.3.2.1a in Traveler Returning to Australia from India, 2024
- Fatal Case of Crimean-Congo Hemorrhagic Fever, Portugal, 2024
- Case Reports of Human Monkeypox Virus Infections, Uganda, 2024
- Equine Encephalomyelitis Outbreak, Uruguay, 2023–2024
- Invasive Group B *Streptococcus* Infections Caused by Hypervirulent Clone of *S. agalactiae* Sequence Type 283, Hong Kong, China, 2021
- Detection and Genomic Characterization of Novel Mammarenavirus in European Hedgehogs, Italy
- Domestic Cat Hepadnavirus Infection in Iberian Lynxes
- Toxigenic *Corynebacterium diphtheriae* Infections in Low-Risk Patients, Switzerland, 2023
- Detection of Prions in Wild Pigs (*Sus scrofa*) from Areas with Reported Chronic Wasting Disease Cases, United States
- Clonal Complex 398 Methicillin-Resistant *Staphylococcus aureus* Producing Panton-Valentine Leukocidin, Czech Republic, 2023
- Fatal Mixed *Plasmodium Infection* in Traveler Returning to Colombia from Comoros Islands, 2024
- Evidence of Influenza A(H5N1) Spillover Infections in Horses, Mongolia
- *Salmonella enterica* Serovar Abony Outbreak Caused by Clone of Reference Strain WDCM 00029, Chile, 2024
- Identification and Characterization of Vancomycin- Resistant *Staphylococcus aureus* (VRSA) CC45/USA600, North Carolina, USA, 2021

EMERGING INFECTIOUS DISEASES

To revisit the January 2025 issue, go to:
https://wwwnc.cdc.gov/eid/articles/issue/31/1/table-of-contents

Model-Based Analysis of Impact, Costs, and Cost-effectiveness of Tuberculosis Outbreak Investigations, United States

Sourya Shrestha, Lucia Cilloni, Garrett R. Beeler Asay, J. Steve Kammerer, Kala Raz, Tambi Shaw, Martin Cilnis, Jonathan Wortham, Suzanne M. Marks, David Dowdy

Outbreak investigation is an essential component of tuberculosis (TB) control in the United States, but its epidemiologic impact and cost-effectiveness have not been quantified. We modeled outbreak investigation activities in the United States during 2023–2032 and estimated corresponding epidemiologic impact, economic costs (in 2022 US$), and incremental cost-effectiveness ratios from the healthcare system perspective (cost per additional quality-adjusted life-year gained). We projected that outbreak investigations would result in 1,030,000 (95% uncertainty interval [UI] 376,000–1,740,000) contacts investigated, leading to 4,130 (95% UI 1,420–7,640) TB diagnoses and 104,000 (95% UI 37,600–181,000) latent TB infection diagnoses, at a total cost of US $219 million (95% UI $80–$387 million). We estimated that 5,560 (95% UI 1,720–11,400) TB cases would be averted through early detection and treatment, and the incremental cost-effectiveness of outbreak investigations, compared with no outbreak investigations, was $27,800 per quality-adjusted life-year gained (95% UI $4,580–$68,700).

Outbreak investigation continues to be an essential part of tuberculosis (TB) control in the United States (*1*–*3*). By promptly detecting and treating TB disease and latent TB infection (LTBI) among contacts of persons with TB or in settings in which TB transmission is likely to be ongoing, outbreak investigations play a critical role in curbing ongoing community transmission. TB incidence in the United States fell by >70% during 1993–2019, and widespread programmatic implementation of contact and outbreak investigations was likely a key contributor to this observed decline (*4*,*5*).

However, TB outbreaks continue to cause substantial illness, particularly in vulnerable populations, which include persons in racial and ethnic minority groups, persons living in congregate settings (such as correctional facilities and homeless shelters), and persons with underlying conditions, who have a higher predisposition to poor TB outcomes (*6*–*9*). Even though a minority of new TB cases (≈14%) in the United States are attributed to recent transmission (*10*,*11*), extensive public health resources are required for TB investigation and control, and outbreak investigations can present substantial financial and workload burdens to frontline public health departments. As such, outbreak prevention and control remain essential to eliminate TB in the United States, and improving the impact of these activities can further accelerate progress toward TB elimination goals. In this model-based analysis, we sought to estimate the epidemiologic effects of control efforts and quantify the cost-effectiveness of TB outbreak response efforts in the United States.

Methods

Projection of TB Outbreaks in the United States

We projected the number of TB cases, the number of TB clusters, and the distribution of cluster sizes in the United States during 2023–2032. TB cases were projected by extrapolating the trend of TB cases during 2014–2019 (1.1% annual decline) (*1*). To allow for additional uncertainty in TB incidence caused by other factors, such as the COVID-19 pandemic–related disruptions, we assumed that, relative to the prepandemic

Author affiliations: Johns Hopkins Bloomberg School of Public Health, Baltimore, Maryland, USA (S. Shrestha, L. Cilloni, D. Dowdy); Centers for Disease Control and Prevention, Atlanta, Georgia, USA (G.R.B. Asay, J.S. Kammerer, K. Raz, J. Wortham, S.M. Marks); California Department of Public Health, Richmond, California, USA (T. Shaw, M. Cilnis)

DOI: https://doi.org/10.3201/eid3103.240633

TB trajectory, from a 5% increase to a 10% decline could be seen in the number of cases projected during the study period (Tables 1, 2). We simulated cluster size distributions of TB outbreaks using a branching process model with a Poisson lognormal distribution (*12*). This model was previously developed and fitted to genotype cluster size distribution data in the United States (*12*), where cases were defined as clustered if they had matching spacer oligonucleotide typing (spoligotype) and 24-locus mycobacterial interspersed repetitive unit–variable number tandem-repeat genotyping results, and they were reported within the same state during 2012–2016 (*29*) (Appendix, https://wwwnc.cdc.gov/EID/article/31/3/24-0633-App1.pdf). Finally, we estimated the number of clusters on the basis of both the projected number of incident cases and the cluster size distribution, such that the sum of cases across simulated clusters equaled the projected number of incident cases.

Epidemiologic Impact of Outbreak Investigation

For the purposes of this analysis, we assumed that all genotype clusters of ≥3 cases would be considered for outbreak investigation response, consistent with assumptions in previous outbreak investigation reviews (*2*). We estimated the number of contacts investigated per case during an outbreak investigation using historical data on outbreak investigations in the United States (*2*,*3*), accounting for contact investigations expected to occur outside of outbreak investigation based on the Aggregate Reports for Program Evaluation (ARPE) from reporting jurisdictions (50 states and 9 cities) to the Centers for Disease Control and Prevention (CDC) (*13*) (Appendix). Among the contacts investigated during the outbreak response, we estimated the number of persons who would be identified as having TB disease and LTBI on the basis of historical data on outbreak investigations and from

Table 1. Descriptions, estimates and uncertainty ranges for parameters describing TB outbreaks and outbreak investigations in study of impact, costs, and cost-effectiveness of TB outbreak investigations, United States*

Model parameters	Point estimate	Lower value	Upper value	Sources and additional notes
Projection of TB cases and outbreaks				
Projected decline in TB cases, year-on-year % decline	1.06%	0%	2%	Based on year-on-year % decline in TB cases in the United States, 2014–2019 (*1*).
Change in TB incidence from the projected baseline because of other factors (e.g., COVID-19 pandemic)	No change	10% decrease	5% increase	Assumption. If r is the annual rate of decline in TB cases before the pandemic, and Δ is the impact of the pandemic, then the number of TB cases projected in the year $y, TB(y)$ is given by: $TB(y) = TB(2019) \times (1-\Delta) \times e^{-r(y-2019)}$.
R_0	0.29	0.19	0.38	Shrestha et al. (*12*)†
Individual level heterogeneity, SD of the Poisson lognormal model	1.9	1.8	2	Shrestha et al. (*12*)†
Characterization of outbreak investigation				
Outbreak investigation threshold		≥3 cases		Assumption, as in Mindra et al. (*2*).
No. contacts investigated per case during outbreak investigation	55	10	78	Mitruka et al. (*3*) reported 42 total contacts investigated per case among 27 outbreaks during 2002–2008; Mindra et al. (*2*) reported 88 contacts per case among 21 outbreaks during 2009–2015. We assumed that on average 10 contacts would be evaluated per case outside of outbreak investigation, on the basis of ARPE report (*13*), and that 5% of the case investigations occur as a part of outbreak investigation (Appendix, https://wwwnc.cdc.gov/EID/article/31/3/24-0633-App1.pdf).
% Contacts evaluated	79%	75%	85%	ARPE report (*13*)
% LTBI diagnoses in evaluated contacts	13%	10%	15%	Mitruka et al. (*3*), ARPE report (*13*)
% Contacts with LTBI initiating LTBI treatment	73%	70%	75%	ARPE report (*13*)
% Contacts with LTBI completing LTBI treatment	57%	55%	65%	ARPE report (*13*); this is a product of the percentage of contacts with LTBI initiating treatment, and percentage of those initiating that complete treatment.
% Evaluated contacts with TB disease	0.5%	0.29%	0.72%	Mitruka et al. (*3*) reports 0.62%; 0.72% by ARPE report (*13*); Mindra et al. (*2*) reports 0.29%.

*3HP, 3 months of isoniazid and rifapentine; 9H, 9 months of isoniazid; ARPE, Aggregate Reports for Program Evaluation; CDC, Centers for Disease Control and Prevention; IGRA, interferon-γ release assay; LTBI, latent TB infection; QALY, quality-adjusted life-years; R_0, basic reproduction number; TB, tuberculosis.

†Based on Poisson lognormal distributions fitted to cluster-size distribution of genotype linked cases in the United States during 2012–2016.

Table 2. Descriptions, estimates and uncertainty ranges for parameters describing TB natural history, costs of TB outbreak investigations, and cost-effectiveness evaluation in study of impact, costs, and cost-effectiveness of TB outbreak investigations, United States*

Model parameters	Point estimate	Lower value	Upper value	Sources and additional notes
Characterization of TB natural history and the impact of intervention				
% Contacts who will develop TB within 5 years after infection	6.6%	3%	15%	Based on estimates of reactivation of LTBI among recent exposure (*14*) and among close contacts of TB patients (*15*). Lower value of 3% reflects uncertainty in the recency of the infection among contacts.
Efficacy of completed LTBI treatment	93%	70%	95%	Estimates from 9H trial and noninferiority of 3HP compared with 9H (*16*,*17*).
R_0 of cases detected during outbreak investigation	0.29	0.15	1.5	R_0 of 0.29 from Shrestha et al. (*12*). Upper value of 1.5 for R_0 reflects outbreak settings with higher transmission.
% Reduction in infectious period through early detection	50%	25%	75%	Modeled as reduction in R_0 based on higher case detection and notification in contact investigations (*18*), resulting in reduction in delays in TB diagnosis, a contributor to outbreaks (*2*).
Unit cost estimates, 2022 US$				
Cost of PCR-based genotyping, per isolate	$35	$25	$50	CDC (culture, typing, and identification by nucleic acid probe, amplified probe technique) (*19*).
Cost of outbreak investigation, cost per contact during outbreak investigation†	$151	$86	$225	Unpublished data from 2 outbreaks in California (average cost of $106 per contact (2014 US$) (T. Shaw, unpub. data) (Appendix, https://wwwnc.cdc.gov/EID/article/31/3/24-0633-App1.pdf); unpublished CDC data reports mean cost of $175.90 ($78.00–$293.50) (2022 US$) (*20*).
Cost of LTBI testing per contact	$71	$60	$80	Includes costs of IGRA LTBI testing, and costs of chest radiograph and TB test to rule out TB disease among those testing positive for IGRA (*19*,*21*,*22*).
Cost of LTBI treatment per infected contact	$515	$300	$700	Includes costs of 3HP (*23*), laboratory testing, and toxicity both requiring and not requiring hospitalization (*24*). Assumes toxicity among 3.2% (*20*) of persons receiving LTBI treatment (*25*), and 0.015% requiring hospitalization (*26*).
Cost of TB treatment per contact with disease	$23,543	$15,000	$30,000	Direct TB treatment costs for non–MDR TB (*27*).
QALY estimates				
Annual discount rate		3%		Assumption
QALYs gained per TB case averted	1.16	0.74	1.39	Assumes 4.7% average mortality among people with TB, 36.3 years of average life expectancy at TB diagnosis, and health utility of 0.76 during TB treatment (*28*).‡
QALYs lost per LTBI treatment	0.002	0.0015	0.0025	Jo et al. (*20*).§

*3HP, 3 months of isoniazid and rifapentine; 9H, 9 months of isoniazid; ARPE, Aggregate Reports for Program Evaluation; CDC, Centers for Disease Control and Prevention; IGRA, interferon-gamma release assay; LTBI, latent TB infection; MDR, multidrug resistant; QALY, quality-adjusted life-years; TB, tuberculosis.
†Excludes costs associated with TB and LTBI treatment.
‡See Appendix for details on TB mortality rates; other data were incorporated to construct the range.
§QALY estimate assumes toxicity among 3.2% of persons receiving LTBI treatment (*25*), and 0.015% requiring hospitalization (26).

contact investigations (*2*,*3*,*13*). For persons who tested positive for LTBI, we also estimated the proportion who would initiate and complete LTBI treatment on the basis of data reported in ARPE (*13*).

We assumed that outbreak investigations would result in earlier detection of TB, thus also preventing further transmission by reducing the number of secondary cases by 50% (with sensitivity analysis including an uncertainty range of 25%–75%). On the basis of historical data (*2*,*3*,*13*), we assumed that TB disease would be diagnosed and treatment would be initiated in 0.5% (uncertainty range 0.29%–0.72%) of contacts; we assumed that LTBI would be diagnosed in 13% (uncertainty range 10%–15%) of contacts, and 57% (uncertainty range 55%–65%) of them would initiate and complete LTBI treatment (*13*) with an efficacy of 93% (uncertainty range 70%–95%) (*16*,*17*). We assumed that 6.6% (uncertainty range 3%–15%) of persons in whom LTBI was diagnosed during an outbreak investigation would develop reactivation TB within 5 years (in the absence of LTBI treatment), on the basis of published estimates of progression after recent exposure or progression specifically among close contacts (*14*,*15*).

Cost-effectiveness of Outbreak Investigation

We used a TB-centered health systems perspective to estimate costs and cost-effectiveness and focused on incorporating costs and benefits that are directly related to TB-related services and outcomes. We relied

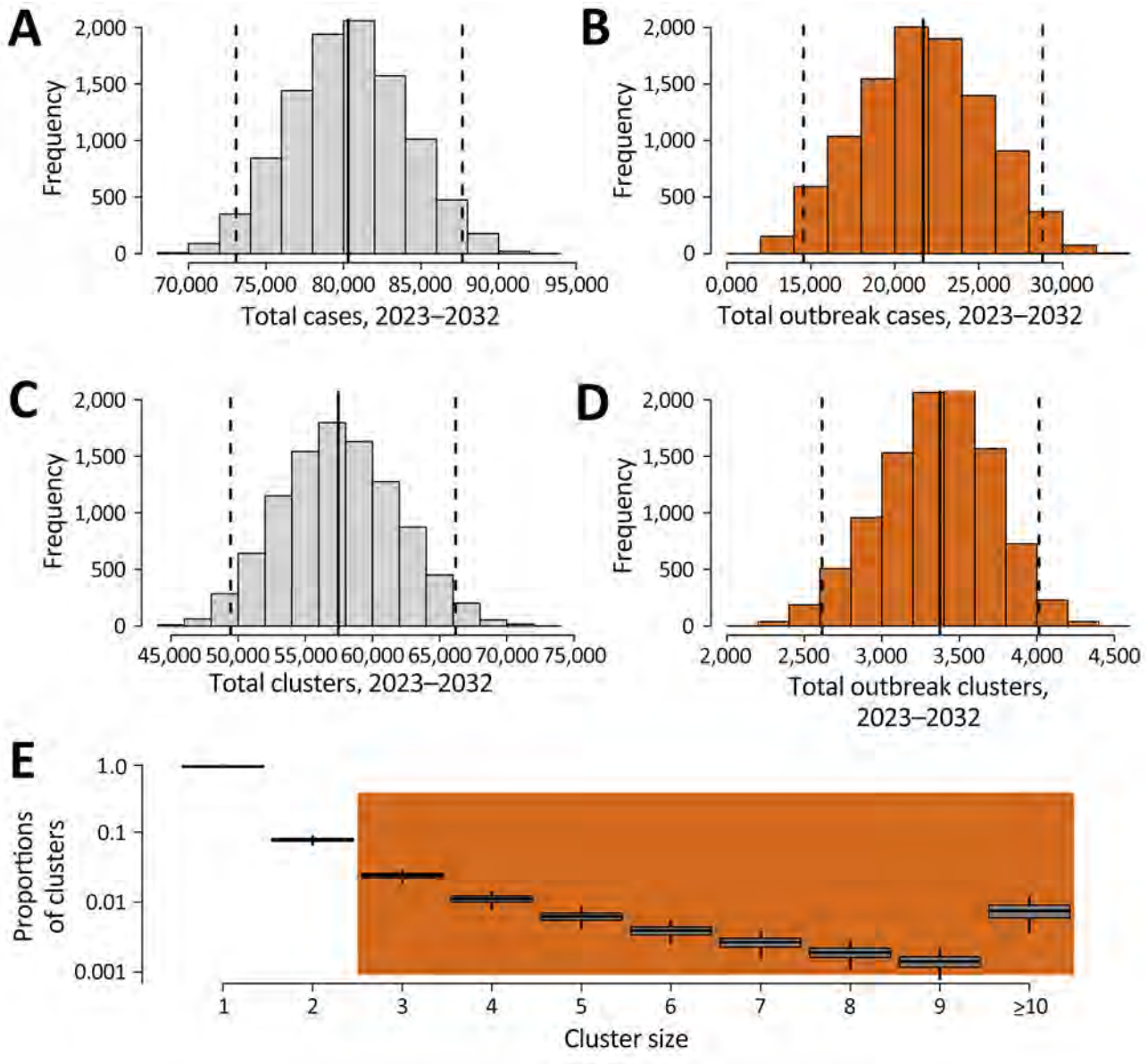

Figure 1. Projected TB cases and outbreaks, 2023–2032, United States, in study of impact, costs, and cost-effectiveness of TB outbreak investigations. Shown are the total number of TB cases (A), the number of TB cases occurring in outbreaks (B), the total number of TB clusters (C), and the number of TB outbreaks (i.e., clusters of ≥3 cases) (D) projected to occur during 2023–2032 and cluster size distributions of the TB clusters (E). Clusters of size 1 are assumed to have no transmission links, and only clusters with ≥3 cases (shaded in orange) are investigated in outbreak investigations.

on published literature and other sources to estimate costs associated with outbreak investigations (Tables 1, 2). We incorporated costs of genotyping, assuming all cases (including those that might end up being part of outbreak investigation) are genotyped; conducting outbreak investigation on all outbreaks of ≥3 cases (excluding TB and LTBI treatment costs); and testing contacts of outbreak TB cases for LTBI and treating persons who tested positive. Unit costs of genotyping included the costs of culturing *Mycobacterium tuberculosis*, genotyping the isolate, and nucleic acid amplification at the CDC laboratory. Outbreak investigation costs were based on 2 sources. The first source was unpublished data from 2 outbreaks in northern California during 2010–2014 (T. Shaw, unpub. data). A total of 276 contacts were investigated across the 2 outbreaks; the corresponding total cost was $29,238 ($106 [in 2014 US dollars] per person investigated), including coordination and communication, analytical activities, case management, contact identification, and evaluation (Appendix). We also used CDC data from Njie et al. (*20*), who reviewed the costs of contact investigations

Table 3. Projected scope of TB outbreak investigations during 2023–2032 in study of impact, costs, and cost-effectiveness of TB outbreak investigations, United States*

Projected outcome	Point estimate	Lower bound	Upper bound
No. TB outbreaks with ≥3 cases investigated	3,350	2,610	4,010
No. outbreak-related TB cases	21,700	14,600	28,800
No. contacts investigated during outbreak investigations	1,030,000	376,000	1,740,000
No. TB cases detected	4,130	1,420	7,640
No. contacts with LTBI detected	104,000	37,600	181,000
No. contacts with LTBI initiating treatment	75,700	27,100	131,000
No. contacts with LTBI completing treatment	61,500	22,000	107,000

*The point estimate is the mean, and the lower and upper bounds represent the 2.5th and 97.5th percentiles across all 10,000 simulations. LTBI, latent TB infection; TB, tuberculosis.

across the United States and estimated the mean cost to be $175.90 (95% CI $78.00–$293.50) per contact. In estimating unit costs of testing and treatment, we assumed that interferon-gamma release assays were used for LTBI testing and that treatment consisted of the 3HP regimen (3 months of self-administered isoniazid and rifapentine) (*21*). We accounted for the costs of chest radiography (*19*,*22*) and laboratory costs (*23*), as well as toxicity and hospitalization during treatment (*24*–*26*). The averted future costs of TB treatment likewise included inpatient and hospitalization costs (*30*,*31*) (Tables 1, 2). We assumed that outbreak investigation costs were distributed evenly over the 10-year analytic period, that future cases resulting from exposure during outbreaks occurred within 5 years of completing the outbreak investigation, and that those cases were distributed exponentially over the 5-year period. We measured all costs from the health system perspective and matched costs to 2022 dollars using the Health Care Price Index for personal consumption expenditures from the US Bureau of Economic Analysis (*32*). We discounted future costs and cost savings at 3% annually.

The primary cost-effectiveness outcome was the incremental cost-effectiveness ratio (ICER) of outbreak investigation activities (cost per quality-adjusted life year [QALY] gained) during 2023–2032, comparing a baseline scenario in which outbreak investigations are conducted (using conventional genotyping) to a counterfactual scenario in which no outbreak investigation activities are conducted. Following the approach taken by Jo et al. (*21*), we estimated the net number of QALYs gained as the difference between the total QALYs gained, resulting from averted future TB cases and averted disabilities among those that are diagnosed during outbreak investigations, and QALYs lost because of the toxicity of treatment. QALY losses associated with TB disease included TB-related mortality rates (*23*) and loss of quality of life during TB treatment (*28*) and QALY losses associated with LTBI treatment, including both toxicity (*25*) and hospitalization (*26*) during treatment (Appendix).

Model Simulation

We used a Monte Carlo approach to generate estimates of our model outcomes. We performed 10,000 model simulations, each using a parameter set generated by probabilistically sampling model parameters. Each model parameter was drawn from a triangular distribution, where the mode of the distribution was taken to be the point estimate, and the range of the distribution varied between the lower and the upper values (Tables 1, 2). For each outcome, we reported the mean and the 95% uncertainty interval (UI; 2.5th–97.5th percentiles) across all model simulations. As a sensitivity analysis of our choice of parameter distribution, we also considered PERT (program evaluation and review technique) distribution and a mixture of PERT and gamma distributions (Appendix). We performed model simulations by using R software (The R Project for Statistical Computing, https://www.r-project.org).

Sensitivity Analyses

We conducted a multivariate sensitivity analysis to explore the sensitivity of the primary outcome to uncertainty in parameter values. We varied all model parameters across specified ranges according to parameter-specific distributional assumptions and

Table 4. Projected epidemiologic impact of TB outbreak investigations, United States, 2023–2032*

Projected outcome	Point estimate	Lower bound	Upper bound
No. TB cases averted from early detection†	1,330	266	3,650
No. TB cases averted through LTBI treatment‡	4,220	1,200	9,090
Total TB cases averted	5,560	1,720	11,400

*The point estimate is the mean, and the lower and upper bounds represent the 2.5th and 97.5th percentiles across all 10,000 simulations. LTBI, latent TB infection; TB, tuberculosis.
†Includes cases expected from transmission that would have occurred within five years, in the absence of outbreak investigation.
‡Includes cases expected to result from reactivation of LTBI that would have occurred within five years among persons who are detected with LTBI and complete LTBI treatment during an outbreak investigation.

Table 5. Cost and cost-effectiveness (in 2022 US dollars) of TB outbreak investigation, United States, 2023–2032*

Projected outcomes	Point estimate	Lower bound	Upper bound
Costs of genotyping, millions	$2.5	$1.85	$3.24
Costs of outbreak investigation, millions	$135.0	$46.6	$251.0
Costs of LTBI testing, millions	$49.0	$17.7	$84.4
Costs of LTBI treatment, millions	$32.4	$11.0	$60.6
Total cost, millions	$219.0	$80.0	$387.0
Averted future costs of TB treatment, millions†	($102.0)	($29.7)	($216.0)
QALYs gained by averted TB	4,890	1,490	103,000
QALYs gained by averted TB-related disabilities through early diagnosis	183	51.4	4020
Total QALYs gained	5,070	1,560	106,000
QALYs lost during LTBI treatment	98.7	34.6	177.0
Cost per QALY gained	$27,800	$4,580	$68,700

*The point estimate is the mean, and the lower and upper bounds represent the 2.5th and 97.5th percentiles across all 10,000 simulations. LTBI, latent TB infection; QLY, quality-adjusted life-years; TB, tuberculosis.
†Future costs of treating future cases are discounted on the basis of their expected time of occurrence up to 5 years into the future.

compared the difference in projected incremental cost-effectiveness between the 1,000 simulations in which the value of the parameter of interest was in the top decile and the 1,000 simulations in which that value was in the bottom decile.

Results

We projected that 3,350 (95% simulation UI 2,610–4,010) outbreaks (clusters with ≥3 TB cases) would occur in the United States over the 10-year period of 2023–2032 and that those outbreaks would include a total of 21,700 (95% UI 14,600–28,800) cases (Figure 1). During this period, we estimated that 1.03 million (95% UI 376,000–1,740,000) persons who had contact with an outbreak TB case would require investigations. Of those persons, we projected that TB disease would be diagnosed in 4,130 (95% UI 1,420–7,640) persons and LTBI would be diagnosed in 104,000 (95% UI 37,600–181,000) persons, reflecting recent infection during the outbreak. Of those persons, we estimated that 61,500 (95% UI 22,000–107,000) would successfully complete LTBI treatment (Table 3).

We estimated that 1,330 (95% UI 266–3,650) cases of future TB would be averted by outbreak investigation through early detection and averted transmission and an additional 4,220 (95% UI 1,200–9,090) cases would be prevented by treating LTBI. Thus, a total of 5,560 (95% UI 1,720–11,400) projected future cases would be averted in the United States through outbreak investigation over the 10-year period of 2023–2032 (Table 4).

We estimated that outbreak investigation activities would cost a total of $219 million (95% UI $80–$387 million) during 2023–2032. This total cost includes the costs of genotyping (1% of the total cost), conducting outbreak investigations (62%), LTBI testing (22%), and LTBI treatment (15%). The estimated (discounted) cost of preventing TB that would be averted through outbreak investigation was $102 million (95% UI $29.7–$216 million), for a net cost of $109 million (95% UI $24.7–$249 million) over 10 years. We estimated the ICER of outbreak investigations compared with no outbreak investigations to be $27,800 per additional QALY gained (95% UI $4,580–$68,700) (Table 5). Our estimates of the epidemiologic effects and cost-effectiveness were robust to the choice of parameter distributions (Appendix).

The factors that were most influential to the estimated cost-effectiveness of outbreak investigation activities consisted of characteristics of outbreak investigations, such as the proportion of contacts that were TB and LTBI cases (Figure 2); epidemiologic quantities, such as the reactivation rate of LTBI cases among outbreak contacts and the number of secondary transmissions per outbreak-related case; and cost-related variables, such as the cost of outbreak investigation (cost per contact) and the cost of treating future TB cases. Under all variations of parameter values evaluated in the sensitivity analysis, the estimated ICER did not exceed $70,000 per additional QALY gained.

Discussion

In this model-based analysis of TB outbreak investigation in the United States during 2023–2032, we projected that outbreak investigation activities could prevent 5,560 cases of TB, a number equal to ≈6% of all incident cases (and ≈40% of all recent transmission cases) expected to occur in the country during that time (*5*,*10*,*11*). Furthermore, compared with other TB interventions in the United States, such as targeted testing and treatment of LTBI that has been previously evaluated as cost-effective in populations at risk for TB (*33*,*34*), outbreak investigation activities are generally more cost-effective at ≈$28,000 per QALY gained in the most likely scenario (<$70,000 per QALY gained in the most pessimistic scenarios). Those results strongly support maintaining TB outbreak response activities in the United States.

Historical data from outbreak investigations in the United States show that outbreak response activities are highly effective in finding both persons with TB disease and those with LTBI (*2*,*3*,*13*,*35*). For example, the prevalence of TB among persons investigated during outbreak investigations is >100 times

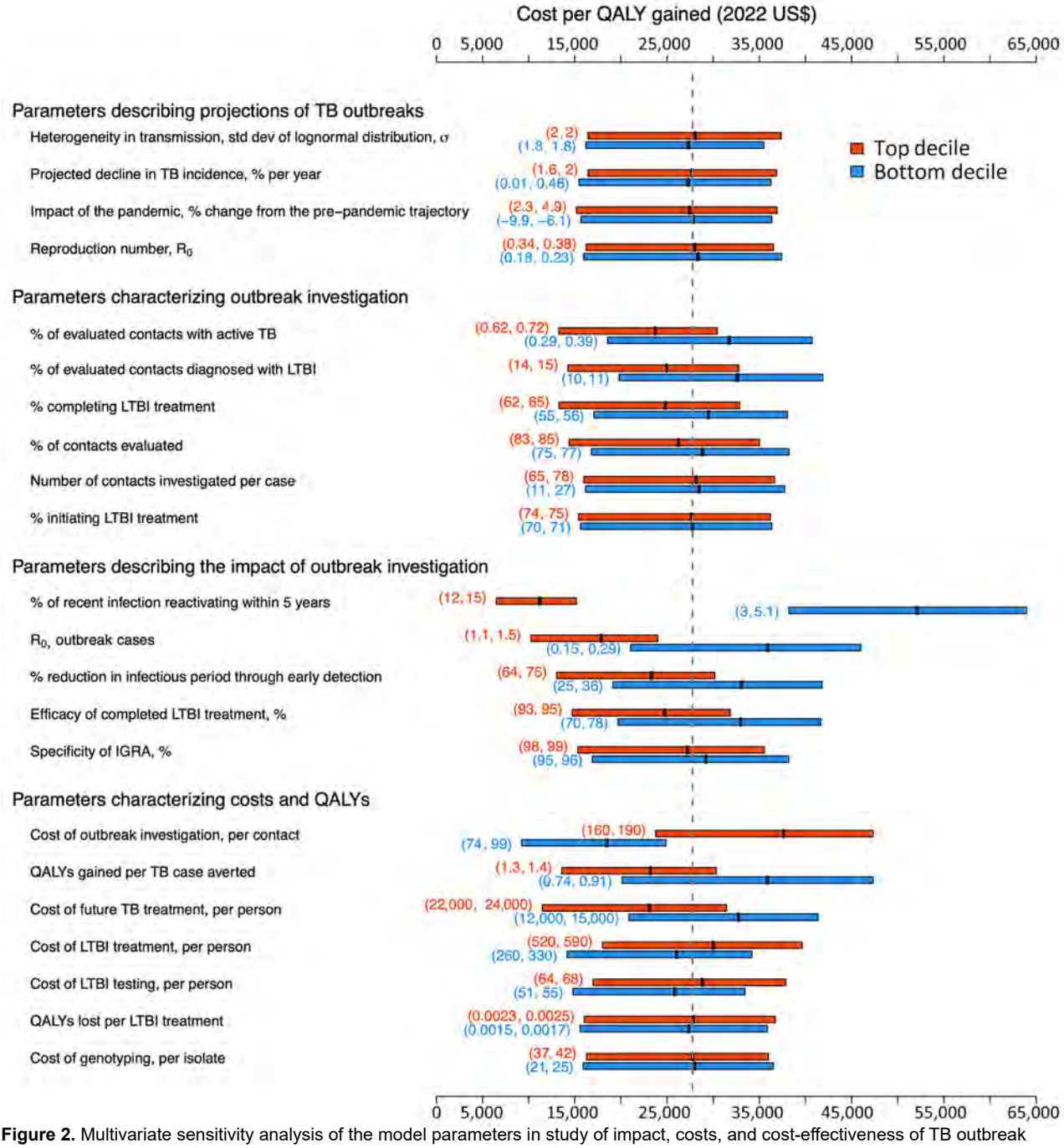

Figure 2. Multivariate sensitivity analysis of the model parameters in study of impact, costs, and cost-effectiveness of TB outbreak investigations, United States. This graph illustrates sensitivity of the incremental cost-effectiveness ratio of TB outbreak investigation in the United States (cost in 2022 US$ per QALY gained, compared with no outbreak investigation) to the values of individual model parameters. Each pair of boxplots shows variation in the outcome when the analysis was limited to either simulations in which the value of the parameter of interest was in the top (red) or bottom (blue) decile of its values across all simulations. The edges of each box represent the lower and upper interquartile range, and the band in the middle represents the mean. The vertical dashed line shows the mean across all simulations ($27,800 per QALY gained, corresponding to the primary outcome). The numbers within parentheses represent the parameter range (up to 2 significant figures) for the top (red) or the bottom (blue) decile. IGRA, interferon-γ release assay; LTBI, latent TB infection; QALY, quality-adjusted life-years; R_0, basic reproduction number; TB, tuberculosis.

the prevalence of TB in the general population, and the prevalence of LTBI is 3–5 times higher (*5*,*36*,*37*). Furthermore, early diagnosis and treatment of TB and LTBI during outbreak investigation are more likely to prevent future TB disease that would have occurred through transmission and reactivation. Factors that contribute to the occurrence of outbreaks, including higher prevalence of known risk factors such as substance use (*7*), barriers in access to care (*38*), and congregate living arrangements (*6*,*9*), also result in higher risks of ongoing transmission if TB is not promptly diagnosed and treated (*39*). In addition, persons in whom LTBI is diagnosed during outbreaks are more likely to have been exposed recently and, therefore, are at substantially higher risk for progression (*14*,*15*). Thus, even as the prevalence of TB in the United States continues to decline, robust outbreak response activities are likely to remain cost-effective.

This analysis assumed conventional PCR-based genotyping methods to define outbreaks. However, in 2018, the CDC began implementing whole-genome sequencing (WGS)–based genotyping methods; the costs associated with using those methods might differ from PCR-based genotyping and might also enable increased discriminatory power, as well as the ability to perform more detailed analyses and exclude genetically distant cases from the outbreak investigation (*40*,*41*). In addition, drug resistance testing can be performed with WGS, reducing the need for separate drug susceptibility testing. Finally, we exclusively modeled 3HP as the LTBI treatment regimen, but other regimens are also being used. Future analyses could refine our estimates by incorporating the costs and benefits of WGS for outbreak investigation and changes in LTBI treatment regimens.

TB outbreaks vary substantially in size and by setting, geography, and context (*12*). Because most outbreak investigations are conducted locally, the costs and extent of outbreak response activities also vary widely from one outbreak to the next and from one location to the next. We relied on historical data, such as those reported in reviews of outbreak investigations (*2*,*3*) and the ARPE (*14*), to estimate the average extent of TB outbreak response activities and used data from a small number of outbreak investigations to estimate corresponding costs. Those outbreak investigations might not be representative of the spectrum of outbreak investigations that are conducted across the country and across a variety of settings. Furthermore, the type of activities that constitute an outbreak investigation, including analytical activities, communication, and coordination, are likely to vary by setting and context. As such, our estimates should not be taken as reflective of any single outbreak investigation in any specified location but rather as an average estimate with substantial variability, as reflected in the uncertainty around our projections. More detailed data are required to better characterize variations in cost and cost-effectiveness of outbreak investigation across the United States, including how costs might scale with the size of the corresponding outbreak. Our projections allow for some uncertainty in the future trends in TB. However, some factors, such as changes in future immigration patterns and their effects, are harder to project.

Our analysis used a TB-centered health systems perspective and excluded patient costs, non-TB related healthcare costs, and other societal costs (e.g., reductions in productivity because of workplace closures during outbreaks or because of TB disease); taking a more comprehensive societal perspective might provide an even stronger rationale for investing in outbreak investigation (*42*). In addition, including potential averted disability resulting from post-TB sequelae might further improve the estimated cost-effectiveness of this intervention (*43*). Conversely, this analysis also did not include public health infrastructural costs that might be required to establish and maintain outbreak investigation and surveillance programs. Such costs could be substantial but are difficult to quantify at the national level. Finally, our approach does not consider the potential value of TB outbreak response activities from the perspective of improving equity (*44*). Given that TB outbreaks disproportionally affect persons in racial and ethnic minority groups and persons affected by poverty (*6*,*7*), TB outbreak investigation activities might also help reduce health disparities.

In conclusion, this model-based analysis predicts that TB outbreak response activities are likely to be both epidemiologically impactful and relatively cost-effective compared with other interventions in the United States over the next decade. A better understanding of the drivers of transmission in outbreaks, concerted efforts to document the scope and costs of outbreak response activities (especially by outbreak setting), and accounting for the use of novel tools such as WGS could further improve future estimates of the effects and cost-effectiveness of TB outbreak response.

Codes, worksheets, and data used for the model simulations are available in the following repository: https://doi.org/10.5281/zenodo.13840138.

This work was supported by the Centers for Disease Control and Prevention, National Center for HIV/AIDS, Viral Hepatitis, STD, and TB Prevention Epidemiologic and

Economic Modeling Agreement (grant no. 5U38PS004646). The findings and conclusions in this report are those of the authors and do not necessarily represent the views or opinions of the California Department of Public Health or the California Health and Human Services Agency.

About the Author

Dr. Shrestha is an assistant scientist in the Department of Epidemiology at Johns Hopkins Bloomberg School of Public Health. His research involves developing mathematical, computational, health economic models of tuberculosis and using them to design and inform public health decision-making.

References

1. Onorato IM. Tuberculosis outbreaks in the United States [The Comstock Lecture]. Int J Tuberc Lung Dis. 2000;4 (Suppl 2):S121–6.
2. Mindra G, Wortham JM, Haddad MB, Powell KM. Tuberculosis outbreaks in the United States, 2009–2015. Public Health Rep. 2017;132:157–63. https://doi.org/10.1177/0033354916688270
3. Mitruka K, Oeltmann JE, Ijaz K, Haddad MB. Tuberculosis outbreak investigations in the United States, 2002–2008. Emerg Infect Dis. 2011;17:425–31. https://doi.org/10.3201/eid1703.101550
4. Armstrong LR, Winston CA, Stewart B, Tsang CA, Langer AJ, Navin TR. Changes in tuberculosis epidemiology, United States, 1993–2017. Int J Tuberc Lung Dis. 2019;23:797–804. https://doi.org/10.5588/ijtld.18.0757
5. Centers for Disease Control and Prevention. Reported tuberculosis in the United States, 2021 [cited 2023 May 22]. https://www.cdc.gov/tb/statistics/reports/2021
6. Wortham JM, Li R, Althomsons SP, Kammerer S, Haddad MB, Powell KM. Tuberculosis genotype clusters and transmission in the U.S., 2009–2018. Am J Prev Med. 2021;61:201–8. https://doi.org/10.1016/j.amepre.2021.02.006
7. Raz KM, Talarico S, Althomsons SP, Kammerer JS, Cowan LS, Haddad MB, et al. Molecular surveillance for large outbreaks of tuberculosis in the United States, 2014–2018. Tuberculosis (Edinb). 2022;136:102232. https://doi.org/10.1016/j.tube.2022.102232
8. Bamrah S, Yelk Woodruff RS, Powell K, Ghosh S, Kammerer JS, Haddad MB. Tuberculosis among the homeless, United States, 1994–2010. Int J Tuberc Lung Dis. 2013;17:1414–9. https://doi.org/10.5588/ijtld.13.0270
9. Haddad MB, Mitruka K, Oeltmann JE, Johns EB, Navin TR. Characteristics of tuberculosis cases that started outbreaks in the United States, 2002–2011. Emerg Infect Dis. 2015;21:508.
10. France AM, Grant J, Kammerer JS, Navin TR. A field-validated approach using surveillance and genotyping data to estimate tuberculosis attributable to recent transmission in the United States. Am J Epidemiol. 2015;182:799–807. https://doi.org/10.1093/aje/kwv121
11. Yuen CM, Kammerer JS, Marks K, Navin TR, France AM. Recent transmission of tuberculosis—United States, 2011–2014. PLoS One. 2016;11:e0153728. https://doi.org/10.1371/journal.pone.0153728
12. Shrestha S, Winglee K, Hill AN, Shaw T, Smith JP, Kammerer JS, et al. Model-based analysis of tuberculosis genotype clusters in the United States reveals high degree of heterogeneity in transmission and state-level differences across California, Florida, New York, and Texas. Clin Infect Dis. 2022;75:1433–41. https://doi.org/10.1093/cid/ciac121
13. Centers for Disease Control and Prevention. 2020 Contact Investigations Report (ARPE Data) [cited 2023 Mar 31]. https://www.cdc.gov/tb/programs/evaluation/arpe-data.htm
14. Menzies NA, Swartwood N, Testa C, Malyuta Y, Hill AN, Marks SM, et al. Time since infection and risks of future disease for individuals with *Mycobacterium tuberculosis* infection in the United States. Epidemiology. 2021;32:70–8. https://doi.org/10.1097/EDE.0000000000001271
15. Trauer JM, Moyo N, Tay E-L, Dale K, Ragonnet R, McBryde ES, et al. Risk of active tuberculosis in the five years following infection . . . 15%? Chest. 2016;149:516–25. https://doi.org/10.1016/j.chest.2015.11.017
16. Sterling TR, Villarino ME, Borisov AS, Shang N, Gordin F, Bliven-Sizemore E, et al.; TB Trials Consortium PREVENT TB Study Team. Three months of rifapentine and isoniazid for latent tuberculosis infection. N Engl J Med. 2011;365:2155–66. https://doi.org/10.1056/NEJMoa1104875
17. International Union Against Tuberculosis Committee on Prophylaxis. Efficacy of various durations of isoniazid preventive therapy for tuberculosis: five years of follow-up in the IUAT trial. Bull World Health Organ. 1982;60:555–64.
18. Velen K, Shingde RV, Ho J, Fox GJ. The effectiveness of contact investigation among contacts of tuberculosis patients: a systematic review and meta-analysis. Eur Respir J. 2021; 58:2100266. https://doi.org/10.1183/13993003.00266-2021
19. US Department of Health and Human Services Center for Medicare Services. Clinical laboratory fee schedule [cited 2024 Aug 16]. https://www.cms.gov/Medicare/Medicare-Fee-for-Service-Payment/ClinicalLabFeeSched/Clinical-Laboratory-Fee-Schedule-Files.html
20. Njie GJ, Young KH, Beeler Asay GR. Estimating tuberculosis contact investigation costs in the United States: a systematic review. Poster presented at: National Tuberculosis Controllers Association Annual Conference; Rancho Mirage, California, USA; 2022 May 23–26.
21. Jo Y, Shrestha S, Gomes I, Marks S, Hill A, Asay G, et al. Model-based cost-effectiveness of state-level latent tuberculosis interventions in California, Florida, New York, and Texas. Clin Infect Dis. 2021;73:e3476–82. https://doi.org/10.1093/cid/ciaa857
22. US Department of Health and Human Services Center for Medicare Services. Physician fee schedule [cited 2024 Aug 16]. https://www.cms.gov/apps/physician-fee-schedule/license-agreement.aspx
23. Shepardson D, Marks SM, Chesson H, Kerrigan A, Holland DP, Scott N, et al. Cost-effectiveness of a 12-dose regimen for treating latent tuberculous infection in the United States. Int J Tuberc Lung Dis. 2013;17:1531–7. https://doi.org/10.5588/ijtld.13.0423
24. Holland DP, Sanders GD, Hamilton CD, Stout JE. Costs and cost-effectiveness of four treatment regimens for latent tuberculosis infection. Am J Respir Crit Care Med. 2009; 179:1055–60. https://doi.org/10.1164/rccm.200901-0153OC
25. Belknap R, Holland D, Feng P-J, Millet J-P, Caylà JA, Martinson NA, et al. Self-administered versus directly observed once-weekly isoniazid and rifapentine treatment of latent tuberculosis infection: a randomized trial. Ann Intern Med. 2017;167:689–97. https://doi.org/10.7326/M17-1150
26. Sotgiu G, Matteelli A, Getahun H, Girardi E, Sañé Schepisi M, Centis R, et al. Monitoring toxicity in individuals receiving treatment for latent tuberculosis infection: a systematic review versus expert opinion. Eur Respir J. 2015;45:1170–3. https://doi.org/10.1183/09031936.00216814

27. Winston CA, Marks SM, Carr W. Estimated costs of 4-month pulmonary tuberculosis treatment regimen, United States. Emerg Infect Dis. 2023;29:2102–4. https://doi.org/10.3201/eid2910.230314
28. Guo N, Marra CA, Marra F, Moadebi S, Elwood RK, Fitzgerald JM. Health state utilities in latent and active tuberculosis. Value Health. 2008;11:1154–61. https://doi.org/10.1111/j.1524-4733.2008.00355.x
29. Kammerer JS, Shang N, Althomsons SP, Haddad MB, Grant J, Navin TR. Using statistical methods and genotyping to detect tuberculosis outbreaks. Int J Health Geogr. 2013;12:15. https://doi.org/10.1186/1476-072X-12-15
30. Marks SM, Flood J, Seaworth B, Hirsch-Moverman Y, Armstrong L, Mase S, et al.; TB Epidemiologic Studies Consortium. Treatment practices, outcomes, and costs of multidrug-resistant and extensively drug-resistant tuberculosis, United States, 2005–2007. Emerg Infect Dis. 2014;20:812–21. https://doi.org/10.3201/eid2005.131037
31. Taylor Z, Marks SM, Ríos Burrows NM, Weis SE, Stricof RL, Miller B. Causes and costs of hospitalization of tuberculosis patients in the United States. Int J Tuberc Lung Dis. 2000;4:931–9.
32. Bureau of Economic Analysis. Personal consumption expenditures price index: health care [cited 2024 Aug 16]. https://www.bea.gov/data/personal-consumption-expenditures-price-index
33. Tasillo A, Salomon JA, Trikalinos TA, Horsburgh CR Jr, Marks SM, Linas BP. Cost-effectiveness of testing and treatment for latent tuberculosis infection in residents born outside the United States with and without medical comorbidities in a simulation model. JAMA Intern Med. 2017;177:1755–64. https://doi.org/10.1001/jamainternmed.2017.3941
34. Menzies NA, Shrestha S, Parriott A, Marks SM, Hill AN, Dowdy DW, et al. The health and economic benefits of tests that predict future progression to tuberculosis disease. Epidemiology. 2022;33:75–83. https://doi.org/10.1097/EDE.0000000000001418
35. Young KH, Ehman M, Reves R, Peterson Maddox BL, Khan A, Chorba TL, et al. Tuberculosis contact investigations—United States, 2003–2012. MMWR Morb Mortal Wkly Rep. 2016;64:1369–74. https://doi.org/10.15585/mmwr.mm6450a1
36. Miramontes R, Hill AN, Yelk Woodruff RS, Lambert LA, Navin TR, Castro KG, et al. Tuberculosis infection in the United States: prevalence estimates from the National Health and Nutrition Examination Survey, 2011–2012. PLoS One. 2015;10:e0140881. https://doi.org/10.1371/journal.pone.0140881
37. Mirzazadeh A, Kahn JG, Haddad MB, Hill AN, Marks SM, Readhead A, et al. State-level prevalence estimates of latent tuberculosis infection in the United States by medical risk factors, demographic characteristics and nativity. PLoS One. 2021;16:e0249012. https://doi.org/10.1371/journal.pone.0249012
38. Labuda SM, McDaniel C, Talwar A, et al. Tuberculosis outbreak associated with delayed diagnosis and long infectious periods in rural Arkansas, 2010–2018. Public Health Rep. 2022;137:94–101. https://doi.org/10.1177/0033354921999167
39. Althomsons SP, Winglee K, Heilig CM, Talarico S, Silk B, Wortham J, et al. Using machine learning techniques and national tuberculosis surveillance data to predict excess growth in genotyped tuberculosis clusters. Am J Epidemiol. 2022;191:1936–43. https://doi.org/10.1093/aje/kwac117
40. Jajou R, de Neeling A, van Hunen R, de Vries G, Schimmel H, Mulder A, et al. Epidemiological links between tuberculosis cases identified twice as efficiently by whole genome sequencing than conventional molecular typing: a population-based study. PLoS One. 2018;13:e0195413. https://doi.org/10.1371/journal.pone.0195413
41. Stucki D, Ballif M, Egger M, Furrer H, Altpeter E, Battegay M, et al. Standard genotyping overestimates transmission of *Mycobacterium tuberculosis* among immigrants in a low-incidence country. J Clin Microbiol. 2016;54:1862–70. https://doi.org/10.1128/JCM.00126-16 PMID 27194683
42. Byford S, Raftery J. Perspectives in economic evaluation. BMJ. 1998;316:1529–30. https://doi.org/10.1136/bmj.316.7143.1529
43. Menzies NA, Quaife M, Allwood BW, Byrne AL, Coussens AK, Harries AD, et al. Lifetime burden of disease due to incident tuberculosis: a global reappraisal including post-tuberculosis sequelae. Lancet Glob Health. 2021;9:e1679–87. https://doi.org/10.1016/S2214-109X(21)00367-3
44. Ryckman T, Robsky K, Cilloni L, Zawedde-Muyanja S, Ananthakrishnan R, Kendall EA, et al. Ending tuberculosis in a post-COVID-19 world: a person-centred, equity-oriented approach. Lancet Infect Dis. 2023;23:e59–66. https://doi.org/10.1016/S1473-3099(22)00500-X

Address for correspondence: Sourya Shrestha, Department of Epidemiology, Johns Hopkins Bloomberg School of Public Health, 615 N Wolfe St, Baltimore, MD 21205, USA; email: sshres14@jh.edu

Mycobacterium nebraskense Isolated from Patients in Connecticut and Oregon, USA

Mark L. Metersky, Ashley J. Losier, David A. Fraulino, Theodore A. Warnock, Cara D. Varley, Angela M. Le, Kevin L. Winthrop, John R. McArdle, Salika M. Shakir, Reeti Khare

Mycobacterium nebraskense infection is rarely encountered; only 7 human cases have been reported worldwide since the initial report of 5 cases in Nebraska, USA, in 2004. We report 9 patients from Connecticut and 2 from Oregon, USA, who had *M. nebraskense* isolated from respiratory secretions; 7 patients met the American Thoracic Society/Infectious Diseases Society of America criteria for nontuberculous mycobacterial pulmonary disease. In 4 cases, the organism was isolated 1 time and caused brief or no symptoms. Most cases in Connecticut were reported after 2017. Antimicrobial drug susceptibility testing of 6 isolates showed clarithromycin susceptibility. In 2 cases, infection was refractory to treatment. The 9 Connecticut patients lived in 8 different towns; thus, a common water supply did not explain the high frequency of *M. nebraskense* isolation. *M. nebraskense* is a clinically significant cause of nontuberculous mycobacterial pulmonary disease in Connecticut; continued surveillance will be needed to determine its frequency and optimum treatment.

Mycobacterium nebraskense is a slow-growing, scotochromogenic mycobacterium first described in 2004 after it was isolated from 5 patients at the University of Nebraska Medical Center in Omaha, Nebraska, USA (*1*). Each patient had symptomatic lung disease; more detailed clinical information was reported for 1 patient with underlying emphysema, bronchiectasis, and a mass-like lung lesion who was thought to have nontuberculous mycobacterial pulmonary disease (NTM-PD) caused by *M. nebraskense* (*2*). Since those initial descriptions, only 7 additional isolates from humans have been reported (*3*); 6 were from different states within the United States, and 1 was from Japan. *M. nebraskense* has rarely been isolated from skin lesions in animals (*4*) or from nonpotable water reservoirs (*5*).

We report 11 patients from Connecticut and Oregon, USA, who had *M. nebraskense* isolated from respiratory samples. This previously rare organism has recently been the third most common nontuberculous mycobacteria (NTM) isolated from patients receiving treatment in a dedicated bronchiectasis center at the University of Connecticut Health Center (after *M. avium* complex [MAC] and *M. gordonae*). The University of Connecticut Health Institutional Review Board (IRB) determined this work was exempt from full IRB review (IRB no. 23X-084-02); the study was also approved by the Oregon Health and Science University IRB (approval no. IRB00003522).

Methods

The Centers for Disease Control and Prevention (Atlanta, GA, USA) identified the Connecticut case (CT-C) 1 isolate by using 16S rRNA gene sequencing (no further details available). ARUP Laboratories (Salt Lake City, UT, USA) identified isolates CT-C2 and CT-C4 by using 16S rRNA Sanger gene sequencing. The first 500 bp of the 16S rRNA gene was sequenced by using 5F-T and 534R-T primers and analyzed by using the RipSeq database (Pathogenomix, https://www.pathogenomix.com). Results were reported in accordance with Clinical and Laboratory Standards Institute criteria for identifying mycobacteria at the species level (*6*) if the sequence was 100% identical. ARUP Laboratories identified 6 CT-C3 respiratory

Author affiliations: University of Connecticut School of Medicine, Farmington, Connecticut, USA (M.L. Metersky, D.A. Fraulino, J.R. McArdle); Yale University School of Medicine, New Haven, Connecticut, USA (A.J. Losier); Oregon Health and Science University, Portland, Oregon, USA (T.A. Warnock, C.D. Varley, A.M. Le, K.L. Winthrop); Portland State University, Portland (T.A. Warnock, C.D. Varley, K.L. Winthrop); University of Utah ARUP Laboratories, Salt Lake City, Utah, USA (S.M. Shakir); National Jewish Health, Denver, Colorado, USA (R. Khare)

DOI: https://doi.org/10.3201/eid3103.240608

isolates by using either 16S rRNA gene sequencing or matrix-assisted laser desorption/ionization time-of-flight mass spectrometry (MALDI Biotyper; Bruker Daltonics, https://www.bruker.com); a score of ≥1.9 was required for positive species level identification. QUEST Laboratories (Secaucus, NJ, USA) identified the CT-C5 isolate by using DNA sequencing with an *M. nebraskense*–specific probe (no further information was available). The Yale New Haven Hospital microbiology laboratory (New Haven, CT, USA) identified CT-C7 and CT-C8 isolates by using 16S rRNA gene sequencing. ARUP Laboratories identified the CT-C9 isolate by using mass spectrometry as described previously. The National Jewish Hospital Advanced Diagnostic Laboratories (Denver, CO, USA) identified the Oregon case (OR-C1 and OR-C2) isolates by using *rpoB* gene Sanger sequencing (732-bp region). Isolates from Oregon were identified by comparing results to sequences in GenBank, requiring a >97% match.

Cases

CT-C1

We evaluated a 61-year-old man in 2008 for productive cough and hemoptysis, as previously described (*7*). He had a history of chronic obstructive pulmonary disease, cardiomyopathy, hypertension, type 2 diabetes, and smoking. His physical examination was unremarkable. A chest computed tomography (CT) scan revealed no infiltrates or bronchiectasis. Pulmonary function tests showed mild to moderate obstruction. Bronchoalveolar lavage (BAL) cultures grew *Aspergillus fumigatus*, *Escherichia coli*, and NTM most consistent with MAC according to high-performance liquid chromatography (HPLC). We did not treat the patient because the CT scan had not revealed bronchiectasis or nodules consistent with NTM-PD.

Fevers, sweats, and increased sputum production developed ≈6 months later. Another chest CT scan revealed ill-defined nodules of various sizes throughout both lungs. After another sputum sample was obtained, we treated the patient with rifampin, ethambutol, and azithromycin for a presumed MAC pulmonary infection. A commercial laboratory using an unknown method identified the organism as *M. interjectum*. Because of uncertainty regarding the identity of the organism, we sent the BAL isolate to the Centers for Disease Control and Prevention; HPLC revealed an organism consistent with *M. scrofulaceum*, but 16S rRNA sequencing identified *M. nebraskense*. The patient's symptoms rapidly improved, a sputum sample obtained 1 month later was acid-fast bacillus (AFB) negative, and a repeat chest CT scan showed near complete resolution of nodules. After ≈2 months, we discontinued ethambutol, and he remained on rifampin and azithromycin for another 10 months.

The patient required bronchial stenting because of stenosis of his left mainstem bronchus, thought to be a result of an endobronchial NTM infection. Samples from 2 bronchoscopies performed after 6 and 7 months of therapy did not grow mycobacteria. An organism consistent with *M. scrofulaceum* (according to HPLC) was cultured from a sputum sample obtained when he had completed ≈1 year of therapy; however, no disease was evident, and we did not reinstitute therapy. Subsequent sputum cultures did not grow mycobacteria, and a chest CT scan performed ≈6 months after therapy completion showed no disease. He remained well for 14 months after completing therapy and was then lost to follow-up.

CT-C2

We evaluated a 69-year-old woman in 2010 for bronchiectasis. Initial sputum mycobacterial cultures were negative; however, MAC grew from 2 sputum sample cultures in 2011. Her chest CT scan showed bronchiectasis and scattered tree-in-bud nodularity (Figure 1, panel A). Because she was doing well clinically, she continued only on an airway clearance regimen. Numerous sputum mycobacterial cultures were negative until 2018, when a sample grew *M. nebraskense*, identified by 16S rRNA gene sequencing. A repeat CT scan showed progression of her tree-in-bud nodularity and bronchiectasis when compared with a 2012 scan. Four sputum mycobacterial cultures during 2019–2022 were negative except for 1 isolation of *M. gordonae*. In January 2023, she reported daily productive cough. She had ovarian cancer and was receiving chemotherapy. She was not regularly performing airway clearance. A sputum culture from January 2023 grew *M. nebraskense*. Antimicrobial susceptibility testing could not be completed because of poor organism growth after using the CLSI approved test method for slow growing mycobacteria. We did not start her on antimycobacterial drug therapy because her symptoms were well controlled with airway clearance, and her CT scan findings had not progressed. She died from ovarian cancer in September 2023.

CT-C3

We saw a 55-year old man who had asthma since childhood. He had a 30 pack-year (1 pack/day for 30 years) history of cigarette smoking but had quit for several years. Cough and congestion persisted despite aggressive asthma treatment. Mycobacterial cultures were negative in 2017, 2018, and 2019.

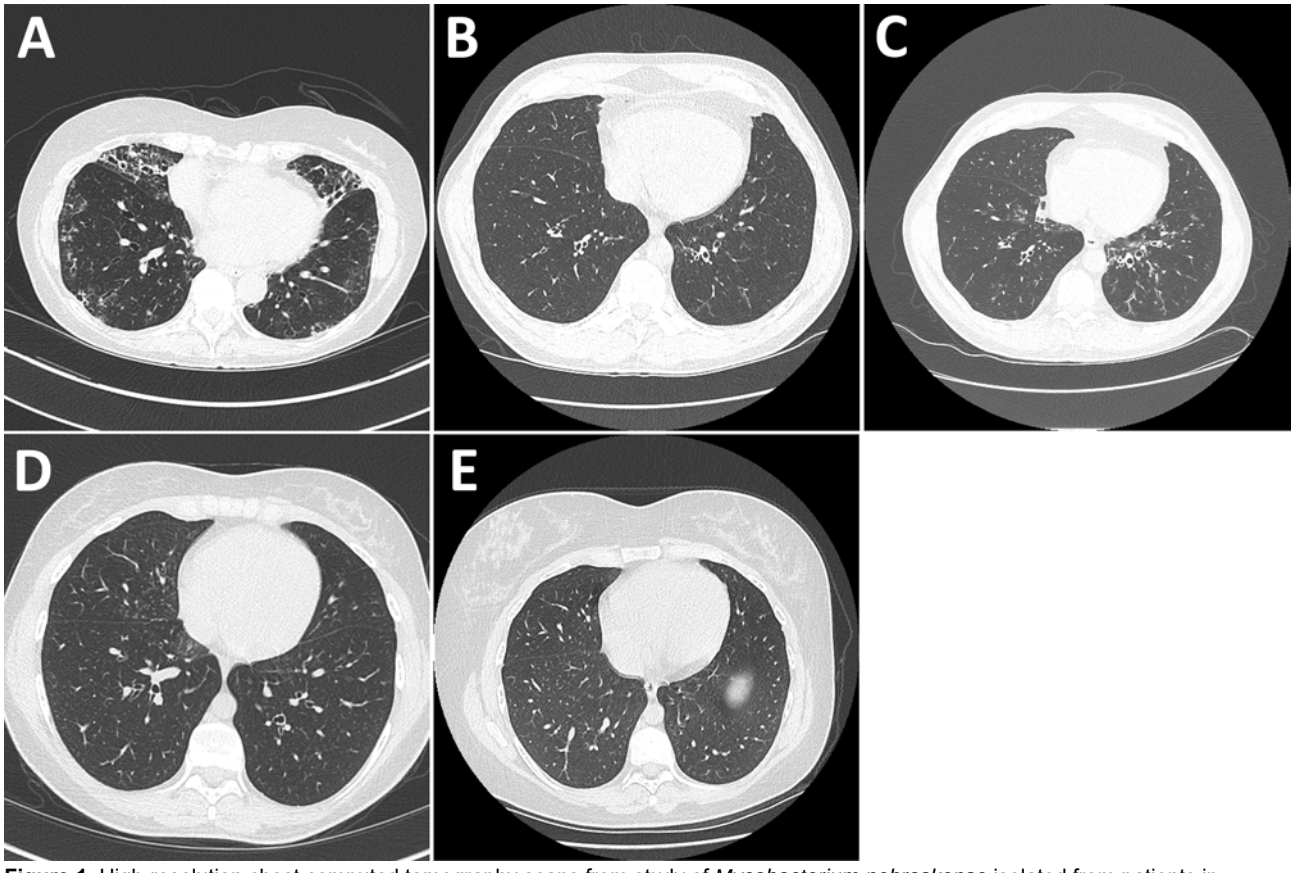

Figure 1. High-resolution chest computed tomography scans from study of *Mycobacterium nebraskense* isolated from patients in Connecticut and Oregon, USA. A) Scan from case 2 in Connecticut showing bronchiectasis in the right middle and lower lobe, left lower lobe, and lingula and tree-in-bud nodularity in the lingula and right and left lower lobes of the lung. B) Scan slice from case 3 in Connecticut through the lower lung lobes showing 1 borderline dilated airway in the left lower lobe, performed in May 2019. C) Scan slice from case 3 at the same anatomic level showing numerous dilated airways and airway wall thickening in the left lower lobe of lung, performed in April 2020 soon after the first isolation of *M. nebraskense*. D) Scan from case 4 in Connecticut showing tree-in-bud nodularity in the right middle and lower lobes of the lung when patient had *M. nebraskense* isolated from her sputum in August 2020. E) Scan from case 4 in Connecticut showing resolution of the tree-in-bud nodularity in the right middle and lower lobes of the lung, performed in December 2022.

In 2020, two sputum cultures grew *M. nebraskense*; drug susceptibility testing could not be done because of poor organism growth. A chest CT scan in 2020 revealed tree-in-bud nodularity, bronchiectasis, and mucus plugging, most prominent in the left lower lobe; most findings were new compared with a 2019 CT scan (Figure 1, panels B, C). We started him on azithromycin, ethambutol, and rifampin. After 12 months of therapy, despite clinical and radiographic improvement, he remained sputum-culture positive. After ≈18 months of therapy, his sputum AFB cultures were negative. Three months later, he had reemergence of cough, and sputum cultures again grew *M. nebraskense*. Drug susceptibility testing revealed susceptibility to all agents tested (Table 1). We treated him with azithromycin, rifampin, ethambutol, and linezolid. We discontinued all therapy in February 2024 because of persistent culture positivity with an acceptable symptom burden. A direct smear of biofilm from a water filter in his house was strongly positive for AFB and grew *M. nebraskense*.

CT-C4

We saw a 19-year-old woman in 2015 with a history of primary ciliary dyskinesia diagnosed at 4 years of age, sinusitis, otitis media, and recurrent *Stenotrophomonas maltophilia* respiratory infections. Her treatment included prophylactic trimethoprim/sulfamethoxazole and airway clearance with a hand-held positive pressure oscillatory device. She had done well for several years, having minimal daily cough and sputum production. A CT scan from 2 years earlier was unremarkable. In 2020, she began having intermittent low-grade fevers and increased cough and sputum production, which persisted for several months. A CT scan showed new areas of tree-in-bud nodularity

Table 1. Antimicrobial drug susceptibility testing results for 6 *Mycobacterium nebraskense* isolates from patients in Connecticut and Oregon, USA*

	MIC, μg/mL					
Drug	CT-C3	CT-C5	CT-C6	OR-C1	OR-C2, pretreatment	OR-C2, during treatment
TMP/SMX	≤0.25/4.75, S	4/76, R	S	NA	NA	NA
Doxycycline	≤0.12, S	NA	NA	NA	NA	NA
Linezolid	≤1, S	2, S	NA	2.0, S	NA	64.0, R
Rifabutin	≤0.12, S	0.25, S	S	≤0.25, S	>0.5, R	>8.0, R
Amikacin	≤1, S	2, S	8, S	4.0, I	4.0, I	16.0, R
Moxifloxacin	0.03, S	0.03, S	S	0.25, S	≤0.5, S	16.0, S
Ciprofloxacin	≤0.12, S	1, S	S	0.5, S	2.0, I	8.0, R
Clarithromycin	≤0.06, S	0.12, S	0.5, S	0.12, S	≤4.0, S	8.0, S
Minocycline	0.5, S	0.03, S	NA	NA	NA	NA
Rifampin	0.12, S	1, S	S	0.5, S	1.0, S	16.0, R

*CT-C, Connecticut-case; I, intermediate; NA, not applicable; OR-C, Oregon-case; R, resistant; S, susceptible; TMP/SMX, trimethoprim-sulfamethoxazole.

in the right middle and lower lobes (Figure 1, panel D). A sputum mycobacterial culture from August 2020 grew *M. nebraskense*, identified by partial 16S rRNA gene sequencing. Antimicrobial susceptibility testing could not be completed because of poor organism growth. A sputum bacterial culture revealed normal oral flora. Her symptoms persisted; a repeat mycobacterial culture from December 2020 was negative and, over several months, her fevers and cough improved. A repeat CT scan in 2022 showed resolution of the tree-in-bud nodularity in the right middle and lower lobes (Figure 1, panel E), and she has done well since then.

CT-C5

A 64-year-old woman was referred to us for evaluation of asthma in August 2021. She reported a history of pneumonia and asthma diagnosed at age 7. She had been noticing shortness of breath with exertion during the previous 2–3 years. She reported a chronic cough with sputum production. She had smoked 6 cigarettes per day when she was 16–25 years of age. She had lost ≈10 pounds in body weight during the preceding 2 years and had a body mass index of 16.5 kg/m^3. Medications included inhaled bronchodilators and, for the previous 9 months, inhaled corticosteroids. Spirometry revealed severe obstruction; her oxygen saturation was 86% on room air. A chest CT scan revealed diffuse cylindrical bronchiectasis with marked bronchial wall thickening, multifocal mucoid impaction, and tree-in-bud nodularity. Laboratory evaluation showed no underlying cause for her bronchiectasis. Her sputum culture was positive for multiple gram-negative bacilli, including *Alcaligenes faecalis* and *Pseudomonas aeruginosa*. We treated her with levofloxacin, and she had transient improvement in sputum production.

In February, 2 sputum mycobacterial cultures grew *M. nebraskense*, and drug susceptibility testing was performed (Table 1). Percussion vest therapy was initiated. A repeat sputum bacterial culture was positive for *P. aeruginosa*. We started her on nebulized tobramycin, azithromycin, ethambutol, and rifampin. She was hospitalized for acute respiratory failure, and we treated her with intravenous cefepime in addition to her previous regimen; she showed modest improvement and was discharged on oxygen. She returned to the hospital because of worsening respiratory failure, elected comfort measures, and died 6 weeks after initiating antimycobacterial therapy.

CT-C6

We saw a 44-year-old woman for dyspnea and chronic cough producing yellow sputum in September 2022. A CT scan revealed bilateral interstitial lung disease but no bronchiectasis or nodules. Sputum mycobacterial culture revealed MAC growth. A second mycobacterial culture a month later was negative, whereas a third culture in November 2022 revealed *M. nebraskense* according to DNA sequencing; drug susceptibility testing was performed (Table 1). Further evaluation showed an elevated antinuclear antibody titer of 1:1,250 with a centromere pattern and elevated RNA polymerase III antibody, leading to a presumptive diagnosis of systemic sclerosis. Three subsequent sputum mycobacterial cultures 2, 3, and 6 months later were negative. Her cough persisted but has been less productive.

CT-C7

A 73-year-old woman sought care in August 2020 for recurrent pneumonia, chronic cough with yellow sputum, fatigue, fevers, and weight loss. She had end-stage renal disease secondary to membranoproliferative nephritis status postkidney transplant and was taking prednisone. Results of pulmonary function testing were unremarkable. Her chest CT scan demonstrated bilateral bronchiectasis, tree-in-bud nodules, and mucus plugging. Testing for underlying

etiologies of bronchiectasis was unrevealing. We thought that her bronchiectasis was secondary to recurrent chest infections in an immunocompromised host. We recommended airway clearance therapy. A sputum culture grew *Haemophilus parainfluenzae*; a negative mycobacterial culture was obtained at the time she sought care. During the following year, she had several bronchiectasis exacerbations requiring antimicrobial drugs for coverage of *Staphylococcus aureus*, *P. aeruginosa*, and isolated *M. nebraskense* from sputum samples obtained in November 2021 and April 2022. No drug susceptibility testing was available. We observed progression of bronchiectasis on repeat chest CT imaging. We started her on nebulized tobramycin solution because of frequent bronchiectasis exacerbations and a persistent productive cough. She noted substantial improvement in cough and fatigue, and her body weight stabilized after using an augmented airway clearance regimen and nebulized tobramycin. She has remained without treatment for *M. nebraskense* infection because of stable symptoms.

CT-C8

In March 2021, a 69-year-old man with a history of coronary artery disease, chronic lymphocytic leukemia (treated with ibrutinib), gastroesophageal reflux, diabetes, and allergic rhinitis sought care for chronic productive cough and chest imaging demonstrating bronchiectasis. His physical examination and spirometry results were unremarkable. Evaluation for underlying causes of bronchiectasis was unrevealing. We started him on airway clearance with a hand-held positive expiratory pressure oscillatory device. The lung CT scan showed chronic scattered nodules (<6 mm), mucus impaction, and mild bronchiectasis in the right lower lobe. His cough continued, and a sputum culture in December 2021 grew methicillin-resistant *S. aureus*, *A. fumigatus*, and *M. nebraskense*; drug susceptibility testing was not available. In February 2022, he was hospitalized with *Pneumocystis jirovecii* pneumonia. A mycobacterial culture of a BAL sample was negative. He improved after treatment for pneumonia and remains with mild dyspnea and chronic cough; *M. nebraskense* has not been isolated from subsequent sputum mycobacterial cultures.

CT-C9

We evaluated a 56-year-old woman in April 2023 for cough producing scant sputum, chest pain, and an abnormal CT scan. She had no remarkable medical history. A chest CT scan in February 2023 revealed multifocal patchy consolidation, several areas of tree-in-bud nodularity, and bronchiectasis, most prominent in the right middle and upper lobes and lingula. Pulmonary function testing was unremarkable. A repeat CT scan showed partial improvement of the patchy consolidation and tree-in-bud nodularity. One of 3 sputum mycobacterial cultures from May 2023 grew *M. nebraskense.* Susceptibility testing could not be done by the reference laboratory because of poor organism growth. A respiratory bacterial culture was negative. Evaluation for underlying causes of bronchiectasis was unrevealing. We did not provide specific treatment. By December 2023, her cough had resolved, although a CT scan revealed only partial improvement of some of the tree-in-bud nodularity observed in April. Bronchoscopy was performed in January 2024; a BAL sample was negative for mycobacteria.

OR-C1

In 2013, we evaluated an 80-year-old woman who was born and raised in Oregon for cough that had been present for ≈10 years and for more recent cryptogenic organizing pneumonia, shortness of breath, low-grade fevers, and increased sputum production. She had gastroesophageal reflux and allergies managed by tap water sinus rinses. We obtained 3 sputum mycobacterial cultures; 1 grew *M. lentiflavum*, identified by gene sequencing. Tap water sinus rinses were discontinued, and we started her on daily azithromycin, ethambutol, and rifampin; culture conversion occurred after 5 months of therapy. We performed BAL because of minimal radiologic improvement in the lungs, which yielded negative fungal, bacterial, and mycobacterial cultures. Areas of radiographic progression were more consistent with cryptogenic organizing pneumonia; improvements in imaging findings were more consistent with NTM-PD. We discontinued treatment after 1 year, and within 3 months, her cough and sputum production returned.

In 2015, two sputum mycobacterial cultures grew *M. nebraskense*, which was resistant to ethambutol (but susceptible to rifampin/ethambutol combination), and 1 culture was positive for *M. scrofulaceum*. We resumed daily azithromycin, ethambutol, and rifampin in mid-2016 and observed serial negative mycobacterial cultures. We changed her regimen to azithromycin and rifampin; she completed 1 year of therapy and had radiologic and symptomatic improvement. Surveillance cultures remained negative until 2018, when MAC was identified in 2 sputum samples. Radiologic progression of disease and continued productive cough warranted resumption of her antimicrobial drug regimen in early 2019, completed in late 2021.

OR-C2

A 71-year-old woman, originally from Vietnam, who had a history of colon cancer status postcolectomy and diabetes mellitus had widespread bronchiectasis with tree-in-bud infiltrates that was discovered incidentally on lung CT scan as part of her malignancy evaluation. Mild progression of bronchiectasis was observed mostly in the right middle lobe and lingula on a subsequent CT scan 2 months later, prompting a bronchoscopy in 2014. Cultures revealed mucoid *P. aeruginosa* and were 1+ AFB smear positive and grew *M. nebraskense*, identified by *rpoB* gene sequencing. We began daily rifampin, ethambutol, and azithromycin treatment. After 11 months, another sputum sample was 2+ AFB smear positive

Table 2. Summary of 11 cases of *Mycobacterium nebraskense* infection in Connecticut and Oregon, USA*

Case no.	Year†	Age, y/sex	Underlying illnesses	Immunosuppressed	Met criteria for pulmonary disease‡	Antimycobacterial treatment	Outcome
CT-C1	2008	61/M	Chronic obstructive pulmonary disease	No	Yes, assuming second *M. scrofulaceum* identification was *M. nebraskense*	Yes	Prolonged culture conversion
CT-C2	2018	69/F	Bronchiectasis at initial isolation, ovarian cancer diagnosed in 2019	No initially, then prolonged chemotherapy	Yes	No	Died from ovarian cancer in 2023
CT-C3	2020	57/M	Asthma	No	Yes	Yes	Persistent infection despite prolonged treatment
CT-C4	2020	24/F	Primary ciliary dyskinesia	No	No, characteristic CT findings but only 1 positive culture	No	Spontaneous resolution of symptoms and CT findings, subsequent negative cultures
CT-C5	2022	64/F	Asthma, bronchiectasis	No	Yes	Yes	Died from respiratory failure 6 weeks after initiating treatment
CT-C6	2022	44/F	Interstitial lung disease from systemic sclerosis	No	No	No	Spontaneous culture conversion
CT-C7	2021	71/F	Kidney transplantation	Yes	Yes	No	Symptom control with airway clearance alone
CT-C8	2021	69/M	Chronic lymphocytic leukemia	Yes	No	No	Spontaneous culture conversion
CT-C9	2023	56/F	None	No	No	No	Spontaneous resolution of symptoms and some CT findings, subsequent negative cultures
OR-C1	2015	82/F	Gastroesophageal reflux, hiatal hernia, allergic rhinitis	No	Yes	Yes	Culture conversion during treatment
OR-C2	2014	71/F	Bronchiectasis, type 2 diabetes, colon cancer	No	Yes	Yes	Converted after prolonged therapy, including surgical resection
Overall	NA	60.7 ±15.7 (mean ±SD), 8/11 (73%) female	NA	2/11 (18%) immunosuppressed at initial *M. nebraskenske* isolation	7/11 (64%) met criteria for NTM-PD	5/11 (45%) received antimycobacterial therapy	NA

**Mycobacterium nebraskense* was isolated from respiratory samples. CT-C, Connecticut-case; NA, not applicable; NTM, nontuberculous mycobacteria; NTM-PD, nontuberculous mycobacterial pulmonary disease; OR-C, Oregon-case.
†Year *M. nebraskense* was first isolated.
‡Met the American Thoracic Society/Infectious Disease Society of America criteria for NTM-PD by having ≥2 positive cultures and characteristic CT imaging showing bronchiectasis or tree-in-bud nodularity.

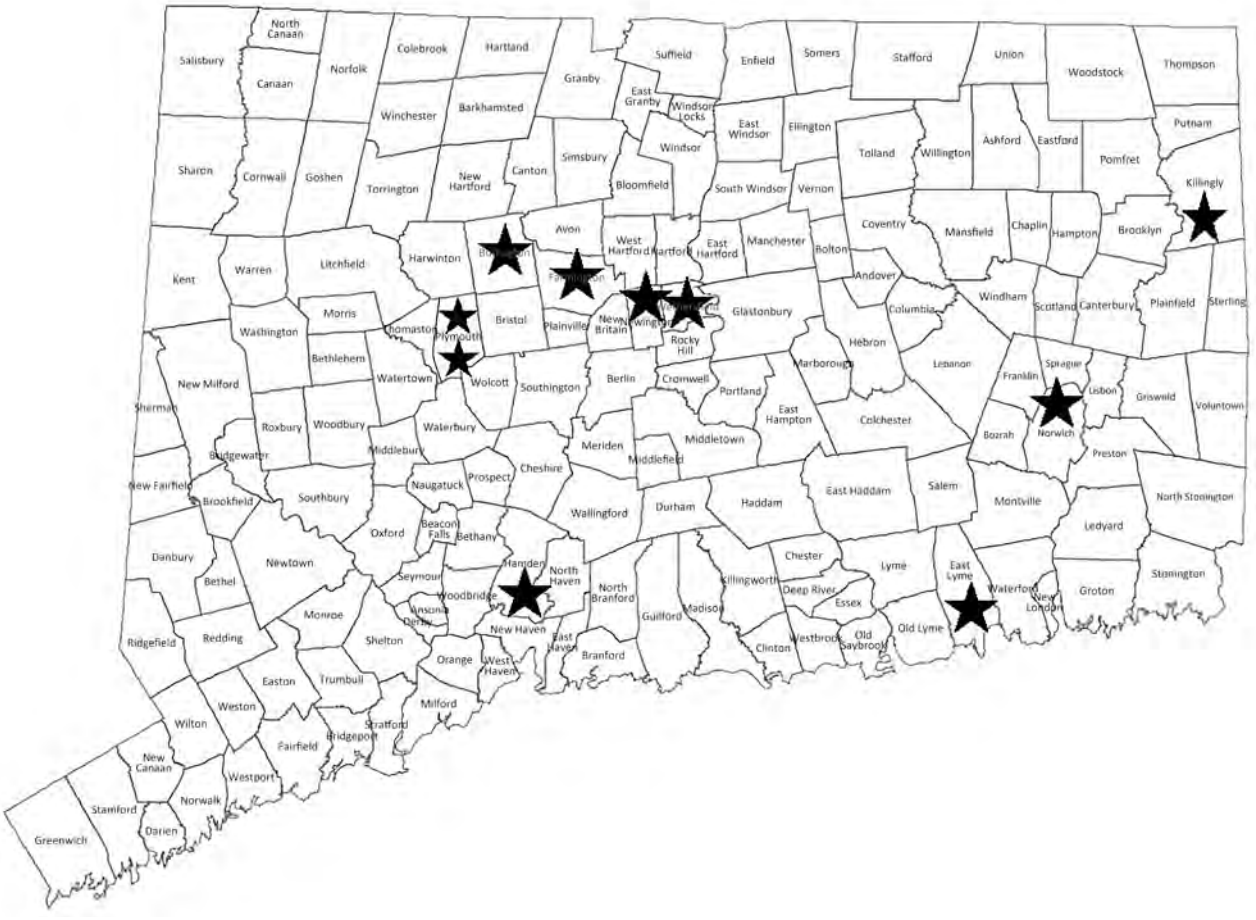

Figure 2. Towns of residence (stars) for 9 patients in Connecticut, USA, who had *Mycobacterium nebraskense* isolated during 2008–2023.

and grew *M. nebraskense* in culture; antimicrobial susceptibility testing showed newly acquired resistance to ethambutol and rifampin, separately or in combination, and macrolide susceptibility (Table 1). We replaced ethambutol with moxifloxacin and referred her for surgical consultation for possible resection of severe bronchiectatic regions and for an enlarging ground-glass nodule in the right lower lung lobe, possibly malignant. After continued culture positivity, despite 21 months of therapy, and the development of antimicrobial drug resistance, we placed her on intravenous amikacin for 2 weeks before and after a right middle lobectomy and right lower lobe wedge resection in 2016. Histopathology confirmed stage IA pulmonary adenocarcinoma; mycobacterial cultures were negative. We discontinued treatment after 25 months. She subsequently required treatment for frequent exacerbations related to *P. aeruginosa* and NTM-PD caused by *M. paraffinicum* and MAC.

Results

We summarized the clinical characteristics of each case (Table 2). Eight (73%) of 11 patients were female, 3 (27%) male. Underlying bronchiectasis was present in 6 (55%) patients; 7 (64%) patients met the American Thoracic Society/Infectious Disease Society of America criteria for NTM-PD. Initial antimicrobial susceptibility testing of 6 isolates revealed uniform macrolide susceptibility (Table 1). The 2 isolates from Oregon had intermediate sensitivity to amikacin, and 1 of those had in vitro resistance to rifampin. Five (45%) patients received antimycobacterial drug treatment; 2 required prolonged therapy because of rapidly recurrent disease after initial completion of treatment for 18 and 21 months.

Most Connecticut patients lived in various locales (Figure 2); thus, they did not all share the same household water supply. Two patients lived in the same small town (population ≈5,000), suggesting a possible common environmental source of mycobacteria. None of the 11 patients had medical visits on the same day, making nosocomial patient-to-patient transmission unlikely.

M. nebraskense isolates were processed in several different laboratories over several years and thus, a

pseudo-outbreak related to contaminated laboratory reagents was unlikely. However, we performed mycobacterial cultures on reagents potentially subject to contamination at the University of Connecticut Health Center mycobacteriology laboratory, where most isolates in this series were processed: NACPAC NALC tablets, NPC-67 neutralizing buffer, and PRB pellet resuspension buffer (Alpha-Tec Systems, https://www.alphatecsystems.com); antibiotic mixture consisting of polymyxin B, trimethoprim, amphotericin B, azlocillin, nalidixic acid; and oleic albumin dextrose catalase growth supplement. All cultures were negative.

Discussion

M. nebraskense infections were first described in 2004 in Nebraska (*1*), and only 7 additional cases have been reported worldwide since then. We report a series of 11 patients who had *M. nebraskense* isolated from respiratory samples; 9 were from Connecticut. Seven cases met the criteria for NTM-PD. Two patients remained refractory to treatment with 4 antimycobacterial drugs for extended periods of time. Two patients (CT-C4 and CT-C9) who had subacute symptoms and a CT scan suggestive of NTM-PD cleared their sputum and had improvement of their symptoms and CT findings without treatment, suggesting that *M. nebraskense* might cause self-limiting infection and symptoms, similar to a previously reported case (*8*). We observed a wide range of clinical manifestations in our case series, including patients with a single isolate and no obvious clinical sequela and those with progressive bronchiectasis and treatment-refractory disease. Temporal association with progressive bronchiectasis (CT-C3) and bronchial stenosis (CT-C1) suggests that *M. nebraskense* can directly damage large airways. CT scan results were also variable and included bronchiectasis, tree-in-bud nodularity, and large nodules.

Although most patients did not have systemic immunosuppression, immunocompetent patients had conditions thought to increase the risk for NTM-PD, such as bronchiectasis (*9*), gastroesophageal reflux (*10*), and inhaled corticosteroid use (*11*). Those factors likely increased risk for NTM-PD by impairing local airway host defenses against infection (*12*) and in the case of gastroesophageal reflux, by increasing airway exposure to NTM.

Despite the pathogenicity of *M. nebraskense* in several patients, others had only a single positive culture and no persistent symptoms. This result demonstrates that initial isolation of this organism does not always indicate the presence of NTM-PD and should generally not prompt antimycobacterial therapy, similar to other NTM such as MAC. Serial mycobacterial cultures and careful clinical assessment and follow-up are indicated before deciding if treatment is warranted.

Drug susceptibility testing revealed uniform in vitro susceptibility to clarithromycin, similar to prior case reports (*3*), but some isolates were resistant to other first-line NTM drugs, including rifamycins and amikacin. In 3 cases, the reference laboratory was not able to perform susceptibility testing because of poor growth of the organism after identification.

In conclusion, *M. nebraskense* has only been reported in rare single case reports, except for the initial report in 2004 from Nebraska (*1*). We report that this organism can be a clinically critical pathogen in Connecticut and has caused sporadic disease in at least 1 other US state. It is unclear whether the increased isolation frequency of this organism in Connecticut represents a true increase in prevalence or is a result of increased availability of molecular methods to identify NTM. Increased research on NTM-PD will be needed to improve diagnosis and treatment of *M. nebraskense* and other NTM infections.

Addendum

Since submission of this manuscript, 2 more patients from Connecticut have had *M. nebraskense* isolated from their sputum, 1 at Yale University (isolated 1×) and 1 at University of Connecticut (isolated 2×) (A.J. Losier, M.L. Metersky, unpub. data). Including those 2 patients, *M. nebraskense* has now been isolated from a total of 11 patients from Connecticut, 10 since 2018.

Acknowledgments

We thank Estelle Maule for assistance with the mycobacterial cultures and Thomas Rivera for assistance with formatting the CT scan images.

M.M. receives personal consulting income from Insmed, Boehringer Ingelheim, and Tactile Inc; clinical trial support to University of Connecticut from Insmed and Armata Pharmaceuticals; and is on data safety monitoring boards for Renovion and AN2 Therapeutics, resulting in personal income. K.L.W. receives research support from Insmed, Paratek, AN2, Renovion, Spero, and Mannkind Corp. and personal consulting income from Insmed, Paratek, AN2 Therapeutics, Renovion, Spero, and Mannkind Corp. C.D.V. receives salary support from National Institutes of Health, National Heart, Lung, and Blood Institute (grant no. K23HL161495). R.K. conducts laboratory contracted research from Insmed, Paratek, AN2 Therapeutics, Spero, Mannkind Corp., Bruker, and Illumina Corp.

About the Author

Dr. Metersky is chief of the Division of Pulmonary, Critical Care and Sleep Medicine at the University of Connecticut School of Medicine and director of the University of Connecticut Center for Bronchiectasis Care in Farmington, Connecticut, USA. His research interests include pulmonary infectious diseases, including pneumonia, bronchiectasis, and NTM pulmonary disease, as well as quality/performance measurements.

References

1. Mohamed AM, Iwen PC, Tarantolo S, Hinrichs SH. *Mycobacterium nebraskense* sp. nov., a novel slowly growing scotochromogenic species. Int J Syst Evol Microbiol. 2004;54:2057–60. https://doi.org/10.1099/ijs.0.63126-0
2. Iwen PC, Tarantolo SR, Mohamed AM, Hinrichs SH. First report of *Mycobacterium nebraskense* as a cause of human infection. Diagn Microbiol Infect Dis. 2006; 56:451–3. https://doi.org/10.1016/j.diagmicrobio.2006.06.020
3. Rajani AJ, Roach D, Raval D, Amin J, Kempaiah P, Chitale R, et al. A systemic review of *Mycobacterium nebraskense* case reports up to October 2023, featuring our unique case study. Int J Mycobacteriol. 2023; 12:443–7. https://doi.org/10.4103/ijmy.ijmy_167_23
4. Niederhäuser S, Klauser L, Bolliger J, Friedel U, Schmitt S, Ruetten M, et al. First report of nodular skin lesions caused by *Mycobacterium nebraskense* in a 9-year-old cat. JFMS Open Rep. 2018;4:2055116918792685. https://doi.org/10.1177/2055116918792685
5. Makovcova J, Slany M, Babak V, Slana I, Kralik P. The water environment as a source of potentially pathogenic mycobacteria. J Water Health. 2014;12:254–63. https://doi.org/10.2166/wh.2013.102
6. Clinical and Laboratory Standards Institute. Interpretive criteria for identification of bacteria and fungi by targeted DNA sequencing, second edition (MM18). Wayne (PA): The Institute; 2018.
7. Puthalapattu S, Metersky ML. *Mycobacterium nebraskense* as a cause of nodular pulmonary disease. Conn Med. 2011;75:527–9.
8. Nomura Y, Chibana K, Umetsu T, Takeda K, Shimizu Y, Numao T. A rare case of pulmonary *Mycobacterium nebraskense* infection outside of North America, who was improved without treatments in Japan. In: Abstracts of the American Thoracic Society 2020 International Conference, Philadelphia, PA, USA; 2020 May 15–20. Abstract A7353. New York: American Thoracic Society; 2020. https://doi.org/10.1164/ajrccm-conference.2020.201.1_MeetingAbstracts.A7353
9. Schildknecht K, Winthrop KL, Prevots DR, Blakney R, Henkle E. Nontuberculous mycobacterial pulmonary disease incidence among elderly patients with bronchiectasis. Eur Respir J. 2022;59:2200018. https://doi.org/10.1183/13993003.00018-2022
10. Kim Y, Yoon JH, Ryu J, Yang B, Chung SJ, Kang HK, et al. Gastroesophageal reflux disease increases susceptibility to nontuberculous mycobacterial pulmonary disease. Chest. 2023;163:270–80. https://doi.org/10.1016/j.chest.2022.08.2228
11. Loebinger MR, Quint JK, van der Laan R, Obradovic M, Chawla R, Kishore A, et al. Risk factors for nontuberculous mycobacterial pulmonary disease: a systematic literature review and meta-analysis. Chest. 2023;164:1115–24. https://doi.org/10.1016/j.chest.2023.06.014
12. Metersky ML, Barker AF. The pathogenesis of bronchiectasis. Clin Chest Med. 2022;43:35–46. https://doi.org/10.1016/j.ccm.2021.11.003

Address for correspondence: Mark L. Metersky, University of Connecticut School of Medicine, 263 Farmington Ave, Farmington, CT 06030-1321, USA; email: metersky@uchc.edu

Genomic Characterization of Circulating Dengue Virus, Ethiopia, 2022–2023

Adugna Abera,[1] Houriiyah Tegally,[1] Geremew Tasew, Eduan Wilkinson, Abraham Ali, Feyisa Regasa, Molalegne Bitew, Mahlet Belachew, Lucious Chabuka, Gaspary Mwanyika, Derek Tshiabuila, Jennifer Giandhari, Sureshnee Pillay, Jenicca Poogavanan, Monika Moir, Moritz U.G. Kraemer, Kamran Khan, Carmen Huber, Getachew Tollera, Tobias F. Rinke de Wit, Cheryl Baxter, Richard Lessells, Dawit Wolday, Dereje Beyene,[2] Tulio de Oliveira,[2] and CLIMADE Consortium[3]

In Ethiopia, dengue virus (DENV) infections have been reported in several regions; however, little is known about the genetic diversity of circulating viruses. We conducted clinical surveillance of DENV during the 2023 nationwide outbreak in Ethiopia. We enrolled patients at 3 sentinel hospital sites. Using reverse transcription PCR, we screened serum samples for 3 arboviruses and then serotyped and whole-genome sequenced DENV-positive samples. We detected DENV-1 and DENV-3 serotypes. Phylogenetic analysis identified 1 transmission cluster for DENV-1 (genotype III major lineage A) and 2 clusters for DENV-3 (genotype III major lineage B). The first DENV-3 cluster was closely related to an isolate from a 2023 dengue outbreak in Italy; the second cluster was related to isolates from India. Cocirculation of DENV-1 and DENV-3 in Ethiopia highlights the potential for severe dengue. Intensified surveillance and coordinated public health responses are needed to address the threat of severe dengue outbreaks.

Dengue virus (DENV) is primarily transmitted by *Aedes* spp. mosquitoes and causes considerable epidemics in tropical and subtropical regions. In 2023, the World Health Organization African Region reported 171,991 suspected cases, 70,223 of which were confirmed cases with 753 deaths (*1*,*2*). Outbreaks have been reported in 15 countries in Africa; Burkina Faso accounted for 85% of cases, followed by Ethiopia (8.2%), Mali (2.5%), and Côte d'Ivoire (2.2%) (*1*,*2*).

Ethiopia has had several outbreaks of dengue fever since 2013. The first recorded outbreak was reported in Dire Dawa and affected 9,441 persons (*3*). A second outbreak occurred in Godey (Somali Region) in 2014 and Afar Region in 2015 (*4*). Since 2015, an increase in the number of severe febrile illness cases has been observed in Godey, Dire Dawa, and Afar Region with no apparent cause. A dengue outbreak began in April 2023 in Afar Region, followed by Dire Dawa and the neighboring regions of Amhara and Oromia. A total of 27,577 cases and 21 deaths in 12 districts have been reported in the eastern part of Ethiopia (*1*,*5*).

DENV is a single-stranded, positive-sense RNA virus with 4 serotypes, DENV-1–4 (*6*,*7*). The risk of severe dengue increases after infections with different serotypes. Each serotype is further divided into several genotypes. However, different genotypes of the same serotype might vary in their ability to infect host cells and cause severe forms of disease. According to genetic characterization, DENV-1 has 5 defined genotypes, DENV-2 has 6 defined genotypes, DENV-3

Authors affiliations: Ethiopian Public Health Institute, Addis Ababa, Ethiopia (A. Abera, G. Tasew, A. Ali, F. Regasa, M. Belachew, G. Tollera, D. Wolday); Addis Ababa University, Addis Ababa (A. Abera, D. Beyene); Centre for Epidemic Response and Innovation, School of Data Science and Computational Thinking, Stellenbosch University, Stellenbosch, South Africa (H. Tegally, E. Wilkinson, L. Chabuka, G. Mwanyika, D. Tshiabuila, J. Poogavanan, M. Moir, C. Baxter, T. de Oliveira); Bio and Emerging Technology Institute, Addis Ababa (M. Bitew); University of KwaZulu-Natal, Durban, South Africa (J. Giandhari, S. Pillay, R. Lessells, T. de Oliveira); University of Oxford, Oxford, UK (M.U.G. Kraemer); University of Toronto, Toronto, Ontario, Canada (K. Khan); BlueDot, Toronto (K. Khan, C. Huber); University of Amsterdam, Amsterdam, the Netherlands (T.F. Rinke de Wit); McMaster University, Hamilton, Ontario, Canada (D. Wolday)

DOI: https://doi.org/10.3201/eid3103.240996

[1]These authors contributed equally to this article.

[2]These senior authors contributed equally to this article.

[3]Members of the CLIMADE consortium are listed in the Appendix (https://wwwnc.cdc.gov/EID/article/31/3/24-0996-App1.pdf).

has 5 defined genotypes, and DENV-4 has 4 defined genotypes (*8*–*11*). A nomenclature system has been recently proposed to further subdivide genotypes into major and minor lineages to aid global monitoring efforts (*12*).

During dengue outbreaks, the emergence of new virus serotypes or changes in circulating genotypes in a particular region can lead to more severe outbreaks (*13*,*14*). Because no approved medical countermeasures for treating severe dengue exist, little is known about the efficacy of dengue vaccines and potential antiviral drugs. Therefore, it is crucial to continuously monitor the genetic diversity of circulating DENVs in dengue-endemic areas. Surveillance will be instrumental in developing and evaluating vaccines and treatments (*15*) and responding effectively to dengue outbreaks.

Although multiple outbreaks and geographic expansion of DENV in Ethiopia have occurred, diversity of circulating DENVs in this country has not been characterized, and whole-genome sequences have not been publicly available. We addressed this information gap by identifying circulating DENV serotypes and genotypes among patients with febrile illness in 3 hospital-based sentinel sites in Ethiopia. Furthermore, we conducted phylogenetic analyses to determine spatial and temporal patterns of dengue transmission in Ethiopia. The study was approved by Addis Ababa University (approval no. CNCSDO/175/15/2023) and the Institutional Review Board of the Ethiopian Public Health Institute (EPHI; approval no. EPHI-IRB-536–2023).

Methods

Patient Characteristics and Study Settings

We conducted a cross-sectional hospital-based study at 3 major public hospitals in Dubti (Afar Region), Dire Dawa, and Gambela (Appendix Figure 1). Those hospitals serve as sentinel sites for acute febrile illnesses in Ethiopia and were selected because of their history monitoring arbovirus outbreaks and collecting serologic evidence for arboviruses (*5*,*16*). During December 2022–November 2023, we enrolled outpatients and inpatients who had fevers >37.5°C. We obtained informed consent from all participants ≥18 years of age. For persons 1–17 years of age, we obtained informed consent from a parent or guardian and assent from the child, when appropriate.

Eligibility/Exclusion Criteria

The inclusion criterion for the study was a fever of >37.5°C according to the 2009 World Health Organization dengue classification (*17*). We excluded patients with severe and established chronic clinical illnesses, such as persons living with HIV, malignancies, and known metabolic disorders.

Sample Collection and Processing

At each study site, 5 mL of whole blood was collected from each participant into serum separator tubes. At the Afar site, blood samples were collected during April 25–May 15, 2023. Serum samples were isolated and collected in tubes containing 1 mL DNA/RNA Shield (Zymo Research, https://www.zymoresearch.com) and stored at −20°C during field collections. The field samples were transported in a cold chain to the EPHI laboratory, where we stored them at −20°C until PCR and sequencing analyses. The blood samples from Dire Dawa and Gambela sites were collected during June–October 2023; serum samples were isolated and stored at −20°C and were then shipped in a cold chain to the EPHI laboratory, where we stored them at −80°C until analysis.

RNA Extraction and PCR Amplification

We performed RNA extraction at EPHI within 5 days of receiving the serum samples from each site by using a Bioer NPA-32P instrument (Bioer Technology, https://www.bioer.com.cn) according to the manufacturer's instructions; final volume of RNA extract was 70 μL. We stored the remaining serum samples from Afar Region at −20°C for whole-genome sequencing and stored remaining samples from the Dire Dawa and Gambela sites at −80°C.

On the same day we extracted RNA, we used the US Centers for Disease Control and Prevention (CDC) Trioplex Real-Time RT-PCR Assay to screen for arboviral infections, including those caused by DENV, chikungunya virus (CHIKV), and Zika virus (ZIKV). This assay includes a set of published oligonucleotide primers and dual-labeled hydrolysis Taqman probes. In brief, we combined 10 μL of RNA sample with 12.5 μL of PCR master mix reaction buffer (Thermo Fisher Scientific, https://www.thermofisher.com), 1 μmol/L virus-specific primers, 0.3 μmol/L dengue-specific probe, 0.15 μmol/L CHIKV-specific probe, 0.15 μmol/L ZIKV-specific probe, and nuclease-free water in a 96-well optical PCR plate to make a final reaction volume of 25 μL. We captured the fluorescent signal intensity by using the QuantStudio 5 Real-Time PCR System (Thermo Fisher Scientific).

DENV Serotyping

After PCR screening, we serotyped DENV-positive samples by using the same RNA extract and the

CDC DENV-1-4 rRT-PCR Multiplex Assay on the QuantStudio 5 Real-Time PCR System. This assay uses specific primers and probes to detect DENV-1–4. To perform the assay, we mixed 5 μL of extracted RNA with 12.5 μL of master mix (Thermo Fisher Scientific), according to the manufacturer's protocol, and DENV-1–4 primers and probes provided by CDC.

DENV Sequencing

After serotyping, we selected specimens with PCR cycle thresholds (Cts) of <26 for sequencing. Technical support staff from KwaZulu-Natal Research Innovation and Sequencing Platform, University of KwaZulu-Natal, and Centre for Epidemic Response and Innovation, Stellenbosch University, performed sequencing. The primer scheme for DENV sequencing and other arboviruses is available on the CLIMADE GitHub (https://github.com/CERI-KRISP/CLIMADE/tree/master/Protocols/Arboviruses). We adapted the COVIDSeq protocol to perform the library preparation, followed by sequencing on the Illumina Miseq platform (Illumina, https://www.illumina.com). The sequencing protocol is also available on the CLIMADE GitHub (https://protocols.io/view/pathogen-whole-genome-sequencing-multiplexed-ampli-cgwbtxan).

We prepared libraries by using the Illumina COVIDSeq protocol. In brief, we reverse transcribed RNA to cDNA by using random hexamers and amplified the DENV genome by using 2 pools of primers specific for the DENV-1–4 serotypes. We used enrichment bead-linked transposomes (Illumina) to tagment PCR amplicons and further amplified adaptor-ligated amplicons by using the unique 10 bp Index 1 (i7) adapters and Index 2 (i5) adapters (Illumina-PCR Indexes Set 1; Illumina) for each sample. We quantified the pooled amplicon library by using a Qubit 2.0 fluorometer (Thermo Fisher Scientific) and diluted the library to 4 nmol/L. We then denatured the library and diluted it to a final loading concentration of 12 pmol/L. We performed dual indexed paired-end sequencing on an Illumina Miseq instrument with a v3 600-cycle flow cell.

Bioinformatics Analysis

After base calling and demultiplexing of the sequence runs, we processed fastq files by using the Genome Detective version 2.13.3 (https://www.genomedetective.com) analysis pipeline. We retrieved consensus fasta and binary alignment map files for each sample from Genome Detective and performed sequence genotyping and lineage classification by using the Genome Detective Dengue Typing Tool according to a newly developed nomenclature for DENV classification (*12*). We submitted all genomic sequences to the GISAID Epi-Arbo database (https://www.gisaid.org; accession nos. EPI_ISL_19229161–193).

Sequence Alignment and Phylogenetic Analysis

We retrieved DENV reference sequence datasets from GenBank and the GISAID Epi-Arbo database and removed duplicate entries. We subjected the retrieved sequences to initial quality control by removing unverified sequences and incomplete records (i.e., geographic location and sampling dates). The final dataset used for phylogenetic analyses consisted of 33 sequences generated from Ethiopia as well as 2,348 publicly available sequences of DENV-3 genotype III major lineage B and 990 sequences of DENV-1 genotype III major lineage A, corresponding to transmission lineages detected in Ethiopia. We aligned the DENV-1 and DENV-3 datasets from this study with the appropriate DENV serotype reference genomes (DENV-1, GenBank accession no. NC_001477.1; DENV-3, accession no. NC_001475.2) by using the Nextalign version 1.3.0 alignment tool (*18*).

We generated maximum-likelihood trees for each of the 2 genotypes by using IQ-TREE version 2.2.2.2 and 1,000 bootstraps (*19*). Using ModelFinder in IQ-TREE, we selected the following nucleotide substitution models: transition 2 plus base frequencies plus proportion of invariable sites plus gamma distribution 4 model for DENV-1 and the general time reversible plus base frequencies plus proportion of invariable sites plus gamma distribution 4 model for DENV-3, according to Bayesian information criterion (*19*). We evaluated the molecular clock signal by using TempEst v1.5.3 (*20*) and removed potential outliers that violated the molecular clock assumption before inferring a time-scaled tree by using TreeTime version 0.10.0 (*21*). We used molecular clock rates of 5.015×10^{-4} (for DENV-1) and 1.225×10^{-4} (for DENV-3) nucleotide substitutions per site per year, determined by the clock function in TreeTime.

Time-Calibrated Bayesian Phylogenies

We constructed time-calibrated Bayesian phylogenetic trees to estimate the time to the most common recent ancestor (tMRCA) (i.e., time of emergence) of the DENV lineages circulating during the 2023 outbreak and likely introduction routes. We used BEAST version 1.10.4 along with the BEAGLE library version 3.2.0 to improve computational speed (*22*,*23*).

We applied a relaxed clock model for all analyses along with the Hasegawa-Kishino-Yano plus gamma distribution plus proportion of invariable sites nucleotide substitution model and used a constant population coalescent model assumption. Subsequently, we performed all analyses in 2 independent runs with 100 million iterations each. We checked convergence of Markov chain Monte Carlo chains by using Tracer version 1.7.1 (*24*) and discarded 10% of initial chains as burn-ins. We pooled postburn-in samples to summarize parameter estimates by using LogCombiner and TreeAnnotator tools in BEAST, including posterior probability for each parameter and maximum-clade credibility trees. We visualized phylogenetic trees by using Figtree version 1.4.4 (http://tree.bio.ed.ac.uk/software/figtree) and other figures by using R (The R Project for Statistical Computing, https://www.r-project.org) and ggplot (*25*).

Air Travel Data

We analyzed travel data from the International Air Transport Association (https://www.iata.org) to determine the volume of passengers arriving from international airports. Those data accounted for ≈90% of passenger travel itineraries on commercial flights, excluding transportation via unscheduled charter flights. The remaining 10% of commercial flights is modeled by using market intelligence.

Results

We recruited study participants during a recorded DENV infection outbreak in Ethiopia (Appendix Figure 1). Cases were recorded in multiple regions of the country by the Ministry of Health in Ethiopia starting in early 2023; Afar Region and Dire Dawa were the 2 most affected regions (Figures 1, 2). A first peak in cases occurred in Afar Region during April–August 2023; low level transmission occurred in Dire Dawa during that period. A second prominent peak was observed in Dire Dawa during October 2023–January 2024. Our clinical surveillance was able to detect acute dengue infections from both regions; detection in Dire Dawa intensified before the peak in recorded cases (Figure 1).

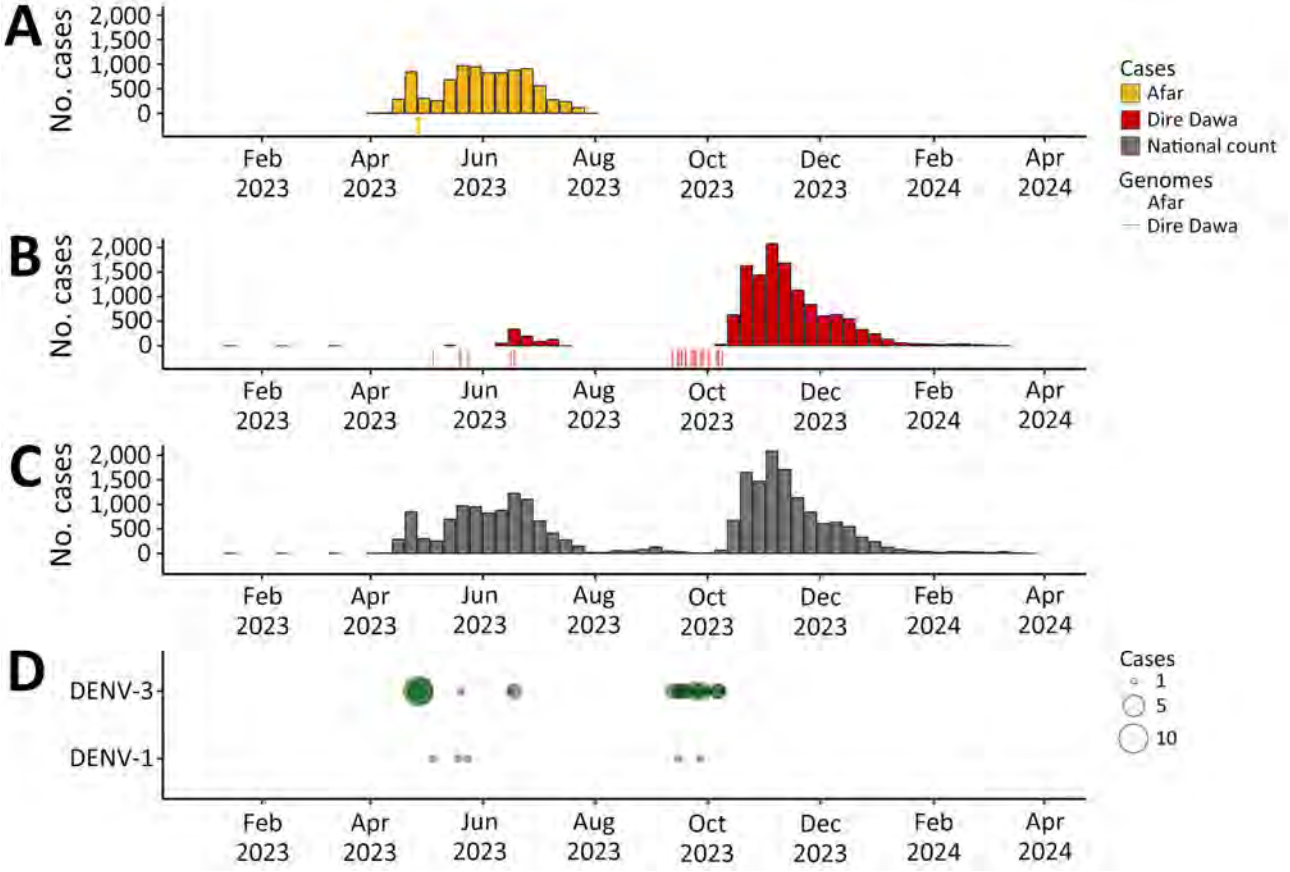

Figure 1. Spatiotemporal distribution of dengue cases in study of genomic characterization of circulating DENV, Ethiopia, 2022–2023. A–C) Number of dengue cases in Ethiopia in Afar Region during April 2023–August 2023 outbreak (A), Dire Dawa during June 2023–April 2024 outbreak (B), and national count during 2023–2024 (C). Each colored vertical line under bars indicates 1 sequenced genome. D) DENV serotype distribution of sampled cases. Size of circles indicates number of genotyped cases for each serotype. DENV, dengue virus.

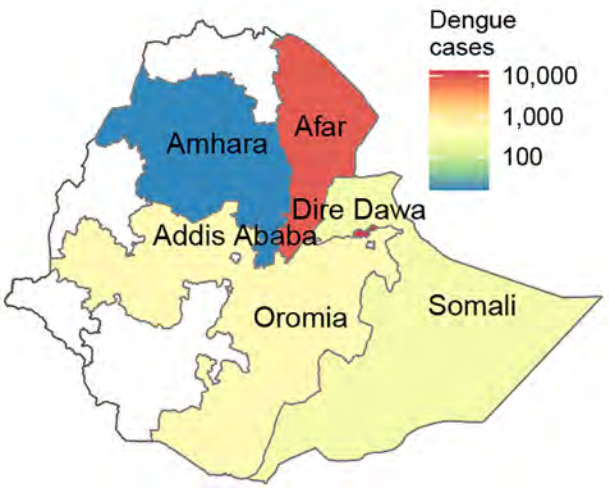

Figure 2. Number of dengue cases in different regions of Ethiopia during 2023–2024 in study of genomic characterization of circulating dengue virus. Only dengue virus (DENV) serotype 3 was found in Afar Region; both DENV-1 and DENV-3 were isolated in the city of Dire Dawa.

Sample Collection and Epidemiology

Of 891 febrile patients screened for DENV, CHIKV, and ZIKV infections, only DENV was detected. The percentage of patients with a positive PCR for DENV was 10.4% (93/891). The test positivity was slightly higher in men than women (Table; Figure 3). DENV was isolated from 2 of the 3 sites; the percentages of patients with a positive DENV PCR were 13.7% (41/300) in Afar Region and 17.9% (52/291) in Dire Dawa. None of the 300 samples from Gambela were positive for DENV. Virus genotyping showed evidence of co-circulation of DENV-1 and DENV-3 throughout the outbreak period (Figure 1, panel D). Among 93 PCR-positive isolates, we identified 88 (94.6%) as DENV-3 and 5 (5.4%) as DENV-1. At the Afar site, only DENV-3 was detected (n = 41), whereas in Dire Dawa, both DENV-1 (n = 5) and DENV-3 (n = 47) were detected (Table).

Virus Genome Sequencing

We selected 55 virus isolates for sequencing on the basis of their PCR Cts. Cts ranged from 15.5 to 25.6. We selected 20 DENV-3 isolates from Afar Region and 35 (5 DENV-1 and 30 DENV-3) from Dire Dawa for sequencing. Of those, 54 isolates were successfully sequenced; 1 sample failed to be sequenced because of low sample volume. Among the successfully sequenced isolates, 33 gave near whole-genome sequences (>90% genome coverage). Of those 33, we identified all 5 DENV-1 as DENV-1 genotype III lineage A and the remaining 28 as DENV-3 genotype III lineage B (1 isolate from Afar Region and 27 from Dire Dawa) (Figure 4).

Samples collected from Dire Dawa showed an expected association between a high virus load (lower Ct values) and high sequence coverage, whereas most samples from Afar Region produced low sequence coverage genomes, despite low Cts. PCR was not repeated after storing the serum samples; we only used Cts from the first screening PCR. Sample collection and storage freezers used at both sites were different. The samples from Afar Region were collected in DNA/RNA Shield during the outbreak in May 2023 and stored for a long period at −20°C, during which intermittent temperature fluctuations of the freezer were noted. In contrast, samples collected from Dire Dawa and Gambela were relatively recent and stored at −80°C until they were sequenced.

Phylogenetic Analysis

We constructed a time-scaled phylogenetic tree by aligning 990 global DENV-1 genotype III lineage A sequences along with 5 sequences from Ethiopia obtained in this study (Figure 5, panel A). For this lineage, all sequences from Ethiopia belonged to a single transmission cluster, which clustered monophyletically with other sequences from Africa, suggesting

Table. Characteristics of patients with DENV infections in study of genomic characterization of circulating dengue virus, Ethiopia, 2022–2023*

Parameters	No. dengue tests		Total no. tests	% Positive tests	DENV serotypes, no. patients		
	Positive	Negative			DENV-1	DENV-3	Total
Sex							
M	49	400	449	10.91	2	47	49
F	44	398	442	9.95	3	41	44
Region							
Afar	41	259	300	13.67	0	41	41
Dire Dawa	52	239	291	17.87	5	47	52
Gambela	0	300	300	0	0	0	0
Age, y							
0–4	0	27	27	0	0	0	0
5–14	2	40	42	4.8	0	2	2
15–29	41	393	434	9.4	2	40	42
30–44	28	228	256	10.9	1	27	28
>45	21	111	132	15.9	2	19	21

*DENV, dengue virus.

cryptic transmission in the region since 2019 (Figure 5, panel B). tMRCA indicated that emergence of the clade from Ethiopia occurred during mid-2021 (Figure 5, panel B). Sequences originating mostly from Asia are basal to the clade from Africa, suggesting an introduction into Africa from Asia in 2018 (Figure 5, panel B). For DENV-3 genotype III lineage B, we constructed a time-scaled phylogenetic tree by using 2,348 global sequences along with sequences from Ethiopia (Figure 5, panel C). Those sequences from Ethiopia belonged to 2 distinct clades (Figure 5, panels D, E). Whereas the first clade consisted of sequences generally from Asia and Africa, sequences from this study had tMRCA in early 2021 (95% highest posterior density [HPD] 2020–2022) and clustered monophyletically with a sequence from Italy's 2023 dengue outbreak (*26*). We infer that the common ancestor for the isolates from Ethiopia and Italy existed around mid-2019 (95% HPD mid-2017–2021) with long branches separating the 2 locations. The Ethiopia/Italy clade was supported with >70% posterior support at the relevant internal nodes on the maximum-clade credibility tree, suggesting some level of cryptic transmission in unsampled areas where both Ethiopia and Italy could have received virus introductions. However, given historical ties between the 2 countries and continued high connectivity, an introduction into Ethiopia from Italy is plausible; Italy has the second highest number of air travel passengers into Ethiopia of all countries within Europe (Appendix Figure 2). The second relevant clade of this lineage indicates a clear introduction from Asia into Ethiopia in late 2021 (95% HPD 2021–2023) and a potentially persistent transmission since then (Figure 3, panel E). Although the closest relatives to this second clade from Ethiopia are sequences from India, it remains possible that intermediate unsampled regions are involved because of the long branch lengths on the tree, including Saudi Arabia (*27*), which has the second largest air travel passenger volume into Ethiopia overall (Appendix Figure 2).

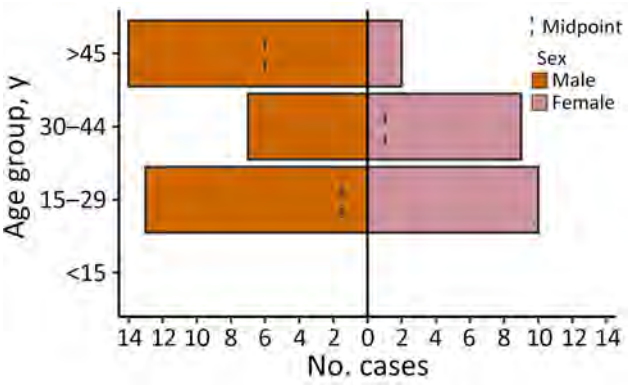

Figure 3. Demographic distribution of patients with dengue virus infections in study of genomic characterization of circulating dengue virus, Ethiopia, 2022–2023.

Discussion

We investigated the genomic epidemiology of DENV in 3 areas of Ethiopia and determined the distribution of serotypes, genotypes, and lineages circulating in Ethiopia, identified by whole-genome sequencing. Our findings showed that 2 serotypes, DENV-1 and DENV-3, were isolated in Dire Dawa, whereas only DENV-3 was isolated in Afar Region. Those data suggest a need for more comprehensive epidemiologic or genomic surveillance and strengthened systems for

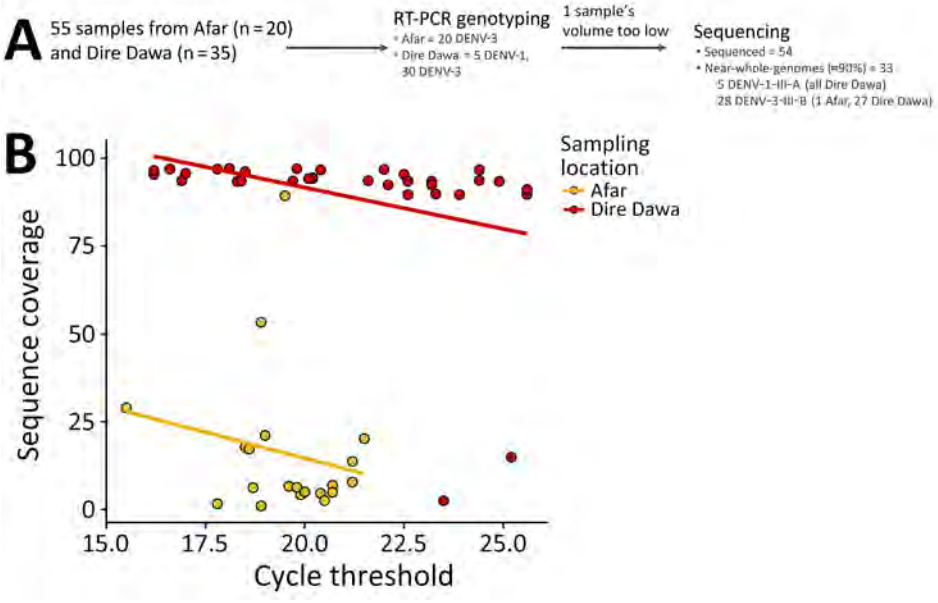

Figure 4. Sequencing process and coverage results in study of genomic characterization of circulating DENV, Ethiopia, 2022–2023. A) Patient sample selection, genotyping, and sequencing workflow. B) PCR cycle thresholds compared with sequence coverage for all sequenced specimens from Afar Regions and Dire Dawa. DENV, dengue virus; III-A, genotype III lineage A; III-B, genotype III lineage B; RT-PCR, reverse transcription PCR.

severe dengue surveillance because of the potential health risks from multiple serotypes or genotypes. In Africa, all 4 DENV serotypes have been detected in both humans and *Aedes* spp. mosquitoes (*28*). DENV-2 is the most prevalent serotype in East Africa. The virus caused outbreaks in Ethiopia in 2013, Kenya in 2013, Tanzania in 2014, and Mozambique in 2014–2015 and has remained prevalent in those areas (*29*–*31*). DENV-1 infection outbreaks have been detected at different times in Angola, Kenya, Senegal, and Somalia (*32*). The current DENV-1 serotype might have been historically co-circulating with DENV-2 or might have been a recent introduction into Dire Dawa. The current dengue fever outbreak in Ethiopia first began in the Mile district of Afar Region in April 2023; the outbreak was caused by DENV-3 and has since spread to ≥5 other regions in the eastern part of the country (*33*).

Phylogenetic analysis revealed that DENV-1 isolates from this study belong to genotype III major lineage A; circulation of this lineage during the 2023 outbreak corresponds to a single transmission cluster.

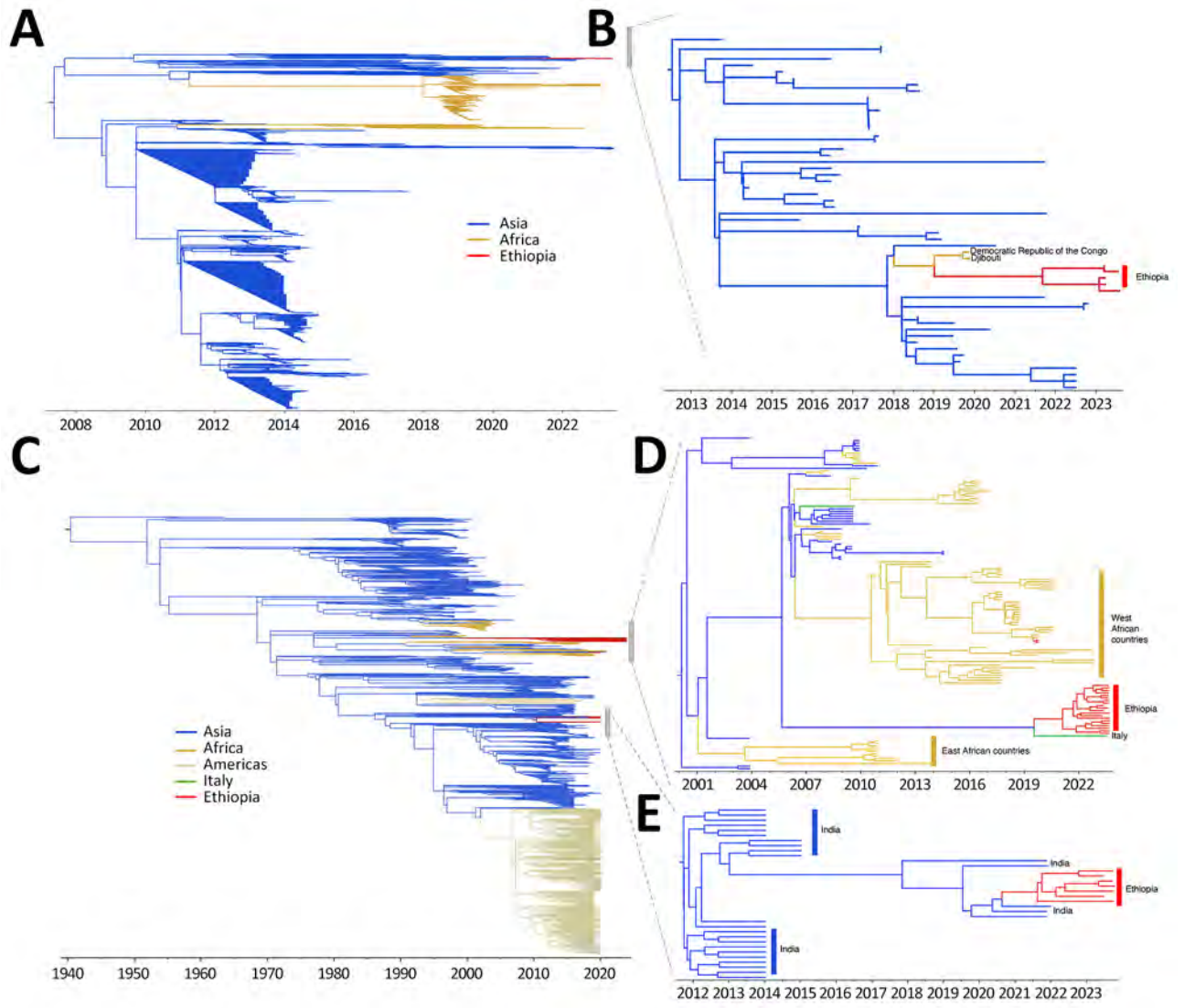

Figure 5. Time-scaled phylogenetic analysis of genomes from Ethiopia in study of genomic characterization of circulating dengue virus (DENV), 2022–2023. A) Time-scaled maximum-likelihood phylogeny of DENV-1 genotype III major lineage A clade sequences containing sequenced genomes from this study. B) Time-scaled phylogeny of subclade of tree in panel A, indicating close evolutionary relationships of DENV-1 sequences from Ethiopia. C) Time-scaled maximum-likelihood phylogeny of DENV-3 genotype III major lineage B clade sequences containing sequenced genomes from this study. D) Time-scaled maximum clade credibility tree of subclade from tree in panel C indicating phylogenetic relationships of cluster 1 of DENV-3 genomes from Ethiopia. E) Time-scaled maximum clade credibility tree of subclade from tree in panel C indicating phylogenetic relationships of cluster 2 of DENV-3 genomes from Ethiopia. Colors indicate country or continent origin of sequences used in trees.

It seems that this cluster was introduced into Ethiopia from Asia via other countries in Africa. DENVs belonging to the same genotype were sequenced during the 2023 dengue outbreak in Chad (*2*). However, the genomes generated in this study are not directly linked to the Chad outbreak, which originated from a large outbreak in Tanzania in 2019 via Nigeria (*34*). The phylogenetic reconstruction from available DENV-1 genomic data in Africa, which we have supplemented with our sequences, indicate several distinct lineages are currently circulating on the continent. All known DENV-1 strains from Central Africa belong to genotype V African lineage; the oldest strains of this lineage were isolated in Nigeria in 1968 (*35*). However, the lack of publicly available data limits our understanding of the dynamics of DENV-1 within Africa.

DENV-3 viruses sequenced during Ethiopia's 2023 dengue outbreak belonged to genotype III major lineage B, and phylogenetic reconstructions revealed 2 transmission clusters circulating in Ethiopia. Cluster 1 is closely related to a DENV-3 from Italy sequenced in 2023 (Figure 5, panel D) (*28*), highlighting the possibility that the virus might have been introduced into Ethiopia from Italy. Because we have no previous sequence information, we cannot exclude the possibility that transmission from Ethiopia to Italy might also have occurred. DENV-3 genotype III exists in neighboring countries, including Sudan, Kenya, Djibouti, and Somalia (*36*). However, the current DENV-3 genotype III in Ethiopia is not directly related to the other isolates from Africa. Cluster 2 appears to have been introduced from India perhaps via secondary locations (Figure 5, panel E). Phylogenetic analysis of DENV-3 in India has shown that outbreaks during 2017–2018 were caused by genotype III (*37*).

By whole-genome sequencing, only 33 samples from this study resulted in >90% genome coverage. Thirty-two (5 DENV-1 and 27 DENV-3) of those samples were from Dire Dawa, but only 1 sample gave ≈90% genome coverage from Afar Region. Serum samples from Afar Region were collected during the outbreak and sent to the EPHI laboratory for DENV detection and serotyping. The remaining samples were then stored at −20°C for ≈11 months before sequencing. The limited genome coverage in some samples could be attributed to extended storage under unsuitable conditions. In contrast, serum samples obtained from Dire Dawa were stored at −80°C for ≈4–8 months, which likely resulted in greater sequence coverage.

The first limitation of our study is that poor sequencing outcomes were encountered, possibly because of inadequate sample storage in Afar Region. Improved sample storage conditions could have led to better whole-genome sequencing results. Second, the limited availability of DENV sequences continentally and globally restricted our ability to infer global transmission dynamics and direct introduction routes. However, we were able to identify circulating genotypes and lineages and infer possible introduction routes and timing.

In conclusion, we characterized DENV genomic epidemiology during the 2023 dengue outbreak in Ethiopia. Our findings highlight the utility of comprehensive disease surveillance, including pathogen genome sequencing, to elucidate DENV transmission dynamics in Ethiopia and elsewhere during emerging outbreaks. Regular active surveillance of dengue through highly connected sentinel sites as well as at ports of entry can improve response time and reduce the likelihood of dengue outbreaks.

Acknowledgments

We thank the US CDC for supplying DENV detection and serotyping kits. We gratefully acknowledge the authors from the originating and submitting laboratories for the reference sequence data in the GISAID EpiArbo database on which our DENV genomic data are partially based.

This work was supported by Ethiopian Public Health Institute and Addis Ababa University. Sequencing and modeling activities at KwaZulu-Natal Research Innovation and Sequencing Platform, University of KwaZulu-Natal and the Centre for Epidemic Response and Innovation, Stellenbosch University, are supported in part by grants from the Rockefeller Foundation (grant no. HTH 017), Abbott Pandemic Defense Coalition, US National Institutes of Health (grant no. U01 AI151698) for the United World Antivirus Research Network, South African Medical Research Council South African mRNA Vaccine Consortium, Global Health European and Developing Countries Clinical Trials Partnership 3 Joint Undertaking, the Bill & Melinda Gates Foundation (grant no. 101103171), European Union' (EU) Horizon Europe Research and Innovation Programme (grant no. 101046041), Health Emergency Preparedness and Response Umbrella Program managed by the World Bank Group (grant no. TF0B8412), Deutsche Gesellschaft für Internationale Zusammenarbeit GmbH commissioned by the Government of the Federal Republic of Germany, UK Medical Research Foundation (grant no. MRF-RG-ICCH-2022-100069), Wellcome Trust for the Global.health Project (grant no. 228186/Z/23/Z), Novo Nordisk Foundation (grant no. NNF24OC0094346), and the EU project EpiGen (https://epigenethiopia.org). M.U.G.K. acknowledges funding from The Rockefeller

Foundation (PC-2022-POP-005), Google.org, the Oxford Martin School Programmes in Pandemic Genomics & Digital Pandemic Preparedness, EU Horizon Europe programme projects MOOD (#874850) and E4Warning (#101086640), Wellcome Trust grants 303666/Z/23/Z, 226052/Z/22/Z & 228186/Z/23/Z, the United Kingdom Research and Innovation (#APP8583), the Medical Research Foundation (MRF-RG-ICCH-2022-100069), UK International Development (301542-403), the Bill & Melinda Gates Foundation (INV-063472), and Novo Nordisk Foundation (NNF24OC0094346). K.K is the founder of BlueDot and C.H. is employed at BlueDot.

About the Author

Dr. Abera is a senior research scientist at the Ethiopian Public Health Institute. His research interests focus on molecular epidemiology, drug resistance, diagnostics, and metagenomics research applied to malaria, neglected tropical diseases, and arboviral diseases in Ethiopia.

References

1. World Health Organization. Disease outbreak news; dengue—global situation. 2023 [cited 2024 May 20]. https://www.who.int/emergencies/disease-outbreak-news/item/2023-DON498
2. World Health Organization African Region. Health emergency situation report: multi-country outbreak of dengue, consolidated regional situation report 001. 2023 [cited 2024 May 20]. https://iris.who.int/handle/ 10665/375392
3. World Health Organization. Ethiopia steps up actions for dengue prevention and control. 2014 [cited 2024 May 20]. https://www.afro.who.int/news/ethiopia-steps-actions-dengue-prevention-and-control
4. Ahmed YM, Salah AA. Epidemiology of dengue fever in Ethiopian Somali region: retrospective health facility based study. Central African J Public Health. 2016;2:51–6. https://doi.org/10.11648/j.cajph.20160202.12
5. Gutu MA, Bekele A, Seid Y, Mohammed Y, Gemechu F, Woyessa AB, et al. Another dengue fever outbreak in Eastern Ethiopia—an emerging public health threat. PLoS Negl Trop Dis. 2021;15:e0008992. https://doi.org/10.1371/journal.pntd.0008992
6. Murugesan A, Manoharan M. Dengue virus. In: Ennaji MM, editor. Emerging and reemerging viral pathogens. Vol. 1. Fundamental and basic virology aspects of human, animal and plant pathogens. New York: Academic Press; 2020. p. 281–359.
7. Mustafa MS, Rasotgi V, Jain S, Gupta V. Discovery of fifth serotype of dengue virus (DENV-5): a new public health dilemma in dengue control. Med J Armed Forces India. 2015;71:67–70. https://doi.org/10.1016/j.mjafi.2014.09.011
8. Poltep K, Phadungsombat J, Nakayama EE, Kosoltanapiwat N, Hanboonkunupakarn B, Wiriyarat W, et al. Genetic diversity of dengue virus in clinical specimens from Bangkok, Thailand, during 2018–2020: co-circulation of all four serotypes with multiple genotypes and/or clades. Trop Med Infect Dis. 2021;6:162. https://doi.org/10.3390/tropicalmed6030162
9. Calvez E, Somlor S, Viengphouthong S, Balière C, Bounmany P, Keosenhom S, et al. Rapid genotyping protocol to improve dengue virus serotype 2 survey in Lao PDR. PLoS One. 2020;15:e0237384. https://doi.org/10.1371/journal.pone.0237384
10. Li L, Guo X, Zhang X, Zhao L, Li L, Wang Y, et al. A unified global genotyping framework of dengue virus serotype-1 for a stratified coordinated surveillance strategy of dengue epidemics. Infect Dis Poverty. 2022;11:107. https://doi.org/10.1186/s40249-022-01024-5
11. Naveca FG, Santiago GA, Maito RM, Ribeiro Meneses CA, do Nascimento VA, de Souza VC, et al. Reemergence of dengue virus serotype 3, Brazil, 2023. Emerg Infect Dis. 2023;29:1482–4. https://doi.org/10.3201/eid2907.230595
12. Hill V, Cleemput S, Pereira JS, Gifford RJ, Fonseca V, Tegally H, et al. A new lineage nomenclature to aid genomic surveillance of dengue virus. PLoS Biol. 2024;22:e3002834. https://doi.org/10.1371/journal.pbio.3002834
13. Rahim R, Hasan A, Phadungsombat J, Hasan N, Ara N, Biswas SM, et al. Genetic analysis of dengue virus in severe and non-severe cases in Dhaka, Bangladesh, in 2018–2022. Viruses. 2023;15:1144. https://doi.org/10.3390/v15051144
14. Ahamed SF, Rosario V, Britto C, Dias M, Nayak K, Chandele A, et al. Emergence of new genotypes and lineages of dengue viruses during the 2012–15 epidemics in southern India. Int J Infect Dis. 2019;84S:S34–43. https://doi.org/10.1016/j.ijid.2019.01.014
15. Durbin AP, Whitehead SS. Next-generation dengue vaccines: novel strategies currently under development. Viruses. 2011;3:1800–14. https://doi.org/10.3390/v3101800
16. Asebe G, Michlmayr D, Mamo G, Abegaz WE, Endale A, Medhin G, et al. Seroprevalence of yellow fever, chikungunya, and Zika virus at a community level in the Gambella Region, South West Ethiopia. PLoS One. 2021;16:e0253953. https://doi.org/10.1371/journal.pone.0253953
17. Horstick O, Martinez E, Guzman MG, Martin JL, Ranzinger SR. WHO dengue case classification 2009 and its usefulness in practice: an expert consensus in the Americas. Pathog Glob Health. 2015;109:19–25. https://doi.org/10.1179/2047773215Y.0000000003
18. Aksamentov I, Roemer C, Hodcroft EB, Neher RA. Nextclade: clade assignment, mutation calling and quality control for viral genomes. J Open Source Softw. 2021;6:3773. https://doi.org/10.21105/joss.03773
19. Nguyen LT, Schmidt HA, von Haeseler A, Minh BQ. IQ-TREE: a fast and effective stochastic algorithm for estimating maximum-likelihood phylogenies. Mol Biol Evol. 2015;32:268–74. https://doi.org/10.1093/molbev/msu300
20. Rambaut A, Lam TT, Max Carvalho L, Pybus OG. Exploring the temporal structure of heterochronous sequences using TempEst (formerly Path-O-Gen). Virus Evol. 2016;2:vew007. https://doi.org/10.1093/ve/vew007
21 Sagulenko P, Puller V, Neher RA. TreeTime: maximum-likelihood phylodynamic analysis. Virus Evol. 2018;4:vex042. https://doi.org/10.1093/ve/vex042
22. Suchard MA, Lemey P, Baele G, Ayres DL, Drummond AJ, Rambaut A. Bayesian phylogenetic and phylodynamic data integration using BEAST 1.10. Virus Evol. 2018;4:vey016. https://doi.org/10.1093/ve/vey016
23. Ayres DL, Darling A, Zwickl DJ, Beerli P, Holder MT, Lewis PO, et al. BEAGLE: an application programming interface and high-performance computing library for statistical phylogenetics. Syst Biol. 2012;61:170–3. https://doi.org/10.1093/sysbio/syr100
24 Rambaut A, Drummond AJ, Xie D, Baele G, Suchard MA. Posterior summarization in Bayesian phylogenetics using Tracer 1.7. Syst Biol. 2018;67:901–4. https://doi.org/10.1093/sysbio/syy032

25. Wickham H. ggplot2: elegant graphics for data analysis. 2nd ed. New York: Springer; 2016
26. Branda F, Nakase T, Maruotti A, Scarpa F, Ciccozzi A, Romano C, et al. Dengue virus transmission in Italy: historical trends up to 2023 and a data repository into the future. Sci Data. 2024;11:1325. https://doi.org/10.1038/s41597-024-04162-7
27. Hashem AM, Sohrab SS, El-Kafrawy SA, Abd-Alla AMM, El-Ela SA, Abujamel TS, et al. Diversity of dengue virus-3 genotype III in Jeddah, Saudi Arabia. Acta Trop. 2018;183:114–8. https://doi.org/10.1016/j.actatropica.2018.04.002
28. Amarasinghe A, Kuritsk JN, Letson GW, Margolis HS. Dengue virus infection in Africa. Emerg Infect Dis. 2011;17:1349–54. https://doi.org/10.3201/eid1708.101515
29. Woyessa AB, Mengesha M, Kassa W, Kifle E, Wondabeku M, Girmay A, et al. The first acute febrile illness investigation associated with dengue fever in Ethiopia, 2013: a descriptive analysis. Ethiop J Health Dev. 2014;28:155–61.
30. Ellis EM, Neatherlin JC, Delorey M, Ochieng M, Mohamed AH, Mogeni DO, et al. A household serosurvey to estimate the magnitude of a dengue outbreak in Mombasa, Kenya, 2013. PLoS Negl Trop Dis. 2015;9:e0003733. https://doi.org/10.1371/journal.pntd.0003733
31. Mboera LEG, Mweya CN, Rumisha SF, Tungu PK, Stanley G, Makange MR, et al. The risk of dengue virus transmission in Dar es Salaam, Tanzania during an epidemic period of 2014. PLoS Negl Trop Dis. 2016;10:e0004313. https://doi.org/10.1371/journal.pntd.0004313
32. Diallo D, Diouf B, Gaye A, NDiaye EH, Sene NM, Dia I, et al. Dengue vectors in Africa: a review. Heliyon. 2022;8:e09459. https://doi.org/10.1016/j.heliyon.2022.e09459
33. World Health Organization Regional Office for Africa. Weekly bulletin on outbreaks and other emergencies, week 21: 15–21 May 2023 [cited 2025 Feb 8]. https://iris.who.int/bitstream/handle/10665/368189/OEW21-1521052023.pdf
34. World Health Organization Regional Office for Africa. Weekly bulletin on outbreaks and other emergencies, week 46. November 11–17, 2019 [cited 2024 May 20]. https://iris.who.int/bitstream/item/334140/OEW46-18112019.pdf
35. Carey DE, Causey OR, Reddy S, Cooke AR. Dengue viruses from febrile patients in Nigeria, 1964–68. Lancet. 1971;1:105–6. https://doi.org/10.1016/S0140-6736(71)90840-3
36. Selhorst P, Lequime S, Dudas G, Proesmans S, Lutumba P, Katshongo F, et al. Phylogeographic analysis of dengue virus serotype 1 and cosmopolitan serotype 2 in Africa. Int J Infect Dis. 2023;133:46–52. https://doi.org/10.1016/j.ijid.2023.04.391
37. Padhi A, Gupta E, Singh G, Parveen S, Islam A, Tarai B. Circulation of DENV-3 genotype 3 during 2017 to 2018 in Delhi: a single-center hospital-based study. J Lab Physicians. 2021;14:21–26. https://doi.org/10.1055/s-0041-1734017

Addresses for correspondence: Adugna Abera, Department of Microbial, Cellular, and Molecular Biology, College of Natural and Computational Sciences, Addis Ababa University, NBH1, 4killo King George VI St, Addis Ababa, Ethiopia, and Ethiopian Public Health Institute, Arbagnoch St, Addis Ababa, Ethiopia; email: adugnabe@yahoo.com; Houriiyah Tegally, Centre for Epidemic Response and Innovation (CERI), School of Data Science and Computational Thinking, Stellenbosch University, Hammanshand Rd, Stellenbosch Central, Stellenbosch, 7600, South Africa; email: houriiyah@sun.ac.za

High Prevalence of *atpE* Mutations in Bedaquiline-Resistant *Mycobacterium tuberculosis* Isolates, Russia

Danila Zimenkov, Anastasia Ushtanit, Elizaveta Gordeeva, Elena Guselnikova, Yakov Schwartz, Natalia Stavitskaya

Bedaquiline is a cornerstone drug for treating drug-resistant tuberculosis. We analyzed 11 isolates from 9 patients who were treated with a bedaquiline-based regimen and remained culture-positive long after treatment start. In 4 of 8 resistant isolates, we found substitutions in AtpE, which encodes subunit *c* of the *Mycobacterium tuberculosis* ATP synthase and is rarely identified in clinical isolates. We found Ile66Met and Glu61Asp substitutions in 2 cases each. Additional mutations in *mmpL5*, *mmpL4*, and *atpB* genes could affect the susceptibility to bedaquiline. MmpL5(Asn772Thr) emerged during bedaquiline treatment, whereas AtpB(Val165Leu) was found in 1 case simultaneously with the loss-of-function *mmpR5* mutation in a susceptible strain. The loss-of-function mutation in the *mmpL4* efflux gene was identified in the mixed state, pointing to ongoing selection in a bedaquiline-resistant isolate. Another case of the emergence of the *mmpL4* mutation, accompanied by a proportional increase in bedaquiline MIC, was identified by retrospective analysis of genomes from bedaquiline-resistant isolates.

Drug-resistant tuberculosis (TB) remains a major problem of the public health system. In 2022, TB was newly diagnosed and officially notified in ≈7.5 million persons, and the total number of deaths caused by TB was 1.30 million. In 2019, TB was the 13th leading cause of death worldwide and the leading cause of death from a single infectious agent (*1*). The incidence of drug-resistant TB is estimated to be >400,000 new cases (*1*).

Author affiliations: Center for Precision Genome Editing and Genetic Technologies for Biomedicine, Engelhardt Institute of Molecular Biology, Russian Academy of Sciences, Moscow, Russia (D. Zimenkov, A. Ushtanit); Federal State Budgetary Institution Novosibirsk TB Research Institute, Ministry of Health, Novosibirsk, Russia (E. Gordeeva, E. Guselnikova, Y. Schwartz, N. Stavitskaya)

DOI: https://doi.org/10.3201/eid3103.241488

The limited number of effective TB drugs has pushed the development of new candidates. Bedaquiline, introduced in 2012, began the new era of therapy and was successfully used in combinations with linezolid, clofazimine, and pretomanid/delamanid in new regimens, including all-oral short-course regimens for drug-resistant TB (*2*).

Bedaquiline has a novel distinct mode of action on bacterial physiology by blocking the ATP synthase of *Mycobacterium tuberculosis*, thus causing the decrease of the ATP pool (*3*) and consequent cell death (*4*). Two main mechanisms of bedaquiline resistance by alteration of the target and drug efflux were identified in vitro (*3*,*5*) and, subsequently, in clinical isolates (*6*–*9*).

In the first main mechanism of resistance, the iron-scavenger siderophore transporter complex MmpS5/L5 (*10*) provides bedaquiline efflux from the cytoplasm. Mutations in the repressor gene *mmpR5*(*rv0678*) lead to derepression of the operon *mmpS5-mmpL5*, thus lowering the bedaquiline concentration inside the cell (*5*). Mutations are spread along the open reading frame and include insertions, deletions, premature stop-codons, and amino acid substitutions (*11*). The most prevalent type of mutations is nucleotide insertion or deletion in homopolymeric sequences in the gene (*12*). Drug-resistant isolates with *mmpR5* mutations that emerged during bedaquiline treatment have been described in many regions of the world (*13*–*15*).

The second type of mutations leading to bedaquiline resistance occur in the *c* subunit of ATP synthase, encoded by the *atpE* gene (*3*). Amino acid substitutions at particular positions in the protein prevent the drug binding (*16*) and are rarely identified in clinical strains (*12*). Isolates with *atpE* mutations possess higher bedaquiline MICs and are supposed to emerge after repressor-inactivating mutations in clinical strains (*17*).

Other genetic traits have been proposed to cause bedaquiline resistance; however, the number of such cases is low, and the World Health Organization (WHO) has associated substitutions in only *atpE*, *mmpR5*, and *pepQ* genes with resistance to bedaquiline (*18*). Most of those mutations are in interim status because of insufficient statistics of characterized isolates with a particular mutation. Only the combined category of loss-of-function mutations in the *mmpR5* gene and selected frameshifting mutations in hot spots are classified as category 1 mutations. WHO experts indicate that the functionality of the *mmpS5* and *mmpL5* genes should also be validated because of epistatic interactions with repressor mutations (*19*). In this study, we analyzed bedaquiline-resistant clinical strains isolated at Novosibirsk TB Research Institute (Novosibirsk, Russia), analyzed mutation profiles using whole-genome sequencing, and proposed the participation of novel determinants of bedaquiline resistance. The study protocol was approved by the Ethical Committee of the Federal State Budgetary Institution Novosibirsk TB Research Institute (protocol no. #52/1, May 5, 2021).

Methods

Clinical Isolates and Drug Susceptibility Testing

Clinical isolates were obtained from patients of the Novosibirsk TB Research Institute in whom TB had first been diagnosed during 2006–2018 (Table 1). In the study period (2021–2022), those patients received treatment with a bedaquiline and linezolid–based regimen. Isolates were obtained using liquid media in the Bactec MGIT 960 system (BD, https://www.bd.com) and were further used for drug susceptibility tests, storage, and DNA isolation for molecular tests.

We performed bedaquiline and linezolid susceptibility tests using the modified proportional method in the automatic Bactec MGIT 960 system. Russia's national guidelines for TB treatment are in accordance with WHO guidelines (*20*), and we used currently approved critical concentrations for bedaquiline and linezolid of 1 mg/L for both tests. We dissolved and diluted bedaquiline (Molekula Ltd., https://molekula.com) in DMSO and added 100 µL per MGIT tube. We dissolved linezolid (Glenmark Pharmaceuticals, https://glenmarkpharma.com) in sterile H_2O as recommended in the guidelines.

Whole-Genome Sequencing

The strains for whole-genome sequencing were recultured on solid Lowenstein-Jensen medium for ≈4 weeks at 37°C and then heat inactivated. We extracted genomic DNA using the Gentra Puregene Yeast/

Table 1. Clinical characteristics of TB cases and resistance to bedaquiline and linezolid determined by phenotypic and genotypic methods in study of high prevalence of *atpE* mutations in bedaquiline-resistant *Mycobacterium tuberculosis* isolates, Russia*

	Isolate identification								
Category	#1	#2	#3	#4	#5	#6	#7	#8	#9c
Year of TB diagnosis	2017	2006	2015	2010	2018	2017	2017	2012	2007
HIV status	Yes	No	No	No	Yes	No	No	Yes	No
Source of the culture	Sputum	Surgery	Sputum	Wound exudate	Sputum	Sputum	Wound exudate	Sputum	Sputum
No. days from treatment start	92	718	196	1,045	206	558	866	609	1,154
Treatment outcome	Treatment failed	Not evaluated	Treatment failed	Death from TB	Death from TB	Treatment failed	Treatment failed	Treatment failed	Treatment failed
Sublineage	B0	B0	B0	CA/R	B0	B0	B0	B0	B0
Bedaquiline phenotype	R	R	R	S	R	R	R	R	R
AtpE Glu61Asp, g>t							100%		
AtpE Glu61Asp, g>c									59%
AtpE Ile66Met					100%			100%	
MmpR5 Cys46fs						21%			
MmpR5 Asp47fs	52%								
MmpR5 Glu49fs	42%			97%					
MmpR5 Ser63Gly			75%						
MmpR5 Ile67fs		97%							96%
MmpR5 Gln76stop						28%			
MmpR5 Leu143_Glu147dup						22%			
MmpL4 Leu130fs†		91%							
MmpL5 Asn772Thr†									37%
AtpB Val165Leu†				100%					
Linezolid phenotype	S	S	S	R	S	S	S	R	R
RplC Cys154Arg				100%				100%	100%

*Percentages indicate relative number of reads with mutations. ID, identification; R, resistant; S, susceptible; TB, tuberculosis.
†Mutations in candidate genes associated with resistance to bedaquiline.

Bact. Kit B (QIAGEN, https://www.qiagen.com). We prepared the DNA libraries using the Illumina DNA Prep kit and performed sequencing using the MiniSeq High Output Kit (300 Cycles) on the MiniSeq platform (Illumina, https://www.illumina.com).

We analyzed sequencing data in FastQ format using the Galaxy web platform (https://usegalaxy.org). We trimmed the reads using the Trimmomatic tool (https://toolshed.g2.bx.psu.edu/repository?repository_id=ef9e620e9ac844b3), mapped them to the reference genome of *M. tuberculosis* H37Rv (GenBank accession no. NC_000962.3) with BWA-MEM2 (https://toolshed.g2.bx.psu.edu/repository?repository_id=48f9d7927f0fd013), and refined using BamLeftAlign (https://toolshed.g2.bx.psu.edu/repository?repository_id=903c3759b76db034). We performed variant calling using FreeBayes (https://toolshed.g2.bx.psu.edu/repository?repository_id=491b7a3fddf9366f) and filtered using the VCFlib toolkit (https://toolshed.g2.bx.psu.edu/repository?repository_id=db548aefa5e7e768). The variants annotation was performed using SnpEff (https://toolshed.g2.bx.psu.edu/repository?repository_id=93a5efea7e957b53). We performed further bioinformatic analysis of the obtained single-nucleotide polymorphisms with custom Python scripts. Alternatively, we used the genome of *M. tuberculosis* B0/W148 (GenBank accession no. CP012090.1) as a reference for the second round of alignment of raw reads for the validation of mutations located in highly repetitive genomic loci.

Analysis of the CRyPTIC Database

For phylogenetic and mutation frequency analysis, we used a dataset consisting of 9,941 of 12,288 isolates that were sequenced and analyzed by the CRYpTIC Consortium (*21*). The remaining 2,347 isolates had an ambiguous description of amino acid substitutions and were omitted. We built the phylogenetic tree by nearest-neighbor method in MEGA 11 software (https://www.megasoftware.net) using the pairwise distances calculated from genome mutations. We omitted highly repetitive PE, PPE, PE-PGRS genes, and insertion elements (Appendix Figure, https://wwwnc.cdc.gov/EID/article/31/3/24-1488-App1.pdf). We verified the reliability of the phylogenetic tree by clonal distribution of selected lineage-specific single-nucleotide polymorphisms. We assembled data consisting of the phylogenetic tree, isolate susceptibility profiles, and mutation profiles in a local database, powered by custom Python scripts.

Results

Molecular Determinants of Resistance to Bedaquiline and Linezolid

During June 2021–May 2022, we identified 9 cases of culture positivity long after the initiation of treatment with bedaquiline plus linezolid–based regimens. We performed drug susceptibility tests for bedaquiline and linezolid using the proportion method. Of the 9 isolates, 8 were resistant to bedaquiline; 2 of the 8 bedaquiline-resistant isolates and the 1 bedaquiline-susceptible isolate were resistant to linezolid (Table 1).

In all 9 isolates, including the susceptible isolate, we identified mutations in either *mmpR5* or *atpE* genes (Table 1). Most of the mutations identified were in mixed state with wild-type sequence, so the allele frequencies were estimated by calculating the relative number of reads with mutations. Unexpectedly, 4 of the 8 resistant strains had substitutions in 61 and 66 codons of the *atpE* gene, which are rarely reported in bedaquiline-resistant isolates. The 100% mutated allele frequency at the *atpE* locus correlated with the absence of substitutions in the *mmpR5* gene in 3 isolates (#5, #7, and #8). Another isolate (#9c) in addition to AtpE Glu61Asp in the mixed state also had the loss-of-function frameshifting MmpR5 Ile67fs and substitution MmpL5 Asn772Thr, which could affect bedaquiline resistance.

In 6 of 9 isolates, we observed variable mutations of *mmpR5*, predominately leading to frameshifts. Single-nucleotide insertions were located in 2 hot spots: around codons 46–49 (3 cases) and 67 (2 cases). Another type of mutations, the amino acid substitution Ser63Gly in MmpR5, was observed only in 1 case with an allele frequency of ≈75%. Serine 63 is located in the turn part of the HTH DNA binding domain of the MmpR5 repressor (*22*), providing the rationale for the effect of substitutions at this point on bedaquiline resistance. One isolate susceptible to bedaquiline had an inactivating mutation in the *mmpR5* gene with an allele frequency close to 100% and mutation Val165Leu in the *atpB* gene encoding the *a* subunit of ATPsynthase and located just upstream of the *atpE* gene (Table 1). This isolate belongs to the Central Asia/Russian genotype, contrary to Beijing B0/W148 for all other isolates. Resistance to linezolid in 3 isolates was caused by the canonical substitution Cys154Arg in the ribosomal protein RplC (*23*).

Candidate Markers of Resistance to Bedaquiline

We also sequenced 3 consequent isolates from the same patient, who was treated with a bedaquiline-based regimen. Although they were isolated during

Table 2. Allele frequencies change in sequential isolates from patient #9 during treatment in study of high prevalence of *atpE* mutations in bedaquiline-resistant *Mycobacterium tuberculosis* isolates, Russia

Gene or intergenic region	Amino acid substitution	Isolate 9a, day 1,004	Isolate 9b, day 1,037	Isolate 9c, day 1,154	Associated with resistance
atpE	Glu61Asp			59%	Bedaquiline
mmpR5 (Rv0678)	Ile67fs	18%	15%	96%	Bedaquiline
	Leu143stop	80%	63%		
mmpL5	Asn772Thr			37%	Bedaquiline
alr	Glu6Gln	78%	65%		D-cycloserine
gabD2	Val153fs			39%	D-cycloserine
Rv2690c	Gly191Arg			26%	(Pyrazinamide)
pncA	Met1Thr	100%	100%	100%	Pyrazinamide
ceoC	Ala130Thr			25%	(Isoniazid)
PPE8	Asp1235fs	64%	63%		
PPE35	Leu939fs		18%	96%	
Rv2298	Gly16Glu			23%	
moeW-mmpL9		71%	64%		
sigL	Leu120Leu			63%	
purM	Pro290Pro			22%	
Rv3083	Leu439Leu		6%	22%	

only half a year, we observed the dynamic change in *mmpR5* mutations and the emergence of AtpE(Glu61Asp) amino acid substitution (Table 2). Thus, in the latest sample, allele frequency of AtpE(Glu61Asp) was 59%, and MmpR5(Ile67fs) was ≈100%. Another mutation MmpR5(Leu143stop) was highly represented in the first sample in the series and then gradually disappeared. Of note, we observed that the additional substitution in the efflux pump subunit MmpL5(Asn772Thr) emerged simultaneously with the AtpE substitution.

Allele frequencies of mutations associated with resistance to other drugs and mutations in genes possibly associated with virulence and host-adaptation also changed in sequential isolates. Furthermore, 3 synonymous amino acid substitutions were recorded in the latest isolate #9c.

In addition to the isolates from case #9, isolates #2 and #4 also had mutations that could be associated with bedaquiline resistance. In those cases, the reference susceptible strains isolated before the start of the treatment were not available, and the emergence of mutations cannot be confirmed directly. The bedaquiline susceptible isolate #4 had Val165Leu substitution in *a* subunit of ATPase, encoded by the *atpB* gene, in addition to the loss-of-function MmpR5(Glu49fs) (Table 1). Another bedaquiline-resistant isolate (#2) had a frameshifting mutation in the *mmpL4* gene together with a loss-of-function mutation in *mmpR5*.

Discussion

Resistance of *M. tuberculosis* to bedaquiline is driven by 2 main mechanisms, drug efflux by the MmpS5-MmpL5 complex and alteration of its binding site in the rotor part of ATP synthase (*3*,*5*). Mutations in both repressor gene *mmpR5* and *atpE* encoding the *c* subunit emerge during bedaquiline treatment. Mutations in *mmpR5* are distributed along the open reading frame, lead to an increase in MIC, and are found more frequently in clinical strains.

We identified a high prevalence of the *atpE* mutations in clinical isolates from patients who were treated with the bedaquiline-linezolid treatment scheme and remained culture-positive long after the start of the treatment. Most isolates developed phenotypic resistance to bedaquiline detected by Bactec MGIT 960 with a recommended critical concentration of 1 mg/L. Four of 8 bedaquiline-resistant strains had amino acid substitutions Glu61Asp or Ile66Met of the *c* subunit in positions that are responsible for the direct interaction with bedaquiline. Those substitutions are classified by the WHO as associated with resistance-interim (*18*).

Only 17 clinical MTB isolates with *atpE* mutations have been described in 9 studies (*9*,*12*,*24*–*30*). Another study from China also describes the existence of AtpE Asp28Gly and Ala63Pro substitutions in clinical strains resistant to bedaquiline; however, the number of such isolates cannot be extracted from the published data (*31*). The most frequent mutation in AtpE was Ile66Met, found in 6 cases. The same dominance was also found in this study: 2 of 4 isolates bore the same substitution. It could be assumed that this mutation provides the best balance between loss of susceptibility to bedaquiline and fitness cost of altered structure of ATP synthase. However, in a report from France, such *atpE* mutation was transient in a series of clinical isolates from 1 patient and was lost in subsequent isolates; the patient was successfully cured (*28*).

The effect of particular mutations in *mmpR* and *atpE* on the bedaquiline MIC value is variable. Part of mutations in the *mmpR5* repressor gene lead to a

modest increase in MIC close to the borderline value and thus are considered not associated with resistance (*32*). Of note, even loss-of-function mutations in the repressor, which are supposed to lead to complete derepression of the efflux operon *mmpS5-mmpL5*, do not invariantly lead to resistance, as was found for an isolate in this study. In this case, the determination of MIC could have been particularly beneficial to estimate the effect of mutation on phenotype; the proportion method with currently approved critical concentration definitely limits the study.

Other genetic traits could affect the phenotype by epistatic interaction, as was shown for the isolate with both derepression of the efflux operon and the inactivated efflux gene (*19*). In general, the particular genotype of the pathogen could have an effect not only on transmission dynamics but also on the speed of resistance acquisition and survival under drug-induced stresses (*33*). In Russia, 2 main genotypes of lineage 2 are associated with resistance to many drugs and rapid transmission in the population, B0/W148 and Central Asia/Russia (*34*). At least 12 of 17 previously reported *atpE* mutants belong to either of these sublineages; 10 of them were reported in different regions of Russia. Only 2 strains belong to lineage 4 (*24*) and lineage 3 (*27*). All bedaquiline-resistant isolates reported here belong to Beijing B0/W148, whereas the single susceptible isolate belongs to the Beijing Central Asia/Russia sublineage.

The recommended critical concentration of 1 mg/L for resistance determination using the Bactec MGIT 960 is probably too high (*32*). A substantial overlap of MIC values at 0.125 mg/L and 0.25 mg/L was previously reported for pairs of exposed and nonexposed and wild-type and mutated isolates (*12*). On the basis of those observations, the critical concentration should be lowered to at least 0.25 mg/L for better differentiation of resistant and susceptible isolates. The current value enables identification of strains with substantially elevated MIC, whereas intermediate resistance is missed by the phenotypic method. Thus, the detection of a considerable number of isolates with AtpE substitutions, which are associated with high bedaquiline MICs, was not unexpected. In addition, we identified strains with *mmpR5* mutations only, including both frameshifting and amino acid substitutions such as Ser63Gly, which occurred in the HTH DNA binding domain of the repressor.

Contrary to several previous reports, we did not find *pepQ* or *rv1979c* mutations in bedaquiline-resistant isolates (*15*,*35*–*37*). Although the isolated mutations in *pepQ* are rare and usually are accompanied with *mmpR5* mutations, WHO has stated that *pepQ* mutations are associated with resistance (*18*). We propose that *mmpL5*, *mmpS4-mmpL4*, and *atpB* genes could also affect the bedaquiline-resistance phenotype from the analysis of microevolution events and the identification of mutations in single isolates in heteroresistant state, which also point to the ongoing evolution of the pathogen.

We observed mutations in genes that encode the siderophore export transport proteins MmpL5/S5 and MmpL4/S4 (*10*). First, the amino acid substitution Asn772Thr of the efflux MmpL5 emerged in the latest of series of 3 consequent isolates from 1 patient, together with fixation of loss-of-function variant of the *mmpR5* gene and the emergence of AtpE Glu61Asp. The *mmpR5* mutation has an allele frequency close to 100%, pointing to the fixation of resistance-associated variant. The allele frequency of MmpL5 Asn772Thr was 40% and for AtpE Glu61Asp was 60%, resulting in a total of 100%. Therefore, we could speculate the existence of 2 strains, 1 with the simultaneous presence of MmpR5(Ile67fs) and AtpE(Glu61Asp) and the other with MmpR5(Ile67fs) and MmpL5(Asn772Thr). If substitution in MmpL5 decreases susceptibility to bedaquiline, both strains would survive better during bedaquiline treatment and have higher MICs than the parental mutant *mmpR5* strain.

Recently, the cryo-EM structure of MmpL5 from *M. smegmatis* was determined, and possible root of transport of mycobactin and other molecules was proposed on the basis of channel prediction, molecular modeling, and docking calculations (*38*). Of note, Ala774 of the *M. smegmatis,* which corresponds to Asn772 of *M. tuberculosis*, is located in the transmembrane domain TM8, responsible for opening and closing of the channel (Figure 1). More precisely, Ala774 is located in the cavity that forms the channel inlet and the narrowest region of the channel together with Tyr767, Gln771, Tyr417, and Trp835, highlighted in the study (*38*). This model should nevertheless be used with caution, taking into account the MmpS5-guided trimerization of MmpL5 and anchoring of the complex in membrane, which is necessary for bedaquiline efflux (*39*).

Mutations in the *mmpL5* are not frequent; however, MmpL5/S5 efflux does not appear to be indispensable, since a substantial number of frameshift mutations were found in different sublineages of *M. tuberculosis* (*19*), and cell wall morphology is not affected in strains with deletion of *mmpL5* or *mmpS5* (*39*). According to the WHO, mutation in the same

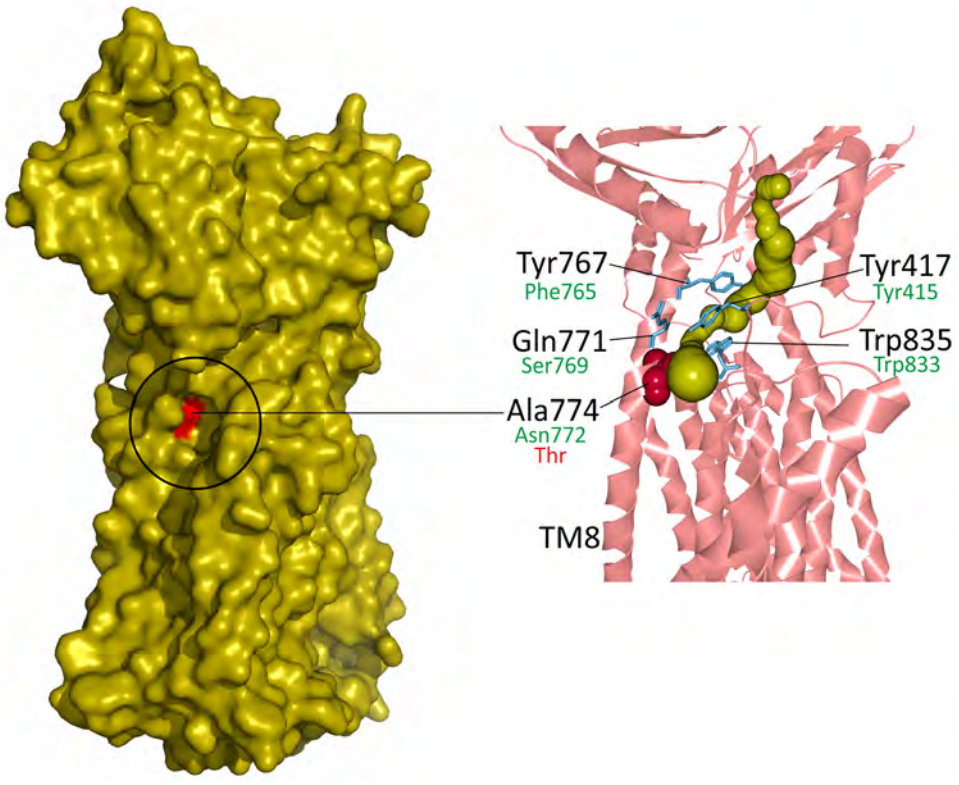

Figure 1. Mapping of the candidate substitution Asn722Thr on the atomic model of *Mycobacterium smegmatis* MmpL5 transporter (PDB: 9B46) in study of high prevalence of *atpE* mutations in bedaquiline-resistant *M. tuberculosis* isolates, Russia. The proposed channel inlet is indicated on the surface model of the MmpL5. The channel model (olive) is shown on the cartoon model of the MmpL5 fragment. Red coloring and text indicates Ala774, located in the transmembrane domain TM8. Green text indicates residues and numbering for *M. tuberculosis*.

codon was found earlier; MmpL5(Asn772Ser) has uncertain significance in the resistance to bedaquiline and clofazimine (*18*). Two strains with this mutation in the CRyPTIC database have a low bedaquiline MIC of 0.03 mg/L (*21*).

More notably, the loss-of-function mutation of *mmpL4* was found in a bedaquiline-resistant isolate together with frameshift in the *mmpR5*. Both the MmpL5/MmpS5 and MmpL4/MmpS4 transporter complexes secrete iron-scavenging siderophores mycobactin and carboxymycobactin (*10*). Although the role of MmpL5/MmpS5 in bedaquiline and clofazimine resistance is well established as the export pump of the drugs, mutations in *mmpS4/L4* were not previously associated with bedaquiline resistance. However, a recent study has shown that deletion of *mmpS4* or *mmpL4* increases bedaquiline MIC from 2 to 4 times in vitro, probably because of the compensatory upregulation of the *mmpS5-mmpL5* operon (*40*). The 91% allele frequency of the frameshifting variant of *mmpL4* found in isolate #2 points to its recent emergence.

To confirm the significance of our findings, we retrospectively analyzed the genomes of clinical isolates of patients treated with bedaquiline from our previous reports (*9*,*12*). Indeed, in a series of consequent isolates from a patient who was treated with a bedaquiline-containing regimen, a similar loss-of-function mutation of *mmpL4* caused by frameshift in the 341 codon emerged (Table 3). The strain already had a high bedaquiline MIC caused by the presence of amino acid substitutions in AtpE and MmpR5. However, in the 2 latest isolates, the emergence of the mutation in *mmpL4* was accompanied by a further increase in bedaquiline MIC, proportional to the allele frequencies, thus

Table 3. Bedaquiline MIC values and allele frequencies of mutations in genes associated with bedaquiline resistance for sequential isolates for patient from study of high prevalence of *atpE* mutations in bedaquiline-resistant *Mycobacterium tuberculosis* isolates, Russia*

Gene or intergenic region	Amino acid substitution	Isolate Af.102, day 236	Isolate Af.103, day 406	Isolate Af.104, day 580	Isolate Af.105, day 672	Isolate Af.106, day 1,489
Bedaquiline MIC (7H11)		0.25	0.25	0.25	1	1
Bedaquiline MIC (MGIT 960)		2	4	4	8	16
AtpE	Ala63Val	99%	100%		99%	100%
MmpR5 (Rv0678)	Leu142Arg	100%	99%	98%	100%	100%
MmpL4	Val341fs				75%	98%

*Patient described by Peretokina et al. (*12*). Percentages indicate relative number of reads with mutations.

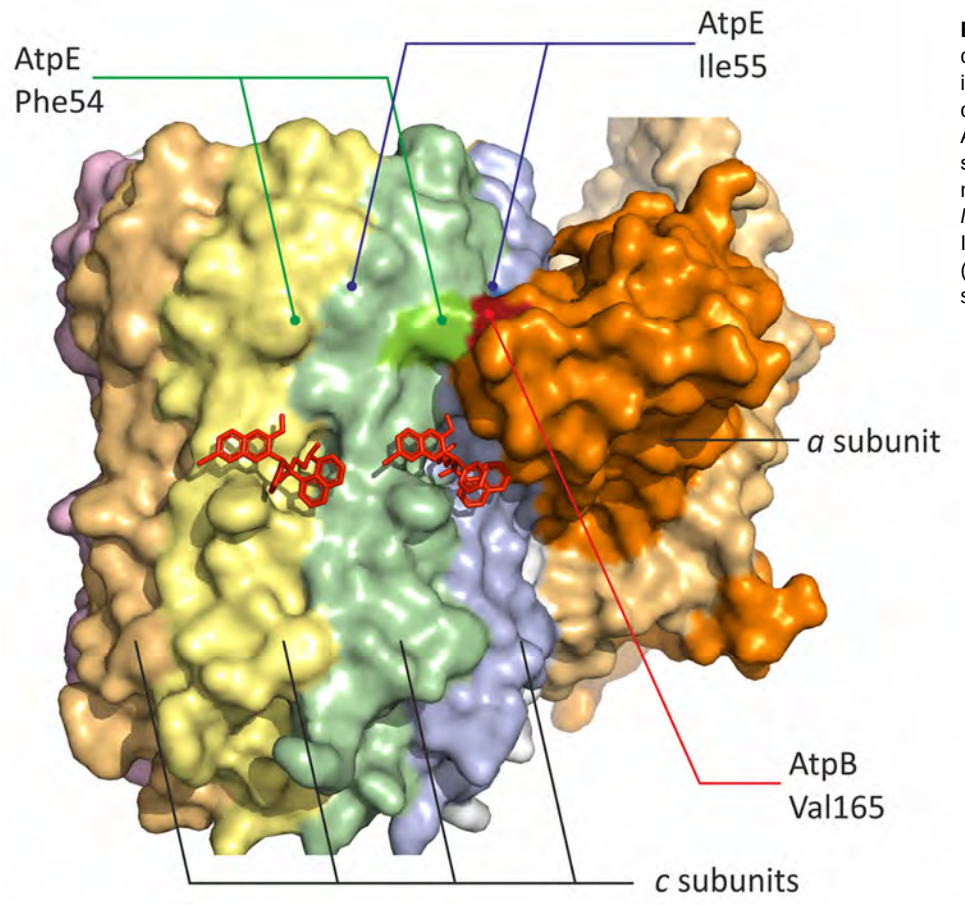

Figure 2. Mapping of the candidate substitution Val165Ile in AtpB on the atomic model of *Mycobacterium tuberculosis* ATP synthase (PDB: 8J0S) in study of high prevalence of *atpE* mutations in bedaquiline-resistant *M. tuberculosis* isolates, Russia. Identical *c* subunits of the rotor (encoded by the *atpE* gene) are shown with distinct colors.

confirming the effect of loss-of-function mutations in the *mmpL4* gene.

The third gene, which was also supposed to have an effect on bedaquiline resistance, was the *atpB* gene encoding *a* subunit of the ATP synthase. This subunit is a part of the stator, lying in tight contact with the rotor, which consists of 9 identical *c* subunits encoded by the *atpE* gene. Moreover, in the ATP synthase operon *atpB* gene is positioned right upstream of *atpE*, and mutations in bedaquiline resistant isolates were already described (*24*). However, those mutations were found close to the 3′ end of the gene (codons 222, 244, and 250) and were supposed to alter the transcription of the downstream *atpE* gene.

We identified the substitution of Val165, which is located at the *a*/*c* interface close to the lagging binding site of bedaquiline in ATP synthase (*41*). It interacts with Phe54 and Ile55 of the *c* subunit, and substitution for a larger Leucine could change the structure substantially (Figure 2). This strain also had a loss-of-function mutation of *mmpR5* and was susceptible to bedaquiline. Therefore, the particular role of AtpB Val165Ile cannot be established from our data.

The CRyPTIC database contains 18 isolates with the neighboring AtpB(Thr166Met) (*21*). They belong to the same clone inside lineage 3 isolated in different laboratories (Appendix Figure). They do not contain mutations in genes associated or involved in bedaquiline resistance: *atpE*, *mmpR5*, *pepQ*, *mmpL5*, *mmpS5*, *mmpL4*, and *mmpS4*. Furthermore, no other isolates with other mutations in *atpB* were found in the CRyPTIC study. The MIC values of those isolates were slightly shifted toward higher values compared with the entire set of strains, pointing to the possible involvement of this substitution in decreased susceptibility to bedaquiline (Table 4).

Table 4. Bedaquiline MIC values for isolates from the CRyPTIC study with mutation in *atpB* gene in study of high prevalence of *atpE* mutations in bedaquiline-resistant *Mycobacterium tuberculosis* isolates, Russia

	Bedaquiline MIC, mg/L											
Isolates	≤0.008	≤0.015	0.015	0.03	0.06	0.12	0.25	0.5	1	>1	2	>2
All isolates	337	1199	851	3405	3082	603	194	54	26	5	3	5
AtpB (Thr166Met)					3	8	4		3			

The frequencies of mutations, associated with resistance to other drugs, also changed in the series obtained from 1 patient. Therefore, the substitution in the *alr* gene encoding alanine racemase (*42*,*43*), associated with resistance to D-cycloserine, has disappeared in the third isolate #9c, which probably points to its high fitness cost. However, another mutation in the *gabD2* gene, previously associated with resistance to D-cycloserine (*44*), emerged. The lineage 4 strains with the loss-of-function *gabD2* mutation were more frequently identified in patients in the epidemiologic study from Colombia (*45*), thus associated with success in transmission, which could be affected also by reduced susceptibility to drugs.

Mutated variants of 2 genes, *rv2690c* and *ceoC*, previously associated with resistance to pyrazinamide (for *rv2690c*) (*46*) and isoniazid (for *ceoC*) (*47*), emerged in the latest isolate. Those genes could be responsible for virulence and host adaptation also (*48*,*49*). Other genes associated with virulence, such as *rv2298* and 2 PPE genes, also changed the frequencies of mutated alleles in sequential isolates.

Research of the microevolution of the pathogen within the host has allowed for clarity into genetic traits related to resistance and host adaptation, thus complementing the massive body of genome-wide association studies. However, it is hard to discern whether the mutations emerged internally, under selective pressures from treatment or the immune system of the host, or are neutral, from genetic drift caused by spread in the general population. In addition, the exact pressure is not known because of poor adherence to treatment in most chronic cases and individual variability in pK/pD (*50*).

This work was supported by the Russian Science Foundation (grant no. 22-15-00432).

All raw sequence reads were submitted to the National Center for Biotechnology Sequence Read Archive database and are available under accession no. PRJNA1167223 for isolates analyzed in this study and accession no. PRJNA768108 for isolates from the earlier study from Moscow. Strain identifications in the database are the same as used in the articles.

About the Author

Dr. Zimenkov is a senior scientist at the Engelhardt Institute of Molecular Biology, Moscow. His research is focused on genomics of *M. tuberculosis*, molecular mechanisms of drug tolerance and resistance, and bioinformatic genome-wide association studies.

References

1. World Health Organization. Global tuberculosis report 2023. Geneva: The Organization; 2023.
2. Dartois V, Rubin EJ. Shortening tuberculosis treatment—a strategic retreat. N Engl J Med. 2023;388:939–41. https://doi.org/10.1056/NEJMe2300413
3. Andries K, Verhasselt P, Guillemont J, Göhlmann HWH, Neefs JM, Winkler H, et al. A diarylquinoline drug active on the ATP synthase of *Mycobacterium tuberculosis*. Science. 2005;307:223–7. https://doi.org/10.1126/science.1106753
4. Koul A, Vranckx L, Dhar N, Göhlmann HWH, Özdemir E, Neefs JM, et al. Delayed bactericidal response of *Mycobacterium tuberculosis* to bedaquiline involves remodelling of bacterial metabolism. Nat Commun. 2014;5:3369. https://doi.org/10.1038/ncomms4369
5. Hartkoorn RC, Uplekar S, Cole ST. Cross-resistance between clofazimine and bedaquiline through upregulation of MmpL5 in *Mycobacterium tuberculosis*. Antimicrob Agents Chemother. 2014;58:2979–81. https://doi.org/10.1128/AAC.00037-14
6. Andries K, Villellas C, Coeck N, Thys K, Gevers T, Vranckx L, et al. Acquired resistance of *Mycobacterium tuberculosis* to bedaquiline. PLoS One. 2014;9:e102135. https://doi.org/10.1371/journal.pone.0102135
7. Somoskovi A, Bruderer V, Hömke R, Bloemberg GV, Böttger EC. A mutation associated with clofazimine and bedaquiline cross-resistance in MDR-TB following bedaquiline treatment. Eur Respir J. 2015;45:554–7. https://doi.org/10.1183/09031936.00142914
8. Bloemberg GV, Keller PM, Stucki D, Trauner A, Borrell S, Latshang T, et al. Acquired resistance to bedaquiline and delamanid in therapy for tuberculosis. N Engl J Med. 2015;373:1986–8. https://doi.org/10.1056/NEJMc1505196
9. Zimenkov DV, Nosova EY, Kulagina EV, Antonova OV, Arslanbaeva LR, Isakova AI, et al. Examination of bedaquiline- and linezolid-resistant *Mycobacterium tuberculosis* isolates from the Moscow region. J Antimicrob Chemother. 2017;72:1901–6. https://doi.org/10.1093/jac/dkx094
10. Wells RM, Jones CM, Xi Z, Speer A, Danilchanka O, Doornbos KS, et al. Discovery of a siderophore export system essential for virulence of *Mycobacterium tuberculosis*. PLoS Pathog. 2013;9:e1003120. https://doi.org/10.1371/journal.ppat.1003120
11. Miotto P, Cirillo DM, Schön T, Köser CU. The exceptions that prove the rule-a historical view of bedaquiline susceptibility. Genome Med. 2024;16:39. https://doi.org/10.1186/s13073-024-01311-w
12. Peretokina IV, Krylova LY, Antonova OV, Kholina MS, Kulagina EV, Nosova EY, et al. Reduced susceptibility and resistance to bedaquiline in clinical *M. tuberculosis* isolates. J Infect. 2020;80:527–35. https://doi.org/10.1016/j.jinf.2020.01.007
13. Kaniga K, Lounis N, Zhuo S, Bakare N, Andries K. Impact of *Rv0678* mutations on patients with drug-resistant TB treated with bedaquiline. Int J Tuberc Lung Dis. 2022;26:571–3. https://doi.org/10.5588/ijtld.21.0670
14. Hu Y, Fan J, Zhu D, Liu W, Li F, Li T, et al. Investigation of bedaquiline resistance and genetic mutations in multi-drug resistant *Mycobacterium tuberculosis* clinical isolates in Chongqing, China. Ann Clin Microbiol Antimicrob. 2023;22:19. https://doi.org/10.1186/s12941-023-00568-0
15. Derendinger B, Dippenaar A, de Vos M, Huo S, Alberts R, Tadokera R, et al. Bedaquiline resistance in patients with drug-resistant tuberculosis in Cape Town, South Africa:

a retrospective longitudinal cohort study. Lancet Microbe. 2023;4:e972–82. https://doi.org/10.1016/S2666-5247(23)00172-6
16. Koul A, Dendouga N, Vergauwen K, Molenberghs B, Vranckx L, Willebrords R, et al. Diarylquinolines target subunit c of mycobacterial ATP synthase. Nat Chem Biol. 2007;3:323–4. https://doi.org/10.1038/nchembio884
17. Mallick JS, Nair P, Abbew ET, Van Deun A, Decroo T. Acquired bedaquiline resistance during the treatment of drug-resistant tuberculosis: a systematic review. JAC Antimicrob Resist. 2022;4:dlac029. https://doi.org/10.1093/jacamr/dlac029
18. World Health Organization. Catalogue of mutations in *Mycobacterium tuberculosis* complex and their association with drug resistance. 2nd edition. Geneva: The Organization: 2023.
19. Vargas R Jr, Freschi L, Spitaleri A, Tahseen S, Barilar I, Niemann S, et al. Role of epistasis in amikacin, kanamycin, bedaquiline, and clofazimine resistance in *Mycobacterium tuberculosis* complex. Antimicrob Agents Chemother. 2021;65:e0116421. https://doi.org/10.1128/AAC.01164-21
20. World Health Organization. Technical report on critical concentrations for drug susceptibility testing of medicines used in the treatment of drug-resistant tuberculosis. Geneva: The Organization; 2018.
21. The CRyPTIC Consortium. A data compendium associating the genomes of 12,289 *Mycobacterium tuberculosis* isolates with quantitative resistance phenotypes to 13 antibiotics. PLoS Biol. 2022;20:e3001721. https://doi.org/10.1371/journal.pbio.3001721
22. Radhakrishnan A, Kumar N, Wright CC, Chou TH, Tringides ML, Bolla JR, et al. Crystal structure of the transcriptional regulator Rv0678 of *Mycobacterium tuberculosis*. J Biol Chem. 2014;289:16526–40. https://doi.org/10.1074/jbc.M113.538959
23. Beckert P, Hillemann D, Kohl TA, Kalinowski J, Richter E, Niemann S, et al. rplC T460C identified as a dominant mutation in linezolid-resistant *Mycobacterium tuberculosis* strains. Antimicrob Agents Chemother. 2012;56:2743–5. https://doi.org/10.1128/AAC.06227-11
24. Martinez E, Hennessy D, Jelfs P, Crighton T, Chen SCA, Sintchenko V. Mutations associated with in vitro resistance to bedaquiline in *Mycobacterium tuberculosis* isolates in Australia. Tuberculosis (Edinb). 2018;111:31–4. https://doi.org/10.1016/j.tube.2018.04.007
25. Mokrousov I, Akhmedova G, Molchanov V, Fundovnaya E, Kozlova E, Ostankova Y, et al. Frequent acquisition of bedaquiline resistance by epidemic extensively drug-resistant *Mycobacterium tuberculosis* strains in Russia during long-term treatment. Clin Microbiol Infect. 2021;27:478–80. https://doi.org/10.1016/j.cmi.2020.08.030
26. Chesov E, Chesov D, Maurer FP, Andres S, Utpatel C, Barilar I, et al. Emergence of bedaquiline resistance in a high tuberculosis burden country. Eur Respir J. 2022;59:2100621. https://doi.org/10.1183/13993003.00621-2021
27. Ghodousi A, Hussain Rizvi A, Khanzada FM, Akhtar N, Ghafoor A, Trovato A, et al. In vivo microevolution of *Mycobacterium tuberculosis* and transient emergence of atpE_Ala63Pro mutation during treatment in a pre-XDR TB patient. Eur Respir J. 2022;59:2102102. https://doi.org/10.1183/13993003.02102-2021
28. Le Ray LF, Aubry A, Sougakoff W, Revest M, Robert J, Bonnet I, et al. atpE mutation in *Mycobacterium tuberculosis* not always predictive of bedaquiline treatment failure. Emerg Infect Dis. 2022;28:1062–4. https://doi.org/10.3201/eid2805.212517
29. Shang Y, Chen S, Shi W, Nie W, Jing W, Huo F, et al. Bedaquiline resistance pattern in clofazimine-resistant clinical isolates of tuberculosis patients. J Glob Antimicrob Resist. 2023;33:294–300. https://doi.org/10.1016/j.jgar.2023.04.003
30. Umpeleva T, Chetverikova E, Belyaev D, Eremeeva N, Boteva T, Golubeva L, et al. Identification of genetic determinants of bedaquiline resistance in *Mycobacterium tuberculosis* in Ural region, Russia. Microbiol Spectr. 2024;12:e0374923. https://doi.org/10.1128/spectrum.03749-23
31. Peng Y, Li C, Hui X, Huo X, Shumuyed NA, Jia Z. Phenotypic and genotypic analysis of drug resistance in *M. tuberculosis* isolates in Gansu, China. PLoS One. 2024;19:e0311042. https://doi.org/10.1371/journal.pone.0311042
32. Köser CU, Miotto P, Ismail N, Anthony RM, Utpatel C, Merker M, et al. A composite reference standard is needed for bedaquiline antimicrobial susceptibility testing for *Mycobacterium tuberculosis* complex. Eur Respir J. 2024;64:2400391. https://doi.org/10.1183/13993003.00391-2024
33. Zhu C, Yang T, Yin J, Jiang H, Takiff HE, Gao Q, et al. The global success of Mycobacterium tuberculosis modern Beijing family is driven by a few recently emerged strains. Microbiol Spectr. 2023;11:e0333922. https://doi.org/10.1128/spectrum.03339-22
34. Vyazovaya A, Gerasimova A, Mudarisova R, Terentieva D, Solovieva N, Zhuravlev V, et al. Genetic diversity and primary drug resistance of *Mycobacterium tuberculosis* Beijing genotype strains in northwestern Russia. Microorganisms. 2023;11:255. https://doi.org/10.3390/microorganisms11020255
35. Kadura S, King N, Nakhoul M, Zhu H, Theron G, Köser CU, et al. Systematic review of mutations associated with resistance to the new and repurposed *Mycobacterium tuberculosis* drugs bedaquiline, clofazimine, linezolid, delamanid and pretomanid. J Antimicrob Chemother. 2020;75:2031–43. https://doi.org/10.1093/jac/dkaa136
36. Wu SH, Chan HH, Hsiao HC, Jou R. Primary bedaquiline resistance among cases of drug-resistant tuberculosis in Taiwan. Front Microbiol. 2021;12:754249. https://doi.org/10.3389/fmicb.2021.754249
37. Shi J, Liu Y, Wu T, Li L, Han S, Peng X, et al. Spontaneous mutational patterns and novel mutations for bedaquiline and clofazimine resistance in *Mycobacterium tuberculosis*. Microbiol Spectr. 2023;11:e0009023. https://doi.org/10.1128/spectrum.00090-23
38. Maharjan R, Zhang Z, Klenotic PA, Gregor WD, Tringides ML, Cui M, et al. Structures of the mycobacterial MmpL4 and MmpL5 transporters provide insights into their role in siderophore export and iron acquisition. PLoS Biol. 2024;22:e3002874. https://doi.org/10.1371/journal.pbio.3002874
39. Yamamoto K, Nakata N, Mukai T, Kawagishi I, Ato M. Coexpression of MmpS5 and MmpL5 contributes to both efflux transporter MmpL5 trimerization and drug resistance in *Mycobacterium tuberculosis*. MSphere. 2021;6:e00518–20. https://doi.org/10.1128/mSphere.00518-20
40. Meikle V, Zhang L, Niederweis M. Intricate link between siderophore secretion and drug efflux in *Mycobacterium tuberculosis*. Antimicrob Agents Chemother. 2023;67:e0162922. https://doi.org/10.1128/aac.01629-22
41. Zhang Y, Lai Y, Zhou S, Ran T, Zhang Y, Zhao Z, et al. Inhibition of *M. tuberculosis* and human ATP synthase by BDQ and TBAJ-587. Nature. 2024;631:409–14. https://doi.org/10.1038/s41586-024-07605-8

42. Awasthy D, Bharath S, Subbulakshmi V, Sharma U. Alanine racemase mutants of *Mycobacterium tuberculosis* require D-alanine for growth and are defective for survival in macrophages and mice. Microbiology (Reading). 2012;158:319–27. https://doi.org/10.1099/mic.0.054064-0
43. Coll F, Phelan J, Hill-Cawthorne GA, Nair MB, Mallard K, Ali S, et al. Genome-wide analysis of multi- and extensively drug-resistant *Mycobacterium tuberculosis*. Nat Genet. 2018;50:307–16. https://doi.org/10.1038/s41588-017-0029-0
44. Chen J, Zhang S, Cui P, Shi W, Zhang W, Zhang Y. Identification of novel mutations associated with cycloserine resistance in *Mycobacterium tuberculosis*. J Antimicrob Chemother. 2017;72:3272–6. https://doi.org/10.1093/jac/dkx316
45. Hurtado-Páez U, Álvarez Zuluaga N, Arango Isaza RE, Contreras-Moreira B, Rouzaud F, Robledo J. Pan-genome association study of *Mycobacterium tuberculosis* lineage-4 revealed specific genes related to the high and low prevalence of the disease in patients from the North-Eastern area of Medellín, Colombia. Front Microbiol. 2023; 13:1076797. https://doi.org/10.3389/fmicb.2022.1076797
46. Thiede JM, Dillon NA, Howe MD, Aflakpui R, Modlin SJ, Hoffner SE, et al. Pyrazinamide susceptibility is driven by activation of the SigE-dependent cell envelope stress response in *Mycobacterium tuberculosis*. MBio. 2021;13:e0043921. https://doi.org/10.1128/mbio.00439-21
47. Vilchèze C, Jacobs WR. Resistance to isoniazid and ethionamide in *Mycobacterium tuberculosis*: genes, mutations, and causalities. Microbiol Spectr. 2014;2:MGM2–0014–2013.
48. Dutta NK, Mehra S, Didier PJ, Roy CJ, Doyle LA, Alvarez X, et al. Genetic requirements for the survival of tubercle bacilli in primates. J Infect Dis. 2010;201:1743–52. https://doi.org/10.1086/652497
49. Salina EG, Waddell SJ, Hoffmann N, Rosenkrands I, Butcher PD, Kaprelyants AS. Potassium availability triggers *Mycobacterium tuberculosis* transition to, and resuscitation from, non-culturable (dormant) states. Open Biol. 2014;4:140106. https://doi.org/10.1098/rsob.140106
50. Alffenaar JC, de Steenwinkel JEM, Diacon AH, Simonsson USH, Srivastava S, Wicha SG. Pharmacokinetics and pharmacodynamics of anti-tuberculosis drugs: an evaluation of in vitro, in vivo methodologies and human studies. Front Pharmacol. 2022;13:1063453. https://doi.org/10.3389/fphar.2022.1063453

Address for correspondence: D.V. Zimenkov, Engelhardt Institute of Molecular Biology, Russian Academy of Sciences, 32 Vavilov St, 119991 Moscow, Russia; email: z@biochip.ru

etymologia revisited

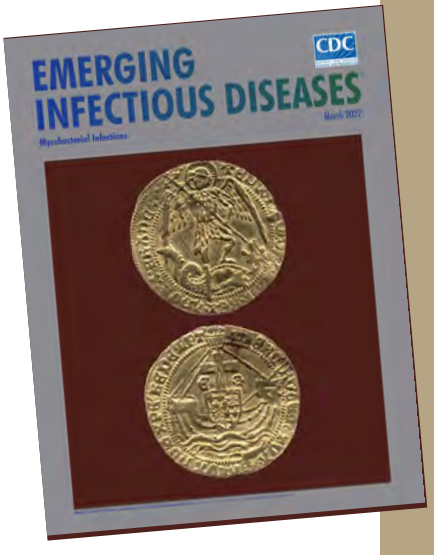

Originally published in March 2022

Schizophyllum commune

[skiz-of′-ĭ-ləm kom′-yoon]

Schizophyllum commune, or split-gill mushroom, is an environmental, wood-rotting basidiomycetous fungus. *Schizophyllum* is derived from "*Schíza*" meaning split because of the appearance of radial, centrally split, gill like folds; "*commune*" means common or shared ownership or ubiquitous. Swedish mycologist, Elias Magnus Fries (1794–1878), the Linnaeus of Mycology, assigned the scientific name in 1815. German mycologist Hans Kniep in 1930 discovered its sexual reproduction by consorting and recombining genomes with any one of numerous compatible mates (currently >2,800).

References

1. Chowdhary A, Kathuria S, Agarwal K, Meis JF. Recognizing filamentous basidiomycetes as agents of human disease: a review. Med Mycol. 2014;52: 782–97. https://doi.org/10.1093/mmy/myu047
2. Cooke WB. The genus *Schizophyllum*. Mycologia. 1961;53:575–99. https://doi.org/10.1080/00275514.1961.12017987
3. Greer DL. Basidiomycetes as agents of human infections: a review. Mycopathologia. 1978;65:133–9. https://doi.org/10.1007/BF00447184
4. O'Reilly P. *Schizophyllum commune*, split gill fungus, 2016 [cited 2021 Aug 23]. https://www.first-nature.com/fungi/schizophyllum-commune.php
5. Raper CA, Fowler TJ. Why study *Schizophyllum*? Fungal Genet Rep. 2004;51:30–6. https://doi.org/10.4148/1941-4765.1142

https//wwwnc.cdc.gov/eid/article/28/3/et-2803_article

A 28-Year Multicenter Cohort Study of Nontuberculous Mycobacterial Lymphadenitis in Children, Spain

Aina Martínez-Planas, Fernando Baquero-Artigao, Ana Méndez-Echevarría, Teresa Del Rosal, Paula Rodríguez-Molino, Carlos Toro-Rueda, Matilde Bustillo-Alonso, Miguel Lafuente, Anna Canet, Ángela Manzanares, Alfredo Tagarro, Francisco José Sanz-Santaeufemia, Sara Guillén-Martín, María José Cilleruelo, Lola Falcón-Neyra, Begoña Santiago, Elena Rincón, Miguel Lillo, Antoni Soriano-Arandes, Luigi Sedda, Clàudia Fortuny, Manuel Monsonís, Julián González-Martín, Marc Tebruegge,[1] Antoni Noguera-Julian,[1] Spanish Pediatric Tb Research Network, The European Nontuberculous Mycobacterial Lymphadenitis In Children Study[2]

We describe the epidemiology, diagnosis, and management of nontuberculous mycobacterial lymphadenitis cases detailed in a 28-year (1996–2023) multicenter cohort from Spain. The case numbers remained stable during the initial prospective phase (2013–2020), but a sharp decline was observed during 2021–2022. Disease onset occurred during spring or June in 45.9% of cases. *Mycobacterium avium* complex (43.1%) and *M. lentiflavum* (39.9%) were the most common species detected. *M. lentiflavum* affected mostly younger children from central Spain. The most common treatment strategy was complete surgical resection with (n = 80) or without (n = 88) antimicrobial drug treatment, followed by antimicrobial drugs alone (n = 76). Facial palsy developed in 10.4% of surgical cases. Adverse events because of antimicrobial drugs were uncommon. New fistula formation during follow-up occurred more in children managed with observation alone than in those treated with antimicrobial drugs alone (relative risk 2.7 [95% CI 1.3–5.3]; p = 0.014).

Author affiliations: Institut de Recerca Pediàtrica Sant Joan de Déu, Barcelona, Spain (A. Martínez-Planas, C. Fortuny, M. Monsonís, A. Noguera-Julian); La Paz Research Institute, Madrid, Spain (F. Baquero-Artigao, A. Méndez-Echevarría, T. Del Rosal, P. Rodríguez-Molino); Universidad Autónoma de Madrid, Madrid (F. Baquero-Artigao, A. Méndez-Echevarría, T. Del Rosal, P. Rodríguez-Molino); Hospital La Paz, Madrid (F. Baquero-Artigao, A. Méndez-Echevarría, T. Del Rosal, P. Rodríguez-Molino, C. Toro-Rueda); Centro de Investigación Biomédica en Red en Enfermedades Infecciosas, Madrid (F. Baquero-Artigao, A. Méndez-Echevarría, P. Rodríguez-Molino, B. Santiago, J. González-Martín); Centro de Investigación Biomédica en Red en Enfermedades Raras, Madrid (T. Del Rosal); Hospital Universitario Miguel Servet, Zaragoza, Spain (M. Bustillo-Alonso, M. Lafuente); Hospital Universitario 12 de Octubre, Madrid, Spain (A. Canet, A. Manzanares); Instituto de Investigación 12 de Octubre, Madrid (A. Tagarro); Hospital Universitario Infanta Sofía, Madrid (A. Tagarro); Universidad Europea de Madrid, Madrid (A. Tagarro); Hospital Universitario Niño Jesús, Madrid (F.J. Sanz-Santaeufemia); Hospital Universitario de Getafe, Getafe, Spain (S. Guillén-Martín); Hospital Universitario Puerta de Hierro, Majadahonda, Spain (M.J. Cilleruelo); Hospital Virgen del Rocío, Seville, Spain (L. Falcón-Neyra); Instituto de Investigación Sanitaria Gregorio Marañón, Madrid (B. Santiago); Hospital Gregorio Marañón, Madrid (B. Santiago, E. Rincón); Hospital General Universitario de Albacete, Albacete, Spain (M. Lillo); Hospital Vall d'Hebron, Barcelona, Spain (A. Soriano-Arandes); Lancaster University, Lancaster, UK (L. Sedda); Centro de Investigación Biomédica en Red en Epidemiología y Salud Pública, Madrid (C. Fortuny, A. Noguera-Julian); Universitat de Barcelona, Barcelona, Spain (C. Fortuny, A. Noguera-Julian); Hospital Clínic, Barcelona (J. González-Martín); Austrian Reference Centre for Childhood Tuberculosis, Vienna, Austria (M. Tebruegge); Vienna Healthcare Group, Vienna (M. Tebruegge); Royal Children's Hospital Melbourne, University of Melbourne, Melbourne, Victoria, Australia (M. Tebruegge); UCL Great Ormond Street Institute of Child Health, London, UK (M. Tebruegge).

DOI: https://doi.org/10.3201/eid3103.241254

[1]These senior authors contributed equally to this article.

[2]Members of the European Nontuberculous Mycobacterial Lymphadenitis in Children Study are listed at the end of this article.

Nontuberculous mycobacteria (NTM) are ubiquitous in soil, water, foodstuffs, and domestic and wild animals. There are ≥190 known species of NTM (*1*). Cervicofacial lymphadenitis is the most common clinical manifestation of NTM infection in young immunocompetent children (*2*). Cervicofacial lymphadenitis typically manifests with a nontender neck mass that progressively becomes violaceous and fluctuant and often fistulizes (*1*,*3*).

Mycobacterium avium complex (MAC) is reported as the most common causative species of NTM lymphadenitis across various geographic locations, accounting for 70%–80% of cases, followed by *M. malmoense*, *M. hemophilum*, and *M. kansasii* (*4*–*8*). *M. lentiflavum*, which is part of the *M. simiae* complex, is a slow-growing NTM species first described in 1996 (*9*,*10*). *M. lentiflavum* is typically isolated from water and soil samples but has increasingly been reported as a pathogenic NTM species in humans over the past 15 years (*4*).

In children, the sensitivity of classical microbiological methods, such as staining techniques and cultures, by using lymph node biopsies or caseum is ≈50%–60% (*11*–*13*). Molecular methods have demonstrated improved sensitivity compared with culture, ≈70%–80% in some studies, although molecular accuracy is limited by species diversity, the lack of commercially available assays and variable performance, and often inadequate sample volumes (*3*,*12*,*14*). In the absence of microbiological confirmation, the presumptive clinical diagnosis of NTM lymphadenitis remains complex and relies on the clinical manifestations, imaging findings, and tuberculosis (TB) immunodiagnostic tests. Recent systematic reviews have recommended the combined use of the tuberculin skin test (TST) and an interferon-γ release assay (IGRA), concluding that a TST+/IGRA– constellation is strongly indicative of NTM lymphadenitis (*13*,*14*), but data to support this strategy are still limited. TST has shown high specificity and positive predictive value in the diagnosis of NTM lymphadenitis in children without TB risk factors or prior bacillus Calmette-Guérin (BCG) vaccination in a country with low TB prevalence (*15*). We previously reported IGRA assay specificity rates and positive predictive values >95% in distinguishing between patients with TB and MAC lymphadenitis (*16*). However, those results cannot necessarily be extrapolated to other geographic settings, such as regions with high TB prevalence, or to other NTM species.

A recent consensus statement of the International Pediatric Otolaryngology Group did not reach an agreement on the single best treatment modality for NTM lymphadenitis (*17*). A meta-analysis published in 2015 reported the highest cure rate by using complete excision, compared with prolonged antimicrobial treatment or observation alone (*6*). However, complete excision was associated with a 10% risk for facial nerve palsy. Currently, the optimal combination of antimycobacterial drugs and treatment duration remains uncertain, as does whether antimycobacterial drug treatment confers advantages over observation alone (*18*).

This study aimed to describe the epidemiologic, clinical, and microbiological characteristics of NTM lymphadenitis in Spain over a 28-year period, to assess the diagnostic value of combined TST and IGRAs use, and to summarize the treatment strategies most used and the related outcomes. Because of the limited data on *M. lentiflavum*, we sought to describe any differences between *M. lentiflavum* and MAC lymphadenitis patients.

Patients and Methods

Study Design

The European nontuberculous mycobacterial lymphadenitis in children (ENSeMBLE) study is a multinational, multicenter, cross-sectional observational study comprising centers and investigators within the Spanish Network for the Study of Pediatric Tuberculosis (*19*), the Paediatric Tuberculosis Network European Trials group (*20*), and the European Nontuberculous Mycobacteria Network European Trials group. The study involves a convenience sample of patients <18 years of age at diagnosis with culture- or PCR-confirmed peripheral NTM lymphadenitis, collected retrospectively during 1996–2012 and prospectively since 2013. All diagnostic and therapeutic decisions were made independently at each center by the patient's physician. We obtained study data exclusively from routine care and collected by using REDCap electronic data capture tools (*21*), hosted at Instituto de Investigación Sanitaria Gregorio Marañón (Madrid, Spain). Ethics approval for this study was obtained from Hospital Sant Joan de Déu (Barcelona, Spain) Ethics Committee (reference no. EPA 04–15). In the prospective study arm, informed consent from parents or legal guardians was obtained before inclusion. Only patients recruited at centers in Spain, representing >90% of patients in the ENSeMBLE study, were included in this report. In Spain, a low TB prevalence country, the pediatric TB incidence was <10 cases/100,000 persons throughout the study period. Neonatal BCG vaccination was discontinued nationwide in 1980, except in Basque Country, which continued until 2013.

Data Collection

Clinical and epidemiologic data (age, sex, country of birth, underlying medical conditions, TB infection risk factors, and BCG vaccination history) were recorded at diagnosis by the clinical care team. We classified the clinical manifestations according to affected sites, laterality (unilateral or bilateral), lymph node size assessed clinically or by ultrasound (in centimeters), duration of illness (in weeks), and clinical stage (I, painless, firm, adherent to overlying skin, increased vascularity; II, fluctuance; III, skin changes, violaceous discoloration, thinning of the skin, parchment-like changes, shiny appearance; IV, fistulization) (*22*). We also collected details about treatment strategies (observation only, antimicrobial drugs, surgery, or a combination of treatments), total duration of follow-up after diagnosis, complications (surgical site infection, drug adverse events, new fistula formation, recurrent NTM infection, and paradoxical worsening), and sequelae at the end of follow-up (hypertrophic scar or keloid, changes in skin color, and transient or permanent facial nerve palsy).

Immunological and Microbiological Tests

TST were performed by intradermal injection of 2 tuberculin units of purified protein derivative (Statens Serum Institut, https://en.ssi.dk), with results read after 48–72 hours. As per national guidelines, an induration of ≥5 mm diameter is considered positive, irrespective of prior BCG vaccination (*23*). All IGRA assays, including the QuantiFERON-TB (QFT) assays QFT Gold (used before 2007), QFT Gold-in-Tube (used during 2007–2016), and QFT Gold Plus (used since 2016) (all Cellestis, https://www.cellectis.com) and T-SPOT.*TB* (Oxford Immunotec LTD., https://www.oxfordimmunotec.com), were performed in fully-accredited diagnostic laboratories at each participating institution and interpreted according to the manufacturer's instructions. Cultures and molecular assays for NTM were also performed at fully accredited clinical laboratories at the participating institutions or at regional reference laboratories.

Statistical Analysis

We present categorical data as absolute numbers and proportions, continuous variables as medians and interquartile ranges (IQRs). We compared groups by using Student *t*-test or Mann-Whitney U test for continuous variables and χ^2 tests for categorical variables. Because patients from provinces surrounding Madrid are usually referred to hospitals in Madrid, we categorized geographic origin dichotomously as central (Madrid and surrounding areas) and peripheral regions in Spain. We determined the onset of symptoms by subtracting the illness duration (available for 268 cases) from the date of microbiological diagnosis. We defined the seasons of the year as spring, March–May; summer, June–August; autumn, September–November; and winter, December–February.

We handled missing data with the complete case analysis method. We defined statistical significance as a 2-sided p value <0.05. We conducted statistical analyses by using SPSS Statistics 29.0 (IBM, https://www.ibm.com).

Results

By May 2023, a total of 311 case-patients (53.7% female, 46.3% male; median [IQR] age at diagnosis 2.4 [1.7–3.2] years) with microbiologically confirmed NTM lymphadenitis were contributed to the EN-SeMBLE study by 33 centers in Spain from 13 of 17 administrative regions; the earliest retrospective case was discovered in 1996 (Table 1; Figure 1). Most cases (63.0%, n = 196) were contributed during the prospective phase of the study, January 2013–2023. The number of cases remained stable from 2013–2020, but a sharp decrease was observed in 2021 and 2022 (Figure 1). Symptom onset occurred during the spring months or June in almost half the patients (45.9%, n = 123) (Figure 2).

Most children were born in Spain (95.8%, n = 298) and were not BCG-vaccinated (96.1%, n = 299). Four (1.3%) patients had underlying medical conditions (Appendix Table 1, https://wwwnc.cdc.gov/EID/article/31/3/24-1254-App1.pdf); no underlying medical conditions were discovered in the remaining children. Risk factors for TB infection were identified in 3.5% (n = 11) of children, including contact with a smear-positive TB patient (n = 5) and birth in or travel to a high TB prevalence country (n = 6).

NTM disease predominantly affected the cervicofacial region (99.0%, n = 308). Only 2 patients had lymphadenitis in the axillary region and 3 patients had lymphadenitis in the inguinal region. In most cases, lymphadenitis only occurred at a single site (77.8%, n = 242) and was unilateral (90.7%, n = 282) (Table 1). The most affected site was the submandibular region (63.3%, n = 197).

At initial examination, the median (IQR) duration of symptoms was 4 weeks (2–6, data available in n = 268 cases), and the maximum lymph node diameter was 3.0 cm (2.1–4.0, n = 108). Almost half the cases were in Penn Stage I upon initial examination (Table 1). Similar results were observed when the retrospective and prospective phases of the study were analyzed separately (Appendix Tables 2, 3).

Causative NTM Species

Microbiological confirmation was obtained at the site of disease (lymph node biopsy, fine needle aspiration, or discharge fluid) in all cases. Mycobacterial cultures were positive in 96.8% (n = 300) of cases and molecular assays were positive in 48.8% (n = 40) of cases when performed; in patients in whom both culture and a molecular test were performed, both techniques yielded a positive result in 35.8% (n = 29) of the time (Appendix Table 4). The most frequently identified

Table 1. Baseline characteristics, clinical manifestations, treatment, outcomes, and comparisons of MAC and *M. lentiflavum* lymphadenitis cases from a 28-year multicenter cohort study of NTM lymphadenitis in children, Spain*

Characteristics	All, n = 311	MAC, n = 134	*M. lentiflavum*, n = 124	p value†
Sex				
F	167 (53.7)	77 (57.5)	67 (54.0)	0.579
M	144 (46.3)	57 (42.5)	57 (46.0)	
Age, y, median (IQR)	2.4 (1.7–3.2)	2.7 (2.0–3.8)	1.9 (1.6–2.6)	<0.001
Patients <5 y of age at diagnosis	26 (8.4)	14 (10.4)	4 (3.2)	0.042
Prospective phase	196 (63.0)	78 (58.2)	88 (71.0)	0.041
Season at symptom onset‡				0.338
Spring	102 (38.1)	39 (33.6)	42 (38.5)	
Summer	58 (21.6)	22 (19.0)	28 (25.7)	
Autumn	46 (17.2)	23 (19.8)	17 (15.6)	
Winter	62 (23.1)	32 (27.6)	22 (20.2)	
Reported in central Spanish regions	189 (60.8)	52 (38.8)	107 (86.3)	<0.001
TB infection risk factors	11 (3.5)	4 (3.0)	2 (1.6)	0.685
Positive TST	168/278 (60.4)	76/118 (64.4)	62/111 (55.9)	0.186
TST induration, mm, median (IQR)	7.0 (0–10)	7.5 (4–11)	7.0 (0–10)	0.055
NTM lymphadenitis disease characteristics				
Unilateral disease	282 (90.7)	124 (92.5)	111 (89.5)	0.395
Single site disease	242 (77.8)	106 (79.1)	90 (72.6)	0.220
Symptom duration, wks, median (IQR)	4.0 (2.0–6.0)	4.0 (2.0–7.3)	3.0 (2.0–4.0)	0.001
Maximum lymph node diameter, cm, median (IQR)	3.0 (2.1–4.0)	3.0 (2.0–4.0)	3.0 (2.1–4.0)	0.558
Clinical stage§				0.926
Stage I	148 (48.6)	62 (47.3)	62 (50.8)	
Stage II	27 (8.8)	13 (9.9)	13 (10.7)	
Stage III	105 (34.4)	44 (33.6)	37 (30.3)	
Stage IV	25 (8.2)	12 (9.2)	10 (8.2)	
Affected site				
Submandibular	197 (63.3)	74 (55.2)	91 (73.4)	0.002
Superficial/deep cervical	81 (26.0)	39 (29.1)	28 (22.6)	0.247
Preauricular	44 (14.1)	13 (9.7)	25 (20.2)	0.019
Parotid	28 (9.0)	10 (7.5)	12 (9.7)	0.523
Jugulodigastric	22 (7.1)	15 (11.2)	6 (4.8)	0.062
Other¶	22 (7.1)	15 (11.2)	3 (2.4)	0.119
Treatment and outcomes				
Initial treatment strategy				0.006
Observation alone	25 (8.0)	15 (11.2)	5 (4.0)	
Antimicrobial drugs alone	76 (24.5)	22 (16.4)	35 (28.2)	
Drainage alone	6 (1.9)	2 (1.5)	2 (1.6)	
Drainage + antimicrobial drugs	29 (9.3)	14 (10.5)	10 (8.1)	
Complete resection alone	80 (25.7)	46 (34.3)	25 (20.2)	
Complete resection + antimicrobial drugs	88 (28.3)	32 (23.9)	43 (34.7)	
Not reported	7 (2.3)	3 (2.2)	4 (3.2)	
Lost to follow-up	23 (7.4)	12 (9.0)	9 (7.3)	0.618
Recurrent NTM lymphadenitis	16 (5.6)	10 (8.2)	6 (5.2)	0.257
New fistulization#	36 (12.9)	20 (18.2)	9 (8.6)	0.042
Sequelae				
None	188 (65.3)	78 (63.4)	76 (66.7)	0.600
Hypertrophic scar	52 (18.1)	25 (20.5)	15 (13.0)	0.126
Skin discoloration	27 (9.4)	13 (10.7)	12 (10.4)	0.956
Transient facial palsy	23 (8.0)	11 (9.0)	10 (8.7)	0.931
Permanent facial palsy	7 (2.4)	1 (0.8)	5 (4.3)	0.093
Frey syndrome	1 (0.3)	0 (0)	1 (0.9)	0.986

*Values are no. (%) except as indicated. Groups were compared with Student *t*-tests or Mann-Whitney U tests for continuous variables and χ^2 tests for categorical variables. MAC, *Mycobacterium avium* complex; NTM, nontuberculous mycobacteria; TB, tuberculosis; TST, tuberculin skin test.
†Comparison between MAC and *M. lentiflavum* cases.
‡Available in 268 cases in the whole cohort (116 MAC and 109 *M. lentiflavum* cases).
§Available in 305 cases in the whole cohort (131 MAC and 122 *M. lentiflavum* cases).
¶Includes posterior cervical (n = 6), occipital (n = 5), postauricular (n = 4), inguinal (n = 3), axillar (n = 2), and supraclavicular (n = 2).
#Excludes patients with clinical stage IV (fistulization) at initial examination.

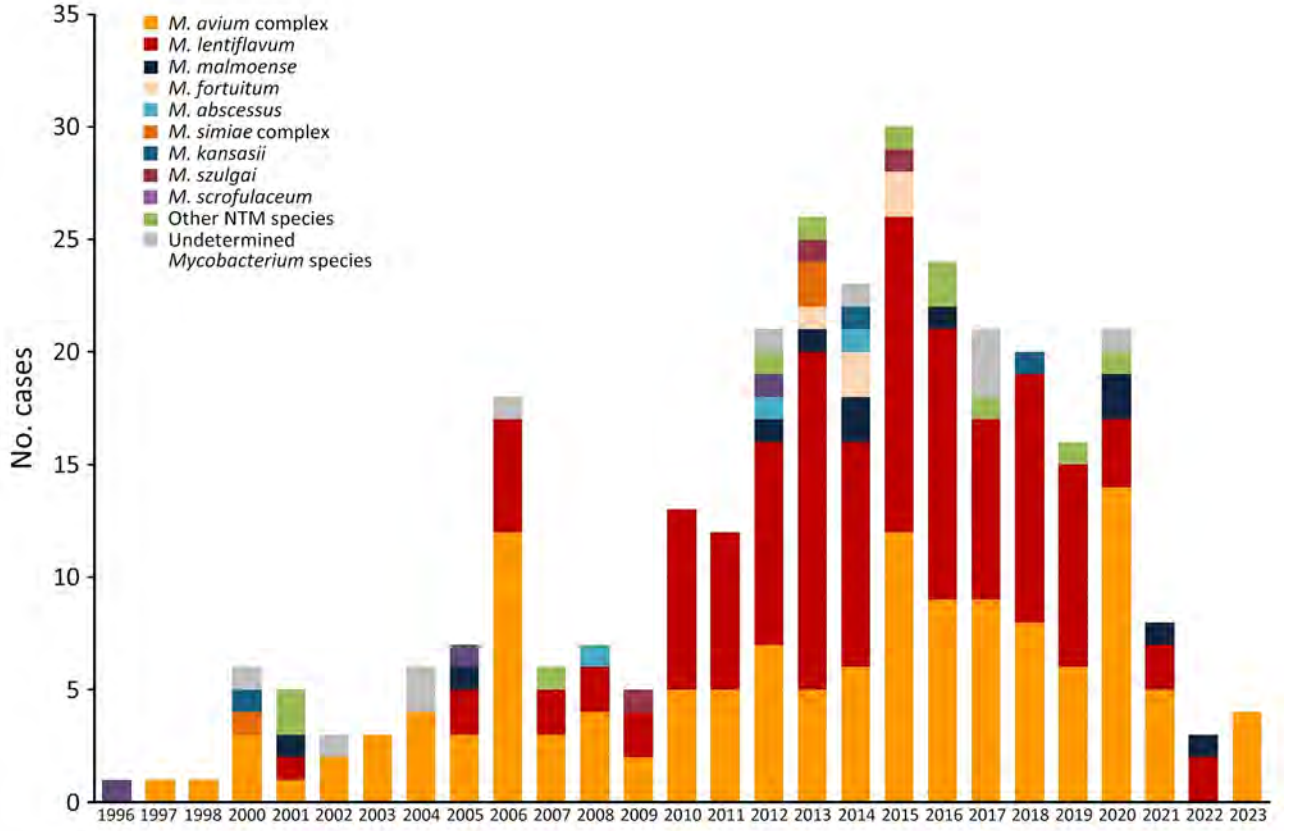

Figure 1. Annual case numbers of NTM lymphadenitis and the causative species in a 28-year multicenter cohort study of NTM lymphadenitis in children in Spain, 1996–2023. NTM, nontuberculous mycobacteria.

NTM species were MAC (43.1%, n = 134) and *M. lentiflavum* (39.9%, n = 124), followed by *M. malmoense* (3.5%, n = 11); *M. fortuitum* (1.6%, n = 5); *M. abscessus*, *M. kansasii*, *M. scrofulaceum*, *M. simiae* complex, and *M. szulgai* (1.0%, n = 3 each); *M. interjectum* (0.6%, n = 2); and *M. chelonae*, *M. colombiense*, *M. mageritense*, *M. marinum*, *M. mucogenicum*, *M. triplex*, and *M. xenopi* (0.3%, n = 1 each). In 13 (4.2%) patients, the NTM species could not be determined. NTM species are widely distributed geographically in Spain (Figure 3).

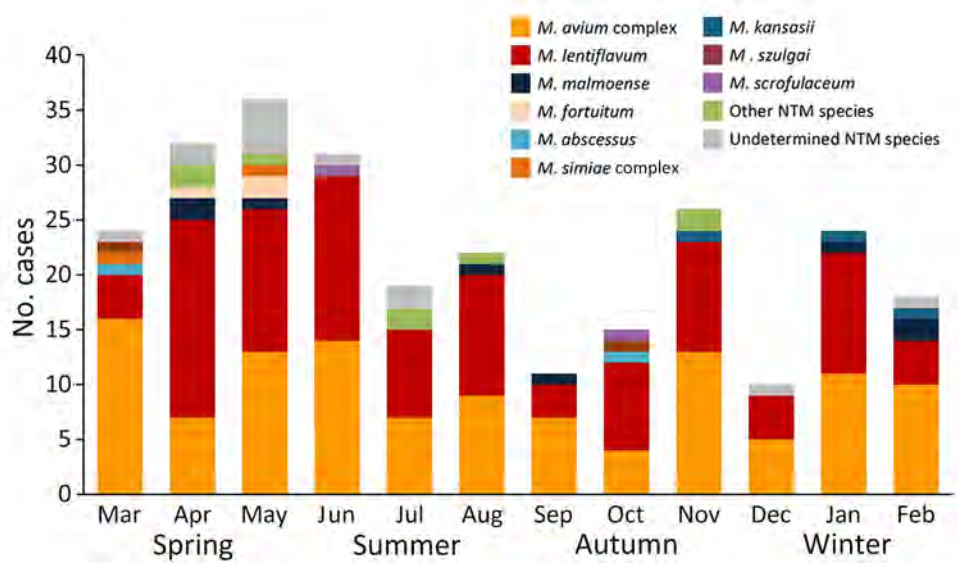

Figure 2. Seasonality of symptom onset, stratified by NTM species, in a 28-year multicenter cohort study of NTM lymphadenitis in children, Spain. NTM, nontuberculous mycobacteria.

Immunologic Tests

TSTs were performed in 89.4% (n = 278) of cases and reported positive in 168 cases, corresponding to a test sensitivity of 60.4% (95% CI 54.4%–66.2%) (Table 1). IGRA assays were performed in 44.4% (n = 138) of cases (QFT assays only, n = 111; T-SPOT.*TB* only, n = 11; both assays, n = 16). Of those cases, 89.9% (n = 124) were negative, 6.5% (n = 9) were positive, and 3.6% (n = 5) had an indeterminate test result. Overall, 138 cases were tested with both the TST and an IGRA assay, 67.4% (n = 93) had a TST+/IGRA– constellation (Appendix Table 5). Among children with a positive IGRA result (Appendix Table 6), epidemiologic risk factors for TB infection were identified in 3 patients. In addition, 4 patients with positive results underwent repeat assays that yielded negative results. *M. kansasii* (n = 3), *M. szulgai* (n = 3), and *M. marinum* (n = 1) are all NTM species that are known to express the ESAT-6 protein and potentially cause false-positive IGRA results (*24*,*25*). An IGRA assay was performed in 1 case caused by *M. szulgai* and was positive.

Treatment and Outcomes

Various treatment strategies were used with differing outcomes in cases of NTM lymphadenitis (Table 1). The most common treatment strategy consisted of complete surgical resection with (n = 88) or without (n = 80) antimycobacterial antimicrobial drugs, followed by antimicrobial drug therapy alone (n = 76). Pyogenic surgical site superinfection occurred in 3.4% (n = 7) of cases who underwent surgery. Overall, 62.1% (n = 193) patients initially received antimicrobial drugs for a median (IQR) time of 16 (8–24) weeks; the most used regimens were a macrolide combined with ciprofloxacin (49.2%, n = 95), rifampin (10.4%, n = 20), ethambutol (9.3%, n = 18) or rifabutin (5.7%, n = 11). Of the cases treated with antimicrobial drugs, 8.3% (n = 16) were treated with clarithromycin only, 7.3% (n = 14) received 3-drug regimens, and 1.6% (n = 3) received 4-drug regimens (Appendix Table 7). No cases of paradoxical worsening were reported. Adverse events because of antimicrobial drugs were uncommon (gastrointestinal symptoms n = 3; neutropenia n = 3; hearing loss n = 1; lethargy n = 1).

Follow-up data were available for 92.6% (n = 288) of cases (median [IQR] follow-up time from diagnosis 0.6 [0.3–1.0] years) (Table 2). Unplanned treatment during follow-up was performed in 18.4% (n = 53) cases and included surgery with (n = 3) or without (n = 44) antimicrobial drugs or antimicrobial drugs alone (n = 6) (Appendix Table 7). Among 280 cases with Penn clinical stages I to III at initial examination, fistula formation occurred in 12.9% (n = 36) of cases. Of those cases, children who were managed with observation alone had a significantly higher risk for fistula formation than those treated with antimicrobial drugs alone (45.0% [n = 9] vs. 16.4% [n = 10]; relative risk 2.7 [95% CI 1.3–5.3]; p = 0.014). Recurrent NTM lymphadenitis after resolution of symptoms and signs of the initial clinical manifestation occurred in 5.6% (n = 16) children.

At the last available follow-up, 65.3% (n = 188) children were reported to have no sequelae.

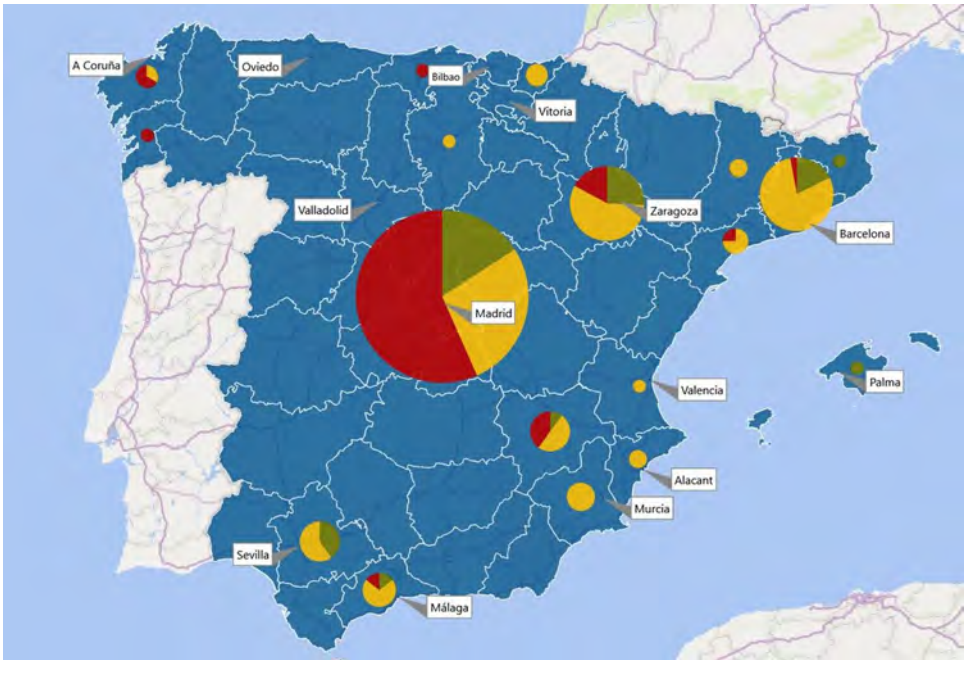

Figure 3. Geographic distribution of nontuberculous mycobacterial lymphadenitis cases in Spain. The pie charts show the species in each region: yellow, *Mycobacterium avium* complex; red, *Mycobacterium lentiflavum*; green, all other species. The size of each pie chart is proportional to the number of cases reported in the respective region.

Table 2. Complication details during follow-up by initial therapeutic strategy at initial examination of patients from a 28-year multicenter cohort study of NTM lymphadenitis in children, Spain*

Characteristics	Observation	Antimicrobial drugs alone	Drainage alone	Drainage + antimicrobial drugs	Complete resection alone	Complete resection + antimicrobial drugs	p value
Need for unplanned treatment	1/25 (4.0)	20/72 (27.8)	3/6 (50.0)	13/29 (44.8)	4/77 (5.2)	11/88 (12.5)	0.033
New fistula formation†	9/20 (40.0)	10/61 (16.4)	2/5 (40.0)	3/20 (15.0)	2/71 (2.8)	10/82 (12.2)	0.002
Recurrent NTM infection	0/21 (0)	1/67 (1.5)	2/6 (33.3)	0/27 (0)	2/76 (2.6)	10/87 (11.5)	0.020
Sequelae							
None	15/21 (71.4)	48/67 (71.6)	5/6 (83.3)	13/27 (48.1)	55/76 (72.4)	48/87 (55.2)	0.073
Hypertrophic scar	2/21 (9.5)	11/67 (16.4)	1/6 (16.7)	8/27 (29.6)	9/76 (11.8)	21/87 (24.1)	0.244
Skin discoloration	4/21 (19.0)	8/67 (11.9)	0/6 (0)	3/27 (11.1)	5/76 (6.6)	7/87 (8.0)	0.122
Transient facial palsy	0/21 (0)	2/67 (3.0)	0/6 (0)	4/27 (14.8)	8/76 (10.5)	9/87 (10.3)	0.025
Permanent facial palsy	0/21 (0)	1/67 (1.5)	0/6 (0)	0/27 (0)	1/76 (1.3)	5/87 (5.7)	0.089
Facial palsy	0/21 (0)	3/67 (4.5)‡	0/6 (0)	4/27 (14.8)	9/76 (11.8)	14/87 (16.1)	0.004

*Values are no. patients/total no. evaluated (%). NTM, nontuberculous mycobacteria
†Excludes patients with clinical stage grade IV (with fistula) at initial examination.
‡All 3 patients were initially managed only with antimycobacterial antimicrobial drugs, but subsequently underwent surgery; facial palsy developed only after the surgical intervention.
Patients with preexisting medical conditions at diagnosis (n = 4) were excluded from this analysis. Groups were compared by using chi-square test

Among children with sequelae, the most common findings were hypertrophic scar or keloid (18.1%, n = 52) and skin discoloration (9.4%, n = 27). Transient facial palsy occurred in 8.0% (n = 23) of cases, and permanent facial palsy occurred in 2.4% (n = 7) of cases. All case-patients had undergone surgery either when diagnosed or during follow-up. The affected sites were submandibular (n = 20), parotid (n = 6), superficial or deep cervical (n = 6), jugulodigastric (n = 5), and preauricular (n = 4). Frey syndrome developed after excisional surgery in a patient with *M. lentiflavum* cervical and preauricular lymphadenitis.

After excluding patients with underlying medical conditions, patients treated with antimicrobial drugs alone or drainage (with or without antimicrobial drugs) more often required unplanned treatment, which included surgery in most cases (Table 2). No significant differences between initial treatment strategies were observed regarding aesthetic sequelae, but facial palsy was significantly more common among patients who had undergone surgery at diagnosis (Table 2). Further detailed analyses revealed no other risk factors associated with the development of sequelae (Appendix Table 8). A subgroup analysis including only children with clinical stage I lymphadenitis at initial clinical examination showed similar results (Appendix Table 9).

Comparison between Dominant Species MAC and *M. lentiflavum*

Children with lymphadenitis caused by *M. lentiflavum* were younger at initial clinical examination, more often reported in the prospective phase of the study, and more common in central Spain (86.3%, n = 107 isolates), whereas MAC was more prevalent in the peripheral regions (61.2%, n = 82 isolates) (Table 1; Figure 3). The duration of symptoms before initial examination was shorter in *M. lentiflavum* cases, and submandibular and preauricular sites tended to be more commonly affected (Table 1). Differences were observed in the initial treatment strategies and the rate of new fistula formation, which was more common in MAC cases.

Discussion

This large study of children with microbiologically confirmed NTM lymphadenitis resulted from collaboration between 3 large mycobacterial research networks. Because of the participation of 33 tertiary and quaternary units providing healthcare for children with NTM infections distributed widely across Spain, we were able to identify several epidemiologic trends. First, the number of NTM lymphadenitis cases in the prospective phase initially remained stable until 2020, followed by a sharp decline coinciding with the COVID-19 pandemic, a trend observed in many other childhood infections (*26*). Because our study was on the basis of a convenience sample, we were not able to calculate incidence rates, but previous studies from the Netherlands, Germany, Wisconsin (USA), and Australia have reported incidences of 0.8–3.3 cases/100,000 children, although each study used different inclusion criteria (*2*,*27*–*29*). Of note, the ENSeMBLE study was deliberately designed to have stringent entry criteria that included the presence of microbiological confirmation, which led to high validity of our data but also resulted in a smaller cohort than if cases solely identified on clinical grounds were included. Second, our data confirm the observation that case numbers of NTM lymphadenitis typically

peak in spring in countries with moderate climate, a phenomenon that was first described by a single-center study from Australia (*3*). Third, geographic differences in the distribution of causative NTM species across the country were observed; *M. lentiflavum* was responsible for most cases in the central regions of Spain, whereas MAC predominated in almost all other regions.

In our cohort, *M. lentiflavum* was almost as common as MAC, which was the predominant agent in almost all previous studies on NTM lymphadenitis (*3*,*27*–*29*). Until the early 21st Century, *M. lentiflavum* was rarely reported as a causative agent of disease in humans. A meta-analysis in 2015 identified only 1 case (of 1,274) of lymphadenitis caused by *M. lentiflavum* (*6*). Nevertheless, this NTM species was described as an emerging pathogen in several small case series of NTM lymphadenitis in southern Europe over the past decade (*4*,*30*–*32*) and in cystic fibrosis patients (*33*–*35*). It was hypothesized that *M. lentiflavum* emergence might be because of improvements in identification techniques such as molecular tests and sequencing, rather than the result of an ecologic evolution (*30*). Of note, when we compared the 2 most prevalent species in our study, *M. lentiflavum* tended to affect younger patients, mainly occurred in the center of the country, had a faster disease course, and predominantly involved submandibular and preauricular lymph nodes compared with MAC. Our findings suggest that a combination of bacterial, host, and environmental factors might play a role in the recent emergence of *M. lentiflavum* (*36*).

In this study, IGRA assays yielded negative results in almost 90% of cases, but a TST+/IGRA– constellation was only observed in two thirds of the cases that underwent both tests. Our results support the dual immunodiagnostic strategy previously reported (*1*,*13*,*14*), but also highlight several limitations. First, we did not include an uninfected control group and therefore could not calculate specificity rates. Second, IGRA assays are not universally available, particularly in low-resource settings where TB lymphadenitis plays a greater role. Third, positive IGRA results were observed in 9 patients in our cohort and were because of different reasons: infection by *M. szulgai*, an NTM species known to express ESAT-6 (*24*,*25*); probable concomitant TB infection (in children with epidemiologic risk factors); and false-positive IGRA results with borderline interferon-γ responses that reverted to negative upon repeat testing. Finally, TST results were negative in 39.6% (n = 110) of cases in which this test was performed. This finding aligns with data from previous studies, which have reported TST results to be negative in 30%–50% of patients with NTM lymphadenitis (*1*). Nevertheless, in the absence of microbiological confirmation in a child with compatible symptoms and signs, a TST+/IGRA– result constellation supports the diagnosis of NTM lymphadenitis. However, such findings should be considered together with the results of other investigations as part of a comprehensive diagnostic work-up.

Our study was observational, with small sample sizes for some treatment options and a risk of confounding bias; therefore, the treatment and outcome data must be interpreted with caution. In contrast with 2 studies from the same group, we found that antimycobacterial treatment was generally well tolerated and that adverse events were rare and typically short-lived (*37*,*38*). In comparison, excisional surgery was associated with a substantial risk for facial nerve palsy, of which 8.0% of cases were transient and 2.4% permanent. Those data are similar to data from a previous meta-analysis documenting 7.6% transient facial nerve palsy and 2.1% permanent facial nerve palsy (*6*). As previously reported, our data also confirm that drainage alone is an inadequate management option, because most patients require further interventions (*39*–*41*). Furthermore, in children without fistula at initial clinical examination, those managed with observation alone had an almost 3-fold higher risk for developing a fistula during the disease course compared with children treated with antimycobacterial antimicrobial drugs alone. Ultimately, treatment decisions should consider diagnostic certainty, location and extent of the disease, local surgical experience, and parental preferences (*1*,*17*,*18*).

Our study is limited as an ambispective observational design, inevitably resulting in some data not being available. During the prospective phase of the study, two thirds of the total cases were reported, likely because of ascertainment bias. Also, we did not collect data on acid-fast staining, culture media, or the molecular assays used across different sites, some assays being noncommercial in-house assays. Although <50% of cases had both TST and IGRA testing completed, the cohort size enabled us to produce meaningful data. Randomized trials would be beneficial to clarify the optimal therapeutic strategy for NTM lymphadenitis, ideally with stratification according to clinical stage at initial clinical examination.

In conclusion, in this 28-year national cohort of microbiologically confirmed NTM lymphadenitis, *M. lentiflavum* emerged as a major causative species. Temporal analyses revealed seasonal peaks in spring and troughs in autumn. Our data support the combined

use of TST and an IGRA assay in the diagnostic work-up of protracted cervical lymphadenitis in young children pending microbiological results, although positive IGRA results can occur and require careful interpretation. Complete surgical resection was associated with a substantial risk for facial nerve palsy. Observation alone was associated with a higher risk for new fistula formation than treatment with antimycobacterial antimicrobial drugs, which were overall well tolerated.

Members of the European Nontuberculous Mycobacterial Lymphadenitis in Children Study: Carmelo Gutiérrez-Abad (Burgos, Spain); César Gavilán (Alicante, Spain); Teresa Valmanya, Laura Minguell-Domingo (Lleida, Spain); María José Mellado, Javier Álvarez, Enrique Villalobos-Pinto, Beatriz Pérez-Gorricho, Sonia Rodríguez, David Torres, Daniel Blázquez-Gamero, Luis Prieto, Beatriz Ruiz, Mar Santos, Teresa Hernández-Sanpelayo, Isabel Romero Blanco, Miguel Roa, Amanda Bermejo Gómez, Ana Morales, Santiago Rueda (Madrid, Spain); Ines Galé, Carmelo Guerrero-Laleona, Sheila Miralbés Terraza, Jesús Viñuelas, Ramiro Álvarez (Zaragoza, Spain); Marta Ruiz, Juana Cacho Calvo (Getafe, Spain); Olaf Neth (Sevilla, Spain); Antonio Cepillo (Albacete, Spain); Andrea Martín-Nalda, María Espiau, Pere Soler-Palacín (Barcelona, Spain); David Moreno, Esmeralda Núñez (Málaga, Spain); Ana Menasalvas-Ruiz (Murcia, Spain); Federico Martinón-Torres, Ana Dacosta-Urbieta (Santiago De Compostela, Spain); Olga Calavia, Rebeca Lahoz (Tarragona, Spain); José Javier Korta Murua, Marta Alonso (San Sebastián, Spain); Mireia Arroyo (Avilés, Spain); Irene Pomar, Susana Herrero (Palma De Mallorca, Spain); Amparo Pérez-Tamarit, Ana Piqueras, Carmen Otero, Mamen Carreras (València, Spain); Cristina Álvarez (Santander, Spain); Zulema Lobato (Manresa, Spain); Lourdes Garcia (Mataró, Spain); Neus Rius (Reus, Spain); Borja Guarch (Girona, Spain); Jose Couceiro (Pontevedra, Spain); Jakko van Ingen (Nijmegen, The Netherlands).

P.R.-M. is funded by Instituto de Salud Carlos III-Spanish Ministry of Health and Fondos Feder of the European Union (grant no. CM21/00174). This study was supported in part by the Carlos III Institute of Health, Ministry of Economy and Competitiveness of Spain (grant no. PI22/00766), and by the Spanish Society of Pneumology and Thoracic Surgery (grant no. 169-2022).

About the Author

Dr. Martínez-Planas is a pediatrician working at Hospital Sant Joan de Déu, a pediatric-only referral center in Barcelona, Spain. Her primary research interests are respiratory infections in children.

References

1. Tebruegge M, Curtis N. Nontuberculous mycobacterial infections. In: Long SS, Prober CG, Fischer M, editors. Principles and practice of pediatric infectious diseases. New York: Elsevier/Saunders; 2017. p. 806–12.
2. Haverkamp MH, Arend SM, Lindeboom JA, Hartwig NG, van Dissel JT. Nontuberculous mycobacterial infection in children: a 2-year prospective surveillance study in the Netherlands. Clin Infect Dis. 2004;39:450–6. https://doi.org/10.1086/422319
3. Tebruegge M, Pantazidou A, MacGregor D, Gonis G, Leslie D, Sedda L, et al. Nontuberculous mycobacterial disease in children—epidemiology, diagnosis & management at a tertiary center. PLoS One. 2016; 11:e0147513. https://doi.org/10.1371/journal.pone.0147513
4. Le Naour S, Boyer J, Malard O, Guillouzouic A, Aubry A, Launay E, et al. Cervicofacial nontuberculous mycobacteria in children: clinical, microbiological and therapeutic features. A retrospective study and literature review. Ann Dermatol Venereol. 2020;147:618–28. https://doi.org/10.1016/j.annder.2020.06.024
5. Faria S, Joao I, Jordao L. General overview on nontuberculous mycobacteria, biofilms, and human infection. J Pathogens. 2015;2015:809014. https://doi.org/10.1155/2015/809014
6. Zimmermann P, Tebruegge M, Curtis N, Ritz N. The management of non-tuberculous cervicofacial lymphadenitis in children: a systematic review and meta-analysis. J Infect. 2015;71:9–18. https://doi.org/10.1016/j.jinf.2015.02.010
7. Pham-Huy A, Robinson JL, Tapiéro B, Bernard C, Daniel S, Dobson S, et al. Current trends in nontuberculous mycobacteria infections in Canadian children: a pediatric investigators collaborative network on infections in Canada (PICNIC) study. Paediatr Child Health. 2010;15:276–82. https://doi.org/10.1093/pch/15.5.276
8. Cruz AT, Ong LT, Starke JR. Mycobacterial infections in Texas children: a 5-year case series. Pediatr Infect Dis J. 2010; 29:772–4. https://doi.org/10.1097/INF.0b013e3181da5795
9. Wetzstein N, Diricks M, Andres S, Kuhns M, Marschall L, Biciusca T, et al. Genomic diversity and clinical relevance of *Mycobacterium simiae*. ERJ Open Res. 2024;10:00773–02023. https://doi.org/10.1183/23120541.00773-2023
10. Springer B, Wu WK, Bodmer T, Haase G, Pfyffer GE, Kroppenstedt RM, et al. Isolation and characterization of a unique group of slowly growing mycobacteria: description of *Mycobacterium lentiflavum* sp. nov. J Clin Microbiol. 1996;34:1100–7. https://doi.org/10.1128/jcm.34.5.1100-1107.1996
11. Olivas-Mazón R, Blázquez-Gamero D, Alberti-Masgrau N, López-Roa P, Delgado-Muñoz MD, Epalza C. Diagnosis of nontuberculous mycobacterial lymphadenitis: the role of fine-needle aspiration. Eur J Pediatr. 2021;180:1279–86. https://doi.org/10.1007/s00431-020-03875-2
12. Bruijnesteijn Van Coppenraet ES, Lindeboom JA, Prins JM, Peeters MF, Claas EC, Kuijper EJ. Real-time PCR assay using fine-needle aspirates and tissue biopsy specimens for rapid diagnosis of mycobacterial lymphadenitis in children. J Clin Microbiol. 2004;42:2644–50. https://doi.org/10.1128/JCM.42.6.2644-2650.2004
13. Willemse SH, Oomens MAEM, De Lange J, Karssemakers LHE. Diagnosing nontuberculous mycobacterial cervicofacial lymphadenitis in children: a systematic review. Int J Pediatr Otorhinolaryngol. 2018;112:48–54. https://doi.org/10.1016/j.ijporl.2018.06.034
14. Saba ES, Ansari G, Hoerter J, Schloegel L, Zim S. The diagnosis of nontuberculous cervicofacial lymphadenitis:

a systematic review. Am J Otolaryngol. 2024;45:104030. https://doi.org/10.1016/j.amjoto.2023.104030
15. Lindeboom JA, Kuijper EJ, Prins JM, Bruijnesteijn van Coppenraet ES, Lindeboom R. Tuberculin skin testing is useful in the screening for nontuberculous mycobacterial cervicofacial lymphadenitis in children. Clin Infect Dis. 2006;43:1547–51. https://doi.org/10.1086/509326
16. Martínez-Planas A, Baquero-Artigao F, Santiago B, Fortuny C, Méndez-Echevarría A, Del Rosal T, et al.; Spanish Pediatric TB Research Network (pTBred) and the European NontuberculouS MycoBacterial Lymphadenitis in childrEn (ENSeMBLE) Study. Interferon-gamma release assays differentiate between *Mycobacterium avium* complex and tuberculous lymphadenitis in children. J Pediatr. 2021; 236:211–218.e2. https://doi.org/10.1016/j.jpeds.2021.05.008
17. Roy CF, Balakrishnan K, Boudewyns A, Cheng A, Chun RH, Daniel SJ, et al.; International Pediatric Otolaryngology Group. International pediatric otolaryngology group: consensus guidelines on the diagnosis and management of non-tuberculous mycobacterial cervicofacial lymphadenitis. Int J Pediatr Otorhinolaryngol. 2023;166:111469. https://doi.org/10.1016/j.ijporl.2023.111469
18. Zimmermann P, Curtis N, Tebruegge M. Nontuberculous mycobacterial disease in childhood—update on diagnostic approaches and treatment. J Infect. 2017;74(Suppl 1):S136–42. https://doi.org/10.1016/S0163-4453(17)30204-9
19. Soler-Garcia A, Gamell A, Pérez-Porcuna T, Soriano-Arandes A, Santiago B, Tórtola T, et al.; QFT-Plus Study Group of the Spanish Pediatric TB Research Network. Performance of QuantiFERON-*TB* Gold Plus assays in children and adolescents at risk of tuberculosis: a cross-sectional multicentre study. Thorax. 2022;77:1193–201. https://doi.org/10.1136/thoraxjnl-2021-217592
20. Rodríguez-Molino P, Tebruegge M, Noguera-Julian A, Neth O, Fidler K, Brinkmann F, et al. Tuberculosis disease in immunocompromised children and adolescents: a pediatric tuberculosis network European trials group multicenter case-control study. Clin Infect Dis. 2024;79:215–22. https://doi.org/10.1093/cid/ciae158
21. Harris PA, Taylor R, Thielke R, Payne J, Gonzalez N, Conde JG. Research electronic data capture (REDCap)—a metadata-driven methodology and workflow process for providing translational research informatics support. J Biomed Inform. 2009;42:377–81. https://doi.org/10.1016/j.jbi.2008.08.010
22. Penn R, Steehler MK, Sokohl A, Harley EH. Nontuberculous mycobacterial cervicofacial lymphadenitis—a review and proposed classification system. Int J Pediatr Otorhinolaryngol. 2011;75:1599–603. https://doi.org/10.1016/j.ijporl.2011.09.018
23. Baquero-Artigao F, Del Rosal T, Falcón-Neyra L, Ferreras-Antolín L, Gómez-Pastrana D, Hernanz-Lobo A, et al. Update on the diagnosis and treatment of tuberculosis. An Pediatr. (Engl Ed.) 2023;98:460–9.
24. van Ingen J, de Zwaan R, Dekhuijzen R, Boeree M, van Soolingen D. Region of difference 1 in nontuberculous Mycobacterium species adds a phylogenetic and taxonomical character. J Bacteriol. 2009;191:5865–7. https://doi.org/10.1128/JB.00683-09
25. Hermansen TS, Thomsen VØ, Lillebaek T, Ravn P. Non-tuberculous mycobacteria and the performance of interferon gamma release assays in Denmark. PLoS One. 2014;9:e93986. https://doi.org/10.1371/journal.pone.0093986
26. Kadambari S, Goldacre R, Morris E, Goldacre MJ, Pollard AJ. Indirect effects of the covid-19 pandemic on childhood infection in England: population based observational study. BMJ. 2022;376:e067519. https://doi.org/10.1136/bmj-2021-067519
27. Vonasek BJ, Gusland D, Tans-Kersten J, Misch EA, Gibbons-Burgener SN. Nontuberculous mycobacterial infection in Wisconsin children and adolescents. J Clin Tuberc Other Mycobact Dis. 2024;36:100456. https://doi.org/10.1016/j.jctube.2024.100456
28. Blyth CC, Best EJ, Jones CA, Nourse C, Goldwater PN, Daley AJ, et al. Nontuberculous mycobacterial infection in children: a prospective national study. Pediatr Infect Dis J. 2009;28:801–5. https://doi.org/10.1097/INF.0b013e31819f7b3f
29. Reuss AM, Wiese-Posselt M, Weissmann B, Siedler A, Zuschneid I, An der Heiden M, et al. Incidence rate of nontuberculous mycobacterial disease in immunocompetent children: a prospective nationwide surveillance study in Germany. Pediatr Infect Dis J. 2009;28:642–4. https://doi.org/10.1097/INF.0b013e3181978e8e
30. Lacroix A, Piau C, Lanotte P, Carricajo A, Guillouzouic A, Peuchant O, et al.; MYCOMED Group. Emergence of nontuberculous mycobacterial lymphadenitis in children after the discontinuation of mandatory Bacillus calmette and guérin immunization in France. Pediatr Infect Dis J. 2018;37:e257–60. https://doi.org/10.1097/INF.0000000000001977
31. Miqueleiz-Zapatero A, Santa Olalla-Peralta C, Guerrero-Torres MD, Cardeñoso-Domingo L, Hernández-Milán B, Domingo-García D. *Mycobacterium lentiflavum* as the main cause of lymphadenitis in pediatric population. Enferm Infecc Microbiol Clin (Engl Ed). 2018;36:640–3. https://doi.org/10.1016/j.eimce.2018.07.009
32. Jiménez-Montero B, Baquero-Artigao F, Saavedra-Lozano J, Tagarro-García A, Blázquez-Gamero D, Cilleruelo-Ortega MJ, et al. Comparison of *Mycobacterium lentiflavum* and *Mycobacterium avium-intracellulare* complex lymphadenitis. Pediatr Infect Dis J. 2014;33:28–34. https://doi.org/10.1097/INF.0000000000000007
33. Moreno Ortega M, Quintana Gallego ME, Carrasco Hernández L, Pérez Borrego E, Delgado Pecellín I. *Mycobacterium lentiflavum* in cystic fibrosis subjects. a colonizer or a true pathogen? Arch Bronconeumol (Engl Ed). 2018;54:639–40. https://doi.org/10.1016/j.arbr.2018.10.002
34. Phelippeau M, Dubus JC, Reynaud-Gaubert M, Gomez C, Stremler le Bel N, Bedotto M, et al. Prevalence of *Mycobacterium lentiflavum* in cystic fibrosis patients, France. BMC Pulm Med. 2015;15:131. https://doi.org/10.1186/s12890-015-0123-y
35. Satana D, Erkose-Genc G, Tamay Z, Uzun M, Guler N, Erturan Z. Prevalence and drug resistance of mycobacteria in Turkish cystic fibrosis patients. Ann Clin Microbiol Antimicrob. 2014;13:28. https://doi.org/10.1186/1476-0711-13-28
36. van Ingen J, van Soolingen D. Cervicofacial lymphadenitis caused by nontuberculous mycobacteria; host, environmental or bacterial factors? Int J Pediatr Otorhinolaryngol. 2011;75:722–3, reply 723–4. https://doi.org/10.1016/j.ijporl.2011.01.032
37. Lindeboom JA, Kuijper EJ, Bruijnesteijn van Coppenraet ES, Lindeboom R, Prins JM. Surgical excision versus antibiotic treatment for nontuberculous mycobacterial cervicofacial lymphadenitis in children: a multicenter, randomized, controlled trial. Clin Infect Dis. 2007;44:1057–64. https://doi.org/10.1086/512675
38. Lindeboom JA. Conservative wait-and-see therapy versus antibiotic treatment for nontuberculous mycobacterial cervicofacial lymphadenitis in children. Clin Infect Dis. 2011;52:180–4. https://doi.org/10.1093/cid/ciq070

39. Zeharia A, Eidlitz-Markus T, Haimi-Cohen Y, Samra Z, Kaufman L, Amir J. Management of nontuberculous mycobacteria-induced cervical lymphadenitis with observation alone. Pediatr Infect Dis J. 2008;27:920–2. https://doi.org/10.1097/INF.0b013e3181734fa3
40. Flint D, Mahadevan M, Barber C, Grayson D, Small R. Cervical lymphadenitis due to non-tuberculous mycobacteria: surgical treatment and review. Int J Pediatr Otorhinolaryngol. 2000;53:187–94. https://doi.org/10.1016/S0165-5876(00)82006-6
41. Lindeboom JA. Surgical treatment for nontuberculous mycobacterial (NTM) cervicofacial lymphadenitis in children. J Oral Maxillofac Surg. 2012;70:345–8. https://doi.org/10.1016/j.joms.2011.02.034

Address for correspondence: Antoni Noguera-Julian, Hospital Sant Joan de Déu, Passeig Sant Joan de Déu 2, 08950 Esplugues de Llobregat, Barcelona, Spain; email: antoni.noguera@sjd.es

December 2024

Zoonotic Infections

- Homelessness and Organ Donor–Derived *Bartonella quintana* Infection
- *Bartonella quintana* Infection in Kidney Transplant Recipients from Donor Experiencing Homelessness, United States, 2022
- Increase in Adult Patients with Varicella Zoster Virus–Related Central Nervous System Infections, Japan
- Historical Assessment and Mapping of Human Plague, Kazakhstan, 1926–2003
- *Bartonella quintana* Endocarditis in Persons Experiencing Homelessness, New York, New York, USA, 2020–2023
- Ophthalmic Sequelae of Ebola Virus Disease in Survivors, Sierra Leone
- Highly Pathogenic Avian Influenza A(H5N1) Virus Infection in Cats, South Korea, 2023
- Human Circovirus in Patients with Hepatitis, Hong Kong
- Rio Mamore Hantavirus Endemicity, Peruvian Amazon, 2020
- Novel Mastadenovirus Infection as Cause of Pneumonia in Imported Black-and-White Colobuses (*Colobus guereza*), Thailand
- Effect of Sexual Partnerships on Zika Virus Transmission in Virus-Endemic Region, Northeast Brazil
- Concurrent Rabies and Canine Distemper Outbreaks and Infection in Endangered Ethiopian Wolves
- Autochthonous *Blastomyces* Dermatitidis, India
- *Ehrlichia canis* in Human and Tick, Italy, 2023

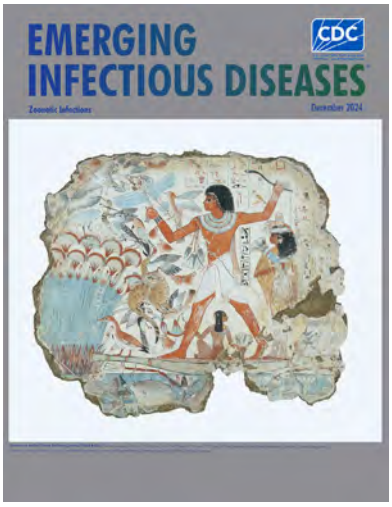

- Clinical Manifestations, Antifungal Drug Susceptibility, and Treatment Outcomes for Emerging Zoonotic Cutaneous Sporotrichosis, Thailand
- Dogs as Reservoirs for *Leishmania donovani*, Bihar, India, 2018–2022
- Mpox Vaccine Acceptance, Democratic Republic of the Congo
- Incursion of Novel Eurasian Low Pathogenicity Avian Influenza H5 Virus, Australia, 2023
- Heartland Virus Infection in Elderly Patient Initially Suspected of Having Ehrlichiosis, North Carolina, USA
- *Mycobacterium leprae* in Nine-Banded Armadillos (*Dasypus novemcinctus*), Ecuador
- Human and Canine Blastomycosis Cases Associated with Riverside Neighborhood, Wisconsin, USA, December 2021–March 2022

- Lack of Lloviu Virus Disease Development in Ferret Model
- Umatilla Virus in Zoo-Dwelling Cape Penguins with Hepatitis, Germany
- Influenza A Virus Antibodies in Ducks and Introduction of Highly Pathogenic Influenza A(H5N1) Virus, Tennessee, USA
- Cost-effectiveness Analysis of Japanese Encephalitis Vaccination for Children <15 Years of Age, Bangladesh
- Feline Panleukopenia Virus in a Marsican Brown Bear and Crested Porcupine, Italy, 2022–2023
- Lobomycosis in Amazon Region, Bolivia, 2022
- Experimental Infection of Reindeer with Jamestown Canyon Virus
- Transmission of Swine Influenza A Viruses along Pig Value Chains, Cambodia, 2020–2022
- Transboundary Movement of Yezo Virus via Ticks on Migratory Birds, Japan, 2020–2021
- Chikungunya Outbreak Risks after the 2014 Outbreak, Dominican Republic
- Replication-Competent Oropouche Virus in Semen of Traveler Returning to Italy from Cuba, 2024
- Bacteriologic and Genomic Investigation of *Bacillus anthracis* Isolated from World War II Site, China
- Canine Multidrug-Resistant *Pseudomonas aeruginosa* Cases Linked to Human Artificial Tears–Related Outbreak
- Possible New Focus of Diphyllobothriasis, Central Europe

EMERGING INFECTIOUS DISEASES

To revisit the December 2024 issue, go to:
https://wwwnc.cdc.gov/eid/articles/issue/30/12/table-of-contents

Diphtheria Outbreak among Persons Experiencing Homelessness, 2023, Linked to 2022 Diphtheria Outbreak, Frankfurt am Main, Germany

Jonas Haller,[1] Anja Berger,[1] Alexandra Dangel,[1] Katja Bengs, Imke Friedrichs, Christian Kleine, Dorothee Schmidt, Maria Goetzens, Udo Goetsch, Michael Hogardt, Andreas Sing

After 3 cases of *Corynebacterium diphtheriae* infection associated with intravenous drug use among persons experiencing homelessness (PEH) were reported to the Health Protection Authority in Frankfurt am Main, Germany, in 2023, we examined pathogen spread among PEH. Furthermore, we investigated a possible link with the 2022 outbreak of diphtheria in Europe. From swab samples collected during August–November 2023 from 36 PEH and cutaneous lesions, we detected 3 additional cases of cutaneous toxigenic *C. diphtheriae*. Sequence type 574 was identified in 5 case-isolates and is genetically associated with 1 of the predominant clusters in identified in the 2022 outbreak. Our findings demonstrate the need for increased detection and monitoring of cutaneous diphtheria and boosting immunity against diphtheria in groups with increased risk for infection. Genomic analyses are valuable for identifying genetic relationships between outbreaks, even when epidemiologic data are scarce.

Diphtheria is a vaccine-preventable disease, caused most often by toxigenic strains of *Corynebacterium diphtheriae*. Diphtheria is a worldwide public health threat that may affect the respiratory tract, especially the larynx or the skin, and may rarely cause ocular, otic, or genital disease (*1*–*3*). *C. diphtheriae* is almost exclusively harbored by humans, and transmission is primarily through airborne respiratory droplets or direct contact with cutaneous lesions or contaminated objects and fomites (*1*,*3*). The incubation period for diphtheria is typically 2–5 days (range 1–10 days) (*3*–*5*). In wound infections, *C. diphtheriae* is frequently found along with other skin pathogens such as *Streptococcus pyogenes* or *Staphylococcus aureus* (*6*).

Cutaneous wounds colonized or infected by toxigenic *C. diphtheriae* are a concerning potential source of severe respiratory diphtheria infections, which can lead to high mortality rates when untreated (*7*). The primary treatment available to neutralize the effects of the toxin is equine diphtheria antitoxin, which should ideally be administered within 48 hours of initial symptom onset. However, the production, supply, and availability of equine diphtheria antitoxin have declined over the past decade because of low demand across Europe, leading to shortages in many countries in Europe (*4*,*8*,*9*).

The World Health Organization aimed to eliminate diphtheria by 2000; thus, a worldwide immunization program was initiated in the late 1970s. As a result, diphtheria cases have substantially decreased in many countries (*10*,*11*). Full vaccination, typically requiring ≥3 doses of a diphtheria toxoid–containing vaccine, provides robust protection: 87% against symptomatic disease and 93% against death (*5*).

In Europe, diphtheria affects mainly persons insufficiently immunized before travel to regions where

Author affiliations: Robert Koch Institute, Berlin, Germany (J. Haller); European Centre for Disease Prevention and Control, Stockholm, Sweden (J. Haller); Gesundheitsamt Frankfurt am Main, Frankfurt am Main, Germany (J. Haller, C. Kleine, D. Schmidt, M. Goetzens, U. Goetsch); Bavarian Health and Food Safety Authority, Oberschleißheim, Germany (A. Berger, A. Dangel, K. Bengs, A. Sing); Laborarztpraxis Rhein-Main MVZ GbR, Frankfurt am Main (I. Friedrichs); Elisabethen Straßenambulanz, Frankfurt am Main (M. Goetzens); University Hospital Frankfurt, Frankfurt am Main (M. Hogardt)

DOI: https://doi.org/10.3201/eid3103.241217

[1]These first authors contributed equally to this article.

diphtheria is endemic (e.g., Africa, the Eastern Mediterranean, and Southeast Asia) and vaccination coverage is historically low (*1*,*4*,*12*–*15*). In 2015, the European Centre for Disease Prevention and Control issued a rapid risk assessment concerning the potential occurrence of cutaneous diphtheria among migrants originating from diphtheria-endemic regions and unvaccinated travelers returning from those areas (*16*). Since 2022, cases of cutaneous diphtheria have notably increased across numerous countries in Europe among migrant populations, particularly affecting young men originating from Syria and Afghanistan. Furthermore, instances of respiratory diphtheria, some resulting in fatalities, have also been documented (*1*–*24*).

Outbreaks have, however, also been observed in other population groups. An outbreak of cutaneous diphtheria caused by toxigenic *C. diphtheriae* in a group of persons with alcohol use disorder in Sweden has been described, and nontoxigenic *C. diphtheriae* has frequently been found in the wounds of persons associated with intravenous drug use (IVDU) (*19*). Because persons with alcohol and substance use disorders often have difficulty accessing reliable medical care, underreporting might be a substantial problem, potentially increasing the risk for diphtheria transmission (*18*–*21*).

In Germany, diphtheria is a notifiable disease. In February 2023, a case of respiratory diphtheria was reported to the Health Protection Authority in Frankfurt am Main (hereafter abbreviated as Frankfurt), followed by 2 cases of cutaneous diphtheria in June and July 2023. In both cases, the infections were characterized by superficial ulceration and abscess formation, primarily in the groin area. Both patients had mixed wound infections with *S. aureus*, *S. pyogenes*, or both. One patient died of *S. aureus* sepsis. For all 3 patients, the time since last vaccination against *C. diphtheriae* was either unknown or confirmed to be >10 years. The patients experienced homelessness, spent time around the central station in Frankfurt, and engaged in IVDU. None of the 3 patients had traveled outside of Germany within 10 days before the sample collection date. Unfortunately, further epidemiologic investigation and contact tracing was not possible.

Until the report of a respiratory diphtheria case in a person with IVDU and experiencing homelessness in February 2023, no isolates from non–travel-related patients with *tox* gene have been reported in Frankfurt since 2014. The PCR test for the diphtheria *tox* gene in all 3 isolates was positive; the number of cases in the nonmigrant population of Frankfurt was higher than expected. We investigated the extent of the outbreak and its genetic relationship with other cases reported in Germany.

Material and Methods

Case Definition

We defined a suspected case as illness in any person experiencing homelessness who had typical skin lesions and was notified during August 1, 2023–October 31, 2023, while residing in Frankfurt am Main and without having returned from a diphtheria-endemic area within the 10 days before testing. We defined a probable case as illness in a person with a suspected case and a positive culture result for *C. diphtheriae*. We defined a confirmed case as illness in any person with a probable case and a *C. diphtheriae tox* gene–positive (*tox*+) isolate, which includes the 3 confirmed case-patients reported earlier in the year (February, June, and July 2023). We did not classify probable cases with a *C. diphtheriae* isolate that tested negative for the *tox* gene (*tox*–) as confirmed cases. Although the definitions of probable and confirmed case were applied to the August–October 2023 period, the inclusion of earlier cases enabled comprehensive knowledge of the outbreak.

Notifiable Disease

The first 3 PCR-positive (*tox*+) cases during February–July 2023 were reported to the Health Protection Authority in Frankfurt by various local hospitals. The first case was identified by PCR and clinical signs/symptoms but without any further typing. The other isolates were sent to the German National Consiliary Laboratory for Diphtheria at the Bavarian Health and Food Safety Authority and World Health Organization Collaborating Centre for Diphtheria (Landesamt *für Gesundheit und* Lebensmittelsicherheit) in Bavaria for toxigenicity testing and whole-genome sequencing (WGS).

Patients were isolated and treated in single rooms in the hospitals and, when possible, interviewed by staff of the Health Protection Authority with regard to possible contact persons. We collected information on age, sex, duration of illness at first visit, clinical manifestations, and vaccination history from medical records.

Epidemiologic Investigation

For further investigation and to determine the extent of the outbreak, we initiated active case finding in collaboration with 3 aid organizations for persons experiencing homelessness (PEH), persons with and without concomitant drug dependence close to the central railway station, or both, as follows. First, we gave the aid organizations information about the potential risk of PEH contracting diphtheria. Then, during August 2023–October 2023, the public health authority of Frankfurt supplied the homeless aid organizations

with the necessary material to systematically screen all patients with skin lesions for *C. diphtheriae*. Patients with open skin wounds were medically examined by a doctor and informed about the screening, which was followed by simultaneous collection of wound and throat swab samples. Last, persons exhibiting clinical signs of respiratory diphtheria or severe skin lesions were promptly directed to the nearest hospital for further evaluation to confirm or rule out suspicion of diphtheria and to receive treatment. In addition to the age, sex, and location of the affected persons, we also received information about their medical history, including possible dependency disorders, vaccination status, and signs/symptoms.

Vaccination

Among the ≈300 PEH in Frankfurt, vaccination coverage against diphtheria is mostly unknown because of lost vaccination cards and sporadic visits to medical aid facilities. Therefore, we conducted a vaccination campaign in collaboration with the Elisabethen Street Ambulance (ESA), one of the aid organizations for PEH. In December 2023, the local health authorities provided ESA with 50 doses each of diphtheria-tetanus and influenza vaccine. To ensure comprehensive coverage, a mobile team of streetworkers and a medical doctor from ESA made weekly outreach visits to the central railway station area via a specialized bus to reach persons who did not have easy access to the ESA facility

Furthermore, we conveyed essential knowledge about diphtheria to the staff members within various homeless aid organizations, raising awareness about diphtheria and encouraging them to confirm their vaccination status. Following the Germany national guidelines for a proven case of diphtheria, we recommended that in-contact persons whose last vaccination for diphtheria was >5 years ago should receive a booster, as opposed to the standard interval of 10 years for boosters (*25*). Staff members of the aid organizations were instructed to self-report any typical signs/symptoms to their family doctor for further diagnosis after having close contact with persons with suspected cases.

Microbiological and Genomic Analyses

At the Laborarztpraxis Rhein-Main MVZ GbR in Frankfurt, we cultured samples on 5% sheep blood and serum tellurite agar plates (both BD, https://www.bd.com). After colony incubation for a minimum of 3 days, we subjected colonies that exhibited characteristics suggestive of coryneform bacteria to matrix-assisted laser desorption/ionization time-of-flight mass spectrometry with VITEK MS PRIME (bioMérieux, https://www.biomerieux.com), followed by microbiological susceptibility testing, which was performed according to the guidelines from the European Committee on Antimicrobial Susceptibility Testing for all isolates (https://www.eucast.org/clinical_breakpoints) (*1*,*17*,*26*).

To verify toxigenicity and perform WGS, we sent all cultivated *C. diphtheriae* isolates except the respiratory *C. diphtheriae* isolate of the first observed case to the German National Consiliary Laboratory on Diphtheria at the Bavarian Health and Food Safety Authority and World Health Organization Collaborating Centre for Diphtheria in Bavaria. The German National Consiliary Laboratory on Diphtheria verified toxigenicity by using real-time PCR (*27*) and the optimized Elek test (*28*), after which WGS was performed on 5 *tox*+ *C. diphtheriae* strains (*16*). We analyzed WGS data by using multilocus sequence typing (MLST) of target loci *atpA*, *dnaE*, *dnaK*, *fusA*, *leuA*, and *odhA* (*25*) and also by core-genome MLST (cgMLST) by using the *C. diphtheriae* cgMLST scheme of 1,553 target loci (*17*) implemented in Ridom SeqSphere+ software (Ridom GmbH, https://www.ridom.de) for centralized complex type (CT) nomenclature and minimum spanning tree visualization. We performed microbiological susceptibility testing according to the guidelines from the European Committee on Antimicrobial Susceptibility Testing for all isolates (https://www.eucast.org/clinical_breakpoints) (*29*).

We defined a genetic cluster/relationship as cgMLST profiles of isolates with a common CT, with the empirical threshold of a maximum of 14 allelic distances of the total 1,553 typed loci to the CT-founder isolate that established the CT. We included published *C. diphtheriae* isolates of the same sequence type (ST) from Frankfurt and Europe in the cgMLST analysis for genetic relatedness.

Results

Outbreak Outline

During August 1, 2023–October 31, 2023, a total of 36 suspected cases were identified. None of the patients refused testing. Of the 36 suspected cases, 13 had probable cases, determined by a positive culture for *C. diphtheriae*. Three confirmed cutaneous diphtheria cases were identified, along with the 3 previously reported cases from earlier in the year, bringing the total number of confirmed cases to 6: 1 respiratory case and 5 cutaneous cases. Of the 10 nonconfirmed case-patients harboring *tox*– *C. diphtheriae* isolates, 7 swab samples were from wounds (Figure 1). Except for the first reported case in February 2023, no patient exhibited clinical signs of respiratory diphtheria. Only 1

patient exhibited severe skin inflammation and was hospitalized (Figure 1). Other skin pathogens (e.g., *S. pyogenes* or *S.* aureus) were isolated from most swab samples. All strains were resistant to trimethoprim/sulfamethoxazole, but we did not observe any antimicrobial resistance against benzylpenicillin (high dosage), erythromycin¸ clindamycin, or tetracycline.

We describe all 6 confirmed cases of diphtheria detected in 2023 because they belonged to 1 outbreak. Most confirmed (5/6) and probable (12/16) case-patients were male; median age was 40 years for the probable case-patients (interquartile range 38–43) (Table). Country of origin was Germany (n = 8), Poland (n = 4), or unknown (n = 4). All 16 patients with a positive culture for *C. diphtheriae* experienced homelessness. Among them, 10 were associated with IVDU, 6 had an alcohol dependency disorder, and 4 had both dependency disorders. The exact date of symptom onset could not be determined because most wound infections had occurred weeks to months earlier. Vaccination status was also unknown because of missing vaccination records. No deaths were reported, and no secondary cases were detected among persons working in the health aid organizations (Table). Furthermore, no further cases of wound/pharyngeal diphtheria in the general population of Frankfurt were notified during the study period.

Laboratory Analysis and Phylogeny

In 5 of the toxigenic outbreak isolates, MLST identified the common ST574. Therefore, those isolates were analyzed by cgMLST and results were compared with the database of sequenced *C. diphtheriae* genomes of the Consiliary Laboratory on Diphtheria. The 5 ST574 isolates showed very close genetic relatedness; total allelic distances from each other were 0–4. Furthermore, the isolates were genetically linked to a cluster of ST574 isolates from the 2022 outbreak among migrants in Europe (*23*) (Figure 2), which also comprised 4 cases among young migrants from the same geographic region of Frankfurt. The 5 current outbreak isolates from PEH in Frankfurt showed a total of 4–13 allelic distances from the migration-associated isolates of that cluster and, within that, 4–8 allelic distances from the Frankfurt-based young migrants (Figure 2). All isolates showed common CT 79, which means that each isolate that harbors the CT has an allelic distance less than or equal to the CT threshold of 14 alleles to the CT-founder isolate that established the CT.

Treatment and Isolation of Case-Patients

In accordance with the National Guidelines (*25*), case-patients received azithromycin (500 mg/d for 3 days). Azithromycin was preferred to other antimicrobial drugs because its treatment duration is shorter and it needs to be administered only once per day. Because of difficult living conditions, only wound coverage and antimicrobial treatment were provided; no swab samples were collected to confirm pathogen eradication.

Outbreak Intervention

By the end of January 2024, a total of 26 PEH had received 1 dose of diphtheria-tetanus vaccine and 1 dose of influenza vaccine, administered according to the national recommendations for vaccinations in Germany. We have no records of how many persons out of the study population refused vaccination.

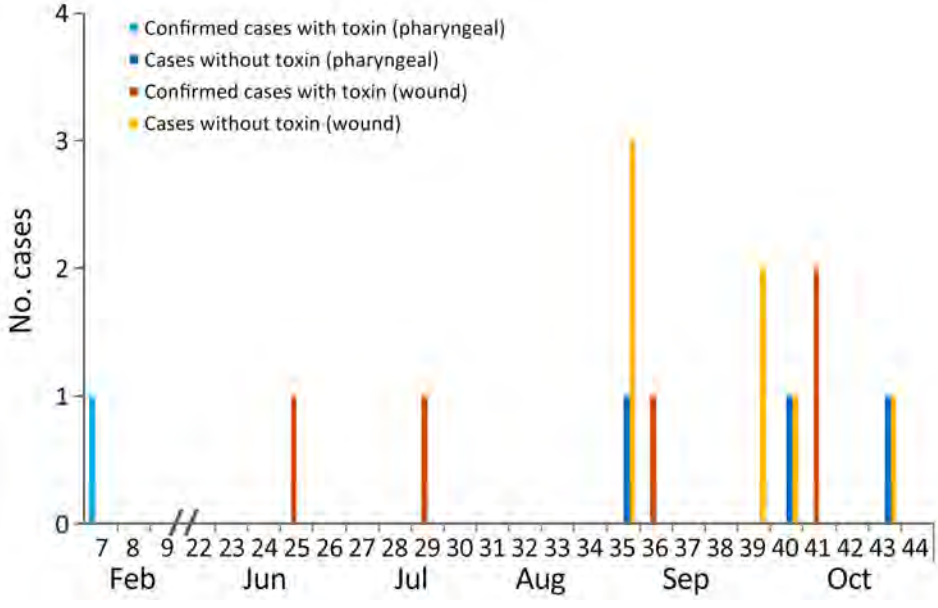

Figure 1. Details on 16 cases of dipththeria in persons experiencing homelessness, by sampling week, toxigenicity (positive/negative), and place of infection, Frankfurt am Main, Germany, February–October 2023.

Table. Demographic and clinical characteristics of 16 *Corynebacterium diphtheriae* cases among persons experiencing homelessness, Frankfurt am Main, Germany, February–October 2023*

	Demographics			Toxigenic status		Symptoms		Substance abuse	
Case no.	Age group, y	Sex	Country of origin	Pharynx	Wound	Respiratory	Wound	Alcohol	IV drugs
1†	26–35	F	Germany	+	UNK	Y	Y	N	Y
2†	26–35	M	Afghanistan	–	+	N	Y	N	Y
3†	36–45	M	Germany	–	+	N	Y	Y	Y
4†	>60	M	Poland	–	+	N	Y	Y	N
5†	36–45	F	Poland	–	+	N	Y	Y	N
6†	46–60	M	Poland	–	+	N	Y	Y	N
7	26–35	M	Germany	–	–	N	Y	N	Y
8	36–45	M	Germany	–	–	N	Y	Y	Y
9	36–45	F	Germany	–	–	Y	Y	Y	N
10	46–60	F	UNK	–	–	N	Y	Y	N
11	36–45	M	UNK	–	–	Y	Y	N	Y
12	46–60	M	UNK	–	–	N	Y	Y	Y
13	46–60	M	Poland	–	–	N	Y	Y	N
14	46–60	M	Germany	–	–	Y	Y	N	Y
15	36–45	M	Germany	–	–	N	Y	Y	Y
16	36–45	M	Germany	–	–	N	Y	N	Y

*Probable and confirmed cases are shown. IV, intravenous; UNK, unknown.
†Previously reported confirmed cases.

Discussion

In recent decades, the incidence of toxigenic *C. diphtheriae* cases in Germany has been low because most persons are vaccinated. However, sporadic cases of imported diphtheria in travelers (*30*–*32*) show that booster vaccination is needed to provide sustained protection against the disease. In PEH who have an IVDU or alcohol dependency disorder, single cases and outbreaks have been reported repeatedly (*33*,*34*). Among PEH and persons who use substances, most cases were cutaneous wound infections colonized by nontoxigenic *C. diphtheriae* (*17*,*35*,*36*).

The unexpected notification of 3 cases of *tox*+ diphtheria in PEH in Frankfurt in early 2023 was the reason for initiating active case finding among PEH in Frankfurt. Our study identified predominantly *tox*− strains, with 6 *tox*+ cases among PEH in Frankfurt. That pattern aligns with findings from other studies

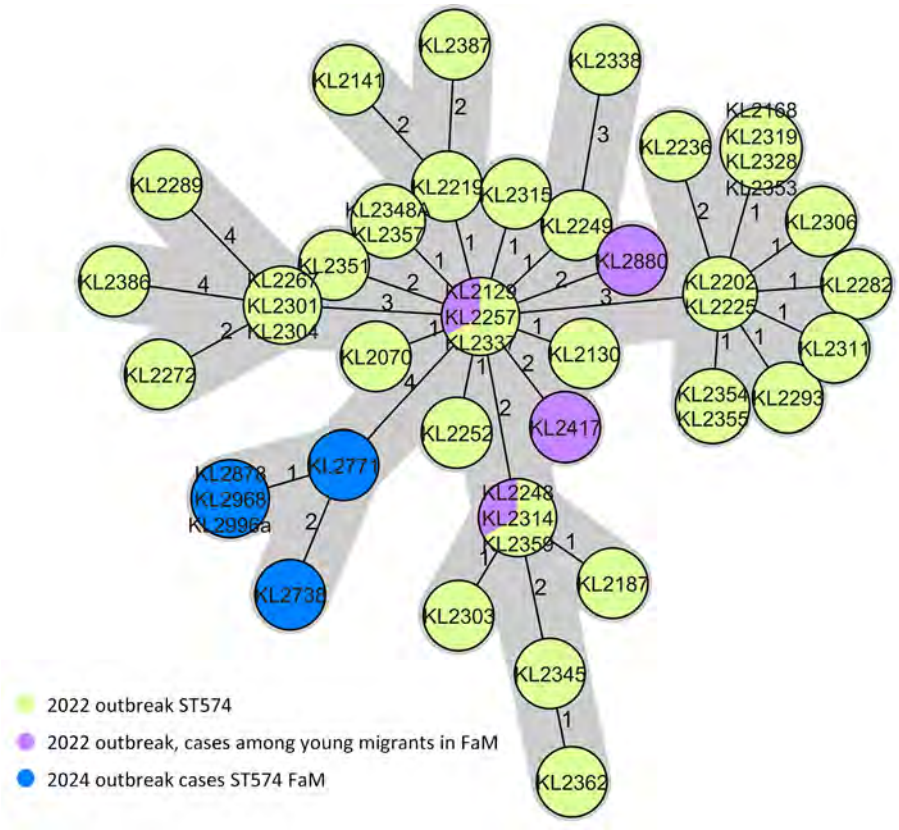

Figure 2. Minimum-spanning tree of core-genome multilocus sequence type analysis of toxigenic *Corynebacterium diphtheria*, with 1,553 target loci of the whole-genome sequencing-obtained genomes of the toxigenic *C. diphtheriae* isolates from an outbreak in 2023 compared with genomes of an outbreak cluster of the same ST (ST574) from a previously reported outbreak among migrants (*23*). Single-linkage allelic distances are illustrated as a measure of genetic related. FaM, Frankfurt am Main; ST, sequence type.

in which cutaneous manifestations of *C. diphtheriae* rather than pharyngeal infections were found to be prevalent, particularly among at-risk groups (*37*–*39*). Cutaneous diphtheria is often observed in populations with limited healthcare access, including those with high rates of alcohol dependency and IVDU, because wounds can serve as entry points for infection (*37*,*40*). The skin lesions make person-to-person transmission easier and can harbor both toxigenic and nontoxigenic strains, increasing the risk for broader community spread (*37*).

Active case finding, in collaboration with medical aid facilities, proved essential for identifying and managing diphtheria cases among PEH. Those facilities, often the primary contact points for vulnerable populations, provided a trusted environment that enable testing, treatment, and vaccination efforts. Given the limited healthcare access and high prevalence of comorbid conditions such as substance use disorders within this population, conventional healthcare systems alone may struggle to effectively reach such persons (*40*,*41*). By engaging medical aid organizations and outreach services, we were able to reach persons whose illness might otherwise remain undiagnosed, thereby reducing potential transmission risks and improving outbreak containment.

Genetic analysis revealed notable similarity among isolates from PEH, suggesting transmission within this group despite the absence of clearly documented direct contacts. Sequence-based comparisons showed that cases shared close genetic profiles (AD 0–4), indicating the likely circulation of *C. diphtheriae* strains (ST574) within that population. That finding highlights the value of genomic surveillance as an epidemiologic tool, providing insights into transmission pathways that may not be captured by standard contact tracing alone and underscores the value of targeted interventions within at-risk populations to mitigate further spread.

A plausible epidemiologic link between the diphtheria outbreak among migrants in 2022 and the recent outbreak among the community of PEH in Frankfurt is suggested by identification of a ST574 cluster; the close genetic relationship that was subsequently identified between ST574 isolates from the 2023 outbreak and ST574 isolates from the 2022 outbreak among young migrants; and the close relationship of ST574 with CT-79. Our hypothesis is further supported by epidemiologic evidence indicating mobility and intermingling between those populations, particularly within urban centers (*42*). The genetic congruence between the isolate genomes implies a direct or indirect transmission pathway, whereby ST574 was introduced from case-patients from the 2022 outbreak into the community of PEH, either through direct contact or within shared environments, such as shelters, aid facilities, or communal spaces.

During the diphtheria outbreak in Frankfurt, the treatment strategy of azithromycin once daily was preferred over multiple daily doses of erythromycin or penicillin; outcomes were positive (*1*,*43*). Both the national guidelines for Germany (*29*) and the recently published World Health Organization guidelines (February 2024) recommend the primary use of azithromycin to treat confirmed cases (*44*). That regimen, with its shorter duration and once-daily dosing, was specifically chosen to improve treatment compliance.

Improving data on vaccination coverage among PEH is essential. In this study, we were able to vaccinate only 26 of ≈300 persons in our potential target group. Many patients faced challenges with regard to adhering to further treatments (e.g., vaccinations), potentially influenced by underlying mental health conditions and other socio-environmental factors. Understanding barriers to vaccine uptake in this community is crucial. A mixed-methods approach involving qualitative interviews with PEH and outreach staff could identify specific challenges (e.g., limited vaccine access, hesitancy, or inability to track vaccinations). Findings could guide strategies to improve access (e.g., mobile vaccination units) and education to address vaccine concerns. Furthermore, obtaining reliable data on the vaccination status of PEH was difficult because of a lack of vaccination documents and a national vaccination register in Germany. Similar problems were encountered during investigations of the outbreak among migrants in 2022 (*1*,*16*,*23*); migrants receive the basic vaccinations in the initial reception facilities in Germany.

In conclusion, our study underscores the challenges inherent in investigating and controlling diphtheria outbreaks among PEH in a bustling urban center such as Frankfurt am Main. Our findings demonstrate that active case finding for diphtheria among persons in those populations is both feasible and more successful when conducted in collaboration with medical aid facilities dedicated to serving them. By leveraging trusted access points, early detection and intervention efforts can reach at-risk persons more effectively, underscoring the value of engaging community health resources.

Sustained awareness and vigilance are crucial, particularly within medical aid facilities serving high-

risk populations. Those facilities, in collaboration with public health organizations, must establish and maintain ongoing partnerships. Such continuous engagement enables both parties to stay informed about emerging public health threats and enhances their preparedness for potential outbreaks. That approach ensures that healthcare providers and the community are more proactive and ready to respond to future infectious disease risk.

Last, molecular typing has proven to be an invaluable asset for providing information about transmission pathways within at-risk populations. By analyzing the genetic profiles of diphtheria strains, health authorities can gain critical insights into potential links between cases, even when direct contact tracing is not possible, thereby enhancing knowledge of disease spread and the effectiveness of outbreak control efforts.

BioSample sequences used in this study are shown in the Appendix (https://wwwnc.cdc.gov/EID/article/31/3/24-1217-App1.xlsx).

Acknowledgments

The authors thank all involved local aid organizations for persons experiencing homelessness for taking swab samples and supporting the active case finding. We also acknowledge the LGL teams of bacteriology and NGS Core Unit for laboratory work and sample management and the infectious diseases department team at the Municipal Health Protection Authority in Frankfurt for supporting the active case finding and data collection. Finally, we thank Sofie Gillesberg Raiser for her supervising role and Christa Bedwin for editing.

About the Author

Mr. Haller works in the Department of Infectious Diseases at the Protection Authority in Frankfurt am Main. He has a master's degree in biology and is attending the German Fellowship for applied Epidemiology (PAE) as a fellow. His main research interests are vaccine-preventable and vectorborne diseases.

References

1. Jacquinet S, Martini H, Mangion JP, Neusy S, Detollenaere A, Hammami N, et al. Outbreak of *Corynebacterium diphtheriae* among asylum seekers in Belgium in 2022: operational challenges and lessons learnt. Euro Surveill. 2023;28:2300130. https://doi.org/10.2807/1560-7917.ES.2023.28.44.2300130
2. Centers for Disease Control and Prevention. The Pink Book: Diphtheria [cited 2024 Apr 25]. https://www.cdc.gov/vaccines/pubs/pinkbook/dip.html
3. Bennett JE, Dolin RD, Blaser R. Mandell, Douglas and Bennett's Principles and Practice of Infectious Diseases, 8th ed. Philadelphia: Elsevier Saunders;2015.
4. Meinel DM, Kuehl R, Zbinden R, et al. Outbreak investigation for toxigenic *Corynebacterium diphtheriae* wound infections in refugees from Northeast Africa and Syria in Switzerland and Germany by whole genome sequencing. Clin Microbiol Infect, 2016;22:1003.e1–1003.e8. https://doi.org/10.1016/j.cmi.2016.08.010
5. Truelove SA, Keegan LT, Moss WJ, Chaisson LH, Macher E, Azman AS, et al. Clinical and epidemiological aspects of diphtheria: a systematic review and pooled analysis. Clin Infect Dis. 2020;71:89–97. 10.1093/cid/ciz808 https://doi.org/10.1093/cid/ciz808
6. Hamborsky J, Kroger A, Wolfe C, editors. Centers for Disease Control and Prevention Epidemiology and Prevention of Vaccine-Preventable Diseases, vol. 13. Washington (DC): Public Health Foundation; 2015
7. Lowe CF, Bernard KA, Romney MG. Cutaneous diphtheria in the urban poor population of Vancouver, British Columbia, Canada: a 10-year review. J Clin Microbiol. 2011;49:2664–6. https://doi.org/10.1128/JCM.00362-11
8. European Centre for Disease Prevention and Control. Increase of reported diphtheria cases among migrants in Europe due to *Corynebacterium diphtheriae*, 2022 [cited 2022 Oct 6]. https://www.ecdc.europa. eu/sites/default/files/documents/diphtheriacases-migrantseurope-corynebacterium-diphtheriae-2022.pdf
9. European Centre for Disease Prevention and Control. Gap analysis on securing diphtheria diagnostic capacity and diphtheria antitoxin availability in the EU/EEA [cited 2017 Jul 12]. https://www.ecdC.europa.eu/sites/default/files/documents/Diphtheria%20Gap%20Analysis%20final%20with%20cover%20for%20web.pdf
10. Polonsky JA, Ivey M, Mazhar MKA, Rahman Z, le Polain de Waroux, et al. Epidemiological, clinical, and public health response characteristics of a large outbreak of diphtheria among the Rohingya population in Cox's Bazar, Bangladesh, 2017 to 2019: a retrospective study. PLoS Med. 2021;18:e1003587.
11. de Benoist AC, White JM, Efstratiou A, Kelly C, Mann G, Nazareth B, et al. Imported cutaneous diphtheria, United Kingdom. Emerg Infect Dis. 2004;10:511–3. 10.3201/eid1003.030524 https://doi.org/10.3201/eid1003.030524
12. Dangel A, Berger A, Konrad R, Bischoff H, Sing A. Geographically diverse clusters of nontoxigenic *Corynebacterium diphtheriae* infection, Germany, 2016-2017. Emerg Infect Dis. 2018;24:1239–45. https://doi.org/10.3201/eid2407.172026
13. World Health Organization. Weekly Epidemiological Record. Geneva: The Organization; 2006. pp. 24–32.
14. Mahomed S, Archary M, Mutevedzi P, Mahabeer Y, Govender P, Ntshoe G, et al. An isolated outbreak of diphtheria in South Africa, 2015. Epidemiol Infect. 2017; 145:2100–08. https://doi.org/10.1017/S0950268817000851
15. European Centre for Disease Prevention and Control. Diphtheria—annual epidemiological report for 2018 [cited 2025 Feb 9]. https://www.ecdc.europa.eu/sites/default/files/documents/diphtheria-annual-epidemiological-report-2018.pdf
16. Badenschier F, Berger A, Dangel A, Sprenger A, Hobmaier B, Sievers C, et al. Outbreak of imported diphtheria with *Corynebacterium diphtheriae* among migrants arriving in Germany, 2022. Euro Surveill. 2022;27:2200849. https://doi.org/10.2807/1560-7917.ES.2022.27.46.2200849
17. Arguni E, Karyanti MR, Satari HI, Hadinegoro SR. Diphtheria outbreak in Jakarta and Tangerang, Indonesia: epidemiological and clinical predictor factors for death.

PLoS One. 2021;16:e0246301. https://doi.org/10.1371/journal.pone.0246301
18. Badell E, Alharazi A, Criscuolo A, Almoayed KAA, Lefrancq N, Bouchez V, et al.; NCPHL diphtheria outbreak working group. Ongoing diphtheria outbreak in Yemen: a cross-sectional and genomic epidemiology study. Lancet Microbe. 2021;2:e386–96. https://doi.org/10.1016/S2666-5247(21)00094-X
19. Björkholm B, Böttiger M, Christenson B, Hagberg L. Antitoxin antibody levels and the outcome of illness during an outbreak of diphtheria among alcoholics. Scand J Infect Dis. 1986;18:235–9. https://doi.org/10.3109/00365548609032332
20. Funke G, Altwegg M, Frommelt L, von Graevenitz A. Emergence of related nontoxigenic *Corynebacterium diphtheriae* biotype mitis strains in Western Europe. Emerg Infect Dis. 1999;5:477–80. https://doi.org/10.3201/eid0503.990326
21. Gubler J, Huber-Schneider C, Gruner E, Altwegg M. An outbreak of nontoxigenic *Corynebacterium diphtheriae* infection: single bacterial clone causing invasive infection among Swiss drug users. Clin Infect Dis. 1998;27:1295–8. https://doi.org/10.1086/514997
22. European Centre for Disease Prevention and Control. Cutaneous diphtheria among recently arrived refugees and asylum seekers in the EU [cited 2024 May 8]. https://www.ecdC.europa.eu/sites/default/files/media/en/publications/Publications/Diphtheria-cutaneous-EU-July-2015.pdf
23. Kofler J, Ramette A, Iseli P, Stauber L, Fichtner J, Droz S, et al. Ongoing toxin-positive diphtheria outbreaks in a federal asylum centre in Switzerland, analysis July to September 2022. Euro Surveill. 2022;27:2200811. https://doi.org/10.2807/1560-7917.ES.2022.27.44.2200811
24. European Centre for Disease Prevention and Control. Increase of reported diphtheria cases among migrants in Europe due to *Corynebacterium diphtheriae*, 2022. [cited 2022 Nov 1]. https://www.ecdc.europa.eu/sites/default/files/documents/diphtheriacases-migrantseurope-corynebacterium-diphtheriae-2022.pdf
25. Robert Koch Institute. National guidelines for diphtheria [in German] [cited 2025 Feb 9]. https://edoc.rki.de/bitstream/handle/176904/3683/diphtherie.pdf
26. Konrad R, Berger A, Huber I, Boschert V, Hörmansdorfer S, Busch U, et al. Matrix-assisted laser desorption/ionisation time-of-flight (MALDI-TOF) mass spectrometry as a tool for rapid diagnosis of potentially toxigenic Corynebacterium species in the laboratory management of diphtheria-associated bacteria. Euro Surveill. 2010;15:19699.
27. Schuhegger R, Lindermayer M, Kugler R, Heesemann J, Busch U, Sing A. Detection of toxigenic *Corynebacterium diphtheriae* and *Corynebacterium ulcerans* strains by a novel real-time PCR. J Clin Microbiol. 2008;46:2822–3. https://doi.org/10.1128/JCM.01010-08
28. Melnikov VG, Berger A, Sing A. Detection of diphtheria toxin production by toxigenic corynebacteria using an optimized Elek test. Infection. 2022;50:1591–5. https://doi.org/10.1007/s15010-022-01903-x
29. Berger A, Badell E, Åhman J, Matuschek E, Zidane N, Kahlmeter G, et al. *Corynebacterium diphtheriae* and *Corynebacterium ulcerans*: development of EUCAST methods and generation of data on which to determine breakpoints. J Antimicrob Chemother. 2024;79:968–76. https://doi.org/10.1093/jac/dkae056
30. Gautret P, Botelho-Nevers E, Brouqui P, Parola P. The spread of vaccine-preventable diseases by international travellers: a public-health concern. Clin Microbiol Infect. 2012;18(Suppl 5):77–84. https://doi.org/10.1111/j.1469-0691.2012.03940.x
31. Jong EC. Immunizations for international travel. Infect Dis Clin North Am. 1998;12:249–66. https://doi.org/10.1016/S0891-5520(05)70004-0
32. Shandera WX. Travel-related diseases: injury and infectious disease prevention. J Wilderness Med. 1993;4:40–61. https://doi.org/10.1580/0953-9859-4.1.40
33. Ly TDA, Castaneda S, Hoang VT, Dao TL, Gautret P. Vaccine-preventable diseases other than tuberculosis, and homelessness: a scoping review of the published literature, 1980 to 2020. Vaccine. 2021;39:1205–24. https://doi.org/10.1016/j.vaccine.2021.01.035
34. Badiaga, Sékéné, Didier Raoult, and Philippe Brouqui. Preventing and controlling emerging and reemerging transmissible diseases in the homeless. Emerg Infect Dis. 2008:14:1353–9.
35. Xiaoli L, Benoliel E, Peng Y, Aneke J, Cassiday PK, Kay M, et al. Genomic epidemiology of nontoxigenic *Corynebacterium diphtheriae* from King County, Washington State, USA, between July 2018 and May 2019. Microbial Genomics. 2020;6:e000467.
36. Gruner E, Opravil M, Altwegg M, von Graevenitz A. Nontoxigenic Corynebacterium *diphtheriae* isolated from intravenous drug users. Clin Infect Dis. 1994;18:94–6. https://doi.org/10.1093/clinids/18.1.94
37. Gaillet M, Hennart M, Sainte Rose V, Badell E, Michaud C, Blaizot R, et al. Retrospective study of infections with *Corynebacterium diphtheriae* species complex, French Guiana, 2016–2021. Emerg Infect Dis. 2024;30:1545–54.
38. Chêne L, Morand J-J, Badell E, Toubiana J, Janvier F, Marthinet H, et al. Cutaneous diphtheria from 2018 to 2022: an observational, retrospective study of epidemiological, microbiological, clinical, and therapeutic characteristics in metropolitan France. Emerg Microbes Infect. 2024; 13:2408324.
39. Ikejezie J, Adebusoye B, Ekezie W, Langley T, Lewis S, Phalkey R. Modifiable risk factors for diphtheria: a systematic review and meta-analysis. Glob Epidemiol. 2023;5:100100. https://doi.org/10.1016/j.gloepi.2023.100100
40. Ozawa S, Yemeke TT, Evans DR, Pallas SE, Wallace AS, Lee BY. Defining hard-to-reach populations for vaccination. Vaccine. 2019;37:5525–34. https://doi.org/10.1016/j.vaccine.2019.06.081
41. Vaughan E, Tinker T. Effective health risk communication about pandemic influenza for vulnerable populations. Am J Public Health. 2009;99(Suppl 2):S324–32. https://doi.org/10.2105/AJPH.2009.162537
42. Melo JS, Mittal ML, Horyniak D, Strathdee SA, Werb D. Injection drug use trajectories among migrant populations: a narrative review. Subst Use Misuse. 2018;53:1558–70. https://doi.org/10.1080/10826084.2017.1416404
43. United Nations International Children's Emergency Fund. COVID-19 pandemic fuels largest continued backslide in vaccinations in three decades [cited 2022 Jul 22]. https://www.unicef.org/press-releases/WUENIC2022release
44. World Health Organization. Clinical management of diphtheria: guideline, 2 February 2024. Geneva: The Organization; 2024.

Address for correspondence: Jonas Haller, Gesundheitsamt Frankifurt am Main–Infectious Diseases, Breite Gasse 28, Frankfurt am Main Hessen 60313, Germany; email: jonas.haller@stadt-frankfurt.de

Macrolide-Resistant *Mycoplasma pneumoniae* Infections among Children after COVID-19 Pandemic, Ohio, USA

Amy L. Leber, Tori Embry, Kathy Everhart, Jeanette Taveras, Sophonie J. Oyeniran, Huanyu Wang

Mycoplasma pneumoniae infections decreased in Ohio, USA, during the COVID-19 pandemic but reemerged in 2023; >2,000 cases were reported during September 2023–September 2024. Of 995 *M. pneumoniae*–positive samples, 24 (2.4%) had mutations for macrolide-resistant *M. pneumoniae* (MRMp). MRMp rates are low but increasing. MRMp surveillance is crucial for monitoring antimicrobial resistance.

Mycoplasma pneumoniae is a major pathogen of community-acquired respiratory infection in school-age children, accounting for 10%–40% of community-acquired pneumonia among hospitalized children (*1*). *M. pneumoniae* is endemic worldwide, and epidemics occur every few years (*1*). During the COVID-19 pandemic, public health measures taken to reduce transmission of SARS-CoV-2 also decreased *M. pneumoniae*, and we saw almost no *M. pneumoniae* activity in pediatric patients at Nationwide Children's Hospital (NCH), Columbus, Ohio, USA. Since the fall of 2023, reports of *M. pneumoniae* infection have increased worldwide (*2*). In central Ohio, we observed a reemergence of *M. pneumoniae* activity in children beginning in September 2023 and a sharp increase in the summer of 2024.

Macrolides are the drug of choice for treating *M. pneumoniae* infections (*3*). Macrolide resistance is conferred by point mutations within the V region of 23S rRNA, which interferes with bacterial protein synthesis leading to organism death. The most common mutation is the change of A to G at location 2063 of the gene (A2063G), accounting for >95% of the *M. pneumoniae* variants in the United States, along with the A2064G mutation (*4*). During 2015–2018, macrolide-resistant *M. pneumoniae* (MRMp) rates in the United States ranged from 2.1% to 18.3% (*5*); in a similar period, we reported a 2.8% MPMp rate in our pediatric population (*6*). With the reemergence of *M. pneumoniae*, we sought to determine the rate of MRMp infections in children in central Ohio.

Author affiliations: Nationwide Children's Hospital, Columbus, Ohio, USA (A.L. Leber, T. Embry, K. Everhart, J. Taveras, S.J. Oyeniran, H. Wang); The Ohio State University, Columbus (A.L. Leber, J. Taveras, S.J. Oyeniran, H. Wang)

DOI: https://doi.org/10.3201/eid3103.241570

The Study

The microbiology laboratory at NCH offers 2 tests to detect *M. pneumoniae*: FilmArray Respiratory Panel version 2.1 (RP2.1; BioFire Diagnostics, https://www.biofiredx.com) (*7*) and a standalone laboratory-developed PCR (*8*,*9*). During September 1, 2023–September 30, 2024, we identified patients ≤21 years of age testing positive for *M. pneumoniae* by RP2.1 or PCR. Patient sample collection occurred in inpatient, outpatient, and emergency department (ED) settings (Appendix Table 1, https://wwwnc.cdc.gov/EID/article/31/3/24-1570-App1.pdf). We retrieved a subset of remnant specimens for further characterization, as previously described (*6*) (Appendix).

We collected data on patient demographics, symptoms, clinical and laboratory findings, and hospitalization status from electronic health records. We analyzed age by Kruskal-Wallis test and reported medians and interquartile ranges (IQRs). We analyzed categorical variables by χ^2 test and conducted analyses by using GraphPad (GraphPad Software Inc., https://www.graphpad.com).

During the study period, the NCH microbiology laboratory performed 18,035 tests and identified 2,616 (14.5%) *M. pneumoniae*–positive samples from 2,469 unique patients during 2,478 medical encounters

Table 1. Dates and characteristics of testing for macrolide-resistant *Mycoplasma pneumoniae* infections among children after COVID-19 pandemic, Ohio, USA*

Date	Total no. tested	*M. pneumoniae*–positive, no. (%)	No. (%) sequenced	Macrolide-resistant, no. (%)
2023				
Sep	818	5 (0.6)	0	NA
Oct	1,001	29 (2.9)	0	NA
Nov	1,348	59 (4.4)	0	NA
Dec	1,697	62 (3.7)	0	NA
2024				
Jan	1,388	57 (4.1)	6 (10.5)	0
Feb	1,303	29 (2.3)	6 (20.7)	0
Mar	1,085	45 (4.2)	1 (2.2)	0
Apr	965	56 (5.8)	27 (48.2)	0
May	1,045	106 (10.1)	47 (44.3)	0
Jun	1,020	266 (28.1)	145 (54.1)	1 (0.7)
Jul	1,318	407 (30.9)	226 (55.5)	2 (0.9)
Aug	2,009	642 (32.0)	285 (44.4)	10 (3.9)
Sep	3,038	853 (28.1)	252 (29.5)	11 (4.4)
Total	18,035	2,616 (14.5)	995 (38.0)	24 (2.4)

*NA, not applicable.

(Table 1; Figure). *M. pneumoniae* positivity rates remained steady during September 2023–May 2024, then rose sharply in early June 2024. The median age of *M. pneumoniae*–positive patients was 8.8 (IQR 5.8–11.6) years; 1,317 (53.3%) were male and 1,152 (46.7%) female (Table 2). Among patients, 304 (12.3%) were hospitalized and 53 (2.1%) required intensive care unit (ICU) admission. Among the 359 *M. pneumoniae*–positive patients who had RP2.1 testing or RP2.1 and PCR testing, 129 (35.9%) had codetection of other respiratory pathogens on the panel; all were viruses (Table 2). The most common codetections were rhinovirus/enterovirus (n = 93, 72.0%) and adenovirus (n = 15, 11.6%).

During January 2024–September 2024, we attempted to sequence 1,096 (41.9%) of 2,616 positive samples and successfully sequenced 995 (91%). Among successfully sequenced samples, 85 (35.4%) were from inpatients, 787 (39.8%) from outpatients, and 123 (30.9%) from ED patients. We detected mutations associated with MRMp in 24 (2.4%) samples; 22 were A2063G, 1 A2064G, and 1 A2064T. The percentage of resistance detected differed by month, and the highest rate (4.4%) was detected in September 2024 ($p = 0.0466$) (Table 1; Figure). The median age of those 24 patients was 8.4 (IQR 5.0–9.8) years; 15 (62.5%) were male and 9 (37.5%) female. Among MRMp–positive patients, 5 (20.8%) had previous azithromycin

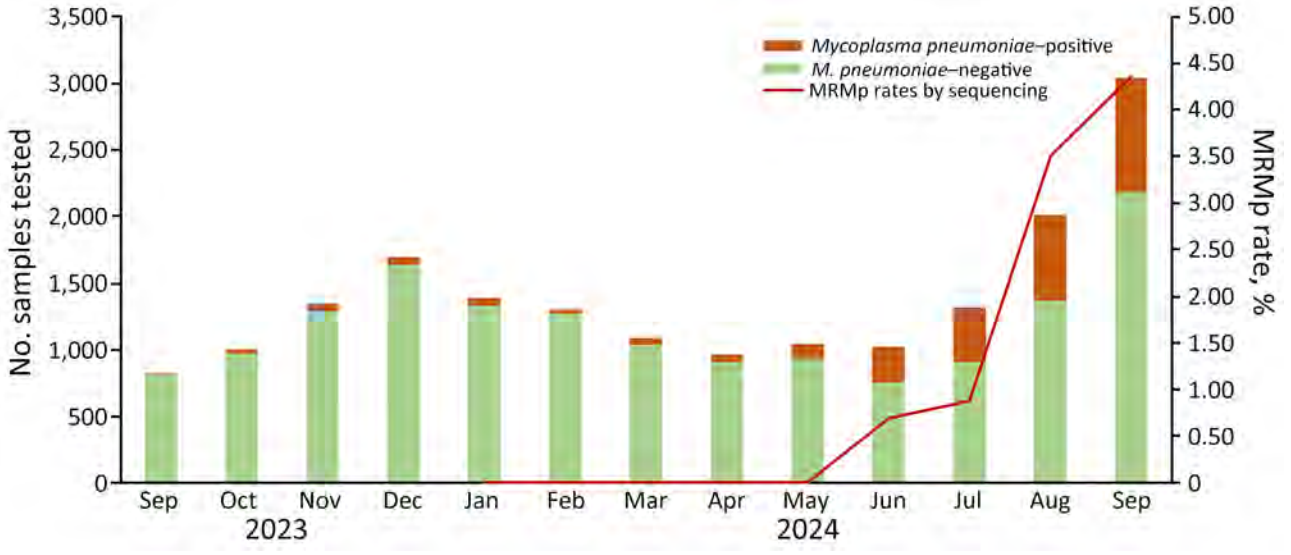

Figure. Monthly testing volumes and rates of MRMp infections among children after COVID-19 pandemic, Ohio, USA. Samples were tested for *Mycoplasma pneumoniae* infection during September 2023–September 2024 by FilmArray Respiratory Panel version 2.1 (BioFire Diagnostics, https://www.biofiredx.com), an in-house *M. pneumonia* PCR, or both. Macrolide resistance was determined in a subset of samples. MRMp rates were not available during September 2023–December 2023. MRMp, macrolide-resistant *Mycoplasma pneumoniae*.

Table 2. Laboratory characteristics for macrolide-resistant *Mycoplasma pneumoniae* infections among children after COVID-19 pandemic, by age group, Ohio, USA*

Characteristics	Total no.	Age group, y				p value
		<2	2 to <6	6 to <10	≥10	
No. samples tested	18,035	5,288	4,373	3,401	4,973	NA
M. pneumoniae–positive	2,616 (14.5)	109 (2.1)	601 (13.7)	904 (26.6)	1,002 (20.1)	<0.0001
Sequenced	995 (38.0)	30 (27.5)	224 (37.3)	363 (40.2)	378 (37.7)	NA
Macrolide-resistant	24 (2.4)	1 (3.3)	6 (2.7)	12 (3.3)	6 (1.6)	NS
No. positive unique patients	2,469	82	572	865	950	NA
Sex						
M	1,317 (53.3)	48 (58.5)	319 (55.8)	457 (52.8)	493 (51.9)	NS
F	1,152 (46.7)	34 (41.4)	253 (44.2)	408 (47.2)	457 (48.1)	
No. medical encounters	2,478	83	575	866	954	NA
Hospitalization	304 (12.3)	23 (27.7)	91 (15.8)	81 (9.4)	109 (11.4)	<0.0001
Intensive care unit admission	53 (2.1)	6 (7.2)	19 (3.3)	14 (1.6)	14 (1.5)	0.0009
RP2.1 tested	359	31	98	100	130	NA
Codetection†	129 (35.9)	19 (61.3)	51 (52.0)	31 (31.0)	28 (21.5)	<0.0001

*Values are no. (%) except as indicated. NA, not applicable; NS, not statistically significant; RP2.1, FilmArray Respiratory Panel version 2.1 (BioFire Diagnostics, https://www.biofiredx.com).
†Codetection of *M. pneumoniae* and other viruses.

exposure, and 5 required hospitalization (Appendix Table 2). Two patients had another *M. pneumoniae*–positive sample collected 3–4 weeks before the sample from which mutations were detected. In both cases, we sequenced the prior sample and detected no mutations. Those 2 patients received azithromycin at both of their clinical encounters.

M. pneumoniae positivity rates were significantly higher among children >6 years of age (p<0.0001). The rate among children <2 years of age was 2.1% compared with 26.6% among children 6–10 years of age. In contrast, the hospital and ICU admission rates were higher for children <2 years of age (p<0.001) (Table 2). Younger children also had higher rates of codetection; 61.3% of children <2 years of age had other respiratory pathogens detected (p<0.001) (Table 2). Mutations were detected in all age groups.

During the COVID-19 pandemic, introduction of nonpharmaceutical interventions interrupted epidemics of other respiratory pathogens, resulting in a substantial decline of respiratory infections worldwide (*10*). Since 2021, other respiratory pathogens have resurged after those interventions were lifted and community transmission returned (*11*). However, we detected little *M. pneumoniae* activity in our patient population until September 2023. That delayed reemergence has also been reported from other parts of the world (*11*). Unlike other areas where *M. pneumoniae* has reemerged with case numbers similar to or slightly higher than prepandemic times (*12*,*13*), the ongoing *M. pneumoniae* surge in our patient population is the largest we have seen in the past 10 years, >2,000 cases in 4 months (June 2024–September 2024), compared with 1,350 total cases during January 2012–January 2019.

Although more children were infected with *M. pneumoniae* in 2024, the hospitalization and ICU admission rates were lower than our previous prepandemic report (*6*). That reduction is possibly because of the increased availability of molecular testing and greater awareness of *M. pneumoniae* testing during periods of heightened activity; 70% of testing orders came from outpatient or ED visits. The progression and severity of this *M. pneumoniae* reemergence has yet to be evaluated.

Surveillance data from the Centers for Disease Control and Prevention (https://www.cdc.gov/mycoplasma/php/surveillance) suggest that the 2024 *M. pneumoniae* surge involved more young children (2–4 years). However, incidence of *M. pneumoniae* infection in our cohort remained highest among school-age children and adolescents. The median age of *M. pneumoniae*–positive children in this study was similar to our previous prepandemic report (*6*). Other countries also observed higher detection among school-age children and adolescents during the 2023–2024 *M. pneumoniae* surge (*12*,*14*).

MRMp has been reported globally and rates vary between regions. Few data are available in the United States, particularly after the COVID-19 pandemic. One report from southeast Germany showed a 2.6% resistance rate among 2023–2024 *M. pneumoniae* strains (*15*); another study from southern China found a 96.4% resistance rate after COVID-19 (*12*). We found that the MRMp rate remains low in this study population; only 2.4% of detected *M. pneumoniae* carried the mutation. However, MRMp rates increased in September 2024 (4.4%) compared with June 2024 (0.7%) and May 2024 (n = 0) (p = 0.0466). We sequenced 38.0% of *M. pneumoniae*–positive samples across all age groups and clinical settings, thus reflecting MRMp rates across the patient population. More work is needed to understand MRMp in different patient populations and geographic locations and its effects on patient care.

One limitation of this study is that it was a single-center study; thus, MRMp rates might not reflect other US regions in or different populations. The data may continue to evolve because the *M. pneumoniae* surge is ongoing.

Conclusions

In summary, we report macrolide resistance in *M. pneumoniae* after COVID-19 in our community. Although MRMp remains low, MRMp is trending upward, underscoring the need for vigilant surveillance to provide accurate information for management of children with *M. pneumoniae* infection and maintain awareness of antimicrobial resistance.

This study was approved by the institutional review board of Nationwide Children's Hospital (NCH), Columbus, Ohio, USA (approval no. STUDY00004480).

A.L.L. received research funding from BioFire, Cepheid, and Luminex, and consulting fees from Medscape, BioRad, and QIAGEN. The remaining authors have no conflicts of interest.

About the Author

Dr. Leber is the director of clinical microbiology and immunoserology and professor of pathology and pediatrics, The Ohio State University. Her research interests include development of molecular infectious disease testing and sexually transmitted disease detection in adolescents and children.

References

1. Waites KB, Xiao L, Liu Y, Balish MF, Atkinson TP. *Mycoplasma pneumoniae* from the respiratory tract and beyond. Clin Microbiol Rev. 2017;30:747–809. https://doi.org/10.1128/CMR.00114-16
2. Edens C, Clopper BR, DeVies J, Benitez A, McKeever ER, Johns D, et al. Notes from the field: Reemergence of *Mycoplasma pneumoniae* infections in children and adolescents after the COVID-19 pandemic, United States, 2018–2024. MMWR Morb Mortal Wkly Rep. 2024;73:149–51. https://doi.org/10.15585/mmwr.mm7307a3
3. Bradley JS, Byington CL, Shah SS, Alverson B, Carter ER, Harrison C, et al.; Pediatric Infectious Diseases Society and the Infectious Diseases Society of America. The management of community-acquired pneumonia in infants and children older than 3 months of age: clinical practice guidelines by the Pediatric Infectious Diseases Society and the Infectious Diseases Society of America. Clin Infect Dis. 2011;53:e25–76. https://doi.org/10.1093/cid/cir531
4. Kim K, Jung S, Kim M, Park S, Yang HJ, Lee E. Global trends in the proportion of macrolide-resistant *Mycoplasma pneumoniae* infections: a systematic review and meta-analysis. JAMA Netw Open. 2022;5:e2220949. https://doi.org/10.1001/jamanetworkopen.2022.20949
5. Waites KB, Ratliff A, Crabb DM, Xiao L, Qin X, Selvarangan R, et al. Macrolide-resistant *Mycoplasma pneumoniae* in the United States as determined from a national surveillance program. J Clin Microbiol. 2019;57:e00968-19. https://doi.org/10.1128/JCM.00968-19
6. Lanata MM, Wang H, Everhart K, Moore-Clingenpeel M, Ramilo O, Leber A. Macrolide-resistant *Mycoplasma pneumoniae* infections in children, Ohio, USA. Emerg Infect Dis. 2021;27:1588–97. https://doi.org/10.3201/eid2706.203206
7. Leber AL, Everhart K, Daly JA, Hopper A, Harrington A, Schreckenberger P, et al. Multicenter evaluation of BioFire FilmArray Respiratory Panel 2 for detection of viruses and bacteria in nasopharyngeal swab samples. J Clin Microbiol. 2018;56:e01945-17. https://doi.org/10.1128/JCM.01945-17
8. Hardegger D, Nadal D, Bossart W, Altwegg M, Dutly F. Rapid detection of *Mycoplasma pneumoniae* in clinical samples by real-time PCR. J Microbiol Methods. 2000;41:45–51. https://doi.org/10.1016/S0167-7012(00)00135-4
9. Leber AL, Oyeniran SJ, Wang H. Reduced sensitivity of a multiplex commercial respiratory panel for detection of *Mycoplasma pneumoniae* is due to specimen type. J Clin Microbiol. 2024;62:e0113924. https://doi.org/10.1128/jcm.01139-24
10. Meyer Sauteur PM, Beeton ML, Uldum SA, Bossuyt N, Vermeulen M, Loens K, et al.; ESGMAC–MyCOVID Study Team. *Mycoplasma pneumoniae* detections before and during the COVID-19 pandemic: results of a global survey, 2017 to 2021. Euro Surveill. 2022;27:1–3. https://doi.org/10.2807/1560-7917.ES.2022.27.19.2100746
11. Meyer Sauteur PM, Beeton ML, Pereyre S, Bébéar C, Gardette M, Hénin N, et al.; European Society of Clinical Microbiology and Infectious Diseases (ESCMID) Study Group for Mycoplasma and Chlamydia Infections (ESGMAC), and the ESGMAC Mycoplasma pneumoniae Surveillance (MAPS) study group. *Mycoplasma pneumoniae*: delayed re-emergence after COVID-19 pandemic restrictions. Lancet Microbe. 2024;5:e100–1. https://doi.org/10.1016/S2666-5247(23)00344-0
12. Zhu X, Liu P, Yu H, Wang L, Zhong H, Xu M, et al. An outbreak of *Mycoplasma pneumoniae* in children after the COVID-19 pandemic, Shanghai, China, 2023. Front Microbiol. 2024;15:1427702. https://doi.org/10.3389/fmicb.2024.1427702
13. You J, Zhang L, Chen W, Wu Q, Zhang D, Luo Z, et al. Epidemiological characteristics of *Mycoplasma pneumoniae* in hospitalized children before, during, and after COVID-19 pandemic restrictions in Chongqing, China. Front Cell Infect Microbiol. 2024;14:1424554. https://doi.org/10.3389/fcimb.2024.1424554
14. Nordholm AC, Søborg B, Jokelainen P, Lauenborg Møller K, Flink Sørensen L, Grove Krause T, et al. *Mycoplasma pneumoniae* epidemic in Denmark, October to December, 2023. Euro Surveill. 2024;29:1–3. https://doi.org/10.2807/1560-7917.ES.2024.29.2.2300707
15. Dumke R. The high-incidence period of *Mycoplasma pneumoniae* infections 2023/2024 in southeast Germany was associated with a low level of macrolide resistance. Infection. 2024;52:2525–7. https://doi.org/10.1007/s15010-024-02336-4

Address for correspondence: Huanyu Wang, Department of Pathology & Laboratory Medicine, Nationwide Children's Hospital, 700 Children's Dr, Columbus, OH 43205, USA; email: huanyu.wang@nationwidechildrens.org

Simultaneous Detection of *Sarcocystis hominis*, *S. heydorni*, and *S. sigmoideus* in Human Intestinal Sarcocystosis, France, 2021–2024

Maxime Moniot, Patricia Combes, Damien Costa, Nicolas Argy, Marie-Fleur Durieux, Thomas Nicol, Céline Nourrisson, Philippe Poirier

To elucidate the epidemiology of *Sarcocystis* spp. parasites in human intestinal infections, we used high-throughput sequencing to investigate human intestinal sarcocystosis cases identified by microscopy in France during 2021–2024. Our results indicate that humans are a definitive host of *S. sigmoideus* parasites and that occurrence of multiple species in 1 patient is common.

The coccidian parasite *Sarcocystis* is one of the most frequently identified protozoa of warm-blooded and poikilothermic animals worldwide, causing an intestinal infection in the definitive host or an extraintestinal infection in the intermediate host (*1*). Human intestinal sarcocystosis (i.e., humans as the definitive host) is rarely reported (*2*–*6*); only 3 of nearly 200 described *Sarcocystis* species have been identified as responsible for human intestinal infections (*1*). Infection is acquired by ingesting raw or undercooked meat containing cysts of the parasite, such as pork for *S. suihominis* or beef for *S. hominis* and *S. heydorni* (*1*,*7*). One human case involving *S. cruzi* infection was also reported, but the presence of this species, for which canids are the definitive host, has yet to be confirmed in humans (*2*,*8*).

Genetic characterization of *Sarcocystis* spp. is commonly based on the mitochondrial cytochrome c oxidase subunit I (COI) gene sequence. Recently, Rubiola et al. described a new species that infects bovine muscle, named *S. sigmoideus* (*9*). Retrospective analyses of genomic data available in GenBank revealed that this species previously had been detected in 2 other carcasses in Italy and 6 in Belgium (*10*–*12*). The definitive host for this new species was still unknown (*9*). Here, we report the presence of *S. sigmoideus* sporocysts in feces from several human patients in France. We also report cases of *S. heydorni* infections and highlight a high frequency of patients infected with multiple species simultaneously.

According to the French Ministry of Health, data for these patients were collected as part of routine surveillance and epidemiologic investigations by the National Reference Center for Cryptosporidiosis, Microsporidia and Other Digestive Protozoa (Public Health Code Article L 1413-3, https://www.santepubliquefrance.fr/a-propos/nos-principes-fondateurs/centres-nationaux-de-reference-pour-la-lutte-contre-les-maladies-transmissibles-cnr). Therefore, this study is exempt from institutional review board review.

Author affiliations: CHU Clermont-Ferrand Service de Parasitologie-Mycologie, Clermont-Ferrand, France (M. Moniot); CHU Clermont-Ferrand Centre National de Référence des cryptosporidioses, microsporidies et autres protozooses digestives, Clermont-Ferrand (M. Moniot, P. Combes, D. Costa, C. Nourrisson, P. Poirier); Université Rouen Normandie, Rouen, France (D. Costa); CHU Rouen Centre National de Référence Cryptosporidioses, Microsporidies et autres protozooses digestives (Centre coordonnateur), Rouen (D. Costa); Hopital Bichat-Claude Bernard, Paris, France (N. Argy); MERIT UMR 216, IRD, Faculté de pharmacie de Paris, Université Paris Cité, Paris (N. Argy); Centre de biologie et de recherche en santé, Hôpital Universitaire Dupuytren, Limoges, France (M. Durieux); CHU Angers, Angers, France (T. Nicol); Microbes, Intestin, Inflammation et Susceptibilité de l'Hôte, UMR Inserm/Université Clermont Auvergne U1071, USC INRAE 1382, Clermont-Ferrand (C. Nourrisson, P. Poirier)

DOI: https://doi.org/10.3201/eid3103.241640

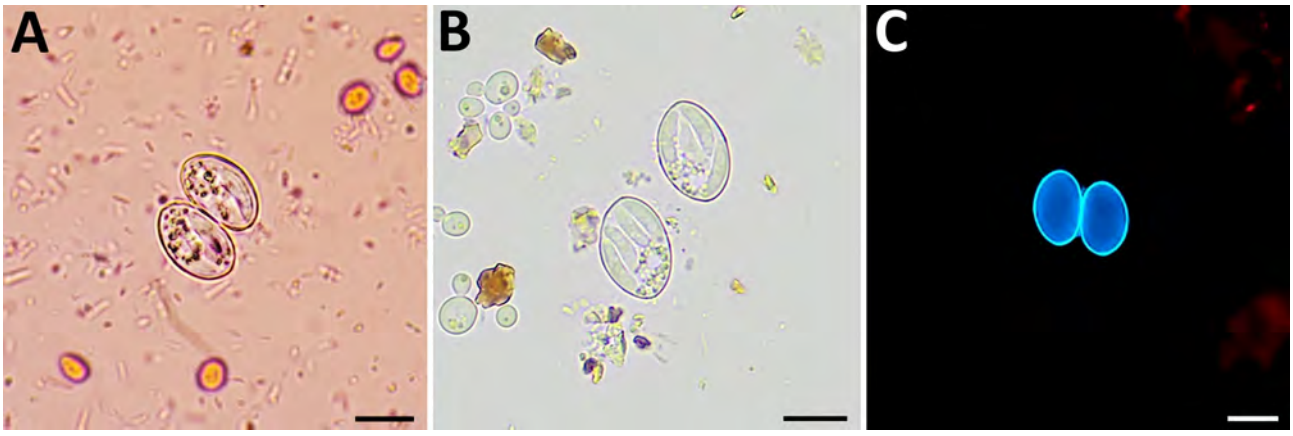

Figure 1. Oocysts of *Sarcocystis* spp. from patients with human intestinal sarcocystosis, France, 2021–2024. A) Concentrated stool smear stained using the merthiolate-iodine-formaldehyde method. Sporulated oocysts are colorless and contain 2 elongated sporocysts. The oocyst wall is thin and often invisible in wet mount. B) Wet mount. Each sporocyst contains 4 banana-shaped sporozoites and a granular sporocyst residuum, which may be compact or dispersed. The 4 sporozoites are rarely seen in a single plane of focus. C) Fresh homogenized stool smear under fluorescent microscopy. Individual sporocysts are autofluorescents and will appear blue with an excitation filter of 330–365 nm. Scale bars indicate 10 μm.

The Study

The patients included in this study underwent testing for intestinal parasites during October 2021–July 2024 because of gastrointestinal disorders or for systematic screening. Testing was performed in medical analysis laboratories by microscopic examination of fresh homogenized stool samples highlighting *Sarcocystis* spp. oocysts, sporocysts, or both (Figure 1). Oocysts/sporocysts were observed in 19 patients (Table), 8 women and 11 men, ranging in age from 19 to 94 years, all living in France. Of the 19 patients, 17 had reported acute, chronic, or occasional diarrhea lasting up to several months; the remaining 2 patients (case identification nos. S01-05 and S01-14) had infection diagnosed during systematic screening. No apparent cause other than *Sarcocystis* infection has been reported to explain the gastrointestinal disorders, except in 2 patients, 1 with concomitant *Salmonella* infection (case identification no. S01-03) and 1 with concomitant *Taenia saginata* infection (case identification no. S01-19). Some other symptoms were occasionally observed, such as abdominal pain, constipation, weight loss, nausea, ileitis, eosinophilia, or blood in stool (Table).

A total of 23 stool samples from the 19 patients were prospectively sent to the French National Reference Center for Cryptosporidiosis, Microsporidia and Other Digestive Protozoa for further molecular analysis (Appendix, https://wwwnc.cdc.gov/EID/article/31/3/24-1640-App1.pdf). In brief, high-throughput sequencing (HTS) was performed on a 332-bp region of the mitochondrial cytochrome c oxidase subunit I gene. We constructed a phylogenetic tree on the basis of the partial gene sequence from the 41 characterized *Sarcocystis* spp. isolates and reference sequences from GenBank by using the neighbor-joining method (Figure 2). The different *Sarcocystis* spp. contigs clustered with the reference sequences with a maximum variation of 2 nt over the 332-bp sequence analyzed (Table). Most (11/19) patients were co-infected with multiple *Sarcocystis* species (*S. hominis* was most frequently detected); *S. sigmoideus* infection was detected in 9 patients and *S. heydorni* infection in 5 patients.

Conclusions

Among the *Sarcocystis* parasite species present in beef meat (i.e., cattle as intermediate host), *S. hominis* was the first species reported to infect humans as the definitive host (*8*). Then, *S. heydorni* was indirectly considered to infect humans after it was observed in calves fed with sporocysts from the feces of a human volunteer (*7*). Our results expand on that previous report of human *S. heydorni* infection by identifying 5 more human cases. Recently, *S. sigmoideus* was described as a novel species in bovine carcasses. Felids were hypothesized to be the definitive hosts for this species, whereas identical samples harboring both *S. sigmoideus* and *S. hominis* suggested a potential zoonotic role (*9*). Here, we confirm at least the second hypothesis by reporting that humans are a definitive host of *S. sigmoideus*.

During the study period, we performed molecular analyses on microscopically positive fecal samples (i.e., detection of oocysts/sporocysts) from 19 patients and detected *S. sigmoideus* parasites in 9 of them. An association with *S. hominis* parasites was detected in 6 patients and with *S. hominis* plus *S. heydorni* parasites in 3 patients.

A limitation of our study is that we could not microscopically distinguish between sporocysts of different species because most patients were co-infected. We also had to consider that, after ingestion of infected meat, some transient *Sarcocystis* DNA resulted in HTS reads that were not associated with the sporocysts seen in the fecal samples. However, we excluded that possibility because repeated stools spaced over 3 to 24 days for 3 co-infected patients showed the same species in the same proportions (data not shown). Also, in the 19 cases analyzed, we never detected reads from *S. cruzi*, which is highly prevalent in beef meat but does not infect humans. To definitively confirm that hypothesis, future attempts should be made to perform single-cell sequencing on sporocysts/oocysts isolated from microscopy or by species-specific labeling with species-specific hybridization probes.

Table. Clinical manifestations and molecular findings for 19 cases of human intestinal sarcocystosis, France, 2021–2024*

Case ID	Age, y/sex	Signs/symptoms	Sample date	HTS		*Sarcocystis* species	GenBank accession no. of reference sequence
				Contigs	No. (%) reads		
S01-01	71/F	Acute diarrhea	2021 Oct 25	Contig 1	4,405 (83.2)	*S. sigmoideus*	OR543013
				Contig 2	730 (13.8)	*S. hominis*	OR543019
S01-02	94/F	Chronic diarrhea, alternating constipation	2022 Jan 22	Contig 1	2,470 (46.1)	*S. sigmoideus*	OR543013
				Contig 2	1,582 (29.5)	*S. hominis*	OR543021
				Contig 3	342 (6.4)	*S. hominis*	MK497842
S01-03	33/F	Acute diarrhea, abdominal pain, ileitis, *Salmonella* infection	2022 Aug 21	Contig 1	5,768 (64.7)	*S. hominis*	OR543021
				Contig 2	2,993 (33.6)	*S. hominis*	MK497842
S01-04	48/M	Abdominal pain, anal itching	2023 Feb 23	Contig 1	3,065 (56.1)	*S. hominis*	OR543021
				Contig 2	2,399 (43.9)	*S. hominis*	MK497842
S01-05	35/F	None†	2023 Mar 16	Contig 1	2,674 (73.4)	*S. hominis*	MK497842
				Contig 2	914 (25.1)	*S. heydorni*	KX057995
S01-06	73/M	Chronic diarrhea, abdominal pain, weight loss, eosinophilia	2023 May 9	Contig 1	4,767 (95.2)	*S. sigmoideus*	OR543013
				Contig 2	99 (2.0)	*S. hominis*	OR543021
S01-08	24/F	Acute diarrhea, nausea	2023 Jun 19	Contig 1	3,213 (68.5)	*S. hominis*	OR543019
				Contig 2	750 (16.0)	*S. heydorni*	KX057995
				Contig 3	673 (8.0)	*S. hominis*	MK497842
S01-09	76/F	Chronic diarrhea, abdominal pain	2023 Aug 30	Contig 1	2,787 (50.6)	*S. hominis*	OR543019
				Contig 2	1,881 (34.2)	*S. hominis*	MK497842
				Contig 3	603 (11.0)	*S. sigmoideus*	OR543013
S01-10	22/F	Chronic diarrhea, asthenia, multiple food intolerances, fibroscopic gastritis and rectitis	2023 Nov 14	Contig 1	5,049 (100)	*S. hominis*	OR543021
S01-11	19/M	Occasional diarrhea, sometimes blood in feces	2023 Nov 18	Contig 1	1,653 (39.5)	*S. sigmoideus*	OR543013
				Contig 2	1,049 (25.1)	*S. hominis*	OR543021
				Contig 3	927 (22.2)	*S. heydorni*	KX057995
S01-12	68/F	Chronic diarrhea, abdominal pain	2023 Dec 11	Contig 1	2,410 (48.8)	*S. hominis*	OR543021
				Contig 2	961 (19.4)	*S. hominis*	MK497842
				Contig 3	869 (17.6)	*S. sigmoideus*	OR543013
S01-13	26/M	Abdominal pain	2023 Dec 18	Contig 1	5,072 (99.9)	*S. hominis*	OR543021
S01-14	57/M	None‡	2024 Jan 9	Contig 1	4,246 (97.4)	*S. hominis*	OR543019
S01-15	79/M	Chronic diarrhea, abdominal pain, CDP 10 y prior	2024 Apr 3	Contig 1	1,428 (36.1)	*S. hominis*	OR543021
				Contig 2	767 (19.4)	*S. hominis*	MK497842
				Contig 3	696 (17.6)	*S. heydorni*	KX057995
				Contig 4	662 (16.7)	*S. sigmoideus*	OR543013
S01-16	62/M	Chronic diarrhea, abdominal pain	2024 Jun 12	Contig 1	1,171 (28.6)	*S. hominis*	MK497842
				Contig 2	1,153 (28.2)	*S. sigmoideus*	OR543013
				Contig 3	641 (15.7)	*S. heydorni*	KX057995
				Contig 4	590 (16.9)	*S. hominis*	OR543021
S01-18	73/M	Acute diarrhea, weight loss	2023 Jan 10	Contig 1	4,103 (100)	*S. hominis*	MK497842
S01-19	52/M	Chronic diarrhea, abdominal pain, weight loss, ulcerative colitis, *Taenia saginata* infection	2023 Sep 29	Contig 1	7,302 (100)	*S. hominis*	OR543019
S01-27	63/M	Abdominal pain, nausea, eosinophilia	2024 Jul 10	Contig 1	4,696 (99.9)	*S. hominis*	OR543021
S01-28	48/M	Chronic diarrhea, rectal cancer diagnosis	2024 Jul 22	Contig 1	3,976 (57.2)	*S. sigmoideus*	OR543013
				Contig 2	2,578 (37.1)	*S. hominis*	OR543021

*CDP, cephalic duodenopancreatectomy; HTS, high-throughput sequencing; ID, identification.
†Preemployment medical screening of food industry worker.
‡Systematic screening in kidney transplantation.

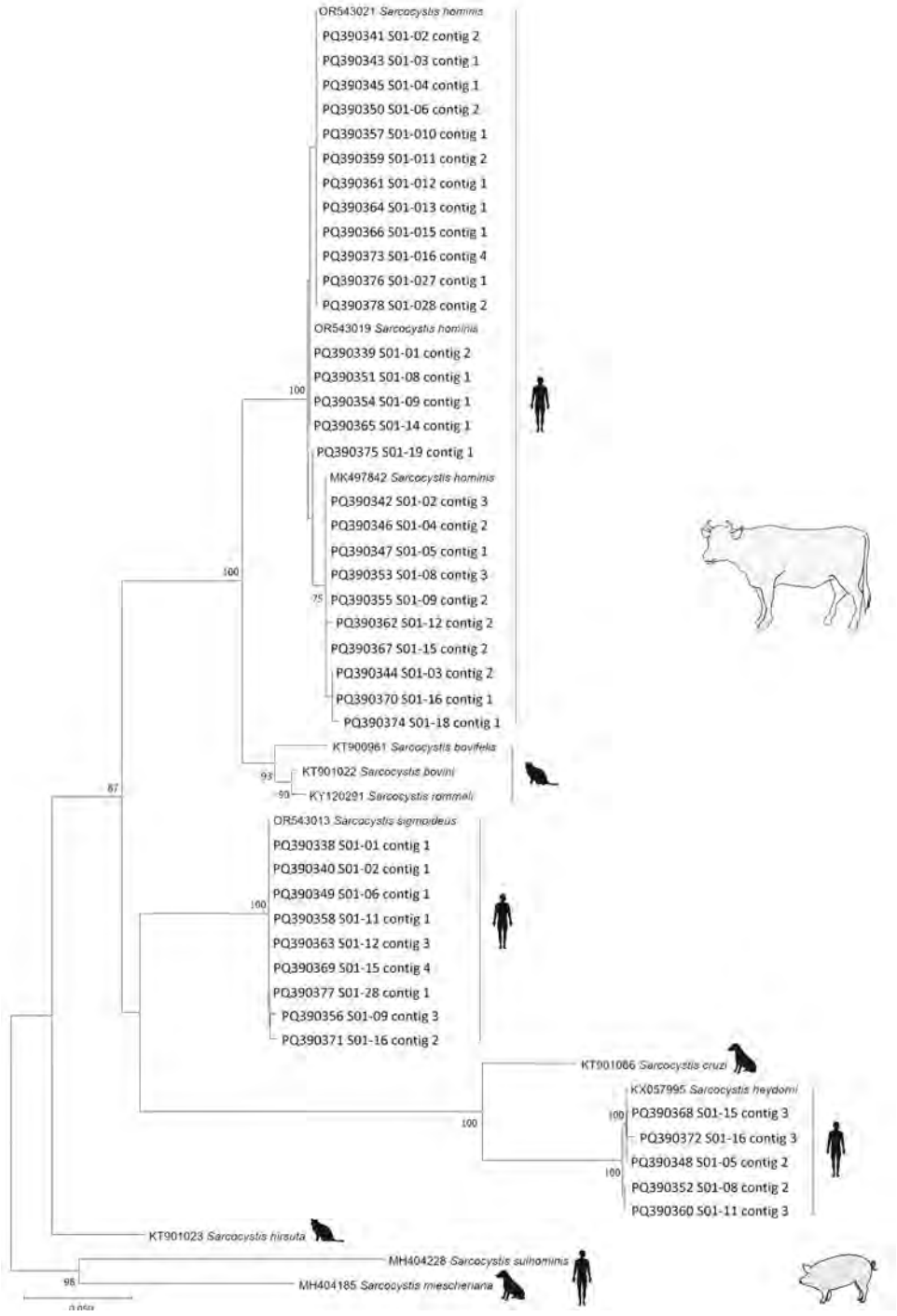

Figure 2. Phylogenetic tree for human *Sarcocystis* spp. from human intestinal sarcocystosis, France, 2021–2024. Tree is based on 54 partial mitochondrial cytochrome c oxidase subunit I gene sequences from patients compared with reference sequences from GenBank. The 41 sequences of 332 bp generated in this study are identified by patient numbers (i.e., S01-02); GenBank accession numbers are provided for reference sequences. This analysis included the 10 taxa described in pigs and cattle (intermediate hosts, blank illustrations) with the corresponding definitive host (humans, felids, or canids, black illustrations). The tree was inferred by using the neighbor-joining method and rooted on the species whose pigs serve as the intermediate hosts, *S. miescheriana* and *S. suihominis*. Evolutionary distances were computed using the Tamura-Nei method. Branch consensus support is expressed as percentage from 1,000 bootstraps and is reported next to the branches; branch support values <75% were not included. Scale bar indicates base substitutions per site.

The prevalence of *S. sigmoideus* parasites in cattle has been reported to be low, but it is likely to be underestimated, as suggested by the number of infected patients (9 of 19) in our study (*9*). Further molecular studies in cattle and human stool are needed to better estimate the real prevalence of *S. sigmoideus* parasites.

We used HTS for molecular analysis of *Sarcocystis* spp. parasites in human stools and found that human intestinal sarcocystosis is mainly caused by multiple species simultaneously (11 of 19 patients were co-infected). That finding is in accordance with recent veterinary data that detected *Sarcocystis* spp. parasites in 64% of randomly sampled cattle carcasses and mixed infections of up to 3 species simultaneously (including *S. sigmoideus* and *S. hominis*) in 25% of intralesional samples and in 5.8% of extralesional samples from

carcasses condemned because of the presence of bovine eosinophilic myositis (*9*,*10*).

S. hominis parasites are considered mildly pathogenic in humans, whereas *S. suihominis* infection is more virulent (*1*). However, data about *Sarcocystis* pathogenicity are scarce, outdated, and mostly derived from volunteers who ingested experimentally infected meat (*1*). The pathogenicity of *S. heydorni* and *S. sigmoideus* parasites is unknown, and further studies are required to address that issue. In conclusion, our data demonstrate that humans are a definitive host for *S. sigmoideus* parasites and that intestinal sarcocystosis frequently results from infection with multiple species.

The datasets generated and analyzed during the study are available from the corresponding author on reasonable request.

This work was supported by internal laboratory funding. This research did not receive any specific grant from funding agencies in the public, commercial, or not-for-profit sectors.

The authors declare no conflict of interest. The authors declare that no chatbot or artificial intelligence tool was used for any part of the work.

Author contributions: P.P., C.N., and M.M. conceived and designed the study. M.M., D.C., N.A., M.-F.D., and T.N. collected data. M.M. conducted the literature search and drafted the manuscript. P.C. performed sequencing experimentation. All authors edited and approved the final manuscript.

About the Author

Dr. Moniot is a parasitologist and mycologist working in the University Hospital of Clermont-Ferrand, France. His research interests are focused on the epidemiological investigation of parasitic diseases.

References

1. Dubey JP, Calero-Bernal R, Rosenthal BM, Speer CA, Fayer R. Sarcocystosis of animals and humans. Boca Raton (FL): CRC Press; 2015.
2. Agholi M, Shahabadi SN, Motazedian MH, Hatam GR. Prevalence of enteric protozoan oocysts with special reference to *Sarcocystis cruzi* among fecal samples of diarrheic immunodeficient patients in Iran. Korean J Parasitol. 2016;54:339–44. https://doi.org/10.3347/kjp.2016.54.3.339
3. Agholi M, Taghadosi Z, Mehrabani D, Zahabiun F, Sharafi Z, Motazedian MH, et al. Human intestinal sarcocystosis in Iran: there but not seen. Parasitol Res. 2016;115:4527–33. https://doi.org/10.1007/s00436-016-5244-6
4. Rubiola S, Civera T, Ferroglio E, Zanet S, Zaccaria T, Brossa S, et al. Molecular differentiation of cattle *Sarcocystis* spp. by multiplex PCR targeting 18S and COI genes following identification of *Sarcocystis hominis* in human stool samples. Food Waterborne Parasitol. 2020;18:e00074. https://doi.org/10.1016/j.fawpar.2020.e00074
5. Van Den Broucke S, Dorny P, Van Esbroeck M, Bottieau E. Microscopic detection of intestinal *Sarcocystis* infection diagnosed in international travelers at the Institute of Tropical Medicine, Antwerp, Belgium, from 2001 to 2020. Am J Trop Med Hyg. 2023;109:327–31. https://doi.org/10.4269/ajtmh.22-0577
6. Fayer R, Esposito DH, Dubey JP. Human infections with *Sarcocystis* species. Clin Microbiol Rev. 2015;28:295–311. https://doi.org/10.1128/CMR.00113-14
7. Dubey JP, van Wilpe E, Calero-Bernal R, Verma SK, Fayer R. *Sarcocystis heydorni*, n. sp. (Apicomplexa: Sarcocystidae) with cattle (*Bos taurus*) and human (*Homo sapiens*) cycle. Parasitol Res. 2015;114:4143–7. https://doi.org/10.1007/s00436-015-4645-2
8. Dubey JP, Rosenthal BM. Bovine sarcocystosis*: Sarcocystis* species, diagnosis, prevalence, economic and public health considerations, and association of *Sarcocystis* species with eosinophilic myositis in cattle. Int J Parasitol. 2023;53:463–75. https://doi.org/10.1016/j.ijpara.2022.09.009
9. Rubiola S, Moré G, Civera T, Hemphill A, Frey CF, Basso W, et al. Detection of *Sarcocystis hominis*, *Sarcocystis bovifelis*, *Sarcocystis cruzi*, *Sarcocystis hirsuta* and *Sarcocystis sigmoideus* sp. nov. in carcasses affected by bovine eosinophilic myositis. Food Waterborne Parasitol. 2024;34:e00220. https://doi.org/10.1016/j.fawpar.2024.e00220
10. Zeng H, Van Damme I, Kabi TW, Šoba B, Gabriël S. *Sarcocystis* species in bovine carcasses from a Belgian abattoir: a cross-sectional study. Parasit Vectors. 2021;14:271. https://doi.org/10.1186/s13071-021-04788-1
11. Vangeel L, Houf K, Geldhof P, De Preter K, Vercruysse J, Ducatelle R, et al. Different *Sarcocystis* spp. are present in bovine eosinophilic myositis. Vet Parasitol. 2013;197:543–8. https://doi.org/10.1016/j.vetpar.2013.06.001
12. Rubiola S, Civera T, Panebianco F, Vercellino D, Chiesa F. Molecular detection of cattle *Sarcocystis* spp. in North-West Italy highlights their association with bovine eosinophilic myositis. Parasit Vectors. 2021;14:223. https://doi.org/10.1186/s13071-021-04722-5

Address for correspondence: Philippe Poirier, Service de Parasitologie Mycologie, 58 rue Montalembert, CHU Gabriel Montpied, 63003 Clermont-Ferrand CEDEX 1, France; email: ppoirier@chu-clermontferrand.fr

National Active Case-Finding Program for Tuberculosis in Prisons, Peru, 2024

Esther Jung, Valentina A. Alarcón, Wilfredo Santos Solís Tupes, Tatiana Avalos-Cruz, Marco Tovar, Erika Abregu, Max Z. Yang, Jason R. Andrews,[1] Moises A. Huaman[1]

During January–September 2024, a national active case-finding program in Peru's prisons screened >38,000 persons for tuberculosis (TB) using chest radiography with automated interpretation and rapid molecular tests. The program found high percentages of TB, rifampin-resistant TB, and asymptomatic infections, demonstrating the urgent need for systematic screening among incarcerated populations.

Global tuberculosis (TB) incidence declined over the past decade, but incidence in prisons remained high, and incidence increased in Latin America (*1*). Overcrowding, poor ventilation, and diagnostic delays amplify TB transmission, and incidence among incarcerated persons in Latin America is 27 times higher than among the general population (*2*). The rise in TB in Latin America's prisons has more than offset reductions in the general population, undermining progress toward international goals to end TB (*3*).

To address the disproportionate TB burden among incarcerated persons, the World Health Organization (WHO) recommended active case-finding for TB in prisons (*4*). However, few standardized nationwide screening efforts have been made in prisons in low- and middle-income countries (LMICs). In Peru, TB screening and treatment has primarily relied on symptom-based screening or passive case detection, without a systematic screening program irrespective of symptoms. In 2023, the Peruvian National TB Program (DPCTB) initiated countrywide screening using chest radiography with computer-detection software, clinical evaluation, and rapid molecular diagnostic testing in high TB–burdened prisons. We evaluated the programmatic yield of that initiative and assessed how each screening component contributed to case identification.

The Study

Peru has a population of 34 million, among whom 96,805 are incarcerated (*5*,*6*). In 2022, national TB incidence was estimated at 153 cases/100,000 person-years (*6*), but incidence in the prison population was 2,746 cases/100,000 person-years (*7*). In September 2023, DPCTB initiated an active case-finding program in 12 male, 1 co-ed, and 5 female prisons chosen for size, TB burden, and accessibility for DPCTB staff (Figure 1).

We analyzed programmatic data from persons ≥18 years of age not treated for active TB and screened with chest radiography during January–September 2024. Screening teams included a physician, nurse, and radiology technician. Participants were interviewed for demographic, clinical, and symptom information, then screened with portable digital radiographs that were evaluated by Computer-Aided Detection for Tuberculosis (CAD4TB) version 7.0 (Delft Imaging Systems, https://delft.care). CAD4TB scores radiographs on the basis of abnormalities suggestive of TB. All participants were evaluated by a physician.

Participants with CAD4TB scores ≥40 (considered abnormal) were asked to produce a sputum sample; participants with scores <40 were only asked

Author affiliations: Stanford University School of Medicine, Stanford, California, USA (E. Jung, M.Z. Yang, J.R. Andrews); Dirección de Prevención y Control de Tuberculosis (DPCTB), Ministerio de Salud, Lima, Peru (V.A. Alarcón, W.S. Solís Tupes, T. Avalos-Cruz, E. Abregu); Instituto de Investigación Nutricional, Lima (M. Tovar); Escuela de Medicina, Universidad Peruana de Ciencias Aplicadas, Lima (M. Tovar); University of Cincinnati College of Medicine, Cincinnati, Ohio, USA (M.A. Huaman)

DOI: https://doi.org/10.3201/eid3103.241727

[1]These senior authors contributed equally to this article.

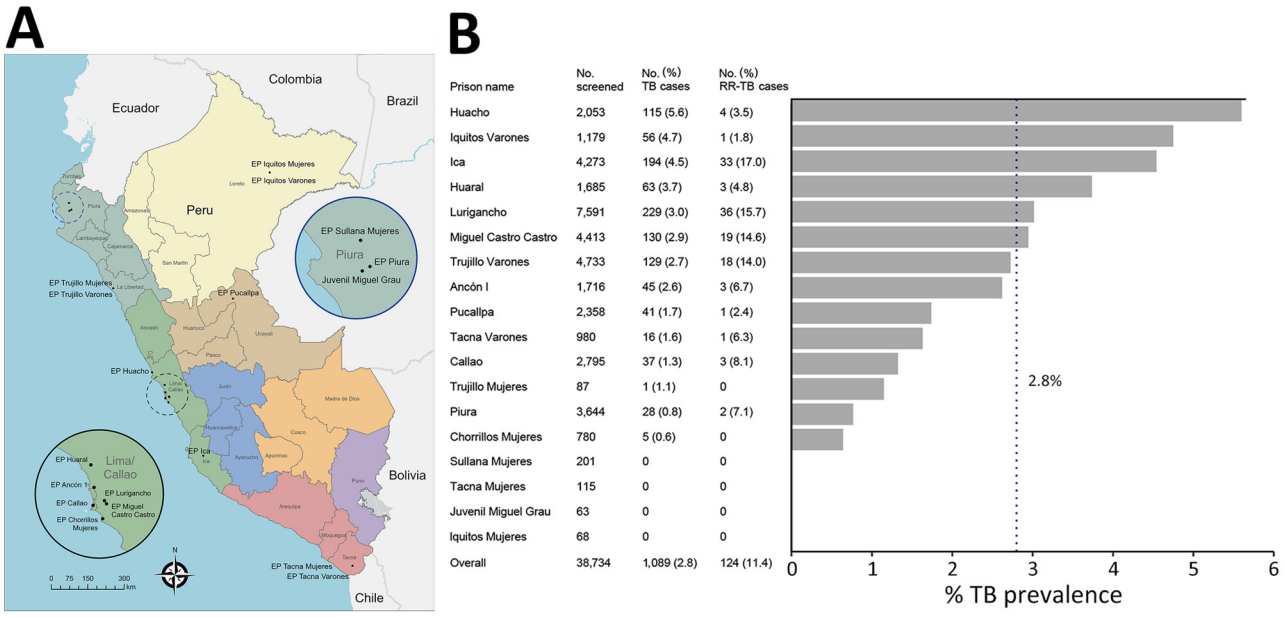

Figure 1. Locations and screening results in a national active case-finding program for TB in prisons, Peru, 2024. A) Locations of 18 facilities included in screening procedures; insets magnify Lima/Callao and Piura departments. B) Bar diagram displaying TB and RR-TB prevalence by prison, sorted by descending TB prevalence. RR-TB percentage is of total TB cases. Dotted line shows overall TB prevalence of 2.8% across all prisons. TB cases were defined as any positive or trace result via Xpert MTB/RIF Ultra (Cepheid, https://www.cepheid.com). EP, Establecimiento Penitenciario (penitentiary establishment); Juvenil Miguel Grau, Centro Juvenil de Diagnóstico y Rehabilitación Miguel Grau; Mujeres, women's prison, RR-TB, rifampin-resistant TB; TB, tuberculosis; Varones, men's prison.

for a sputum sample if the physician suspected TB on the basis of symptoms or evaluation. Teams performed rapid molecular diagnostic testing on sputum samples by using Xpert MTB/RIF Ultra assay (hereafter Xpert; Cepheid, https://www.cepheid.com). We defined a TB case as any Xpert-positive result or Xpert result indicating trace *Mycobacterium tuberculosis* DNA levels. All persons with confirmed TB, including drug-resistant TB, received free treatment through directly observed therapy in prison clinics and were isolated in dedicated cells.

During January–September 2024, DPCTB screened 38,734 eligible participants, representing >80% of the population (48,376 persons) across 18 study prisons (*8*). We collected sputum from 7,291 (18.8%) participants, and 6,873 (94.3%) samples produced valid Xpert results; supply issues at the time of screening prevented Xpert testing for 308 samples (Figure 2). To evaluate demographic and clinical characteristics, we used multivariable logistic regression with fixed effects for prisons to estimate crude odds ratios (ORs) and adjusted ORs (aORs) and 95% CIs, accounting for age, sex, TB history, TB contact, and Peru birth. We calculated sputum positivity and TB case percentages by combinations of symptom screening and CAD4TB results. We used R version 4.4.1 (The R Project for Statistical Computing, https://www.r-project.org) for statistical analyses.

Among participants, 96% were male, 4% were female, 94% were born in Peru, and median age was 35 (IQR 27–43) years. In addition, 16% of participants reported TB history and 40% shared a cell with a known case (Table 1). We diagnosed TB in 1,089 (2.8%) participants. Prevalence ranged from no cases in small prisons (those with <250 persons) to 5.6% in Huacho (population of 2,053). Female prisons had prevalences <1.5%, and 8 of 12 male prisons had prevalences >2%. Among Xpert-positive samples, 11.4% (124/1,089) were rifampin-resistant TB (RR-TB); 4 prisons recorded >10% RR-TB (Figure 1).

Among participants, 15.3% (5,908) had abnormal CAD4TB scores, and 11.9% (4,613) reported symptoms in the 2 weeks before participation. Among participants providing sputum samples, Xpert positivity varied substantially by symptom and radiograph status: 6.8% of participants with symptoms but CAD4TB scores <40 accounted for 7.8% of detected cases, 12.2% with abnormal scores but no symptoms accounted for 40.9% of cases, and 26.2% with symptoms and abnormal scores comprised 49.8% of cases (Table 2). Odds of TB were higher among participants with TB history (aOR 2.75, 95% CI 2.41–3.13) and TB contact (aOR 1.90, 95% CI 1.56–2.30) (Table 1). Odds of RR-TB were higher among persons with TB history (aOR 1.96 95% CI 1.32–2.91) (Appendix Table, https://wwwnc.cdc.gov/EID/article/31/3/24-1727-App1.pdf).

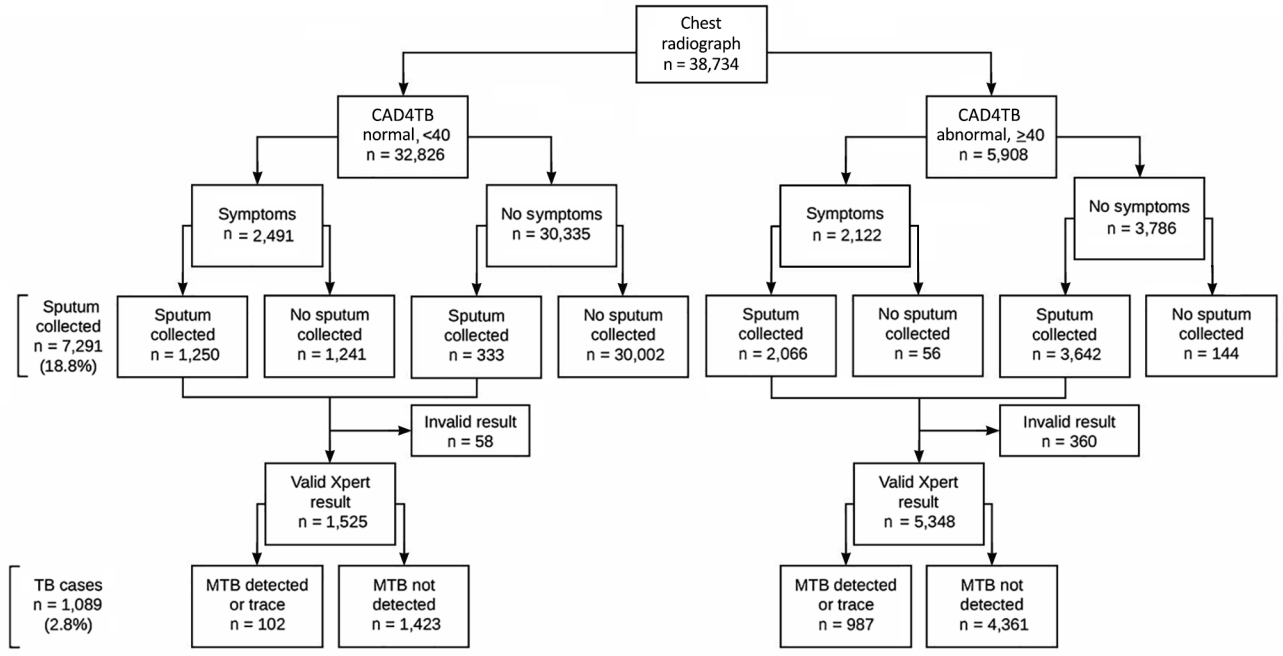

Figure 2. Flowchart for TB screening in a national active case-finding program for tuberculosis in prisons, Peru, 2024. The algorithm shows screening among included participants across 18 study prisons. TB cases were defined as any positive or trace result via Xpert MTB/RIF Ultra (Cepheid, https://www.cepheid.com). CAD4TB, Computer-Aided Detection for Tuberculosis version 7.0 (Delft Imaging Systems, https://delft.care); MTB, *Mycobacterium tuberculosis*; TB, tuberculosis; Xpert, Xpert MTB/RIF Ultra (Cepheid, https://www.cepheid).

One limitation of this study is that we did not analyze HIV; however, HIV testing was performed on <5% of participants and prevalence was low (0.01% self-reported; 0 cases among 1,165 screened), consistent with national reports (*9*). Another limitation is that we did not analyze other TB risk factors because of missing or sparse data; however, this implementation study focused on describing the TB burden among the incarcerated population. In addition, the lack of genotype data prevented distinguishing relapse from reinfection, despite previous TB being high among both drug-sensitive and drug-resistant cases. Finally, this study was limited to 18 high-burden prisons, hindering generalizability to other

Table 1. Multivariable logistic regression analysis of demographic characteristics and risk factors for tuberculosis in a national active case-finding program for TB in prisons, Peru, 2024*

Risk factor	No. tested	No. (%) TB confirmed	OR (95% CI)	p value	aOR (95% CI)†	p value
Age group, y						
18–29	11,193	382 (3.4)				
30–44	17,557	486 (2.8)	0.81 (0.70–0.92)	0.002	0.68 (0.59–0.78)	<0.001
45–60	7,708	169 (2.2)	0.64 (0.53–0.77)	<0.001	0.54 (0.45–0.65)	<0.001
>60	2,274	52 (2.3)	0.67 (0.49–0.88)	0.006	0.58 (0.42–0.77)	<0.001
NA	2	0				
Sex						
M	37,227	1,081 (2.9)	5.61 (3.00–12.33)	<0.001	3.78 (1.20–22.94)	0.062
F	1,507	8 (0.5)				
TB history						
Y	6,232	397 (6.4)	3.16 (2.78–3.58)	<0.001	2.75 (2.41–3.13)	<0.001
N	32,502	692 (2.1)				
TB contact						
Y	15,459	556 (3.6)	1.61 (1.43–1.82)	<0.001	1.90 (1.56–2.30)	<0.001
N	23,275	533 (2.3)				
Peru origin						
Y	36,596	1,054 (2.9)	1.80 (1.30–2.57)	0.001	1.67 (1.20–2.41)	0.004
N	2,138	35 (1.6)				

*The program screened 38,734 incarcerated persons during January–September 2024. aOR, adjusted odds ratio; NA, not available; OR, odds ratio; TB, tuberculosis.
†aORs include fixed effects for prison and are adjusted for age, sex, TB history, TB contact, and Peru origin.

Table 2. Predictive value of CAD4TB, symptom screening, and sputum testing among participants in a national active case-finding program for TB in prisons, Peru, 2024*

CAD4TB score	Symptoms	No. (%)	Sputum collected	TB confirmed		
				No. confirmed	% TB cases (95% CI)†	% Sputum positivity (95% CI)‡
<40						
	N	30,335 (78.3)	333	17	1.6 (0.9–2.5)	5.1 (3.0–8.1)
	Y	2,491 (6.4)	1,250	85	7.8 (6.3–9.6)	6.8 (5.5–8.3)
≥40						
	N	3,786 (9.8)	3,642	445	40.9 (37.9–43.9)	12.2 (11.2–13.3)
	Y	2,122 (5.5)	2,066	542	49.8 (46.8–52.8)	26.2 (24.4–28.2)
Total		38,734	7,291	1,089		

*CAD4TB, Computer-Aided Detection for Tuberculosis version 7.0 (Delft Imaging Systems, https://delft.care); TB, tuberculosis.
†TB case defined as any positive or trace result via Xpert MTB/RIF Ultra (Cepheid, https://www.cepheid.com).
‡Sputum positivity calculated as percentage of individuals with sputum collected who are confirmed to have TB via Xpert MTB/RIF Ultra (Cepheid).

facilities in Peru, and the absence of disease duration data restricted comparisons between study prevalence and prior incidence estimates.

Nonetheless, this study provides TB prevalence estimates in Peru's carceral system on the basis of molecular testing covering nearly half of the country. Since 2020, Peru has remained among WHO's 30 countries with the highest burden of drug-resistant TB, and ≈8.3% of new diagnoses annually are drug-resistant (*6*,*10*). Our study detected high (2,800/100,000 persons) TB and RR-TB (11.4%) prevalences. Those findings likely are underestimated because we did not screen persons with previously diagnosed TB or persons on TB treatment, and we only collected sputum from participants with radiographic anomalies, symptoms, or clinical suspicion of TB. In addition, 200 persons with abnormal chest radiographs were not able to provide sputum. Including clinical inference as a criterion would likely have captured additional TB.

Asymptomatic TB is a hidden threat in high-transmission settings like LMIC prisons. Previous estimates suggest that asymptomatic TB represents a considerable proportion of active disease and transmission in general and incarcerated populations (*11*,*12*). In this study, 42.5% of TB cases were asymptomatic, likely an underestimate because of symptom criteria in the screening algorithm, suggesting that symptom-only case-finding would greatly delay or miss active TB infections among incarcerated populations.

Conclusions

Effective, scalable, active case-finding models are critically needed in LMIC prisons, where nearly half of TB cases go undetected annually (*13*). In Peru, mobile health teams screened >38,000 incarcerated persons in 8 months, covering 40% of the national incarcerated population. That large-scale implementation of active case-finding revealed high prevalences of RR-TB and undiagnosed TB. In addition, 42.5% of persons with Xpert-confirmed TB had no clinical symptoms. Those findings illustrate the importance of systematic TB screening in prisons, particularly for asymptomatic persons.

In summary, our data demonstrated that active case-finding can identify large reservoirs of undiagnosed TB and be performed efficiently at scale in prisons by teams of health professionals. Because TB and RR-TB prevalence is high, intensive screening, including annual or biannual mass screenings, and targeted interventions like TB preventive therapy are essential (*14*,*15*). Such strategies and sustainable financing need to be incorporated into national TB programs to establish, implement, and maintain programs in LMIC prisons, where the TB burden demands urgent attention.

This article was preprinted at https://www.medrxiv.org/content/10.1101/2024.11.08.24317002v1.

Acknowledgments

We thank the Peruvian National TB Program team for providing data and assistance during this study.

This study was reviewed by the Stanford Institutional Review Board and was determined not to be human subjects research. This project has been registered in the INS-Peru study registry (PRISA) (no. EI00000003259).

About the Author

Ms. Jung is a research program coordinator at Stanford University School of Medicine, Stanford, California, USA. Her research interests include environmental and infectious disease epidemiology in marginalized populations.

References

1. Walter KS, Martinez L, Arakaki-Sanchez D, Sequera VG, Estigarribia Sanabria G, Cohen T, et al. The escalating tuberculosis crisis in central and South American prisons. Lancet. 2021;397:1591–6. https://doi.org/10.1016/S0140-6736(20)32578-2

2. Cords O, Martinez L, Warren JL, O'Marr JM, Walter KS, Cohen T, et al. Incidence and prevalence of tuberculosis in incarcerated populations: a systematic review and meta-analysis. Lancet Public Health. 2021;6:e300–8. https://doi.org/10.1016/S2468-2667(21)00025-6
3. World Health Organization. The End TB Strategy: global strategy and targets for tuberculosis prevention, care and control after 2015 [cited 2024 Aug 23]. https://www.who.int/publications/i/item/WHO-HTM-TB-2015.19
4. World Health Organization. Consolidated guidelines on tuberculosis: Module 2: screening—systematic screening for tuberculosis disease [cited 2024 Aug 2]. http://www.ncbi.nlm.nih.gov/books/NBK569338
5. World Prison Brief. Peru [cited 2024 Jul 13]. https://www.prisonstudies.org/country/peru
6. World Health Organization. TB profile [cited 2025 Jan 6]. https://worldhealthorg.shinyapps.io/tb_profiles/?_inputs_&entity_type=%22country%22&iso2=%22PE%22&lan=%22EN%22
7. Ministerio de Salud del Perú. Dashboard Directorate of Tuberculosis Prevention and Control [in Spanish] [cited 2025 Jan 6]. http://www.tuberculosis.minsa.gob.pe/DashboardDPCTB/Dashboard.aspx
8. Peruvian National Penitentiary Institute (INPE). Statistical panel of the prison population [in Spanish] [cited 2024 Dec 20]. https://app.powerbi.com/view?r=eyJrIjoiMTE4M-ThmYTUtODEwZi00NTBmLWEyNTktNzFlNzc2ZGY2NzQ0IiwidCI6IjdlYzgyZDIwLTE0NmItNDZjNS04MDg2LTYyYjY1NjBhMTI0MiJ9&pageName=ReportSection38a5a6e96e0ed1e30e01
9. Hernández-Vásquez A, Huarez B. HIV in prison: results from a national prison census in Peru. Int J STD AIDS. 2018;29:203–5. https://doi.org/10.1177/0956462417744372
10. World Health Organization. Global tuberculosis report 2023 [cited 2024 Jul 23]. https://www.who.int/teams/global-tuberculosis-programme/tb-reports/global-tuberculosis-report-2023
11. Frascella B, Richards AS, Sossen B, Emery JC, Odone A, Law I, et al. Subclinical tuberculosis disease—a review and analysis of prevalence surveys to inform definitions, burden, associations, and screening methodology. Clin Infect Dis. 2021;73:e830–41. https://doi.org/10.1093/cid/ciaa1402
12. Kendall EA, Shrestha S, Dowdy DW. The epidemiological importance of subclinical tuberculosis. A critical reappraisal. Am J Respir Crit Care Med. 2021;203:168–74. https://doi.org/10.1164/rccm.202006-2394PP
13. Martinez L, Warren JL, Harries AD, Croda J, Espinal MA, Olarte RAL, et al. Global, regional, and national estimates of tuberculosis incidence and case detection among incarcerated individuals from 2000 to 2019: a systematic analysis. Lancet Public Health. 2023;8:e511–9. https://doi.org/10.1016/S2468-2667(23)00097-X
14. Charalambous S, Velen K, Rueda Z, Croda J, Herce ME, Shenoi SV, et al. Scaling up evidence-based approaches to tuberculosis screening in prisons. Lancet Public Health. 2023;8:e305–10. https://doi.org/10.1016/S2468-2667(23)00002-6
15. World Health Organization. WHO consolidated guidelines on tuberculosis: module 1: prevention—tuberculosis preventive treatment, second edition [cited 2024 Dec 9]. https://www.who.int/publications/i/item/9789240096196

Address for correspondence: Esther Jung, Stanford University School of Medicine, 240 Pasteur Dr, Stanford, CA 94304-1049, USA; email: esthjung@stanford.edu

EID Spotlight Topic

Tuberculosis

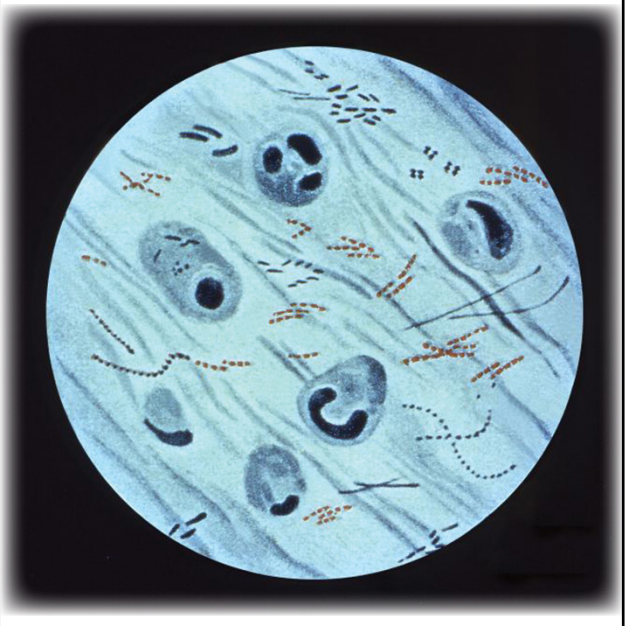

World TB Day, falling on March 24th each year, is designed to build public awareness that tuberculosis today remains an epidemic in much of the world, causing the deaths of nearly one-and-a-half million people each year, mostly in developing countries. It commemorates the day in 1882 when Dr. Robert Koch astounded the scientific community by announcing that he had discovered the cause of tuberculosis, the TB bacillus. At the time of Koch's announcement in Berlin, TB was raging through Europe and the Americas, causing the death of one out of every seven people. Koch's discovery opened the way towards diagnosing and curing TB.

http://wwwnc.cdc.gov/eid/page/world-tb-day

EMERGING INFECTIOUS DISEASES®

Mycobacterium ulcerans in Possum Feces before Emergence in Humans, Australia

Bridgette J. McNamara, Jack Cornish, Kim R. Blasdell, Eugene Athan, Naomi E. Clarke, Tiffany Pe, Mohammad Akhtar Hussain, Michael Muleme, Ee Laine Tay, Michael Dunn, Victoria Boyd, Anjana Karawita, Daniel P. O'Brien

We describe emergence of Buruli ulcer in urban Geelong, Victoria, Australia, and examine timing and proximity of human cases to detection of *Mycobacterium ulcerans* DNA in possum feces. *M. ulcerans*–positive feces preceded human cases by up to 39 months, constituting an early warning of impending risk for Buruli ulcer.

Buruli ulcer is a neglected tropical disease and remains a public health issue across south-eastern Australia (*1*). Manifesting as a necrotizing ulcer, Buruli ulcer is caused by the environmental pathogen *Mycobacterium ulcerans* (*2*). Although global case numbers are falling, the ongoing epidemic in Victoria, Australia, appears to be worsening (*3*), with a record 362 notified cases in Victoria in 2023. Historically concentrated in coastal areas in Victoria, more recent cases have emerged within noncoastal urban suburbs of Melbourne and Geelong (*4*); the reasons remain unclear. Temporal analysis of the phylogenic trees of Victoria *M. ulcerans* isolates suggests a 7- to 9-year lag time between the bacterium's arrival in an area and the emergence of human cases (*5*). Human acquisition routes may include mosquito bites (*6*), direct trauma, or contact with contaminated substrates, particularly in limb areas with exposed skin (*2*,*7*). Unlike in Africa, Australia shows evidence of zoonotic transmission, notably from native ringtail (*Pseudocheirus peregrinus*) and brushtail (*Trichosurus vulpecula*) possums, which inhabit native habitat across coastal and inland areas of Australia (*8*). Possum feces testing positive for *M. ulcerans* DNA found at residential properties correlated with higher likelihood of Buruli ulcer among residents (*9*); surveillance in possums enhances case prediction in humans (*10*), yet the timing of infection in possum populations related to the emergence of human cases has not been described. We describe the emergence of human Buruli ulcer cases in Geelong, Victoria, Australia, and their timing and proximity to *M. ulcerans*–positive possum feces.

The Study

We conducted a descriptive epidemiologic study, including a spatiotemporal clustering analysis of laboratory-confirmed and probable Buruli ulcer cases notified to the Department of Health Victoria during January 1, 2011–December 31, 2022, to identify new endemic areas in suburbs of Geelong, a city of ≈250,000 persons in southwest Victoria, Australia (Figure 1). We examined aggregate case numbers and incidence per 100,000 estimated resident population (*11*) at Australian Bureau of Statistics (ABS) Statistical Areas 2 (SA2) for the central Geelong suburbs and known endemic areas of the Bellarine Peninsula and Surf Coast. We examined geographic clustering of Geelong cases, mapped to ABS Meshblocks (small geographic areas, 3–40 dwellings), in a space-time analysis using Poisson models in SatScan (http://www.satscan.org). The models scan across geographic locations over time to detect areas and time periods where reported case numbers significantly exceed expected case numbers.

We used data from a systematic possum fecal survey conducted in Geelong suburbs in 2020 (*10*), as well as follow-up surveys conducted in a more restricted area of Geelong at 3, 6, and 24 months

Author affiliations: Barwon Health, Geelong, Victoria, Australia (B.J. McNamara, J. Cornish, E. Athan, N.E. Clarke, T. Pe, M.A. Hussain, M. Muleme, D.P. O'Brien); Centre for Innovation in Infectious Disease and Immunology Research, Geelong (B.J. McNamara, E. Athan, M.A. Hussain, M. Muleme, D.P. O'Brien); The University of Melbourne, Melbourne, Victoria, Australia (B.J. McNamara, D.P. O'Brien); CSIRO Australian Centre for Disease Preparedness, Geelong (K.R. Blasdell, M. Dunn, V. Boyd, A. Karawita); Deakin University, Geelong (E. Athan, T. Pe, M.A. Hussain); Victoria Department of Health, Melbourne (E.L. Tay)

DOI: https://doi.org/10.3201/eid3103.240657

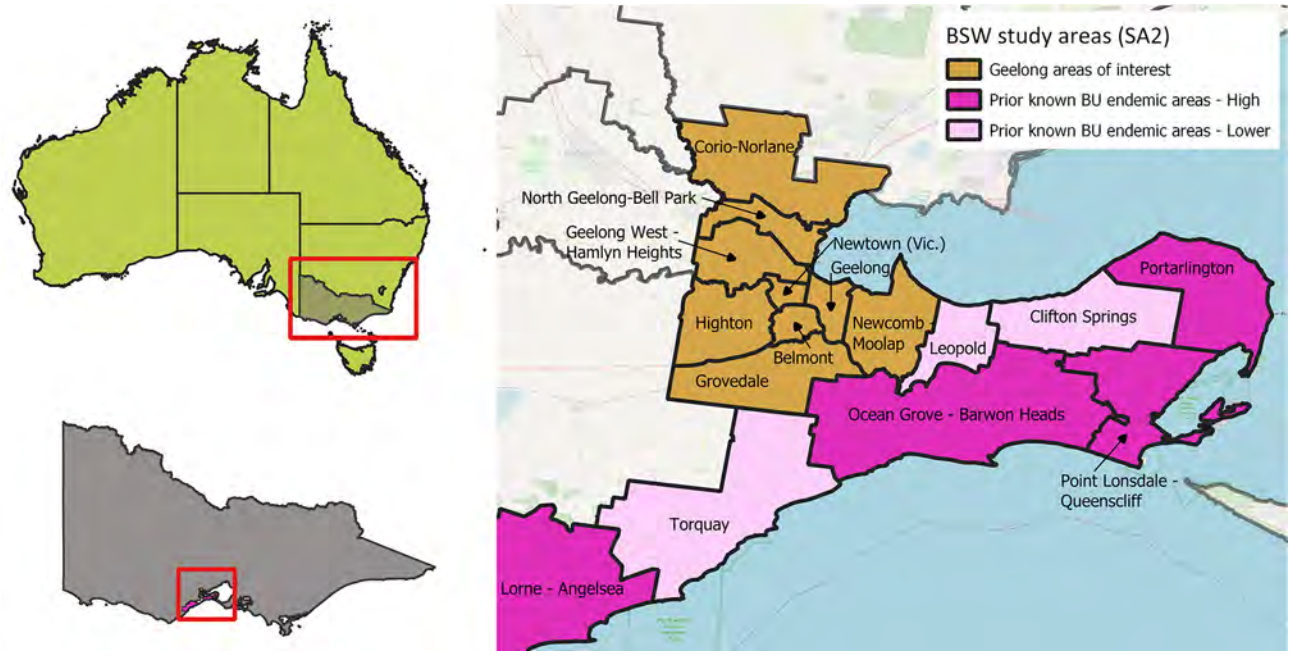

Figure 1. Location of central Geelong suburbs in Victoria, Australia, and prior known endemic areas in the Bellarine Peninsula and Surf Coast (higher case numbers dark pink, lower case numbers in light pink). We defined high incidence as >10 cases/100,000 population in 2017–2019. Belmont with the central Geelong suburbs also meets this criterion. SA2, Australian Bureau of Statistics Statistical Area 2.

later and several samples from Belmont in the pre-survey period in September 2019 (Appendix Figure 1, https://wwwnc.cdc.gov/EID/article/31/3/24-0657-App1.pdf). Fecal survey collection methods have been published previously (*10*,*12*). We used the data to examine the proximity and timing of human Buruli ulcer cases notified in 2020–2022 to feces from *M. ulcerans*–infected possums by calculating distance from Buruli ulcer case residence (in meters) and timing (in months) from the most proximal possum fecal sample collection to human case at notification.

During 2011–2022, a total of 402 Buruli ulcer cases were reported in the Barwon South West (BSW) catchment, including 80 cases within the SA2 locations of interest in central Geelong. We observed increasing case numbers and incidence in Belmont during 2017–2022 and in Highton and Newtown areas during 2020–2022 (Table 1); we identified 3 clusters where reported case numbers exceeded the number expected (Figure 2, panel C).

Of the 49 Buruli ulcer cases diagnosed since 2020 in Geelong suburbs, 39 case-patients resided within

Table 1. Cases and incidence of Buruli ulcer in a noncoastal urban area, Australia, 2011–2022*

Location	2020 population†	No. cases (no. per 100,000 patient-years)			
		2011–2013	2014–2016	2017–2019	2020–2022
Geelong SA2					
Belmont	14,829	3 (7.2)	0 (0.0)	9 (**20.5**)	24 (**53.5**)
Corio–Norlane	27,622	0 (0.0)	0 (0.0)	2 (2.4)	0 (0.0)
Geelong	13,781	2 (5.3)	0 (0.0)	1 (2.5)	1 (2.4)
Geelong West–Hamlyn Heights	21,272	2 (3.4)	0 (0.0)	0 (0.0)	2 (3.1)
Grovedale	31,579	0 (0.0)	0 (0.0)	3 (3.6)	4 (4.0)
Highton	23,869	3 (4.9)	1 (1.5)	1 (1.4)	12 (**16.6**)
Newcomb–Moolap	15,089	3 (6.7)	0 (0.0)	0 (0.0)	0 (0.0)
Newtown (Victoria.)	10,945	0 (0.0)	0 (0.0)	1 (3.1)	6 (**18.1**)
North Geelong–Bell Park	15,757	0 (0.0)	0 (0.0)	0 (0.0)	0 (0.0)
Bellarine and Surf Coast endemic SA2					
Ocean Grove–Barwon Heads	29,382	45 (**76.8**)	28 (**41.0**)	37 (**46.2**)	47 (**51.0**)
Point Lonsdale–Queenscliff	4,746	38 (**303.3**)	20 (**157.9**)	7 (**53.0**)	21 (**144.3**)
Portarlington	8,541	0 (0.0)	5 (**22.8**)	4 (**16.8**)	4 (**15.2**)
Lorne–Angelsea‡	5,615	0 (0.0)	0 (0.0)	6 (**37.1**)	8 (**46.8**)

*Data presented are for regions of interest in SA2 of Geelong and other recognized Bellarine Peninsula and Surf Coast disease-endemic areas. Bold text indicates incidence >10 per 100,000 person-years. SA2, Australian Bureau of Statistics Statistical Area 2.
†Australian Bureau of Statistics estimated resident population for 2020.
‡Includes Aireys Inlet, Angelsea, Lorne. Aireys Inlet, 7 cases since 2017; Anglesea, 5 cases since 2017.

areas included in the 2020 possum excreta survey (Figure 2). The median distance from case-patient residence to *M. ulcerans*–positive possum feces was 283 meters (Table 2). In all, 16/39 (41%) of the cases resided within 200 meters of a positive possum sample. The median distance to a positive possum sample was lower for cases within the identified clusters in Belmont, Highton, and Newtown (199 meters; 50% of case-patients resided within 200 meters of a positive possum sample) than cases who were not within the identified clusters (median 1,177 meters; 23% within 200 meters; p = 0.040 by rank-sum test). For cases within the central areas sampled in both 2020 and 2022 fecal surveys, the median distance from a case residence to a prior positive possum sample was only 108 meters (interquartile range [IQR] 82–263 meters).

The most geographically proximal detections of *M. ulcerans* in possum fecal samples preceded the emergence of human Buruli ulcer cases by up to 39 (IQR 8–29) months (Table 2). For cases in identified clusters, the most geographically proximal positive possum fecal samples to cases occurred with an IQR of 7–31 months before the case diagnosis, apart from 2 cases in which the closest positive detection (<100 meters) occurred after case diagnosis. For those cases, other positive possum feces within 250 meters of the case residence were detected 16 and 18 months before the case diagnosis. Of note, we observed few Buruli ulcer cases in the northern suburbs of Geelong during 2011–2022. Possum population density was lower in these suburbs; few to no possum feces were present during the 2020 excreta survey (Appendix Figure 1).

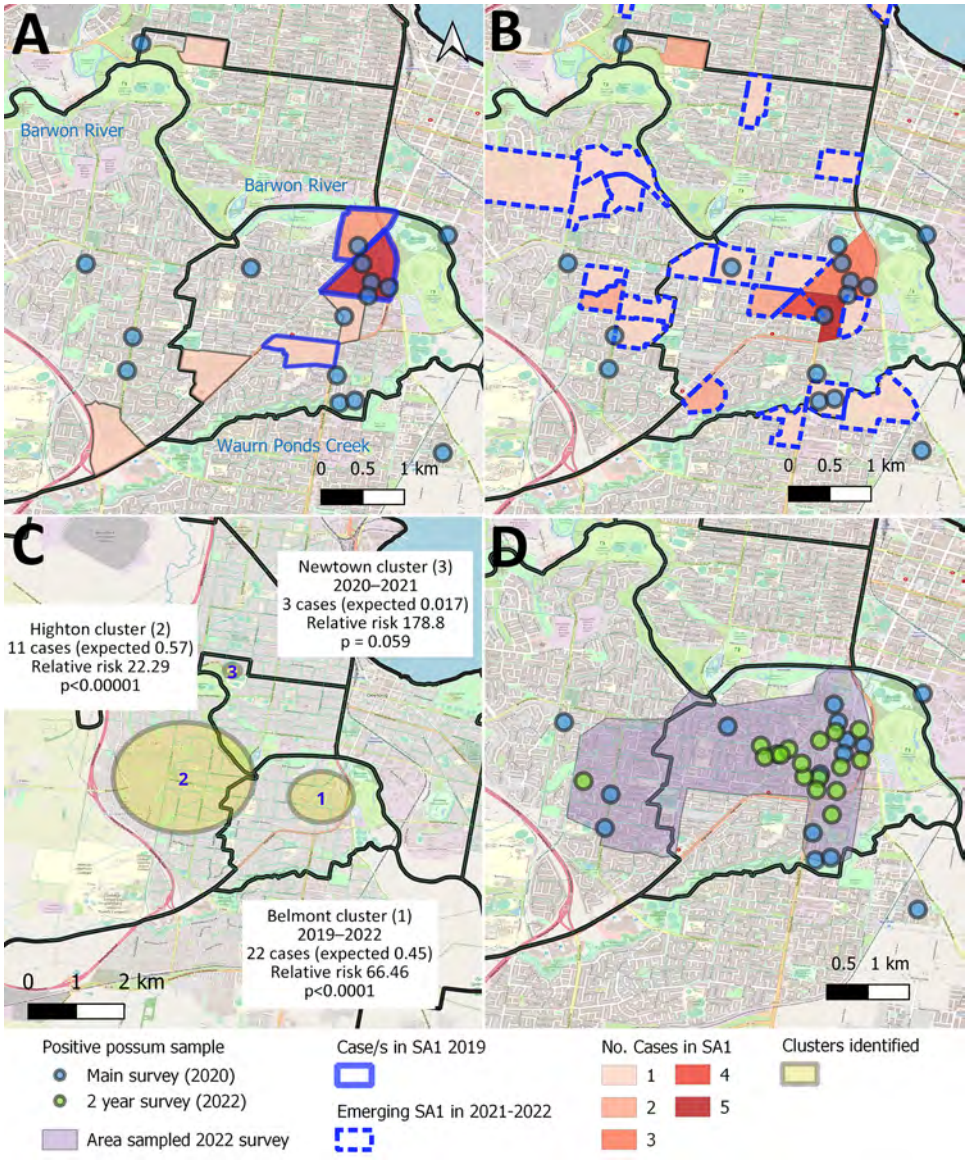

Figure 2. Distribution, clustering, and timing of Buruli ulcer cases in relation to *Mycobacterium ulcerans*–positive possum fecal samples, Victoria, Australia. A) Number and home location of human Buruli ulcer cases in Statistical Area SA1 in 2019–2020, compared with the distribution of *M. ulcerans*–positive possum fecal samples collected in the systematic main survey in 2020. Solid blue outline indicates areas in 2019 in which cases were tightly clustered during 2019; colored areas without borders had cases in 2020 only, B) Number and home location of human Buruli ulcer cases in Statistical Area SA1 in 2021–2022, compared with the distribution of *M. ulcerans*–positive possum fecal samples collected in the systematic main survey in 2020. Dashed blue outline indicates areas with cases only in 2021–2022 and not 2019–2020. Blue circles indicate 100-meter radius around the collection location. C) Spatiotemporal clustering of human Buruli ulcer cases from 2011–2022 in Geelong suburbs, Australia. The observed number of cases within each cluster are compared to the expected number for the estimated resident population of the area during the period (*3*), under the null hypothesis (no spatiotemporal clustering). D) Changing distribution of positive possum fecal samples from 2020 (blue) and 2022 (green).

Table 2. Proximity and timing of human cases of Buruli ulcer in areas with *Mycobacterium ulcerans*–positive possum fecal samples collected in 2020 and 2022, Australia*

Characteristic	Cases diagnosed since 2020	Cases within detected clusters	Cases not in detected clusters	Cases in 2-year follow-up survey area
Total cases	39	26	13	24
Distance from positive possum fecal sample, meters				
Median (IQR)	283 (92–1,025)	199 (88–393)	1177 (209–1,256)	108 (82–263)
Range	35–1,867	35–1,531	70–1,867	35–405
Proximity				
≤200 meters	16 (41)	13 (50)	3 (23)	16 (67)
≤500 meters	26 (67)	20 (77)	6 (46)	24 (100)
Months between possum detections and cases, median (IQR)	17 (8–29)	19 (8–31)	16 (11–26)	12 (7–28)

*Values are no. (%) except as indicated. Clusters here include the 3 identified clusters (Belmont, Highton, Newtown, as presented in Figure 2, panel C). All fecal samples positive by IS2404 from any of the surveys (presurvey samples September 2019, main 2020 survey, 3-mo, 6-mo, or 24-mo follow-up) were included in the measurement of proximity; the closest sample contributing to these summary measures.
†Month calculated as days divided by 30. Two cases with closest proximity samples <100 meters in 2022 (postdiagnosis in 2021) have been excluded from this time calculation, although both had relatively proximal detections (<250 meters) before diagnosis also.

No cases were reported in North Geelong-Bell Park SA2; 1 of the 2 cases reported in 2018 in Corio-Norlane SA2 resided within 344 meters of the subsequent single *M. ulcerans*–positive possum fecal detection in 2020. Analysis examining the timeliness of diagnosis in BSW demonstrated delays in Buruli ulcer diagnosis in emerging endemic areas.

Conclusions

Buruli ulcer endemicity in Victoria, Australia, is evolving. Our multidisciplinary investigation of human Buruli ulcer cases and *M. ulcerans* shedding in local possums describes the speed and pattern of spread in a large noncoastal urban center in Victoria. Since 2017, Buruli ulcer cases have increased and clustered within 3 Geelong suburbs, predominantly near possums shedding *M. ulcerans* in feces. Possum detection precedes human cases by months to years, suggesting that possum fecal surveillance for *M. ulcerans* may be useful in identifying emerging areas before the onset of human cases. Our findings support a recently published statistical model to predict the location of future human Buruli ulcer cases based on previous human cases and the location of positive possum fecal specimens (*10*); here, we defined the temporal relationship whereby infection appears in possums before humans in an emerging disease area. Furthermore, we quantified the time between the positive detections in possum populations and subsequent human cases. Our results suggest that possum fecal positivity may provide an early warning signal of emerging at-risk areas for Buruli ulcer. In Geelong, the Barwon South West Public Health Unit, established in late 2020, uses this information (*13*) to inform targeted efforts to enhance community awareness and clinician knowledge of the condition in relation to recommended behaviors aimed at disease prevention (*7*) and for testing for more timely diagnosis (*14*). Evidence that such recommendations reduce Buruli ulcer incidence is limited; further research is required to investigate this possibility. As human cases emerge, *M. ulcerans* detections in possum feces may help delineate new areas of local transmission from travel-related acquisition within known endemic areas, assisted by research into the ecology and transmission pathways of Buruli ulcer to develop interventions to reduce disease in both human and wildlife populations. Early detection of *M. ulcerans* shedding in possums may inform decisions on target areas to implement and evaluate any such potential future interventions in Victoria.

This article was preprinted at https://medrxiv.org/cgi/content/short/2024.05.03.24306731v1.

Acknowledgments

We acknowledge the work of the public health officers (K. Cham, B. Eedara, S. Fletcher, J. FitzGibbon, S. Howard, L. Nolte, T. Pe, S. Thompson, L. Veenhuizen, R. Ward, I. Caple) and team leaders (L. Farnsworth, S. Hallissey, A. Kelly, J. O'Neill) within the BSW Public Health Unit for their follow-up of notified cases since July 2022 and assistance with the current epidemiological investigation, as well as the Department of Health Victoria Health Protection team for follow-up of cases prior to 2022 and guidance in the response to the emerging areas. We acknowledge the field researchers at CSIRO involved in collection and testing of the possum fecal samples in Geelong.

The Barwon Health Human Research Ethics Committee granted ethical approval for our analyses under a negligible-risk application (Project 23/10).

Deidentified human case data used in this publication may be requested from the Department of Health Victoria (infectious.diseases@health.vic.gov.au), contingent on approval of an analysis plan by this Department and

relevant ethical approval. Possum fecal data may be shared, after publication, on a collaborative basis upon reasonable request made to Kim Blasdell (kim.blasdell@csiro.au).

The data collection and analysis of the possum fecal surveys were funded as part of the NHMRC Partnership Project Grant 2018–2020 (GNT1152807) led by Tim Stinear.

Author contributions: B.J.M., J.C., K.R.B., and D.P.O. conceived and designed the study. B.J.M., T.P., N.E.C., and E.L.T. conducted data collection from human cases and K.R.B., M.D., V.B., and A.K. from possum excreta. B.J.M. conducted epidemiologic analysis; V.B. and K.R.B. conducted fecal PCR analysis; and J.C., K.R.B., E.A., N.E.C., T.P., M.A.H., M.M., and D.P.O. interpreted results. B.J.M. and J.C. prepared the draft manuscript. All authors reviewed the results and approved the final version of the manuscript.

About the Author

Dr. McNamara is an epidemiologist at the Barwon South West Public Health Unit and honorary senior research fellow at the Centre for Epidemiology and Biostatistics at the University of Melbourne. Her research interests focus on social and health equity and applied epidemiology for disease outbreak management and primary prevention, particularly for Buruli ulcer and COVID-19.

References

1. World Health Organization. Working to overcome the global impact of neglected tropical diseases: first WHO report on neglected tropical diseases. Geneva: The Organization; 2010.
2. Merritt RW, Walker ED, Small PL, Wallace JR, Johnson PD, Benbow ME, et al. Ecology and transmission of Buruli ulcer disease: a systematic review. PLoS Negl Trop Dis. 2010;4:e911. https://doi.org/10.1371/journal.pntd.0000911
3. O'Brien DP, Jeanne I, Blasdell K, Avumegah M, Athan E. The changing epidemiology worldwide of *Mycobacterium ulcerans*. Epidemiol Infect. 2019;147:e19. https://doi.org/10.1017/S0950268818002662
4. Loftus MJ, Tay EL, Globan M, Lavender CJ, Crouch SR, Johnson PDR, et al. Epidemiology of Buruli ulcer infections, Victoria, Australia, 2011–2016. Emerg Infect Dis. 2018;24:1988–97. https://doi.org/10.3201/eid2411.171593
5. Buultjens AH, Vandelannoote K, Meehan CJ, Eddyani M, de Jong BC, Fyfe JAM, et al. Comparative genomics shows that *Mycobacterium ulcerans* migration and expansion preceded the rise of Buruli ulcer in southeastern Australia. Appl Environ Microbiol. 2018;84:e02612-17. https://doi.org/10.1128/AEM.02612-17
6. Mee PT, Buultjens AH, Oliver J, Brown K, Crowder JC, Porter JL, et al. Mosquitoes provide a transmission route between possums and humans for Buruli ulcer in southeastern Australia. Nat Microbiol. 2024;9:377–89. https://doi.org/10.1038/s41564-024-01693-y
7. McNamara BJ, Blasdell KR, Yerramilli A, Smith IL, Clayton SL, Dunn M, et al. Comprehensive case-control study of protective and risk factors for Buruli ulcer, southeastern Australia. Emerg Infect Dis. 2023;29:2032–43. https://doi.org/10.3201/eid2910.230011
8. Fyfe JA, Lavender CJ, Handasyde KA, Legione AR, O'Brien CR, Stinear TP, et al. A major role for mammals in the ecology of *Mycobacterium ulcerans*. PLoS Negl Trop Dis. 2010;4:e791. https://doi.org/10.1371/journal.pntd.0000791
9. Blasdell KR, McNamara B, O'Brien DP, Tachedjian M, Boyd V, Dunn M, et al. Environmental risk factors associated with the presence of *Mycobacterium ulcerans* in Victoria, Australia. PLoS One. 2022;17:e0274627. https://doi.org/10.1371/journal.pone.0274627
10. Vandelannoote K, Buultjens AH, Porter JL, Velink A, Wallace JR, Blasdell KR, et al. Statistical modeling based on structured surveys of Australian native possum excreta harboring *Mycobacterium ulcerans* predicts Buruli ulcer occurrence in humans. eLife. 2023;12: e84983. https://doi.org/10.7554/eLife.84983
11. Australian Bureau of Statistics. Regional population, estimated residential population 2001–2020. Canberra: The Bureau; 2022.
12. Blasdell KR, McNamara B, O'Brien DP, Tachedjian M, Boyd V, Dunn M, et al. Environmental risk factors associated with the presence of *Mycobacterium ulcerans* in Victoria, Australia. PLoS One. 2022;17:e0274627. https://doi.org/10.1371/journal.pone.0274627
13. Department of Health Victoria. Local public health units. 2023 [cited 2024 Feb 5]. https://www.health.vic.gov.au/local-public-health-units
14. Coutts SP, Lau CL, Field EJ, Loftus MJ, Tay EL. Delays in patient presentation and diagnosis for Buruli ulcer (*Mycobacterium ulcerans* infection) in Victoria, Australia, 2011–2017. Trop Med Infect Dis. 2019;4:100. https://doi.org/10.3390/tropicalmed4030100

Address for correspondence: Bridgette McNamara, Barwon South West Public Health Unit, Barwon Health, PO Box 281, Geelong, VIC 3220, Australia; email: bridgette.mcnamara@barwonhealth.org.au

Extended-Spectrum β-Lactamase–Producing Enterobacterales in Municipal Wastewater Collections, Switzerland, 2019–2023

Lisandra Aguilar-Bultet,[1] Elena Gómez-Sanz,[1] Ana B. García-Martín, Monica Alt Hug, Reto Furger, Lucas Eichenberger, Claudia Bagutti,[2] Sarah Tschudin-Sutter[2]

We quantified presumptive extended-spectrum β-lactamase–producing *Escherichia coli* and *Klebsiella*, *Enterobacter*, *Serratia*, and *Citrobacter* group colonies from wastewater in Basel, Switzerland, across 3 years to represent before, during, and after the COVID-19 pandemic. Wastewater surveillance might be a noninvasive, sensitive, rapid, and cost-effective instrument for early detection and monitoring local epidemiology.

Extended-spectrum β-lactamase–producing Enterobacterales (ESBL-PE), particularly *Escherichia coli* and species of the *Klebsiella*, *Enterobacter*, *Serratia*, and *Citrobacter* (KESC) group, are bacteria that contribute to the global antimicrobial resistance burden (*1*–*3*). A comprehensive understanding of the sources of the bacteria and relevant expansion factors is imperative.

The COVID-19 pandemic caused unprecedented challenges at a global scale by overwhelming healthcare systems and causing disruption of infection control and preventive measures (*4*,*5*). Antibiotic drugs were overprescribed for patients with COVID-19 because of concerns about secondary infections and co-infections (*4*,*6*,*7*). Such overuse of antibiotic drugs might have caused the emergence of multidrug-resistant pathogens. However, measures such as general lockdowns, social distancing, vaccination, reduced antibiotic drug use in the outpatient sector, extensive implementation of hand hygiene and face masks, decreased elective hospital procedures, and limited global international travel and migration reduced local antimicrobial resistance severity during the pandemic (*8*).

Author affiliations: University Hospital Basel, Basel, Switzerland (L. Aguilar-Bultet, E. Gómez-Sanz, Ana B. García-Martín, S. Tschudin-Sutter); State Laboratory Basel-City, Basel (M. Alt Hug, R. Furger, L. Eichenberger, C. Bagutti)

DOI: https://doi.org/10.3201/eid3103.240099

Returning travelers have been recorded as a source of ESBL-PE (*9*). Thus, the influence of COVID-19 on ESBL-PE remains unclear, and surveillance data from clinical samples might be biased because of reduced patient care during the pandemic. In contrast, wastewater surveillance is independent of diagnostic tests and is increasingly recognized as a tool to track circulating bacterial and viral pathogens and drug resistance determinants (*10*,*11*). Here, we leveraged and applied an established wastewater surveillance system (*12*) to assess changes in the number of presumptive ESBL-producing *E. coli* and KESC in municipal wastewater before (2019), during (2021), and after (2023) the COVID-19 pandemic in Basel, Switzerland.

The Study

We collected 125 wastewater samples distributed across Basel, Switzerland, for 3 consecutive months (April–June) in 2021 (n = 62 [33.0% of samples]) and 2023 (n = 63 [33.5% of samples]) using a systematic approach (Appendix, https://wwwnc.cdc.gov/EID/article/31/3/24-0099-App1.pdf) (*12*). To represent the baseline, we retrospectively included the quantification results of presumptive ESBL-producing *E. coli* and KESC of wastewater samples collected from the same wastewater sampling sites during a 12-month period covering 2018–2019. Those samples were collected as part of an earlier study on ESBL-PE in municipal wastewater and used the same sampling approach and methods (*12*) (Appendix). For the primary analyses, we chose not to incorporate all results from that earlier study because of differences in the timing of sample collection (Appendix Table

[1]These first authors contributed equally to this article.

[2]These senior authors contributed equally to this article.

Table 1. Quantification over 3 years of presumptive extended-spectrum β-lactamase–producing Enterobacterales in municipal wastewater collections, Switzerland, 2019–2023*

	2019, n = 63		2021, n = 62		2023, n = 63	
Colony	Median CFU/mL (IQR)	Range, CFU/mL	Median CFU/mL (IQR)	Range, CFU/mL	Median CFU/mL (IQR)	Range, CFU/mL
ESBL *Escherichia coli*	60 (8–180)	0–15,480	193 (50–520)	0–18,100	195 (58–708)	0–125,300
ESBL KESC	10 (0–83)	0–9,700	178 (51–731)	0–11,400	110 (13–373)	0–5,550
ESBL *E. coli* + KESC	120 (28–283)	0–15,480	473 (191–1,403)	0–11,400	475 (80–1,585)	0–125,300

*Comparisons for 2019 versus 2021 versus 2023 by Friedman test. All colony p values were statistically significant at <0.001. ESBL, extended-spectrum β-lactamase; IQR, interquartile range; KESC, *Klebsiella*, *Enterobacter*, *Serratia*, and *Citrobacter* group.

1). We analyzed samples collected within the same months (April–June) throughout the study period because we previously found differences in ESBL-PE counts across sampling months when analyzing ESBL-PE counts across an entire year (*12*).

Municipal wastewater samples were taken at 21 different sewer sampling points representing the 10 postal codes of Basel, as previously described (*12*). We categorized sites as urban (81.0%, n = 17), representing a community without wastewater from

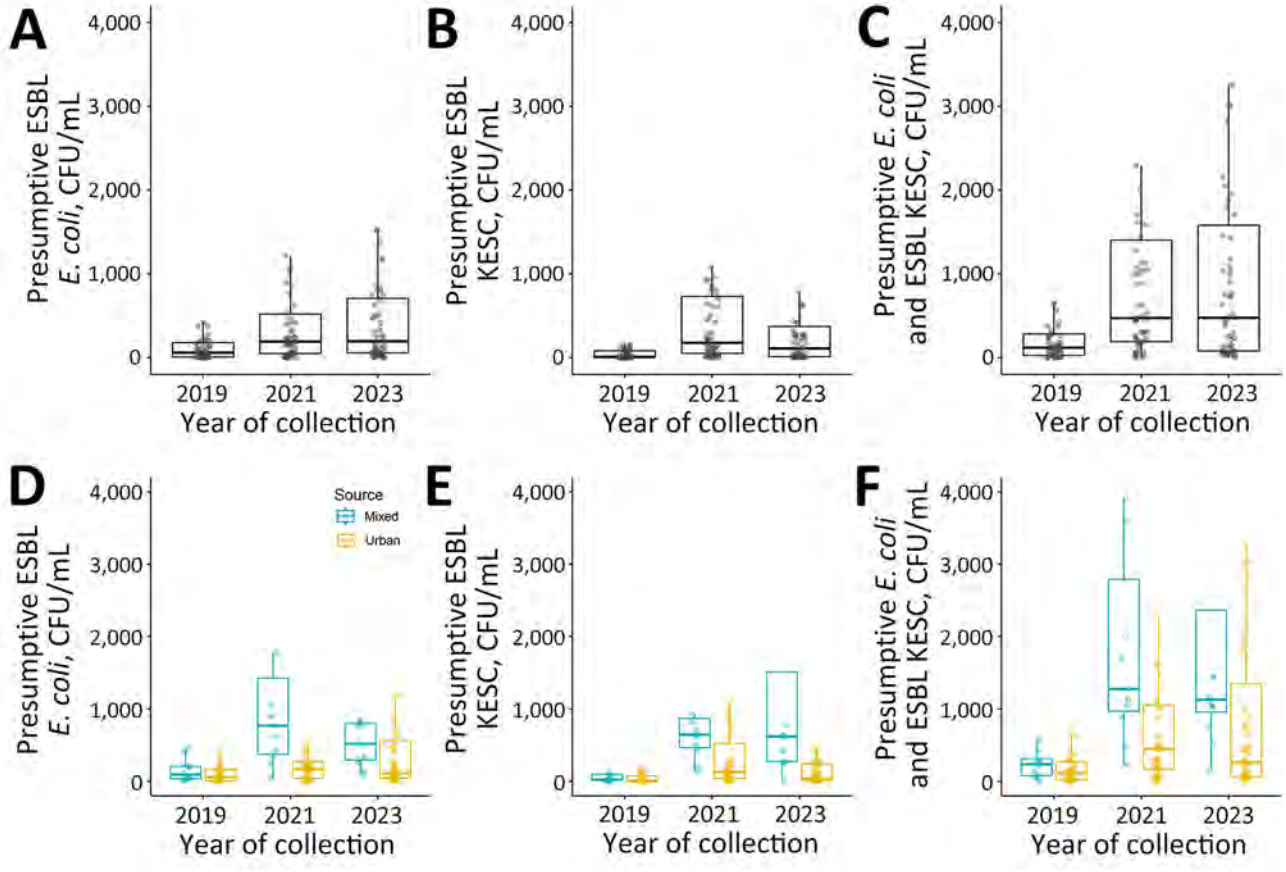

Figure. Temporal quantification of extended-spectrum β-lactamase–producing Enterobacterales in municipal wastewater collections, Switzerland, 2019–2023. A–C) Temporal distribution of presumptive ESBL-producing *Escherichia coli* (A), presumptive ESBL-producing KESC (B), and presumptive ESBL-producing *E. coli* plus KESC (C). Data from the 3-month sampling across the 21 sampling points distributed across Basel, Switzerland (representing 44% of the Basel population), are collapsed and represented by year: 2019, n = 63; 2021, n = 62; 2023, n = 63. Friedman test p values for all categories are <0.001. Quantification stratified by sample source. D–F) Temporal distribution by source, urban or mixed (community and hospital) effluents, of presumptive ESBL-producing *E. coli* (D) presumptive ESBL-producing KESC (E), and presumptive ESBL-producing *E. coli* plus KESC (F). Data from the 3-month sampling across the 17 urban (n = 51 per year) and 4 mixed (n = 12 per year, except for 1 data point missing in April 2021) sampling points are combined and represented per year. Box tops and bottoms indicate interquartile ranges; bold lines, medians; whiskers, 1.5 times the interquartile range. Jitter plots indicate individual data points. Outliers were removed for readability. Mann-Whitney sum U test p values stratified by mixed versus urban samples per chromogenic group (per year): *E. coli,* p = 0.654 (2019), 0.107 (2021), 0.371 (2023); KESC: 0.420 (2019), 0.179 (2021), 0.0251 (2023); *E. coli* plus KESC, p = 0.531 (2019), 0.283 (2021), 0.128 (2023). ESBL extended-spectrum β-lactamase; ESBL-PE, extended-spectrum β-lactamase–producing Enterobacterales; KESC, *Klebsiella, Enterobacter, Serratia,* and *Citrobacter.*

healthcare settings; and mixed (19.1%, n = 4), both community and healthcare settings (Appendix Table 2). The samples were collected by the Civil Engineering Department of the Canton of Basel-Stadt following the recommendations of the World Health Organization and processed as previously detailed (*12*).

We assessed differences in the number of presumptive ESBL-producing *E. coli*, KESC, and *E. coli* plus KESC by using the Friedman test, which is a nonparametric alternative to the repeated-measures analysis of variance and Kruskal-Wallis test for comparisons stratified by month. We compared urban versus mixed sites per sampling year for each bacterial group by using the Mann-Whitney U test. To account for the repeated testing of the sampling sites, we calculated the mean of 3 CFU/mL counts measured over the 3-month sampling period per sampling site and year (Appendix Table 3). We used Stata version 16.1 (StataCorp LLC, https://www.stata.com) to perform analyses. Reported p values are 2-sided and considered significant at <0.05.

Median total counts combined across the 3 years were as follows: 140 CFU/mL, presumptive ESBL *E. coli*; 70 CFU/mL, KESC group; and 270 CFU/mL, *E. coli* plus KESC. For all 3 comparisons, we observed significant differences (p<0.001) (Table 1; Figure, panels A–C). For analyses stratified by the 3 sampling months, median counts statistically differed for May and June (p<0.05) (Appendix Table 4). For the data stratified by mixed (n = 35 [18.6% of samples]) versus urban (n = 153 [81.4% of samples]) sites, sites that included hospital sewage had higher counts overall (Figure 1, panels D–F). We detected larger values of presumptive ESBL-producing KESC colonies in sampling sites including hospital sewage compared with sampling sites receiving only community wastewater (2023 median counts: 620 CFU/mL mixed, 40 CFU/mL urban; p = 0.025) (Table 2; Figure 1, panels D–F), whereas Mann-Whitney U tests showed no statistically significant differences for other comparisons. Analyses stratified per month supported higher counts for mixed compared with urban sites during and after the pandemic (Appendix Table 5, Figures 1–4).

One limitation of the study was the small number of wastewater samples, and we acknowledge that the prepandemic phase was represented by samples collected within 12 months spanning 2018 and 2019. To ensure comparability between the sample years, the main comparisons were made for April, May, and June because data were only available for those 3 months in 2019, 2021, and 2023 (Appendix Table 1). The samples collected in 2019 might not accurately reflect the baseline presence of ESBL-PE before the pandemic. Also, collection of specimens in 2020 and 2022 could have further substantiated a conclusion that the changes were caused by factors related to the pandemic. Another limitation of the study was that we could not collect samples in 2020 and 2022 because of a lack of resources.

Conclusions

Our wastewater surveillance showed increased presumptive ESBL-producing *E. coli* and KESC counts during and after the COVID-19 pandemic compared with the prepandemic period. Prevalence of ESBL-producing *Klebsiella pneumoniae* in humans has doubled in Switzerland since 2019, particularly in the northwest region where Basel is located (5% in 2019; 8% in 2021; 11% in

Table 2. Quantification across 3 years of presumptive extended-spectrum β-lactamase–producing Enterobacterales in municipal wastewater collections, Switzerland, 2019–2023, stratified by source*

Characteristics	ESBL *E. coli*		ESBL KESC		ESBL *E. coli* + KESC	
	Mixed	Urban	Mixed	Urban	Mixed	Urban
2019						
Sample size	n = 12	n = 51	n = 12	n = 51	n = 12	n = 51
Median CFU/mL (IQR)	90 (36–210)	55 (5–165)	23 (13–94)	5 (0–75)	238 (79–318)	115 (18–273)
Range, CFU/mL	5–455	0–15,480	0–840	0–9,700	5–885	0–15,480
p value	0.654		0.420		0.531	
2021						
Sample size	n = 11	n = 51	n = 11	n = 51	n = 11	n = 51
Median CFU/mL (IQR)	770 (375–1,428)	170 (40–278)	645 (465–870)	130 (40–528)	1,275 (970–2,793)	445 (170–1,058)
Range, CFU/mL	40–4,200	0–18,100	140–3,900	0–11,400	230–8100	0–18,300
p value	0.107		0.179		0.283	
2023						
Sample size	n = 12	n = 51	n = 12	n = 51	n = 12	n = 51
Median CFU/mL (IQR)	515 (296–798)	110 (43–563)	620 (275–1,511)	40 (10–243)	1,130 (956–2,365)	260 (63–1,348)
Range, CFU/mL	85–3,490	0–125,300	15–5,550	0–3,830	155–7,195	5–125,300
p value	0.371		**0.025**		0.128	

*Mixed versus urban by Mann-Whitney U test. Bold text indicates statistically significant value. ESBL, extended-spectrum β-lactamase; IQR, interquartile range; KESC, *Klebsiella*, *Enterobacter*, *Serratia*, and *Citrobacter* group.

2023) (*13*). Highest presumptive ESBL-KESC counts in wastewater in 2021 might be related to the overwhelming global situation in the healthcare system, implying predominance of hospital-acquired infections, such as those caused by ESBL-producing *K. pneumoniae* (*14*,*15*). We observed an increase of presumptive ESBL-producing *E. coli* during 2021, without a subsequent decrease in 2023. Of note, the overall ESBL-producing *E. coli* resistance rates in humans in Switzerland have remained stable since 2015 (10%–11%) (*13*).

Our results suggest that the COVID-19 pandemic exacerbated the differences in ESBL-PE abundance between urban and mixed sites. That increase might be caused by the rise in ESBL-PE prevalence in local hospitals compared with before the pandemic, as is the case for ESBL *K. pneumoniae*, together with a slight increase detected in consumption of third- and fourth-generation cephalosporins in German-speaking Switzerland in the inpatient sector (defined daily dose per 100 bed-days: 2019, 6.5; 2020, 7.0; 2021, 6.8; 2022, 7.0) (*13*). Social distancing, travel restrictions, and decreases in third- and fourth-generation cephalosporin use (defined daily dose per 1,000 inhabitants per day: 2019, 0.05; 2021, 0.03) observed in the outpatient sector in the region during the years of the COVID-19 pandemic (*13*) might have promoted the disparity of presumptive ESBL-KESC abundance between urban and mixed wastewater samples in 2023.

In summary, we showed an increase in presumptive ESBL-producing *E. coli* and KESC in 2021 and 2023, particularly in samples containing hospital wastewater, suggesting a disproportionate increase of ESBL KESC within healthcare settings compared with the community and possibly explained by less adherence to infection prevention and control procedures. Social distancing, travel restriction measures, and reduced antibiotic drug use in the community during the pandemic might have prevented further ESBL-PE increases in community settings. Wastewater ESBL-PE surveillance may serve as a noninvasive, sensitive, rapid, and cost-effective instrument for early detection and monitoring the local epidemiology of ESBL-PE.

Acknowledgments

We thank the team of the Civil Engineering Department of the canton of Basel-Stadt for providing access and collecting wastewater samples and the Statistical Office of the canton of Basel-Stadt for analyzing the sewer catchment areas and number of inhabitants.

This work was supported by the University Hospital Basel, the University of Basel, and the Swiss National Science Foundation (grant no. 407240_167060).

About the Authors

Dr. Aguilar-Bultet is a research associate at the Department of Infectious Diseases and Hospital Epidemiology of the University Hospital Basel, Switzerland. Her primary research interest is bacterial genomics applied to epidemiology. Dr. Gómez-Sanz is a senior research associate at the Department of Infectious Diseases and Hospital Epidemiology of the University Hospital Basel. Her primary research lies in defining the pathways for transmission and persistence of bacterial antimicrobial resistance from a One Health perspective.

References

1. Kaarme J, Riedel H, Schaal W, Yin H, Nevéus T, Melhus Å. rapid increase in carriage rates of Enterobacteriaceae producing extended-spectrum β-lactamases in healthy preschool children, Sweden. Emerg Infect Dis. 2018;24:1874–81. https://doi.org/10.3201/eid2410.171842
2. Antimicrobial Resistance Collaborators. Global burden of bacterial antimicrobial resistance in 2019: a systematic analysis. Lancet. 2022;399:629–55. https://doi.org/10.1016/S0140-6736(21)02724-0
3. Cassini A, Högberg LD, Plachouras D, Quattrocchi A, Hoxha A, Simonsen GS, et al.; Burden of AMR Collaborative Group. Attributable deaths and disability-adjusted life-years caused by infections with antibiotic-resistant bacteria in the EU and the European Economic Area in 2015: a population-level modelling analysis. Lancet Infect Dis. 2019;19:56–66. https://doi.org/10.1016/S1473-3099(18)30605-4
4. Centers for Disease Control and Prevention. COVID-19: U.S. impact on antimicrobial resistance, special report 2022. Atlanta (GA): The Centers; 2022.
5. Tomczyk S, Taylor A, Brown A, de Kraker MEA, El-Saed A, Alshamrani M, et al.; WHO AMR Surveillance and Quality Assessment Collaborating Centres Network. Impact of the COVID-19 pandemic on the surveillance, prevention and control of antimicrobial resistance: a global survey. J Antimicrob Chemother. 2021;76:3045–58. https://doi.org/10.1093/jac/dkab300
6. Langford BJ, So M, Simeonova M, Leung V, Lo J, Kan T, et al. Antimicrobial resistance in patients with COVID-19: a systematic review and meta-analysis. Lancet Microbe. 2023;4:e179–91. https://doi.org/10.1016/S2666-5247(22)00355-X
7. Suleiman AS, Islam MA, Akter MS, Amin MR, Werkneh AA, Bhattacharya P. A meta-meta-analysis of co-infection, secondary infections, and antimicrobial resistance in COVID-19 patients. J Infect Public Health. 2023;16:1562–90. https://doi.org/10.1016/j.jiph.2023.07.005
8. Monnet DL, Harbarth S. Will coronavirus disease (COVID-19) have an impact on antimicrobial resistance? Euro Surveill. 2020;25:2001886. https://doi.org/10.2807/1560-7917.ES.2020.25.45.2001886
9. Arcilla MS, van Hattem JM, Haverkate MR, Bootsma MCJ, van Genderen PJJ, Goorhuis A, et al. Import and spread of extended-spectrum β-lactamase-producing Enterobacteriaceae by international travellers (COMBAT study): a prospective, multicentre cohort study. Lancet Infect Dis. 2017;17:78–85. https://doi.org/10.1016/S1473-3099(16)30319-X
10. Bagutti C, Alt Hug M, Heim P, Maurer Pekerman L, Ilg Hampe E, Hübner P, et al. Wastewater monitoring of

SARS-CoV-2 shows high correlation with COVID-19 case numbers and allowed early detection of the first confirmed B.1.1.529 infection in Switzerland: results of an observational surveillance study. Swiss Med Wkly. 2022;152:w30202. https://doi.org/10.4414/SMW.2022.w30202
11. Aarestrup FM, Woolhouse MEJ. Using sewage for surveillance of antimicrobial resistance. Science. 2020;367:630–2. https://doi.org/10.1126/science.aba3432
12. Gómez-Sanz E, Bagutti C, Roth JA, Alt Hug M, García-Martín AB, Maurer Pekerman L, et al. Spatiotemporal dissemination of ESBL-producing Enterobacterales in municipal sewer systems: a prospective, longitudinal study in the city of Basel, Switzerland. Front Microbiol. 2023; 14:1174336. https://doi.org/10.3389/fmicb.2023.1174336
13. Federal Office of Public Health and Federal Food Safety and Veterinary Office. Swiss antibiotic resistance report 2024. Usage of antibiotics and occurrence of antibiotic resistance in bacteria from humans and animals in Switzerland. Bern (Switzerland): The Office; 2024.
14. Holt KE, Wertheim H, Zadoks RN, Baker S, Whitehouse CA, Dance D, et al. Genomic analysis of diversity, population structure, virulence, and antimicrobial resistance in *Klebsiella pneumoniae*, an urgent threat to public health. Proc Natl Acad Sci U S A. 2015;112:E3574–81. https://doi.org/10.1073/pnas.1501049112
15. Moradigaravand D, Martin V, Peacock SJ, Parkhill J. Evolution and epidemiology of multidrug-resistant *Klebsiella pneumoniae* in the United Kingdom and Ireland. MBio. 2017;8:e01976-16. https://doi.org/10.1128/mBio.01976-16

Address for correspondence: Sarah Tschudin-Sutter, University Hospital Basel, Department of Infectious Diseases and Hospital Epidemiology, Petersgraben 4, Basel CH-4031, Switzerland; email: sarah.tschudin@usb.ch

World TB Day

World TB Day, falling on March 24th each year, is designed to build public awareness that tuberculosis today remains an epidemic in much of the world, causing the deaths of nearly one-and-a-half million people each year, mostly in developing countries. It commemorates the day in 1882 when Dr. Robert Koch astounded the scientific community by announcing that he had discovered the cause of tuberculosis, the TB bacillus. At the time of Koch's announcement in Berlin, TB was raging through Europe and the Americas, causing the death of one out of every seven people. Koch's discovery opened the way towards diagnosing and curing TB.

Access the link below for *Emerging Infectious Diseases* articles and podcasts and to learn more about the latest information and emerging trends in TB.



EMERGING INFECTIOUS DISEASES®

http://wwwnc.cdc.gov/eid/page/world-tb-day

Haemophilus influenzae Type b Meningitis in Infants, New York, New York, USA, 2022–2023

Anne Ewing, Sydney Haldeman, Megan J. Job, Caitlin Otto, Adam J. Ratner

Two unvaccinated infants residing in the same borough of New York, New York, USA, had *Haemophilus influenzae* type b meningitis develop 1 year apart. Whole-genome sequencing and phylogenetic analysis revealed the isolates shared a previously undescribed multilocus sequence type and were more closely related to each other than to other sequenced strains.

Haemophilus influenzae type b (Hib) invasive infections and upper respiratory tract colonization have declined since the introduction of polysaccharide conjugate Hib vaccines, but sporadic cases still occur, leading to serious illness or death, especially in young children (*1*,*2*). Undervaccinated communities can serve as reservoirs for Hib colonization. Prior investigations of invasive Hib case clusters identified the same multilocus sequence type (ST) in multiple cases within undervaccinated Amish communities 14 years apart (*3*). Our medical center in New York, New York, USA, received 2 unvaccinated infants with Hib meningitis in 2022–2023, both of whom resided in the same borough, prompting further investigation.

The Study

Case-patient 1, a 3-month-old, previously healthy, unvaccinated girl, came to our facility with 2 days of fever and lethargy. Physical examination revealed a full fontanelle, right upward gaze deviation, and focal seizure activity. She required noninvasive respiratory support for hypoxia and fluid resuscitation for septic shock. We administered vancomycin and ceftriaxone and admitted her to the intensive care unit. Blood and cerebrospinal fluid (CSF) cultures grew *H. influenzae*, later identified by the New York City Department of Health and Mental Hygiene as type b. Complications impeding treatment included seizures and bilateral subdural empyemas, requiring surgical drainage. She completed 4 weeks of ceftriaxone with clinical improvement and returned home on a continuing course of antiepileptic medication.

Case-patient 2, a 5-month-old, unvaccinated boy, came to our facility with a history of prematurity and 3 days of fever, lethargy, and acute perioral cyanosis. He was in septic shock, requiring vasopressor support with hypoxic respiratory failure and encephalopathy requiring endotracheal intubation. Shortly after admission to the intensive care unit, the patient's pupils became fixed and dilated. Computed tomographic imaging of the brain revealed diffuse cerebral edema. Blood and CSF cultures grew *H. influenzae*, later identified as Hib by New York City Department of Health and Mental Hygiene. A multiplex PCR panel from the nasopharynx detected rhinovirus and enterovirus. The patient underwent initial treatment with linezolid and cefepime and then transitioned to ceftriaxone for 10 days. He also completed a 7-day course of metronidazole for presumed aspiration pneumonia. His severe neurologic injury with absence of brain stem reflexes did not improve. After 1 month of hospitalization, the patient transitioned to a rehabilitation facility, still requiring invasive mechanical ventilation.

We performed a retrospective chart review of pediatric patients (0–5 years of age) with a sterile-site culture positive for Hib who were seen in our health system during January 1, 2013–December 31, 2023. We also conducted whole-genome sequencing of Hib isolates from the 2 case-patients in this study. We isolated bacterial DNA as previously described and performed short-read sequencing on the NovaSeq 6000 platform (Illumina, https://www.illumina.com) for both the blood and CSF isolates from the 2 patients (*4*). We performed long-read sequencing on the blood isolates by using the Oxford Nanopore Technologies platform R10.4.1 (Oxford Nanopore

Author affiliation: New York University Grossman School of Medicine, New York, New York, USA

DOI: http://doi.org/10.3201/eid3103.240946

Technologies, https://nanoporetech.com), conducting hybrid assembly with Trycycler (https://github.com/rrwick/Trycycler) and polishing with polypolish 0.6.0 (https://github.com/rrwick/Polypolish), resulting in closed, error-corrected genomes (*5*,*6*). We submitted genome sequences to the National Center for Biotechnology Information (https://www.ncbi.nlm.nih.gov) (GenBank accession nos. CP148001 and CP148002). We determined multilocus sequence types (STs) by using the PubMLST server (*7*). We detected single-nucleotide polymorphisms and insertions/deletions with snippy 4.6.0 (https://software.cqls.oregonstate.edu/updates/snippy-4.6.0). We downloaded all available *H. influenzae* genome sequences from GenBank (n = 2,199) by using National Center for Biotechnology Information Datasets command line tools 16.0.0 (https://www.ncbi.nlm.nih.gov/datasets/docs/V2). In silico serotype prediction using hicap 1.0.3 (https://github.com/scwatts/hicap) generated a dataset of 73 nonredundant Hib genomes (*8*). We constructed a genetic distance tree, including those 73 genomes plus the 2 newly generated genomes by using mashtree 1.2.0 and visualized that tree in Microreact (*9*,*10*).

The 2 cases we describe were the only invasive pediatric (0–5 years of age) cases of Hib identified at our institution during the 10-year span we investigated. We obtained antibiotic susceptibility data for the 2 cases we studied (Appendix Table 1, https://wwwnc.cdc.gov/EID/article/31/3/24-0946-App1.pdf) and generated high-quality closed genome sequences from the 2 Hib isolates. Both strains belonged to a previously unreported ST, newly assigned the identifier ST2832 within the ST6 clonal complex (Appendix Table 2). Analysis with hicap confirmed that each isolate contained 2 copies of the type b capsule locus, one of which had a truncation in the *bexA* gene (Appendix Figure). In a comparative genomic analysis of the 2 ST2832 isolates and the 73 genomes in our dataset, we enumerated core single-nucleotide

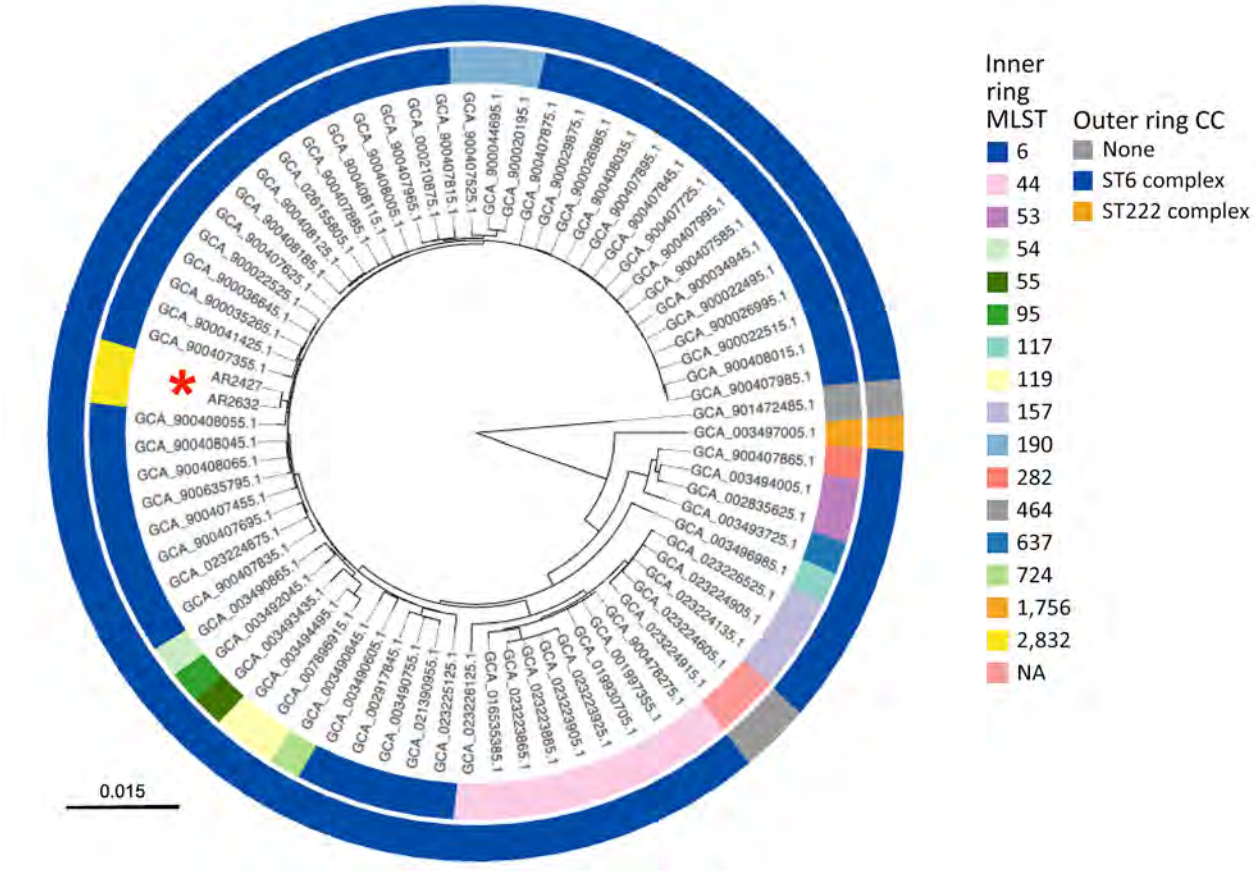

Figure. Genetic distance tree constructed to assess genetic relatedness among strains in study of *Haemophilus influenzae* type b (Hib) meningitis in infants, New York, New York, USA, 2022–2023. We constructed the tree using Mashtree *(10)* for Hib strains from the 2 New York patients (red asterisk) and reference sequences from GenBank (Appendix Table). Rings are color-coded to indicate MLST (inner ring) and CC (outer ring). Tree was rooted using the genome for NCTC 8468 (GenBank accession nos. GCA_90147285.1), a division II, *sodC*-containing Hib strain distantly related to other sequenced Hib isolates. Branch lengths represent mash distances. CC, clonal complex; MLST, multilocus sequence type; NA, not available.

polymorphisms among the Hib strains (Appendix Table 2). We also performed short-read sequencing on matched CSF isolates for each case and detected no variants between the blood and CSF isolates within either individual case. A genetic distance tree (Figure) demonstrated that the 2 ST2832 isolates from this study were more closely related to each other than to any other Hib genomes in the dataset.

Conjugate vaccination programs have been highly successful in decreasing the burden of invasive Hib disease, in part through reduction of nasopharyngeal carriage among vaccine recipients (*2*,*11*). However, even in the setting of widespread vaccination, sporadic cases occur among unvaccinated infants, older adults, and immunocompromised patients (*1*,*2*,*12*). Among children born in New York, New York, in 2021, less than 65% received their primary series of Hib vaccination on schedule (by 7 months of age), despite eventual coverage of ≈90% by 13 months of age (*13*). The basic reproductive rate of Hib has been estimated to be 3.3, implying a target immunization rate of ≥70% for disease control (*14*). Adequate primary series vaccination, boosters, and catchup programs are critical for herd immunity. Susceptible infants acquire Hib from colonized persons (generally young children), and such colonization is more common within underimmunized communities (*11*). Thus, sporadic invasive Hib cases, especially with related strains, may be sentinel events that indicate increased colonization within local populations, possibly owing to decreased immunization rates.

Limitations of our analysis include the small number of identified strains and limited whole-genome sequencing data from invasive Hib strains in the United States, requiring our comparisons to include both colonizing and invasive strains. Our observations are reminiscent of a report of 3 unvaccinated children hospitalized with invasive Hib disease within 5 months in 2014 (*3*). Two of those children were from the same Amish community and had Hib strains with a shared ST (ST45), described 14 years earlier in Amish communities in Pennsylvania, USA.

Vaccination rates are not the sole determinants of community levels of Hib carriage. In some populations with adequate vaccination coverage, factors like crowding might contribute to high colonization rates. Nolen et al. described 33 cases of invasive Hib over 14 years in Alaska, 27 of which were in Alaska native children, all originating from high-density indigenous communities despite ≈90% vaccination coverage in that population (*15*). That research group identified multiple distinct Hib STs in their analysis, implicating factors other than clonal spread in Hib carriage. Robust local surveillance of Hib vaccination coverage and routine whole-genome sequencing of isolates from invasive Hib disease would aid early identification of inadequate herd immunity and potential outbreaks. Studies of Hib colonization, particularly in communities with low uptake of routine childhood vaccinations, are urgently needed, as are ongoing efforts to combat vaccine hesitancy.

Conclusions

We identified Hib meningitis in 2 geographically linked, unimmunized infants over the course of ≈1 year. Our findings, including the newly described ST and the relatedness of the 2 isolates, suggest ongoing colonization and transmission of this strain in New York communities. Despite the small number of cases described in this report, our findings raise concern for ongoing transmission of potentially virulent Hib strains in New York, New York, placing unvaccinated children at risk.

Acknowledgments

We are grateful for sequencing support from the Antimicrobial Resistant Pathogens Program at New York University.

This study was supported by the Department of Pediatrics at New York University Grossman School of Medicine. The New York University Grossman School of Medicine Internal Review Board approved this study.

About the Author

Dr. Ewing is a pediatric infectious diseases fellow at Hassenfeld Children's Hospital and Bellevue Hospital Center. Her research focuses on genomic epidemiology of vaccine-preventable pathogens.

References

1. Briere EC, Rubin L, Moro PL, Cohn A, Clark T, Messonnier N; Division of Bacterial Diseases, National Center for Immunization and Respiratory Diseases, CDC. Prevention and control of *Haemophilus influenzae* type b disease: recommendations of the advisory committee on immunization practices (ACIP). MMWR Recomm Rep. 2014;63:1–14.
2. Gilsdorf JR. Hib vaccines: their impact on *Haemophilus influenzae* type b disease. J Infect Dis. 2021;224(Suppl 4): S321–30. https://doi.org/10.1093/infdis/jiaa537
3. Myers AL, Jackson MA, Zhang L, Swanson DS, Gilsdorf JR. *Haemophilus influenzae* type b invasive disease in Amish children, Missouri, USA, 2014. Emerg Infect Dis. 2017;23:112–4. https://doi.org/10.3201/eid2301.160593
4. Hanze Villavicencio KL, Job MJ, Burghard AC, Taffet A, Banda FM, Vurayai M, et al. Genomic analysis of group B *Streptococcus* carriage isolates from Botswana reveals distinct local epidemiology and identifies novel strains. Open Forum

Infect Dis. 2023;10:ofad496. https://doi.org/10.1093/ofid/ofad496
5. Bouras G, Judd LM, Edwards RA, Vreugde S, Stinear TP, Wick RR. How low can you go? Short-read polishing of Oxford Nanopore bacterial genome assemblies. Microb Genom. 2024;10:001254. https://doi.org/10.1099/mgen.0.001254
6. Wick RR, Judd LM, Cerdeira LT, Hawkey J, Méric G, Vezina B, et al. Trycycler: consensus long-read assemblies for bacterial genomes. Genome Biol. 2021;22:266. https://doi.org/10.1186/s13059-021-02483-z
7. Jolley KA, Bray JE, Maiden MCJ. Open-access bacterial population genomics: BIGSdb software, the PubMLST.org website and their applications. Wellcome Open Res. 2018;3:124. https://doi.org/10.12688/wellcomeopenres.14826.1
8. Watts SC, Holt KE. hicap: *In silico* serotyping of the *Haemophilus influenzae* capsule locus. J Clin Microbiol. 2019;57:e00190-19. https://doi.org/10.1128/JCM.00190-19
9. Argimón S, Abudahab K, Goater RJE, Fedosejev A, Bhai J, Glasner C, et al. Microreact: visualizing and sharing data for genomic epidemiology and phylogeography. Microb Genom. 2016;2:e000093. https://doi.org/10.1099/mgen.0.000093
10. Katz LS, Griswold T, Morrison SS, Caravas JA, Zhang S, den Bakker HC, et al. Mashtree: a rapid comparison of whole genome sequence files. J Open Source Softw. 2019;4:1762. https://doi.org/10.21105/joss.01762
11. Adegbola RA, Secka O, Lahai G, Lloyd-Evans N, Njie A, Usen S, et al. Elimination of *Haemophilus influenzae* type b (Hib) disease from The Gambia after the introduction of routine immunisation with a Hib conjugate vaccine: a prospective study. Lancet. 2005;366:144–50. https://doi.org/10.1016/S0140-6736(05)66788-8
12. Blain A, MacNeil J, Wang X, Bennett N, Farley MM, Harrison LH, et al. Invasive *Haemophilus influenzae* disease in adults ≥65 years, United States, 2011. Open Forum Infect Dis. 2014;1:ofu044. https://doi.org/10.1093/ofid/ofu044
13. Centers for Disease Control and Prevention. ChildVaxView [cited 2024 Oct 01]. https://www.cdc.gov/childvaxview
14. Coen PG, Heath PT, Barbour ML, Garnett GP. Mathematical models of *Haemophilus influenzae* type b. Epidemiol Infect. 1998;120:281–95. https://doi.org/10.1017/S0950268898008784
15. Nolen LD, Topaz N, Miernyk K, Bressler S, Massay SC, Geist M, et al. Evaluating a cluster and the overall trend of invasive *Haemophilus influenzae* serotype b in Alaska 2005-2019. Pediatr Infect Dis J. 2022;41:e120–5. https://doi.org/10.1097/INF.0000000000003470

Address for correspondence: Adam J. Ratner, New York University Grossman School of Medicine, 430 East 29th St (Alexandria West 505), New York, NY 10016, USA; email: adam.ratner@nyulangone.org

EID Podcast A Worm's Eye View

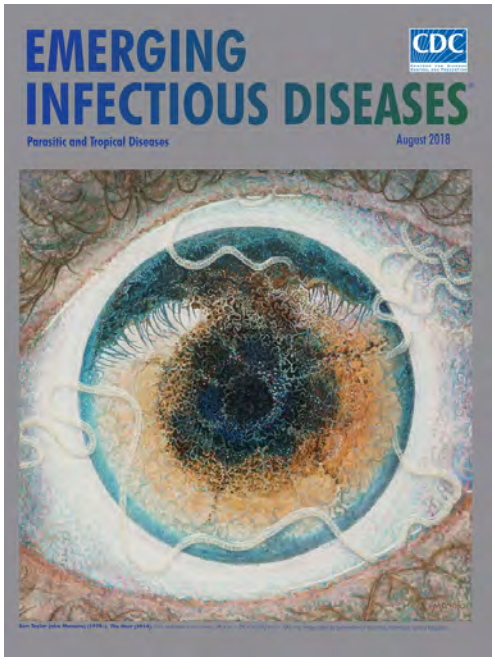

Seeing a several-centimeters-long worm traversing the conjunctiva of an eye is often the moment when many people realize they are infected with *Loa loa*, commonly called the African eyeworm, a parasitic nematode that migrates throughout the subcutaneous and connective tissues of infected persons. Infection with this worm is called loiasis and is typically diagnosed either by the worm's appearance in the eye or by a history of localized Calabar swellings, named for the coastal Nigerian town where that symptom was initially observed among infected persons. Endemic to a large region of the western and central African rainforests, the *Loa loa* microfilariae are passed to humans primarily from bites by flies from two species of the genus *Chrysops*, *C. silacea* and *C. dimidiate*. The more than 29 million people who live in affected areas of Central and West Africa are potentially at risk of loiasis.

Ben Taylor, cover artist for the August 2018 issue of EID, discusses how his personal experience with the *Loa loa* parasite influenced this painting.

Visit our website to listen:
https://tools.cdc.gov/medialibrary/index.aspx#/media/id/392605

EMERGING INFECTIOUS DISEASES

Meningococcal Sepsis in Patient with Paroxysmal Nocturnal Hemoglobinuria during Pegcetacoplan Therapy

Leo Starck, Vuokko Nummi, Eira Poikonen, Anna-Elina Lehtinen, Pia Kivelä, Nathalie Friberg, Jukka Torvikoski, Maija Toropainen, Seppo Meri

Complement C5 inhibitors bring an increased risk for *Neisseria* infections. A novel complement C3 inhibitor, pegcetacoplan, was recently approved to treat paroxysmal nocturnal hemoglobinuria, a condition commonly treated with complement C5 inhibitors. We present a case of meningococcal sepsis in a pegcetacoplan-treated patient with aplastic anemia and paroxysmal nocturnal hemoglobinuria.

Paroxysmal nocturnal hemoglobinuria (PNH) is a rare, acquired disorder caused by a de novo mutation in the *PIG-A* gene. This mutation occurs in a hematopoietic stem cell and causes a clonal loss of the glycosylphosphatidylinositol anchor from the surfaces of affected blood cells (*1*). Complement decay-accelerating factor (*2*) and protectin (*3*) are bound to cell membranes by the glycosylphosphatidylinositol anchor. Thus, glycosylphosphatidylinositol-deficient blood cells are vulnerable to complement attack, leading to hemolytic anemia, thrombi, and other PNH-related complications.

Complement inhibition is a logical therapy for PNH. In 2007, the US Food and Drug Administration and the European Medicines Agency licensed an anti-C5 monoclonal antibody, eculizumab, and in 2018–2019, the longer-acting ravulizumab. Deficiencies of the terminal complement pathway increase the risk for *Neisseria* infections (*4*). C5 inhibitor decreases the ability of human blood to kill serogroup B meningococci despite vaccination (*5*); investigators have described sepsis caused by nonencapsulated *N. meningitidis* in a patient with PNH during ravulizumab therapy (*6*).

In 2021, pegcetacoplan was the first C3 inhibitor authorized by the US Food and Drug Administration and the European Medicines Agency. Phase III clinical trial data and postmarketing safety surveillance studies revealed no invasive *N. meningitidis* infections in patients (*7*–*9*). We describe invasive *N. meningitidis* infection in a patient with PNH during pegcetacoplan therapy.

Case Report

A 16-year-old girl received a diagnosis of aplastic anemia and PNH. The next year, her granulocyte PNH clone size increased from 1% to 98%. To address chronic, severe hemolysis, physicians prescribed ravulizumab therapy in April 2023. The patient received a dose of meningococcal conjugate vaccine (covering serogroups A, C, Y, and W-135 and a dose of meningococcal group B vaccine (4CMenB) in April 2023; she received a dose of each again in June 2023, ≈8 months before meningococcal sepsis onset. In December 2023, physicians switched the patient's therapy from ravulizumab to pegcetacoplan (1,080 mg 2×/wk) because of extravascular hemolysis; the last ravulizumab infusion was 78 days before the onset of her infection, corresponding to 1.5 times the half-life of ravulizumab. The patient's medications for aplastic anemia included eltrombopag (125 mg 1×/d), cyclosporine (100 mg 2×/d), and folic acid (5 mg 1×/d). She also used lynestrenol. At a follow-up appointment in January 2024, the patient's test results showed leukopenia: total leukocyte count of 1.8 × 10^9 cells/L (reference range 3.4–8.2 × 10^9 cells/L) and neutrophils at 0.60 × 10^9 cells/L (reference range 1.5–6.7 × 10^9 cells/L).

Author affiliations: University of Helsinki, Helsinki, Finland (L. Starck, S. Meri); Helsinki University Central Hospital, Helsinki (V. Nummi, E. Poikonen, A.-E. Lehtinen, P. Kivelä, N. Friberg, J. Torvikoski, S. Meri); Finnish Institute for Health and Welfare, Helsinki (M. Toropainen)

DOI: http://doi.org/10.3201/eid3103.241182

In February 2024, three days after a student celebration on an international cruise ship, the patient, then 18 years of age, visited the emergency department with signs of septic infection: occipital headache, fever 39.5°C, tachycardia 110 beat/min, and blood pressure 105/67 mm Hg. Physical examination revealed no petechiae; thorax radiograph and urinalysis results were unremarkable. We performed blood culture and started the patient on antimicrobial therapy (cefuroxime 1.5 g 3×/d). Tests showed a total leukocyte count of 2.5×10^9 cells/L and neutrophils at 1.90×10^9 cells/L. The patient's hemoglobin level was 86 g/L (reference 117–155 g/L), and lactate dehydrogenase (LDH) was 398 U/L (reference 115–235 U/L) (Tables 1, 2).

During the first inpatient morning, the patient's temperature peaked at 40.1°C, but she remained hemodynamically stable and in good consciousness. Her LDH increased to 463 U/L and hemoglobin decreased to 73 g/L. A transfusion of 1 unit of packed red blood cells was administered. Pegcetacoplan was continued at the same dose. Thromboprophylaxis with enoxaparin was initiated. Approximately 24 hours after admission, the patient's blood culture sample became positive, with an unclear finding in gram-staining. A commercial multiplex-PCR array (Biofire FilmArray Blood Culture Identification Panel 2; bioMérieux, https://www.biomerieux.com) yielded no identification. Dosing of cefuroxime was increased to 4 times a day.

On the second day, matrix-assisted laser desorption/ionization time-of-flight mass spectrometry (VITEK MS; bioMérieux) identified *N. meningitidis,* but capsule agglutination was inconclusive. An in-house meningococcus-specific PCR remained negative. The multiplex PCR repeatedly returned a negative result for all targets. Cefuroxime was switched to ceftriaxone (2 g 2×/d), a medication more appropriate for treating meningococcal sepsis. Subsequent laboratory tests revealed a decrease in hemoglobin to 72 g/L and an increase in LDH to 726 U/L, indicating active hemolysis. She received another infusion of packed red blood cells.

Epidemiologic contact tracing and distribution of antimicrobial prophylaxis to close contacts commenced. The meningococcal isolate was sent to the Finnish Institute for Health and Welfare for verification, serogrouping, and characterization by whole-genome sequencing that included genes of the 4CMenB vaccine antigens. The isolate autoagglutinated and was not groupable using a latex agglutination test (BioRad Laboratories, https://www.bio-rad.com).

On the third day of her hospital stay, the patient remained clinically stable, and her LDH level decreased to 619 U/L. On the fourth day, a slight drooping of the left side of her mouth was noticed. Magnetic resonance imaging of her brain revealed no abnormalities. The patient recovered fully and was discharged in good health after a 7-day course of intravenous antimicrobial drugs. She continued pegcetacoplan therapy for PNH. At discharge, the patient was prescribed amoxicillin/clavulanate (875/125 mg) to be started in duplicate in case of a sudden onset of fever at distance from hospital. On a follow-up visit for PNH, the patient gave informed consent for publication of a case report.

Whole-genome sequencing revealed a nonencapsulated *N. meningitidis*, harboring the capsule null locus (cnl) allele 2. The strain designation of the isolate was sequence type 198, clonal complex 198 (cnl: P1.18,25–1: F5–5: ST198 (cc198) (capsule group:PorA type:FetA type:sequence type [clonal complex]). The isolate contained neisserial heparin binding antigen peptide 10 and factor H binding protein peptide 94 but lacked neisserial adhesin A. The genetic Meningococcal Antigen Typing System (*10*) predicts isolate coverage by 4CMenB because of cross-reactive neisserial heparin binding antigen. Blocking of complement C3 probably hinders killing by both opsonophagocytosis and the complement terminal pathway (*11*), although there is also evidence for serum killing during C3 blockade through a C3 bypass pathway (*12*). The negative diagnostic PCR and latex agglutination test results were likely due to lack of capsular transport and biosynthesis genes, including the PCR-targeted *ctrA* (*13*).

Infections caused by nonencapsulated *N. meningitidis* are rare. The epidemiology of cnl invasive

Table 1. Blood test results and body temperature of case patient from study of meningococcal sepsis in patient with paroxysmal nocturnal hemoglobinuria during pegcetacoplan therapy*

Parameter	Reference range	Day −29	Day 0	Day 1	Day 2	Day 3	Day 4	Day 5
Hemoglobin, g/L	117–155	94	86	73†	72†	80	76†	99
Total leukocytes, $\times 10^9$ cells/L	3.4–8.2	1.8	2.5	1.8	3.1	2.3	2.2	3.4
Neutrophils, $\times 10^9$ cells/L	1.5–6.7	0.60	1.90	1.46	2.02	1.33	0.89	1.81
CRP, g/L	<4	<4	21	67	202	102	54	32
LDH, U/L	115–235	362	398	463	726	619	493	452
Fever, °C	36–37	NA	39.5	40.1	<38	<37.5	NA	NA

*Day 0 indicates day patient sought hospital care. CRP, C-reactive protein; LDH, lactate dehydrogenase; NA, not available.
†Packed red blood cell transfusions.

Table 2. Case patient diagnostic and hospital course highlights from study of meningococcal sepsis in patient with PNH during pegcetacoplan therapy*

Treatment day	Microbiology	Treatment	Diagnostic tests and additional treatments
Day 0	Blood culture	Cefuroxime 1.5 g × 3	
Day 1	Positive blood culture; Gram staining, challenging interpretation; BCID2 PCR, negative	Cefuroxime 1.5 g × 4	Pegcetacoplan 1,080 mg; prophylactic enoxaparin started; PRBC transfusion
Day 2	Identification (MALDI-TOF mass spectrometry), *Neisseria meningitidis*; in-house PCR, negative; serogrouping, inconclusive results; preliminary report, nongroupable *N. meningitidis*	Ceftriaxone 2 g × 2	PRBC transfusion, contact tracing, prophylactic antimicrobial drugs distributed
Day 4	NA	NA	Brain magnetic resonance imaging (PNH), PRBC transfusion
Day 5	NA	NA	Pegcetacoplan 1,080 mg
Day 9	Whole-genome sequencing, nonencapsulated *N. meningitidis* harboring capsule null locus	NA	NA

*Day 0 indicates day patient sought hospital care. BCID2, bioMérieux (https://www.biomerieux.com) Biofire Blood Culture Identification 2 Panel; MALDI-TOF, matrix-assisted laser desorption/ionization time-of-flight; NA, not applicable; PNH, paroxysmal nocturnal hemoglobinuria; PRBC, 1 unit packed red blood cells.

meningococci is difficult to ascertain. The 2022 European Centre for Disease Prevention and Control Surveillance Report for Invasive Meningococcal Disease (*14*) listed serotypes A, X, Z, 29E, nongroupable, and others in the same category (n = 63 in Europe in 2022). The US Centers for Disease Control and Prevention categorized cnl meningococci as nongroupables (n = 30) and other/unknowns (n = 40) in 2022. The PubMLST database (https://pubmlst.org/neisseria), however, received >100 reports of invasive infections by cnl meningococci, most belonging to the same strain designation as the isolate infecting our patient. As whole-genome sequencing becomes more common, allowing a more detailed characterization than the agglutination test, cnl and other nongroupable meningococci will likely become more frequently recognized and differentiated.

Conclusions

Our patient had aplastic anemia and associated PNH, with relative leukopenia and complement inhibition, increasing her susceptibility to meningococcal infections. Iatrogenic complement inhibition with pegcetacoplan and potential residual ravulizumab predisposed this patient to an unusual septic infection by nonencapsulated *N. meningitidis*, despite immunization with 4CMenB 10 months and 8 months earlier. We faced some clinical challenges in diagnosing and treating this patient. First, several meningococcal identification tests returned negative results. Second, because complement C3 inhibitor therapy hampers protection against meningococci conferred by 4CMenB immunization, patients who suffer severe infections must sometimes compromise continuity of complement inhibitor treatment. Finally, with evidence lacking about efficacy and safety of antimicrobial prophylaxis in complement inhibitor recipients (*15*), physicians lack guidance regarding appropriate prophylactic antimicrobial drugs after severe infections in patients with PNH. Our case sheds light on the obstacles involved in both diagnosing and treating neisserial infections in complement inhibitor recipients and demonstrates the importance of vigilance and rapid administration of effective antimicrobial drugs.

This work was conducted as part of routine employment. S.M. is supported by the Sigrid Jusélius Foundation and the Helsinki University Hospital Funds (TYH2019311 and TYH202322).

About the Author

Dr. Starck is a researcher at the Department of Bacteriology and Immunology, University of Helsinki, Finland, whose primary interests are complement and bacterial research.

References

1. Takeda J, Miyata T, Kawagoe K, Iida Y, Endo Y, Fujita T, et al. Deficiency of the GPI anchor caused by a somatic mutation of the PIG-A gene in paroxysmal nocturnal hemoglobinuria. Cell. 1993;73:703–11. https://doi.org/10.1016/0092-8674(93)90250-t
2. Nicholson-Weller A, March JP, Rosenfeld SI, Austen KF. Affected erythrocytes of patients with paroxysmal nocturnal hemoglobinuria are deficient in the complement regulatory protein, decay accelerating factor. Proc Natl Acad Sci U S A. 1983;80:5066–70. https://doi.org/10.1073/pnas.80.16.5066
3. Yamashina M, Ueda E, Kinoshita T, Takami T, Ojima A, Ono H, et al. Inherited complete deficiency of 20-kilodalton homologous restriction factor (CD59) as a cause of paroxysmal nocturnal hemoglobinuria. N Engl J Med. 1990; 323:1184–9. https://doi.org/10.1056/NEJM199010253231707

4. Fijen CAP, Kuijper EJ, Hannema AJ, Sjöholm AG, van Putten JPM. Complement deficiencies in patients over ten years old with meningococcal disease due to uncommon serogroups. Lancet. 1989;2:585–8. https://doi.org/10.1016/s0140-6736(89)90712-5
5. Langereis JD, van den Broek B, Franssen S, Joosten I, Blijlevens NMA, de Jonge MI, et al. Eculizumab impairs *Neisseria meningitidis* serogroup B killing in whole blood despite 4CMenB vaccination of PNH patients. Blood Adv. 2020;4:3615–20. https://doi.org/10.1182/bloodadvances.2020002497
6. Galli N, Pettine L, Panigada M, Daprai L, Suriano G, Grancini A, et al. Non-capsulated *Neisseria meningitidis* sepsis in a paroxysmal nocturnal hemoglobinuria patient treated with ravulizumab: case report and review of the literature. Front Immunol. 2023;14:1269325. https://doi.org/10.3389/fimmu.2023.1269325
7. Hillmen P, Szer J, Weitz I, Röth A, Höchsmann B, Panse J, et al. Pegcetacoplan versus eculizumab in paroxysmal nocturnal hemoglobinuria. N Engl J Med. 2021;384:1028–37. https://doi.org/10.1056/NEJMoa2029073
8. de Castro CM, Dingli D, Al-Adhami M, Mulherin B, Yeh M, Lallier S, et al. A real-world evidence review of post-marketing safety and compliance with pegcetacoplan in patients with paroxysmal nocturnal hemoglobinuria (PNH) in the US. Blood. 2023;142(Supp 1):5647. https://doi.org/10.1182/blood-2023-181917
9. Patriquin CJ, Bogdanovic A, Griffin M, Kelly RJ, Maciejewski JP, Mulherin B, et al. Safety and efficacy of pegcetacoplan in adult patients with paroxysmal nocturnal hemoglobinuria over 48 weeks: 307 open-label extension study. Adv Ther. 2024;41:2050–69. https://doi.org/10.1007/s12325-024-02827-8
10. Muzzi A, Brozzi A, Serino L, Bodini M, Abad R, Caugant D, et al. Genetic Meningococcal Antigen Typing System (gMATS): a genotyping tool that predicts 4CMenB strain coverage worldwide. Vaccine. 2019;37:991–1000. https://doi.org/10.1016/j.vaccine.2018.12.061
11. Konar M, Granoff DM. Eculizumab treatment and impaired opsonophagocytic killing of meningococci by whole blood from immunized adults. Blood. 2017;130:891–9. https://doi.org/10.1182/blood-2017-05-781450
12. Ispasanie E, Muri L, Schmid M, Schubart A, Thorburn C, Zamurovic N, et al. In vaccinated individuals serum bactericidal activity against B meningococci is abrogated by C5 inhibition but not by inhibition of the alternative complement pathway. Front Immunol. 2023;14:1180833. https://doi.org/10.3389/fimmu.2023.1180833
13. Sirluck-Schroeder I, Al-Rawahi GN, Gadkar V, Hoang L, Tsang R, Tilley P. Limitation of *ctrA* as a target for Neisseria meningitidis identification and potential alternative targets. J Clin Microbiol. 2022;60:e0015222.
14. European Centre for Disease Prevention and Control. Invasive meningococcal disease—annual epidemiological report for 2022. Stockholm: The Centre; 2024 [cited 2024 Sep 5]. https://www.ecdc.europa.eu/en/publications-data/invasive-meningococcal-disease-annual-epidemiological-report-2022
15. Crew PE, McNamara L, Waldron PE, McCulley L, Christopher Jones S, Bersoff-Matcha SJ. Antibiotic prophylaxis in vaccinated eculizumab recipients who developed meningococcal disease. J Infect. 2020;80:350–71. https://doi.org/10.1016/j.jinf.2019.11.015

Address for correspondence: Seppo Meri, Haartman-Institute, Haartmaninkatu 3 (PL 21), 00014 Helsinki, Finland; email: seppo.meri@helsinki.fi

EID Podcast

Isolation Cocoon, May 2020—After Zhuangzi's Butterfly Dream

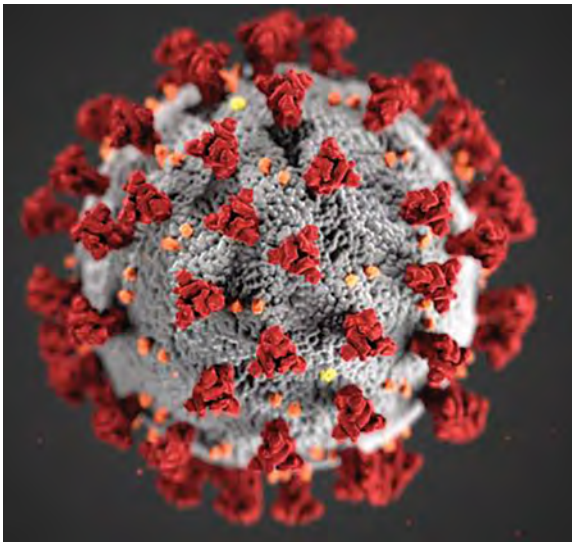

For many people, the prolonged period of social distancing during the coronavirus disease pandemic felt frightening, uncanny, or surreal.

For Ron Louie, the sensation was reminiscent of a moth taking refuge in its cocoon, slumbering in isolation as he waited for better days ahead.

In this EID podcast, Dr. Ron Louie, a clinical professor in Pediatrics Hematology-Oncology at the University of Washington in Seattle, reads and discusses his poem about the early days of the pandemic.

Visit our website to listen: https://go.usa.gov/x6W9A

EMERGING INFECTIOUS DISEASES®

Donor-Derived Ehrlichiosis Caused by *Ehrlichia chaffeensis* from Living Donor Kidney Transplant

Michael J. Scolarici,[1] Daniel Kuehler,[1] Rebecca Osborn, Annie Doyle, Elizabeth K. Schiffman, Alex Garvin, Julian A. Villalba, Carmen J. Ramos, Christopher D. Paddock, Pallavi D. Annambhotla, Marissa Taylor, Johanna S. Salzer, Christopher Saddler, Carrie Thiessen, Raja Kandaswamy,[2] Jon Odorico[2]

Tickborne infections are challenging to diagnose, particularly among solid organ transplant recipients. We report a US case of donor-derived ehrlichiosis from a living kidney donation that highlights how screening for living donors may miss tickborne infections. Clinicians should consider the epidemiology of the donor when screening donations and evaluating recipients for donor-derived infection.

Ehrlichia chaffeensis ehrlichiosis is a tickborne bacterial infection transmitted by the lone star tick (*Amblyomma americanum*) endemic to the southeastern and south-central United States (*1*). Because organ transplant–associated transmission is rare, screening of organ donors for ehrlichiosis is not routine, but infection in transplant recipients is possible (*2*–*5*). We report a case of donor-derived *E. chaffeensis* ehrlichiosis in a Wisconsin, USA, resident from a living kidney donor in Minnesota, USA.

The Study

The living donor was a 33-year-old man with obesity and unremarkable preoperative examination and serologies who underwent laparoscopic hand-assisted right nephrectomy for National Kidney Registry living unrelated kidney transplant donation at the University of Minnesota (Minneapolis, MN, USA) in June 2023. The donor had an uncomplicated nephrectomy; the total operative time was 4 hours and 29 minutes. On postoperative day (POD) 0, a new erythematous rash on the left hip and lower flank with accompanying myalgia and weakness developed on the donor. His urine output substantially decreased and became cola colored. Creatine kinase (CK) level was 41,155 U/L (reference range 30–200 U/L). Rhabdomyolysis was diagnosed, and the patient received aggressive fluid replacement. Urine myoglobin and CK levels steadily improved, and the donor was discharged on POD 6.

The recipient was a 24-year-old man with end-stage kidney disease secondary to IgA nephropathy who was on peritoneal dialysis. He underwent a National Kidney Registry transplant from the described unrelated donor to the right iliac fossa with antithymocyte globulin induction and peritoneal catheter removal at the University of Wisconsin (Madison, WI, USA). He had an uncomplicated postoperative recovery and was discharged to home on POD 3 with a creatinine level of 1.8 mg/dL (reference range 0.73–1.18 mg/dL) and maintenance immunosuppression (mycophenolate mofetil, tacrolimus, prednisone) and antimicrobial prophylaxis (valganciclovir, trimethoprim/sulfamethoxazole).

A week later, the recipient was readmitted with a fever of 100.7°F (38.2°C), generalized malaise, joint pain, and a perinephric fluid collection measuring 4.9 × 5.1 × 3.8 cm with 69 nucleated cells, predominately macrophages. He received empiric intravenous piperacillin/tazobactam and vancomycin for 48 hours that was then discontinued because admission cultures

Author affiliations: University of Wisconsin–Madison School of Medicine and Public Health, Madison, Wisconsin, USA (M.J. Scolarici, C. Saddler, C. Thiessen, J. Odorico); University of Minnesota, Minneapolis, Minnesota, USA (D. Kuehler, A. Doyle, R. Kandaswamy); Wisconsin Department of Health Services, Madison (R. Osborn); Minnesota Department of Health, St. Paul, Minnesota, USA (E.K. Schiffman, A. Garvin); Centers for Disease Control and Prevention, Atlanta, Georgia, USA (J.A. Villalba, C.J. Ramos, C.D. Paddock, P.D. Annambhotla, M. Taylor, J.S. Salzer)

DOI: https://doi.org/10.3201/eid3103.241723

[1]These first authors contributed equally to this article.

[2]These senior authors contributed equally to this article.

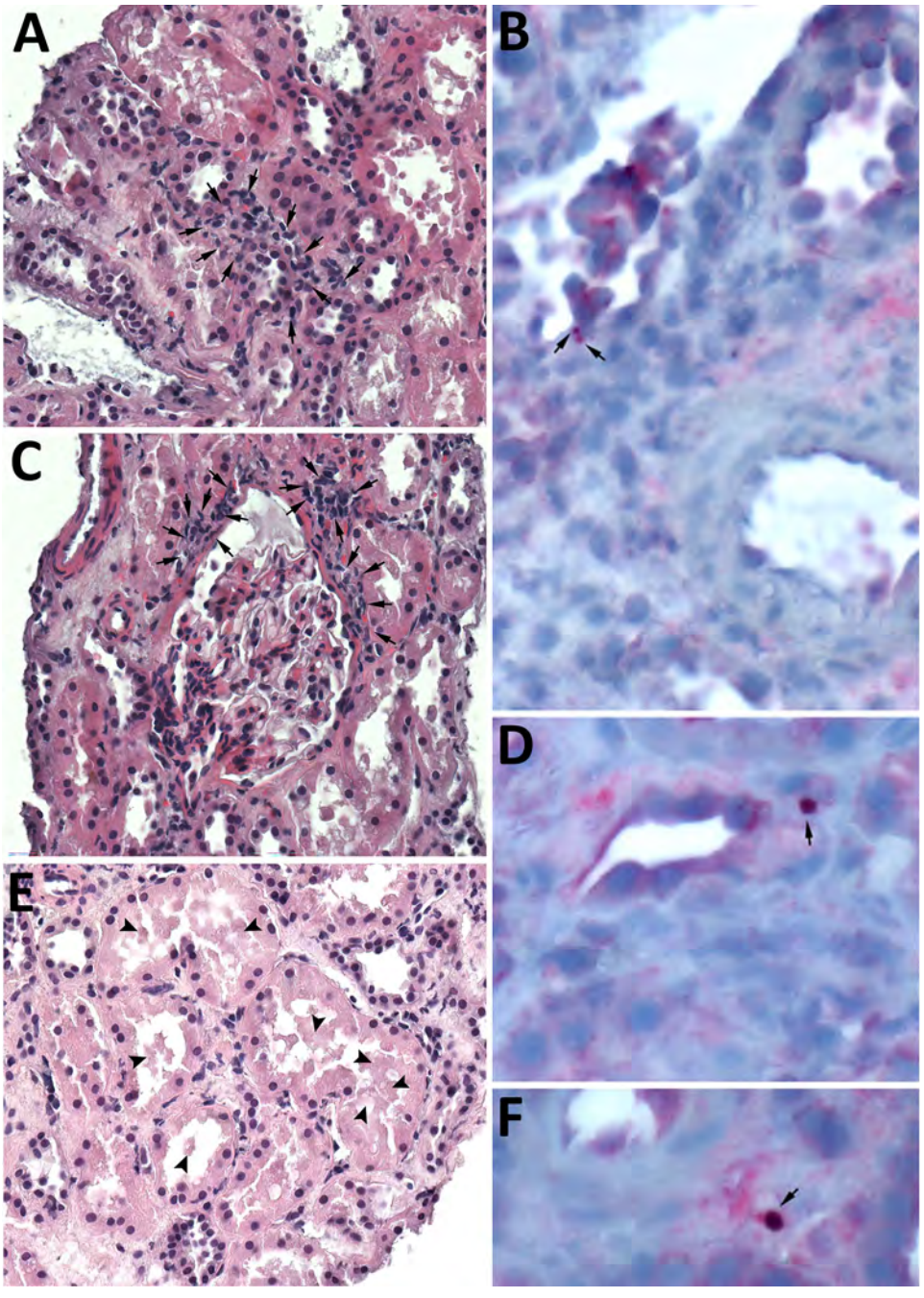

Figure. Histopathologic and immunohistochemical staining of renal graft biopsy from donor-derived ehrlichiosis caused by *Ehrlichia chaffeensis* from living donor kidney transplant. We performed an immunohistochemical (IHC) assay using an immunoperoxidase technique, with naphthol fast-red substrate, light hematoxylin counterstaining, and an antibody raised against *E. canis* but known to cross-react with other *Ehrlichia* species, including *E. chaffeensis* and *E. ewingii*, among others. A) Interstitial peritubular mononuclear cell infiltrate (arrows). Hematoxylin and eosin (H&E) stain; original magnification ×400. B) Immunostaining of bacterial antigens from *Ehrlichia* species within 2 morulae in the cytoplasm of reactive endothelial cells of a renal venule (arrows). Original magnification ×630. C) Periglomerular focal interstitial mononuclear cell inflammation (arrows). H&E stain; original magnification ×400. D) Magnification of IHC assay of kidney biopsy indicating a granular immunostaining pattern within intracellular morulae (arrows). Original magnification ×1,000. E) Renal tubules displaying some features of acute tubular necrosis including epithelial cells with condensed chromatin and sloughing of cells into lumina. The tubular lumina are filled with sloughed-off necrotic tubular epithelial cells (arrowheads). Some tubules show near complete luminal occlusion. Casts are not identified. H&E stain; original magnification ×630. F) Another intracellular morulae seen on kidney biopsy by IHC assay (arrow). Original magnification ×1,000.

remained negative. Because of persistent fever that increased to 103°F (39.4°C), worsening renal function, and onset of neutropenia and thrombocytopenia, we performed broad-range 16S rRNA gene PCR on the perinephric fluid, serum Lyme PCR, whole-blood *Babesia* spp. PCR, and whole blood *Ehrlichia* and *Anaplasma* spp. PCR. Progressive kidney injury prompted a graft biopsy.

Further patient history revealed no new sexual partners, no international travel, and minimal outdoor exposure before or after transplantation. Neither he nor his dogs had known recent tick exposures.

The whole-blood *E. chaffeensis* PCR result was positive, and the 16S rRNA gene PCR, followed by sequencing of the perinephric fluid collection, detected *E. chaffeensis*. The patient started oral doxycycline with defervescence within 12 hours. His pancytopenia and renal function improved, and he was discharged on hospitalization day 9 with a creatinine level of 3.6 mg/dL. Two weeks after starting

doxycycline, his perinephric drain was removed; doxycycline was stopped 7 days later, for a total 21-day course. Six weeks after transplant, he had a creatinine level of 1.1 mg/dL, as well as unremarkable leukocyte and platelet counts.

Ehrlichiosis is a nationally notifiable disease; therefore, the recipient's positive *E. chaffeensis* PCR result was reported through the Wisconsin Electronic Disease Surveillance System, initiating a routine investigation by the Wisconsin Department of Health Services. During the interview, the recipient denied recent travel outside his Wisconsin county of residence, outdoor activities, or tick exposures. His recent organ transplantation triggered a multiagency investigation. The donor, a Minnesota resident, reported the following to the Minnesota Department of Health: outdoor exposure in Minnesota and travel to Kansas to hunt 3 weeks before the transplant. While in Kansas, which is an *E. chaffeensis*–endemic state, the donor removed several ticks crawling on his body and clothing, including 1 attached tick; he then experienced an illness the donor attributed to food poisoning the week before transplant.

Tissue biopsies from the transplanted kidney sent to the Centers for Disease Control and Prevention (CDC) revealed mild-to-moderate acute tubular injury and necrosis (Figure, panels A, C, E). Because of clinical and epidemiologic concerns for transplant-transmitted infection of *E. chaffeensis*, we performed an immunohistochemical assay raised against *E. canis* that is known to cross-react with other *Ehrlichia* species, including *E. chaffeensis* (*6*). The immunohistochemical assay highlighted antigens of *Ehrlichia* spp. in intracellular morulae located within circulating and interstitial mononuclear inflammatory cells and endothelial cells of periglomerular capillaries (Figure, panels B, D, F). IgG against *E. chaffeensis* was detected in archived predonation donor serum samples at a titer of 1:128, increasing 4-fold to 1:512 in postdonation donor serum collected on POD 119. The recipient's pretransplant serum samples were all PCR negative for *E. chaffeensis* (Table).

The laboratory evidence, exposure history, and epidemiology of ehrlichiosis strongly support donor-derived transmission of *E. chaffeensis* initially acquired by the donor through a tick bite in Kansas 3 weeks before donation (*7*). That case highlights the importance of rapid communication between transplant centers when donor-derived infections are suspected and the value of a parallel surveillance system for tickborne infections leading to a comprehensive investigation between 2 state health departments and the assistance of CDC reference laboratories.

Although routine screening of all living donors for laboratory evidence of ehrlichiosis is not justified, this case study emphasizes the importance of asking living donors and deceased donor next of kin about recent travel and tick exposures, given the perioperative risk to both living donors and recipients. Donor-derived infection from a living donor is unique and is definitive evidence that acute infection with *Ehrlichia* spp. preoperatively developed in the donor. A prior report showed posttransplant ehrlichiosis in 2 kidney recipients with no exposure to ticks transmitted from a deceased donor with increased risk for tickborne disease but no positive donor testing (*5*). Another study highlighted 2 clusters of donor-derived ehrlichiosis from 2 deceased donors found to have attached ticks on postmortem exam; 1 donor had perimortem serum IgG positive for *E. chaffeensis* but no convalescent titers (*8*).

Table. Summary of *Ehrlichia* testing of living donor and recipient from donor-derived ehrlichiosis caused by *Ehrlichia chaffeensis* from living donor kidney transplant*

Days from kidney donation	Specimen	IgG IFA titer†	Real-time PCR‡	16S rRNA gene PCR§	Immunohistochemical assay¶
Donor					
−10	Serum	1:128	Negative	ND	ND
0	Serum	1:128	Negative	ND	ND
20	Serum	1:256	ND	ND	ND
119	Serum	1:512	ND	ND	ND
Recipient					
−15	Serum	ND	Negative	ND	ND
0	Serum	ND	Negative	ND	ND
11	Perinephric fluid	ND	ND	*E. chaffeensis* detected	ND
14	Blood	ND	Positive	ND	ND
16	Renal tissue biopsy	ND	ND	ND	*Ehrlichia* spp. antigens detected

*IFA, indirect fluorescent antibody; ND, not done.
†Testing performed at the Centers for Disease Control and Prevention.
‡Testing performed at the Centers for Disease Control and Prevention and Mayo Clinic Laboratories. Negative results defined as no bacterial DNA detected by real-time PCR.
§Testing performed at University of Wisconsin Hospital Laboratory.
¶Testing performed at the Centers for Disease Control and Prevention.

This recipient's perinephric fluid 16S rRNA gene PCR was sent for evaluation for typical etiologies of surgical site infection, but it detected *E. chaffeensis*. We cannot determine whether that evaluation represents infected fluid or contamination from the recipient's circulating infected mononuclear cells. However, that evaluation prompted extended therapy beyond the CDC recommendation of ≥3 days of doxycycline after defervescence and until clinical improvement (typically a minimum of 5–7 days) (*9*).

Previously published cases have suggested that trimethoprim/sulfamethoxazole use may increase the severity of ehrlichiosis, although an analysis in 2020 did not find a major association between trimethoprim/sulfamethoxazole use and need for intensive care after controlling for underlying conditions and doxycycline treatment delay (*10*). In addition, this case highlights rhabdomyolysis, a relatively uncommon and serious complication of ehrlichiosis (*11*,*12*). This donation surgery was not prolonged, and the CK level was higher than expected for routine postoperative rhabdomyolysis. Recognition of a disproportionately high CK level should trigger further evaluation for a secondary cause such as infection.

Conclusions

In summary, clinicians should remain vigilant for tickborne infections in potential organ donors, particularly those with known exposure to common disease vectors. Clinicians should maintain a broad differential when evaluating solid organ recipients with febrile syndrome shortly after transplantation, even if the donor, recipient, or both reside in areas where potential pathogens are not endemic.

About the Author

Dr. Scolarici is a transplant infectious disease physician at the University of Wisconsin in Madison. His primary research interest revolves around the optimization of care for solid organ transplant recipients.

References

1. Dumler JS, Madigan JE, Pusterla N, Bakken JS. Ehrlichioses in humans: epidemiology, clinical presentation, diagnosis, and treatment. Clin Infect Dis. 2007;45:S45–51. https://doi.org/10.1086/518146
2. Thomas LD, Hongo I, Bloch KC, Tang Y-W, Dummer S. Human ehrlichiosis in transplant recipients. Am J Transplant. 2007;7:1641–7. https://doi.org/10.1111/j.1600-6143.2007.01821.x
3. Mowla SJ, Drexler NA, Cherry CC, Annambholta PD, Kracalik IT, Basavaraju SV. Ehrlichiosis and anaplasmosis among transfusion and transplant recipients in the United States. Emerg Infect Dis. 2021;27:2768–75. https://doi.org/10.3201/eid2711.211127
4. Adachi JA, Grimm EM, Johnson P, Uthman M, Kaplan B, Rakita RM. Human granulocytic ehrlichiosis in a renal transplant patient: case report and review of the literature. Transplantation. 1997;64:1139–42. https://doi.org/10.1097/00007890-199710270-00010
5. Sachdev SH, Joshi V, Cox ER, Amoroso A, Palekar S. Severe life-threatening *Ehrlichia chaffeensis* infections transmitted through solid organ transplantation. Transpl Infect Dis. 2014;16:119–24. https://doi.org/10.1111/tid.12172
6. Dawson JE, Paddock CD, Warner CK, Greer PW, Bartlett JH, Ewing SA, et al. Tissue diagnosis of *Ehrlichia chaffeensis* in patients with fatal ehrlichiosis by use of immunohistochemistry, in situ hybridization, and polymerase chain reaction. Am J Trop Med Hyg. 2001;65:603–9. https://doi.org/10.4269/ajtmh.2001.65.603
7. Centers for Disease Control and Prevention. Ehrlichiosis epidemiology and statistics [cited 2024 May 9]. https://www.cdc.gov/ehrlichiosis/stats/index.html
8. Saha A, Browning C, Dandamudi R, Barton K, Graepel K, Cullity M, et al. Donor-derived ehrlichiosis: 2 clusters following solid organ transplantation. Clin Infect Dis. 2022;74:918–23. https://doi.org/10.1093/cid/ciab667
9. Biggs HM, Behravesh CB, Bradley KK, Dahlgren FS, Drexler NA, Dumler JS, et al. Diagnosis and management of tickborne rickettsial diseases: Rocky Mountain spotted fever and other spotted fever group rickettsioses, ehrlichioses, and anaplasmosis—United States. MMWR Recomm Rep. 2016;65:1–44. https://doi.org/10.15585/mmwr.rr6502a1
10. Kuriakose K, Pettit AC, Schmitz J, Moncayo A, Bloch KC. Assessment of risk factors and outcomes of severe ehrlichiosis infection. JAMA Netw Open. 2020;3:e2025577. https://doi.org/10.1001/jamanetworkopen.2020.25577
11. Overmiller AC, Bitter CC. Rhabdomyolysis and multisystem organ failure due to fulminant ehrlichiosis infection. Wilderness Environ Med. 2021;32:226–9. https://doi.org/10.1016/j.wem.2021.01.009
12. Shea KW, Calio AJ, Klein NC, Cunha BA. Rhabdomyolysis associated with *Ehrlichia chaffeensis* infection. Clin Infect Dis. 1995;21:1056–7. https://doi.org/10.1093/clinids/21.4.1056

Address for correspondence: Michael Scolarici, University of Wisconsin Hospital and Clinics, 600 Highland Ave, Madison, WI 53792, USA; email: mscolarici@uwhealth.org

Cefotaxime-Resistant *Neisseria meningitidis* Sequence Type 4821 Causing Fulminant Meningitis

Youxing Shao,[1] Mingliang Chen,[1] Jiehao Cai, Yohei Doi, Min Chen, Minggui Wang, Mei Zeng, Qinglan Guo

We explored the role of commensal *Neisseria* in the emergence of third-generation cephalosporin-resistant *N. meningitidis*. Cefotaxime resistance–conferring *penA795* was prevalent among commensal *Neisseria* isolates in Shanghai, China, and was acquired by a serogroup C quinolone-resistant sequence type 4821 *N. meningitidis*, Nm507, causing fulminant meningitis in an unvaccinated 2-year-old child.

Invasive meningococcal disease (IMD) is a severe infection caused by *Neisseria meningitidis*. Early empiric treatment with penicillin or third-generation cephalosporins (3GCs) including ceftriaxone and cefotaxime, is crucial (*1*). Over the past 2 decades, the spread of the hyperinvasive and quinolone-resistant *N. meningitidis* clone China$^{CC4821\text{-}R1\text{-}C/B}$ (sublineage L44.1, mainly serogroup C) within clonal complex (CC) 4821 has resulted in ≈70% fluoroquinolone resistance among meningococci in China (*2*). More recently, penicillin nonsusceptiblity has increased rapidly among meningococci in China (*3*–*5*). We recently reported acquisition of penicillin and cefotaxime resistance by CC4821 (*3*).

The *penA* gene (around 1,746 bp, NEIS1753) encodes penicillin binding protein 2 (PBP2), a 2-domain protein (*6*). A 402-bp region (nucleotides 1321–1722, amino acids 441–574) is commonly used to determine *penA* alleles in meningococci. Five well-characterized alterations in the C-terminal catalytic transpeptidase of PBP2 (PBP2-TPase) are primarily responsible for penicillin nonsusceptibility in meningococci (*7*). A series of additional mutations in PBP2-TPase contribute to ceftriaxone resistance in the globally disseminated *N. gonorrhoeae* FC428 clone (*8*,*9*). Three cefotaxime-resistant meningococci isolates were reported in China during 2017–2019 (*3*). The case reported in this article involves, 1 of those 3 isolates, Nm507, serogroup C quinolone-resistant sequence type (ST) 4821 (C: P1.21–2,9:F3–3:ST4821, L44.1), which led to a rare fulminant case of IMD (Appendix, https://wwwnc.cdc.gov/EID/article/31/3/24-1493-App1.pdf). This study was approved by the Institutional Review Board of Children's Hospital of Fudan University (approval no. 2023–111).

The Study

A 2-year-old child was initially infected with influenza A virus and subsequently developed purpura fulminans, progressing to septic shock and disseminated intravascular coagulation. Mechanical ventilation, fluid resuscitation, and vasoactive drugs were administered to stabilize his vital signs. After 1 dose of penicillin, antimicrobial therapy was changed to ceftriaxone for 14 days (Appendix Figure 1). The child recovered fully. Previous influenza A virus infection is hypothesized to increase the risk for IMD because it disrupts the nasopharyngeal epithelium and normal flora (*10*).

We isolated 3 *N. meningitidis* isolates from the patient: Nm507 (blood), Nm508 (cerebrospinal fluid), and Nm509 (nasopharynx). Antimicrobial susceptibility testing showed the 3 *N. meningitidis* isolates were resistant to penicillin (MICs 0.75 μg/mL),

Author affiliations: Institute of Antibiotics, Huashan Hospital, Fudan University, Shanghai, China (Y. Shao, M. Wang, Q. Guo); Key Laboratory of Clinical Pharmacology of Antibiotics, National Heath Commission of the People's Republic of China, Shanghai (Y. Shao, M. Wang, Q. Guo); Minhang Hospital, Fudan University, Shanghai (M. Chen); Children's Hospital of Fudan University, Shanghai (J. Cai, M. Zeng); University of Pittsburgh School of Medicine, Pittsburgh, Pennsylvania, USA (Y. Doi); Fujita Health University School of Medicine, Toyoake, Japan (Y. Doi); Shanghai Municipal Center for Disease Control and Prevention, Shanghai (M. Chen)

DOI: https://doi.org/10.3201/eid3103.241493

[1]These authors contributed equally to this article.

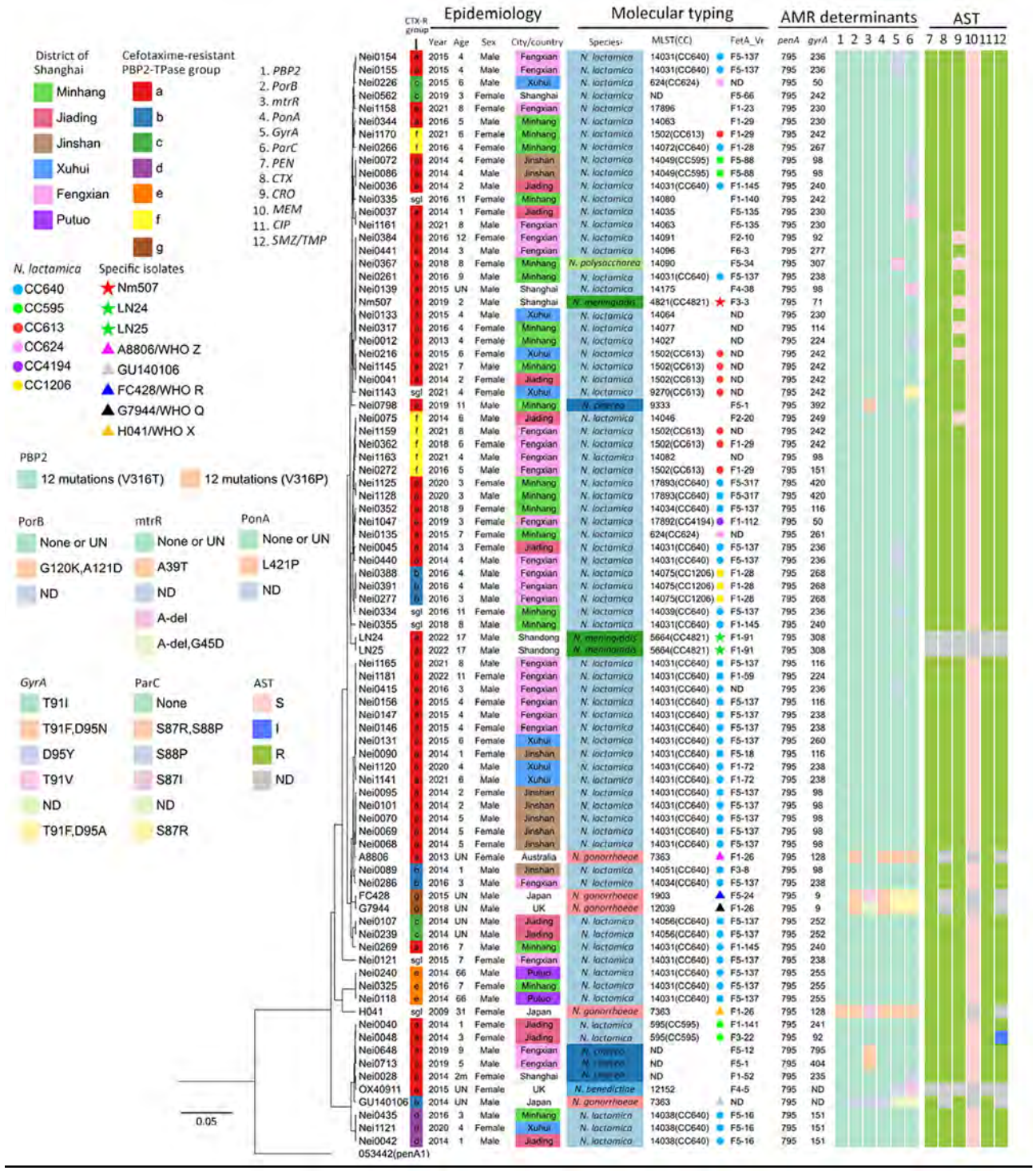

Figure 1. Epidemiologic and molecular characterizations of *penA795*-bearing *Neisseria meningitidis*, *N. gonorrhoeae*, and *Neisseria* commensals in study of cefotaxime-resistant *N. meningitidis* sequence type 4821 causing fulminant meningitis. Epidemiology, molecular typing, antimicrobial resistance determinants, and antimicrobial susceptibility testing results of 85 *penA795*-bearing *Neisseria* isolates are shown. The leftmost tree depicts the phylogeny of the PBP2-TPase region (*penA* 718 to 1,746 bp). Analysis of mutations in antimicrobial resistance-associated genes/determinants is provided in the Appendix (https://wwwnc.cdc.gov/EID/article/31/3/24-1493-App1.pdf). Scale bar indicates number of nucleotide substitutions per site. AMR, antimicrobial resistance; AST, antimicrobial susceptibility testing; CC, clonal complex; CIP, ciprofloxacin; CRO, ceftriaxone; CTX, cefotaxime; MEM, meropenem; MLST, multilocus sequence type; I, intermediate; ND, not determined; PEN, penicillin; R, resistant; sgl, singleton; S, susceptible; UN, unknown.

cefotaxime (MICs 0.25 μg/mL), ciprofloxacin (MICs 0.5 μg/mL), and trimethoprim/sulfamethoxazole (MICs >2/38 μg/mL) and had reduced susceptibility to ceftriaxone (MICs 0.125 μg/mL) and meropenem (MICs 0.047 μg/mL). The 3 isolates were genetically identical and harbored *penA795*, which contained 12 mutations associated with penicillin and 3GCs resistance in the PBP2-TPase. These mutations included 5 classic penicillin-resistance–associated mutations (F504L, A510V, I515V, H541N, and I566V) (*7*) and the A549T mutation, which contributes to penicillin nonsusceptibility (*3*). In addition, they contained 6 mutations found in *N. gonorrhoeae* strain FC428 associated with resistance to 3GCs (A311V, I312M, V316T, T483S, N512Y, and G545S) (*8*,*9*), without any other determinants conferring resistance to 3GCs. Natural transformants, obtained from previous research (*3*), harbored mosaic *penA*, and the segments containing *penA795* were transferred from 3 commensal *Neisseria* species to penicillin- and 3GCs-susceptible recipient *N. meningitidis* Nm040 (penicillin MIC 0.032 μg/mL, cefotaxime MIC 0.008 μg/mL). All natural transformants showed penicillin nonsusceptibility (MIC 0.19–0.38 μg/mL) and cefotaxime resistance (MIC 0.25–0.5 μg/mL). In addition, MICs were elevated by 32–62-fold (0.064–0.125 μg/mL) for ceftriaxone and by 2–5-fold (0.023–0.064 μg/mL) for meropenem compared with recipient Nm040 (ceftriaxone MIC ≤0.002 μg/mL, meropenem MIC 0.012 μg/mL) (Appendix Table 1).

We cataloged the *penA* alleles in 1,032 local commensal *Neisseria* isolates (commensals) and observed *penA795* in 76/1,032 (7.4%) isolates. The 76 *penA795*-bearing commensals included *N. lactamica* (n = 71), *N. cinerea* (n = 4), and *N. polysaccharea* (n = 1) (Figure 1). Among the 71 *N. lactamica* isolates, CC640 dominated (54.9%, 39 isolates; 27 isolates were ST14031). Those *penA*795-bearing commensals were collected from 6 districts of Shanghai (Figures 1, 2); they were isolated from persons of various ages, mainly children 3–6 years of age (n = 42), students 7–11 years of age (n = 18), and children <3 years of age (n = 10), over a 10-year period (2013–2022) (Figures 1, 3). All 76 *penA795*-bearing commensals were resistant to penicillin, cefotaxime, and ciprofloxacin and nonsusceptible (75/76 resistant, 1 intermediate) to trimethoprim/sulfamethoxazole but susceptible to meropenem. Seventy-one isolates (93%, 71/76) were resistant to ceftriaxone (Figure 1; Appendix Table 2).

We identified the *penA795* allele among 6 *Neisseria* species (85 isolates, including 76 from this study) through searches in PubMLST (https://pubmlst.org/neisseria) and PubMed (*8*,*11*–*14*). Of note, *penA795* has been transferred among unrelated *N. gonorrhoeae* clones such as H041 (World Health Organization gonococcal reference strain X [WHO X], 2009, Japan)

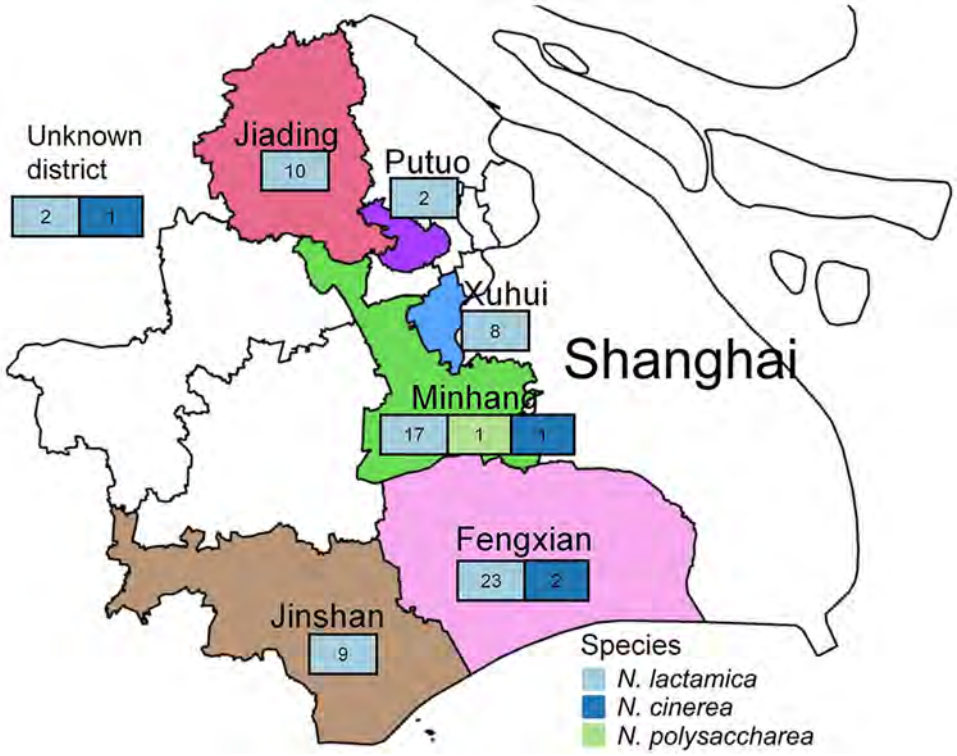

Figure 2. Sampling locations of 76 *penA795*-bearing *Neisseria* commensals in 6 districts of Shanghai, China, in study of cefotaxime-resistant *Neisseria meningitidis* sequence type 4821 causing fulminant meningitis.

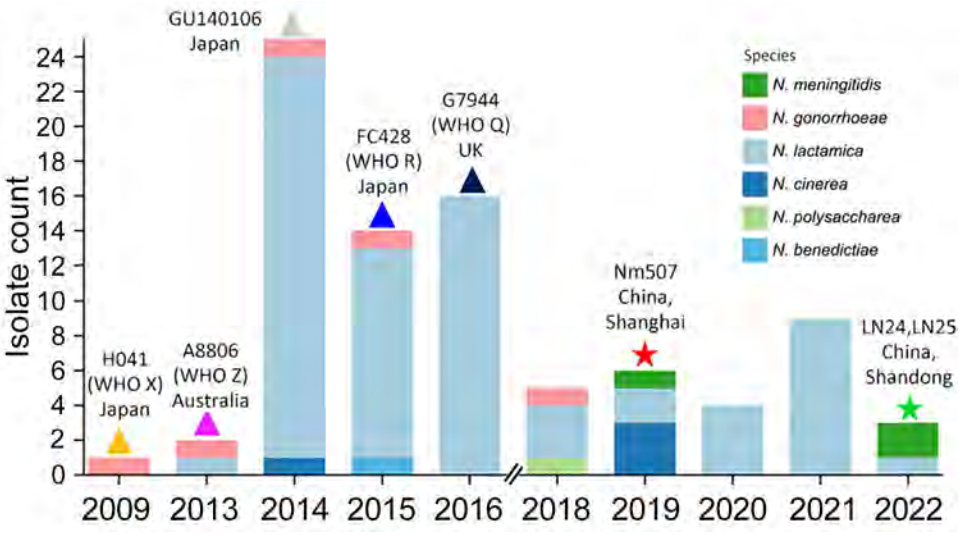

Figure 3. Timeline of 85 *penA795*-bearing *Neisseria* isolates from China and elsewhere during 2009–2022 in study of cefotaxime-resistant *Neisseria meningitidis* sequence type 4821 causing fulminant meningitis. WHO, World Health Organization.

(*11*), A8806 (WHO Z, 2013, Australia) (*12*), GU140106 (2014, Japan) (*13*), the FC428 international clone (WHO R, 2015, Japan) (*8*), and G7944 (WHO Q, 2018, United Kingdom) (*14*) (Figures 1, 3; Appendix Table 1). Only 3 *penA795*-bearing *N. meningitidis* isolates have been reported: Nm507 from Shanghai in 2019 and LN24 and LN25 (PubMLST identifications 133563 and 133564) from Shandong Province, China, in 2022. LN24 and LN25 exhibit identical molecular characteristics as B: P1.20,23–1: F1–91:ST5664 (CC4821, L44.2) (Figures 1, 3). MIC data for LN24 and LN25 are unavailable. We extracted the full-length *penA* (NEIS1753) sequences from 85 *penA795*-bearing *Neisseria* isolates and divided them at nucleotide position 718, according to the N terminal (*penA* 1–717) and C terminal (*penA* 718–1,746) encompassing the 3 conserved motifs of the PBP2-TPase domain of PBP2 (Appendix Figures 2, 3) (*6*). The +718 to +900 region possessed 1%–28% nucleotide variations. Except for H041, which had an amino acid alternation of V316P, all isolates harbored the 12 resistance-associated mutations in PBP2-TPase described in Nm507 and FC428 (Appendix Table 1, Figure 3). We classified 85 *penA795*-bearing *Neisseria* isolates into 7 groups (a–g) and 6 singletons based on PBP2-TPase sequences associated with cefotaxime resistance (*penA* 901–1,746, covering 12 resistance-associated mutations) (Figure 1). Nm507 shared an identical cefotaxime-resistant PBP2-TPase sequence with 50 *penA795*-bearing commensals, as well as LN24, LN25, and A8806 (CTX-R group a), suggesting likely horizontal gene transfer among different *Neisseria* species, especially from *N. lactamica* to *N. meningitidis*. Natural transformation experiments (*3*) reproduced the horizontal gene transfer event of *N. meningitidis* acquiring the *penA795*-bearing segment from *Neisseria* commensals.

Commensal *Neisseria*, with a 100% carriage rate, serve as an ideal reservoir of antimicrobial resistance genetic elements for local meningococci. The widespread presence of *penA795*-bearing *N. lactamica* CC640, exhibiting multidrug resistance to penicillin, cefotaxime, ceftriaxone, ciprofloxacin, and trimethoprim-sulfamethoxazole in Shanghai, raises substantial concerns over its role in fostering the emergence of multidrug-resistant *N. meningitidis*. Moreover, the increase of international travel heightens the risk for both meningococcal and multidrug-resistant commensal colonization. Of note, *penA795*-bearing *N. meningitidis* (LN24 and LN25) in Shandong were recovered sharing identical PBP2-TPase sequences associated with cefotaxime resistance with commensals from Shanghai.

Conclusions

Our study reveals widespread presence of the *penA795* allele, which encodes PBP2-TPase associated with cefotaxime resistance, among *Neisseria* commensals in Shanghai, China. The *penA795* fragment has been captured by the hyperinvasive, quinolone-resistant NmC *N. meningitidis* ST4821, causing life-threatening meningitis. In China, scheduled meningococcal vaccines include the group A polysaccharide vaccine (MPV-A, 2 doses at 6 and 9 months) and the bivalent NmA and NmC polysaccharide vaccine (MPV-AC, administered at 3 and 6 years of age). This patient had received only 2 doses of MPV-A, because MPV-AC is not licensed for young children (<2–3 years of age). A recent study has just reported an outbreak of NmC caused by multidrug-resistant ST4821 isolates in Fiji (*15*). Promoting coverage with meningococcal polysaccharide conjugate vaccine (MPCV), such

as MPCV-AC or MPCV-ACYW, will be imperative to effectively reduce illness and deaths caused by *N. meningitidis*, particularly the emerging multidrug-resistant invasive NmC clone.

This study used *Neisseria* genomic data deposited in the PubMLST database (https://pubmlst.org/neisseria), sited at the University of Oxford (Jolley & Maiden, 2018, Wellcome open research, 3:124).

This work was supported by the National Natural Science Foundation of China (grant nos. 82373918, 82272381, 81872909, and 82472322). The funders played no role in the study design, data collection, and interpretation, or the decision to submit the work for publication.

About the Author

Dr. Shao is a PhD candidate from Institute of Antibiotics, Huashan Hospital, Fudan University. His research interests include bacterial antimicrobial resistance mechanisms.

References

1. Hasbun R. Progress and challenges in bacterial meningitis: a review. JAMA. 2022;328:2147–54. https://doi.org/10.1001/jama.2022.20521
2. Chen M, Harrison OB, Bratcher HB, Bo Z, Jolley KA, Rodrigues CMC, et al. Evolution of sequence type 4821 clonal complex hyperinvasive and quinolone-resistant meningococci. Emerg Infect Dis. 2021;27:1110–22. https://doi.org/10.3201/eid2704.203612
3. Chen M, Shao Y, Luo J, Yuan L, Wang M, Chen M, et al. Penicillin and cefotaxime resistance of quinolone-resistant *Neisseria meningitidis* clonal complex 4821, Shanghai, China, 1965–2020. Emerg Infect Dis. 2023;29:341–50. https://doi.org/10.3201/eid2902.221066
4. Xu L, Zhu B, Xu Z, Gao Y, Shao Z. Analysis on antibiotic susceptibility of Neisseria meningitidis isolates in China, 2003–2012 [in Chinese]. Dis Surveill. 2015;30:316–20.
5. Xu L, Han FY, Wu D, Zhu BQ, Gao WY, Gao Y, et al. Analysis on antimicrobial sensitivity of *Neisseria meningitidis* in China from 2005 to 2019 [in Chinese]. Zhonghua Yu Fang Yi Xue Za Zhi. 2021;55:207–11.
6. Powell AJ, Tomberg J, Deacon AM, Nicholas RA, Davies C. Crystal structures of penicillin-binding protein 2 from penicillin-susceptible and -resistant strains of *Neisseria gonorrhoeae* reveal an unexpectedly subtle mechanism for antibiotic resistance. J Biol Chem. 2009;284:1202–12. https://doi.org/10.1074/jbc.M805761200
7. Shao Y, Chen M, Luo J, Li D, Yuan L, Yang X, et al. Serogroup Y clonal complex 23 meningococcus in China acquiring penicillin resistance from commensal *Neisseria lactamica* species. Antimicrob Agents Chemother. 2022;66:e0238321. https://doi.org/10.1128/aac.02383-21
8. Nakayama S, Shimuta K, Furubayashi K, Kawahata T, Unemo M, Ohnishi M. New ceftriaxone- and multidrug-resistant *Neisseria gonorrhoeae* strain with a novel mosaic *penA* gene isolated in Japan. Antimicrob Agents Chemother. 2016;60:4339–41. https://doi.org/10.1128/AAC.00504-16
9. Kanesaka I, Ohno A, Morita M, Katsuse AK, Morihana T, Ito T, et al. Epigenetic effects of ceftriaxone-resistant *Neisseria gonorrhoeae* FC428 mosaic-like sequences found in PenA sequences unique to *Neisseria subflava* and related species. J Antimicrob Chemother. 2023;78:2683–90. https://doi.org/10.1093/jac/dkad281
10. Salomon A, Berry I, Tuite AR, Drews S, Hatchette T, Jamieson F, et al. Influenza increases invasive meningococcal disease risk in temperate countries. Clin Microbiol Infect. 2020;26:1257.e1–7. https://doi.org/10.1016/j.cmi.2020.01.004
11. Ohnishi M, Golparian D, Shimuta K, Saika T, Hoshina S, Iwasaku K, et al. Is *Neisseria gonorrhoeae* initiating a future era of untreatable gonorrhea?: detailed characterization of the first strain with high-level resistance to ceftriaxone. Antimicrob Agents Chemother. 2011;55:3538–45. https://doi.org/10.1128/AAC.00325-11
12. Lahra MM, Ryder N, Whiley DM. A new multidrug-resistant strain of *Neisseria gonorrhoeae* in Australia. N Engl J Med. 2014;371:1850–1. https://doi.org/10.1056/NEJMc1408109
13. Deguchi T, Yasuda M, Hatazaki K, Kameyama K, Horie K, Kato T, et al. New clinical strain of *Neisseria gonorrhoeae* with decreased susceptibility to ceftriaxone, Japan. Emerg Infect Dis. 2016;22:142–4. https://doi.org/10.3201/eid2201.150868
14. Eyre DW, Sanderson ND, Lord E, Regisford-Reimmer N, Chau K, Barker L, et al. Gonorrhoea treatment failure caused by a *Neisseria gonorrhoeae* strain with combined ceftriaxone and high-level azithromycin resistance, England, February 2018. Euro Surveill. 2018;23:1800323. https://doi.org/10.2807/1560-7917.ES.2018.23.27.1800323
15. Strobel AG, Sahukhan A, Ratu A, Kailawadoko J, Koroituku I, Singh S, et al. Meningococcal C disease outbreak caused by multidrug-resistant *Neisseria meningitidis*, Fiji. Emerg Infect Dis. 2025;31:32–40. https://doi.org/10.3201/eid3101.240476

Address for correspondence: Qinglan Guo, Institute of Antibiotics, Huashan Hospital, Fudan University, 12 Middle Wulumuqi Rd, Shanghai 200040, China; email: qinglanguo@fudan.edu.cn; Mei Zeng, Children's Hospital of Fudan University, 399 Wanyuan Rd, Shanghai 201102, China; email: zengmeigao@aliyun.com

Tsukamurella tyrosinosolvens Respiratory Infection in Immunocompetent Man

Aidan Clifford, Jenny Siaw Jin Wong, Ben Aw-Yeong, Kerrie Lea, Maria Globan, Benjamin Smith

Tsukamurella spp. are an infrequent and underdiagnosed cause of bacterial respiratory infection, usually occurring in patients with structural lung disease or immune compromise. We describe *T. tyrosinosolvens* respiratory infection in a patient in Australia without structural lung disease or known immune deficiency. The patient was successfully treated with oral ciprofloxacin and clarithromycin.

Tsukamurella spp. are variably or weakly acid-fast, gram-positive, non–spore-forming, obligate aerobic actinomycetes and are typically isolated from water, soil, and other terrestrial samples. *Tsukamurella* infections are rare but, when reported, are often associated with indwelling vascular or peritoneal catheters (*1*). *Tsukamurella* spp. also have been described as causative agents in respiratory infection, meningitis, keratitis, cutaneous infection, and acute otitis media (*1*,*2*). Nonpathogenic respiratory colonization by *Tsukamurella* spp. also has been described (*1*). *Tsukamurella* respiratory infection probably is underidentified because of clinical, radiologic, and morphologic similarities with related, more common organisms such as *Mycobacterium tuberculosis*. The advent of DNA and RNA sequencing techniques and matrix-assisted laser desorption/ionization time-of-flight (MALDI-TOF) mass spectrometry has enabled an increase in diagnosis of *Tsukamurella* infection (*2*,*3*).

Tsukamurella spp. respiratory infection might be clinically indistinguishable from pulmonary tuberculosis (TB); symptoms include cough, hemoptysis, and weight loss (*1*). Current understanding of risk factors is limited; however, 38% of previously described cases were associated with immune compromise and 69% with underlying structural lung disease (*1*,*4*–*13*) (Appendix, https://wwwnc.cdc.gov/EID/article/31/3/24-1365-App1.pdf). *Tsukamurella* pulmonary co-infection with other aerobic actinomycetes also has been described (*13*).

Because reported cases are rare, awareness of *Tsukamurella* spp. infection among clinicians is limited, and evidence to guide empiric management is scarce. We describe a case of *T. tyrosinosolvens* respiratory infection in an apparently immunocompetent patient in Australia without underlying structural lung disease.

The Case-Patient

A 25-year-old man, 3 years postmigration from India, was referred to our hospital with right apical nodular opacities on chest radiograph performed during routine migrant screening, which were presumed to be attributable to TB. He was asymptomatic, with no cough, dyspnea, fevers, night sweats, or recent weight loss. The patient had no remarkable medical history and did not take medications regularly. He reported no smoking or recreational drug use. He had no history of immune deficits such as HIV infection, malignancy, stem cell or solid organ transplant, steroid or other immunosuppressive drug use, diabetes mellitus, alcoholism, renal failure, liver failure, or previous splenectomy. He worked in manufacturing and had exposure to diesel engines and reported no exposure to soil, animals, or wastewater.

At initial assessment, the patient was afebrile and had no focal respiratory signs. Initial blood testing results were unremarkable; C-reactive protein and leukocyte counts were within reference ranges.

Author affiliations: Western Health, Melbourne, Victoria, Australia (A. Clifford, B. Smith); Dorevitch Pathology, Melbourne (J. Siaw Jin Wong, B. Aw-Yeong); Victorian Infectious Disease Reference Laboratory at the Peter Doherty Institute for Infection and Immunity, Melbourne (K. Lea, M. Globan)

DOI: https://doi.org/10.3201/eid3103.241365

Results of assay tests for TB and HIV were negative. Sputum specimens collected on 3 consecutive days were smear-negative for acid-fast bacilli (AFB) with auramine-rhodamine stain.

Computed tomography (CT) of the chest showed variable-sized pulmonary nodules in the right lung apex and surrounding tree-in-bud changes (Figure). CT also identified 2 cavities; the larger cavity measured 25 mm and contained an air-fluid level. The remaining lung was clear. Cultures of all 3 sputum samples indicated *Tsukamurella* spp. most closely related to *T. tyrosinosolvens*. We performed species identification through targeted Sanger DNA sequencing of a 550-bp fragment of the 16S rRNA gene, followed by BLAST analysis (https://blast.ncbi.nlm.nih.gov) to determine the most closely matched species. Given radiologic findings consistent with active infection and repeated isolation of *Tsukamurella* spp., we decided to treat empirically with ciprofloxacin and clarithromycin (both 500 mg 2/d).

Subsequent sensitivity testing through broth microdilution demonstrated susceptibility to a broad range of antimicrobial drugs, intermediate susceptibility to doxycycline, and resistance to amoxicillin/clavulanic acid and tobramycin (Table). Given the lack of clinical data to support development of validated MIC breakpoints for *Tsukamurella* spp., we interpreted susceptibilities by using MIC breakpoints for *Nocardia* spp. by Clinical and Laboratory Standards Institute guidelines (*14*). Two further sputum samples collected 1 month later also were AFB smear-negative; however, we cultured *Mycobacterium fortuitum* from a single specimen, which was not considered causative or otherwise clinically important.

After 3 months of treatment, the patient remained asymptomatic and reported no adverse events associated with treatment. Repeat CT showed interval reduction of the cavitating lesion from 25 to 17 mm (Figure). Treatment was continued for another 3 months, at which time the nodules had further reduced in size; the cavitating lesion measured 10 mm (Figure). After 6 months of macrolide and fluoroquinolone therapy, treatment was stopped. We noted no radiologic signs of infection recurrence on repeat CT at 6 months after treatment cessation.

Conclusions

We describe a case of *T. tyrosinosolvens* infection as a cause of cavitating respiratory disease in an immunocompetent and otherwise healthy young man. This case challenges the characterization of *Tsukamurella* spp. as opportunistic pathogens and should raise awareness of *Tsukamurella* respiratory infection. Although *Tsukamurella* pulmonary infection is rare, the number of reports is increasing, and most cases have been published within the last decade (Appendix). The emergence of *Tsukamurella* bacteria as a cause of human infection probably reflects advances in laboratory methods and increased recognition of a previously misdiagnosed disease. Although the true prevalence remains unclear, epidemiologic studies in China indicated that 1% of presumed nontuberculous *Mycobacteria* respiratory samples were *Tsukamurella* spp. when they were retrospectively analyzed using molecular methods (*15*).

Underrecognition occurs for several reasons. Lack of awareness among clinicians and the practice of treating AFB culture-positive infection as presumed TB in some clinical settings contribute

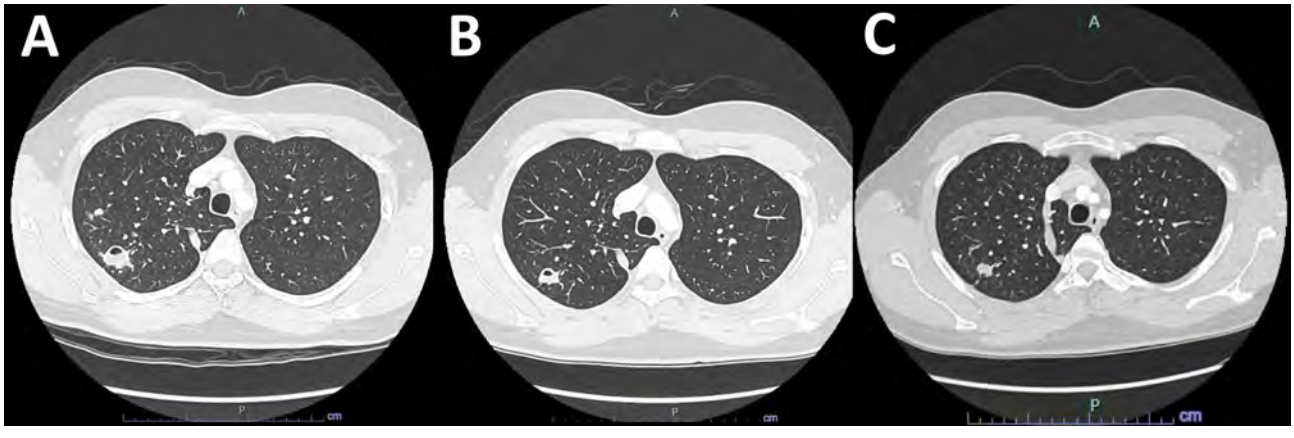

Figure. Computed tomography (CT) scans for reported case of *Tsukamurella tyrosinosolvens* infection in 25-year-old immunocompetent man. A) Initial CT showing 25-mm cavitating right apical lesion. B) Repeat CT after 6 months of treatment, indicating interval cavitary lesion reduction to 10 mm and resolution of the second smaller cavitation seen on original CT. C) Final CT 6 months after treatment cessation, indicating further cavity resolution without evidence of infection recurrence.

Table. Antimicrobial susceptibility testing results for reported case of *Tsukamurella tyrosinosolvens* infection in 25-year-old immunocompetent man, with tentative interpretation based on *Nocardia* spp. breakpoints (*14*)*

Agent	MIC, μg/mL	Tentative interpretation
Amikacin	1	S
Amoxicillin/clavulanic acid	64/32	R
Ceftriaxone	4	S
Ciprofloxacin	0.5	S
Clarithromycin	2	S
Doxycycline	4	I
Imipenem	2	S
Linezolid	2	S
Minocycline	1	S
Moxifloxacin	0.25	S
Tobramycin	16	R
Trimethoprim/sulfamethoxazole	0.25/4.75	S

*I, intermediate; R, resistant; S, sensitive.

to misdiagnosis (*2*,*7*). Because *Tsukamurella* spp. respiratory infection might be clinically, radiologically, and morphologically indistinguishable from pulmonary TB and might also respond to treatment with first-line TB therapy, the risk for misdiagnosis is high in the absence of microbiologic confirmation. A broader differential including other aerobic actinomycetes could be beneficial, especially in patients not responding to initial therapy. *Tsukamurella* resistance to first-line TB treatment agents has been described (*2*). Misdiagnosis has been shown to lead to excess disease and death in some case reports (*7*) and can also lead to use of unnecessary, toxicity-prone TB treatment regimens.

Microbiologic diagnosis often is resource-intensive. Standard laboratory phenotypic and biochemical methods might be inadequate to distinguish *Tsukamurella* from other aerobic actinomycetes. The advent of MALDI-TOF mass spectrometry and molecular techniques such as 16S rRNA and DNA sequencing have enabled accurate identification of *Tsukamurella* genus (*2*). Although 16S sequencing is an effective technique for identifying *Tsukamurella* genus, it often is insufficient to achieve species-level identification because of the high genetic conservation between species and lack of sequences available on public databases for comparison. Sequencing of additional housekeeping genes (e.g., *groEL*, *sec*A, and *rpoB*) might be necessary for *Tsukamurella* species identification. Although some literature describes low diagnostic accuracy of *Tsukamurella* spp. with MALDI-TOF mass spectrometry, recent database improvements have demonstrated species-level identification with 98% accuracy (*3*). Therefore MALDI-TOF mass spectrometry might be an efficacious and cost-effective diagnostic method compared with DNA and RNA sequencing techniques. Unfortunately, those methods might not be routinely available outside metropolitan clinical microbiology and reference laboratories and can be impractical in settings with high TB prevalence.

Even once diagnosis is made, evidence to guide antibiotic choice and duration of therapy is scarce. Empiric regimens are based on previous case reports, and duration must be guided by clinical response. In the absence of validated MIC breakpoints, correlation between in vivo and in vitro sensitivities might be poor. Current Clinical and Laboratory Standards Institute guidelines provide tentative breakpoints for interpreting *Tsukamurella* spp. susceptibility testing on the basis of *Nocardia* spp. breakpoints (*14*); however, patients should be monitored to ensure appropriate clinical response.

Acknowledgments

We thank the staff at Footscray Hospital for their tireless commitment to patient care.

The patient has provided consent for the publication of this case report.

We declare no conflict of interest, and the authors received no financial support for this work.

About the Author

Dr. Clifford is a medical registrar at Western Health. His primary research interests include infectious disease and global health.

References

1. Safaei S, Fatahi-Bafghi M, Pouresmaeil O. Role of *Tsukamurella* species in human infections: first literature review. New Microbes New Infect. 2018;22:6–12. https://doi.org/10.1016/j.nmni.2017.10.002
2. Yu S, Ding X, Hua K, Zhu H, Zhang Q, Song X, et al. Systematic investigation of the emerging pathogen of *Tsukamurella* species in a Chinese tertiary teaching hospital. Microbiol Spectr. 2023;11:e0164423. https://doi.org/10.1128/spectrum.01644-23
3. Teng JLL, Tang Y, Wong SSY, Fong JYH, Zhao Z, Wong CP, et al. MALDI-TOF MS for identification of *Tsukamurella* species: *Tsukamurella tyrosinosolvens* as the predominant species associated with ocular infections. Emerg Microbes Infect. 2018;7:80. https://doi.org/10.1038/s41426-018-0083-4
4. Romano L, Spanu T, Calista F, Zappacosta B, Mignogna S, Sali M, et al. *Tsukamurella tyrosinosolvens* and *Rhizobium radiobacter* sepsis presenting with septic pulmonary emboli. Clin Microbiol Infect. 2011;17:1049–52. https://doi.org/10.1111/j.1469-0691.2010.03396.x
5. Yang L, Cao Y, Dan Z, Wang Z, Wang X. Community-acquired *Tsukamurella* pneumonia in a young immunocompetent adult: a case misdiagnosed as pulmonary tuberculosis and literature review. Postgrad Med. 2017;129:563–6. https://doi.org/10.1080/00325481.2017.1344513

6. Sandhu JE, Ariyaratnam J. D Trandafirescu T. *Nocardia Tsukamurella*: an atypical pneumonia. Chest. 2022;162 (Supplement):A561. https://doi.org/10.1016/j.chest.2022.08.435
7. Liu X, Shi J, Wang X, Chen Y, Zheng L. *Tsukamurella* pneumonia misdiagnosed as pulmonary tuberculosis. Lancet Infect Dis. 2022;22:1090. https://doi.org/10.1016/S1473-3099(22)00134-7
8. Kuge T, Fukushima K, Matsumoto Y, Saito H, Abe Y, Akiba E, et al. Chronic pulmonary disease caused by *Tsukamurella toyonakaense*. Emerg Infect Dis. 2022;28:1437–41. https://doi.org/10.3201/eid2807.212320
9. Gotoh K, Mayura IPB, Hagiya H, Obata K, Ogawa T, Iio K, et al. Septic pulmonary emboli caused by *Tsukamurella inchonensis*: A case report. J Infect Chemother. 2021;27:369–72. https://doi.org/10.1016/j.jiac.2020.09.024
10. Swier R, Jakharia KK. Acid-fast bacteria in bronchiectasis: if the glass slipper does not fit, non-TB mycobacteria, consider Tsukamurella. Chest. 2022;162:A573. https://doi.org/10.1016/j.chest.2022.08.444
11. Manek G, Shah N, Krishnan AM, Anthony P. A case of *Tsukamurella pulmonis* masquerading as pleural TB in an immunocompetent patient. Chest. 2019;156(Supplement): A252. https://doi.org/10.1016/j.chest.2019.08.302
12. Akkineni S, Calderon Candelario RA, Mirsaeidi M. Acute COPD exacerbation associated with a rare pathogen: a case of *Tsukamurella pulmonis*. Am J Respir Crit Care Med. 2019;199:A6448. https://doi.org/10.1164/ajrccm-conference.2019.199.1_MeetingAbstracts.A6448
13. Rao S, Paz M, Nugent K. *Tsukamurella* and *Mycobacterium tuberculosis* pneumonia co-infection. Am J Med Sci. 2023; 365:S163-S. https://doi.org/10.1016/S0002-9629 (23)00312-9
14. Clinical and Laboratory Standards Institute. Susceptibility testing of mycobacteria, Nocardiae, and other aerobic actinomycetes. 2nd edition. Wayne (PA): The Institute; 2011 [cited 2024 Sep 24]. https://www.ncbi.nlm.nih.gov/books/NBK544374
15. Sun Q, Yan J, Liao X, Wang C, Wang C, Jiang G, et al. Trends and species diversity of non-tuberculous Mycobacteria isolated from respiratory samples in Northern China, 2014-2021. Front Public Health. 2022;10:923968. https://doi.org/10.3389/fpubh.2022.923968

Address for correspondence: Aidan Clifford, Sunshine Hospital, 176 Furlong Rd, St Albans, VIC 3021, Australia; email: aidan.clifford@wh.org.au

etymologia revisited

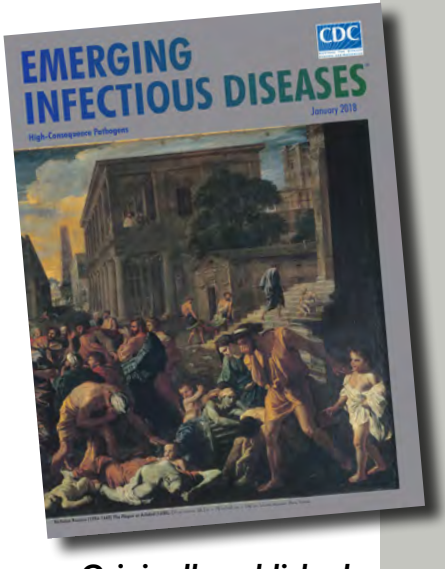

Originally published in January 2018

Plague
[plāg]

Plague (from the Latin *plaga*, "stroke" or "wound") infections are believed to have been common since at least 3000 BCE. Plague is caused by the ancestor of current *Yersinia* (named for Swiss bacteriologist Alexandre Yersin, who first isolated the bacterium) *pestis* strains. However, this ancestral *Y. pestis* lacked the critical *Yersinia* murine toxin (*ymt*) gene that enables vectorborne transmission. After acquiring this gene (sometime during 1600–950 BCE), which encodes a phospholipase D that protects the bacterium inside the flea gut, *Y. pestis* evolved the ability to cause pandemics of bubonic plague. The first recorded of these, the Justinian Plague, began in 541 ACE and eventually killed more than 25 million persons.

References:

1. Alexandre Yersin BW. Etymologia: yersinia. Emerg Infect Dis. 2010;16:496.
2. Centers for Disease Control and Prevention. History of plague [cited 2017 Oct 19]. https://www.cdc.gov/plague/history/index.html.
3. Rasmussen S, Allentoft ME, Nielsen K, Orlando L, Sikora M, Sjögren K-G, et al. Early divergent strains of Yersinia pestis in Eurasia 5,000 years ago. Cell. 2015;163:571–82.

https://wwwnc.cdc.gov/eid/article/24/1/et-2401_article

etymologia

Tsukamurella tyrosinosolvens
(tsū-kə-mə-rel′lə tī′-r.-sē-nō-sol′vins)

Clyde Partin

The species name for the bacterium *Tsukamurella tyrosinosolvens* was accepted in 1997 on the basis of biochemical attributes: *tyrosina*, from the amino acid tyrosine in cheese (*tyros*, Greek for cheese), which imparts a crystalline texture. The hydrolysis, or dissolving of tyrosine—thus, *tyrosinosolvens*—is a species characteristic.

The genus *Tsukamurella* consists of commensal bacteria with a propensity to cause opportunistic infections in immunocompromised patients, especially those with chronic lung disease. *Tsukamurella* bacteria are related to the genera *Nocardia*, *Mycobacterium*, *Corynebacterium*, and *Gordonia*. *Gordonia aurantiaca* was initially isolated in 1971 by renowned Japanese physician-microbiologist and *Mycobacteria* taxonomist Michio Tsukamura at Nagoya University in Nagoya, Japan. In 1988, he was honored with the genus name *Tsukamurella*.

Tsukamurella, retrospectively isolated by Edward A. Steinhaus in 1941 from the mycetoma and ovaries of the bedbug, was originally misidentified as *Corynebacterium paurometabolum*. *Tsukamurella* are weakly acid-fast; therefore, clinical manifestations can be confused with those of tuberculosis and create microbiological misidentification with *Mycobacterium* and *Corynebacterium* spp.

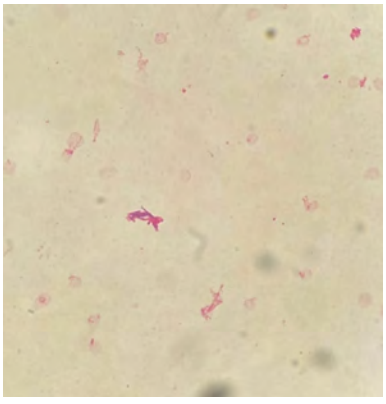

Figure. Gram staining from aerobic blood cultures (×1,000 magnification) showing numerous long, slightly curved, thin, nonbranching, and gram-positive rods, confirmed as *Tsukamurella tyrosinosolvens*. Image from (*2*); licensed by CC by 4.0 (https://creativecommons.org/licenses/by/4.0).

Tsukamurella infections are rare and usually associated with immune-suppressed patients, but severe infections have occurred in immunocompetent patients. Currently, of 17 known species, 12 cause human disease. Although *Tsukamurella* infections have been increasingly reported in Europe, Asia, America, and Africa, *T. tyrosinosolvens* has been the most common species observed.

Sources

1. Genus *Tsukamurella*. LPSN—List of Prokaryotic names with Standing in Nomenclature [cited 2024 Dec 27]. https://lpsn.dsmz.de/genus/tsukamurella
2. Mizuno S, Tsukamura Y, Nishio S, Ishida T, Hasegawa D, Kosaka Y, et al. Catheter-related bloodstream infection caused by *Tsukamurella tyrosinosolvens* identified by *secA1* sequencing in an immunocompromised child: a case report. Ann Clin Microbiol Antimicrob. 2023;22:97. https://doi.org/10.1186/s12941-023-00651-6
3. Species *Tsukamurella tyrosinosolvens*. LPSN—List of Prokaryotic names with Standing in Nomenclature [cited 2024 Dec 27]. https://lpsn.dsmz.de/species/tsukamurella-tyrosinosolvens
4. Steinhaus EA. A study of the bacteria associated with thirty species of insects. J Bacteriol. 1941;42:757–90. https://doi.org/10.1128/jb.42.6.757-790.1941
5. Teng JLL, Tang Y, Wong SSY, Fong JYH, Zhao Z, Wong C-P, et al. MALDI-TOF MS for identification of *Tsukamurella* species: *Tsukamurella tyrosinosolvens* as the predominant species associated with ocular infections. Emerg Microbes Infect. 2018;7:80. https://doi.org/10.1038/s41426-018-0083-4
6. Usuda D, Tanaka R, Suzuki M, Shimozawa S, Takano H, Hotchi Y, et al. Obligate aerobic, gram-positive, weak acid-fast, nonmotile bacilli, *Tsukamurella tyrosinosolvens*: minireview of a rare opportunistic pathogen. World J Clin Cases. 2022;10:8443–9. https://doi.org/10.12998/wjcc.v10.i24.8443
7. Yu S, Ding X, Hua K, Zhu H, Zhang Q, Song X, et al. Systematic investigation of the emerging pathogen of *Tsukamurella* species in a Chinese tertiary teaching hospital. Microbiol Spectr. 2023;11:e0164423. https://doi.org/10.1128/spectrum.01644-23

Address for correspondence: Clyde Partin, Emory Clinic, 1365 Clifton Rd NE, Bldg A, 1st Fl, Atlanta, GA 30322, USA; email: wpart01@emory.edu

Author affiliation: Emory University School of Medicine, Atlanta, Georgia, USA

DOI: https://doi.org/10.3201/eid3103.242004

Outbreak Caused by Multidrug-Resistant *Mycobacterium Tuberculosis* with Unusual Combination of Resistance Mutations, Northern Argentina, 2006–2022

Roxana Paul,[1] Federico Lorenzo,[1] Beatriz López, María Gabriela Alegre, David Couvin, Nalin Rastogi, Laura Pérez-Lago, Darío García de Viedma, Ana Gamberale, Norma González, Domingo Palmero, Silvia Altabe, Norberto Simboli, Noemí Kaoru Yokobori

To reconstruct transmission chains of the multidrug-resistant tuberculosis Ch strain, which harbors a unique combination of resistance mutations, we analyzed genomes of 25 isolates from 12 patients with diagnosis during 2006–2022 in Chaco Province, Argentina. Amplification of resistance, high mortality rates, and indications of a wider outbreak raise concerns for surveillance programs.

Argentina is considered a mid-incidence country for tuberculosis (TB); 1% of multidrug-resistant (MDR) cases persist in Argentina. The northern province of Chaco, a province with a top 5 TB burden (*1*), had a low number of MDR TB cases and no prior evidence of local transmission (*2*). MDR TB can affect patients beyond the well-established risk groups, making clinical suspicion essential where universal drug-susceptibility testing (DST) is unavailable. Whole-genome sequencing (WGS) enables timely and precise molecular drug-resistance profiling, but genotype/phenotype correlations need further research, especially for rapidly emerging resistance to second-line drugs (e.g., bedaquiline and linezolid) (*3*).

To reconstruct the transmission chains and drug-resistance profiles, we used WGS to analyze an MDR TB outbreak in Resistencia, Chaco Province, Argentina. The study was performed in accordance with the Helsinki Declaration as revised in 2013. The Research Ethics Committee of the Instituto Nacional de Epidemiologia, ANLIS "Dr. Jara," Buenos Aires, Argentina, approved the project and waived the informed consent requirement (project code YOKOBORI05/2022).

The Study

During 2018–2019, our laboratory received 9 MDR *M. tuberculosis* isolates from 3 patients of Resistencia, Chaco, that had unexpectedly inconsistent PCR-based resistance profiles for rifampin and isoniazid in isolates from the same patient and between 2 patients with close epidemiologic links (Appendix 1, https://wwwnc.cdc.gov/EID/article/31/3/24-1272-App1.pdf; Appendix 2, https://wwwnc.cdc.gov/EID/article/31/3/24-1272-App2.xlsx). A preliminary genomic analysis showed simultaneous presence of the mutations *rpoB*_Asp435His, *rpoB*_His445Asp,

Author affiliations: Instituto Nacional de Enfermedades Infecciosas, ANLIS "Dr. C. G. Malbrán," Buenos Aires, Argentina (R. Paul, F. Lorenzo, B. López, N. Simboli, N.K. Yokobori); Programa de Control de Tuberculosis, Chaco, Argentina (M.G. Alegre, S. Altabe); Université des Antilles, Guadeloupe, France (D. Couvin); Institut Pasteur de Guadeloupe, Abymes, Guadeloupe (D. Couvin, N. Rastogi); Hospital General Universitario Gregorio Marañón, Madrid, Spain (L. Pérez-Lago, D. García de Viedma); Instituto de Investigaciòn Sanitaria Gregorio Marañón, Madrid (L. Pérez-Lago, D. García de Viedma); Instituto de Salud Carlos III, Madrid (D. García de Viedma); CIBER Enfermedades Respiratorias, Madrid (D. García de Viedma);Hospital Muñiz, Buenos Aires (A. Gamberale, D. Palmero); Instituto Vaccarezza, Buenos Aires (A. Gamberale, D. Palmero); Hospital General de Niños "Pedro de Elizalde," Buenos Aires (N. González); National Scientific and Technical Research Council, Buenos Aires (N.K. Yokobori)

DOI: https://doi.org/10.3201/eid3103.241272

[1]These first authors contributed equally to this article.

*fabG1-inhA*_t-8c, and *katG*_Ser315Thr. We studied that possible outbreak because of the unusual combination of mutations, the extended resistance profile, and the critical disease in young patients with no relevant comorbidities (Table 1).

The Mycobacteria Service, Instituto Nacional de Enfermedades Infecciosas, ANLIS "Dr. C. Malbrán," Buenos Aires, Argentina, the national reference laboratory for TB diagnosis, has kept an MDR genotyping database, representing nationwide cases, since 2003. After intense screening of our databases, on the basis of rifampin and isoniazid molecular resistance patterns; province of origin; epidemiologic link, genotype, or both, we identified 29 candidate isolates from 12 patients. Twenty-four isolates were available for WGS analysis (Appendix 1); we assigned an identification number to each isolate. We performed phenotypic DST when we received the isolates unless otherwise stated (Appendixes 1, 2), and we compared spoligotypes with those in the SITVITEXTED database (Appendix 3, https://wwwnc.cdc.gov/EID/article/31/3/24-1272-App3.pdf).

Table 1. Characteristics of patients at time of diagnosis of MDR-TB infection with Ch strain, Argentina, 2006–2022*

ID	Residence	Year	Age, y/sex	DR profile†	DR status	HIV status	Comments
1	Resistencia, Chaco	2006	57/M	STR, INH, RIF, EMB, PZA, ETH	MDR	Unknown	Index case-patient. No previous treatment records. Died 2 months after diagnosis. Treatment was with INH, RIF, PZA, EMB, and STR.
2	Resistencia, Chaco	2008	NA/F	STR, INH, RIF, EMB, PZA, ETH	MDR	Negative	Mother of patients 3, 4, and 9. Worked as a nurse at hospital where patient 1 was assisted. Self-administered the second-line drugs. Smear positive for AFB until 2011.
3	Resistencia, Chaco	2010	14/M	STR, INH, RIF, EMB, PZA, ETH (2LI, FLQ)	MDR (pre-XDR)	Negative	Son of patient 2. Hepatotoxicity associated with TB drugs. Poor adherence to treatment. Problematic substance use. Died in 2016.
4	Resistencia, Chaco	2010	16/M	STR, INH, RIF, EMB, PZA, ETH	MDR	Negative	Son of patient 2. Hepatotoxicity associated with TB drugs.
5	Resistencia, Chaco	2014	66/M	STR, INH, RIF, EMB, PZA, ETH	Pre-XDR	Unknown	Grandfather of patient 6. Repeated treatment changes, suboptimal treatment.
6	Resistencia, Chaco	2014	15/F	STR, INH, RIF, EMB, PZA, ETH, FLQ (LZD‡)	Pre-XDR (XDR)	Negative	Granddaughter of patient 5. Her mother, who had lupus, and brother died of TB (Appendix 2, https://wwwnc.cdc.gov/EID/article/31/3/24-1272-App2.pdf). Discharged in 2016 after sputum tested negative. Relapsed in 2017. Referred to a hospital that specialized in DR-TB in Buenos Aires in 2019. Poor adherence to treatment. Smoker.
7	Corrientes, Corrientes	2014	52/M	STR, INH, RIF, EMB, PZA, ETH	MDR	Positive	Died in 2015.
8	Resistencia, Chaco	2017	43/F	STR, INH, RIF, EMB, PZA, ETH	MDR	Unknown	TB diagnosed in 2016. Had contact with a TB patient in 1999, but the association with the outbreak is unknown.
9	Resistencia, Chaco	2017	18/F	STR, INH, RIF, EMB, PZA, ETH (CAP, ETH)	MDR	Negative	Daughter of patient 2. Irregular treatment and poor adherence. Died in 2021.
10	Resistencia, Chaco	2018	16/F	STR, INH, RIF, EMB, PZA, ETH, FLQ (CFZ, BDQ§)	Pre-XDR (XDR)	Negative	Friend of patient 6, who visited her frequently. Repeated treatment changes. Admitted to a pediatric hospital in Buenos Aires in 2019, where she received CFZ/BDQ. Patient complied with treatment; her condition improved, and she was discharged in December 2019. Relapsed and died in 2020 during social isolation because of COVID-19 pandemic.
11	Resistencia, Chaco	2020	24/F	STR, INH, RIF, EMB, PZA, ETH	MDR	Negative	Irregular treatment. Problematic substance use.
12	Del Viso, Buenos Aires	2021	21/M	STR, INH, RIF, EMB, PZA, ETH	MDR	Unknown	Patient was unavailable for follow-up until mid-2022 when he started second-line treatment. Former resident of Resistencia and declared the same address of patient 2 and her family, but their exact relationship is unknown.

*BDQ, bedaquiline; CAP, capreomycin; CFZ, clofazimine; DR, drug resistance; EMB, ethambutol; ETH, ethionamide; FLQ, fluoroquinolone; INH, isoniazid; NA, not available; MDR, multidrug-resistant; pre-XDR, pre–extensively drug-resistant; PZA, pyrazinamide; RIF, rifampin; STR, streptomycin; XDR, extensively drug-resistant.; 2LI, second-line injectable drugs.
†Consolidated DR profiles based on phenotypic and molecular test results. STR was tested phenotypically in all isolates until 2017. The DR profile and DR status of the last isolate are indicated between brackets.
‡Confirmed phenotypically.
§Tested retrospectively after the detection of the *Rv0678*_114duplC mutation by whole-genome sequencing.

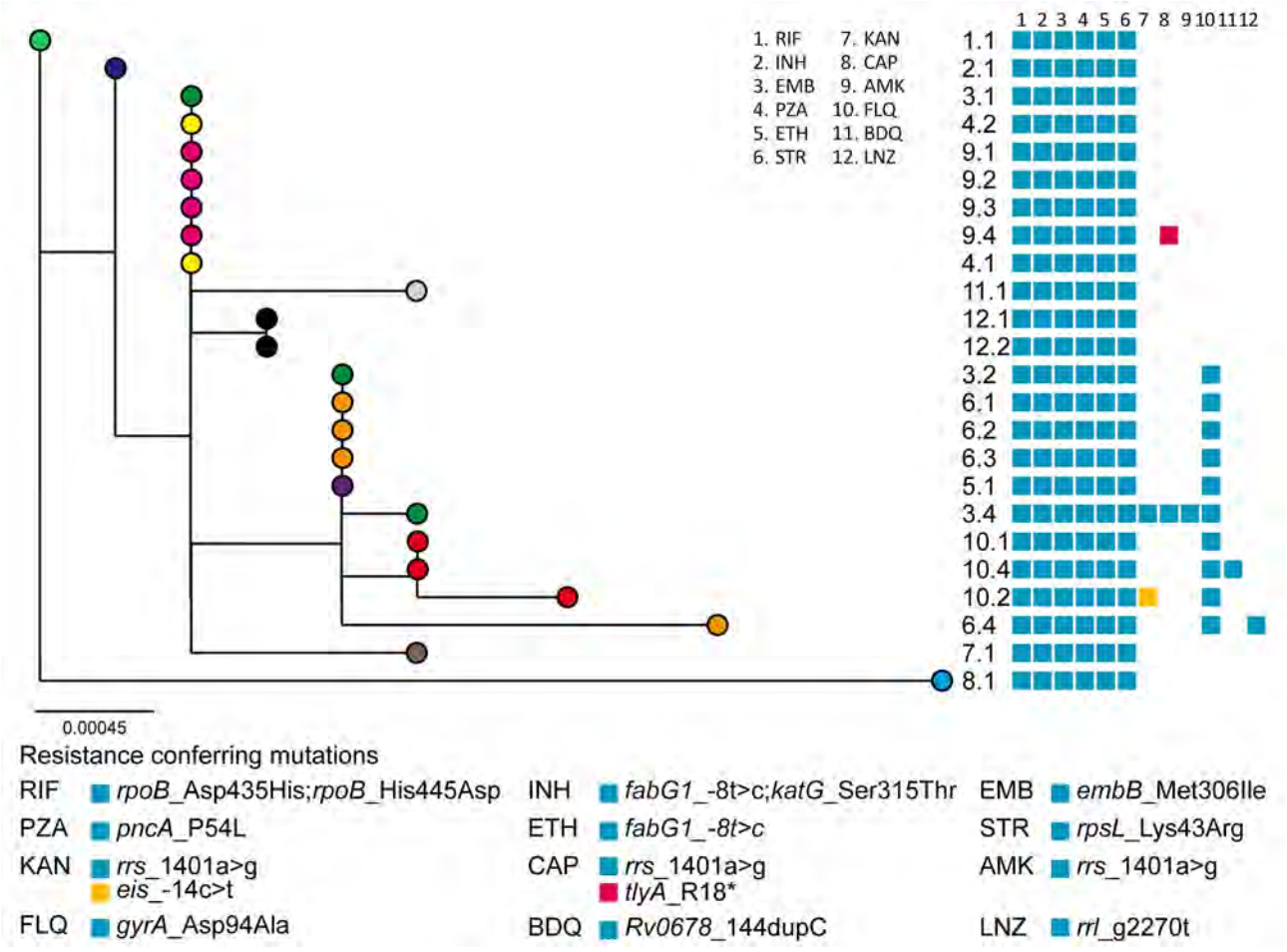

Figure 1. Maximum-likelihood phylogenetic tree of the 24 isolates from the MDR *Mycobacterium tuberculosis* outbreak strain Ch, Chaco, Argentina, 2006–2022, analyzed by whole-genome sequencing. Each patient is represented by a colored dot. Labels indicate the patient and isolate identification numbers. Blocks indicate the resistance-conferring mutations detected in each isolate, as indicated below the tree. Scale bar indicates number of substitutions per variable site. MDR, multidrug-resistant.

All patients were residents of Resistencia, except for a patient from the neighboring Corrientes city and a former resident of Resistencia who received their diagnoses in Buenos Aires (Table 1; Appendix 3). Patient 2, a healthcare worker at the hospital where patient 1 was assisted, was the mother of patients 3, 4, and 9. Patient 6 was the granddaughter of patient 5 and frequently visited her friend, patient 10. The remaining epidemiologic links were unknown. Five patients were teenagers at the time of diagnosis (Table 1).

WGS showed a monophyletic group (Figure 1; Appendix 2). We named the clone the Ch strain, and it belonged to lineage 4.1.1 and to the spoligotype international type (SIT) 119 of the X1 family. The highest number of SIT119 clones in the SITVITEXTEND database in the region, without association with MDR, is in Brazil (Appendix 3). The median pairwise single-nucleotide polymorphism distance among the first isolates from each patient was 3 (range 0–6) (Appendix 2), excluding isolate 8.1, which was 15 single-nucleotide polymorphisms (range 12–17) apart from the others. The most ancestral isolate belonged to the index case-patient, whose diagnosis was made in 2006. Despite the patient having no history of TB treatment, that isolate had the 8 resistance mutations common to the cluster, including the double mutations for isoniazid and rifampin (Table 2; Figure 1), suggesting that the outbreak could have been more extended. Patient 3 was probably the source of 3 secondary pre–extensively drug-resistant cases in the second subcluster. Isolates from the patients with the most recent diagnoses (patients 11 and 12) were closer to the first subcluster (Figure 1).

The resistance mutations had high World Health Organization (WHO) confidence gradings and were concordant with the phenotypic drug-susceptibility testing results (Table 2), except for ethionamide and

Table 2. Resistance conferring mutations found in Ch strain isolates from patients with MDR-TB infection, Argentina, 2006–2022*

Mutation	Drug	Confidence grading	Phenotype/genotype†	Concordance
*rpoB*_Asp435His	RIF	Associated with resistance–interim	24/24	Yes
*rpoB*_His445Asp	RIF	Associated with resistance	24/24	Yes
*fabG1-inhA*_t-8c	INH	Associated with resistance–interim	24/24	Yes
	ETH	Associated with resistance–interim	3/24‡	Partial
*katG*_Ser315Thr	INH	Associated with resistance	24/24	Yes
*embB*_Met306Ile	EMB	Associated with resistance	18/24§	Partial
*embA*_c-11a	EMB	Uncertain significance	NA	NA
*pncA*_Pro54Leu	PZA	Associated with resistance	24/24	Yes
*rpsL*_Lys43Arg	STR	Associated with resistance	24/24	Yes
*rrs*_a1401 g	KAN	Associated with resistance	1/1	Yes
	AMK	Associated with resistance	1/1	Yes
	CAP	Associated with resistance	1/1	Yes
*eis*_c-14t	KAN	Associated with resistance	1/1	Yes
	AMK	Associated with resistance–interim	0/1	No
	CAP	NA	0/1	NA
*tlyA*_Arg18stop (LoF)	KAN	NA	0/1	NA
	AMK	NA	0/1	NA
	CAP	Associated with resistance	1/1	Yes
*gyrA*_Asp94Ala	FLQ	Associated with resistance	10/10¶	Yes
*rrl*_g2270t	LZD	Associated with resistance–interim	1/1#	Yes
*Rv0678*_144dupC (LoF)	BDQ	Associated with resistance	1/1	Yes
	CFZ	Associated with resistance	1/1**	Yes

*Confidence grading according to the World Health Organization Catalogue of Mutations, 2nd Edition (*3*). AMK, amikacin; BDQ, bedaquiline; CAP, capreomycin; CFZ, clofazimine; EMB, ethambutol; ETH, ethionamide; FLQ, fluoroquinolone; INH, isoniazid; LoF, loss of function; LZD, linezolid; NA, not applicable; PZA, pyrazinamide; RIF, rifampin; Stop, stop codon; STR, streptomycin; 2LI, second-line injectable drugs.
†For the isolates studied by whole-genome sequencing; phenotypically resistant isolates/isolates harboring each mutation are indicated.
‡Fifteen isolates were sensitive, 5 isolates had discordant results between methods, and 1 isolate was not tested.
§Two isolates were susceptible, 3 had discordant results between proportion and MGIT methods, and 1 isolate was not studied.
¶Resistance to low dose of moxifloxacin.
#Isolate 6.4 had a MIC of 4 mg/L for LZD (suggested cutoff value 0.5 mg/L).
**Isolate 10.4 had a MIC of 2 mg/L for CFZ (suggested cutoff value 0.25 mg/L). Phenotypic resistance to BDQ was implemented in 2021, and isolate 10.4. was tested in the light of the genomic results.

ethambutol, as expected (*3*). Resistance to the second-line injectable drugs was acquired independently in 3 isolates (Figure 1). Two isolates were extensively drug resistant. Isolate 6.4 had a *rrl*_g2270t mutation, which has recently been associated with linezolid resistance (*3*), and isolate 10.4 had the loss-of-function mutation *Rv0678*_144dupC. Resistance to linezolid and cross-resistance to bedaquiline were confirmed by phenotypic methods (Table 2). Instances of clofazimine/bedaquiline resistance were acquired shortly after their administration under strict supervision (Figure 2).

No compensatory mutations were found in *rpoC* or *rpoA*. Because both mutations in *rpoB* are expected to have a mild to high fitness cost (*4*), their simultaneous presence could constitute a unique compensatory mechanism.

Patient 1 died shortly after diagnosis. The mother of patient 2 had received a TB diagnosis in 2010 but refused treatment and died in 2011. The mother and the brother of patient 6 died in 2013 (Appendix 2). Isolates from those patients were not available. Because isolates 3.2, 5.1, and 6.1 were identical (Figure 1), the other 2 relatives could have acquired their infection from patient 3 (Figure 2), but their epidemiologic link remains unknown. Their close relationship, the contemporaneity, and their fatal outcomes strongly suggest that those patients were part of the outbreak (Figure 2). Patient 9 probably experienced relapse from latency and infected patient 12, who lived at the same address before moving to Buenos Aires. Their relationship remains unclear. Patient 2 administered the medication to her family, including the injectable drugs. Some regimens, especially in the first years of the outbreak, were suboptimal and underwent multiple changes. Reports suggest that empathy from some healthcare providers had been insufficient. Three cohabitants received chemoprophylaxis with isoniazid, and no active disease has been reported (Appendix 2).

Conclusions

The MDR Ch outbreak strain, with its epicenter in Resistencia, Chaco, belonged to the X1, SIT 119 spoligotype, which is infrequent in Argentina (*5*,*6*) (Appendix 3). The X family has been associated with high transmissibility (*7*,*8*), and SIT119 could have been imported from Brazil, considering the frequent cross-border movements to and from Chaco (Appendix 3). Further phylogenomic studies are warranted to determine the precise origin of that MDR strain.

Several factors converged in the outbreak. It started as intrahospital transmission to a healthcare worker, who spread the disease to her cohabitants (Figure 2).

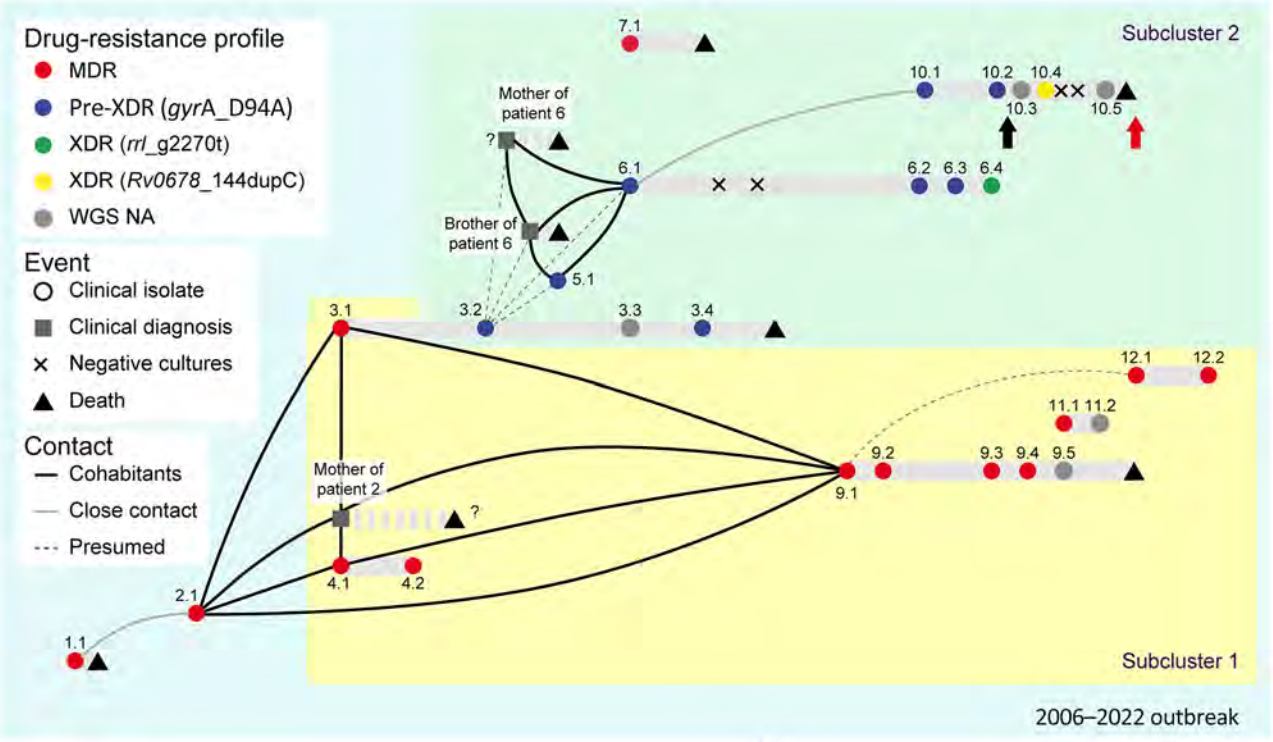

Figure 2. Schematic representations of the timeline and epidemiologic links of the MDR *Mycobacterium tuberculosis* outbreak with strain Ch, Chaco, Argentina, 2006–2022. Two subclusters were defined according to the phylogenetic analysis (Figure 1). The symbols represent epidemiologic events. Patients represented with squares were identified as part of the outbreak after comprehensive epidemiologic research in the light of the genomic results (Appendix 2, https://wwwnc.cdc.gov/EID/article/31/3/24-1272-App2.pdf). They had received a clinical diagnosis, and the drug susceptibility profiles were not available. Dot colors represent the drug-resistance status and the mutation found. The exact date of the events indicated with a question mark is unknown. Black arrow indicates administration of bedaquiline to patient 10, and the red arrow indicates implementation of phenotypic drug-susceptibility testing for that drug in Argentina. MDR, multidrug resistant; WGS NA, whole-genome sequence not available; XDR, extensively multidrug resistant.

Despite her background, the family was poorly receptive to and not compliant with treatment. On the other hand, some healthcare workers were not appropriately prepared to manage MDR TB. Delayed diagnosis, poor compliance, and administration of suboptimal regimens led to long periods of culture positivity, amplification of resistance, and an alarmingly high mortality rate (53%). In addition to lack of effective drugs, host and bacterial genetic factors could have played a role. Several patients were relatives, which suggests genetic susceptibility to TB. Conversely, the observed mortality rate suggests higher virulence of the Ch strain. Although challenging to assess their relative effect, those biological and societal factors collectively shaped the outbreak outcome.

We gained valuable insights from our study. The phylogenetic analysis strongly suggests additional missing cases, and although no new cases were diagnosed, MDR TB surveillance in Chaco must be strengthened. Of note, Ch genotype can be suspected by detecting the *rpoB* double mutation through GeneXpert and other molecular tests (data not shown). Next-generation tools, including novel drugs and WGS, are available, but clinical suspicion of MDR-TB remains crucial for their effective use. Continuing education and active engagement of healthcare professionals and the community are vital for managing future outbreaks.

Acknowledgments

We thank Susana Imaz for the helpful discussion.

This work was supported by PICT-2021-I-GRF1 TI-00049 of the Agencia I+D+i, Argentina. The funder had no role in study design. The authors have no relevant financial or nonfinancial interests to disclose.

Raw sequences were deposited in the European Nucleotide Archive. Accession numbers are available in Appendix 1.

About the Author

Mrs. Paul is a professional of the Servicio de Micobacterias, INEI, ANLIS Dr. "C. G. Malbrán" and the Hospital Piñero, Buenos Aires, Argentina, with a research interest in the microbiological diagnosis of mycobacterial diseases.

References

1. Argentina Ministerio de Salud. Boletín N° 7 tuberculosis y lepra en la argentina coordinación de tuberculosis y lepra [cited 2024 Nov 30]. https://www.argentina.gob.ar/sites/default/files/2024/04/boletin_tuberculosis_2024_1642024.pdf
2. Ritacco V, López B, Ambroggi M, Palmero D, Salvadores B, Gravina E, et al.; National TB Laboratory Network. HIV infection and geographically bound transmission of drug-resistant tuberculosis, Argentina. Emerg Infect Dis. 2012;18:1802–10. https://doi.org/10.3201/eid1811.120126
3. World Health Organization. Catalogue of mutations in *Mycobacterium tuberculosis* complex and their association with drug resistance, 2nd ed. [cited 2024 Nov 30]. https://www.who.int/publications/i/item/9789240082410
4. Gagneux S, Long CD, Small PM, Van T, Schoolnik GK, Bohannan BJM. The competitive cost of antibiotic resistance in *Mycobacterium tuberculosis*. Science. 2006;312:1944–6. https://doi.org/10.1126/science.1124410
5. Yokobori N, Paul R. Informe técnico sobre la tuberculosis multidrogorresistente en la Argentina, 2023 [cited 2024 Nov 30]. https://sgc.anlis.gob.ar/handle/123456789/2618
6. Monteserin J, Paul R, Gravina E, Reniero A, Hernandez T, Mazzeo E, et al. Genotypic diversity of *Mycobacterium tuberculosis* in Buenos Aires, Argentina. Infect Genet Evol. 2018;62:1–7. https://doi.org/10.1016/j.meegid.2018.04.006
7. Comín J, Cebollada A, Ibarz D, Viñuelas J, Vitoria MA, Iglesias MJ, et al. A whole-genome sequencing study of an X-family tuberculosis outbreak focus on transmission chain along 25 years. Tuberculosis (Edinb). 2021 Jan:126:102022.
8. Bishai WR, Dannenberg AM Jr, Parrish N, Ruiz R, Chen P, Zook BC, et al. Virulence of *Mycobacterium tuberculosis* CDC1551 and H37Rv in rabbits evaluated by Lurie's pulmonary tubercle count method. Infect Immun. 1999;67:4931–4. https://doi.org/10.1128/IAI.67.9.4931-4934.1999

Address for correspondence: Noemí Kaoru Yokobori, Servicio de Micobacterias, Departamento de Bacteriología, INEI, ANLIS "Dr. C. G. Malbrán." Vélez Sarsfield 563, Ciudad Autónoma de Buenos Aires, C1282AFF, Argentina; email: nyokobori@anlis.gob.ar

etymologia revisited

Coronavirus

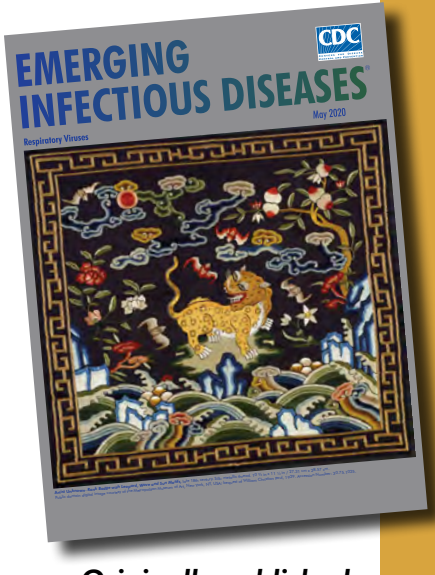

Originally published in May 2020

The first coronavirus, avian infectious bronchitis virus, was discovered in 1937 by Fred Beaudette and Charles Hudson. In 1967, June Almeida and David Tyrrell performed electron microscopy on specimens from cultures of viruses known to cause colds in humans and identified particles that resembled avian infectious bronchitis virus. Almeida coined the term "coronavirus," from the Latin *corona* ("crown"), because the glycoprotein spikes of these viruses created an image similar to a solar corona. Strains that infect humans generally cause mild symptoms. However, more recently, animal coronaviruses have caused outbreaks of severe respiratory disease in humans, including severe acute respiratory syndrome (SARS), Middle East respiratory syndrome (MERS), and 2019 novel coronavirus disease (COVID-19).

References:

1. Almeida JD, Tyrrell DA. The morphology of three previously uncharacterized human respiratory viruses that grow in organ culture. J Gen Virol. 1967;1:175–8. https://doi.org/10.1099/0022-1317-1-2-175
2. Beaudette FR, Hudson CB. Cultivation of the virus of infectious bronchitis. J Am Vet Med Assoc. 1937;90:51–8.
3. Estola T. Coronaviruses, a new group of animal RNA viruses. Avian Dis. 1970;14:330–6. https://doi.org/10.2307/1588476
4. Groupe V. Demonstration of an interference phenomenon associated with infectious bronchitis virus of chickens. J Bacteriol. 1949;58:23–32. https://doi.org/10.1128/JB.58.1.23-32.1949

https://wwwnc.cdc.gov/eid/article/26/5/et-2605_article

Portraying Tuberculosis Through Western Art, 1000–2000 CE

Yousra Kherabi, Philippe Charlier

In 2025, tuberculosis (TB) still maintains its grim distinction as one of the world's most lethal infectious diseases. *Mycobacterium tuberculosis*, the causative agent, infects one fourth of the global population (*1*). However, this statistic offers only a partial understanding of the disease's true effect on humanity.

To assess the burden of TB comprehensively, especially in Europe, we must embark on a historical expedition, retracing our steps to an era when this ailment was a cryptic and seemingly incurable enigma (*2*). During that period, society sought to grapple with the mysteries of tuberculosis through artistic expressions. Representation of TB in art underwent an evolution in tandem with the shifting perceptions of the disease.

Termed under various appellations, such as phthisis, a Greek term denoting wasting, or consumption, TB has long been portrayed across a spectrum of cultural domains from literature and music to movies (*3*,*4*). The confluence of visual arts and TB offers a unique vantage point to examine humanity's enduring confrontation with this disease. In this article, we aim to explore the depiction of TB in Western art across the centuries, shedding light on how it not only reflects a medical journey but also echoes the profound societal shifts accompanying its history.

Methods

Definitions

The primary objective of this study was to conduct a comprehensive review of the representation of TB in Western pictorial arts spanning a millennium. To establish a focused framework, we defined a precise chrono-cultural context, centering on Western art created during 1000–2000 CE. Geographically, this context encompasses Europe, the United States, and Canada. Our review included a diverse range of pictorial art forms, including painting, engraving, sculpture, photography, and posters.

Search Strategy

To identify relevant references for our review, we executed searches across museum databases and national heritage platforms (Appendix, https://wwwnc.cdc.gov/EID/article/31/3/23-1581-App1.pdf). Our search strategy included the use of specific keywords, including tuberculosis, cough, scrofula, consumption, phthisis, king's evil, disease, and healing. To ensure inclusivity, those search terms were translated into the language of each database.

Selection of Artworks

From our extensive search, we selected reference artworks that portrayed TB according to previously published iconodiagnosis guidelines (recommendations for the retrospective diagnosis carried out on a work of art representing a human being) (*5*). We excluded pieces of art that did not unequivocally depict the presence of TB. The process of selection ensured the chosen artworks provided clear and discernible representations of TB within the context of our study.

Results

We classified the selected works of art into 3 different periods of influence (Figure 1). The first period, from the 10th Century through the 18th Century, was marked by the depiction of thaumaturgic kings (i.e., kings with miraculous healing powers); the most famous wonder was the touching of scrofula. This period was followed by a very short but rich second period that flourished at the start of the Industrial Revolution and was full of paradoxes. The third period covered the 20th Century, which was a period of challenge and struggle against an identified scourge: Koch's bacillus.

Author affiliations: Infectious and Tropical Diseases Department, Bichat-Claude Bernard Hospital, Assistance Publique-Hôpitaux de Paris, Université Paris Cité, Paris, France (Y. Kherabi); IAME, INSERM, Université Paris Cité, Paris (Y. Kherabi); Université Paris-Saclay, Montigny-le-Bretonneux, France (P. Charlier); Biologie–Institut de France, Paris (P. Charlier)

DOI: https://doi.org/10.3201/eid3103.231581

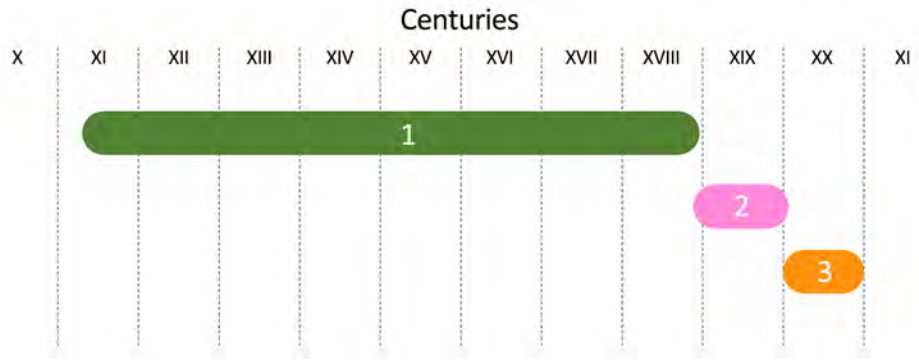

Figure 1. The 3 different periods of consequence in tuberculosis representation in visual art in the Western world, 1000–2000 CE. The first period (10th–18th Centuries) was marked by the magic of "the royal touch." The second period (19th Century) displayed romanticized representations of tuberculosis. The third period (20th Century) depicted the struggle against an identified microbial enemy: Koch's bacillus.

First Period, 10th–18th Centuries

Throughout history, rulers have sought divine approval to legitimize their reign, a phenomenon integral to the governance of many cultures (*6*). Rulers in Europe in particular claimed the divine right to rule, and the belief of the divine right of kings in Britain and France played a major role in shaping the past millennium (*7*).

Figure 2. An engraving by Robert White of Charles II touching a patient to cure them of tuberculosis, or the King's Evil (scrofula), surrounded by courtiers, clergy, and the public. Image from the Wellcome Collection, https://wellcomecollection.org/works/z9hwpcka. Public domain image.

The royal touch, an act by the monarch with which they could seemingly heal the sick, probably dates back to Clovis of France (5th Century) or to Philip I (11th Century) in France and to Edward the Confessor in Britain (11th Century) (*7*, *8*). In Shakespeare's Macbeth, the royal touch is shown as both a medical ritual and a symbol of the monarch's legitimacy (*9*). Afflicted persons often sought the king's miraculous cure for scrofula (tuberculous cervical lymphadenitis), often referred to as the King's Evil. Before the advent of pasteurization, scrofula was predominantly because of the ingestion of dairy products contaminated with *M. bovis* that resulted in local infection of the lymph nodes in proximity to the upper digestive tract (*10*).

In ceremonies, subjects could approach the king to seek the royal touch, hoping to cure their ailments or diseases (Figure 2). Scrofula would manifest itself with painful and visible sores that could spontaneously go into remission and even resolve, giving the impression of a royally induced cure. Frequently during the 15th–17th Centuries, those subjects were also given a hammered gold coin as a gift picturing the winged standing figure of the Archangel Michael slaying a dragon with a spear (*11*).

Second Period, 19th Century

The 19th Century witnessed a rich and paradoxical portrayal of TB in the pictorial arts. As the Industrial Revolution brought about urbanization and widespread poverty, artists began to interpret the disease within this new social context. TB was frequently seen as an ailment of poverty, a theme powerfully encapsulated in Cristobal Rojas' *The Misery* (Figure 3), a poignant painting of the somber reality of TB in the 19th Century. This painting depicts a young man in

Figure 3. *The Misery*, an oil painting by Cristobal Rojas that depicts tuberculosis as a disease of poverty. 1886. Public domain digital image.

a state of despondency next to his wife who has succumbed to the illness amidst the backdrop of squalor. Rojas' work stands as a vivid reminder of the human cost of TB during a time when the disease was a major cause of death in Europe (*12*). Operas such as Verdi's *La Traviata* and Puccini's *La Bohème* also reflected societal views on TB.

Figure 4. A 19th Century painting of Marie Duplessis by Edouard Viénot. Marie Duplessis was a courtesan with tuberculosis whose beauty contributed to romanticizing the infection. Public domain digital image.

Concurrently, with the stark realism of tuberculosis's representation, there emerged a romanticized vision of the disease as a marker of fragile, tragic beauty, a sentiment that became particularly pronounced in the 19th Century (*13*). This idealization of tuberculosis-related frailty was famously captured in the figure of Marie Duplessis, the high-society courtesan whose battle with tuberculosis was immortalized in Alexandre Dumas fils' novel *La Dame aux Camélias* (*15*) (Figure 4). Her portrayal as an ethereal beauty, with her pallor, slimness, and radiant eyes, captivated the societal imagination, encapsulating the era's curious romanticization of consumption. This romanticization was a phenomenon that even Lord Byron alluded to, suggesting that consumption led to a delicate and refined end by enhancing a person's beauty until the last breath; a jarring contradiction to the harsh reality of the disease (*15*) (Figure 5).

Historically, there was a pervasive belief that TB could accentuate artistic talent. The slight fever and toxemia supposedly enabled artists afflicted with TB to see more clearly and to act more decisively, a notion rooted in Greek medical terms that associated phthisis with heightened mental faculties. This idea was further romanticized during the 19th Century and the physical manifestations of the disease, such as lean limbs and a pallid complexion, were often linked to an aesthetic of the ethereal and the sublime, reinforcing the stereotype of the consumptive artist who produced work of profound emotional and artistic depth (*16*). Poets such as Percy Bysshe Shelley and John Keats transformed their personal battles with TB into metaphors for creativity and passion, exemplifying the concept of "spes phthisica," where physical decline spurred artistic brilliance (*17*). This romantic notion, although scientifically unfounded,

Figure 5. A 19th Century engraving of Marie Duplessis' death by H. Linton. Created during the romanticized era of tuberculosis history. Public domain digital image.

contributed to the mythos of the tortured artist, intertwining the suffering and creativity of figures who, despite their illness, were believed to have harnessed their condition to fuel their artistic genius.

The intimate tragedies of TB within familial circles are profoundly rendered in the works of Christian Krohg and Edvard Munch. Krohg's *The Sick Girl* from 1880–1881 is a poignant depiction, where the neutral setting and the subject's simple attire focus the viewer's attention on the emotional gravity of the scene (Figure 6). Nana, the dying girl, sometimes identified as Krohg's sister, daughter, or niece, is prominently placed and engages the viewer in a shared space of death, underscored by the emblematic withering rose that symbolizes the fleeting nature of life. This painting, steeped in personal loss with echoes of Nana's illness and death, is thought to have influenced Edvard Munch. *The Sick Child* by Munch is a series of 6 paintings and various prints created during 1885–1926, depicting the moments before the death of his sister Sophie from tuberculosis (*18*) (Figure 7). Munch revisited this personal trauma in his art for more than 4 decades, portraying Sophie in a chair, in pain, and accompanied by a grieving woman, likely her aunt. Munch's work symbolizes his own experiences with TB and his feelings of despair and guilt for surviving his sister. Obsessively returning to this theme, he produced numerous versions in different formats by using various models (*19*).

Figure 6. *The Sick Girl* is an oil painting by Christian Krohg detailing the familiar heartache experienced by many of losing loved ones to tuberculosis. Public domain digital image.

Figure 7. A painting by Edvard Munch, *The Sick Child*, depicts the moments before the death of his sister Sophie from tuberculosis. Munch portrayed his sister Sophie in a chair, in pain, and accompanied by a grieving woman. Image from The Munch Museum/The Munch-Ellingsen Group/Artist Rights Society, NY. Image copyright, Tate, London, 2011. Previously published by Emerging Infectious Diseases (https://wwwnc.cdc.gov/eid/article/17/3/ac-1703_article).

The turn of the 20th Century was marked by noteworthy medical advances in the fight against tuberculosis as depicted in the fine arts of the period. René Laennec's innovation of the stethoscope, a revolutionary breakthrough for the diagnosis of TB, was celebrated in art, which showcased the instrument that became synonymous with medical practice. Furthermore, the artistic engagement with medical progress was epitomized by Jules Adler's *Transfusion of a Goat's Blood* (Figure 8). Commissioned by Dr. Samuel Bernheim, a renowned physician and TB specialist

Figure 8. An 1892 painting by Jules Adler, *Transfusion of a Goat's Blood*. Commissioned by Dr. Samuel Bernheim, a tuberculosis specialist, the painting shows him overseeing a transfusion of goat blood to a patient and demonstrates the engagement of art with medical progress. Copyright © Pittsburgh Post-Gazette, 2010, all rights reserved. Photograph by Alyssa Cwanger, 2006. Previously published by Emerging Infectious Diseases (https://wwwnc.cdc.gov/eid/article/18/8/ac-1808_article).

from Paris, the painting depicts him overseeing a transfusion of goat blood to a patient (*20*, *21*). In the painting's foreground, a woman reclines, enveloped in a pristine white shroud, her complexion ghostly, contrasting with the stark black of her hair and her hand tightly clutches the bed's edge. Adler's work reflects the perception of medical practices as grand historical events, thus bridging the realms of art and the history of medicine. This dualistic artistic depiction of TB traverses the societal spectrum from raw reality to idealized romanticism, juxtaposing the gritty struggle against the disease with an almost paradoxical glorification, all amidst a backdrop of critical medical innovation.

Third Period, 20th Century

The 20th Century marked a shift in the representation of TB because scientific understanding advanced. Robert Koch's discovery of the TB bacillus in 1882 shattered the romanticized image of the disease. The imagery moved from depicting the consumptive beauty to showcasing TB as an enemy of public health (*17*).

During World War I, TB was depicted in propaganda posters from France as a national adversary, akin to the German enemy. One propaganda poster shows the German imperial eagle being struck down by a sword, drawing a parallel between the fight against TB and the war against Germany (Figure 9).

The representation of TB in the 20th Century not only documented a medical battle against a microbial foe but also encapsulated the social and political challenges of the era. The fight against TB was not just in hospitals and sanatoriums but also on the front lines of public consciousness, through stamps, posters, and public campaigns, urging a societal call to arms against this persistent threat to human health.

In the United States, artists such as Alice Neel brought the issue of TB into the context of immigration and the urban experience (*22*). Neel's 1940 painting *TB Harlem* starkly depicts the reality of TB in New York City, portraying Carlos Negrón with a dignified yet afflicted presence postthoracoplasty (Figure 10). Her unsentimental style emphasizes the physical ravages of the disease through distorted anatomy and dark, heavy outlines. Neel's work reflects TB's grim effect in urban settings, particularly within the disadvantaged communities of Harlem.

This representation is complemented by *Recovery*, a life-size wood sculpture by an unnamed TB patient from an English asylum, depicting the patient's own experience with the disease by representing

Figure 9. *L'aigle Boche sera vaincu: la tuberculose doit l'être aussi*, a World War I propaganda poster from France depicting tuberculosis as a national adversary. Public domain digital image

Figure 10. Alice Neels' 1940 painting *TB Harlem* depicting tuberculosis in New York City, portraying Carlos Negrón after thoracoplasty. Image from the National Museum of Women in the Arts, Gift of Wallace and Wilhelmina Holladay. Copyright © The Estate of Alice Neel/Courtesy of David Zwirner, New York. Previously published by Emerging Infectious Diseases (https://wwwnc.cdc.gov/eid/article/19/3/ac-1903_article).

himself with a sunken chest (Figure 11) (*23*). This work underscores the personal narratives of those who endured TB, shifting the focus from mere artistic interpretation to patient-lived reality.

Since the 1980s, TB and HIV have been jointly portrayed in art as twin scourges, reflecting their intertwined epidemiologic effect on global health. Posters and visual campaigns frequently depict them together, symbolizing the compounded vulnerability and the heightened challenge faced by those having both conditions (*24*). This co-representation has served to amplify awareness and galvanize action against the dual public health crises.

Discussion

Our review has traced the evolution of TB's portrayal from a mysterious condition affecting all societal levels to a known pathogen targeted by public health initiatives. Throughout the centuries, the representation of TB in Western art has undergone a profound transformation. This artistic journey through TB's depiction reflects a complex interplay among harsh reality, romantic idealization, and evolving medical understanding, illustrating how deeply TB has been woven into the cultural and artistic fabric of society.

In the organization of this review, we have consciously categorized the artistic representation of TB into 3 distinct periods, a decision driven by our goal to provide clarity and coherence for the reader. Although we acknowledge that the artistic portrayal of TB often transcends strict chronological boundaries and forms a spectrum of evolving expression, this structured approach simplified the complex interplay between art

Figure 11. *Recovery*, a life-size wood sculpture by an unnamed tuberculosis patient from an asylum in England, showcasing the patient's direct experience with the disease as he represented himself with a sunken chest. Copyright © American Visionary Art Museum.

Figure 12. *Don't Speak* is a painting by Paulina Siniatkina. She painted the piece while battling tuberculosis in 2015 to demonstrate how stigmatizing the infection felt. Copyright © Paulina Siniatkina. Previously published by Emerging Infectious Diseases (https://wwwnc.cdc.gov/eid/article/30/3/AC-3003_article).

and the disease. By dividing the material into distinct eras, we aimed to highlight the major shifts in perception and representation that paralleled medical advancements and still appreciate the nuanced continuity present in the artistic narrative of this disease.

Artistic portrayals often showed patients as gaunt or skeletal figures, either bedridden or sitting, their bodies weakened or immobilized. However, as the 20th Century progressed, the visual narrative attributed to TB permeated representations of other diseases. Inspired by the TB attributes, the Spanish influenza after 1918 and cancer after the 1950s were portrayed by using similar visual motifs in artistic representations. This shift coincided with a decline in TB because of increasingly effective public health measures, the devastating effect of the Spanish influenza pandemic, and a rise in cancer diagnoses (*25*,*26*).

The 20th Century has also seen the patient's perspective come to the forefront. Those personal narratives deepen our appreciation for the subjective experience of illness and resonate with contemporary movements in healthcare that emphasize patient-centered perspectives. Those narratives also illustrate how art has not only served as a medium for societal reflection but also provided a therapeutic outlet for persons to process and contend with their conditions (*27*).

Once shrouded in a romanticized veil or seen as an almost divine affliction, TB has now become a stigmatizing disease. In the 21st Century, the works of artists such as Paulina Siniatkina, who, while battling TB herself in 2015, created poignant and powerful paintings during her stay in a TB hospital in Moscow, are particularly illustrative (*28*,*29*) (Figure 12). Her art is a testament to the role of creative expression in coping with illness and stigma, offering both a form of escapism and a way to confront and articulate the reality of living with a chronic condition (*30*).

In conclusion, the intersection of TB and art throughout history highlights the enduring human capacity to find meaning and resilience in the face of suffering. The artistic legacy of TB, from the royal touch to patient-produced artwork, encapsulates a diverse range of human response to this disease. As we continue to grapple with TB in various contexts, art remains a potent form of expression and coping, offering insights into the individual and collective experience of health and disease.

About the Author

Dr. Kherabi is a French infectious diseases specialist particularly interested in tuberculosis management. Dr. Charlier is a physician and director of the Anthropology, Archaeology, and Biology Laboratory at the University of Versailles Saint-Quentin-en-Yvelines. His interests include anthropology and archaeology.

References

1. World Health Organization. Global tuberculosis report 2024 [cited 2025 Feb 20]. https://iris.who.int/bitstream/handle/10665/379339/9789240101531-eng.pdf
2. Morens DM. At the deathbed of consumptive art. Emerg Infect Dis. 2002;8:1353–8. https://doi.org/10.3201/eid0811.020549
3. Vilaplana C. A literary approach to tuberculosis: lessons learned from Anton Chekhov, Franz Kafka, and Katherine Mansfield. Int J Infect Dis. 2017;56:283–5. https://doi.org/10.1016/j.ijid.2016.12.012
4. Kaptein AA, Meulenberg F, Smyth JM. A breath of fresh air: images of respiratory illness in novels, poems, films, music, and paintings. J Health Psychol. 2015;20:246–58. https://doi.org/10.1177/1359105314566613
5. Charlier P, Perciaccante A, Kluger N, Nerlich AG, Appenzeller O, Donell ST, et al. Iconodiagnosis: guidelines and recommendations. Ethics Med Public Health. 2023;31:100951. https://doi.org/10.1016/j.jemep.2023.100951
6. Murray JF, Rieder HL, Finley-Croswhite A. The King's Evil and the royal touch: the medical history of scrofula. Int J Tuberc Lung Dis. 2016;20:713–6. https://doi.org/10.5588/ijtld.16.0229
7. Bloch M. Les rois thaumaturges. Strasbourg (France): Librairie Istra; 1924.
8. USU Digital Exhibits. Clovis I touching for scrofula [cited 2025 Feb 14]. http://exhibits.usu.edu/items/show/16300
9. Xu J. The royal touch: scrofula and defining monarchy. Clin Dermatol. 2023;41:166–70. https://doi.org/10.1016/j.clindermatol.2022.09.009
10. O'Reilly LM, Daborn CJ. The epidemiology of *Mycobacterium bovis* infections in animals and man: a review. Tuber Lung

Dis. 1995;76(Suppl 1):1–46. https://doi.org/10.1016/0962-8479(95)90591-X
11. Krugman J, Chorba T. When a touch of gold was used to heal the king's evil. Emerg Infect Dis. 2022;28:765–7. https://doi.org/10.3201/eid2803.AC2803
12. Chorba T, Breedlove B. Depictions of heroism in battle and anguish from tuberculosis. Emerg Infect Dis. 2016;22:573–4. https://doi.org/10.3201/eid2203.AC2203
13. Day C. Consumptive chic: a history of beauty, fashion, and disease. London: Bloomsbury Academic; 2017. https://doi.org/10.5040/9781350009417
14. Lefebvre T. A famous patient: Marie Duplessis, la dame aux camélias [in French]. Rev Prat. 1998;48:1518–20.
15. Lawlor C, Suzuki A. The disease of the self: representing consumption, 1700–1830. Bull Hist Med. 2000;74:458–94. https://doi.org/10.1353/bhm.2000.0130
16. Lemlein RF. Influence of tuberculosis on the work of visual artists: several prominent examples. Leonardo. 1981;14:114–7. https://doi.org/10.2307/1574402
17. Mahoney D, Chorba T. Romanticism, mycobacterium, and the myth of the muse. Emerg Infect Dis. 2019;25:617–8.
18. Holland JG, editor. The private journals of Edvard Munch: we are the flames which pour out of the earth. Madison (WI): University of Wisconsin Press; 2005.
19. Chorba T, Jereb J. Keeping it in the family: the childhood burden of tuberculosis. Emerg Infect Dis. 2017;23:561–2.
20. Potter P. Heart fastened to a dying animal. Emerg Infect Dis. 2012;18:1394–5.
21. Lefrère J-J, Danic B. Pictorial representation of transfusion over the years. Transfusion. 2009;49:1007–17. https://doi.org/10.1111/j.1537-2995.2008.02068.x
22. National Museum of Women in the Arts. Alice Neel, TB Harlem [cited 2024 Jan 12]. https://nmwa.org/art/collection/tb-harlem
23. American Visionary Art Museum. Recovery [cited 2024 Jan 12]. https://www.avam.org/art/recovery
24. National Library of Medicine. TB, HIV: double trouble [cited 2024 Jan 12]. https://collections.nlm.nih.gov/catalog/nlm:nlmuid-101450773-img
25. Goldstein JL. The Spanish 1918 flu and the COVID-19 disease: the art of remembering and foreshadowing pandemics. Cell. 2020;183:285–9. https://doi.org/10.1016/j.cell.2020.09.030
26. Kaptein AA, Thong MSY. Portraying a grim illness: lung cancer in novels, poems, films, music, and paintings. Support Care Cancer. 2018;26:3681–9. https://doi.org/10.1007/s00520-018-4222-1
27. Stuckey HL, Nobel J. The connection between art, healing, and public health: a review of current literature. Am J Public Health. 2010;100:254–63. https://doi.org/10.2105/AJPH.2008.156497
28. Egelund EF, Bucciarelli AL. Art and the fight against tuberculosis. JAMA. 2022;328:509–10. https://doi.org/10.1001/jama.2021.24029
29. Fukunaga R, Moonan PK. Mental health and tuberculosis—holding our breath in isolation. Emerg Infect Dis. 2024;30:627–8. https://doi.org/10.3201/eid3003.AC3003
30. World Health Organization. "Hold your breath", paintings made by Russian artist while in a TB clinic [cited 2023 Nov 10]. https://www.who.int/news-room/photo-story/photo-story-detail/hold-your-breath-paintings-made-by-russian-artist-while-in-a-tb-clinic

Address for correspondence: Yousra Kherabi, Bichat-Claude Bernard Hospital, 46 rue Henri Huchard, 75018 Paris, France; email: yousra.kherabi@aphp.fr

EID Podcast

Emerging Infectious Diseases Cover Art

Byron Breedlove, managing editor of the journal, elaborates on aesthetic considerations and historical factors, as well as the complexities of obtaining artwork for Emerging Infectious Diseases.

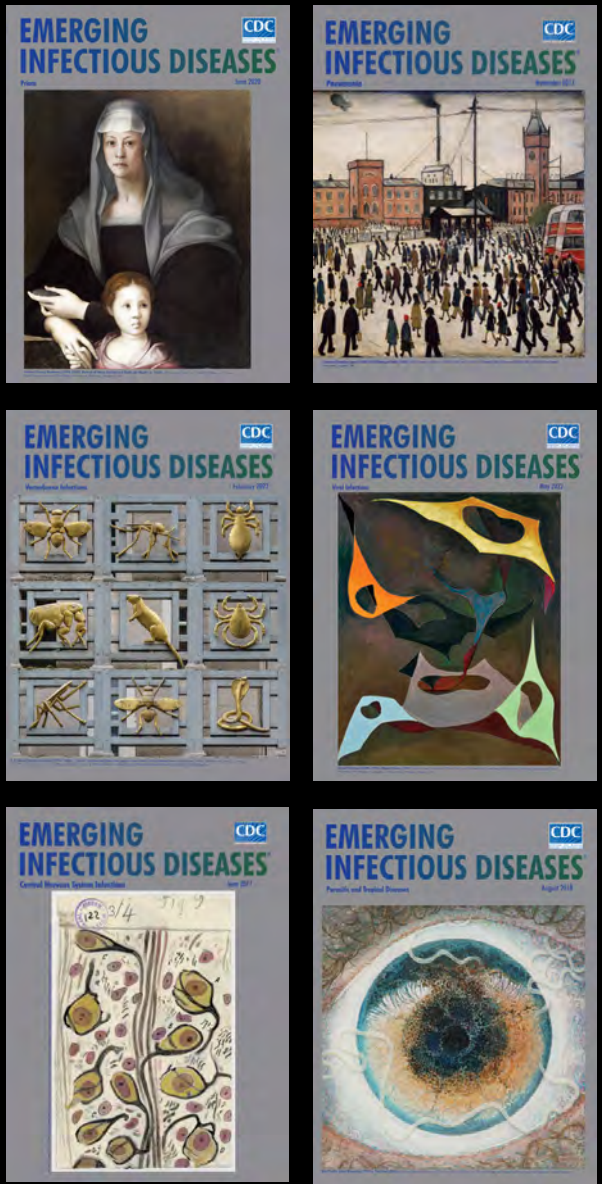

Visit our website to listen:

https://www2c.cdc.gov/podcasts/player.asp?f=8646224

EMERGING INFECTIOUS DISEASES

Fluoroquinolone Resistance in Drug-Resistant Tuberculosis, Kharkiv, Ukraine, 2019–2023

Olha Konstantynovska, Tetiana Synenko, Alla Honcharenko, Olha Volobuieva, Tetiana Liadova, Maja Reimann, Christoph Lange, Dumitru Chesov

Author affiliations: Imperial College London, London, UK (O. Konstantynovska); Kharkiv Regional Phthisiopulmonological Center, Kharkiv, Ukraine (O. Konstantynovska, T. Synenko, A. Honcharenko, O. Volobuieva); V.N. Karazin Kharkiv National University, Kharkiv (O. Konstantynovska, O. Volobuieva, T. Liadova); Leibniz Lung Center, Borstel, Germany (M. Reimann, C. Lange, D. Chesov); German Center for Infection Research (DZIF), Hamburg-Lübeck-Borstel-Riems, Germany (M. Reimann, C. Lange, D. Chesov); University of Lübeck, Lübeck, Germany (C. Lange); Baylor College of Medicine and Texas Children's Hospital, Global Tuberculosis Program, Houston, Texas, USA (C. Lange); Nicolae Testemitanu State University of Medicine and Pharmacy, Chisinau, Moldova (D. Chesov)

DOI: https://doi.org/10.3201/eid3103.241675

Rifampin-resistant *Mycobacterium tuberculosis* was identified by the World Health Organization as a pathogen of public health critical importance. During 2014–2023, an increase in fluoroquinolone resistance in rifampin-resistant *M. tuberculosis* from Kharkiv, Ukraine, was observed. Efforts to mitigate factors contributing to resistance should be prioritized to prevent further escalation of that threat.

In 2024, the World Health Organization (WHO) officially recognized rifampin-resistant *Mycobacterium tuberculosis* as 1 of 4 antibiotic drug–resistant pathogens of critical global priority (*1*). According to WHO's 2024 Global TB report, 400,000 persons worldwide develop tuberculosis (TB) caused by a multidrug-resistant/rifampin-resistant (MDR/RR) *M. tuberculosis* (*2*). Of note, the estimated proportion of MDR/RR TB among all new TB cases is 3.2%, whereas among previously treated cases, that figure was 16% (*2*). Regional disparities in the global burden of MDR/RR TB are profound. The greatest incidence is observed in Eastern Europe and Central Asia, where up to 20% of new TB cases and >50% of previously treated cases exhibit MDR/RR TB. Those regions face considerable challenges in implementing effective TB control measures (*2*).

WHO's 2024 recommendations for drug-resistant TB management included several short treatment regimens, which have shown high efficacy in curing MDR/RR TB. Treatment durations are 6–9 months, which are substantially shorter than the standard 18–20-month regimen (*3*). Eligibility for shorter regimens requires confirmation of drug susceptibility within the regimen. In cases where resistance to agents used in 6- and 9-month regimens is confirmed or suspected, patients must undergo the longer 18-month course. However, emerging resistance to key second-line TB treatment agents in multiple regions threatens the real-world effectiveness of those treatment approaches (*4*).

The objective of this study was to assess resistance rates to second-line TB treatment drugs in the Kharkiv region of Ukraine (2.6 million inhabitants in 2023), which is a country with a high burden of drug-resistant TB, and to compare those findings with our previously reported data from the same region (*5*). We analyzed data from phenotypic drug susceptibility testing, as recorded in the Electronic Register of the TB-Control Program in Kharkiv, for the specified period. Results indicated that 23.1%–31.2% of patients in Kharkiv affected by MDR/RR TB during 2019–2023 had additional resistance to levofloxacin at ≈3-fold greater level than the 10% observed in 2014. Similarly, resistance to moxifloxacin ranged from 10.6% to 20.9% and was the highest rate recorded in the past 2 years, suggesting a notable upward trend in fluoroquinolone resistance (Table). Conversely, resistance to other group A agents (bedaquiline and linezolid) and group B agents (clofazimine and cycloserine) remained low at <1%. We observed high levels of resistance for pyrazinamide (a drug belonging to group C on the WHO drug list), which is a component medicine in the 2024 WHO-recommended 9-month MDR TB regimens. Resistance to pyrazinamide ranged from 54.3% to 58.7% during 2019–2023, compared with 69.6% in 2014.

The substantial increase in fluoroquinolone resistance observed in this study is particularly alarming. Fluoroquinolones play a critical role in MDR/RR TB treatment. Resistance to those agents is a key criterion for defining pre–extensively drug-resistant TB. That resistance is also a noteworthy factor linked to poorer outcomes in patients with MDR/RR TB (*6*). Consequently, because up to 30% of patients in Kharkiv with MDR/RR TB are infected with *M. tuberculosis* strains exhibiting fluoroquinolone resistance, effective TB control faces considerable challenges at times of military oppression. A contributing factor to the rise in fluoroquinolone resistance is likely the insufficient availability or improper use of second-line TB medications (*7*). Our 2014 data indicated deficiencies

Table. Resistance to second-line drugs in a study of fluoroquinolone resistance in drug-resistant TB, Kharkiv, Ukraine, 2019–2023*

Category	2014	2019	2020	2021	2022	2023	Kendall τ
No. patients with MDR/RR TB	169	333	231	243	155	262	0.07
New TB patients with MDR/RR TB, no. (%)	104 (61.5)	256 (76.9)	178 (77.1)	173 (71.2)	125 (80.6)	187 (71.4)	0.07†
Group A drugs, % resistant							
Moxifloxacin	14.9	NT	15.0	10.6	20.8	20.9	0.6
Levofloxacin	10.0	23.1	27.2	26.9	31.2	28.2	0.73
Bedaquiline	NT	NT	0	0	0.7	0.4	0.55
Linezolid	2.9	0.3	0	0.5	2.7	0.4	−0.07
Group B drugs, % resistant							
Clofazimine	NT	0	0	0	0	0.4	0.63
Cycloserine	5.8	0	NT	NT	NT	NT	NA
Group C drugs, % resistant							
Ethambutol	66.3	75.4	60.1	37.9	49.4	54.4	−0.47
Delamanid	NT	0	1.8	0.9	0.7	1.7	0.2
Pyrazinamide	69.6	54.9	54.9	54.3	55.3	58.6	0
Imipenem/meropenem	NT	NT	NT	NT	NT	NT	NA
Amikacin	23.4	12.4	13.2	18.5	20.4	18.0	0.07
Streptomycin	95.9	75.3	78.4	NT	NT	NT	−0.33
Ethionamide	33.6	32.7	26.1	24.4	27.3	NT	−0.6
Para-aminosalicylic acid	3.1	NT	NT	NT	NT	NT	NA

*Results referred to phenotypic drug susceptibility testing, performed by using the BACTEC MGIT960 culture system (Becton Dickinson, https://www.bd.com), applying World Health Organization–recommended critical concentrations. Drug groups are from the World Health Organization (*3*). MDR/RR, multidrug resistant/rifampin resistant; NA, not applicable; NT, not tested; TB, tuberculosis.
†The Kendal τ coeficient for the trend for the percentage of new TB patients over the study period 2014 and 2019–2023 was 0.33.

in MDR/RR TB management at the Kharkiv TB Dispensary, suggesting that the high rates of fluoroquinolone resistance observed during 2019–2023 could be a consequence of suboptimal possibilities for the management of patients with drug-resistant TB in previous years.

In addition to their role in MDR/RR TB treatment, fluoroquinolones are frequently prescribed empirically for common bacterial infections, such as pneumonia and sinusitis. In cases where fluoroquinolones are used as monotherapy for patients with undiagnosed TB, that practice may contribute to bacillary resistance across that drug class (*8*). The resulting symptom relief can delay TB diagnosis, thereby increasing community transmission risk (*9*). In Ukraine, the unregulated use of antibiotic drugs is common practice (*10*), adding to the increase in *M. tuberculosis* resistance to fluoroquinolones. The rapid development of resistance observed here should serve as a cautionary example as new MDR/RR TB drugs, such as bedaquiline, are introduced into clinical settings. Rapid resistance development poses a potential threat to the efficacy of newly implemented TB treatment drugs such as bedaquiline, even if data from this study do not yet reflect such resistance.

In conclusion, given the ongoing military conflict in the region, heightened vigilance regarding the potential for worsening drug resistance among patients with MDR TB in Kharkiv is essential. Additional efforts to mitigate factors that may contribute to rising resistance should be prioritized to prevent further escalation of the public health threat.

D.C. and C.L. are supported by the German Center of Infection Research (grant agreement no. 02.709).

About the Author

Dr. Konstantynovska is an associate professor at the Department of Infectious Diseases and Clinical Immunology of V.N. Karazin Kharkiv National University's Medical School in Ukraine. Her research and clinical interests focus on molecular genetics, tuberculosis, pulmonology, genetic factors in drug resistance against antimycobacterial agents, and infections caused by nontuberculous mycobacteria.

References

1. World Health Organization. WHO bacterial priority pathogens list, 2024: bacterial pathogens of public health importance to guide research, development and strategies to prevent and control antimicrobial resistance. Geneva: The Organization; 2024.
2. World Health Organization. Global tuberculosis report 2024. Geneva: The Organization; 2024.
3. World Health Organization. Key updates to the treatment of drug-resistant tuberculosis: rapid communication. Geneva: The Organization; 2024.
4. Chesov E, Chesov D, Maurer FP, Andres S, Utpatel C, Barilar I, et al. Emergence of bedaquiline resistance in a high tuberculosis burden country. Eur Respir J. 2022;59:2100621. https://doi.org/10.1183/13993003.00621-2021
5. Butov D, Lange C, Heyckendorf J, Kalmykova I, Butova T, Borovok N, et al. Multidrug-resistant tuberculosis in the Kharkiv Region, Ukraine. Int J Tuberc Lung Dis. 2020;24:485–91. https://doi.org/10.5588/ijtld.19.0508
6. Pedersen OS, Holmgaard FB, Mikkelsen MKD, Lange C, Sotgiu G, Lillebaek T, et al. Global treatment outcomes of extensively drug-resistant tuberculosis in adults: a systematic review and meta-analysis. J Infect. 2023;87:177–89. https://doi.org/10.1016/j.jinf.2023.06.014

7. Liu CH, Yang N, Wang Q, Hu YL, Li L, Zhang GY, et al. Risk factors associated with fluoroquinolone-resistant tuberculosis in a Beijing tuberculosis referral hospital. Respirology. 2011;16:918–25. https://doi.org/10.1111/j.1440-1843.2011.01990.x
8. Lee JY, Lee HJ, Kim YK, Yu S, Jung J, Chong YP, et al. Impact of fluoroquinolone exposure prior to tuberculosis diagnosis on clinical outcomes in immunocompromised patients. Antimicrob Agents Chemother. 2016;60:4005–12. https://doi.org/10.1128/AAC.01749-15
9. Chen TC, Lu PL, Lin CY, Lin WR, Chen YH. Fluoroquinolones are associated with delayed treatment and resistance in tuberculosis: a systematic review and meta-analysis. Int J Infect Dis. 2011;15:e211–6. https://doi.org/10.1016/j.ijid.2010.11.008
10. Versporten A, Bolokhovets G, Ghazaryan L, Abilova V, Pyshnik G, Spasojevic T, et al.; WHO/Europe-ESAC Project Group. Antibiotic use in eastern Europe: a cross-national database study in coordination with the WHO Regional Office for Europe. Lancet Infect Dis. 2014;14:381–7. https://doi.org/10.1016/S1473-3099(14)70071-4

Address for correspondence: Dumitru Chesov, Clinical Infectious Diseases, Research Center Borstel, Leibniz Lung Center, Parkallee 35, 23845 Borstel, Germany; email: dchesov@fz-borstel.de

Neurosarcocystosis in Patient with HIV-Induced Immunodeficiency

Tonje Skarpengland,[1] Anders A. Tveita,[1] Christopher F. Berntsen, Erik. E. Christensen, Magnhild E. Macpherson, Birgitte Stiksrud, Nils O. Hermansen, Pitt Niehusmann, Tine S. Oldereid, Espen Stjernstrøm, Hanne Brekke, Henrik V. Nielsen, Frank O.D. Pettersen

Author affiliations: Oslo University Hospital, Ullevål, Oslo, Norway (T. Skarpengland, C.F. Berntsen, E.E. Christensen, M.E. Macpherson, B. Stiksrud, N.O. Hermansen, T.S. Oldereid, E. Stjernstrøm, H. Brekke, F.O.D. Pettersen); Institute of Clinical Medicine, University of Oslo, Oslo (A.A. Tveita); Oslo University Hospital, Rikshospitalet, Oslo (A.A. Tveita, P. Niehusmann); Statens Serum Institut, Copenhagen, Denmark (H.V. Nielsen)

DOI: https://doi.org/10.3203/eid3103.241361

[1]These first authors contributed equally to this article.

Sarcocystis is a genus of protozoan parasites that can infect various vertebrates. In humans, *Sarcocystis* infection usually is asymptomatic but might manifest as a mild gastroenteritis or extraintestinal myositis. We report a case of human central nervous system infection in Norway caused by *S. nesbitti* parasites.

The genus *Sarcocystis* consists of apicomplexan parasites, ≈200 species of which can infect reptiles, birds, and mammals; however, few species are zoonotic (*1*). Humans are definitive hosts of *S. hominis*, *S. suihominis*, and *S. heydorni*, shedding oocysts after ingestion of undercooked meat from intermediate hosts containing tissue cysts (*1*). Gastrointestinal infection is asymptomatic or causes a mild, self-limiting gastroenteritis (*2*). Human muscular sarcocystosis is a rare clinical syndrome associated with *S. nesbitti* infection mostly documented in Malaysia (*2*). The natural reservoirs of *S. nesbitti* parasites are probably reptiles, particularly snakes in Southeast Asia and Australia (*3*,*4*). Intermediate hosts, including humans, might develop tissue sarcocystosis after ingesting *S. nesbitti* sporocysts from fecally contaminated food or water. In Thailand, the prevalence of intestinal sarcocystosis is 7.0%–23.2% (*5*,*6*), but data regarding tissue sarcocystosis and *S. nesbitti* infection are scarce. We report a human case of *S. nesbitti* central nervous system infection in Norway.

The patient, a White male in his 70s, had lived in Norway for ≈40 years and visited Thailand for several months a year for 10 years. While in southern Thailand, he experienced increasing back pain and acute diplopia, aphasia, unilateral hemiparesis, and urinary and fecal incontinence. Imaging conducted in a clinic in Thailand revealed multiple brain lesions, and he returned to Norway for further investigations.

Upon the patient's hospital admission in Norway, initial laboratory workup revealed an undiagnosed HIV infection (viral load 50,000 copies/mL, CD4+ T-cell count 116 cells/mm^3). Magnetic resonance imaging showed numerous cortical and subcortical contrast-enhancing lesions in both cerebral hemispheres, along with multiple cerebellar, cervical, and thoracic spinal cord lesions (Figure). We noted hemorrhagic components and substantial perilesional edema (Figure). 18F-fluorodeoxyglucose (FDG) positron emission tomography–computed tomography demonstrated intense focal FDG uptake corresponding to areas of contrast enhancement found on magnetic resonance imaging. Apart from a diffusely increased signal in gluteal muscles, we noted no abnormal FDG uptake outside the central nervous system (CNS). The overall assessment suggested metastatic cancer, with opportunistic infection as a differential diagnosis.

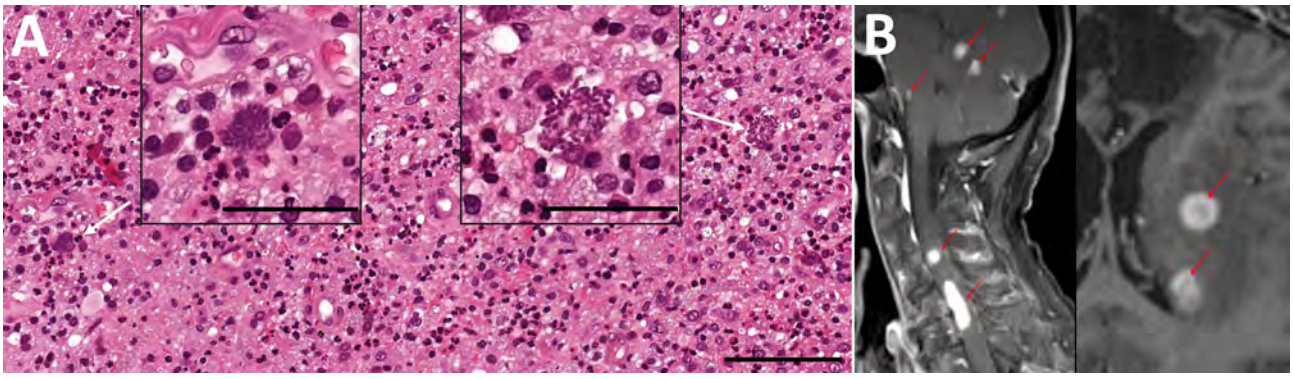

Figure. Microscopic findings and imaging results for patient with HIV-induced immunodeficiency preceding diagnosis of neurosarcocystosis, Norway. A) Light microscopic findings of structures resembling *Toxoplasma gondii* bradozoites (white arrows) in brain biopsy. Hematoxylin and eosin stain. Scale bars of enlarged images indicate 50 μm; scale bar of background image indicates 100 μm. B) Magnetic resonance imaging of cerebral and spinal cord lesions (contrast enhanced sagtittal T1 sequence, left panel, red arrows) and cerebral lesions with slight peripheral ring enhancement (contrast enhanced transversal T1 sequence, right panel, red arrows).

Cerebrospinal fluid (CSF) analysis showed an unremarkable leucocyte count (<4 × 10^6 cells/L), but increased protein level (1.8 g/L) and albumin and IgG indices. Serologic test results were positive for *Toxoplasma gondii* IgG and negative for IgM. Blood and CSF were negative for *T. gondii* DNA. We detected asymptomatic reactivation of Epstein-Barr virus (EBV) and cytomegalovirus in blood. Results of additional microbiologic diagnostic analyses of other viruses, bacteria, fungi, and parasites (e.g., tuberculosis interferon-γ release assay and serologic and molecular testing of blood and CSF) were negative.

Histological examination of brain tissue revealed no signs of malignancy but indicated lymphohistiocytic infiltrates and singular structures resembling *T. gondii* bradyzoites (Figure). However, *T. gondii* immunohistochemical testing was inconclusive, and results for 2 different *T. gondii*–specific PCR assays were negative. Brain tissue PCR results were negative for herpes simplex virus 1 and 2, varicella zoster virus, cytomegalovirus, JC virus, 16S rDNA, internal transcribed spacer 2, and D1D2 fungal DNA. EBV PCR results were positive, but in situ hybridization displayed EBV-positive cells in a minute proportion of infiltrating lymphocytes, compatible with unspecific reactivity. We sent brain tissue and CSF to Statens Serum Institut (Copenhagen, Denmark) for metabarcoding analyses based on 16S and 18S DNA PCR combined with next-generation sequencing (*7*).

Faced with the presence of multiple space-occupying CNS lesions and evolving neurologic symptoms in the patient, we initiated treatment with dexamethasone pending further diagnostic workup. We started the patient on antiretroviral therapy, and after histologic assessment of the brain biopsy, we commenced treatment with high-dose trimethoprim/sulfamethoxazole (5/25 mg/kg × 2/d), because toxoplasmosis was considered the most probable diagnosis. The metabarcoding analyses of brain tissue (but not CSF) yielded a 380-bp consensus sequence of the 18S rRNA gene with 100% similarity to a published *S. nesbitti* sequence (genomic DNA containing 18S rRNA gene; GenBank accession no. HF544323.1). On the basis of metabarcoding analyses and histological findings, we made a final diagnosis of neurosarcocystosis. *Sarcocystis* serologic testing was not obtainable.

The treatment regimen was well-tolerated, and the patient's clinical and radiologic condition improved substantially without signs of immune reconstitution inflammatory syndrome; however, some neurologic sequelae remained. We tapered glucocorticoids gradually and started secondary prophylaxis of trimethoprim/sulfamethoxazole.

To our knowledge, human neurosarcocystosis is not recognized as an opportunistic infection. Given the phylogenetic relationship of *Sarcocystis* with *Toxoplasma*, the patient's condition might represent reactivation of latent sarcocystis infection resulting from HIV-induced immunodeficiency. Because of limited knowledge about the dynamics of extraintestinal sarcocystosis in immunosuppressed hosts, we cannot determine whether this condition represents a primary infection or reactivation. A detailed travel history revealed no visits to *Sarcocystis*-endemic hotspots such as the Pangkor or Tioman Islands of Malaysia (*8*).

We hypothesize that *Sarcocystis* spp. may cause opportunistic CNS infections in immunocompromised persons. Furthermore, neurosarcocystosis might be misdiagnosed as toxoplasmosis clinically, histopathologically, and radiologically. Because both conditions respond to high-dose trimethoprim/sulfamethoxazole, therapeutic efficacy might inadvertently support such a misdiagnosis. This case illustrates that the

true prevalence and disease patterns of opportunistic pathogens are probably underestimated and that routine microbiologic workup might fail to reveal rare and unrecognized opportunistic infections.

Acknowledgments

We thank the patient for providing the written informed consent for publication of this report.

About the Author

Dr. Skarpengland is a specialist in infectious diseases and senior consultant at the Department of Infectious Diseases, Oslo University Hospital, Ullevål, Norway. Her main research interests are immunodeficiency and lipid metabolism. Dr. Tveita is a resident physician at the Department of Rheumatology, Dermatology, and Infectious Diseases, Oslo University Hospital, Rikshospitalet, Norway. His main research interests are cellular immunodeficiencies and immunotherapy.

References

1. Rosenthal BM. Zoonotic *Sarcocystis*. Res Vet Sci. 2021;136:151–7. https://doi.org/10.1016/j.rvsc.2021.02.008
2. Fayer R, Esposito DH, Dubey JP. Human infections with *Sarcocystis* species. Clin Microbiol Rev. 2015;28:295–311. https://doi.org/10.1128/CMR.00113-14
3. Shahari S, Tengku-Idris TI, Fong MY, Lau YL. Molecular evidence of *Sarcocystis nesbitti* in water samples of Tioman Island, Malaysia. Parasit Vectors. 2016;9:598. https://doi.org/10.1186/s13071-016-1883-9
4. Wassermann M, Raisch L, Lyons JA, Natusch DJD, Richter S, Wirth M, et al. Examination of *Sarcocystis* spp. of giant snakes from Australia and Southeast Asia confirms presence of a known pathogen—*Sarcocystis nesbitti*. PLoS One. 2017;12:e0187984. https://doi.org/10.1371/journal.pone.0187984
5. Wilairatana P, Radomyos P, Radomyos B, Phraevanich R, Plooksawasdi W, Chanthavanich P, et al. Intestinal sarcocystosis in Thai laborers. Southeast Asian J Trop Med Public Health. 1996;27:43–6.
6. Tungtrongchitr A, Chiworaporn C, Praewanich R, Radomyos P, Boitano JJ. The potential usefulness of the modified Kato thick smear technique in the detection of intestinal sarcocystosis during field surveys. Southeast Asian J Trop Med Public Health. 2007;38:232–8.
7. Hartmeyer GN, Stensvold CR, Fabricius T, Marmolin ES, Hoegh SV, Nielsen HV, et al. *Plasmodium cynomolgi* as cause of malaria in tourist to Southeast Asia, 2018. Emerg Infect Dis. 2019;25:1936–9. https://doi.org/10.3201/eid2510.190448
8. Abubakar S, Teoh B-T, Sam S-S, Chang L-Y, Johari J, Hooi P-S, et al. Outbreak of human infection with *Sarcocystis nesbitti*, Malaysia, 2012. Emerg Infect Dis. 2013;19:1989–91. https://doi.org/10.3201/eid1912.120530

Address for correspondence: Frank O.D. Pettersen, Oslo University Hospital, Ullevål, Department of Infectious Diseases, Regional Advisory Unit for Imported and Tropical Diseases, PO Box 4950, Nydalen 0424, Oslo, Norway; email: frank.o.pettersen@gmail.com

Lack of Competence of US Mosquito Species for Circulating Oropouche Virus

Anne F. Payne, Jessica Stout, Peter Dumoulin, Timothy Locksmith, Lea A. Heberlein, Molly Mitchell, Arnold Rodriguez-Hilario, Alan P. Dupuis II, Alexander T. Ciota

Author affiliations: Wadsworth Center, New York State Department of Health, Slingerlands, New York, USA (A.F. Payne, J. Stout, A.P. Dupuis II, A.T. Ciota); Florida Department of Health, Tampa, Florida, USA (P. Dumoulin, T. Locksmith, L.A. Heberlein, A. Rodriguez-Hilario); Florida Department of Health, Jacksonville, Florida, USA (M. Mitchell); University at Albany School of Public Health, Rensselaer, New York, USA (A.T. Ciota)

DOI: https://doi.org/10.3201/eid3103.241886

Given recent outbreaks of Oropouche virus in Latin America and >100 confirmed travel-associated cases in the United States, we evaluated the competence of US vectors, including *Aedes albopictus*, *Culex quinquefasciatus*, *Culex pipiens*, and *Anopheles quadrimaculatus* mosquitoes. Results with historic and recent isolates suggest transmission potential for those species is low.

Oropouche virus (OROV) is a negative-sense, segmented RNA virus and a member of the family Peribunaviridae, genus *Orthobunyavirus*. OROV was first identified in Trinidad and Tobago in 1955, and although it was previously detected in several countries in Latin America, large outbreaks have historically been limited to the Amazon region of Brazil (*1*,*2*). In 2024, >10,000 cases were reported, with unprecedented activity outside Brazil (*3*). In addition, 108 imported cases have been identified in travelers or residents returning to the United States. Although most of those cases have been in Florida, cases have also been identified in New York, New Jersey, Kentucky, Colorado, and California (*3*).

OROV infection is generally associated with a mild, self-limiting febrile illness, yet more extensive disease, including fatal infections, has been attributed to the recent outbreak. Furthermore, vertical transmission and associations with congenital abnormalities and fetal death have been reported (*4*,*5*).

Although the primary vector of OROV is *Culicoides paraensis* midges (*6*), mosquitoes have also been implicated, particularly *Culex quinquefasciatus* mosquitoes (*7*). However, experimental assessment of OROV transmission by mosquitoes is limited

(*8*–*10*). We investigated whether prominent US mosquito species have the potential to contribute to local maintenance.

We isolated OROV from reverse transcription PCR–positive serum from a febrile patient from Cuba after amplification on Vero cell culture (OROV 240023). We obtained RNA through the QIAGEN QIAcube using the DSP Viral RNA Mini Kit (https://www.qiagen.com). We completed first and second strand cDNA synthesis with random primers using NEB ProtoScript II First Strand cDNA Synthesis Kit and NEBNext Ultra II Non-Directional RNA Second Strand Synthesis Module (New England BioLabs, https://www.neb.com). We completed purification using AMPure bead-based methods (Beckman Coulter, https://www.beckmancoulter.com) and completed library preparation using the Illumina DNA Prep kit (Illumina, https://www.illumina.com). We completed sequencing on an Illumina NextSeq 1000 with fastq files generated through BaseSpace. We achieved reference-based assembly using an in-house pipeline. We aligned high-quality reads to reference sequences (GenBank accession nos. PQ064919.1, PQ064920.1, and PQ064921.1) and generated consensus sequences. We compared OROV 240023 to the 1955 strain OROV TRVL9760 (GenBank accession no. KC759122–24) after pairwise alignment in Geneious Prime (https://www.geneious.com). OROV 240023 was 6.3% divergent on the nucleotide level and 0% on the amino acid level in the small segment, 5.2% divergent on the nucleotide level and 1.8% on the amino acid level in the medium segment, and 10.9% divergent on the nucleotide level and 2.0% on the amino acid level in the large segment. The 69 unique amino acid residues are dispersed throughout the medium and large peptides.

Using OROV 240023 and TRVL9760, we assessed competence of mosquitoes after feeding on blood meals containing 6.5 $\log_{10}$ PFU/mL with 4 US species: *Aedes albopictus*, *Cx. quinquefasciatus*, *Cx. pipiens*, and *Anopheles quadrimaculatus*. *Ae. albopictus* mosquitoes, F46, were collected in Suffolk County, New York , in 2014. *Cx. quinquefasciatus* mosquitoes, F57, were collected in Chattooga County, Georgia, in 2022. *Cx. pipiens* mosquitoes, F50, were collected in Albany County, New York, in 2022. *An. quadrimaculatus* mosquitoes (BEI Resources, https://www.beiresources.org) were originally collected in Orlando, Florida, in 1930. At 14 days postinfection, we anesthetized mosquitoes and assessed competence using 26–50 mosquitoes/population. We removed legs and placed the proboscises in a capillary tube containing 25% sucrose. After 30 minutes, we collected secretions and bodies and stored all samples −70°C. We thawed bodies and legs, homogenized for 30 seconds with a stainless-steel bead (Daisy, https://www.daisy.com) using a Retsch Mixer Mill (https://www.retsch.com), and centrifuged for 2 min at 10,000 × *g*. We tested samples by plaque assay on Vero cells to determine infectivity (positive body), dissemination (positive legs), and transmission potential (positive saliva).

Our results suggest a general lack of competence for all species with both viral strains (Table). Infection rates for *Ae. albopictus* mosquitoes were 2.0% for TRVL9760 and 0.0% for OROV 240023, for *An. quadrimaculatus* mosquitoes 4.0% for TRVL9760 and 0.0% for OROV 240023, for *Cx. quinquefasciatus* mosquitoes 2.0% for TRVL9760 and 0.0% for OROV 240023, and for *Cx. pipiens* mosquitoes 0.0% for OROV TRVL9760 and 2.0% for OROV 240023. Although strain-dependent, those data represent a single positive mosquito for each species. Of the 3 TRVL9760-positive mosquitoes, 2 had disseminated infections, and no transmission was detected. Our results provide evidence of infectivity of OROV in *Anopheles* mosquitoes, and given the small sample sizes, modest transmission potential is possible for this species. A more comprehensive assessment of competence could be achieved with larger sample sizes.

OROV 240023 infection was only identified for *Cx. pipiens* mosquitoes, the only mosquito with positive saliva, indicating OROV transmission. McGregor et al. (*9*) demonstrated higher OROV TRVL9760 infection levels at the same dose in *Cx. quinquefasciatus* mosquitoes but similarly limited transmission potential. In addition, de Mendonça et al. (*10*) used a

Table. Vector competence of US mosquito species for Oropouche virus

Strain	Input, $\log_{10}$ PFU/mL	Species	% Infected (no. tested)	% Disseminated (no. tested)	% Transmitted (no. tested)
OROV TRVL9760	6.5	*Aedes albopictus*	2 (50)	100 (1)	0 (1)
		Anopheles quadrimaculatus	4 (26)	100 (1)	0 (1)
		Culex. quinquefasciatus	2 (50)	0 (1)	0 (1)
		Cx. pipiens	0 (50)	0	0
OROV 240023	6.5	*Ae. albopictus*	0 (50)	0	0
		An. quadrimaculatus	0 (31)	0	0
		Cx. quinquefasciatus	0 (46)	0	0
		Cx. pipiens	2 (50)	100 (1)	100 (1)

historic sloth isolate, OROV BeAn19991, and found a lack of infectivity in *Cx. quinquefasciatus* mosquitoes. Our data suggest that the currently circulating genotype remains limited in its capacity to infect that species. These results demonstrate some strain-specific variability in competence but suggest the likelihood of these species maintaining OROV in North America remains low.

Acknowledgments

We thank the Wadsworth Center tissue and media core for supplying cells and media for these studies and Ilia Rochlin for kindly providing *Aedes albopictus* eggs. We additionally thank the Centers for Disease Control and Prevention for providing the OROV TRVL9760 isolate.

About the Author

Ms. Payne is a research scientist and laboratory manager in the New York State Department of Health Arbovirus Laboratory at the Wadsworth Center. Her primary research interests are mosquito-borne viruses and vector biology.

References

1. Wesselmann KM, Postigo-Hidalgo I, Pezzi L, de Oliveira-Filho EF, Fischer C, de Lamballerie X, et al. Emergence of Oropouche fever in Latin America: a narrative review. Lancet Infect Dis. 2024;24:e439–52. https://doi.org/10.1016/S1473-3099(23)00740-5
2. Sakkas H, Bozidis P, Franks A, Papadopoulou C. Oropouche fever: a review. Viruses. 2018;10:175. https://doi.org/10.3390/v10040175
3. Centers for Disease Control and Prevention. 2024 Oropouche outbreak. 2024 Dec 31 [cited 2025 Jan 2]. https://www.cdc.gov/oropouche/outbreaks/2024/index.html
4. Pareek A, Singhal R, Pareek A, Chuturgoon A, Apostolopoulos V. Rising threat of Oropouche virus transmission from mother to child: an urgent call for action. Travel Med Infect Dis. 2024;62:102776. https://doi.org/10.1016/j.tmaid.2024.102776
5. Nielsen-Saines K, Brasil P. Oropouche virus and potential birth defects. Lancet Infect Dis. 2024 Oct 15 [Epub ahead of print].
6. Pinheiro FP, Travassos da Rosa AP, Gomes ML, LeDuc JW, Hoch AL. Transmission of Oropouche virus from man to hamster by the midge *Culicoides paraensis*. Science. 1982;215:1251–3. https://doi.org/10.1126/science.6800036
7. Cardoso BF, Serra OP, Heinen LB, Zuchi N, Souza VC, Naveca FG, et al. Detection of Oropouche virus segment S in patients and in *Culex quinquefasciatus* in the state of Mato Grosso, Brazil. Mem Inst Oswaldo Cruz. 2015;110:745–54. https://doi.org/10.1590/0074-02760150123
8. Hoch AL, Pinheiro FP, Roberts DR, Gomes ML. Laboratory transmission of Oropouche virus by *Culex quinquefasciatus* Say. Bull Pan Am Health Organ. 1987;21:55–61.
9. McGregor BL, Connelly CR, Kenney JL. Infection, dissemination, and transmission potential of North American *Culex quinquefasciatus*, *Culex tarsalis*, and *Culicoides sonorensis* for Oropouche virus. Viruses. 2021;13:226. https://doi.org/10.3390/v13020226
10. de Mendonça SF, Rocha MN, Ferreira FV, Leite THJF, Amadou SCG, Sucupira PHF, et al. Evaluation of *Aedes aegypti*, *Aedes albopictus*, and *Culex quinquefasciatus* mosquitoes competence to *Oropouche virus* infection. Viruses. 2021;13:755. https://doi.org/10.3390/v13050755

Address for correspondence: Alexander T. Ciota, Wadsworth Center, New York State Department of Health, Arbovirus Laboratory, 5668 State Farm Rd, Slingerlands, NY 12159, USA; email: alexander.ciota@health.ny.gov

Urban Coatis (*Nasua nasua*) Exposure to *Alphainfluenzavirus influenzae*

Bruna Hermine de Campos, Jéssica de Souza Joaquim, Nadja Simbera Hemetrio, Lara Ribeiro de Almeida, Paula Cristina Senra Lima, Grazielle Cossenzo Florentino Galinari, Marcelo Coelho Lopes, Camila Issa Amaral, Gustavo Canesso Bicalho, Beatriz Senra Santos, Nágila Rocha Aguilar, Maria Isabel Maldonado Coelho Guedes, Danielle Ferreira de Magalhães Soares, Pedro Lúcio Lithg Pereira, Cíntia Aparecida de Jesus Pereira, Walter dos Santos Lima, Camila Stefanie Fonseca de Oliveira, Roselene Ecco, Erica Azevedo Costa, Zélia Inês Portela Lobato, Marcelo Pires Nogueira de Carvalho

Author affiliations: Universidade Federal de Minas Gerais, Belo Horizonte, Brazil (B.H. de Campos, J.S. Joaquim, L.R. de Almeida, G.C.F Galinari, M.C. Lopes, C.I. Amaral, G.C. Bicalho, B.S. Santos, N.R. Aguilar, M.I.M.C. Guedes, D.F.M. Soares, P.L.L. Pereira, C.A.J. Pereira, W.S. Lima, C.S.F. de Oliveira, R. Ecco, E.A. Costa, Z.I.P. Lobato, M.P.N. de Carvalho); Fundação de Parques Municipais e Zoobotânica de Belo Horizonte, Minas Gerais, Brazil (N.S. Hemetrio, P.C.S. Lima)

DOI: https://doi.org/10.3201/eid3103.231640

We detected neutralizing antibodies, viral RNA, and sialic acid receptors for *Alphainfluenzavirus influenzae* in urban coatis (*Nasua nasua*) in Brazil, suggesting exposure and susceptibility. We used hemagglutination inhibition, reverse transcription quantitative PCR, and histochemistry for detection. Increased epidemiologic wildlife surveillance would improve influenza A emergency event response.

Alphainfluenzavirus influenzae, also known as as influenza A virus (IAV), continues to spread globally, causing economic loss and threatening public health (*1*). IAVs can infect a range of species, leading to the emergence of new subtypes with altered host tropism or virulence (*2*). Highly pathogenic avian influenza viruses (HPAIVs) have been detected in wild animals around the world (*3*). Brazil reported its first case of HPAIV in 2023, in a *Thalasseus acuflavidus* bird (*4*).

The expression of an appropriate host cell receptor that viral haemagglutinin (HA) can bind to is the key determinant of IAV ability to infect a species (*5*). Avian influenza viruses preferentially bind to sialic acid (SA) receptors linked to galactose by α-2,3 linkage, whereas human and classical swine influenza show preference for α-2,6 linkage. Mammal hosts that co-express both SA α-2,3 and α-2,6 receptors, primarily in the upper respiratory tract, potentially play a major role in the evolution and transmission of IAVs. Susceptibility to infection by IAVs of different origins (human, avian, or swine) can support rearrangement between IAVs and contribute to the emergence of genetically diverse viruses (*6*).

Coatis (*Nasua nasua*) are carnivores of the Procyonidae family (*7*). Coatis are susceptible to different virus infections, such as SARS-COV-2, and can be sentinels for animal, human, and environmental health (*8*). We investigated coatis IAV exposure and susceptibility from an urban park (Appendix Figure 1, https://wwwnc.cdc.gov/EID/article/31/3/23-1640-App1.pdf), which comprises an intersecting area of urban and wild environments, in Belo Horizonte, Brazil.

Table. Urban coatis (*Nasua nasua*) samples positive for *Alphainfluenzavirus influenzae* viral RNA, demonstrating exposure and susceptibility, Brazil

Coati identification no.	Collection date	Sex	Cycle threshold
343	2021 Jan 18	F	36.7
344	2021 Jan 18	M	37.3
518	2021 Jan 18	M	38.3
520	2021 Jan 18	M	36.6
347	2021 Jun 28	F	37.776
541	2021 Jun 30	F	34.266
531	2021 Jul 9	M	37.436
354	2021 Aug 13	M	38.880
355	2021 Aug 13	F	38.824
356	2021 Aug 13	M	35.462

During 2013, 2014, 2018, 2019, and 2021, we collected samples from wild coatis. We captured coatis respecting Biosafety standards and using personal protective equipment. Ethical approvals were obtained for research development (Appendix). We placed tomahawk (Zootech, https://zootechonline.com.br/armadilhas) traps at strategic points and checked them daily. We physically examined the captured coatis and then gave each an intramuscular injection of Zoletil 100 (Virbac, https://us.virbac.com) at a dose of 7–10 mg/kg. We collected blood samples from the coatis and identified each with a subcutaneous microchip before releasing them.

We collected whole blood samples at a limit of 1% of bodyweight by jugular venipuncture from 145 coatis (Appendix Table). For 63 coatis captured in 2021, we also collected oropharyngeal swab samples and packed them in 3 mL of buffered saline solution with penicillin (200 U/mL) and streptomycin (200 mg/mL). We stored serum samples at −20°C and swabs at −80°C. We used dead coatis (n = 3) found in the park for tissue sample collection. We fixed tissues in 10% buffered formalin, embedded them in paraffin, and sectioned the tissue samples at 4 μm thickness.

We conducted hemagglutination inhibition (HI) assays to detect neutralizing antibodies to IAV (Appendix). We identified antibodies in 92.4% (n = 134) of the samples. Influenza A(H1N1)pdm09 subtype was detected in coatis' samples from each year of the study period. H3N2 virus was detected in samples from 2018, 2019, and 2021, and seasonal human H1N1 virus was detected in 2021 (Appendix Figure 2). None of the captured coatis demonstrated any clinical manifestations of illness.

We performed RNA extraction from swabs by using QIAamp MinElute Virus Spin Kit (QIAGEN, https://www.qiagen.com), and quantitative reverse transcription PCR for universal and subtype detection of IAVs (Appendix). We detected viral RNA in 15.87% of samples from 2021 (Table 1). We detected subtype H3N2 genetic material from coati 347.

To detect α-2,6 and α-2,3 SA receptors, we selected nasal conchae, trachea, and lung tissue for lectin histochemistry technique by using *Maackia amurensis* and *Sambucus nigra* plant lectin (Appendix). We detected positive labels for those receptors in all analyzed tissues. The receptor marking was visualized as a strong brown color at the apical membrane of the nasal ephitelium and ciliated cells of the respiratory

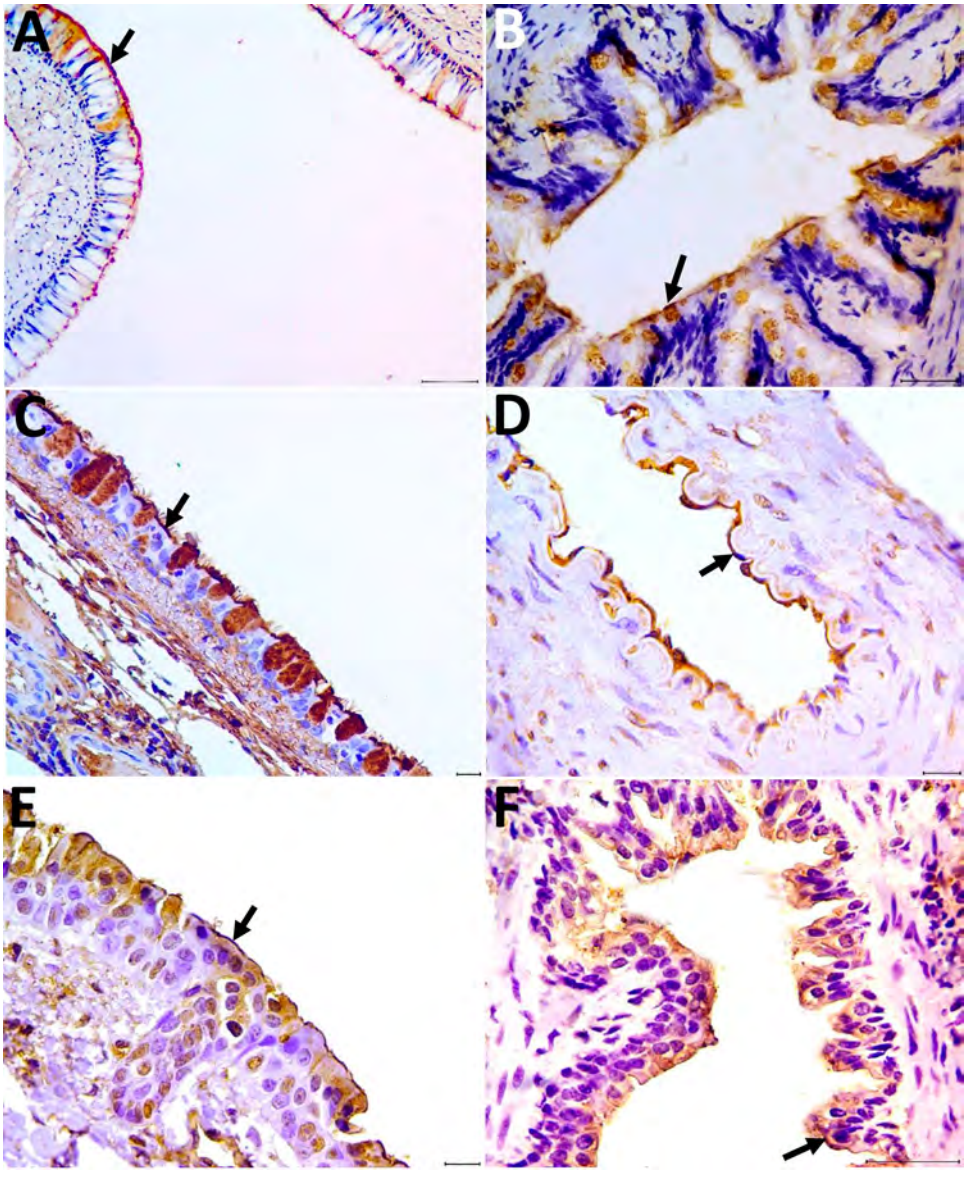

Figure. Detection of α-2,3 and α-2,6 receptors in tissues from the respiratory system of coatis (*Nasua nasua*), Brazil. A–C) Arrows indicate labeling of the α-2,3 receptor in the ciliated epithelium for the lectin *Maackia amurensis* II of the nasal concha (A), lung (bronchiole) tissue (B), and trachea (C). Scale bars = 100 μm in panel A, 50 μm in panel B, and 20 μm in panel C. D–F) Arrows indicate labeling of the α-2,6 receptor in the endothelium for *Sambucus nigra* lectin in the arteriole (D), rostral concha (E), and lung (bronchiole) (F). Scale bars = 20 μm in panels D and E, 50 μm in panel F. Tissue was counterstained with hematoxylin and revealed with diaminobenzidine chromogen.

tract (nasal turbinate, trachea, bronchus and bronchiole), including globet cells, pneumocytes, and pulmonary endothelial cells (Figure). The 2 lectins labeled both receptors with diffuse distribution in the respiratory tissues.

The detection of antibodies against IAV subtypes suggests natural exposure of coatis to IAVs. We were unable to confirm the mode of IAV transmission to coatis; nevertheless, we found evidence of close contact of coatis to contaminated human waste and food, indicating the possibility of human-to-animal transmission.

The seasonal human H1N1 virus subtype, which circulated in Brazil during 2001–2003, was detected in swab samples, suggesting the possible dissemination, maintenance, and transmission capacity of coatis. Those results agree with previously published reports that detected the same viral subtype in wild carnivores during 2009–2011 (*9*). In 2021 and 2022, there were reports of outbreaks in Brazil triggered by the emergence of a new influenza A(H3N2) strain, named Darwin, occurring concurrently with SARS-CoV-2 as co-infection (*10*). The presence of α-2,6 and α-2,3 SA receptors highlight the possibility of co-infection of coatis with different viral lineages, giving the animals a potential role in IAV spillover events. Because of urban coatis' habitats, the absence of signs of clinical illness, and the recent introduction of HPAIV into Brazil, a heightened epidemiologic wildlife surveillance strategy would improve the ability to respond to IAV emergency health events.

Acknowledgments

We thank the ECOS Conservation Medicine Research Group staff for their contributions to assembling the fieldwork team and conducting laboratory analyses. We thank our colleagues and the staff at the Universidade Federal de Minas Gerais Veterinary School for their technical support, sample sharing, and statistical analysis work. We thank the Belo Horizonte Municipal Parks and Zoobotany Foundation for allowing the field work. We thank Augusto Gomes for the coatis photographs.

Technical support was available from the Histopathology Laboratory of the Multidisciplinary Research Unit (MULTILAB), Department of Veterinary Clinic and Surgery, Universidade Federal de Minas Gerais, Belo Horizonte, Brazil.

Financial support for this study was provided by Fundação de Amparo à Pesquisa do estado de Minas Gerais (grant no. APQ-02779-21) and Coordenação de Aperfeiçoamento de Pessoal de Nível Superior.

Author contributions: Original draft, review and editing, data analysis: B.H.D.C., M.P.N.D.C., and R.E.; sample collection: B.H.D.C., J.S.J., M.P.N.D.C., L.R.D.A., N.S.H., and P.C.S.L.; serologic assays: B.H.D.C., G.C.F.G., E.A.C., and Z.I.P.L.; molecular testing: B.H.D.C., B.S.S., N.R.A., D.F.M.S., M.I.M.C.G., E.A.C., and Z.I.P.L.; lectin immunohistochemistry: B.H.D.C., J.S.J., M.C.L., C.I.A., and R.E.; statistical analysis: G.C.B. and C.S.F.D.O.; resources: E.A.C., Z.I.P.L., M.P.N.D.C., and R.E.; study supervision, manuscript writing, review, and editing: D.F.M.S., P.L.L.P., C.S.F.D.O., C.A.J.P., W.S.L., R.E., E.A.C., Z.I.P.L., and M.P.N.D.C. All authors have read and approved the final version of the manuscript.

About the Author:

Dr. de Campos is a veterinarian and PhD student in animal science at Universidade Federal of Minas Gerais. Her primary research interests include virology, viral zoonoses, epidemiology, and wildlife disease.

References

1. Jeong O-M, Kim M-C, Kim M-J, Kang H-M, Kim H-R, Kim Y-J, et al. Experimental infection of chickens, ducks and quails with the highly pathogenic H5N1 avian influenza virus. J Vet Sci. 2009;10:53–60. https://doi.org/10.4142/jvs.2009.10.1.53
2. Chothe SK, Bhushan G, Nissly RH, Yeh YT, Brown J, Turner G, et al. Avian and human influenza virus compatible sialic acid receptors in little brown bats. Sci Rep. 2017;7:660. https://doi.org/10.1038/s41598-017-00793-6
3. Gilbertson B, Subbarao K. Mammalian infections with highly pathogenic avian influenza viruses renew concerns of pandemic potential. J Exp Med. 2023;220:e20230447. https://doi.org/10.1084/jem.20230447
4. Reischak D, Rivetti AV Jr, Otaka JNP, Domingues CS, Freitas TL, Cardoso FG, et al. First report and genetic characterization of the highly pathogenic avian influenza A(H5N1) virus in Cabot's tern (*Thalasseus acuflavidus*), Brazil. Vet Anim Sci. 2023;22:100319. https://doi.org/10.1016/j.vas.2023.100319
5. Lakadamyali M, Rust MJ, Zhuang X. Endocytosis of influenza viruses. Microbes Infect. 2004;6:929–36. https://doi.org/10.1016/j.micinf.2004.05.002
6. Nelli RK, Kuchipudi SV, White GA, Perez BB, Dunham SP, Chang KC. Comparative distribution of human and avian type sialic acid influenza receptors in the pig. BMC Vet Res. 2010;6:4. https://doi.org/10.1186/1746-6148-6-4
7. Whiteside DP. Nutrition and behavior of coatis and raccoons. Vet Clin North Am Exot Anim Pract. 2009;12:187–95, xiii. https://doi.org/10.1016/j.cvex.2009.01.002
8. Stoffella-Dutra AG, de Campos BH, Bastos E Silva PH, Dias KL, da Silva Domingos IJ, Hemetrio NS, et al. SARS-CoV-2 spillback to wild coatis in sylvatic-urban hotspot, Brazil. Emerg Infect Dis. 2023;29:664–7. https://doi.org/10.3201/eid2903.221339
9. Bakken MA, Nashold SW, Hall JS. Serosurvey of coyotes (*Canis latrans*), foxes (*Vulpes vulpes*, *Urocyon cinereoargenteus*), and raccoons (*Procyon lotor*) for exposure to influenza A viruses in the USA. J Wildl Dis. 2020;56:953–5. https://doi.org/10.7589/2019-10-244
10 Santos CAD, Bezerra GVB, Marinho ARRAA, Sena LOC, Menezes VJ, Teixeira DCP, et al. SARS-CoV-2/influenza A (H3N2) virus coinfection: epidemiological surveillance in Northeast Brazil. Rev Soc Bras Med Trop. 2022;55:e0132.

Address for correspondence: Marcelo Pires Nogueira de Carvalho, Universidade Federal de Minas Gerais, Campus Pampulha da, Av. Presidente Antônio Carlos, 6627 São Luiz, Belo Horizonte, Minas Gerais 31270-901, Brazil; email: marcelopnc@yahoo.com.br

Identification of 2 Novel Species, *Mycobacterium novusgordonae* and *M. shingordonae*

Kazuki Hashimoto,[1] Yuko Abe,[1] Kiyoharu Fukushima, Yuki Matsumoto, Haruko Saito, Yuri Akamine, Takayuki Niitsu, June Yamauchi, Tadayoshi Nitta, Michio Tanaka, Takuro Nii, Takanori Matsuki, Daisuke Motooka, Kazuyuki Tsujino, Keisuke Miki, Kozo Morimoto, Atsushi Kumanogoh, Shizuo Akira, Shota Nakamura, Hiroshi Kida

Author affiliations: Osaka University, Osaka, Japan

[1]These authors contributed equally to this article.

(K. Hashimoto, Y. Abe, K. Fukushima, Y. Matsumoto, Y. Akamine, T. Niitsu, M. Tanaka, D. Motooka, A. Kumanogoh, S. Akira, S. Nakamura); Toneyama Medical Center, Osaka (K. Fukushima, H. Saito, J. Yamauchi, T. Nitta, T. Nii, T. Matsuki, K. Tsujino, K. Miki, H. Kida); Fukujuji Hospital, Tokyo, Japan (K. Morimoto)

DOI: https://doi.org/10.3201/eid3103.240174

We identified 2 novel species, *Mycobacterium novusgordonae* and *M. shingordonae*, from sputum specimens of pulmonary disease patients in Japan. Genetic and biochemical analyses revealed a close relationship with *M. paragordonae*. One *M. shingordonae* case-patient experienced severe progressive infection, highlighting the variation in pathogenicity of the *M. gordonae* clade species.

We report identification of *Mycobacterium novusgordonae* and *M. shingordonae*, 2 novel species in the *M. gordonae* clade, in sputum specimens from 5 patients with chronic respiratory disease in Japan. Written informed consent was obtained from all the participants at enrollment. The ethics board of the National Hospital Organization, Osaka Toneyama Medical Center approved the whole-genome sequencing (WGS) analysis of *Mycobacterium* culture isolates (TNH-R-2020020).

During 2021–2024, staff of Toneyama Medical Center (Osaka, Japan), detected novel mycobacteria strains from 3 patients receiving treatment or follow-up for nontuberculous mycobacterial pulmonary disease caused by other species, 1 patient with a clinical diagnosis of nontuberculous mycobacterial pulmonary disease, and 1 immunocompetent patient with progressive pulmonary infectious disease. Here, we discuss the course of illness and testing for the immunocompetent patient (strain MS1); the other patients are described in the Appendix (https://wwwnc.cdc.gov/EID/article/31/3/24-0174-App1.pdf).

A 68-year-old woman with a history of chronic gastritis and allergic rhinitis sought care for a chronic productive cough. Chest computed tomography revealed centrilobular nodules and bronchiectasis in the middle and bilateral lower lobes (Appendix Figure 2). Acid-fast bacilli were detected in 61 sputum culture tests. *M. gordonae* was identified 3 times with DNA–DNA hybridization assays (Kyokuto Pharmaceutical Industrial, https://www.kyokutoseiyaku.co.jp), 13 times using AccuProbe (Gen-Probe Inc., https://www.hologic.com), and 1 time using matrix-assisted laser desorption/ionization time-of-flight (MALDI-TOF) mass spectrometry (Bruker Daltonics, https://www.bruker.com). No other pathogenic bacteria were detected.

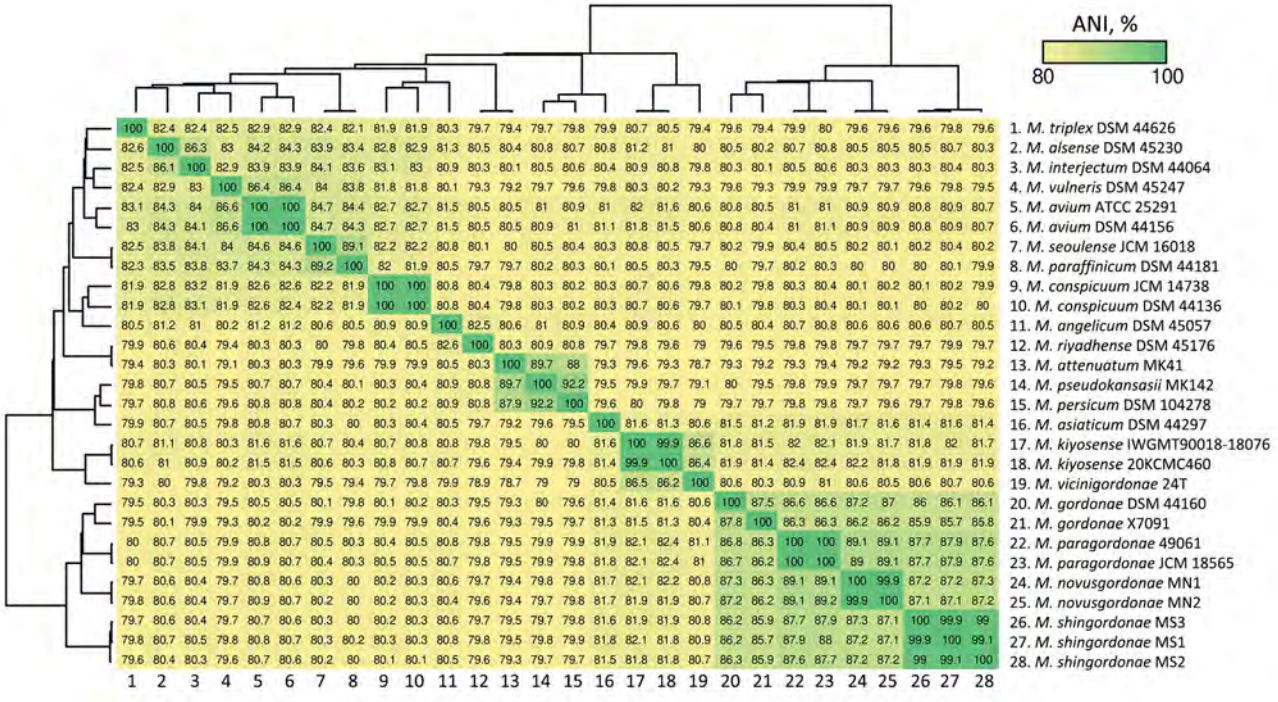

Figure. Heatmap showing average nucleotide identity classification of 2 novel mycobacteria species, *Mycobacterium novusgordonae* and *M. shingordonae*, among other *Mycobacteria* species. Heatmap drawn using FastANI (https://github.com/ParBLiSS/FastANI/releases). Species labels in the heatmap were sorted in the same manner as those in the whole-genome sequence-based phylogenetic tree. Numbers at bottom match numbers at right; 24–28 indicate the strains from this study.

Table. Biochemical assay results for 4 strains of *Mycobacterium* spp. in study identifying 2 novel species*

Characteristic	*M. novusgordonae* (MN1)	*M. shingordonae* (MS1)	*M. paragordonae* (CIP112418)	*M. gordonae* (ATCC 14470)
Growth at 37°C	+	+	–	+
Growth detectable after 7 d	+	+	+w	+
Catalase	+	+	+	+
Urease	–	–	–	–
Nitrate reduction	+	+	+	–
3-d arylsulfatase	+w	+	+	+
Telluric acid reduction	+	+	+	+
Colony color	Yellow	Yellow	Yellow	Orange
Pigmentation	Scoto	Scoto	Scoto	Scoto
Colony morphology	Smooth	Smooth	Smooth	Smooth

*Schoto, scotochromogenic; w, weak; +, positive; −, negative.

The patient initially started clarithromycin monotherapy; her condition progressively worsened. When she was 75 years of age, a left pneumothorax developed that required drainage. At 77 years of age, her providers switched her treatment to erythromycin from clarithromycin because of gastrointestinal intolerance. Despite worsening respiratory symptoms (productive cough, hemoptysis, and dyspnea) and radiologic findings (Appendix Figure 2), she declined the recommended multidrug therapy because of concerns about adverse effects.

We performed MALDI-TOF mass spectrometry, culture of sputum samples, whole-genome sequencing (WGS), and phylogenetic analysis on all 5 identified strains. MALDI-TOF mass spectrometry identified 2 of the strains as *M. gordonae* and the other 3 strains as unidentified. We processed sputum samples in accordance with the guidance in Clinical Microbiology Procedures Handbook, 5th edition (*1*). After processing, we cultured sputum samples on Ogawa medium at 36°C or in mycobacteria growth indicator tube (MGIT) media at 37°C using a BACTEC MGIT 960 system (BD, https://www.bd.com) (*2*). We subsequently pure-cultured 5 strains on Ogawa medium, analyzed them by WGS, and classified them into 2 groups, MN1/MN2 and MS1/MS2/MS3. Genetic similarity was 99.9%–100% between MN1 and MN2 and 99.1%–100% among MS1, MS2, and MS3. All 5 strains showed an average nucleotide identity (ANI) <95% with the closest known species, *M. paragordonae* (Figure). Phylogenetic analysis showed that the 5 strains and *M. paragordonae* belong to different lineages from *M. gordonae*; however, their mutual relationships are unclear (Appendix Table 1, Figure 1).

WGS confirmed that the MS1 isolates collected at 3 different time points and the MS2 isolates collected at 2 different time points belong to the same species (ANI of MS1, 99.1%–100.0%; of MS2, 100.0%). The new species to which MN1 and MN2 belong was named *M. novusgordonae*, strain type MN1 (TY813, RIMD 1378001, and CIP 11419^T), and the other new species to which MS1, MS2, and MS3 belong was named *M. shingordonae* strain type MS1 (TY814; RIMD 1379001; CIP 11420^T) (Appendix). Novus in Latin and shin in Japanese both mean new.

M. gordonae is an environmental acid-fast bacterium traditionally considered to have low virulence and pathogenicity; it primarily causes opportunistic infections in immunocompromised persons (*3*). However, recent studies have identified diverse novel species within this clade, revealing distinct patterns of pathogenicity (*4*–*7*).

We determined MICs on the basis of recommendations of the Clinical and Laboratory Standards Institute (*8*). Of note, the MN1–2 and MS2–3 strains exhibit low MICs for clarithromycin, ethambutol, and rifampin, whereas the MS1 strain showed high MIC for clarithromycin, in parallel with the detection of an A2058G mutation in the *rrl* gene. We performed biochemical tests on 4 strains: MN1 (*M. novusgordonae* type strain), MS1 (*M. shingordonae* type strain), *M. paragordonae* (RIMD 1369002, CIP 112418), and *M. gordonae* (ATCC 14470^T) (Table; Appendix Table 3). The MN1 and MS1 strains were nearly identical; they had similar characteristics as *M. paragordonae* but were distinct in their ability to grow at 37°C. MN1 and MS1 isolates and *M. paragordonae* were positive for nitrate reduction. All strains showed positive reactions for catalase, 3-day arylsulfatase, and telluric acid reduction tests.

In conclusion, we identified 2 novel mycobacteria species within the *M. gordonae* clade that are more closely related to *M. paragordonae* than to *M. gordonae*. One patient experienced a progressive infection, revealing the pathogenicity of this novel strain and diversity within the *M. gordonae* clade.

Acknowledgments

We thank the patients for granting permission to publish their information. We thank Lisa Oberding for editing a draft of this manuscript.

Availability of data and materials: The datasets supporting the conclusions of this article are included within the article. Whole-genome sequences were deposited in the National Center for Biotechnology Information RefSeq assembly database: MN1 (TY813), accession no. GCF_030755155.1; MN2, accession no. GCF_046643285.1; MS1 (TY814), accession no. GCF_030755175.1; MS2 (TY815), accession no. GCF_030755135.1; and MS3, accession no. GCF_046643305.1.

This work was supported in part by Japan Agency for Medical Research and Development (grant nos. JP20fk0108129, JP21fk0108129h0702, JP21lm0203007), a GlaxoSmithKline Research grant (grant no.A-32), JSPS KAKENHI (grant nos. JP21K16118, JP21K08194), Takeda Science Foundation, Uehara Memorial Foundation, MSD Life Science Foundation, Japanese Respiratory Society Boehringer Ingelheim Research Grant Program, Foundation of Kinoshita Memorial Enterprise, Senri Life Science Foundation, Inamori Foundation, and the Japan Intractable Diseases (Nanbyo) Research Foundation (grant no. 2020B02). The funders had no role in the study design, collection, analyses, or interpretation of data, writing of the manuscript, or decision to publish the results.

Author contributions: K.F. designed the study; H.S., J.Y., and T.N. performed mycobacterial culture and analysis of culture isolates; K.F., K.H., and Y.A. performed clinical and laboratory data extraction and analysis; Y.A., T.N., T.M., K.T., and K.M. assisted with data extraction and analysis; Y.M., D.M., and S.N. performed multilocus typing analysis and whole-genome analysis; M.T. analyzed biochemical profiles of the strain; K.H., Y.A., K.F., and S.N. wrote the manuscript; H.K. supervised the study. All authors read and approved the manuscript.

Abut the Author

Dr. Hashimoto is a clinical fellow in respiratory medicine in the Respiratory Medicine department of Osaka University Medical Hospital, Osaka, Japan. His primary research interest is respiratory infections.

References

1. Leber AL, Burnham C-AD. Mycobacteriology and antimycobacterial susceptibility testing. In: Clinical microbiology procedures handbook, 5th edition. Wayne (PA): Clinical and Laboratory Standards Institute; 2023.
2. Lee JJ, Suo J, Lin CB, Wang JD, Lin TY, Tsai YC. Comparative evaluation of the BACTEC MGIT 960 system with solid medium for isolation of mycobacteria. Int J Tuberc Lung Dis. 2003;7:569–74.
3. Eckburg PB, Buadu EO, Stark P, Sarinas PS, Chitkara RK, Kuschner WG. Clinical and chest radiographic findings among persons with sputum culture positive for *Mycobacterium gordonae:* a review of 19 cases. Chest. 2000;117:96–102. https://doi.org/10.1378/chest.117.1.96
4. Kim BJ, Hong SH, Kook YH, Kim BJ. *Mycobacterium paragordonae* sp. nov., a slowly growing, scotochromogenic species closely related to *Mycobacterium gordonae*. Int J Syst Evol Microbiol. 2014;64:39–45. https://doi.org/10.1099/ijs.0.051540-0
5. Mei YM, Zhang Q, Zhang WY, Jiang HQ, Shi Y, Xiong JS, et al. Isolation of novel *Mycobacterium* species from skin infection in an immunocompromised person. Emerg Infect Dis. 2021;27:2944–7. https://doi.org/10.3201//eid2711.210426
6. Armstrong DT, Eisemann E, Parrish N. A brief update on mycobacterial taxonomy, 2020 to 2022. J Clin Microbiol. 2023;61:e0033122. https://doi.org/10.1128/jcm.00331-22
7. Liu G, Yu X, Luo J, Hu Y, Dong L, Jiang G, et al. *Mycobacterium vicinigordonae* sp. nov., a slow-growing scotochromogenic species isolated from sputum. Int J Syst Evol Microbiol. 2021;71. https://doi.org/10.1099/ijsem.0.004796
8. Woods GL, Brown-Elliott BA, Conville PS, Desmond EP, Hall GS, Lin G, et al. Susceptibility testing of Mycobacteria, Nocardiae, and other aerobic Actinomycetes. Wayne (PA): Clinical and Laboratory Standards Institute; 2011 Mar. Report no.: M24–A2.

Address for correspondence: Kiyoharu Fukushima, Department of Respiratory Medicine and Clinical Immunology, Osaka University Graduate School of Medicine, 2-2 Yamadaoka, Suita, Osaka, Japan; email: fukushima@imed3.med.osaka-u.ac.jp

Multidrug-Resistant *Mycobacterium tuberculosis* in a Community Hospital, Luanda, Angola

Ngiambudulu M. Francisco, Alberto Gaviraghi, Francesca Alladio, Ralph Huits, Bruna Carnielli, Elena Salvador, Giacomo Stroffolini, Niccolò Ronzoni, Paolo Cattaneo, Concetta Castilletti, Alberto Kalume, Cristina Mazzi, Alberto Matteelli, Dora Buonfrate, Federico G. Gobbi

Author affiliations: Instituto Nacional de Investigação em Sáude, Luanda, Angola (N.M. Francisco); IRCCS Ospedale Sacro Cuore Don Calabria, Negrar, Italy (A. Gaviraghi, F. Alladio, E. Salvador, G. Stroffolini, N. Ronzoni, P. Cattaneo, C. Castilletti, C. Mazzi, D. Buonfrate, F.G. Gobbi); IRCCS Sacro Cuore Don Calabria Hospital, Verona, Italy (R. Huits); Presidio Ospedale Santa Maria del Prato, Feltre, Italy (B. Carnielli); Hospital Divina Providencia, Luanda (A. Kalume); University of Brescia and Brescia Spedali Civili General Hospital WHO Collaborating Centre for TB/HIV and TB Elimination, Brescia, Italy (A. Matteelli); University of Brescia, Brescia (F.G. Gobbi)

DOI: https://doi.org/10.3201/eid3103.241831

In a longitudinal study in a first-level hospital in Luanda, Angola, we found rifampin-resistant and multidrug-resistant tuberculosis (TB) in 38 (8%, 95% CI 5.7–10.8) of 474 patients with no previous history of TB. Of note, 2 patients (0.4%, 95% CI 0.1–1.5) demonstrated pre–extensively drug-resistant TB.

Tuberculosis (TB) is one of the leading causes of death worldwide, causing an estimated 1.25 million deaths in 2023 (95% uncertainty interval [UI] 1.13–1.37 million) (*1*,*2*). Drug resistance is a major threat to the effective treatment of TB; rifampin-resistant (RR) and multidrug-resistant (MDR; resistance to both rifampin and isoniazid) TB caused an estimated 150,000 (95% UI 94,000–210,000) deaths in 2023 (*2*). Even more worrisome, is the emergence of pre–extensively drug-resistant (pre-XDR; resistance to rifampin and any fluoroquinolone) and extensively drug-resistant (XDR TB; resistance to rifampin, any fluoroquinolone, and ≥1 of bedaquiline or linezolid) strains, which entail the deployment of more expensive and less tolerated drugs (*2*).

Angola is one of 30 countries with high TB burden; ≈22,000 (95% UI 14,000–32,000) deaths were caused by TB in 2023 (*2*,*3*). The incidence rate in the country is 339 cases/100,000 population (95% UI 217–511 cases/100,000 population), which is still far from the 50% incidence rate reduction target set for 2015 (when the rate was 366 cases/100,000 population [95% UI 232–531 cases/100,000 population]) to 2025 by the End TB strategy (*2*,*4*). However, the official data on TB in Angola are based on notifications only; thus, the World Health Organization (WHO) encourages nationwide surveys to collect more reliable data (*2*,*5*).

During November 21, 2023–June 14, 2024, we conducted a study to determine the prevalence of drug-resistant TB at the Hospital Divina Providência, a first-level hospital in the district of Kilamba-Kiaxi, Luanda, Angola. TB cases were diagnosed with GeneXpert Ultra assay (Cepheid, https://www.cepheid.com). Patients who tested positive for RR or MDR TB were referred to the Centro Especializado de Tratamento de Endemias e Pandemias (CETEP) for further management, in accordance with national guidelines. The Ministry of Health Research Ethics Committee, Angola, approved the study (ref. 32/C.E.M.S/2023).

Table 1. Resistance profiles of cases in study of multidrug-resistant tuberculosis, Luanda, Angola

Drug	No. (%) cases showing resistance, N = 474
Rifampin	38 (8.0)
Isoniazid	19 (4.0)
Fluoroquinolones	2 (0.4)
Amikacin	0
Ethionamide	4 (0.8)

We calculated sample size using a conservative percentage of MDR TB and RR-TB of 20%. We calculated a 2-sided 95% CI with a width of 10% for ≥264 TB-infected participants. We measured potential associations between resistance and demographic and clinical variables. We summarized continuous variables by median and interquartile range and categorical variables by number and percentage. We used exact CIs for CI proportions. We calculated odds ratios (ORs) with 95% CIs to identify possible risk factors (age, sex, body mass index, smoking status, alcohol consumption, and HIV infection) associated with *Mycobacterium tuberculosis* infection, RR-MTB, and MDR TB in multivariable logistic regression models. We used R version 4.4.1 (The R Project for Statistical Computing, https://www.r-project.org) for all analyses.

During the study period, 474 cases of TB were confirmed in patients with no history of TB. We detected RR-TB in 38 (8%, 95% CI 5.7%–10.8%) and MDR TB in

Table 2. Multivariable logistic regression models evaluating risk factors for RR and MDR TB, Luanda, Angola*

Characteristic	RR TB		MDR TB	
	OR (95% CI)	p value	OR (95% CI)	p value
Age	1 (0.97–1.03)	0.8	1.02 (0.98–1.06)	0.4
Sex				
M	Referent		Referent	
F	0.59 (0.27–1.25)	0.2	0.39 (0.13–1.07)	0.075
Body mass index	0.96 (0.84–1.08)	0.5	0.91 (0.75–1.07)	0.3
Smoking				
N	Referent		Referent	
Y	0.84 (0.22–2.63)	0.8	0.44 (0.02–2.85)	0.5
Alcohol				
N	Referent		Referent	
Y	1.01 (0.38–2.46)	>0.9	0.85 (0.18–3.01)	0.8
HIV				
Negative	Referent		Referent	
Positive	1.16 (0.26–3.76)	0.8	0.57 (0.03–3.23)	0.6

*MDR, multidrug-resistant; OR, odds ratio; RR, rifampin-resistant; TB, tuberculosis.

19 (4.0%, 95% CI 2.4%–6.2%) of the 474 cases. Of note, 2 cases (0.4%, 95% CI 0.1%–1.5%) showed resistance also to quinolones (pre-XDR TB). No cases of XDR TB were detected (Table 1). None of the considered variables was associated with an increased risk for RR or MDR TB (Table 2).

In our study, the prevalence of RR or MDR TB in patients with no previous history of TB was at least double the estimates reported by WHO for 2023 in Angola (3.29%–3.65%) (*3*). Similarly, a previous study in a rural area (Cubal, in Benguela Province) in 2014 reported prevalence of MDR TB as twice as high as estimates: 8% (95% CI 5.1%–12.3%) (*6*). In 2014, a study carried out at Hospital Divina Providência found 5.6% of RR/MDR TB in 89 patients who were tested for TB (no distinction between new and previously treated cases) (*7*). A retrospective study conducted at the Instituto Nacional de Investigação em Saúde, Angola, found MDR TB in 38 (50%) of 76 patients with previously untreated TB who attended private and public health services in Luanda (*8*). Discrepancies with previous data might be caused by the different settings (rural vs. urban), study designs (prospective vs. retrospective), population (previously infected included or not), and diagnostic methods (GeneXpert vs. BACTEC [BD, https://www.bd.com]).

Because we collected data from a single center, our results should not be generalized as prevalence in Luanda or all of Angola. Despite that limitation, our finding of higher prevalence (8%) of RR/MDR TB in new TB cases compared with the estimates from WHO, together with the existence of pre-XDR TB cases, calls for a nationwide prevalence survey to strengthen epidemiologic monitoring of TB drug resistance in Angola.

Acknowledgments

We thank colleagues from the Instituto Nacional de Investigação em Saúde and from the Hospital Divina Providência for their valuable support and contributions to this project. We also thank all participants who accepted to be enrolled in this study.

This work was partly funded by the Italian Ministry of Health ("Ricerca corrente," Linea 1) to IRCCS Sacro Cuore Don Calabria hospital.

About the Author

Dr. Francisco is a clinical immunologist and head of the department of project management at the National Institute for Health Research in Angola. His current research interests are infectious diseases and molecular and genomic epidemiology.

References

1. World Health Organization. The global health observatory [cited 2024 Nov 25]. https://www.who.int/data/gho
2. World Health Organization. Global tuberculosis report 2024. Geneva: The Organization; 2024 [cited 2024 Nov 25]. https://www.who.int/teams/global-tuberculosis-programme/tb-reports/global-tuberculosis-report-2024
3. World Health Organization. TB country profile 2023. 2024 [cited 2024 Nov 25]. https://www.who.int/teams/global-tuberculosis-programme/tb-reports/global-tuberculosis-report-2023
4. World Health Organization. The End TB strategy [cited 2024 Nov 25]. http://www.who.int/tb/strategy/end-tb
5. Robbiati C, Tosti ME, Mezzabotta G, Dal Maso F, Lulua Sachicola OM, Siene Tienabe P, et al. Improving TB surveillance and patients' quality of care through improved data collection in Angola: development of an electronic medical record system in two health facilities of Luanda. Front Public Health. 2022;10:745928. https://doi.org/10.3389/fpubh.2022.745928
6. Aznar ML, Rando-Segura A, Moreno MM, Soley ME, Igual ES, Bocanegra C, et al. Prevalence and risk factors of multidrug-resistant tuberculosis in Cubal, Angola: a prospective cohort study. Int J J Tuberc Lung Dis. 2019 Jan 1;23:67–72.
7. Perdigão J, Clemente S, Ramos J, Masakidi P, Machado D, Silva C, et al. Genetic diversity, transmission dynamics and drug resistance of *Mycobacterium tuberculosis* in Angola. Sci Rep. 2017;7:42814. https://doi.org/10.1038/srep42814
8. Sebastião CS, Samulengo J, Sacomboio E, Francisco NM, Teixeira C, António S, et al. Epidemiological characteristics and risk factors related to drug-resistant tuberculosis in Luanda, Angola. Am J Trop Med Hyg. 2022;106:779–84. https://doi.org/10.4269/ajtmh.21-0659

Address for correspondence: Federico Gobbi, Department of Infectious, Tropical Diseases and Microbiology, IRCCS Ospedale Sacro Cuore Don Calabria, Via Sempreboni 5, Negrar di Valpolicella, Verona, Italy; email: federico.gobbi@sacrocuore.it

Community-Acquired Pneumonia Caused by Avian *Chlamydia abortus*, the Netherlands

Jairo Gooskens, Einar H.R. van Essen, Margriet E.M. Kraakman, Patrick Wörz, Edou R. Heddema, Stefan A. Boers

Author affiliations: Center of Infectious Diseases (LUCID), Leiden University Medical Center Intensive Care, Leiden (J. Gooskens, M.E.M. Kraakman, P. Wörz, S.A. Boers); Leiden University Medical Center, Leiden, the Netherlands (E.H.R. van Essen); Reference Laboratory for Zoonotic *Chlamydia* Infections, Zuyderland Medical Center, Sittard-Geleen, the Netherlands (E.R. Heddema)

DOI: https://doi.org/10.3201/eid3103.241406

We report avian *Chlamydia abortus* pneumonia in an immunocompetent elderly patient in the Netherlands after environmental exposure to wild aquatic birds, including seabirds. New molecular surveillance studies are needed in wild and captive birds, as well as increased awareness to establish occurrence, clinical manifestations, and geographic distribution of this rare zoonotic disease.

The bacterial genus *Chlamydia* consists of 14 ubiquitous species that affect a wide range of hosts. The species *C. trachomatis*, *C. pneumoniae*, *C. psittaci*, *C. caviae*, *C. felis*, and *C. abortus* are pathogenic to humans after interhuman or zoonotic transmission. Taxonomy studies have identified a new avian *C. abortus* subgroup that is an intermediary related to *C. psittaci* and mammalian *C. abortus* (*1*). In 2024, avian *C. abortus* was associated with human respiratory tract infection and possible human-to-human transmission (*2*). We report a case of severe community-acquired pneumonia caused by an avian *C. abortus* genotype not yet associated with human disease.

A previously healthy 74-year-old man from a residential coastal town in the Netherlands was admitted to the hospital during the winter in 2021 with fever, confusion, and progressive dyspnea of 4-day duration. The patient was a nonsmoker and was vaccinated against seasonal influenza and SARS-CoV-2. He lived a socially withdrawn lifestyle and had no exposure to ruminants or domestic birds, although he regularly fed wild aquatic birds during the winter months. He reported noteworthy exposure to wild birds, including seabirds, which included hand feeding and occasional contact with bird droppings on his clothing.

At hospital admission, a physical examination revealed a body temperature of 39.3°C, pulse of 162 beats/min, blood pressure of 127/77 mm Hg, and respiration rate of 42 breaths/min. Laboratory results showed an unremarkable leukocyte count of 7.49 × 10^9 cells/L (reference range 4.0–10.0 × 10^9 cells/L), acute lymphocytopenia of 0.43 × 10^9 cells/L (reference range 1.0–3.5 × 10^9 cells/L), unremarkable serum creatinine level of 101 μmol/L (reference range 64–104 μmol/L), and elevated C-reactive protein level of 305 mg/L (reference range <5.0 mg/L). Other findings included hyponatremia with a serum sodium level of 129 mmol/L (reference range 136–145 mmol/L) and elevated levels of creatine kinase, 531 U/L (reference range <171 U/L); plasma fibrinogen, 7.3 g/L (reference range 2.1–3.8 g/L); serum lactate dehydrogenase, 397 U/L (reference range <248 U/L); blood urea, 11.7 mmol/L (reference range 2.5–7.5 mmol/L); serum glucose, 10 mmol/L (reference range 3.9–7.7 mmol/L); γ-glutamyl transferase, 71 U/L (reference range <55 U/L); aspartate aminotransferase, of 87 U/L (reference range <35 U/L); and cardiac troponin T, 58 ng/L (reference range <14 ng/L). All other laboratory findings were unremarkable.

The patient was transferred to the intensive care unit because of hypoxemic respiratory failure (SaO_2 <90%) and progressive pulmonary consolidations with pleural effusion (Figure 1) requiring invasive mechanical ventilation. Blood and sputum cultures collected before intravenous cefuroxime and ciprofloxacin empirical therapy showed no microbial pathogens. Bronchial aspirate obtained by fiberoptic bronchoscopy was negative for respiratory viruses,

Figure 1. Chest radiograph of a patient with community-acquired pneumonia caused by avian *Chlamydia abortus*, the Netherlands. The radiograph shows progressive pulmonary consolidations with pleural effusion.

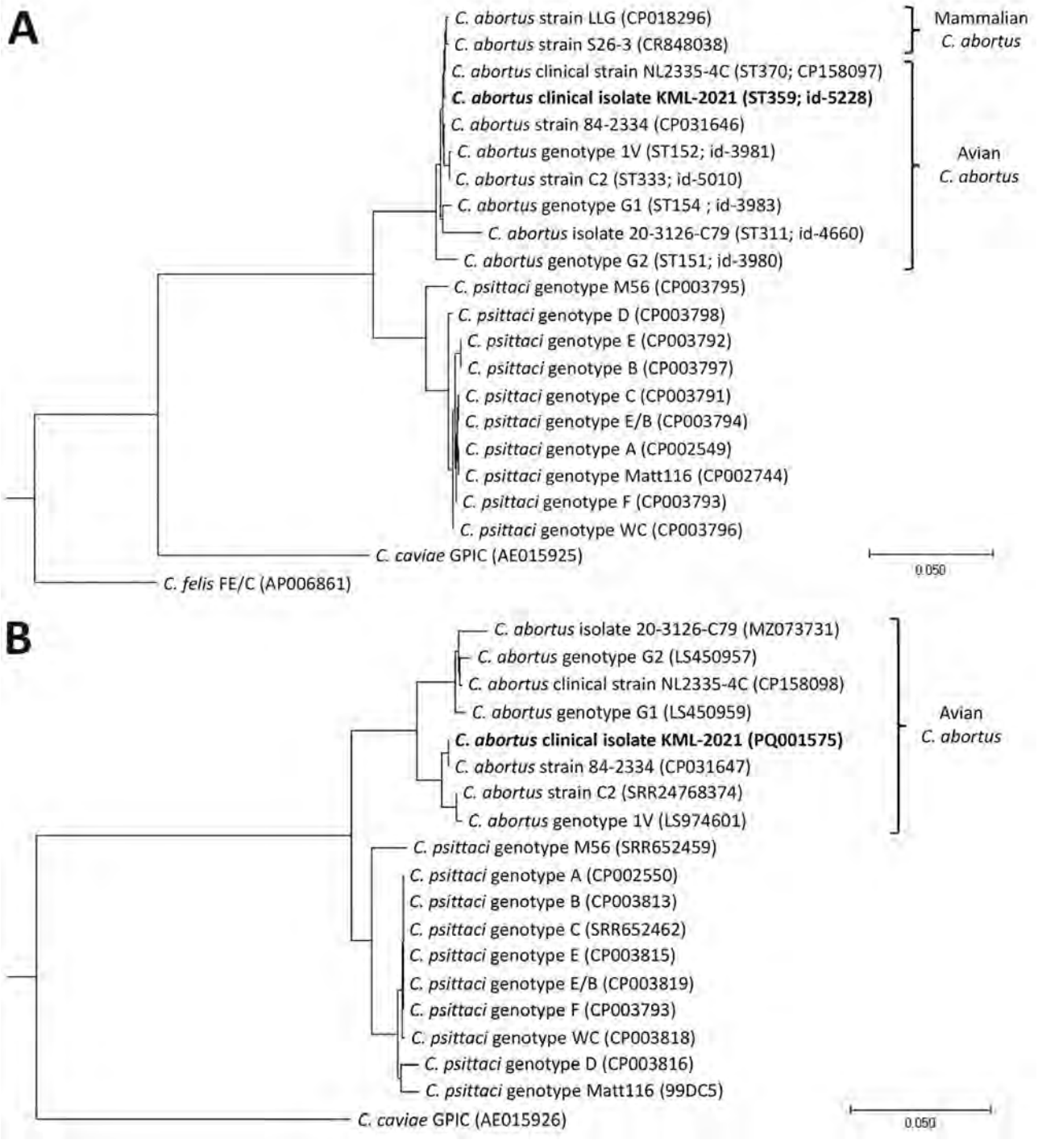

Figure 2. Chlamydial phylogeny of isolates from a patient with community-acquired pneumonia caused by avian *Chlamydia abortus*, the Netherlands, and reference sequences. Chlamydial phylogenetic trees were constructed by using concatenated MLST *gatA, oppA, hflX, gidA, enoA, hemN,* and *fumC* gene sequences (A) or by using plasmid II *xerC* gene sequences (B) of clinical isolate KML-2021 (bold; PubMLST sequence type 359; id-5228, https://pubmlst.org) and reference *Chlamydia* isolates (GenBank accession no. or PubMLST id shown) that were aligned and analyzed in MEGA11 (https://www.megasoftware.net). The phylogenetic tree was constructed by using maximum-likelihood approximation with FastTree v2.1.11 (https://kbase.us/applist/apps/kb_fasttree/run_FastTree/release) and rooted with *C. felis* (FE/C) or *C. caviae* (GPIC reference strains). Scale bar indicates nucleotide substitutions per 100 sites. id, identification; MLST, multilocus sequence typing.

Legionella spp., *Mycoplasma pneumoniae*, and *Chlamydia pneumoniae* by real-time PCR; however, B-CAP real-time PCR (Biolegio, https://www.biolegio.com) detected *Chlamydia* DNA. Quantitative 16S micelle PCR and next-generation sequencing–based (*3*) and metagenomic-based (*4*,*5*) microbiota profiling showed a high relative abundance of *Chlamydia* spp. in the lower respiratory tract; levels were >100 million 16S rRNA gene copies per milliliter of bronchial aspirate (Appendix Figure 1, https://wwwnc.cdc.gov/EID/article/31/3/24-1406-App1.pdf). Metagenomic profiling suggested a high abundance of *Chlamydia* spp. intermediaries related to *C. psittaci* and *C. abortus*. The reference laboratory detected *C. abortus* carrying a plasmid inherent in avian *C. abortus* (*6*). Multilocus sequence typing revealed sequence type 359. Phylogenetic analyses of concatenated multilocus sequence typing and plasmid II *xerC* gene sequences confirmed avian *C. abortus* (Figure 2) (*6*,*7*). Chlamydial outer membrane protein A gene sequencing identified a single *Chlamydia* spp. matching provisional genotype R54 (Appendix Figure 2), previously isolated from migratory seabirds in polar regions but never from humans or other mammals (*8*,*9*). The avian *C. abortus* clinical isolate KML-2021 (GenBank accession nos. OR665720 and PQ001575) obtained from the patient in this study was genetically different from avian *C. abortus* clinical strain NL2335-4C (GenBank accession nos. CP158097 and CP158098) and related clinical isolates or strains from other patients in the Netherlands (Figure 2; Appendix Figure 2) (*2*).

The patient's respiratory condition improved with doxycycline treatment directed at *Chlamydia* spp. At 1-year clinical follow-up, the patient noted no recurrences. The patient provided written informed consent for publication to the treating physician (E.H.R.v.E.) after the 1-year clinical follow-up. All authors confirmed that subject protection guidelines and regulations were strictly followed. We notified the Public Health Service for the Hollands Midden region in Leiden, the Netherlands, of the zoonotic *Chlamydia* spp. infection and did not identify any human-to-human transmission events.

In conclusion, our findings confirm the zoonotic potential of avian *C. abortus* to cause severe community-acquired pneumonia in humans. Increased awareness is warranted to establish the occurrence, clinical manifestations, and global geographic distribution of that rare zoonotic disease. We recommend molecular surveillance studies in wild and captive birds to evaluate sources of contamination of different avian *C. abortus* genotypes.

Acknowledgments

We acknowledge the valuable technical support provided by Miriam Knops. We thank Georg Zeller for methodological guidance on metagenomic sequencing and microbiota profiling. We gratefully acknowledge Marloes Stradmeijer for providing relevant public health data.

E.H.R.v.E. and J.G. provided clinical care to the patient. J.G., M.E.M.K., and S.B. performed chlamydial diagnostics, *ompA* genotyping, multilocus sequence typing genotyping, and phylogenetic analyses. P.W. and S.B. conducted quantitative microbiota profiling using 16S rDNA micelle PCR and metagenomic sequencing. E.H. performed chlamydial plasmid sequencing and reference genotyping.

About the Author

Dr. Gooskens is a clinical microbiologist at the Department of Medical Microbiology, Leiden University Medical Center, Leiden, the Netherlands. His research interests focus on zoonotic *Chlamydia* spp. infections and genomic clinical surveillance of CC398 *Staphylococcus aureus*.

References

1. Borel N, Greub G. International Committee on Systematics of Prokaryotes (ICSP) Subcommittee on the taxonomy of *Chlamydiae*: minutes of the closed meeting, 25 August 2022, ESCCAR Meeting Lausanne, Switzerland. Int J Syst Evol Microbiol. 2023;73:005712. https://doi.org/10.1099/ijsem.0.005712
2. Raven S, Heijne M, Koomen J, Doornenbal G, Mass M, Jacobs P, et al. Circulation of avian Chlamydia abortus in the Netherlands and community-acquired pneumonia: an outbreak investigation and retrospective cohort study. Lancet Infect Dis.2025;25:198–207.https://doi.org/10.1016/S1473-3099(24)00529-2
3. Boers SA, Hiltemann SD, Stubbs AP, Jansen R, Hays JP. Development and evaluation of a culture-free microbiota profiling platform (MYcrobiota) for clinical diagnostics. Eur J Clin Microbiol Infect Dis. 2018;37:1081–9. https://doi.org/10.1007/s10096-018-3220-z
4. van Boheemen S, van Rijn AL, Pappas N, Carbo EC, Vorderman RHP, Sidorov I, et al. Retrospective validation of a metagenomic sequencing protocol for combined detection of RNA and DNA viruses using respiratory samples from pediatric patients. J Mol Diagn. 2020;22:196–207. https://doi.org/10.1016/j.jmoldx.2019.10.007
5. Walker MA, Pedamallu CS, Ojesina AI, Bullman S, Sharpe T, Whelan CW, et al. GATK PathSeq: a customizable computational tool for discovering and identifying microbial sequences in libraries from eukaryotic hosts. Bioinformatics. 2018;34:4287–9. https://doi.org/10.1093/bioinformatics/bty501
6. Aaziz R, Laroucau K, Gobbo F, Salvatore D, Schnee C, Terregino C, et al. Occurrence of Chlamydiae in corvids in northeast Italy. Animals (Basel). 2022;12:1226. https://doi.org/10.3390/ani12101226

7. Szymańska-Czerwińska M, Mitura A, Niemczuk K, Zaręba K, Jodełko A, Pluta A, et al. Dissemination and genetic diversity of chlamydial agents in Polish wildfowl: isolation and molecular characterisation of avian *Chlamydia abortus* strains. PLoS One. 2017;12:e0174599. https://doi.org/10.1371/journal.pone.0174599
8. Herrmann B, Rahman R, Bergström S, Bonnedahl J, Olsen B. *Chlamydophila abortus* in a brown skua (*Catharacta antarctica lonnbergi*) from a subantarctic island. Appl Environ Microbiol. 2000;66:3654–6. https://doi.org/10.1128/AEM.66.8.3654-3656.2000
9. Christerson L, Blomqvist M, Grannas K, Thollesson M, Laroucau K, Waldenström J, et al. A novel Chlamydiaceae-like bacterium found in faecal specimens from sea birds from the Bering Sea. Environ Microbiol Rep. 2010;2:605–10. https://doi.org/10.1111/j.1758-2229.2010.00174.x

Address for correspondence: J. Gooskens, Department of Medical Microbiology, E4-58, Center of Infectious Diseases (LUCID), Leiden University Medical Center, PO Box 9600, 2300 RC, Leiden, the Netherlands; email: j.gooskens@lumc.nl

Evaluation of High-Dose Isoniazid in Multidrug-Resistant Tuberculosis Treatment

Valentina Gerussi, Tania Petersen, Isabelle Bonnet, Alexandra Aubry, Marwa Bachir, Esther Gyde, Florence Morel, Corentin Poignon, Brigitte Rached, Valérie Pourcher, Christophe Rioux, Dorothée Vallois, Nicolas Veziris, Jérôme Robert, Lorenzo Guglielmetti

Author affiliations: Università degli Studi di Trieste, Trieste, Italy (V. Gerussi); Sorbonne Université, Centre National de Référence des Mycobactéries et de la Résistance des Mycobactéries aux Antituberculeux, Assistance Publique–Hôpitaux de Paris, Paris, France (T. Petersen, I. Bonnet, A. Aubry, E. Gyde, F. Morel, C. Poignon, B. Rached, V. Pourcher, N. Veziris, J. Robert, L. Guglielmetti); Centre Hospitalier de Saint-Denis-Centre Hospitalier de Gonesse, Saint-Denis, France (M. Bachir); Université Paris Cité, Paris (C. Rioux, D. Vallois)

DOI: https://doi.org/10.3201/eid3103.241473

High-dose isoniazid is recommended to treat multidrug-resistant tuberculosis (MDR TB). Among 958 MDR TB isolates identified in France during 2008–2022, 93.1% exhibited high-level isoniazid resistance, and molecular testing showed limited diagnostic accuracy in predicting resistance. Clinicians should reconsider using high-dose isoniazid in MDR TB treatment because of suboptimal effect and toxicity concerns.

Despite the turning point represented by the 2022 update in World Health Organization guidelines (*1*), optimal treatment for multidrug-resistant tuberculosis (MDR TB), defined by isoniazid and rifampin resistance, remains a global challenge. The 6-month, all-oral regimen combining bedaquiline, pretomanid, linezolid, and moxifloxacin represents a breakthrough in MDR TB treatment; however, its adoption is limited by cost and access issues. Alternative treatments include the 9-month, all-oral short-course regimen (SCR) and the 18-month, individualized conventional regimen. The SCR is recommended for patients with MDR TB without fluoroquinolone resistance and includes high-dose isoniazid of 10–15 mg/kg. The conventional regimen may also incorporate high-dose isoniazid if there is no confirmation of high-level isoniazid resistance (*1*). The effectiveness of high-dose isoniazid relies on the absence of mutations known to confer phenotypic high-level isoniazid resistance, notably mutations in the *katG* gene (*2*). The high prevalence of such mutations among MDR TB isolates makes the role of high-dose isoniazid in MDR TB regimens questionable (*3*). We quantified the prevalence of high-level isoniazid resistance among MDR TB isolates, particularly isolates from patients eligible for SCR, and evaluated the diagnostic accuracy of molecular testing for predicting high-level isoniazid resistance.

We used data from the comprehensive French national network of the National Reference Centre for Mycobacteria (Paris, France) to perform a retrospective, observational cohort study. We included the isolate obtained at diagnosis from each patient with confirmed pulmonary or extrapulmonary MDR TB identified in France during 2008–2022. We excluded isolates lacking phenotypic drug susceptibility testing (DST) results for isoniazid (0.2 and 1.0 μg/mL) or genotypic data for *inhA*, *katG*, and *gyrA*. For phenotypic DST, solid and liquid cultures were used interchangeably. Testing of solid cultures used the proportion method on Löwenstein-Jensen media, whereas testing of liquid cultures used mycobacteria growth indicator tubes containing Middlebrook 7H9 broth (BD Difco, https://www.bd.com). We defined resistance levels

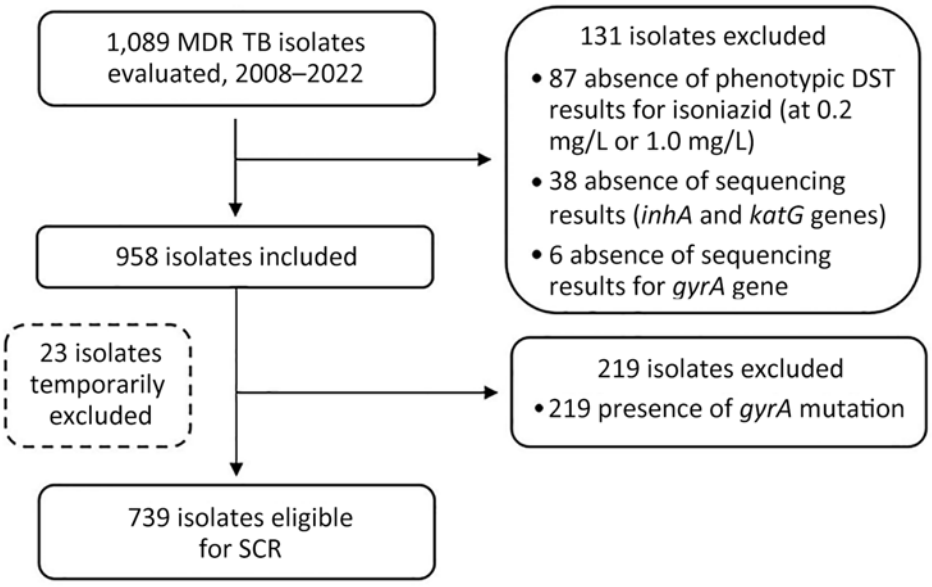

Figure. Flowchart of MDR TB isolates identified in France during 2008–2022 included in an evaluation of high-dose isoniazid in MDR TB treatment. DST, drug susceptibility testing; MDR TB, multidrug-resistant tuberculosis; SCR, short-course regimen.

as low-level (0.2 μg/mL) or high-level (1.0 μg/mL) (*4*). Genotypic DST used GenoType MTBDR*plus* and MTBDR*sl* assays (Bruker, https://www.bruker.com) and Sanger or targeted next-generation sequencing (Deeplex Myc-TB; Genoscreen, https://www.genoscreen.fr) when line-probe assay results were missing or uninterpretable. We interpreted results according to the World Health Organization catalog of resistance-associated genetic variants (*5*). We defined eligibility for SCR as the absence of *gyrA* mutations.

We assessed the diagnostic accuracy of *katG* mutations (with or without mutation in *inhA*) in predicting high-level isoniazid resistance by using phenotypic DST. In the DST calculation, strains without mutations were excluded because they could not be classified as low-level resistance (*inhA* mutation) or high-level resistance (*katG* with or without *inhA* mutation) in phenotypic-genotypic comparisons.

Descriptive statistics included frequency analyses for categorical variables and median and interquartile range for quantitative variables. We calculated 95% CIs for proportions. We used Stata 15.2 (StataCorp LLC, https://www.stata.com) for analyses and considered $p<0.05$ statistically significant. Ethical approval was granted by the ethics review board of the Bligny Hospital, Briis-sous-Forges, France (study design approved by Conseil de Réflexion Ethique on June 27, 2023).

Among 1,089 MDR TB isolates, 958 were included in the study (Figure). Of those isolates, 892 (93.1%, 95% CI 91.5–94.7) exhibited high-level isoniazid resistance (Table). Mutations in *katG* were found in 837 (87.4%) isolates and *inhA* mutations in 259 (27.0%)

Table. Phenotypic and genotypic methods for MDR TB isolates identified in France during 2008–2022 used in evaluation of high-dose isoniazid use in MDR TB treatment*

Isoniazid resistance	All isolates, n = 958	Isolates from patients eligible for SCR, n = 739
Phenotypic isoniazid resistance		
High-level resistance†	892 (93.1; 91.5–94.7)	677 (91.6; 89.6–93.6)
Low-level resistance‡	66 (6.9; 5.3–8.5)	62 (8.4; 6.4–10.4)
Genotypic isoniazid resistance		
katG + *inhA* or its promoter mutation	161 (16.8; 14.4–19.2)	104 (14.1; 11.6–16.6)
katG mutation alone	676 (70.6; 67.7–73.5)	525 (71.0; 67.8–74.3)
inhA or its promoter mutation alone	98 (10.2; 8.3–12.1)	89 (12.1; 9.7–14.4)
No mutation	23 (2.4; 1.4–3.4)	21 (2.8; 1.6–4.0)
Diagnostic accuracy of genotypic testing (*katG* mutation) to predict high-level isoniazid resistance, % (95% CI)		
Sensitivity	93.3 (91.6–94.9)	92.3 (90.4–94.3)
Specificity	86.4 (84.2–88.6)	87.3 (84.8–89.7)
Positive predictive value	99.0 (98.4–99.7)	98.9 (98.1–99.7)
Negative predictive value	46.4 (43.2–49.6)	48.5 (44.8–52.1)

*Values are no. (%; 95% CI) except as indicated. MDR TB, multidrug-resistant TB; SCR, short course regimen.
†Defined as resistance to the 1.0 μg/mL dose.
‡Defined as resistance to the 0.2 μg/mL dose.

isolates. Of note, 828 (98.9%) of the 837 isolates with *katG* mutations showed high-level isoniazid resistance. In addition, we detected high-level isoniazid resistance in 51.0% of isolates with *inhA* mutations and without *katG* mutations. Of the 739 isolates from patients eligible for the SCR (Figure), 677 (91.6%) had high-level isoniazid resistance. The diagnostic accuracy of genotypic testing for predicting high-level isoniazid resistance compared with phenotypic DST was as follows: sensitivity 93.3% (95% CI 91.6–94.9), specificity 86.4% (95% CI 84.2–88.6), positive predictive value 99.0% (95% CI 98.4–99.7), and negative predictive value 46.4% (95% CI 43.2–49.6). Those accuracy metrics were comparable among isolates from patients eligible for SCR (Table).

Our findings indicated that high-dose isoniazid is unlikely to be effective for most patients using the MDR TB regimen because of the high prevalence of high-level isoniazid resistance, including those from patients eligible for SCR. The high frequency of observed *katG* mutations aligns with previous studies; most *katG* mutant isolates exhibited high-level isoniazid resistance (*3*). Furthermore, the absence of *katG* mutations alone does not reliably exclude high-level isoniazid resistance because more than half of strains in our study with *inhA* mutations displayed isoniazid MICs ≥1.0 mg/L. Although high-dose isoniazid was previously considered effective against *inhA* mutant isolates (*6*), more recent research reported MICs >1.0 mg/L in those strains (*7*,*8*), which limits the utility of genotypic testing in predicting low-level isoniazid resistance. Although high-dose isoniazid may still be appropriate in specific cases, the associated toxicity risks suggest that its inclusion in MDR TB regimens may not be warranted (*9*,*10*).

In summary, high-dose isoniazid offers limited benefit for most patients using the MDR TB regimen because of widespread high-level isoniazid resistance. Clinicians should optimize existing regimens, replace high-dose isoniazid with safer, more effective alternatives, and promote global access to new treatments.

Acknowledgments

The authors thank the technical staff of the National Reference Centre for Mycobacteria (Paris, France) for their invaluable and meticulous daily contributions. V. Gerussi thanks Maria Merelli for her support and Carlo Tascini for providing the opportunity to conduct research at the National Reference Centre for Mycobacteria.

V.G., A.A., N.V., and L.G. are members of European Society of Clinical Microbiology and Infectious Diseases Study Group for Mycobacterial Infections.

About the Author

Dr. Gerussi is an infectious diseases specialist at the Infectious Diseases Department of Trieste University Hospital, Trieste, Italy. Her research interests include tubercular infections and antibiotic drug use.

References

1. World Health Organization. WHO consolidated guidelines on tuberculosis. Module 4: treatment—drug-resistant tuberculosis treatment, 2022 update. Geneva: The Organization; 2022.
2. Gausi K, Ignatius EH, De Jager V, Upton C, Kim S, McKhann A, et al. High-dose isoniazid lacks EARLY bactericidal activity against isoniazid-resistant tuberculosis mediated by katG mutations: a randomized, phase 2 clinical trial. Am J Respir Crit Care Med. 2024;210:343–51. https://doi.org/10.1164/rccm.202311-2004OC
3. Chesov D, Ciobanu N, Lange C, Heyckendorf J, Crudu V. High-dose isoniazid in the shorter-course multidrug-resistant tuberculosis regimen in the Republic of Moldova. Eur Respir J. 2017;50:1701340. https://doi.org/10.1183/13993003.01340-2017
4. World Health Organization. Technical report on critical concentrations for drug susceptibility testing of isoniazid and the rifamycins (rifampicin, rifabutin and rifapentine). Geneva: The Organization; 2021.
5. World Health Organization. Catalogue of mutations in *Mycobacterium tuberculosis* complex and their association with drug resistance, 2nd ed. Geneva: The Organization; 2023.
6. Dooley KE, Miyahara S, von Groote-Bidlingmaier F, Sun X, Hafner R, Rosenkranz SL, et al. Early bactericidal activity of different isoniazid doses for drug-resistant TB (INHindsight): a randomized open-label clinical trial. Am J Respir Crit Care Med. 2020;201:1416–24. https://doi.org/10.1164/rccm.201910-1960OC
7. Lale Ngema S, Dookie N, Perumal R, Nandlal L, Naicker N, Peter Letsoalo M, et al. Isoniazid resistance-conferring mutations are associated with highly variable phenotypic resistance. J Clin Tuberc Other Mycobact Dis. 2023;33:100387. https://doi.org/10.1016/j.jctube.2023.100387
8. Ghodousi A, Tagliani E, Karunaratne E, Niemann S, Perera J, Köser CU, et al. Isoniazid resistance in *Mycobacterium tuberculosis* is a heterogeneous phenotype composed of overlapping MIC distributions with different underlying resistance mechanisms. Antimicrob Agents Chemother. 2019;63:e00092-19. https://doi.org/10.1128/AAC.00092-19
9. Katiyar SK, Bihari S, Prakash S, Mamtani M, Kulkarni H. A randomised controlled trial of high-dose isoniazid adjuvant therapy for multidrug-resistant tuberculosis. Int J Tuberc Lung Dis. 2008;12:139–45.
10. Richardson M, Kirkham J, Dwan K, Sloan DJ, Davies G, Jorgensen AL. *NAT2* variants and toxicity related to anti-tuberculosis agents: a systematic review and meta-analysis. Int J Tuberc Lung Dis. 2019;23:293–305. https://doi.org/10.5588/ijtld.18.0324

Address for correspondence: Valentina Gerussi, Infectious and Tropical Diseases Unit, Trieste University Hospital, Via Giuseppe Lorenzo Gatteri 25/1, 34125 Trieste, Italy; email: valentina.gerussi@gmail.com

Annual Hospitalizations for COVID-19, Influenza, and Respiratory Syncytial Virus, United States, 2023–2024

Projections for the US 2023–24 respiratory virus season indicated a 31% decrease to a 55% increase in hospitalizations for respiratory syncytial virus, influenza, and COVID-19 compared with 2022–23, depending on circulating variants and vaccination uptake. The projections captured the tripledemic peak but missed the multiwave seasonality of COVID-19.

Kaiming Bi,[1,2] Shraddha Ramdas Bandekar,[2] Anass Bouchnita, Spencer J. Fox,[3] Lauren Ancel Meyers[3]

Author affiliations: The University of Texas at Austin, Austin, Texas, USA (K. Bi, S.R. Bandekar, L. Ancel Meyers); The University of Texas at El Paso, El Paso, Texas, USA (A. Bouchnita); University of Georgia, Athens, Georgia, USA (S.J. Fox)

DOI: https://doi.org/10.3201/eid3103.240594

Nonpharmaceutical interventions to combat the COVID-19 pandemic disrupted the seasonal transmission of influenza virus and respiratory syncytial virus (RSV). During November 2022–March 2023, co-circulation of SARS-CoV-2, influenza virus, and RSV caused a tripledemic that strained US healthcare systems. By the summer of 2023, global authorities had officially declared the end of the COVID-19 pandemic (*1*), and the recent tripledemic had bolstered populationwide immunity against the 3 viruses, leading to considerable uncertainty about the potential severity of the 2023–24 respiratory virus season and the effects of updated vaccines for SARS-CoV-2 and influenza (*2*), the novel Food and Drug Administration–approved RSV vaccine for older adults and pregnant women, and the novel monoclonal antibody therapy for infants with RSV (*3*). To support national planning, we created a series of scenario projections by using validated models of influenza, SARS-CoV-2, and RSV that track immunity stemming from infection and immunization (Appendix, https://wwwnc.cdc.gov/EID/article/31/3/25-0594-App1.pdf) and compared projected 2023–24 hospitalizations to those reported during the 2022–23 season. We retrospectively evaluated the validity of the assumptions and the consistency of the projections compared with actual epidemiologic trends in the United States during September 1, 2023–March 30, 2024.

The 4 SARS-CoV-2 scenarios assumed that an immune-evasive EG.5-like variant either would or would not emerge in May 2023 and that updated booster vaccines would be recommended for everyone or only for adults ≥65 years of age (Appendix). In retrospect, the scenarios optimistically assumed 52% booster coverage for persons ≥65 years of age and 34% for persons <65 years of age, which are almost double the reported uptake of 28.1% for persons ≥65 years of age and 19.1% for persons <65 years of age (*4*). Moreover, none of the scenarios anticipated the October emergence of the highly transmissible JN.1 variant (*5*). Our projections of 598,000 (95% CI 486,000–692,000) to 1,310,000 (95% CI 1,089,000–1,493,000) total COVID-19 hospitalizations were high compared with the 612,616 eventually reported, and the projected mid-October peak was considerably earlier than the actual December peak (Figure, panel A). Our model cannot explain the persistent 2-wave seasonal dynamics of COVID-19, which could stem from frequent emergence of new variants, durability of infection-acquired and vaccine-acquired immunity, or other unidentified seasonal factors.

The influenza scenarios vary in terms of the dominant subtype (H1N1 vs. H3N2) and national vaccination coverage (40% vs. 60%) (Appendix). In retrospect, the 2023–24 influenza season was dominated by influenza A(H1N1), and an estimated 47.3% of the US population received an influenza vaccine (*6*). Under the best-matching scenario (H1N1 with 40% coverage), daily influenza hospital admissions were projected to peak on December 16 (95% CI November 21–January 25) at 4,100 (95% CI 400–8,700) and to total 210,000 (95% CI 17,000–475,000) (Figure, panel B). In reality, influenza hospital admissions peaked on December 28 at 3,137 and totaled 215,667. Comparing our 2 influenza A(H1N1) scenarios, we estimated that vaccinating 60% versus 40% of the US population would have prevented 27,000 (95% CI 6,000–34,000) influenza-related hospitalizations.

The RSV scenarios assume either a high transmission rate (estimated in 2022–23) or a low transmission rate (estimated before 2020) and either high or low vaccination uptake. Under the high uptake scenario, the new RSV vaccine is recommended

[1]Current affiliation: The University of Texas Health Science Center, Houston, Texas, USA.

[2]These first authors contributed equally to this article.

[3]These authors contributed equally to this article.

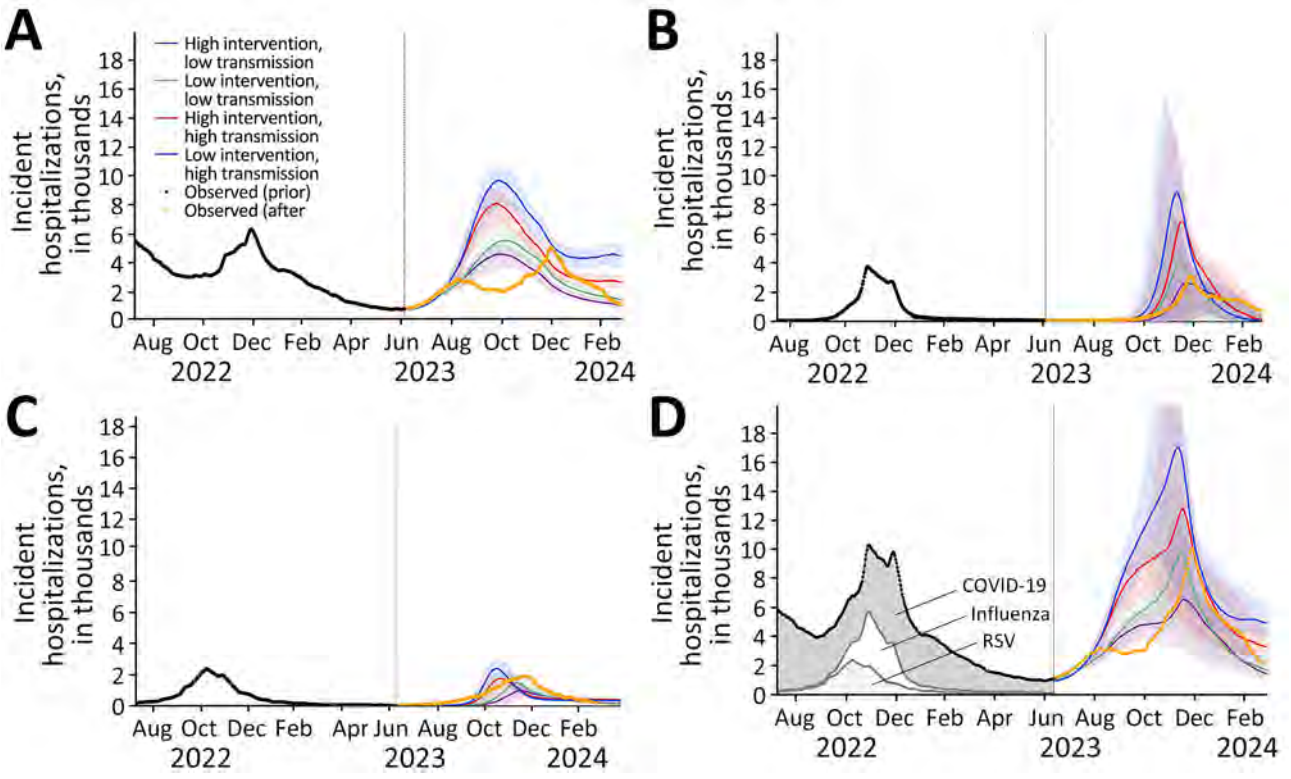

Figure. Projected daily hospital admissions attributable to COVID-19 (A), influenza (B), RSV (C), and COVID-19, influenza, or RSV infections combined (D) under multiple scenarios with varying viral transmission rates and varying effect of medical countermeasures, United States, June 8, 2023–March 30, 2024. Values are the 7-day average number of hospital admissions attributable to infections by the specified viruses. The solid lines indicate medians; shaded ribbons indicate 95% CIs across 200 stochastic simulations. Black dots in all graphs and gray shading in panel D indicate the reported 7-day average hospital admissions for the 3 viruses before the projection period (*9*,*10*); orange lines indicate 7-day average hospital admissions from the projection period that were not available at the time of the initial analysis. RSV, respiratory syncytial virus.

for persons ≥60 years of age (assuming 56.12% uptake based on 2022–23 influenza vaccination coverage), and all infants <8 months of age receive the new monoclonal antibody (Appendix). As of April 2024, only ≈23.6% (95% CI 22.7%–24.5%) of older adults had received the vaccine and 43.0% (95% CI 33.9%–52.1%) of infants had received antibody injections (*7*,*8*). By fitting our model to 2023–24 RSV hospitalization data (Appendix), we estimated that the transmission rate for children <18 years of age was similar to prepandemic levels, whereas that for older persons might have been higher than during the 2022–23 season. Although our scenarios did not anticipate this complexity, the observed trends are roughly consistent with the projections. The scenario assuming a prepandemic transmission rate and low vaccination uptake projected a total of 95,000 (95% CI 52,000–157,000) RSV hospitalizations, peaking on December 12 (95% CI December 5–25) with 1,500 (95% CI 800–2,100) daily admissions. In reality, US RSV hospital admissions peaked on December 30 at 1,911 and totaled 178,000 (Figure, panel C).

We aggregated the individual pathogen scenario projections to estimate overall tripledemic hospitalizations, assuming no epidemiologic interactions among them (Appendix). The subsequently observed trends fell well within the projected CIs (Figure, panel D) and were closest to the scenario assuming low transmission rates and low vaccination uptake for all 3 viruses. Although the scenario assumptions were imperfect, particularly for COVID-19, the projected cumulative hospitalizations of 1,029,000 (95% CI 688,000–1,518,000) and early December peak of 9,800 (95% CI 4,700–15,246) daily admissions are consistent with the observed 1,007,000 total hospitalizations and late December peak of 10,082 (Appendix). Even when the assumptions prove wrong, simulating a range of carefully constructed scenarios can help anticipate the timing and severity of epidemics, assess the probable effect of interventions, and guide healthcare capacity planning.

All data for reproducing the analysis are publicly available at https://github.com/bikaiming93/tripledemic. All code for reproducing the analysis are publicly available at https://github.com/bikaiming93/tripledemic.

This study was supported by funding from the National Institutes of Health (grant no. R01 AI151176-Suppl), the Centers for Disease Control and Prevention (grant no. U01IP001136-Suppl), and the Council of State and Territorial Epidemiologists (grant no. NU38OT000297).

About the Author

Dr. Bi is an assistant professor of Management, Policy, and Community Health at The University of Texas Health Science Center School of Public Health. His research interests include infectious disease modeling, epidemic forecasting, and supporting public health decision-making. Dr. Bandekar is a postdoctoral fellow at The University of Texas at Austin with expertise in infectious disease modeling. Her primary research interests include mathematical and computational modeling of respiratory viruses.

References

1. World Health Organization. Statement on the fifteenth meeting of the IHR (2005) Emergency Committee on the COVID-19 pandemic. 2023 May 5 [cited 2023 Aug 13]. https://www.who.int/news/item/05-05-2023-statement-on-the-fifteenth-meeting-of-the-international-health-regulations-(2005)-emergency-committee-regarding-the-coronavirus-disease-(covid-19)-pandemic
2. Kumari M, Lu RM, Li MC, Huang JL, Hsu FF, Ko SH, et al. A critical overview of current progress for COVID-19: development of vaccines, antiviral drugs, and therapeutic antibodies. J Biomed Sci. 2022;29:68. https://doi.org/10.1186/s12929-022-00852-9
3. Food and Drug Administration. Respiratory syncytial virus (RSV). 2024 Oct 22 [cited 2024 Sep 4]. https://www.fda.gov/consumers/covid-19-flu-and-rsv/respiratory-syncytial-virus-rsv
4. Centers for Disease Control and Prevention. Weekly COVID-19 vaccination dashboard. 2025 Jan 15 [cited 2024 Sep 4]. https://www.cdc.gov/vaccines/imz-managers/coverage/covidvaxview/interactive/vaccination-dashboard.html
5. Kaku Y, Okumura K, Padilla-Blanco M, Kosugi Y, Uriu K, Hinay AA Jr, et al.; Genotype to Phenotype Japan (G2P-Japan) Consortium. Virological characteristics of the SARS-CoV-2 JN.1 variant. Lancet Infect Dis. 2024;24:e82. https://doi.org/10.1016/S1473-3099(23)00813-7
6. Centers for Disease Control and Prevention. Influenza vaccine doses distributed. 2025 Jan 15 [cited 2023 Sep 4]. https://www.cdc.gov/flu/fluvaxview/dashboard/vaccination-doses-distributed.html
7. Centers for Disease Control and Prevention. Infant protection against respiratory syncytial virus (RSV) by maternal RSV vaccination or receipt of nirsevimab, and intent for nirsevimab receipt, United States. 2025 Jan 15 [cited 2023 Aug 13]. https://www.cdc.gov/vaccines/imz-managers/coverage/rsvvaxview/nirsevimab-coverage.html.
8. Centers for Disease Control and Prevention. Respiratory syncytial virus (RSV) vaccination coverage and intent for vaccination, adults 75 years and older and adults 60–74 years with high-risk conditions, United States. 2025 Jan 15 [cited 2024 Sep 4]. https://www.cdc.gov/vaccines/imz-managers/coverage/rsvvaxview/adults-60-coverage-intent.html
9. US Department of Health and Human Services. COVID-19 reported patient impact and hospital capacity by state timeseries (raw). 2024 Jun 28 [cited 2024 May 3]. https://healthdata.gov/Hospital/COVID-19-Reported-Patient-Impact-and-Hospital-Capa/g62h-syeh/about_data
10. Centers for Disease Control and Prevention. RSV-NET interactive dashboard 2024 Oct 10 [cited 2024 Sep 4]. https://www.cdc.gov/rsv/research/rsv-net/dashboard.html

Address for correspondence: Lauren Ancel Meyers, Department of Integrative Biology, The University of Texas at Austin, PAT 656, 2415 Speedway, Austin, TX 78712, USA; email: laurenmeyers@austin.utexas.edu

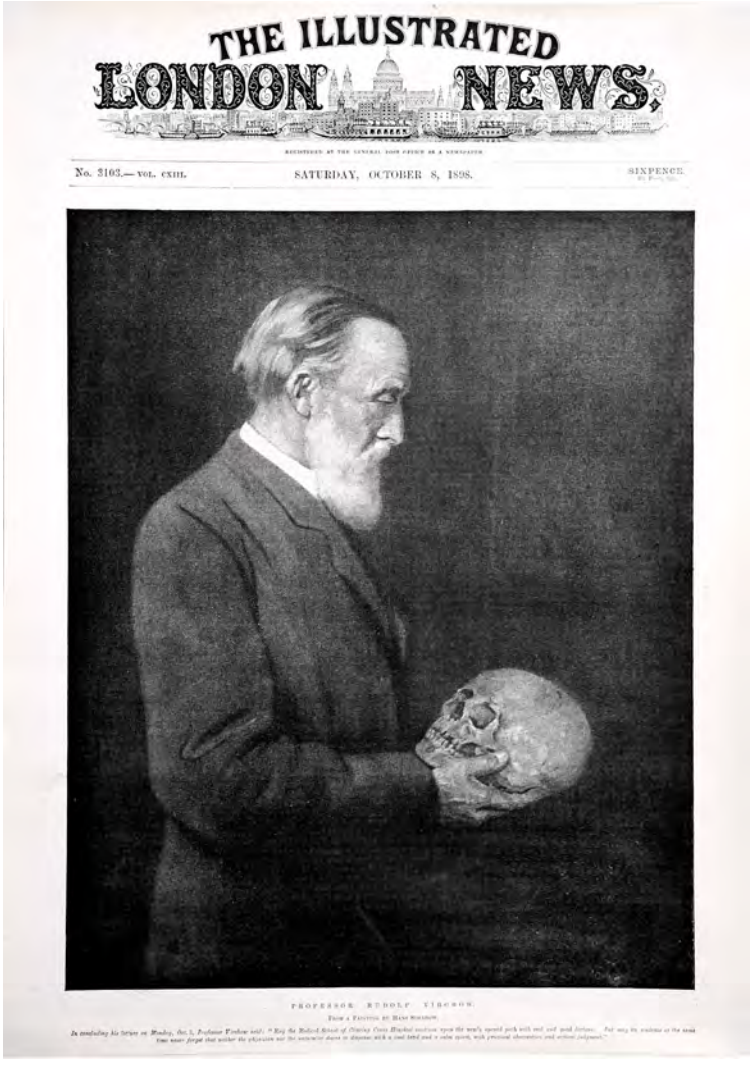

Hans Schadow (1862–1924), print of original oil on canvas portrait of Rudolf Virchow (1896). *The Illustrated London News* (London, UK; October 8, 1898). Private collection, Atlanta, Georgia, USA. Photography by Will Breedlove.

Themes of Holism and Reductionism in the Quest for the Cause of Tuberculosis

Terence Chorba

In 1882, at a time when many prominent physicians, including Rudolf Virchow (1821–1902), had yet to accept the germ theory of disease, 2 contrasting but complementary schools of thought on the etiology of tuberculosis (TB) were dominant. The first was "holistic," focused principally on the host (susceptibility of the exposed individual) and the environment (extrinsic factors that affect the opportunity for exposure and development of disease); its leading proponent was Virchow, a Germ an physician whose seminal work in cellular pathology, social medicine, and public health contributed substantially to the development of modern medicine. The second was "reductionistic," focused on identifying the agent (the organism or event that resulted in disease or disability) and

Author affiliation: Centers for Disease Control and Prevention, Atlanta, Georgia, USA

DOI: https://doi.org/10.3201/eid3103.AC3103

on deconstructing the complex process of infection into its component parts; its leading proponent was Robert Koch (1843–1910), whose crowning achievement—the discovery of the organism—is celebrated annually worldwide in March and is the impetus for dedicating each March issue of this journal to tuberculosis.

Virchow popularized the biological principle that every cell originates from a predecessor cell (omnis cellula e cellula in Latin, a theory originally proposed by physiologist Theodor Schwann and botanist Matthias Schleiden) and held that all disease involves changes in normal cells (i.e., all pathology is cellular pathology). Among Virchow's many achievements as "the father of modern pathology" were the first descriptions of many medical phenomena including leukemia, embolism, and thrombosis. Virchow was also a strong proponent of social medicine, advancing insightful arguments that disease was often caused and exacerbated by social and economic conditions, rather than just biological factors. His belief in the social determinants of health led him to identify nutrition, poverty, and sanitation as influential factors in public health and to advocate for improvements in living and working conditions.

On the evening of March 24, 1882, at the Berlin Institute of Physiology, Robert Koch presented his conclusive work demonstrating that infection with a characteristic bacillus (*Mycobacterium tuberculosis*) was the cause of TB. Koch's conclusion was based on strict criteria or postulates now considered essential for establishing scientific consensus that a given microorganism causes a disease: 1) the organism can be shown to be consistently present in diseased tissue; 2) the organism can be isolated and grown in pure culture; and 3) the organism can be shown experimentally to induce the disease in animal models. The Nobel Prize–winning physician and chemist Paul Ehrlich (1854–1915), who had been an early assistant of Koch and a TB survivor himself, later said of that evening's meeting that it had been "the most important experience of my scientific life."

Koch had much ground to cover in his brief presentation of that reductionist science (i.e., proving TB to be a specific disease with a specific infectious etiology). Although Virchow was in attendance, he remained silent. As a proponent of the societal and environmental causes of disease, Virchow had characterized TB as a social disease strongly linked to poverty and had disputed Koch's germ theory. His holistic recognition of the social determinants of health constituted the basis for advocacy of comprehensive health reforms (i.e., improved housing, sanitation, water supply, and working conditions). In the years immediately following Koch's discovery, there was great interest in seeking nonexclusionary remedies that addressed both the holistic and reductionist views for TB prevention and control. Holistic efforts attempted to avert the societal burden of transmission of the bacillus through public health campaigns to raise awareness of risk factors and to improve living and working conditions. Reductionist efforts were aimed at attenuating the bacillus through use of serum, mostly from infected animals and humans. Both Koch and Virchow achieved great public stature in their lifetimes for their contributions to medical science and public health.

In 1896, Hans Schadow (1862–1924), an accomplished portrait painter born in Berlin, Germany, created a detailed oil-on-canvas portrait of Rudolf Virchow contemplating a human skull; the portrait was commissioned by *The Illustrated London News*, a magazine published weekly during 1842–1971 and then less frequently before ceasing publication altogether in 2003. The magazine itself was revolutionary, as the first fully illustrated weekly newspaper, and took the occasion of Virchow's delivering a medical lecture in London to reproduce Schadow's painting as a print on its front page in 1898, featured again on the cover of this month's journal.

In modern-day TB elimination efforts, effective prevention and control programs have several priority strategies that include identifying and completing treatment of TB disease; finding and screening persons who have been recent contacts of TB patients; and screening, testing, and treating populations at greater risk of having latent TB infection and of developing TB disease. Components of Koch's reductionist approach are fundamental to the identification of persons with TB disease; although a minority of incident TB cases have no bacilli detectable in sputum or in other body fluids, TB disease is usually confirmed by a positive culture or nucleic acid amplification test result for *M. tuberculosis*. However, components of Virchow's holistic approach are essential for identifying, testing, and treating populations at greater risk and for whom testing and treatment are most defensible in a resource-limited environment (e.g., persons from high-burden countries; those who lived or worked with persons with TB disease; or those with immune compromise resulting from diabetes,

smoking, alcohol use disorder, cancer, or HIV infection). Both perspectives have intrinsic relevance to the strategies of health departments in TB elimination efforts.

References

1. Daniel TM. Pioneers of medicine and their impact on tuberculosis. Rochester (NY): University of Rochester Press; 2000. p. 73–79.
2. Dubos RJ, Dubos J. The white plague: tuberculosis, man, and society. New Brunswick (NJ): Rutgers University Press; 1987.
3. Glatman-Freedman A, Casadevall A. Serum therapy for tuberculosis revisited: reappraisal of the role of antibody-mediated immunity against *Mycobacterium tuberculosis*. Clin Microbiol Rev. 1998;11:514–32. https://doi.org/10.1128/CMR.11.3.514
4. Goetz T. The Remedy: Robert Koch, Arthur Conan Doyle, and the quest to cure tuberculosis. New York,: Avery Publishing; .014.
5. Gradmann C. Laboratory disease: Robert Koch's medical bacteriology. Forster E, translator. Baltimore (MD): Johns Hopkins University Press; 2009.
6. Ribatti D. Rudolf Virchow, the founder of cellular pathology. Rom J Morphol Embryol. 2019;60:1381–2.
7. Riccardi N, Canetti D, Martini M, Diaw MM, DI Biagio A, Codecasa L, et al. The evolution of an ancient disease: tuberculosis discoveries in the centuries. J Prev Med Hyg. 2020;61(Suppl 1):E9–12. https://doi.org/10.15167/2421-4248/jpmh2020.61.1s1.1353
8. Schultz M. Rudolf Virchow. Emerg Infect Dis. 2008;14:1480–1. https://doi.org/10.3201/eid1409.086672
9. Tawde PP, Choudhari SG, Quazi Syed Z, Gaidhane A. Rudolf Virchow: integrating medicine and social reform for public health. Cureus. 2024;16:e68161. https://doi.org/10.7759/cureus.68161

Address for correspondence: Terence Chorba, Centers for Disease Control and Prevention, 1600 Clifton Rd NE, Mailstop H24-4, Atlanta, GA 30329-4018, USA; email: tlc2@cdc.gov

The Public Health Image Library

The Public Health Image Library (PHIL), Centers for Disease Control and Prevention, contains thousands of public health–related images, including high-resolution (print quality) photographs, illustrations, and videos.

PHIL collections illustrate current events and articles, supply visual content for health promotion brochures, document the effects of disease, and enhance instructional media.

PHIL images, accessible to PC and Macintosh users, are in the public domain and available without charge.

Visit PHIL at: https://phil.cdc.gov/

EMERGING INFECTIOUS DISEASES®

Upcoming Issue

- Maternal and Fetal Implications of Oropouche Fever, Espírito Santo State, Brazil, 2024
- Erythema Migrans Skin Lesions Less Frequent in Lyme Reinfections, Europe
- Alistipes Bacteremia in Older Patients with Digestive and Cancer Comorbidities, Japan, 2016–2024
- Foodborne Illness Acquired in the United States—Major Pathogens, 2019
- A Population-Based Matched Cohort Study of Healthcare Costs Attributable to COVID-19 in Ontario, Canada
- Detection and Decontamination of Chronic Wasting Disease Prions during Venison Processing
- Epidemiology of Tularemia among Humans and Animals, Baden-Wuerttemberg, Germany, 2012–2022
- Neutralizing Antibodies against California Serogroup Orthobunyaviruses in Human Serum Samples, Montana, USA
- Prevalence of Herpes B Virus in Wild Long-Tailed Macaques, Thailand, 2018–2024
- Predictive Model for Estimating Annual Ebolavirus Spillover Potential
- Oz Virus Infection in Six Animal Species, Including Macaques, Bears, and Companion Animals, Japan
- Reemergence of *Brucella abortus*, Israel, 2021
- Carbapenem-Resistant, Virulence Plasmid–Harboring *Klebsiella pneumoniae,* United States
- Alpha-Gal Syndrome after *Ixodes scapularis* Tick Bite, Maine, USA, 2014–2023
- Onset of Alpha-Gal Syndrome after Tick Bite, Washington, USA
- *Bartonella Quintana* Endocarditis and Pauci-Immune Glomerulonephritis in A Patient
- Dynamics of Bagaza, West Nile, and Usutu Viruses Revealed by Surveillance in Red-Legged Partridges, Portugal, 2018–2022
- Exposure of Wild Mammals Inhabiting Alaska to Influenza A(H5N1) Virus
- Nipah Virus Detection in *Pteropus hypomelanus* Bats in Central Java, Indonesia
- Rabbit Hepatitis E Virus, Ukraine, 2024
- HAdV-B55 Infection in Patient without Recent Travel History, France
- Local Circulation of Sindbis Virus in Wild Birds and Horses, the Netherlands, 2021–2022
- Increased Recognition of Human Anaplasmosis, Ontario, Canada, 2021
- Emerging Trends in Streptococcal Toxic Shock Syndrome, Japan
- Spread of Dual-Resistant *Mycoplasma genitalium* Clone among Men, France, 2021–2022

Complete list of articles in the April issue at https://wwwnc.cdc.gov/eid/#issue-320

Earning CME Credit

To obtain credit, you should first read the journal article. After reading the article, you should be able to answer the following, related, multiple-choice questions. To complete the questions (with a minimum 75% passing score) and earn continuing medical education (CME) credit, please go to http://www.medscape.org/journal/eid. Credit cannot be obtained for tests completed on paper, although you may use the worksheet below to keep a record of your answers.

You must be a registered user on http://www.medscape.org. If you are not registered on http://www.medscape.org, please click on the "Register" link on the right hand side of the website.

Only one answer is correct for each question. Once you successfully answer all post-test questions, you will be able to view and/or print your certificate. For questions regarding this activity, contact the accredited provider, CME@medscape.net. For technical assistance, contact CME@medscape.net. American Medical Association's Physician's Recognition Award (AMA PRA) credits are accepted in the US as evidence of participation in CME activities. For further information on this award, please go to https://www.ama-assn.org. The AMA has determined that physicians not licensed in the US who participate in this CME activity are eligible for *AMA PRA Category 1 Credits*™. Through agreements that the AMA has made with agencies in some countries, AMA PRA credit may be acceptable as evidence of participation in CME activities. If you are not licensed in the US, please complete the questions online, print the AMA PRA CME credit certificate, and present it to your national medical association for review.

Article Title

Efficacy and Safety of 4-Month Rifapentine-Based Tuberculosis Treatments in Persons with Diabetes

CME Questions

1. What were the results of the full patient cohort of the Tuberculosis Trials Consortium Study 31/ AIDS Clinical Trials Group 79 A5349 (S31/A5349) in comparing the rifapentine-moxifloxacin 4-month regimen vs the 6-month control regimen?

A. The rifapentine-moxifloxacin regimen was superior to the control regimen
B. The control regimen was superior to the rifapentine-moxifloxacin regimen
C. The rifapentine-moxifloxacin regimen was similar to the control regimen
D. Only the 4-drug rifapentine regimen was effective in treating tuberculosis

2. Which of the following treatment groups had the highest numerical rate of tuberculosis-related unfavorable outcomes in the current study focused on participants with diabetes?

A. Control regimen
B. Rifapentine-moxifloxacin regimen
C. Rifapentine regimen
D. 5-drug regimen including rifapentine, isoniazid, ethambutol, pyrazinamide, and moxifloxacin

3. Which of the following statements regarding the rate of culture conversion to negative in the current study is most accurate?

A. Culture conversion was most rapid with the control regimen
B. Culture conversion was most rapid with the rifapentine-moxifloxacin regimen
C. Culture conversion was most rapid with the rifapentine regimen
D. The rate of culture conversion was similar in the 3 treatment groups

4. Which of the following severe adverse events was more common in the rifapentine-moxifloxacin group vs the other 2 treatment groups in the current study?

A. Hypertension
B. Poor glycemic control
C. Transaminitis
D. Neuropathy

Emerging Infectious Diseases
Photo Quiz Articles

Volume 14, Number 9
September 2008

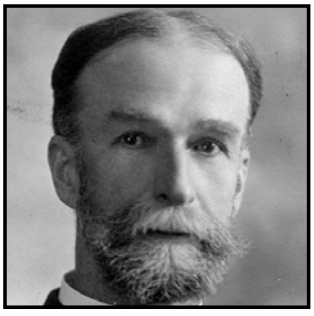

Volume 14, Number 12
December 2008

Volume 15, Number 9
September 2009

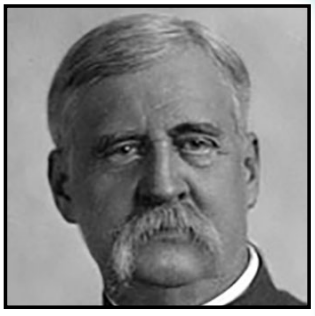

Volume 15, Number 10
October 2009

Volume 16, Number 6
June 2010

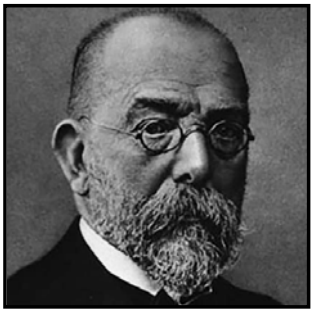

Volume 17, Number 3
March 2011

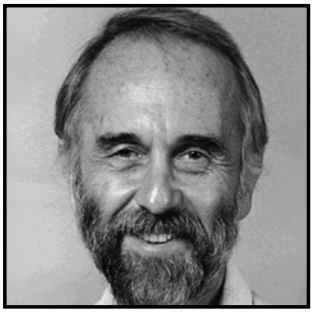

Volume 17, Number 12
December 2011

Volume 19, Number 4
April 2013

Volume 20, Number 5
May 2014

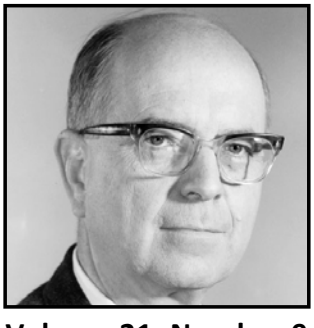

Volume 21, Number 9
September 2015

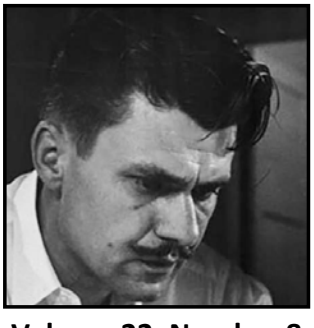

Volume 22, Number 8
August 2016

Volume 28, Number 3
March 2022

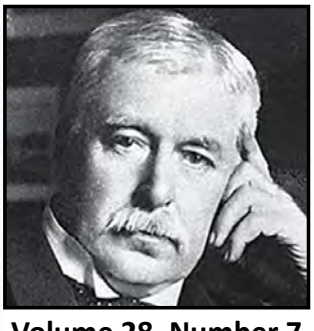

Volume 28, Number 7
July 2022

Click on the link below to read about the people behind the science.

https://bit.ly/3LN02tr

See requirements for submitting a photo quiz to EID.

https://bit.ly/3VUPqfj

EID Journal